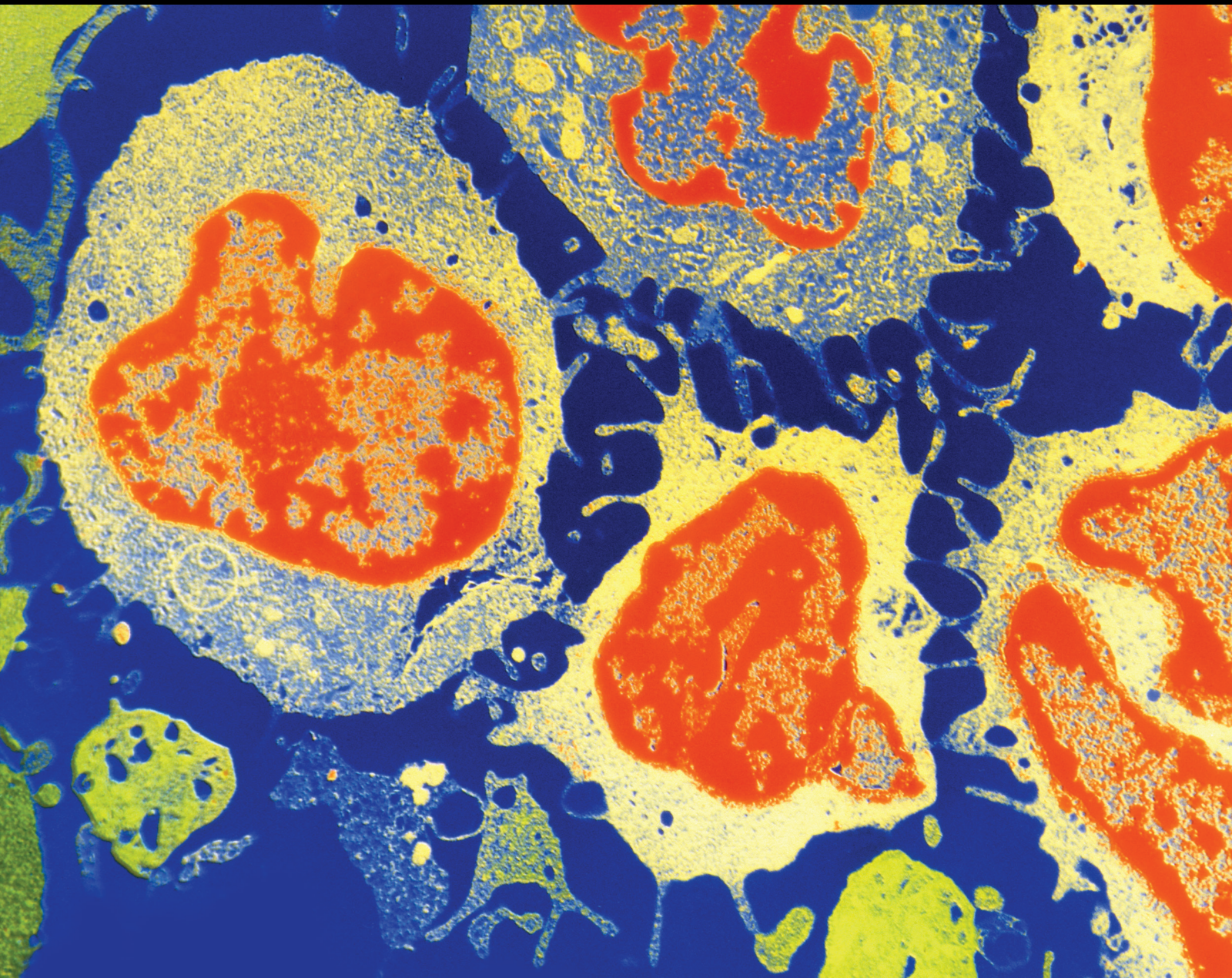# Novel Roles for Genomic Markers in Potential Targeted Therapy for Digestive Cancers

Lead Guest Editor: Xiaodong Li
Guest Editors: Yanqing Liu and Jinping Liu

Novel Roles for Genomic Markers in Potential Targeted Therapy for Digestive Cancers

Novel Roles for Genomic Markers in Potential Targeted Therapy for Digestive Cancers

Lead Guest Editor: Xiaodong Li
Guest Editors: Yanqing Liu and Jinping Liu

Contents

Research Article

Insights into the Oncogenic, Prognostic, and Immunological Role of BRIP1 in Pan-Cancer: A Comprehensive Data-Mining-Based Study

Yongru Liu ⓘ**, Xi Wu** ⓘ**, Yunlu Feng** ⓘ**, Qingwei Jiang** ⓘ**, Shengyu Zhang** ⓘ**, Qiang Wang** ⓘ**, and Aiming Yang** ⓘ

Department of Gastroenterology, State Key Laboratory of Complex Severe and Rare Diseases,
Peking Union Medical College Hospital, Peking Union Medical College and Chinese Academy of Medical Sciences,
Beijing 100730, China

Correspondence should be addressed to Aiming Yang; yangam2020@126.com

Background. BRCA1 interacting helicase 1 (BRIP1), an ATP-dependent DNA helicase which belongs to an Iron-Sulfur (Fe-S) helicase cluster family with a DEAH domain, plays a key role in DNA damage and repair, Fanconi anemia, and development of several cancers including breast and ovarian cancer. However, its role in pan-cancer remains largely unknown. *Methods.* BRIP1 expression data of tumor and normal tissues were downloaded from the Cancer Genome Atlas, Genotype-Tissue Expression, and Human Protein Atlas databases. Correlation between BRIP1 and prognosis, genomic alterations, and copy number variation (CNV) as well as methylation in pan-cancer were further analyzed. Protein-protein interaction (PPI) and gene set enrichment and variation analysis (GSEA and GSVA) were performed to identify the potential pathways and functions of BRIP1. Besides, BRIP1 correlations with tumor microenvironment (TME), immune infiltration, immune-related genes, tumor mutation burden (TMB), microsatellite instability (MSI), and immunotherapy as well as antitumor drugs were explored in pan-cancer. *Results.* Differential analyses showed an increased expression of BRIP1 in 28 cancer types and its aberrant expression could be an indicator for prognosis in most cancers. Among the various mutation types of BRIP1 in pan-cancer, amplification was the most common type. BRIP1 expression had a significant correlation with CNV and DNA methylation in 23 tumor types and 16 tumor types, respectively. PPI, GSEA, and GSVA results validated the association between BRIP1 and DNA damage and repair, cell cycle, and metabolism. In addition, the expression of BRIP1 and its correlation with TME, immune-infiltrating cells, immune-related genes, TMB, and MSI as well as a variety of antitumor drugs and immunotherapy were confirmed. *Conclusions.* Our study indicates that BRIP1 plays an imperative role in the tumorigenesis and immunity of various tumors. It may not only serve as a diagnostic and prognostic biomarker but also can be a predictor for drug sensitivity and immunoreaction during antitumor treatment in pan-cancer.

1. Introduction

Cancer remains a thorny problem which brings immense suffering to individual health and financial burden. Despite the tremendous advances in the detection of novel biomarkers and development of targeted drugs as well as immunotherapies in recent decades, the high morbidity and mortality of cancer is still frustrating. According to the GLOBOCAN 2020 statistics, there were approximately 19.3 million new cases and 10.0 million deaths related to cancer worldwide in 2020, and the global cancer burden was expected to reach 28.4 million cases in 2040 with a rise of 47% from 2020 [1]. Therefore, persistent efforts are urgently needed to understand the complex mechanisms of tumorigenesis and identify novel biomarkers for early diagnosis, clinical prognosis, and therapy response. Thanks to various

public databases, valuable data can be mined and pan-cancer analysis can be conducted for a comprehensive investigation of extracted genes.

BRIP1 (BRCA1 interacting helicase 1), also known as FANCJ (as the gene mutated in the J complementation group of Fanconi anemia) or BACH1 (BRCA1-associated C-terminal helicase), was first discovered in 2001 by its interaction with BRCA1 [2]. BRIP1 is a protein coding gene which encodes for homologous recombination repair (HRR)-related protein and facilitates DNA single-strand break (SSB) and DNA double-strand break (DSB) repair during vital biological processes including DNA replication, transcriptional regulation, and overall metabolic health [3]. BRIP1, whose encoded protein belongs to an Iron-Sulfur (Fe-S) helicase cluster family with a DEAH domain, helps to preserve chromatin structure and function and may also maintain genomic and epigenetic stability. Besides its collaboration with numerous DNA metabolizing proteins implicated in the detection and repair of DNA damage, BRIP1 also participates in cell cycle checkpoint control [4]. Recent studies manifest that BRIP1 took part in miscellaneous tumorigeneses and pathological conditions. The National Comprehensive Cancer Network (NCCN) guidelines identified BRIP1 as a potential risk factor for breast cancer, especially for triple negative breast cancers [5]. In ovarian cancer, a deleterious mutation of BRIP1 was associated with low-grade histology and led to an increased risk of the disease [6]. In endometrial cancer, BRIP1 correlated to tumor recurrence and patients with mutations in BRIP1 might benefit from poly ADP-ribose polymerase (PARP) inhibitors [7]. Mikaeel et al. reported that BRIP1 might be a cancer-predisposing gene in young-onset colorectal cancer [8]. Mani et al. suggested that BRIP1 was of the imperative role in maintaining neuronal cell health and homeostasis by suppressing oxidative stress, excitotoxicity induced DNA damage, and protecting mitochondrial integrity [3]. However, there is a lack of a comprehensive pan-cancer analysis of BRIP1. Hence, we extracted diverse data from The Cancer Genome Atlas (TCGA), Genotype-Tissue Expression (GTEx), Cancer Cell Line Encyclopedia (CCLE), Human Protein Atlas (HPA), cBioPortal and GeneMANIA databases and evaluated the expression, prognosis, and mutation as well as function of BRIP1 in various cancer types. We further carried out immune infiltration analysis, and the relationships between BRIP1 and immune-related genes and tumor mutation burden (TMB)-microsatellite instability (MSI) as well as immunotherapy and targeted drug responses were subsequently analyzed. This in-depth data-mining based study helped us understand the role of BRIP1 in tumorigenesis, provided evidence for its diagnostic and prognostic evaluation in the clinic, and shed light on the novel targeted treatment as well as immunotherapy in pan-cancer.

2. Materials and Methods

2.1. Raw Data Collection and Differential Expression Analysis. The mRNA expression profiles and related clinical information of 33 human cancers and their corresponding normal samples were, respectively, downloaded from TCGA via the UCSC Xena platform (https://xena.ucsc.edu/) [9]. Additional gene expression data were also retrieved from GTEx (https://gtexportal.org/home/datasets) and CCLE (https://sites.broadinstitute.org/ccle). BRIP1 expression was transferred to transcripts per million (TPM) and then evaluated by $\log_2$ transformation. *T*-test was carried out to identify its different expression between tumor and normal tissues as well as between different TNM stages. R software (Version 4.0.3, https://www.Rproject.org) and the "ggplot2" R package (Version 3.3.3) were applied to analyze the data and draw box diagrams. The abbreviations and full names of the various cancer types were listed in Table 1. Besides, to evaluate the differential expression of BRIP1 at the protein level, immunohistochemistry (IHC) images in multiple tumors and normal tissues were downloaded from HPA (https://www.proteinatlas.org/). The antibody used for IHC was HPA005474.

2.2. Prognostic Value of BRIP1 in Pan-Cancer. Overall survival (OS), disease-specific survival (DSS), disease-free interval (DFI), and progression-free interval (PFI) were of vital importance in exploring the association between BRIP1 expression and prognosis. Related survival data were downloaded from the UCSC Xena platform. The Kaplan–Meier (KM) method and log-rank test were utilized to carry out survival analyses in each cancer with the best cut-off value of BRIP1 expression by using R packages "survminer" and "survival." Univariate Cox regression and R package "forestplot" were also used to identify the relevancy between BRIP1 expression and survival in pan-cancer. The hazard ratio (HR) and Cox's regression *P* values were shown in the plot.

2.3. BRIP1 Mutation and Its Correlation with Copy Number Variation and DNA Methylation. To further investigate the modification of BRIP1 gene in pan-cancer, we used the cBioPortal database (https://cbioportal.org) to explore its mutation, structural variant, amplification, deep deletion, and multiple alterations [10]. As copy number variation (CNV) and copy number alteration (CNA) played a critical role in cancer initiation and progression, and promoter methylation was critical in gene silencing and inactivation, related data were downloaded from cBioPortal for further analyses. Association between the expression of BRIP1 and CNV as well as promoter methylation was further evaluated by carrying out Pearson correlation analysis. R software and the "ggplot2" R package were acquired to analyze the data and draw lollipop plots.

2.4. Gene Interaction of BRIP1 and Its Enrichment and Variation Analysis. The GeneMANIA database (https://www.genemania.org) was applied to detect functionally similar genes to BRIP1 and construct the protein-protein interaction (PPI) network [11, 12]. Subsequently, gene set enrichment analysis (GSEA) was performed in pan-cancer based on the Gene Ontology (GO) and Kyoto Encyclopedia of Genes and Genomes (KEGG) database to explore the

TABLE 1: Full names and abbreviations of the tumor types from TCGA and CCLE.

Abbreviation	Full name
ACC	Adrenocortical carcinoma
ALL	Acute lymphoblastic leukemia
BLCA	Bladder urothelial carcinoma
BRCA	Breast invasive carcinoma
CESC	Cervical squamous cell carcinoma and endocervical adenocarcinoma
CHOL	Cholangiocarcinoma
CLL	Chronic lymphoblastic leukemia
COAD	Colon adenocarcinoma
DLBC	Lymphoid neoplasm diffuse large B-cell lymphoma
ESCA	Esophageal carcinoma
GBM	Glioblastoma multiforme
HNSC	Head and neck squamous cell carcinoma kidney
KICH	Kidney chromophobe
KIRC	Kidney renal clear cell carcinoma
KIRP	Kidney renal papillary cell carcinoma
LAML	Acute myeloid leukemia
LCML	Chronic myeloid leukemia
LGG	Brain lower grade glioma
LIHC	Liver hepatocellular carcinoma
LUAD	Lung adenocarcinoma
LUSC	Lung squamous cell carcinoma
MB	Medulloblastoma
MESO	Mesothelioma
MM	Multiple myeloma
NB	Neuroblastoma
OV	Ovarian serous cystadenocarcinoma
PAAD	Pancreatic adenocarcinoma
PCPG	Pheochromocytoma and paraganglioma
PRAD	Prostate adenocarcinoma
READ	Rectum adenocarcinoma
SARC	Sarcoma
SCLC	Small cell lung cancer
SKCM	Skin cutaneous melanoma
STAD	Stomach adenocarcinoma
TGCT	Testicular germ cell tumor
THCA	Thyroid carcinoma
THYM	Thymoma
UCEC	Uterine corpus endometrial carcinoma uterine
UCS	Uterine carcinosarcoma
UVM	Uveal melanoma

biological signalling pathway by using R package "cluster-Profiler," and R package "ridgeplot" was used to draw the ridge plot [13, 14]. We further downloaded the "gmt" file of the 50 hallmark gene sets from the Molecular Signatures Database (MSigDB, via https://www.gsea-msigdb.org/gsea/msigdb/index.jsp) [15, 16] and performed gene set variation analysis (GSVA) using the "GSVA" R package to explore the correlation between BRIP1 expression and 50 hallmark pathways. Pearson correlation analysis was conducted, and the "pheatmap" R package was used to turn the results into heatmap.

2.5. BRIP1 Expression and Its Relationship with Immunity. Tumor microenvironment (TME), a crucial element of tumor, has been reported to play a decisive role in cancer development and therapeutic responses. Hence, we carried out evaluation of the association between BRIP1 expression and the proportion of immune-stromal component in pan-cancer. Data were downloaded from TCGA via the UCSC Xena platform, while R package "ESTIMATE" was used to evaluate the immune score, stromal score, and tumor purity score. Subsequently, the specific tumor-infiltrating immune cells (TIICs) and its correlation to BRIP1 expression were assessed via Tumor Immune Estimation Resource (TIMER) database (https://timer.cistrome.org/) [17]. The TIMER, EPIC, MCPCOUNTER, CIBERSORT, CIBERSORT_ABS, XCELL, and QUANTISEQ algorithms were utilized to estimate the immune infiltration of the 21 TIICs. Relationship between BRIP1 expression and immune-related genes was also evaluated at the pan-cancer level. The visualization of the results was implemented with R packages "ggplot2" and "pheatmap." Besides, TMB, which reflects cancer mutation quantity, has been considered as a leading candidate biomarker for immune checkpoint blockade (ICB) [18].

Meanwhile, MSI, which facilitates mutation and acts as a biomarker of response to immune checkpoint inhibitors (ICPis), plays an important role in improving the possibility of a favorable response to immunotherapy [19]. We thus analyzed the TMB-MSI association with BRIP1 in pan-cancer by Pearson correlation using Sangerbox tools (https://vip.sangerbox.com/home.html), and the results were shown in radar maps.

2.6. BRIP1 Expression and Different Therapies. To further validate the relationship between BRIP1 and ICB therapy response, data from the IMvigor210 cohort, which contains 298 metastatic urothelial cancer cases treated by atezolizumab (an antiprogrammed cell death ligand 1, anti-PD-L1 agent), were obtained and analyzed [20]. Patients were divided into two subgroups, one with a low level of BRIP1 and the other with a high level of BRIP1, according to the best cut-off value identified by the "survminer" R package, and immunotherapy response of BRIP1 was then validated. A chi-square test was carried out to assess the proportion differences of responses between subgroups. Furthermore, relationships between BRIP1 and IC50 of numerous antitumor drugs were explored via the Genomics of Drug Sensitivity in Cancer (GDSC) database (https://www.cancerrxgene.org). A Spearman correlation was used to evaluate the drug resistance.

3. Results and Discussion

3.1. BRIP1 Expression Profile. The expression level of BRIP1 explored via the GTEx transcriptomics dataset indicated it was low in most normal tissues under physiological circumstances, whereas higher in bone marrow than other 30 tissues (Figure 1(a)). Results from CCLE revealed that its expression level was generally increased in various cancer cell lines as the highest expression was in NB, ALL, and SCLC (Figure 1(b)). TCGA data showed a similar expression tendency to that of CCLE, and the highest expression level of BRIP1 was in LAML and genital cancers such as CESC and TGCT (Figure 1(c)). Comparison of the expression level between cancer and normal tissues combing TCGA and GTEx data manifested that BRIP1 was significantly upregulated in 7 digestive tumors (including CHOL, COAD, ESCA, LIHC, PAAD, READ, and STAD) and other 21 tumors (including ACC, BLCA, BRCA, CESC, DLBC, GBM, HNSC, KIRC, KIRP, LGG, LUAD, LUSC, OV, PCPG, PRAD, SARC, SKCM, THCA, THYM, UCEC, and UCS) and downregulated in TGCT (Figure 1(d)), indicating that BRIP1 might play an oncogenic role during carcinogenesis and may function as a potential diagnostic biomarker. Moreover, a noteworthy increase in the expression of BRIP1 was detected in 16 cancers (including BLCA, BRCA, CESC, CHOL, COAD, ESCA, HNSC, KIRC, KIRP, LIHC, LUAD, LUSC, READ, STAD, THCA, and UCEC) between paired tumor tissues and their corresponding normal tissues (Figure S1). When further seeking for the association between BRIP1 expression and different tumor stages, we found that there was a significant difference between stage I, II and stage III, IV in ACC, KIRP, LUAD, and OV

(Figure S2). Subsequently, the protein level of BRIP1 was explored in multiple tumor and normal tissues. Representative IHC images showed that BRIP1 was mostly enriched in the nucleoplasm and nuclear membrane and had a low expression level in normal tissues than that of tumor tissues in breast, cerebellum, cervix, colon, endometrium, kidney, liver, lung, lymph node, ovary, pancreas, prostate, skin, stomach, thyroid gland, and urinary bladder, while high in normal testis tissues than tumor tissues (Figure 2).

3.2. Prognostic Value of BRIP1 across Cancers. Given the aberrant expression of BRIP1 observed in pan-cancer, we wonder its role within prognosis. Therefore, we analyzed the expression of BRIP1 and its association with OS, DSS, DFI, and PFI, respectively. Cox proportional hazards model analysis elucidated BRIP1 expression was correlated with OS in LGG ($P < 0.001$), MESO ($P < 0.001$), KIRP ($P < 0.001$), KICH ($P < 0.001$), ACC ($P < 0.001$), PAAD ($P = 0.003$), LUAD ($P = 0.005$), READ ($P = 0.011$), PRAD ($P = 0.012$), and THYM ($P = 0.044$). BRIP1 was a high-risk factor in LGG, MESO, KIRP, KICH, ACC, PAAD, LUAD, and PRAD, while it was a low-risk factor in READ and THYM. These results are shown in forestplot in Figure 3(a). KM survival analyses illustrated that upregulated BRIP1 was associated with poor OS in ACC, CHOL, KICH, KIRC, KIRP, LGG, LIHC, LUAD, MESO, PAAD, PCPG, PRAD, SKCM, UCEC, and UVM, while downregulated BRIP1 had shorter survival times in BLCA, CESC, COAD, HNSC, OV, READ, SARC, STAD, and THYM (Figures 3(b)–3(y)).

As for DSS, it was associated with BRIP1 in LGG ($P < 0.001$), KIRP ($P < 0.001$), MESO ($P < 0.001$), KICH ($P < 0.001$), ACC ($P = 0.001$), PAAD ($P = 0.002$), PRAD ($P = 0.002$), LUAD ($P = 0.013$), OV ($P = 0.015$), PCPG ($P = 0.029$), and LIHC ($P = 0.031$), among which BRIP1 was considered as a low-risk factor in OV and a high-risk factor in other cancer types (Figure 4(a)). Besides, worse DSS was found in ACC, BLCA, KICH, KIRC, KIRP, LGG, LIHC, LUAD, MESO, PAAD, PCPG, PRAD, SKCM, and UCEC with the increased expression level of BRIP1, while in CESC, COAD, DLBC, HNSC, OV, STAD, THYM and UCS with the decreased expression level of BRIP1 (Figures 4(b)–4(w)).

When considering the relationship between BRIP1 expression and DFI, there was a significant association between them in KIRP ($P < 0.001$), THCA ($P = 0.002$), PAAD ($P = 0.003$), and LIHC ($P = 0.026$). Moreover, BRIP1 was a high-risk factor in all of these four cancers (Figure 5(a)). In addition, poor DFI was perceived in BLCA, KIRP, LIHC, LUAD, LUSC, MESO, PAAD, SARC, and THCA as BRIP1 upregulated in these tumors, while in COAD, DLBC, KIRC, READ, STAD, UCEC, and UCS as BRIP1 downregulated (Figures 5(b)–5(q)).

Regarding PFI, it was correlated with BRIP1 in LGG ($P < 0.001$), KIRP ($P < 0.001$), KICH ($P < 0.001$), ACC ($P < 0.001$), MESO ($P < 0.001$), LIHC ($P < 0.001$), PAAD ($P = 0.001$), UVM ($P = 0.007$), PRAD ($P = 0.017$), OV ($P = 0.040$), and LUAD ($P = 0.048$), among which BRIP1 was regarded as a low-risk factor in OV but a high-risk factor in others (Figure 6(a)). Additionally, increased expression of
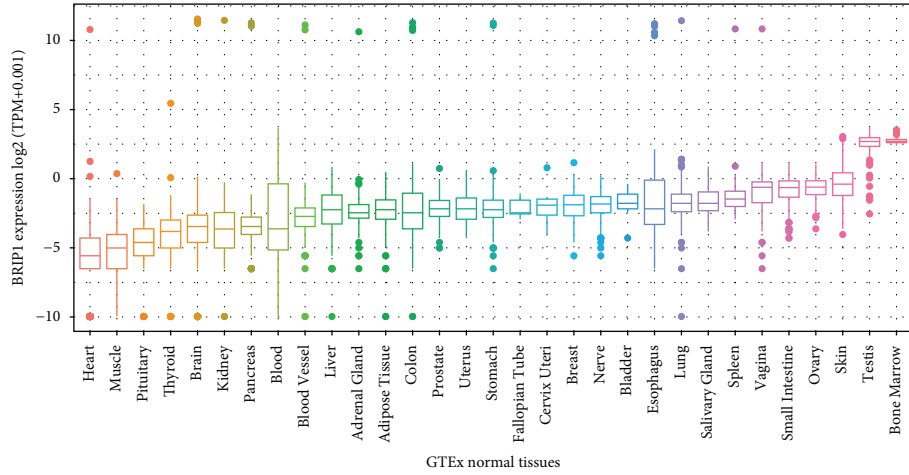
(a)
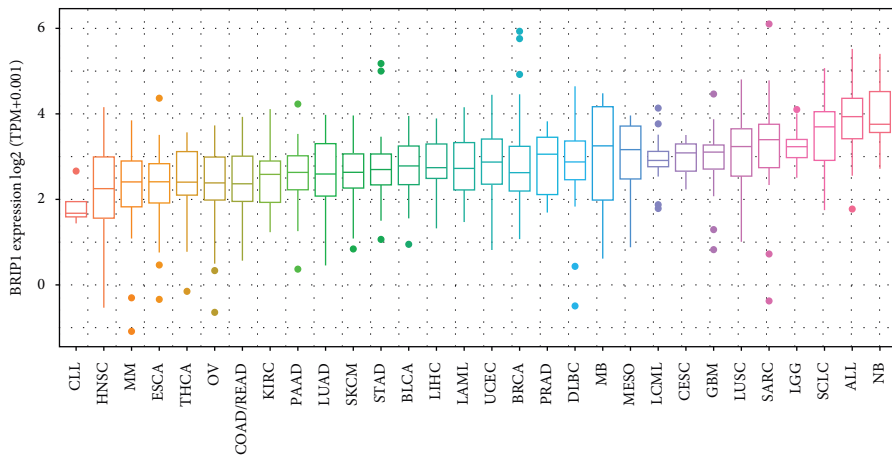
(b)
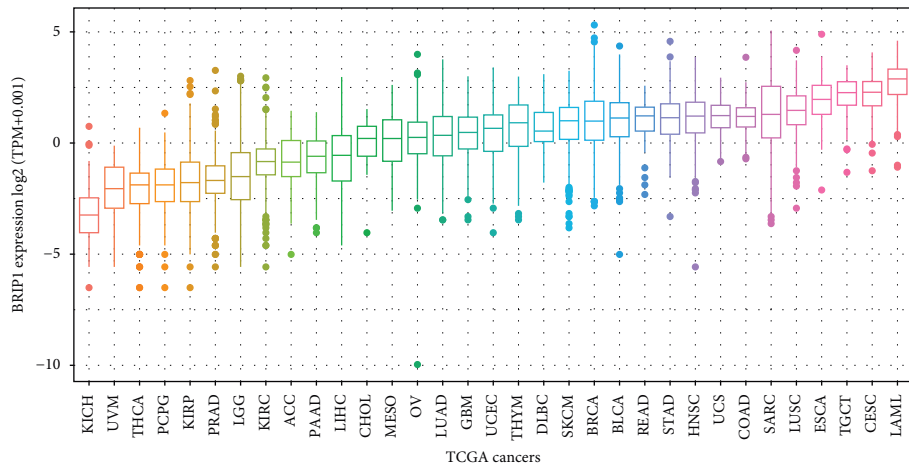
(c)

Figure 1: Continued.
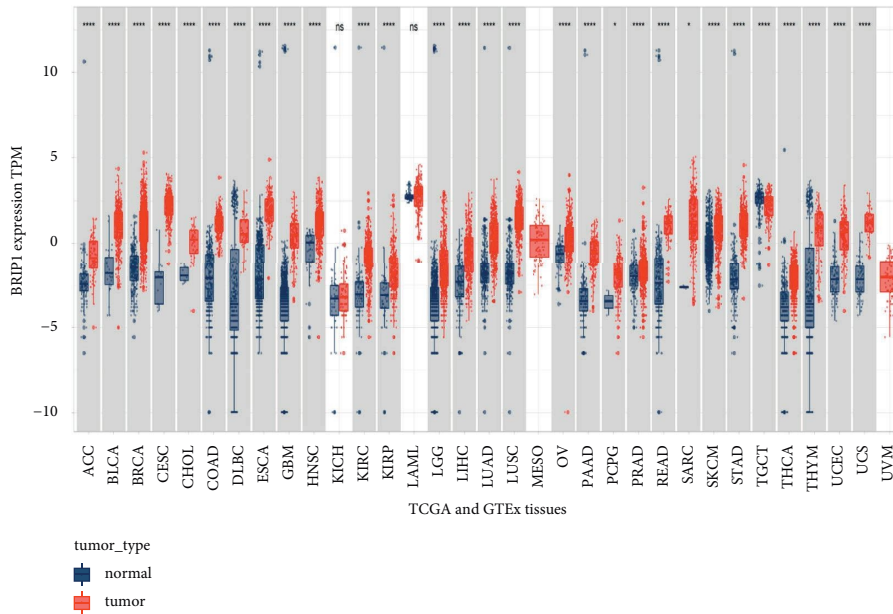
(d)

FIGURE 1: Differential expression level of BRIP1. (a) Expression of BRIP1 in 31 normal tissues from GTEx database. (b) Expression of BRIP1 in 30 cancer cell lines from CCLE database. (c) Expression of BRIP1 in 33 types of cancer from TCGA database. (d) Comparison between tumor and normal tissues of the BRIP1 expression from TCGA and GTEx database. Normalized expression levels of BRIP1 were changed by $\log_2(\text{TPM} + 0.001)$. * represents $P < 0.05$, ** represents $P < 0.01$, *** represents $P < 0.001$, and **** represents $P < 0.0001$. Expression levels of BRIP1 in the first three figures are arranged in ascending order.
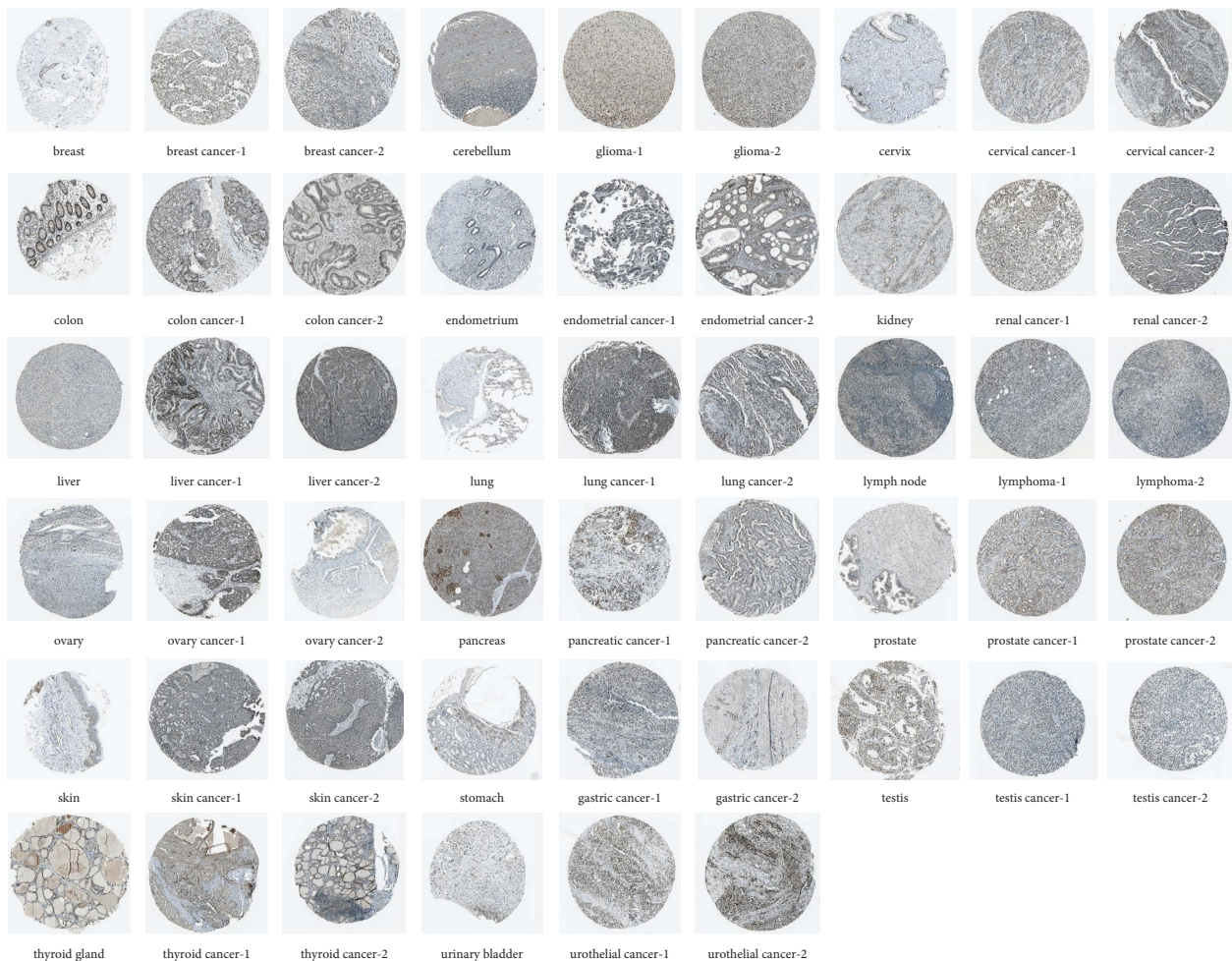
FIGURE 2: Representative IHC images of BRIP1 in normal and tumor tissues from HPA database.
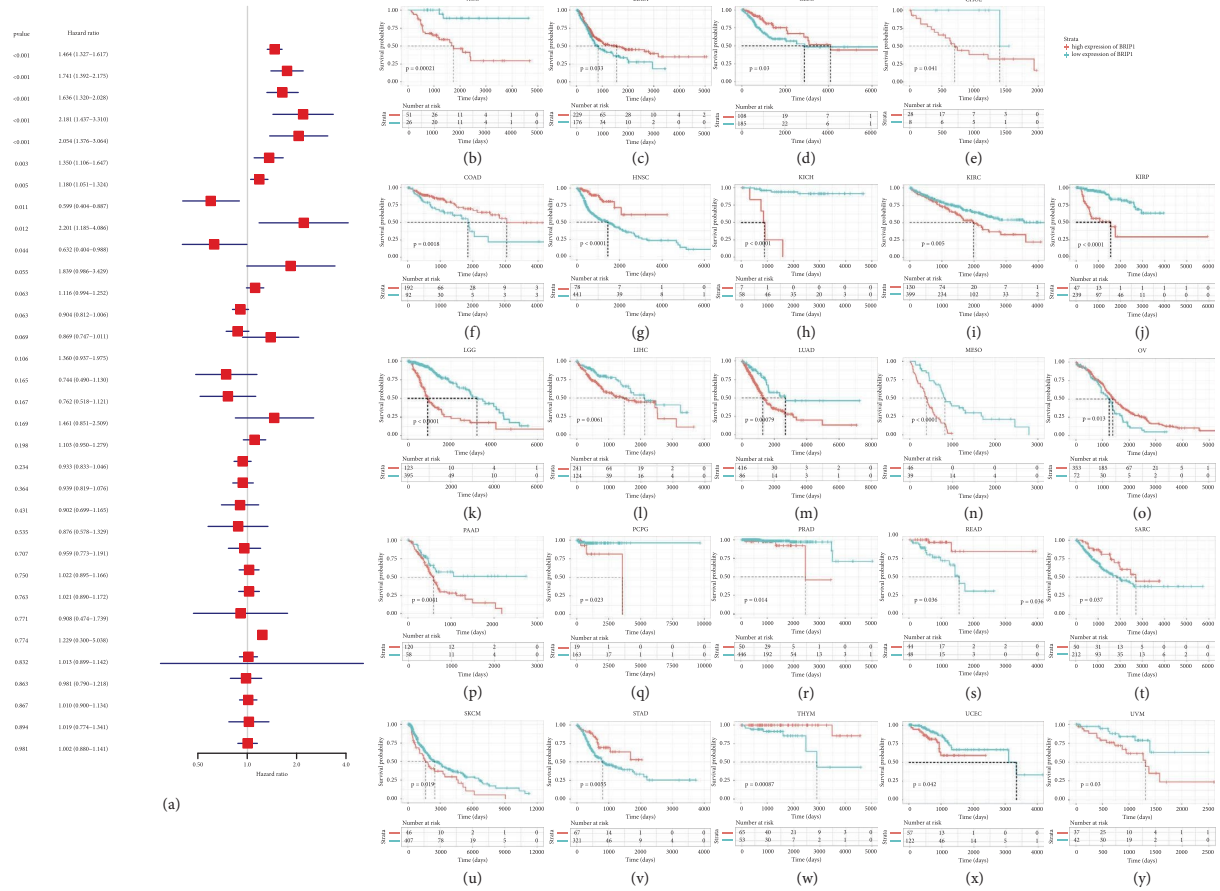
FIGURE 3: Correlation between BRIP1 expression and overall survival (OS). (a) Forest plot of associations between BRIP1 and OS in 33 cancer types. (b–y) KM analysis results of the relationship between BRIP1 level and OS. The high and low expression level of BRIP1 was divided by the best cut-off value.

BRIP1 was associated with poor PFI in ACC, BLCA, HNSC, KICH, KIRP, LGG, LIHC, LUAD, MESO, PAAD, PCPG, PRAD, SARC, SKCM, THCA, and UVM, while its decreased expression was correlated to poor PFI in CESC, COAD, GBM, OV, READ, STAD, and UCEC (Figures 6(b)–6(x)).

In general, BRIP1 expression level was a vital factor influencing the survival of various cancers and it played an important role in the tumor progression and recurrence.

3.3. Correlation between BRIP1 Expression and CNV as well as DNA Methylation in Pan-Cancer.

The previous findings indicated that BRIP1 might play a role in the carcinogeneses and it was widely accepted that the genomic mutation was associated with tumorigenesis. Therefore, a comparative analysis of genomic mutations of BRIP1 in pan-cancer was conducted. Results from the cBioPortal database consisting of 32 cancer types and 10953 tumor samples showed that the amplification of BRIP1 was one of the most vital single factors for alteration. It accounted for 6.92%, 4.6%, and 3.14% in BRCA, MESO, and sarcoma, respectively, as the largest proportion of all mutation types among these tumors (Figure 7(a)). Meanwhile, mutation of BRIP1 became the most important single factor for alteration in UCEC (8.88%), SKCM (5.86%), and BLCA (3.89%). Moreover, there was

a significant positive correlation between CNV and BRIP1 expression in 5 digestive tumors (COAD, ESCA, LIHC, STAD, and READ) and other 18 tumors (UCS, BRCA, LUSC, CESC, OV, BLCA, LUAD, SKCM, UCEC, PRAD, LAML, PCPG, LGG, MESO, KIRC, HNSC, SARC, and KIRP), as shown in the lollipop chart (Figure 7(b)), and the correlation in each specific tumor type was summarized in Figure S3. As for promoter methylation, it was significantly negatively associated with the expression level of BRIP1 in 4 digestive tumors (COAD, ESCA, LIHC, and STAD) and other 12 tumors (LUAD, HNSC, BLCA, SKCM, CESC, UCEC, BRCA, LUSC, SARC, THYM, TGCT, and DLBC) (Figures 7(c) and S4).

3.4. Interacting Genes of BRIP1 and Its Enrichment and Variation Analysis.

The PPI network for BRIP1 and its coexpressed as well as colocalized genes were constructed by GeneMANIA. The results showed the 20 most frequently altered proteins closely linked to BRIP1, in which BRCA1 had the most prominent correlation with BRIP1 as expected. Besides, the functional analysis indicated that BRIP1 and its similar genes had a significant association with DNA recombination, double-strand break repair, and recombinational repair (Figure 8). To uncover the function of
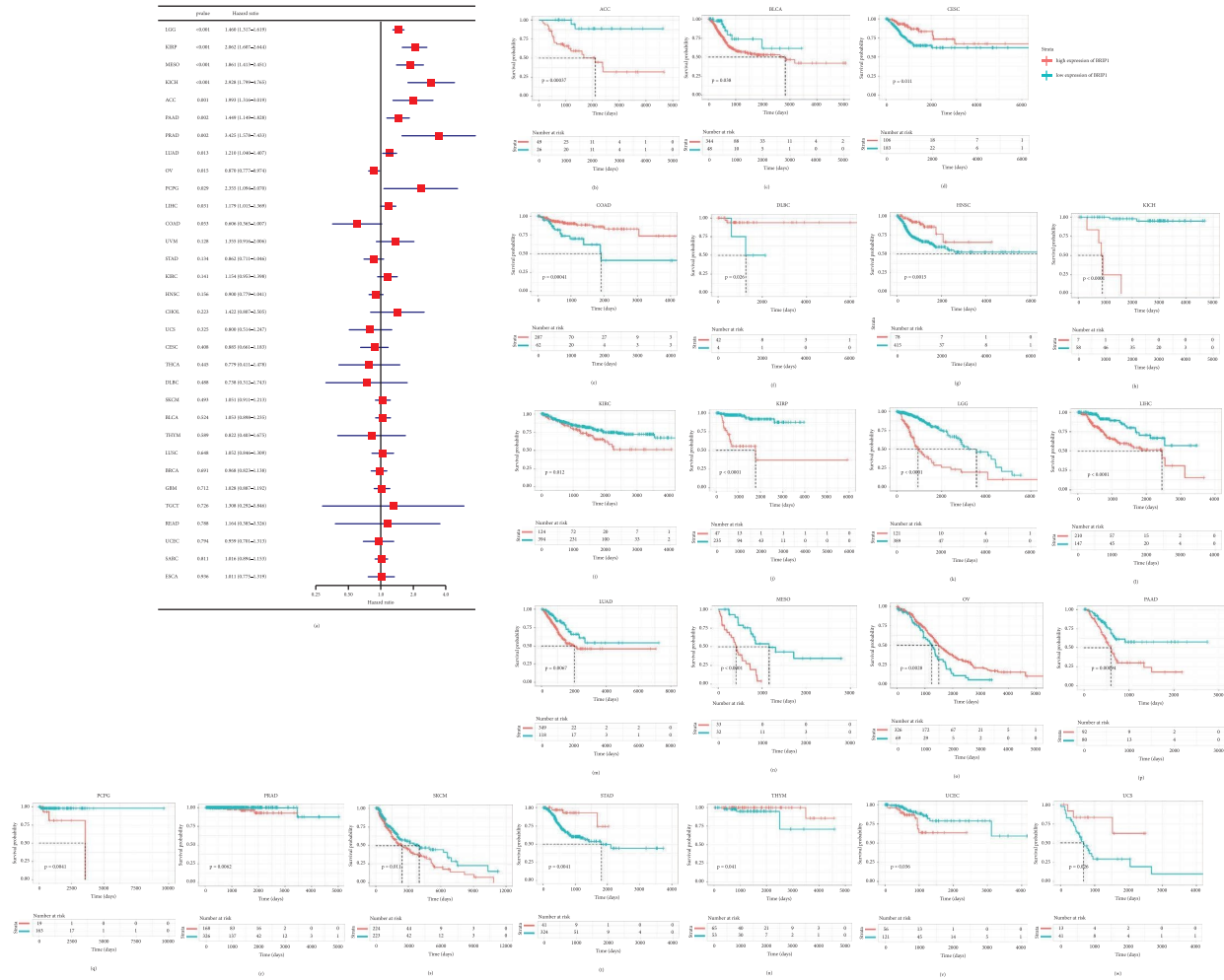
Figure 4: Correlation between BRIP1 expression and disease-specific survival (DSS). (a) Forest plot of associations between BRIP1 and DSS in 33 cancer types. (b–w) KM analysis results of the relationship between BRIP1 level and DSS. The high and low expression level of BRIP1 was divided by the best cut-off value.

BRIP1, we carried out GSEA in 33 cancer types, and the results suggested that the top 6 signalling pathways correlated with BRIP1 among all cancers based on KEGG were DNA replication, cell cycle, spliceosome, nucleocytoplasmic transport, homologous recombination, and Fanconi anemia pathway. The specific 20 signalling pathways associated with BRIP1 in each type of tumor are summarized in Figure S5.

As for GSVA, the relationship between BRIP1 and various hallmark pathways in pan-cancer is shown in the heatmap (Figure 9). It was obvious that BRIP1 had the most significantly positive correlation with G2M checkpoint and E2F targets in ACC, BLCA, LGG, LUSC, PCPG, and THYM, with mitotic spindle and G2M checkpoint in BRCA, ESCA, MESO, OV, PAAD, and PRAD, with mitotic spindle in CESC, CHOL, DLBC, SARC, TGCT, and UCS, with G2M checkpoint in COAD, GBM, STAD, and THCA, with mitotic spindle, G2M checkpoint, and E2F targets in HNSC, KIRC, KIRP, LAML, LIHC, and LUAD, with G2M checkpoint and MYC targets V1 in KICH, with MYC targets V1 in READ and UCEC, with mitotic spindle and MYC targets V1 in SKCM, and with MYC targets V1 and protein secretion in

UVM. Moreover, the most prominently negative correlation between BRIP1 and xenobiotic metabolism lay in ACC, BLCA, DLBC, READ, SARC, and UCEC, between BRIP1 and xenobiotic metabolism as well as myogenesis lay in BRCA, between BRIP1 and coagulation as well as KRAS signalling upregulation lay in CESC, between BRIP1 and xenobiotic metabolism and myogenesis as well as P53 pathway lay in COAD, between BRIP1 and xenobiotic metabolism and adipogenesis as well as complement lay in ESCA, between BRIP1 and xenobiotic metabolism as well as adipogenesis lay in GBM, between BRIP1 and KRAS signalling downregulation lay in HNSC, KICH, and UVM, between BRIP1 and KRAS signalling downregulation as well as oxidative phosphorylation lay in KIRC, between BRIP1 and xenobiotic metabolism as well as oxidative phosphorylation lay in KIRP, between BRIP1 and coagulation as well as P53 pathway lay in LAML, between BRIP1 and bile acid metabolism as well as heme metabolism lay in LGG, between BRIP1 and myogenesis lay in LIHC and STAD, between BRIP1 and bile acid metabolism as well as fatty acid metabolism lay in LUAD, between BRIP1 and
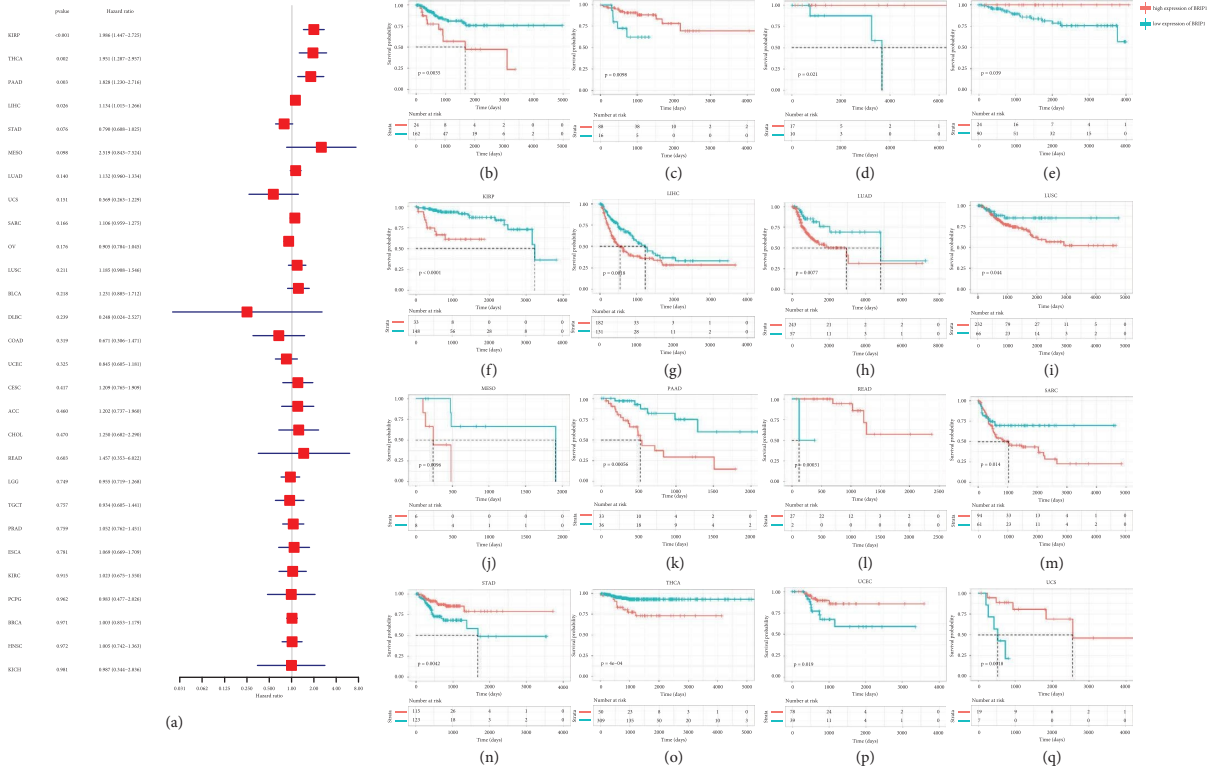
FIGURE 5: Correlation between BRIP1 expression and disease-free interval (DFI). (a) Forest plot of associations between BRIP1 and DFI in 33 cancer types. (b–q) KM analysis results of the relationship between BRIP1 level and DFI. The high and low expression level of BRIP1 was divided by the best cut-off value.

coagulation as well as adipogenesis lay in LUSC, between BRIP1 and xenobiotic metabolism and bile acid metabolism as well as fatty acid metabolism lay in MESO, between BRIP1 and bile acid metabolism lay in OV, between BRIP1 and pancreas beta cells lay in PAAD, between BRIP1 and apical surface lay in PCPG, between BRIP1 and xenobiotic metabolism as well as KRAS signalling downregulation lay in PRAD, between BRIP1 and xenobiotic metabolism, myogenesis as well as KRAS signalling downregulation lay in SKCM, between BRIP1 and P53 pathway lay in TGCT, between BRIP1 and fatty acid metabolism lay in THCA, and between BRIP1 and xenobiotic metabolism, myogenesis, and P53 pathway as well apical junction lay in THYM. In summary, the previous results elucidated the hallmark pathways and potential mechanisms of BRIP1 in pan-cancer. In essence, BRIP1 kept an intimate relationship with HRR, cell cycle, and varied metabolism in different cancers.

3.5. BRIP1 Expression and Its Correlation with TME and Immune Infiltration. Along with the above coexpressed genes and signalling pathways, TME and immune infiltration also take part in the regulation of tumorigenesis. As part of the complex microenvironment, TIICs have a crucial role in cancer progression and therapeutic responses. Accordingly, we explored the correlation between BRIP1 expression and TME by ESTIMATE and evaluated the coefficient of BRIP1 expression and immune infiltration level via TIMER. The results revealed that the expression of BRIP1 had significant correlations with tumor purity and ESTIMATEScore in 19 cancer types (Figure 10). The top three most significant cancers associated with BRIP1 expression were GBM, SARC, and LUSC based on ImmuneScore, StromalScore, and ESTIMATEScore. The higher the level of BRIP1 as these three tumors expressed, the less stromal and immune cells as these tumors had. On the contrary, the higher level of BRIP1 as these tumors expressed, the higher purity as these tumors had. Results of ESTIMATEScore for all tumor types are listed in Figure S6. In addition, BRIP1 expression and its association with TIICs were significant in most cancer types (Figure 11). Especially in THYM, BRIP1 had a positive correlation with B cells, memory and naive CD4+ T cells, CD8+ T cells, myeloid dendritic cells, neutrophils (by CIBERSORT, CIBERSORT_ABS, and TIMER algorithm), common lymphoid progenitor, granulocyte and monocyte progenitor, and a negative correlation with fibroblast, endothelial cell, eosinophil, macrophage, mast cell, monocyte, neutrophil (by XCELL and MCPCOUNTER algorithm), NK cell, and common myeloid progenitor. As for those digestive tumors, the most significant association between BRIP1 and TIICs was found in STAD. A significantly negative correlation was found between BRIP1 and fibroblast as well as hematopoietic stem cell in STAD.
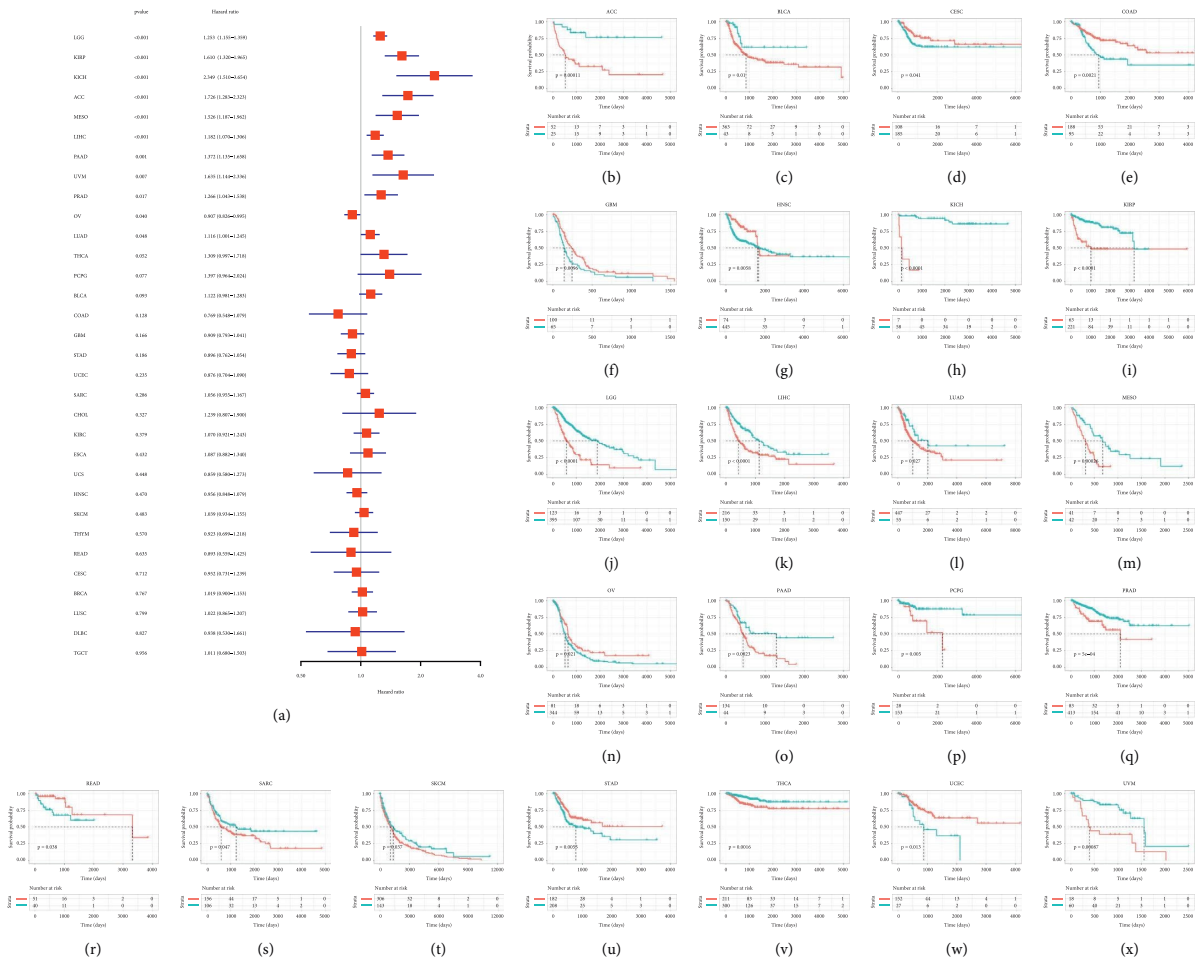
Figure 6: Correlation between BRIP1 expression and progression-free interval (PFI). (a) Forest plot of associations between BRIP1 and PFI in 33 cancer types. (b–x) KM analysis results of the relationship between BRIP1 level and PFI. The high and low expression level of BRIP1 was divided by the best cut-off value.

Moreover, the association between the expression of BRIP1 and immune-related genes including immune-activating genes, immunosuppressive genes, mismatch repair (MMR) genes, and genes encoding the major histocompatibility complex (MHC), chemokine, and chemokine receptor proteins is evaluated (Figure 12). Results indicated that BRIP1 was positively correlated with the majority of immune-activating genes as well as immunosuppressive genes in UVM, KIRC, THCA, KICH, PAAD, HNSC, PRAD, and OV. In HNSC, OV, PRAD, UVM, LAML, TGCT, UCEC, READ, SKCM, LIHC, ESCA, DLBC, LUSC, BLCA, GBM, BRCA, CESC, KICH, STAD, SARC, LGG, PAAD, PCPG, and KIRC, the expression of BRIP1 was positively correlated with most of the MMR genes. As for the correlation between BRIP1 and the majority of genes encoding the chemokine and chemokine receptor proteins, a positive correlation was found in THCA for the former and in KIRC and PRAD for the latter. Besides, there was a positive correlation between BRIP1 and most of the MHC-related genes in KIRC, PAAD, UVM, and THCA, and a negative correlation between BRIP1 and most of the MHC-related genes in THYM, GBM, and LUSC.

3.6. Correlation between BRIP1, TMB/MSI, and Immunotherapy Response.

To discover the role of BRIP1 in predicting the response to ICPis, we assessed the correlation between BRIP1 expression and the two famous biomarkers, TMB and MSI. BRIP1 was positively associated with TMB in 2 digestive tumors (COAD and STAD) and other 7 tumors including KICH, LUAD, ACC, OV, PRAD, KIRC, and SKCM (Figures 13(a) and S7). As for MSI, it was negatively correlated with BRIP1 in DLBC and positively correlated with BRIP1 in 3 digestive tumors (COAD, READ, and STAD) and other 4 tumors including GBM, LUSC, KIRC, and LUAD (Figures 13(b) and S8). As indicated by previous studies that high TMB/MSI-H increased patients' response to ICPis and was correlated to better immunotherapy outcomes, we therefore, downloaded data of the IMvigor210 cohort to investigate the correlation between BRIP1 and treatment response. Results showed that in this urothelial cancer cohort, patients with a high level of BRIP1 had a better response to the treatment and a more favorable survival rate (Figures 13(c) and 13(d)). Moreover, the anti-PD-L1 response rate was 49% among patients with a high expression level of BRIP1, while there were only 19% of the

(a)

(b)

(c)
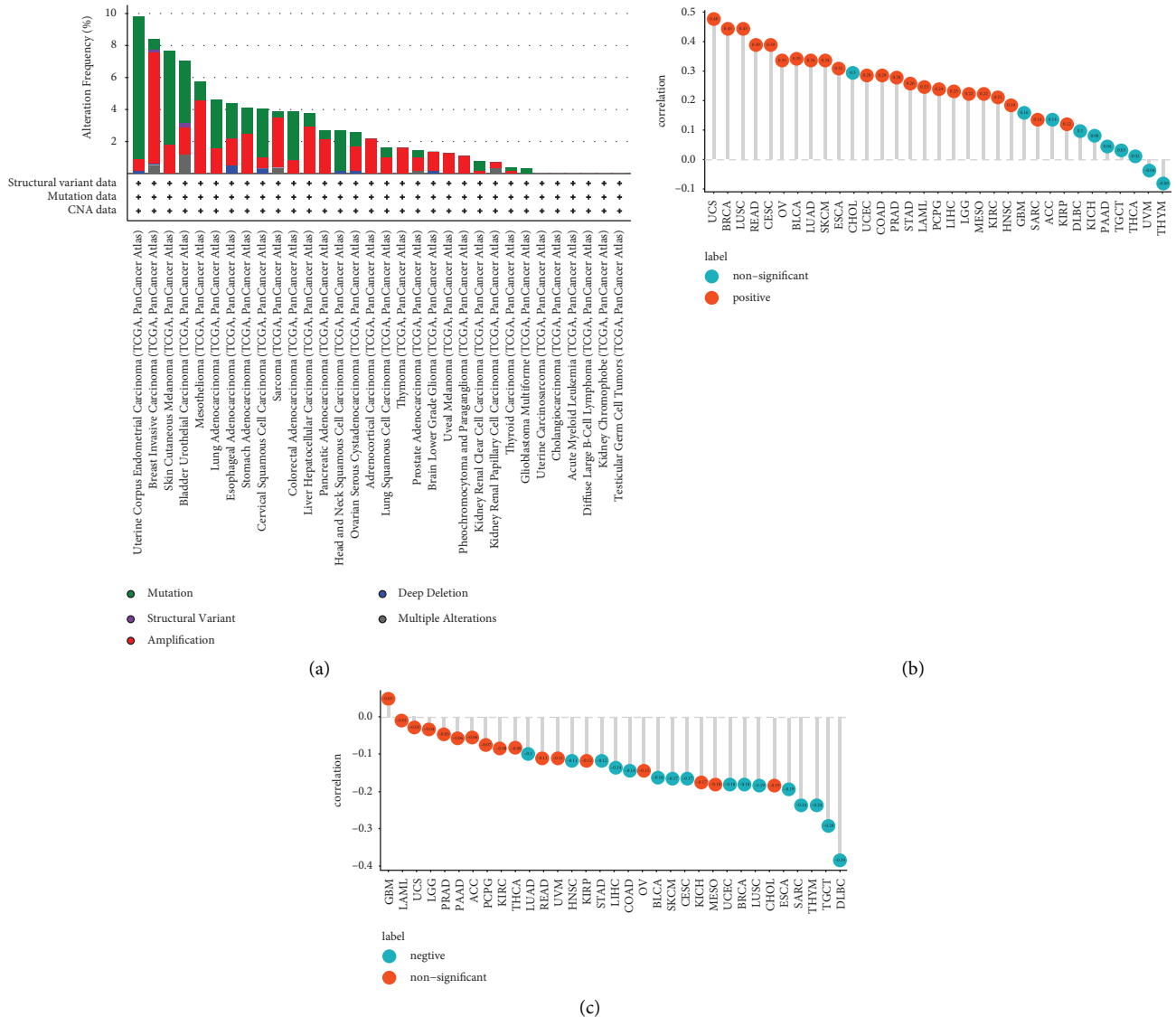
FIGURE 7: Genetic mutation of BRIP1 and its correlation with CNV and DNA methylation. (a) BRIP1 alteration frequency in pan-cancer. (b) Correlation between BRIP1 expression and CNV. (c) Correlation between BRIP1 expression and methylation.

low-BRIP1 patients responding to the treatment (Figure 13(e)). These results showed the potential of BRIP1 in predicting immunotherapy response and BRIP1 could be a promising candidate biomarker for immunotherapy of various cancers.

3.7. BRIP1 and Antitumor Drugs. Other than immunotherapy, the relationships between BRIP1 and IC50 of numerous antitumor drugs are also evaluated (Table S1). Among the 192 antitumor drugs, 141 of them including Olaparib and Niraparib (two PARP inhibitors) were negatively correlated with BRIP1, which indicated a promising response in these treatments. Besides, 7 drugs including Trametinib, SCH772984, ERK_2440, ERK_6604, Selumetinib, Ulixertinib, and VX-11e were positively correlated with BRIP1 which indicated a potential resistance during treatment.

4. Discussion

Cancer is a complex polyfactorial disease with high morbidity and mortality, remaining as an unsolved threaten to human health. Thus, research of effective diagnostic biomarkers and therapeutic targets for tumors has always been a heated focus. With the availability of public databases, cancer-related data can be mined to explore novel biomarkers. Through pan-cancer analysis, BRIP1 emerged from a bunch of candidate genes who were applicable for broad-spectrum tumor diagnosis as it significantly upregulated in most tumors. Herein, we conducted a systematic and comprehensive analysis of BRIP1 in pan-cancer. We validated its differential expression in various cancers between tumor and normal tissues at transcriptional and protein levels. Subsequently, we elucidated its role in prognosis, gene function, and regulatory pathways, and we discovered its
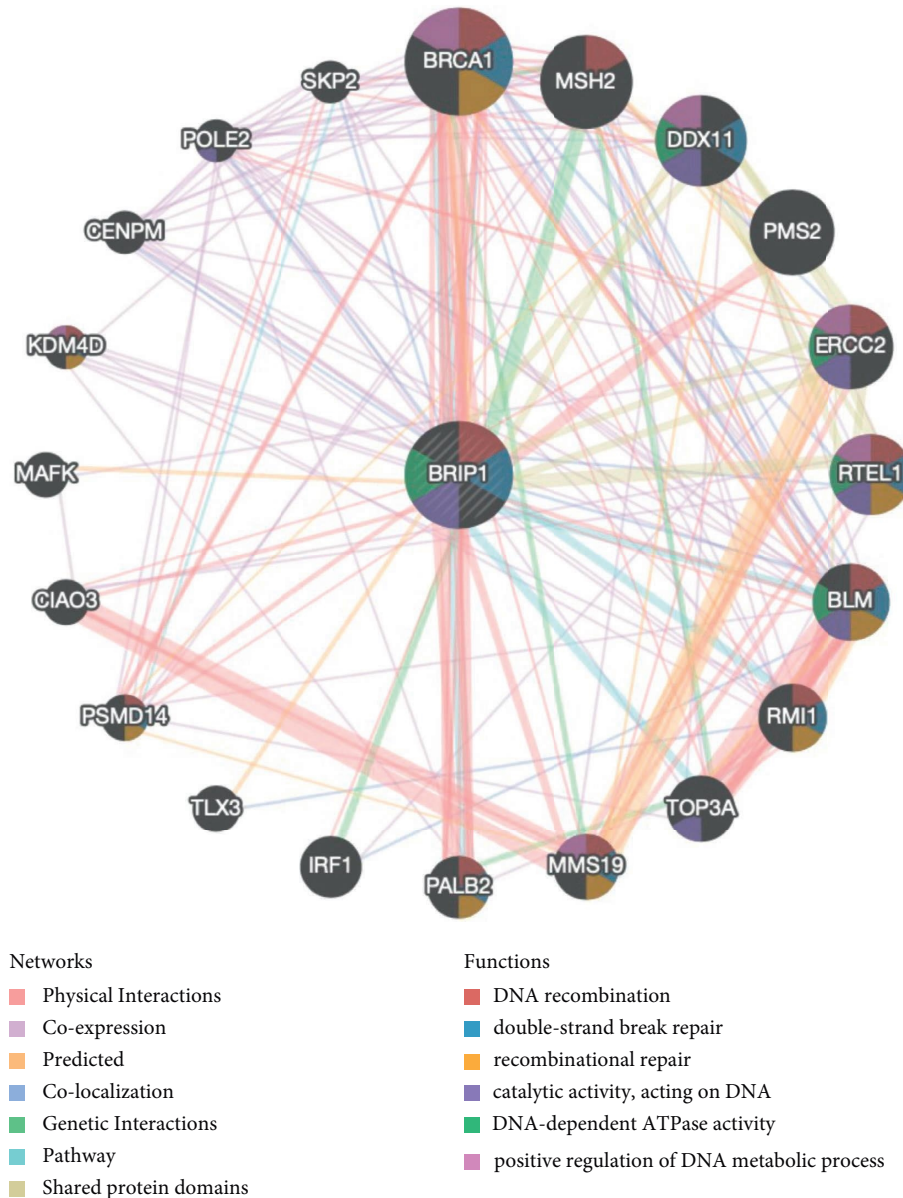
FIGURE 8: The PPI network and function analysis of BRIP1 from GeneMANIA.

association with TME, immune infiltration, immune-related genes, and treatment responses.

BRIP1, with a length of more than 180 kb, is located on chromosome 17q23.2 and encodes a protein of 1249 amino acids. Previous studies regarded BRIP1 as a tumor suppressor gene and revealed its diagnostic role in various types of cancer, such as breast cancer, ovarian cancer, cervical cancer, and colon cancer [21–24]. In our comprehensive data mining-based analysis, by analyzing data from the GTEx, CCLE, and TCGA databases, we revealed that BRIP1 expression was higher in 28 types of cancer tissues (including BRCA, CESC, COAD, and OV, in consistence with previous study results) and only lower in TGCT than in normal tissues. Furthermore, our results of differential expression analysis of paired samples and the results of IHC analysis also confirmed the diagnostic role of BRIP1 in pan-

cancer. Unfortunately, due to the lack of normal sample data, differential expression analysis could not be conducted in MESO and UVM. Accumulating evidence will be needed for further exploration in these two tumors. Besides, we found a significant differential expression between tumor stage I, II and stage III, IV in ACC, KIRP, LUAD, and OV, suggesting the predicting role of BRIP1 in early diagnosis of these cancers is worth looking forward to. Along with its predicting role in diagnosis, we also performed prognostic analyses in pan-cancer based on data from TCGA. Either from OS or DSS, as well as from DFI and PFI, we found a significant correlation between BRIP1 expression and survival probability in various cancers, among which, BRIP1 was basically a high-risk factor. Whether it be OS, DSS, DFI, or PFI, BRIP1 remained as a high-risk factor in KIRP and PAAD. Although our results from TCGA database did not
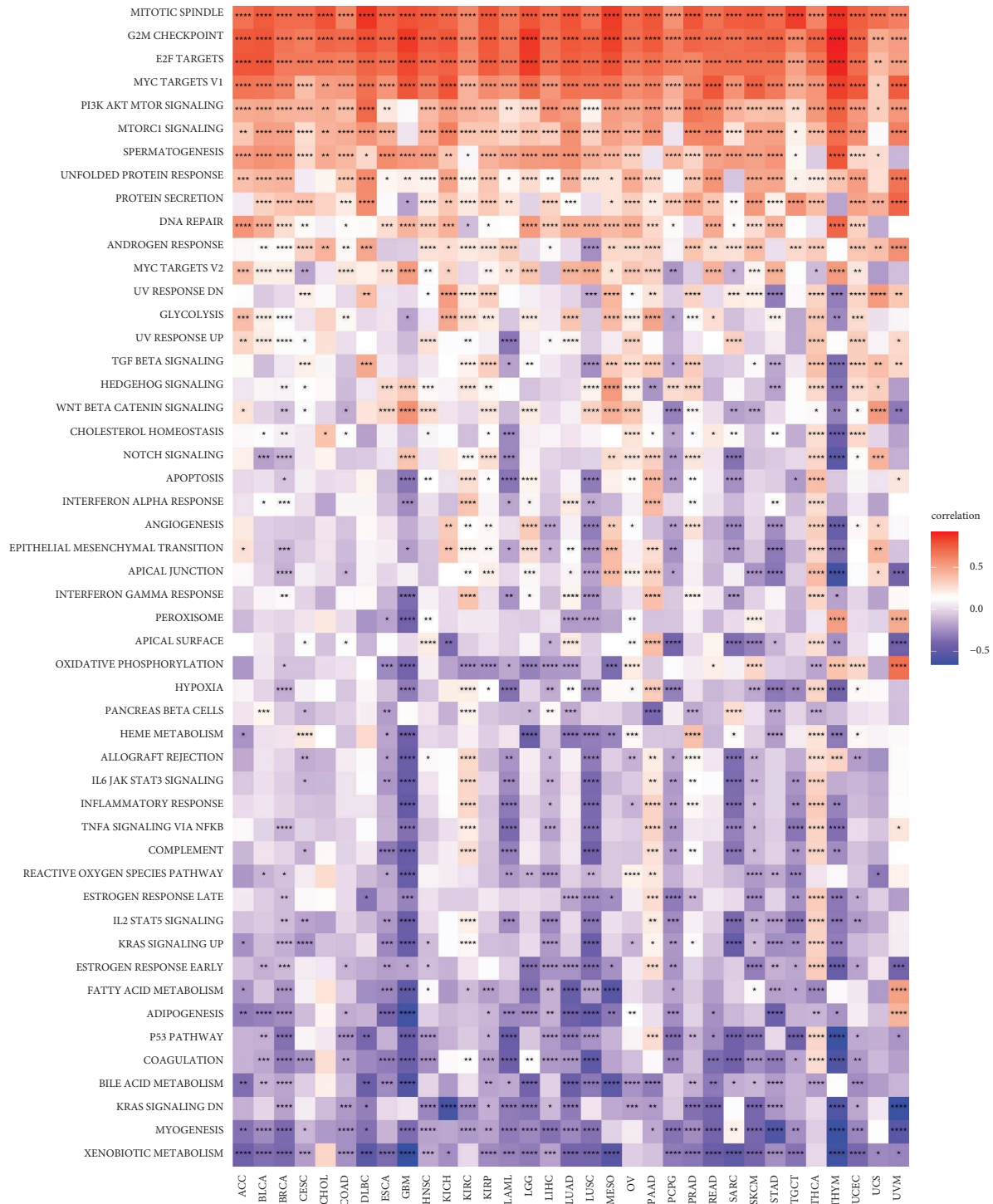
Figure 9: GSVA of BRIP1 in pan-cancer. * represents $P < 0.05$, ** represents $P < 0.01$, *** represents $P < 0.001$, and **** represents $P < 0.0001$.

find a correlation between BRIP1 expression and prognosis of breast cancer patients, a study based specifically on several breast cancer databases exhibited that higher BRIP1 expression was correlated with poor OS, DSS, DFI, and PFI [25]. Another study mining data of LUAD patients from the Genomic Data Commons (GDC) Data Portal indicated that BRIP1 might regulate fibroblast growth factor 22 and affect

MAPK as well as Rap 1 signalling pathways in all tumor stages of LUAD, and a high level of BRIP1 showed boundary significance on OS [26], in consistence with our results. Synthesizing the previous results, we believed that the high expression of BRIP1 could hamper cancer patients' survival and it might be an independent prognostic factor for various tumors. Although BRIP1 seemed to be a novel biomarker of
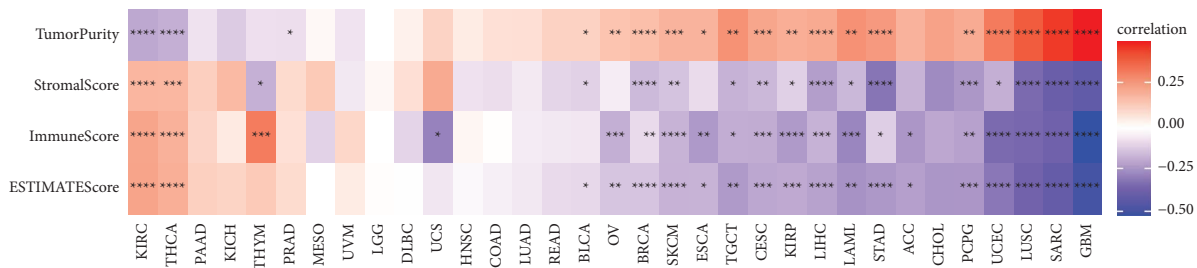
Figure 10: Correlation between BRIP1 expression and TME evaluated by ImmuneScore, StromalScore, and ESTIMATEScore. * represents $P < 0.05$, ** represents $P < 0.01$, *** represents $P < 0.001$, and **** represents $P < 0.0001$.

vital clinical utility in predicting diagnosis and prognosis in pan-cancer, the distinct effects of the differential expression of BRIP1 on protein function in various cancer types remain largely unknown. Previously, a meta-analysis based on 29400 patients with 116000 controls from 63 studies found BRIP1 was associated with a high risk of ovarian cancer and the HRR pathway might be involved [27, 28]. A cohort of more than 117000 patients elucidated the missense variant of BRIP1 conferred risk for ovarian and breast cancer. Researchers further studied the functional characterization of BRIP1, revealing an impaired interstrand crosslink (ICL) repair of DNA due to the missense variants of BRIP1 [29]. In an Asian esophageal squamous cell carcinoma cohort, researchers found that BRIP1 mutant was an adverse factor for OS and the cohort harboured TP53 signalling pathway alterations altered NOTCH, RTK-RAS, and cell cycle pathway, which might explain the phenomenon [30]. As reported by Singh, via quantitative real-time polymerase chain reaction (qRT-PCR) and Caspase-3 immunostaining, they found that the loss of DNA repair genes expression including BRIP1 in testis correlated with increased apoptosis [31]. To sum up, the distinct effects of the differential expression of BRIP1 in various cancer types may rely on different signalling pathways. Furthermore, *in vivo* and *in vitro* experiments are needed to validate the above findings and elucidate the specific underlying mechanisms of BRIP1 in different types of cancer.

The genomic mutation analysis revealed that the amplification of BRIP1 was one of the most vital single factors for alteration. Interestingly, previous studies reported that amplification of the 17q23 region led to a gain of function in lung cancer, liver cancer, pancreatic cancer, bladder cancer, testis cancer, and ovarian cancer [32]. Since this is the region where BRIP1 locates and with our finding of BRIP1 amplification and its role in pan-cancer, the phenomenon shall be explained to some extent. In addition, PPI analysis revealed that BRIP1 was mainly associated with DNA recombination, double-strand break repair, and recombinational repair. Enrichment analysis uncovered its correlation with homologous recombination, DNA replication, cell cycle, and Fanconi anemia. As indicated by previous studies, BRIP1 took part in HRR and helped in reducing the occurrence and persistence of DSB which was

regarded as the last defense against feasibly mutagenic and carcinogenic injury [33]. These might explain the underlying mechanisms of BRIP1 in tumorigenesis and provide a theoretical foundation for the discovery and development of targeted drugs. For example, Hodgson et al. illuminated in their study that ovarian cancer patients with loss-of-function mutations in HRR genes, including BRIP1, would benefit from Olaparib treatment [34]. Our study has evaluated the association between BRIP1 and IC50 of various antitumor drugs via GDSC database and found the same promising response to Olaparib. Except a few of antitumor drugs, there were 141 drugs negatively correlated with BRIP1, which indicated a promising treatment response. Furthermore, clinical trials with different drugs in diverse cancers and research on their targeted signalling pathways are urgently needed to validate effective targeted-therapies.

The cancer-related immune microenvironment was sophisticated and was regarded as the seventh marker feature of cancer [35]. Under normal circumstances, the immune system would recognize and eliminate tumor cells, preventing the invasion and metastasis of tumor cells. However, cancer cells could be subtle and survive the immune supervision by integrating with immune cells, thus restraining the immune system. Under this condition, immunotherapy would restore the normal antitumor immune response. Specifically, ICB therapy showed a remarkable clinical benefit in prolonging patient survival [36]. Immune checkpoints maintained a close correlation with immune cells in TME. Programmed death 1 (PD-1)/PD-L1 was one of the most vital immune checkpoint signalling pathways. Elevated expression of PD-1 and PD-L1 by TIICs was associated with suppression of T cell immune function and poor prognosis in cancer patients [37]. Besides, TMB and MSI were both considered as potential biomarkers for predicting ICB response. In this study, we systematically evaluated the correlation between BRIP1 and TME, TIICs, immune-related genes, as well as TMB-MSI. Results showed that there were close relationships between BRIP1 and various TIICs as well as immune-related genes. Additionally, BRIP1 was intimately correlated with the ESTIMATEScore in 19 cancers and positively associated with TMB in 9 cancers with MSI in 7 cancers, indicating a promising response to ICB therapy in these tumors. Especially in

Figure 11: BRIP1 expression and its association with TIICs from TIMER database.

(a)

(b)

(c)

(d)

(e)

(f)
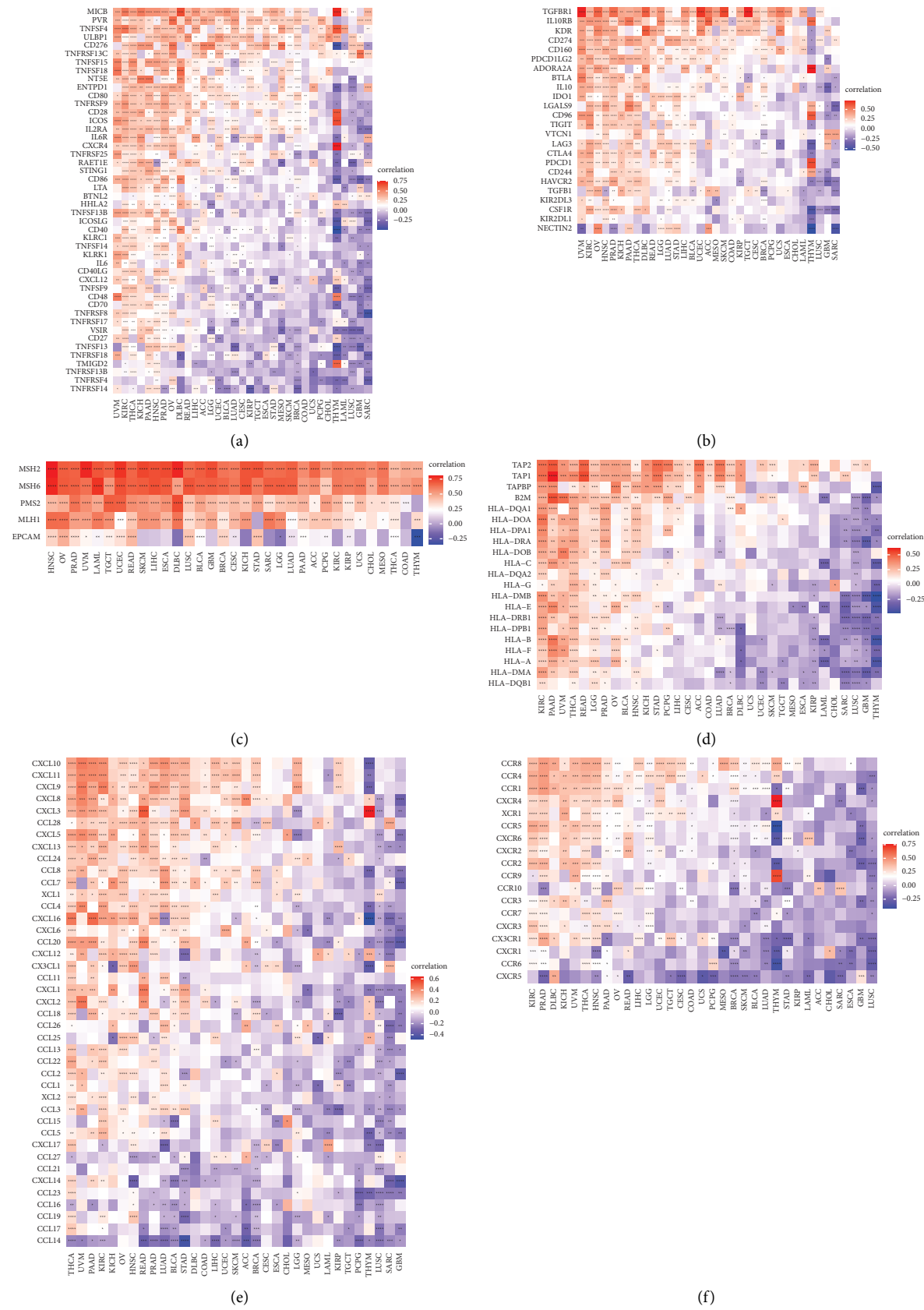
Figure 12: Correlation between BRIP1 and immune-related genes in pan-cancer. (a) Association between expression of BRIP1 and immune-activating genes. (b) Correlation between BRIP1 expression and immunosuppressive genes. (c) BRIP1 expression and its relationship with MMR genes. (d) BRIP1 expression and correlation with genes encoding MHC. (e) Association between BRIP1 expression and chemokine. (f) Correlation between expression of BRIP1 and chemokine receptor proteins. * represents $P < 0.05$, ** represents $P < 0.01$, *** represents $P < 0.001$, and **** represents $P < 0.0001$.

(a)

(b)

(c)

(d)

(e)
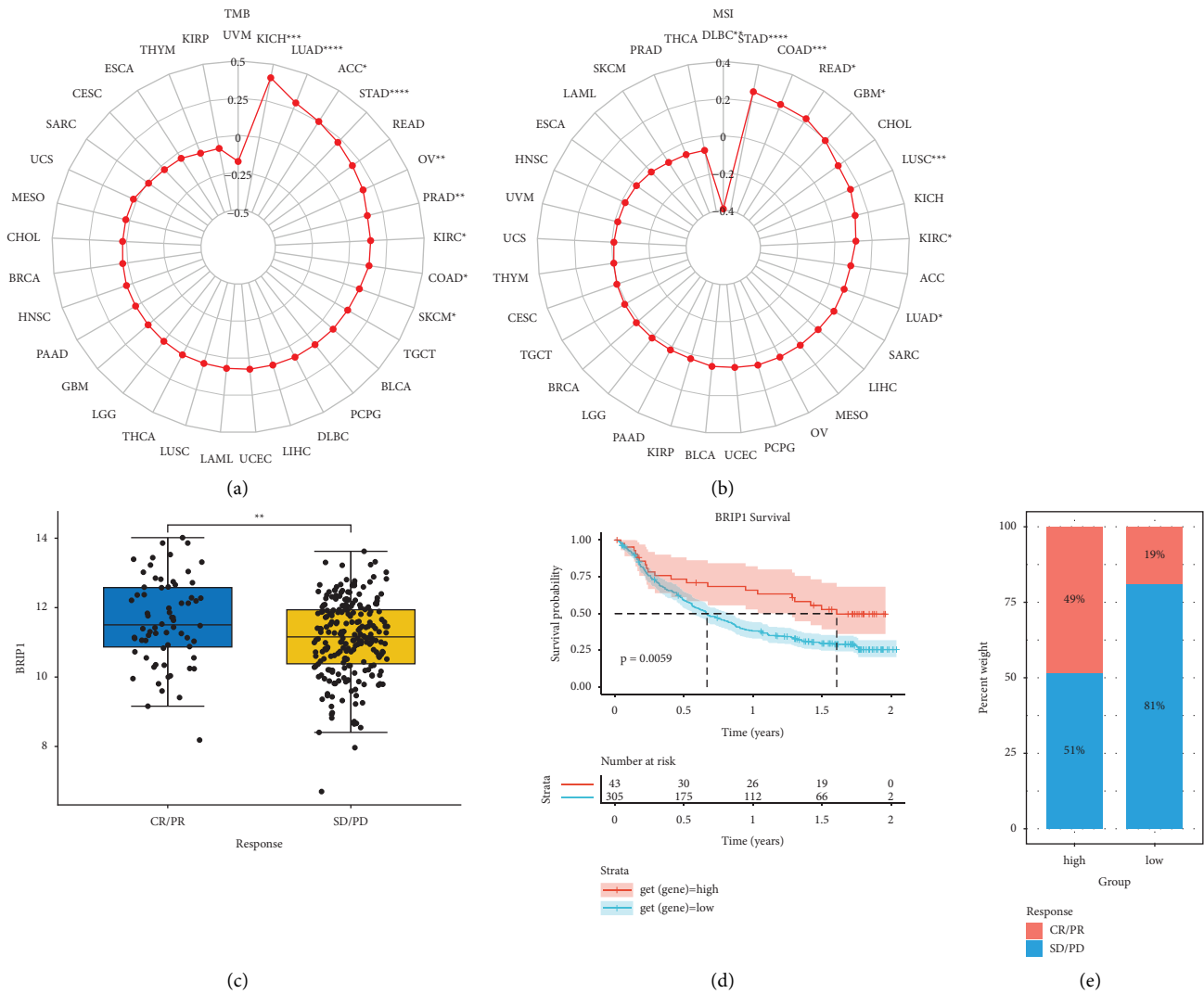
FIGURE 13: Correlation of BRIP1 expression with TMB/MSI and immunotherapy response. (a) Correlation between BRIP1 and TMB in pancancer. (b) Correlation between BRIP1 and MSI in pan-cancer. (c) Association between PD-L1 treatment response and BRIP1 in IMvigor210 cohort. (d) KM curve of the relationship between BRIP1 and survival rate in IMvigor210 cohort. (e) Response rate to PD-L1 therapy in different BRIP1 expression subgroups of IMvigor210 cohort. CR represents complete response, PR represents partial response, PD represents progressive disease, and SD represents stable disease. * represents $P < 0.05$, ** represents $P < 0.01$, *** represents $P < 0.001$, and **** represents $P < 0.0001$.

urothelial cancer, patients with a high level of BRIP1 had a better response to anti-PD-L1 treatment and a more favorable survival rate. Our research shed light on BRIP1 as a latent immunotherapy biomarker.

5. Conclusions

This study highlights the potential role of BRIP1 in pancancer as a predictor for diagnosis, prognosis, and treatment response through in-depth analyses of differential expression, relationships between BRIP1 and different prognostic parameters, gene functions, regulatory pathways, TME, TIICs, immune-related genes, and TMB-MSI as well as anticarcinogen. Furthermore, functional and mechanistic experiments are needed to elucidate the role of BRIP1 in specific cancers.

Data Availability

The original datasets analyzed in this study can be found in the corresponding websites as indicated in the article. Requests for further access to datasets can be directed to the corresponding author.

Conflicts of Interest

The authors declare that they have no conflicts of interest.

Authors' Contributions

L-YR was involved in study design, data acquisition and analysis, result interpretation, and manuscript draft. WX was responsible for result discussion. Z-SY and WQ were

involved in data acquisition. J-QW and F-YL were involved in data analysis. Y-AM was responsible for study concept, critical revision and supervision, and final approval of the submission. All authors have read and approved the final version of our study.

Acknowledgments

Supplementary Materials

Figures S1–S8 are separately uploaded as supplementary materials and figure legends are listed as follows: *Figure S1*. Differential expression of BRIP1 in 16 cancers between paired tumor tissues and their corresponding normal tissues. * represents $P < 0.05$, ** represents $P < 0.01$, *** represents $P < 0.001$, and **** represents $P < 0.0001$. *Figure S2*. Association between BRIP1 expression and different tumor stages. * represents $P < 0.05$, ** represents $P < 0.01$, and **** represents $P < 0.0001$. *Figure S3*. Positive correlation between BRIP1 expression and CNV in 23 specific tumor types including digestive cancers such as COAD, ESCA, LIHC, READ, and STAD. *Figure S4*. Negative association between BRIP1 expression and methylation in 16 specific tumor types including those digestive cancers such as COAD, ESCA, LIHC, and STAD. *Figure S5*. GSEA of BRIP1 based on KEGG in pan-cancer. (A1–A6) GSEA in ACC, BLCA, BRCA, CESC, CHOL, and COAD, respectively. (B1–B6) GSEA in DLBC, ESCA, GBM, HNSC, KICH, and KIRC, respectively. (C1–C6) GSEA in KIRP, LAML, LGG, LIHC, LUAD, and LUSC, respectively. (D1–D6) GSEA in MESO, OV, PAAD, PCPG, PRAD, and READ, respectively. (E1–E6) GSEA in SARC, SKCM, STAD, TGCT, THCA, and THYM, respectively. (F1–F3) GSEA in UCEC, UCS, and UVM, respectively. *Figure S6*. Association between BRIP1 expression and ESTIMATEScore in 33 tumors. (A1–A6) Association between BRIP1 expression and ESTIMATEScore in ACC, BLCA, BRCA, CESC, CHOL, and COAD, respectively. (B1–B6) Association between BRIP1 expression and ESTIMATEScore in DLBC, ESCA, GBM, HNSC, KICH, and KIRC, respectively. (C1–C6) Association between BRIP1 expression and ESTIMATEScore in KIRP, LAML, LGG, LIHC, LUAD, and LUSC, respectively. (D1–D6) Association between BRIP1 expression and ESTIMATEScore in MESO, OV, PAAD, PCPG, PRAD, and READ, respectively. (E1–E6) Association between BRIP1 expression and ESTIMATEScore in SARC, SKCM, STAD, TGCT, THCA, and THYM, respectively. (F1–F3) Association between BRIP1 expression and ESTIMATEScore in UCEC, UCS, and UVM, respectively. *Figure S7*. Correlation between BRIP1 and TMB in 9 tumors including digestive cancers such as COAD and STAD. *Figure S8*. Association between BRIP1 and MSI in 8 tumors including digestive cancers such as COAD, READ, and STAD. *Table S1*. Relationship between BRIP1 and IC50 in pan-cancer. (*Supplementary Materials*)

References

[1] H. Sung, J. Ferlay, R. L. Siegel et al., "Global cancer statistics 2020: GLOBOCAN estimates of incidence and mortality worldwide for 36 cancers in 185 countries," *CA: A Cancer Journal for Clinicians*, vol. 71, no. 3, pp. 209–249, 2021.

[2] S. B. Cantor, D. W. Bell, S. Ganesan et al., "BACH1, a novel helicase-like protein, interacts directly with BRCA1 and contributes to its DNA repair function," *Cell*, vol. 105, no. 1, pp. 149–160, 2001.

[3] C. Mani, G. Acharya, S. Kshirsagar et al., "A novel role for BRIP1/FANCJ in neuronal cells health and in resolving oxidative stress-induced DNA lesions," *Journal of Alzheimer's Disease*, vol. 85, no. 1, pp. 207–221, 2022.

[4] R. M. Brosh Jr. and S. B. Cantor, "Molecular and cellular functions of the FANCJ DNA helicase defective in cancer and in Fanconi anemia," *Frontiers in Genetics*, vol. 5, p. 372, 2014.

[5] M. B. Daly, T. Pal, M. P. Berry et al., "Genetic/familial high-risk assessment: breast, ovarian, and pancreatic, version 2.2021, NCCN clinical practice guidelines in Oncology," *Journal of the National Comprehensive Cancer Network*, vol. 19, no. 1, pp. 77–102, 2021.

[6] A. Turchiano, D. C. Loconte, R. De Nola, F. Arezzo, G. Chiarello, and A. Pantaleo, "Beyond brca1/2: homologous recombination repair genetic profile in a large cohort of apulian ovarian cancers," *Cancers*, vol. 14, 2022.

[7] C. Nero, T. Pasciuto, S. Cappuccio et al., "Further refining 2020 ESGO/ESTRO/ESP molecular risk classes in patients with early-stage endometrial cancer: a propensity score-matched analysis," *Cancer*, vol. 128, no. 15, pp. 2898–2907, 2022.

[8] R. R. Mikaeel, J. P. Young, Y. Li et al., "Survey of germline variants in cancer-associated genes in young adults with colorectal cancer," *Genes, Chromosomes and Cancer*, vol. 61, no. 2, pp. 105–113, 2022.

[9] M. J. Goldman, B. Craft, M. Hastie et al., "Visualizing and interpreting cancer genomics data via the Xena platform," *Nature Biotechnology*, vol. 38, no. 6, pp. 675–678, 2020.

[10] E. Cerami, J. Gao, U. Dogrusoz et al., "The cBio cancer genomics portal: an open platform for exploring multidimensional cancer genomics data," *Cancer Discovery*, vol. 2, no. 5, pp. 401–404, 2012.

[11] D. Warde-Farley, S. L. Donaldson, O. Comes et al., "The GeneMANIA prediction server: biological network integration for gene prioritization and predicting gene function," *Nucleic Acids Research*, vol. 38, no. 2, pp. W214–W220, 2010.

[12] M. Franz, H. Rodriguez, C. Lopes et al., "GeneMANIA update 2018," *Nucleic Acids Research*, vol. 46, no. 1, pp. W60–W64, 2018.

[13] M. Ashburner, C. A. Ball, J. A. Blake et al., "Gene Ontology: tool for the unification of biology," *Nature Genetics*, vol. 25, no. 1, pp. 25–29, 2000.

[14] S. Carbon, E. Douglass, B. M. Good et al., "The Gene Ontology resource: enriching a GOld mine," *Nucleic Acids Research*, vol. 49, no. 1, pp. D325–D334, 2021.

[15] A. Subramanian, P. Tamayo, V. K. Mootha et al., "Gene set enrichment analysis: a knowledge-based approach for interpreting genome-wide expression profiles," *Proceedings of the National Academy of Sciences of the U S A*, vol. 102, no. 43, pp. 15545–15550, 2005.

[16] A. Liberzon, C. Birger, H. Thorvaldsdottir, M. Ghandi, J. P. Mesirov, and P. Tamayo, "The molecular Signatures database hallmark gene set collection," *Cell Systems*, vol. 1, no. 6, pp. 417–425, 2015.

[17] T. Li, J. Fu, Z. Zeng et al., "TIMER2.0 for analysis of tumor-infiltrating immune cells," *Nucleic Acids Research*, vol. 48, no. 1, pp. W509–W514, 2020.

[18] D. J. McGrail, P. G. Pilie, N. U. Rashid et al., "High tumor mutation burden fails to predict immune checkpoint blockade response across all cancer types," *Annals of Oncology*, vol. 32, no. 5, pp. 661–672, 2021.

[19] L. Chang, M. Chang, H. M. Chang, and F. Chang, "Microsatellite instability: a predictive biomarker for cancer immunotherapy," *Applied Immunohistochemistry & Molecular Morphology*, vol. 26, no. 2, pp. e15–e21, 2018.

[20] S. Mariathasan, S. J. Turley, D. Nickles et al., "TGFβ attenuates tumour response to PD-L1 blockade by contributing to exclusion of T cells," *Nature*, vol. 554, no. 7693, pp. 544–548, 2018.

[21] M. Ali, C. D. Delozier, and U. Chaudhary, "BRIP-1 germline mutation and its role in colon cancer: presentation of two case reports and review of literature," *BMC Medical Genetics*, vol. 20, no. 1, p. 75, 2019.

[22] D. Samuel, A. Diaz-Barbe, A. Pinto, M. Schlumbrecht, and S. George, "Hereditary ovarian carcinoma: cancer pathogenesis looking beyond BRCA1 and BRCA2," *Cells*, vol. 11, no. 3, p. 539, 2022.

[23] S. Peleg Hasson, T. Menes, and A. Sonnenblick, "Comparison of patient susceptibility genes across breast cancer: implications for prognosis and therapeutic," *Pharmacogenomics and Personalized Medicine*, vol. 13, pp. 227–238, 2020.

[24] X. D. Ma, G. Q. Cai, W. Zou et al., "First evidence for the contribution of the genetic variations of BRCA1-interacting protein 1 (BRIP1) to the genetic susceptibility of cervical cancer," *Gene*, vol. 524, no. 2, pp. 208–213, 2013.

[25] U. Khan and M. S. Khan, "Prognostic value estimation of BRIP1 in breast cancer by exploiting transcriptomics data through bioinformatics approaches," *Bioinformatics and Biology Insights*, vol. 15, Article ID 117793222110558, 2021.

[26] H. Y. Liu, H. Zhao, and W. X. Li, "Integrated analysis of transcriptome and prognosis data identifies FGF22 as a prognostic marker of lung adenocarcinoma," *Technology in Cancer Research and Treatment*, vol. 18, Article ID 153303381982731, 2019.

[27] M. Suszynska, M. Ratajska, and P. Kozlowski, "BRIP1, RAD51C, and RAD51D mutations are associated with high susceptibility to ovarian cancer: mutation prevalence and precise risk estimates based on a pooled analysis of ~30,000 cases," *Journal of Ovarian Research*, vol. 13, no. 1, p. 50, 2020.

[28] K. P. Pennington, T. Walsh, M. I. Harrell et al., "Germline and somatic mutations in homologous recombination genes predict platinum response and survival in ovarian, fallopian tube, and peritoneal carcinomas," *Clinical Cancer Research*, vol. 20, no. 3, pp. 764–775, 2014.

[29] C. L. Moyer, J. Ivanovich, J. L. Gillespie et al., "Rare BRIP1 missense alleles confer risk for ovarian and breast cancer," *Cancer Research*, vol. 80, no. 4, pp. 857–867, 2020.

[30] H. Dai, Y. Wei, Y. Liu et al., "Pathway-based analysis revealed the role of keap1-nrf2 pathway and PI3K-akt pathway in Chinese esophageal squamous cell carcinoma patients with definitive chemoradiotherapy," *Frontiers in Genetics*, vol. 12, Article ID 799663, 2021.

[31] V. Singh, D. Jaiswal, K. Singh et al., "Azoospermic infertility is associated with altered expression of DNA repair genes," *DNA Repair*, vol. 75, pp. 39–47, 2019.

[32] B. Rizeq, S. Sif, G. K. Nasrallah, and A. Ouhtit, "Novel role of BRCA1 interacting C-terminal helicase 1 (BRIP1) in breast tumour cell invasion," *Journal of Cellular and Molecular Medicine*, vol. 24, no. 19, pp. 11477–11488, 2020.

[33] L. H. Thompson and J. M. Hinz, "Cellular and molecular consequences of defective Fanconi anemia proteins in replication-coupled DNA repair: mechanistic insights," *Mutation Research: Fundamental and Molecular Mechanisms of Mutagenesis*, vol. 668, no. 1-2, pp. 54–72, 2009.

[34] D. R. Hodgson, B. A. Dougherty, Z. Lai et al., "Candidate biomarkers of PARP inhibitor sensitivity in ovarian cancer beyond the BRCA genes," *British Journal of Cancer*, vol. 119, no. 11, pp. 1401–1409, 2018.

[35] M. R. Junttila and F. J. de Sauvage, "Influence of tumour micro-environment heterogeneity on therapeutic response," *Nature*, vol. 501, no. 7467, pp. 346–354, 2013.

[36] J. Zhang, Z. Wang, X. Zhang et al., "Large-scale single-cell and bulk sequencing analyses reveal the prognostic value and immune aspects of CD147 in pan-cancer," *Frontiers in Immunology*, vol. 13, Article ID 810471, 2022.

[37] T. Kamada, Y. Togashi, C. Tay et al., "PD-1(+) regulatory T cells amplified by PD-1 blockade promote hyperprogression of cancer," *Proceedings of the National Academy of Sciences of the USA*, vol. 116, no. 20, pp. 9999–10008, 2019.

Research Article

The Cuproptosis-Related Long Noncoding RNA Signature Predicts Prognosis and Immune Cell Infiltration in Hepatocellular Carcinoma

Ying Li [iD],[1,2] **Kaichao Song** [iD],[1,3] and **Wensheng Zheng** [iD][1]

[1]*Beijing City Key Laboratory of Drug Delivery Technology and Novel Formulation, Institute of Materia Medica, Chinese Academy of Medical Sciences & Peking Union Medical College, Beijing 100050, China*
[2]*Shandong University of Traditional Chinese Medicine, College of Traditional Chinese Medicine, Jinan 250355, China*
[3]*Institute of Medicinal Biotechnology, College of Traditional Chinese Academy of Medical Science and Peking Union Medical College, Beijing 100050, China*

Correspondence should be addressed to Ying Li; 782678245@qq.com, Kaichao Song; kaichao_song@163.com, and Wensheng Zheng; wensheng_zheng@126.com

Background. Hepatocellular carcinoma (HCC), ranking as one of the most common malignant tumors, is one of the leading causes of cancer death, with a poor prognosis. Cuproptosis, a novel programmed cell death modality that has just been confirmed recently, may play an important role in HCC prognosis. Long noncoding RNA (LncRNA) is a key participant in tumorigenesis and immune responses. It may be of great significance to predict HCC based on cuproptosis genes and their related LncRNA. *Methods*. The sample data on HCC patients were obtained from The Cancer Genome Atlas (TCGA) database. Combined with cuproptosis-related genes collected from the literature search, expression analysis was carried out to find cuproptosis genes and their related LncRNAs significantly expressed in HCC. The prognostic model was constructed by least absolute shrinkage and selection operator (LASSO) regression and multivariate Cox regression. The feasibility of these signature LncRNAs used for the evaluation of the overall survival rate in HCC patients as independent factors was investigated. The expression profile of cuproptosis, immune cell infiltration, and the status of somatic mutation were analyzed and compared. *Results*. A prognostic model of HCC consisting of seven cuproptosis gene-related LncRNA signatures was constructed. Multiple verification methods have showed that this model can accurately predict the prognosis of HCC patients. It was showed that the classified high-risk group under the risk score of this model had worse survival status, more significant expression of the immune function, and higher mutation frequency. During the analysis, the cuproptosis gene CDKN2A was found to be most closely related to LncRNA DDX11-AS1 in the expression profile of HCC patients. *Conclusion*. The cuproptosis-related signature LncRNA in HCC was identified, on the basis of which a model was constructed, and it was verified that it can be used to predict the prognosis of HCC patients. The potential role of these cuproptosis-related signature LncRNAs as new targets for disease therapy in antagonizing HCC development was discussed.

1. Introduction

The incidence of liver cancer is increasing year by year [1]. About 1 million people suffer from this disease every year worldwide [2, 3]. Among them, hepatocellular carcinoma (HCC), accounting for 75% to 90%, is the tumor ranking the third in mortality globally [4, 5]. Currently, radiotherapy, chemotherapy, and surgery are often adopted for early HCC, and systemic treatment is used for advanced HCC in clinical practice [6, 7]. However, the early diagnosis of HCC is difficult. Most HCC patients are diagnosed in the late stage, and it is difficult to cure them [8, 9]. Therefore, finding new targets for diagnosis and treatment is crucial for the effective management of HCC.

Cuproptosis is a recently confirmed cell death modality. Copper is one of the essential trace elements for living organisms. It is mainly absorbed through the small intestine and metabolized in the liver and in turn transported to various tissues and organs with the blood for use by cells. Generally, cuproptosis exists widely in body cells in the form of reduced cuprous ions (Cu^+) and oxidized cupric ions (Cu^{2+}), and also it is ingested by the copper transporter (hCtrl) and effluxed by adenosine triphosphatase (ATPase) to its intracellular levels in the body [10, 11]. The homeostasis of copper in the body is associated with many diseases. Existing studies have shown that the destruction of copper homeostasis can lead to the occurrence of multisystem diseases such as anemia [11], Wilson's disease [12], Menkes disease [13, 14], brain disease [15–17], immune system disease [18, 19], and tumors [20, 21]. When the copper ion concentration in the body cells exceeds the threshold of maintaining the homeostasis mechanism, it can directly combine with the fatty acylation components of the tricarboxylic acid cycle, which results in the aggregation of fatty acylated proteins and the loss of iron-sulfur cluster protein, and in turn trigger protein toxic stress and also ultimately cause cell death [22–24].

The long noncoding RNA(LncRNA) is a noncoding RNA with a length of N200 nucleotides. Recent studies have shown that LncRNA plays an important role in the occurrence and development of cancer, and the abnormal expression of LncRNA is associated with malignant tumors, tumor autophagy, tumor resistance, and tumor immunity [25, 26]. So far, it has been found that LncRNA is abnormally expressed in HCC [27], which can play a role in the formation of HCC and the migration of cancer cells, and in turn affect the occurrence, metastasis, and prognosis of HCC. Therefore, many scholars have focused on the value of lncRNA in tumor prognosis, building prognosis models, and developing new diagnostic targets based on the unique expression profile of lncRNA [28, 29]. The development and progression of HCC is a cumulative effect of genetic changes that affect the expression of tumor-related genes [30]. However, as a new mechanism involved in tumor cell death, it is worth paying attention to and discussing whether the influence of the changes of related genes on HCC has far-reaching significance and value.

Therefore, in this study, we used bioinformatics methods, sample data from TCGA public database, combined with cuproptosis-related genes collected by the literature search, to construct a unique expression profile of cuproptosis-related lncRNA, and used machine learning and other methods to screen out lncRNA which is of the great value to the prognosis of HCC and construct a prognosis model. The purpose of this study is to provide more predictive methods for diagnosing and evaluating the prognosis of patients with HCC, and to provide new ideas and support for the development of cuproptosis in HCC.

2. Materials and Methods

2.1. The Collection of Samples and CRGs. The public data on HCC came from The Cancer Genome Atlas (TCGA) database, including the RNA sequence data, clinical information, and tumor mutation data on 424 patients (50 normal and 374 tumor patients). The R language was used to classify protein-coding genes and lncRNAs in RNA sequences. The clinical information collection included gender, age, stage, grade, TNM, survival time, and status. For the accuracy of the study, the unknown part of clinical information was marked uniformly. A total of 19 CRGs were collected through the literature search. The research process is shown in Figure 1.

2.2. Coexpression Analysis of Cuproptosis-Related LncRNAs. The "limma" package in R language was used to extract the expression levels of CRGs and LncRNA from HCC samples. The LncRNAs associated with these CRGs were obtained by coexpression analysis, and also their relationship with HCC was tested by correlation analysis. The absolute value of the correlation coefficient was set to >0.5 and p value <0.001($p < 0.001$). The Sankey diagram is a diagram used to describe the flow direction of values from one group to another. In order to more intuitively show the relationship between CRGs and its related lncRNA, we used dplyr, ggalluvial, and ggplot2 packages in R language to draw the Sankey diagram to visualize the coexpression results.

2.3. Screening and Construction of a Prognostic Cuproptosis-Related lncRNAs Signature. The expression of lncRNA related to cuproptosis in the same sample of patients with HCC was combined with their survival status and survival time data. The lncRNAs related to cuproptosis was randomly divided into a training set (the train group) and a testing set (the test group) ($n = 1$) by the random forest algorithm, and the ratio of the training set to testing set was set to 1 : 1. The cuproptosis-related lncRNAs were filtered using univariate Cox regression analysis for genes that significantly affected the overall survival of patients with HCC (p-value <0.05). The univariate COX results were screened using a least absolute shrinkage and selection operators (LASSO) regression analysis. The multivariate COX regression analysis can detect whether multiple features are related to survival at the same time. In order to make the screened prognosis lncRNAs results more accurate, we further screened it by using multivariate COX regression based on the results of LASSO regression analysis. The screening result was a prognostic lncRNA associated with cuproptosis in HCC. We also constructed a prognostic model based on these key lncRNAs for evaluating the prognostic survival of patients with HCC. The model calculation formula is as follows:

$$\text{risk score} = \sum_{i=1}^{n} \beta_i \times x_i. \tag{1}$$

β_i represents the regression coefficient of each LncRNA, and X_i the expression level of each LncRNA.

The risk scores of the train and test groups were predicted according to the model, and the samples were divided into the high- and low-risk groups according to the median value of the risk scores.
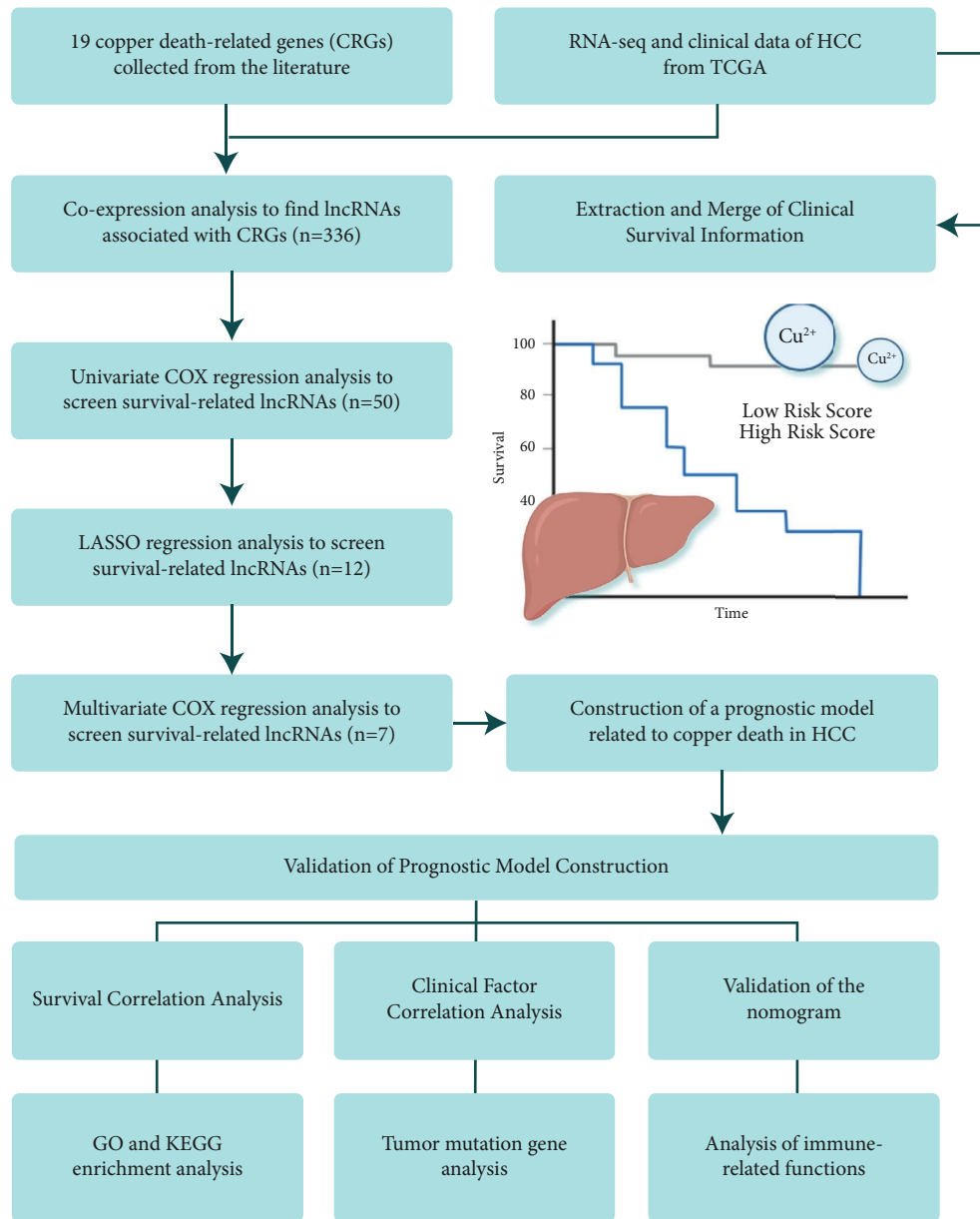
Figure 1: Process flow diagram.

2.4. Survival and Independent Prognostic Analyses. The survival analysis of patients in high- and low-risk groups was performed by models. Progression-free-survival (PFS) is an important index commonly used in clinical practice to judge the survival of malignant tumor patients in addition to OS. It represents the time period from the initial treatment of cancer patients to disease progression or death. The longer the PFS time is, the longer the survival cycle of this patient will be. In this study, the survival analysis was separately performed from two aspects of OS and PFS to evaluate the value of these cuproptosis-related LncRNA markers in HCC survival and prognosis.

Through independent prognostic analysis, it is possible to observe whether the prediction model constructed by us can be used as an independent prognostic factor independently of other clinical traits. The unifactor analysis was adopted to compare each clinical factor with survival time and status, and also the multifactor analysis of the effect on the survival status was analyzed under the interaction of multiple factors. The correlation between CRGs and prognosis-related LncRNA was verified, with the correlation heat map.

In order to verify the accuracy of the prediction model constructed by us, the receiver operating characteristic (ROC) curve of 1-, 3-, and 5-year survival in HCC patients

under the prediction of this model and that under the prediction of it combined with other clinical traits were plotted, respectively. The prediction accuracy of this model was confirmed by interpreting the area under the curve (AUC). Additionally, the concordance index (C-index) curve was plotted to evaluate the probability of consistency between the predicted and actual results. Principal component analysis (PCA) is a multivariate statistical method that can help us to evaluate the expression differences of four variables: whole genes, CRGS, CRGs-related lncRNAs, and characteristic lncRNAs for constructing models.

2.5. The Construction of a Prediction Nomogram. Based on the multifactor regression analysis, scores were assigned to each clinical factor according to the effect of various clinical traits in the prediction model on OS. The 1-, 3-, and 5-year OS of HCC patients was estimated through the relationship between the total score and the probability of outcome event occurrence and displayed in the form of a nomogram.

2.6. Model Validation for Clinical Grouping. By grouping clinical information, it was verified whether our prediction model is suitable for patients with different clinical straits from three aspects of tumor: grade, stage and age. According to the degree of tumor differentiation, G1-G2 patients with a relatively low malignant degree of HCC were grouped into one group, and G3-G4 patients with a high malignant degree were grouped into one group; the early patients in stages I and II were grouped into a group, and the late patients in stage III and IV were grouped one group; they were divided into two groups according to the age of <65 and ≥65, and the survival curve was plotted.

2.7. Risk Differentially Expressed Genes and Their Functional Enrichment Analysis. Through the "limma" package, the gene expression levels of high- and low-risk groups from the sample data were extracted and compared to find the genes with the differential expression between high- and low-risk groups (logFC >1, FDR >0.05). These risks differentially expressed genes may provide new ideas for explaining the HCC progression. Through gene ontology (GO) analysis, these risk differentially expressed genes that are involved in the biological processes of the body could be enriched and found. The biological processes included three aspects, the biological function (BP), cell component (CC), and molecular function (MF). Through the analysis of the Kyoto Encyclopedia of Genes and Genomes (KEGG), the signal pathways related to these differentially expressed genes could be enriched and found.

2.8. Tumor Mutation Analysis. By sorting and analyzing the mutation information in high- and low-risk groups, the genes mutated in the two groups of samples and their mutation frequency could be obtained. Also, the differential analysis of tumor mutation burden between the two groups of HCC patients was performed. It was observed whether the tumor mutations between the two groups were significantly different, and the 15 genes with the highest mutation frequency in HCC were further found for visualization, observation, and interpretation.

2.9. Analysis of the Immune-Related Function. Through gene set variation analysis (GSVA), the immune-related function gene set enriched by a single gene can be used as a signature expression matrix. Also, the difference in the immune function between the two groups by comparing the difference in the gene set expression between high- and low-risk groups was inferred. The difference analysis of immune checkpoint genes can help us observe which immune checkpoint genes are different in high- and low-risk patients to further find the relationship between cuproptosis genes and immune checkpoints.

3. Research Results

3.1. The Consistency Test of Clinical Traits in Patients between the Train and Test Group Cohorts. According to the clinical information, the consistency test on the clinical traits of patients in the train and test groups was carried out. The missing unknown parts of the clinical information were uniformly marked with "unknown." A total of 370 HCC patients were included. The test results are shown in Table 1. It was seen that after the included sample data were randomly assigned to two groups of cohorts, there was no significant difference in clinical traits between the two groups ($p > 0.05$), with the better-randomized grouping.

3.2. The Screening of Cuproptosis-Related LncRNAs and Prognosis-Related LncRNAs in HCC Patients. The biomarkers play an important role in tumor detection and treatment. The risk stratification for screening can be increased by finding new biomarkers that may identify susceptibility or early stages of the disease, either alone or as a complement to existing tests. [15, 30] The cuproptosis-related LncRNAs predicted by coexpression were screened according to the correlation coefficient (>0.5), and finally, 15 CRGs and 336 LncRNAs related to them were obtained (Table S1 and Figure 2(a)). After merging the survival information, 50 lncRNAs with the significant correlation and the overall survival rate of patients were obtained by univariate Cox regression analysis H, and the forest plot of survival results was drawn thereby (Figure 2(b)). The 12 features with the smallest error from the 50 significant lncRNs were screened out by LASSO regression analysis as key lncRNAs (see Figures 2(c) and 2(d)). Finally, further screening by multivariate Cox regression identified seven cuproptosis-related prognostic lncRNAs (lncRNA AC026412.3, PICSAR, AC021188.1, LINC00702, LINC00426, AL031985.3, and DDX11-AS1). The risk score was calculated for the prognostic model construction according to the formula in the Section 2. According to the median value of the risk score, the samples were divided into 191 cases in the high-risk group (92 cases in the train group and 99 cases in the test group) and 179 cases in the low-risk group (93 cases in the train group and 86 cases in the test group). The correlation analysis between CRGs and their related signature LncRNAs showed that there was a significant positive correlation between cyclin-dependent kinase inhibitor

TABLE 1: The consistency test results of HCC clinical traits.

Covariates	Types	Total	Test group	Train group	p value
Age	≤65	232 (62.7%)	107 (57.84%)	125 (67.57%)	0.0676
	>65	138 (37.3%)	78 (42.16%)	60 (32.43%)	
Gender	Female	121 (32.7%)	60 (32.43%)	61 (32.97%)	1
	Male	249 (67.3%)	125 (67.57%)	124 (67.03%)	
Grades	G1	55 (14.86%)	24 (12.97%)	31 (16.76%)	0.7163
	G2	177 (47.84%)	93 (50.27%)	84 (45.41%)	
	G3	121 (32.7%)	60 (32.43%)	61 (32.97%)	
	G4	12 (3.24%)	6 (3.24%)	6 (3.24%)	
	Unknow	5 (1.35%)	2 (1.08%)	3 (1.62%)	
Stages	Stage I	171 (46.22%)	87 (47.03%)	84 (45.41%)	0.7738
	Stage II	85 (22.97%)	42 (22.7%)	43 (23.24%)	
	Stage III	85 (22.97%)	38 (20.54%)	47 (25.41%)	
	Stage IV	5 (1.35%)	3 (1.62%)	2 (1.08%)	
	Unknow	24 (6.49%)	15 (8.11%)	9 (4.86%)	
T	T1	181 (48.92%)	93 (50.27%)	88 (47.57%)	0.7336
	T2	93 (25.14%)	49 (26.49%)	44 (23.78%)	
	T3	80 (21.62%)	36 (19.46%)	44 (23.78%)	
	T4	13 (3.51%)	6 (3.24%)	7 (3.78%)	
	Unknow	3 (0.81%)	1 (0.54%)	2 (1.08%)	
M	M0	266 (71.89%)	137 (74.05%)	129 (69.73%)	1
	M1	4 (1.08%)	2 (1.08%)	2 (1.08%)	
	Unknow	100 (27.03%)	46 (24.86%)	54 (29.19%)	
N	N0	252 (68.11%)	120 (64.86%)	132 (71.35%)	0.5598
	N1	4 (1.08%)	3 (1.62%)	1 (0.54%)	
	Unknow	114 (30.81%)	62 (33.51%)	52 (28.11%)	

2A (CDKN2A) and LncRNA DDX11-AS1, and a close positive correlation between NACHT, LRR, and PYD domains-containing protein 3 (NLRP3) and the LncRNAs(AC02118.1, LINC00426, LINC00702, and PICSAR), while there was a close negative correlation between FDX1 and LncRNA DDX11-AS1 (Figure 3).

3.3. The Survival Outcome and Multifactor Test. The survival curve can show the difference in model prediction of patient OS between the high- and low-risk groups. The OS of HCC patients in the high-risk group was generally lower within ten years, but after ten years, the OS was more stable than that in the low-risk group (Figure 4(a)). PFS analysis shows that the significant expression of prognosis-related lncRNA in the high-risk group is related to the poor survival of patients ($P < 0.001$), as shown in Figure 4(b). Additionally, by the risk distribution of HCC patients and the corresponding survival status chart, it was found that the survival status of patients in the high-risk group was worse and their survival time was shorter than that in the low-risk group (Figures 4(c) and 4(d)). By the heat map of the prognostic LncRNA expression in high- and low-risk groups, it was found that the LncRNAs(AC026412.3, AL031985.3, and DDX11-AS1) were positively correlated with the risk score, while the LncRNAs (AC021188.1, LINC00702, and LINC00426) were negatively correlated with the risk score (Figure 4(e)).

The forest diagram of unifactor and multifactor analyses of independent prognosis showed that the prediction model constructed by us could be used as an independent factor to evaluate the HCC prognosis just like the tumor grade (Figures 5(a) and 5(b); $p < 0.001$). Both the ROC curve and the area under curve (AUC) showed that this prediction model had relatively high accuracy in predicting the prognosis and survival of patients, which is significantly better than the prediction ability of other clinical traits (Figure 5(d)). The time-dependent receiver operating characteristic (ROC) and C-index curves also showed that this model had a good prediction effect, with more sensitivity in the prediction of early HCC patients (Figures 5(c) and 5(e)).

Through principal component analysis (PCA), the ability of cuproptosis genes, cuproptosis-related LncRNAs, and the signature LncRNAs used for model construction in classifying high- and low-risk patients could be judged. The results showed that the classification ability of signature LncRNAs was much better (Figure 6(d)), which demonstrated that it has a good value in prognostic risk prediction of hepatocellular carcinoma(HCC) patients.

3.4. The Nomogram of Prognostic Models. Based on the constructed prediction model based on the cuproptosis-related signature LncRNA and the effects of each clinical trait in the model on HCC, a nomogram was made to evaluate the prognosis of HCC patients for clinical management of HCC patients. The ordinate of the nomogram represents the variables in the prediction model and the abscissa represents the range of values that can be taken for each variable. According to the

(a)

(b)

FIGURE 2: Continued.

(c)
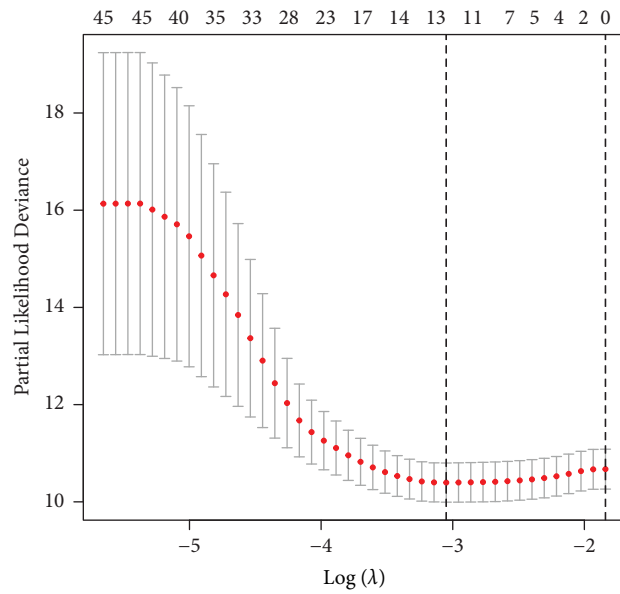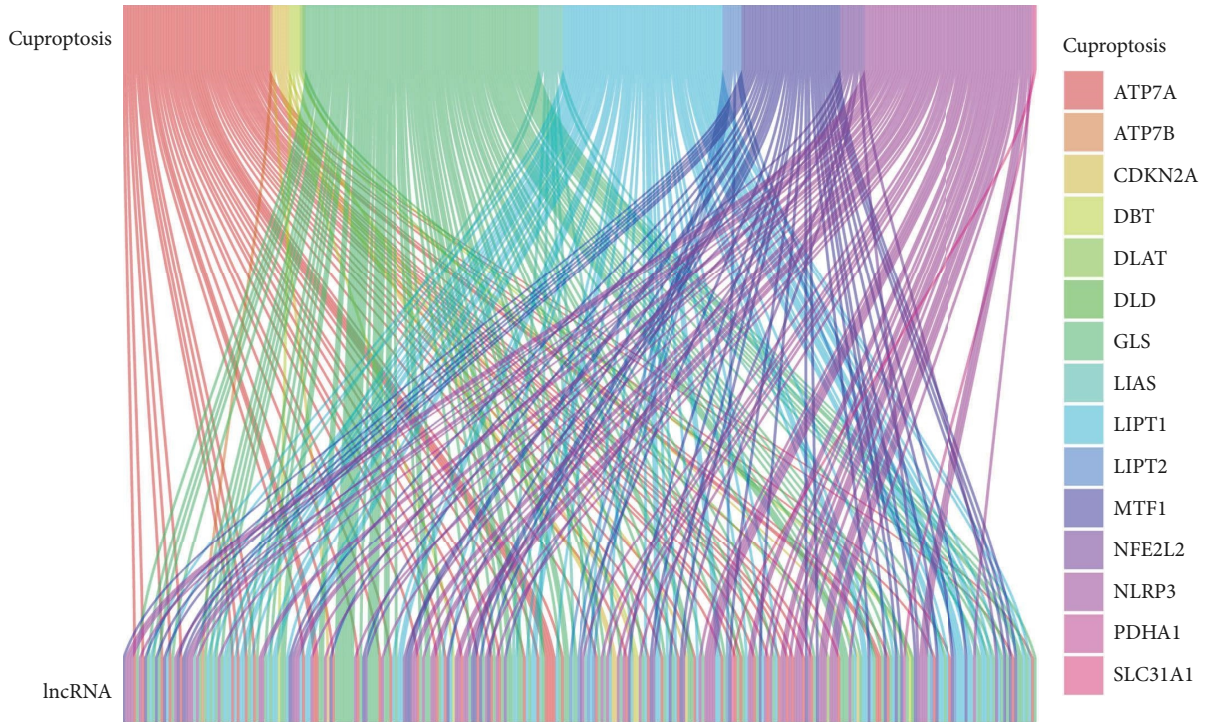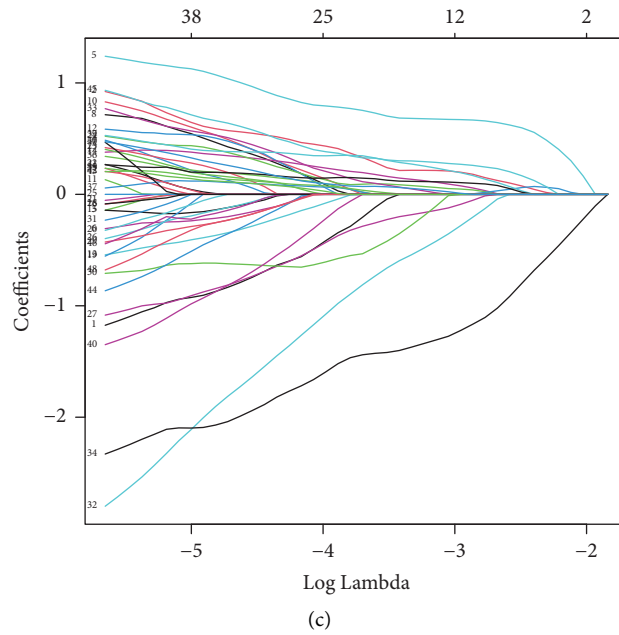
FIGURE 2: (a) Sankey diagram of CRGs and its related lncRNA: the different colors on the right side of the picture represent different CRGs, the top of the picture represents CRGs, and the bottom represents the lncRNA related to cuproptosis. (b) Univariate cox regression analysis forest plot. (c, d) LASSO regression analysis and cross-validation results. The dotted line on the left in (c) shows the number of features with the smallest error. (d) The changing track of each independent variable coefficient.
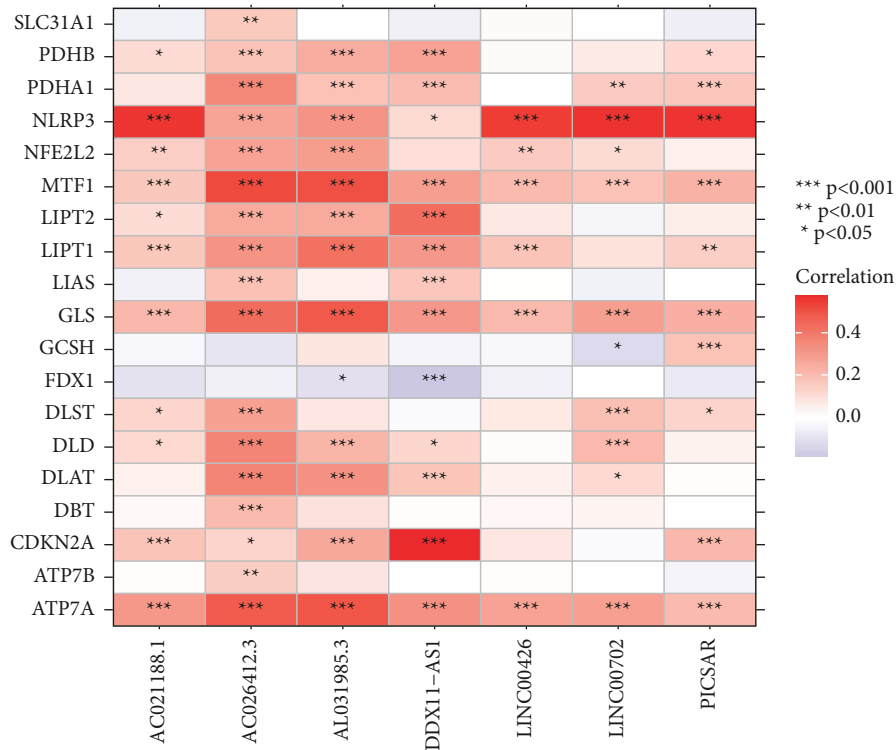
FIGURE 3: The expression heat map of cuproptosis-related genes (CRGs) and their related long noncoding RNAs (LncRNAs). The right side of the map represents different cuproptosis-related genes (CRGs), the lower part of the map represents the cuproptosis gene-related signature long noncoding RNAs (LncRNAs) screened by least absolute shrinkage and selection operator (LASSO) and multifactor regression, and the color represents the correlation between the two. The closer the color is to red, the higher the correlation is, and the closer it is to purple, the lower the correlation is.
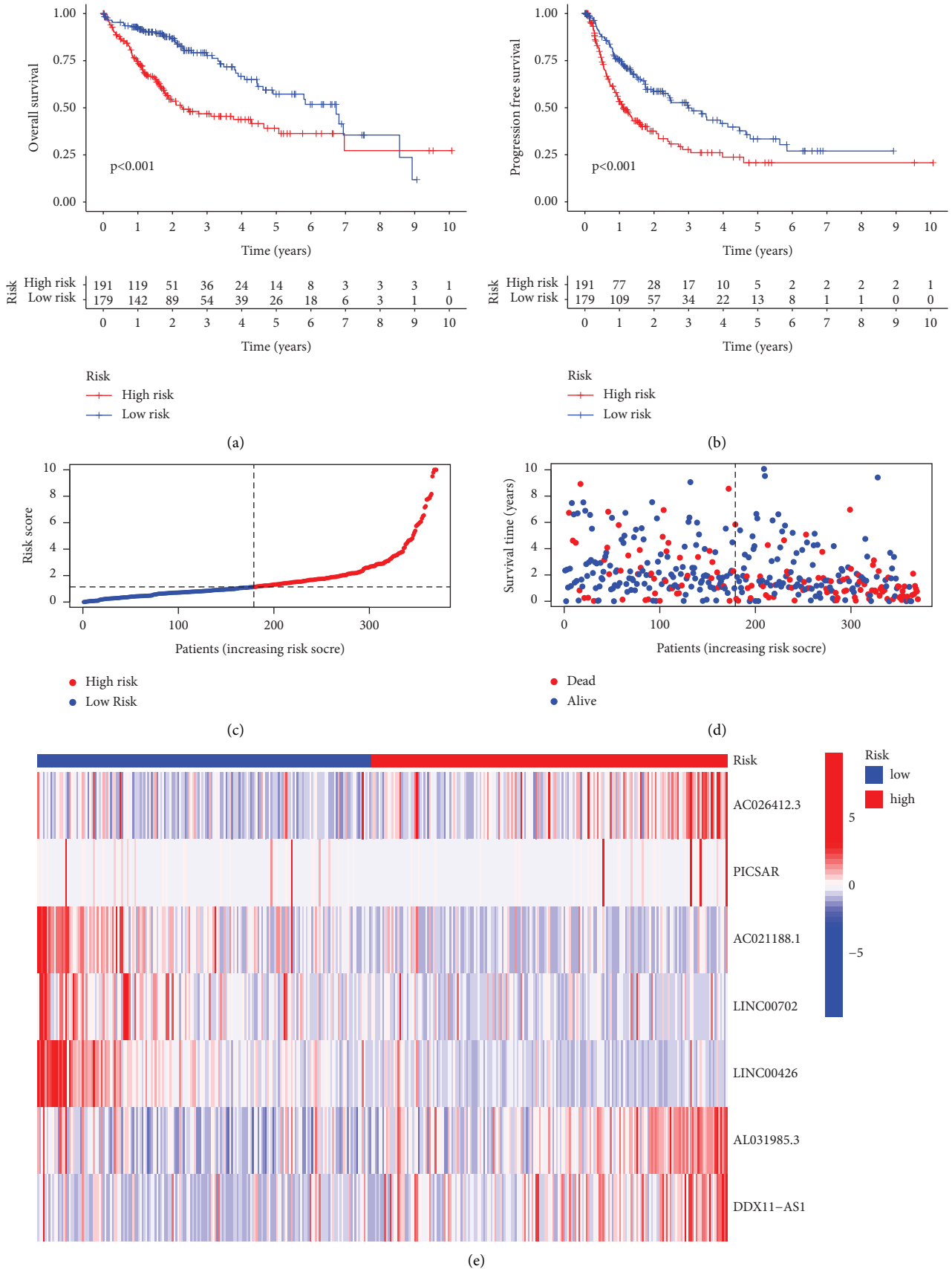
FIGURE 4: The group diagram of survival outcomes. (a) The Kaplan–Meier curve of overall survival (OS) in high- and low-risk groups; (b) the Kaplan–Meier curve of PFS in high- and low-risk groups; (c) the schematic diagram of the high- and low-risk distribution of hepatocellular carcinoma (HCC) patients; (d) the scatter plot of survival status of high- and low-risk groups; (e) the expression heat map of prognosis-related long noncoding RNA(LncRNA) in high- and low-risk groups.

(a)

(b)

AUC at 1 years: 0.736
AUC at 3 years: 0.752
AUC at 5 years: 0.662

(c)

Risk, AUC=0.736   Grade, AUC=0.499
Age, AUC=0.531   Stage, AUC=0.671
Gender, AUC=0.509

(d)

Risk score   Grade
Age   Stage
Gender

(e)
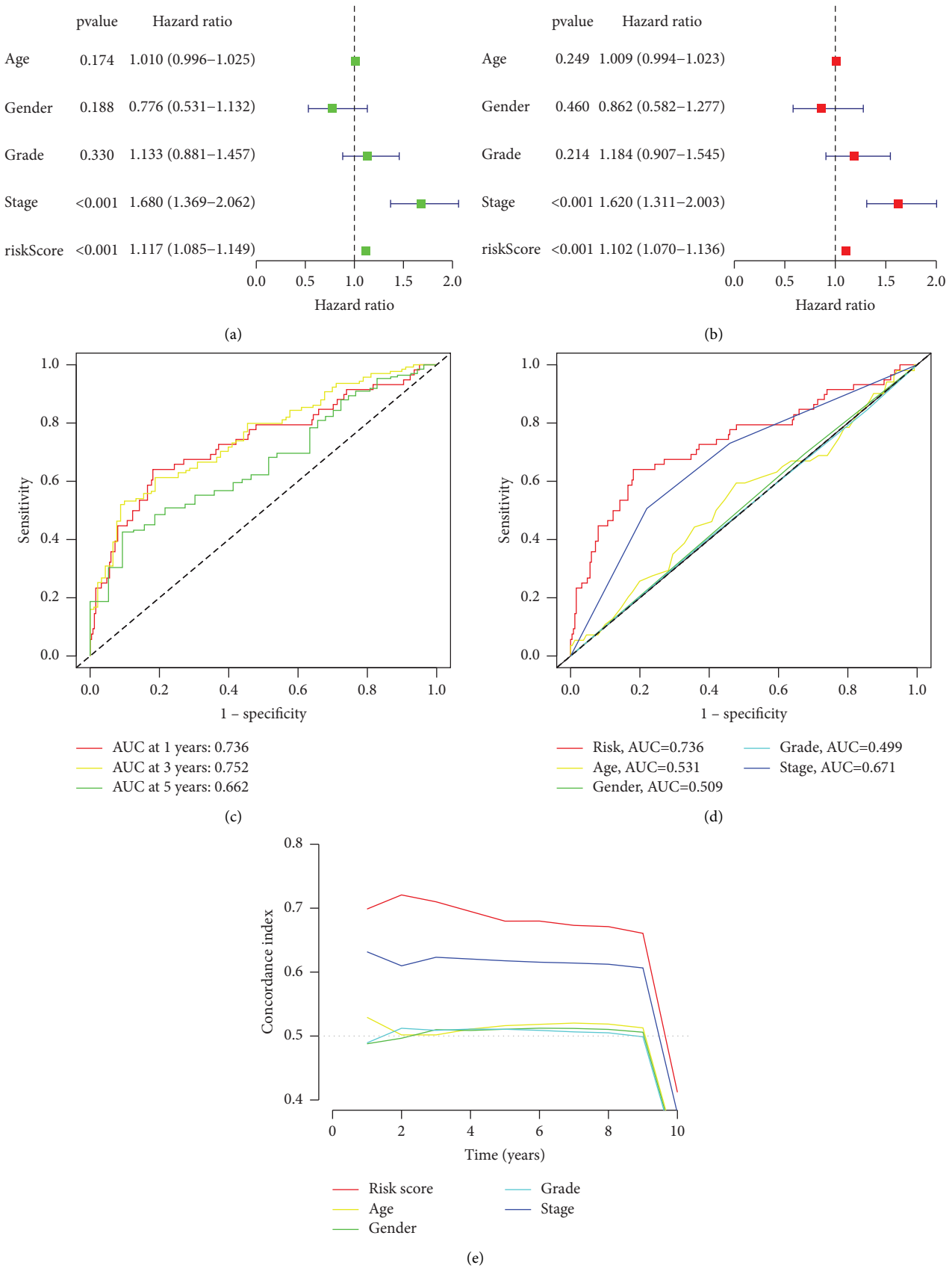
FIGURE 5: The group diagram for testing prognostic models. (a) The forest diagram of unifactor analysis of independent prognosis; (b) the forest diagram of multifactor analysis of independent prognosis; (c) the time-dependent receiver operating characteristic (ROC) curve diagram for validation of prognostic model risk scores; (d) the receiver operating characteristic (ROC) curve diagram of the accuracy of prediction ability of each clinical trait; and (e) the C-index curve diagram of the accuracy of prediction ability of each clinical trait.
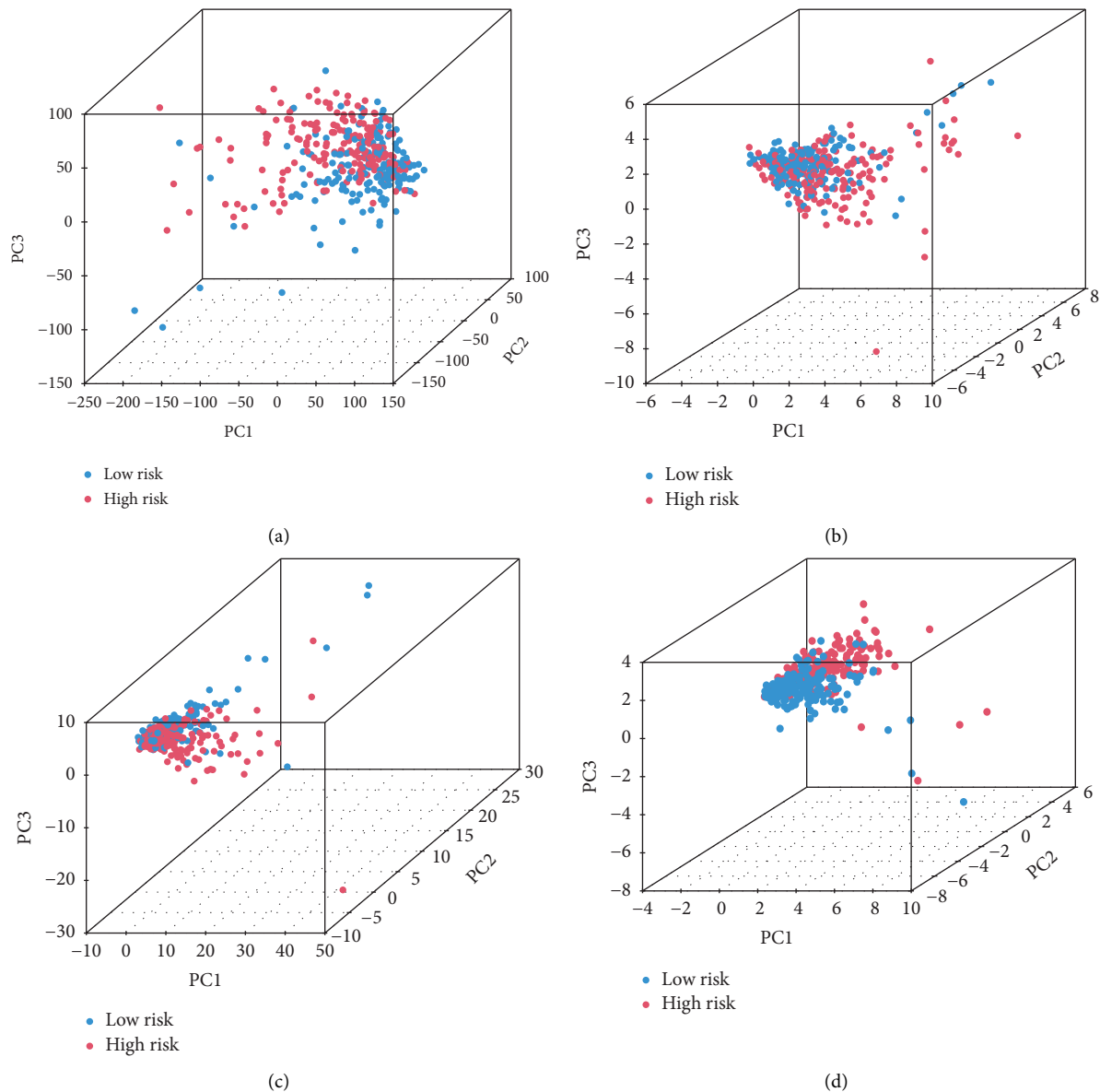
FIGURE 6: The group diagram of principal component analysis (PCA). (a) The whole gene expression in hepatocellular carcinoma (HCC) patients in two high- and low-risk groups; (b) the expression of cuproptosis genes; (c) the expression of cuproptosis-related long noncoding RNAs (LncRNAs); and (d) the expression of signature long noncoding RNAs(LncRNAs) for model construction.

number of the sample data above the vertical corresponding scale point on the horizontal axis of the variable, the score of the single variable of the sample can be obtained. The vertically correspond survival probability value can be found by calculating that total score of variable, thereby judging the survival condition of the patient. One patient sample was randomly selected from the samples for prediction, and its 1-, 3-and 5-year prediction scores are shown in Figure 7. The model showed that the total score of the patient was 391, and the survival probability was 93.6% after one year, 89.6% after three years, and 82.0% after five years after the diagnosis of HCC.

3.5. Clinical Grouping for Model Verification. As shown in Figure 5, this prediction model can be used as an independent factor to evaluate the prognosis of HCC and has better prediction ability compared with tumor staging. The samples were grouped according to the clinical information, and the performance of the prognostic model was verified by grouping in terms of stage, age, and grade. According to the clinical information, the samples were separately grouped from three aspects of grade, stage, and age to verify the accuracy of the model in predicting the prognosis of patients. In the survival curve drawn according to tumor stage factors, it can be seen that the patients in the high-risk group divided by the model showed worse survival status in both early and late stages of the tumor (Figures 8(a) and 8(b)). The same situation also appeared in the survival curves obtained by age grouping (Figures 8(c) and 8(d)). However, the results of grouping verification according to tumor differentiation levels were slightly different. According to the results of the C-index curve, we can find that the tumor
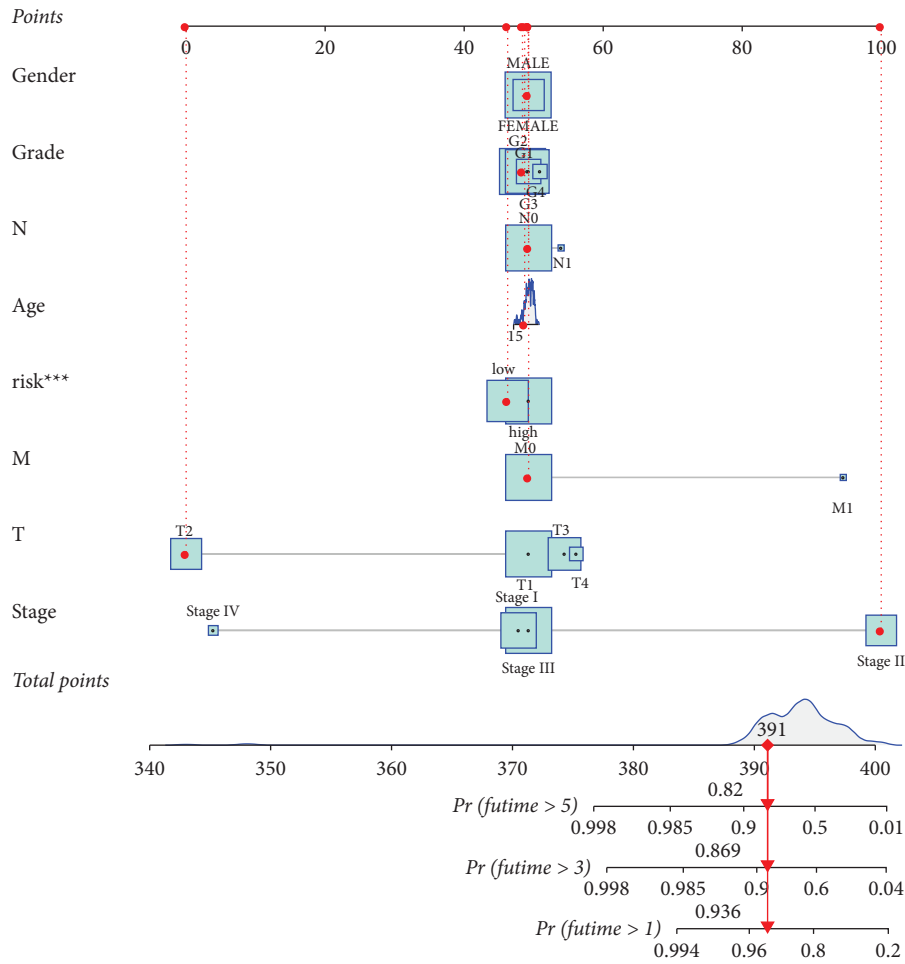
FIGURE 7: The nomogram of each clinical trait and prognostic cuproptosis-related long noncoding RNA (LncRNA).

grade (grade) has poor ability to judge the prognosis and survival of patients with HCC. Patients with high- and low-risk scores showed significant differences between the G1-G2 groups ($P < 0.001$), as shown in Figure 8(e). However, among the more differentiated G3-G4 groups, there was no significant difference in survival condition between the high- and low-risk groups ($P > 0.05$). The Kaplan–Meier curve shows that our model still has good discrimination ability in the early stage of the disease in patients with poorly differentiated HCC, as shown in Figure 8(f). However, it lacks sensitivity in the long-term prediction in patients with poorly differentiated HCC. We believe that although the public database contains data on all stages of the tumor, the prognosis of HCC patients with low differentiation and high malignancy is often worse, and their long-term survival performance is unoptimistic. Therefore, there is a lack of long-term survival data from poorly differentiated patients, resulting in a mediocre performance of the model in patients during this period. This suggests that in order to increase the credibility of the model, more sample data should be included in future research.

3.6. Analysis of Risk-Differential Genes and Their Functional Enrichment. Through risk differential analysis, a total of 598 genes with the differential expression were screened in high- and low-risk groups. The top ten with the highest significance among the gene ontology (GO) enrichment analysis results were selected and sorted according to the number of target genes enriched in them, and they were integrated into a classification histogram (Figure 9(a)). As can be seen in the figures, in BP, these differential genes were mainly involved in these biological functions such as lymphocyte-mediated immunity, B cell-mediated immunity, immunoglobulin-mediated immune responses, regulation of B cell activation, the B cell receptor signaling pathway, complement activation, humoral immune response mediated by circulating immunoglobulin, phagocytosis recognition, and complement activation of the classical pathways; in CC, cell components such as the immunoglobulin complex, external side of the plasma membrane and the plasma membrane signaling receptor complex, and blood microparticles were involved; in MF, these risk differentially expressed genes were mainly involved in molecular functions such as antigen binding, immunoglobulin receptor binding, glycosaminoglycan binding, heparin-binding, immune receptor activity, chemokine receptor binding, chemokine activity, CCR chemokine receptor binding, chemokine binding, and C–C chemokine binding.

(a)

(b)

(c)

(d)

Figure 8: Continued.

(e)

(f)
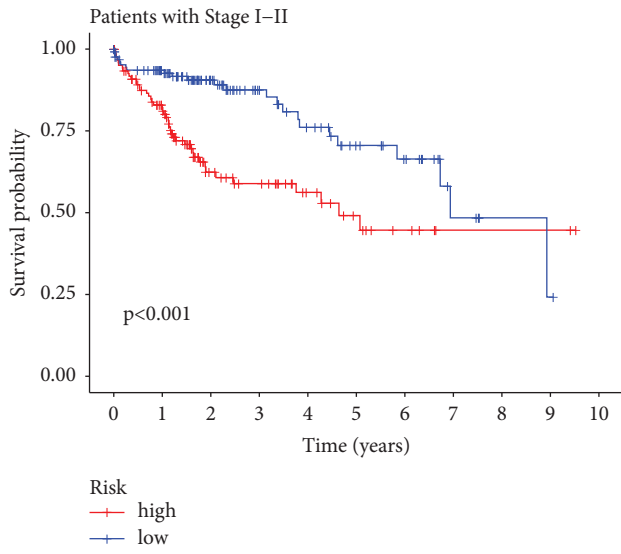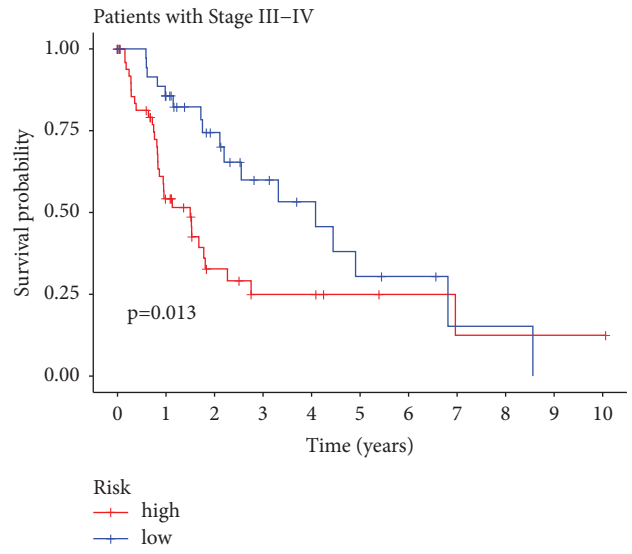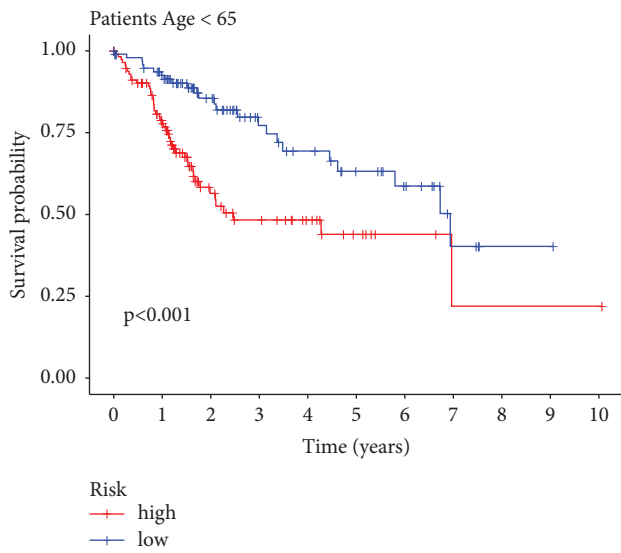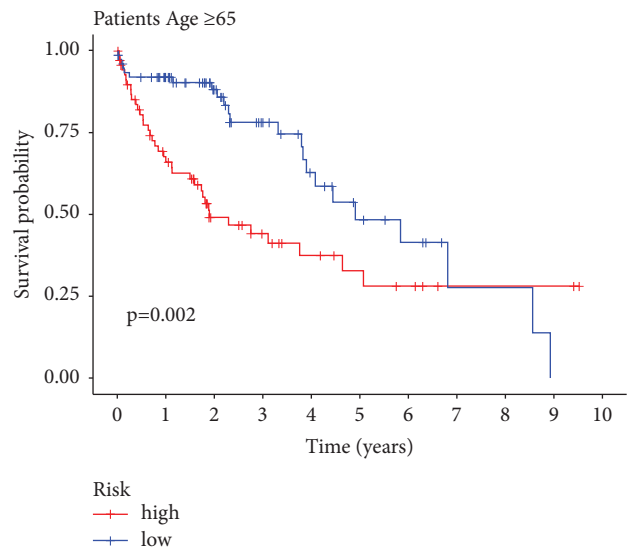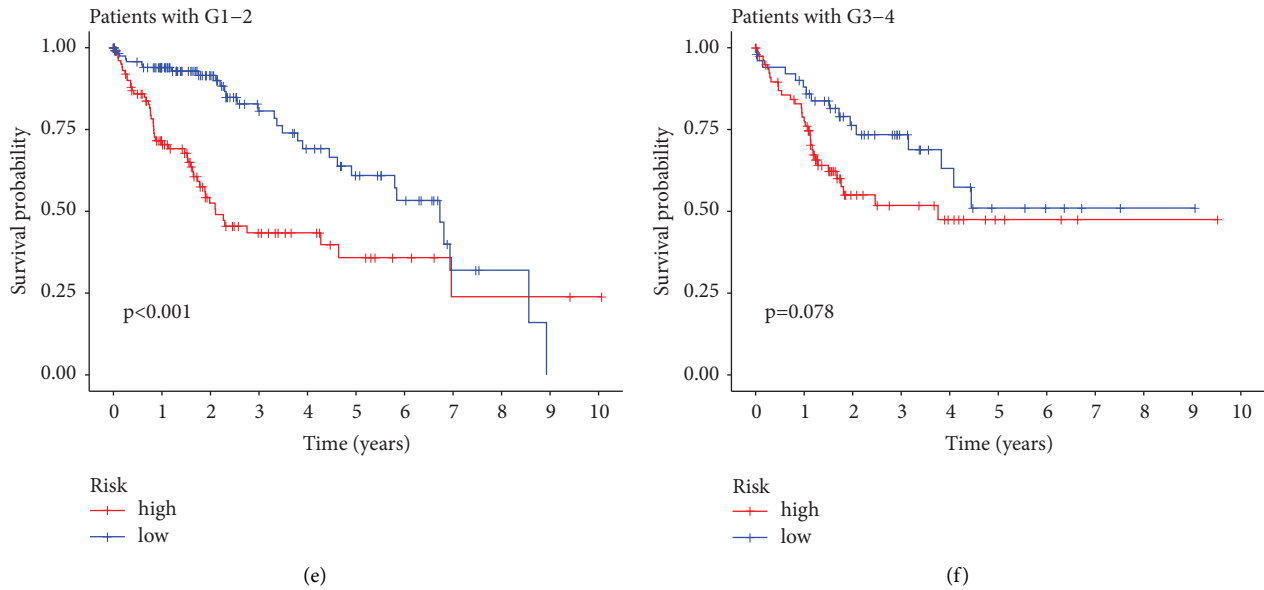
FIGURE 8: The Kaplan–Meier curve of verification of model-predicted overall survival by grouping according to clinical trait. (a, b) the survival analysis curve of high- and low-risk groups grouped according to the tumor stage, I-II (early stage) and III-IV (latestage). (c, d) the survival analysis curve of high- and low-risk groups grouped according to age. (e, f) the survival analysis curve of high- and low-risk groups grouped according to tumor differentiation levels. G1-G2 represent medium and high differentiation levels, with low malignancy, and G3-G4 represent low or undifferentiated levels, with high malignancy.

Kyoto Encyclopedia of Genes and Genomes (KEGG) pathway enrichment analysis showed that the pathways closely related to these risk differentially expressed genes included those such as hsa04060 cytokine-cytokine receptor interaction, hsa04640 hematopoietic cell lineage, hsa04061 viral protein interaction with cytokine, and cytokine and hsa05340 primary immunodeficiency (Figure 9(b); supplementary Table S2).

3.7. Mutation Gene Analysis. After analyzing mutation information between the high-risk group and the low-risk group, we found that there was no significant difference in the tumor mutation load between these two groups, which meant that the difference in the number of gene mutation sites in HCC cells between these two groups was insignificant, as shown in Figure 10(a). The survival analysis was performed according to the mutation burden, and it can be seen from Figure 10(b) that the survival status of patients in the high burden group was worse ($P < 0.05$). From the survival analysis results based on tumor mutation burden combined with the patient risk, it can be seen that there were significant differences between all the four groups ($P < 0.001$), and the patients in the high-risk group all showed a poor survival status regardless of the high or low level of the tumor mutation burden. This indicates from the side that the prediction model we constructed has a certain value in the analysis of patient survival prognosis (Figure 10(c)).

The waterfall plot of the two groups of mutated genes shows that they had a higher mutation frequency in the high-risk group. Among them, the genes such as TP53 (cellular tumor antigen p53), CTNNB1 (catenin beta-1),

TTN (titin), and MUC16 (mucin-16) had a very high mutation rate in HCC, with their mutation methods all mainly missense mutation, and some genes were also mutated by such methods as frame shift mutation and nonsense mutation. Among them, the variation frequency of GTNNB1, TTN, and MUC16 in the low-risk group was higher than that in the high-risk group, and on the contrary, TP53 is more prone to mutation in the high-risk group (Figures 10(d) and 10(e)).

3.8. The Analysis of Immune-Related Functions. Tumor immunotherapy is considered as a promising method for tumor treatment, and it has become an important method and research focus of tumor treatment [31, 32]. Through the analysis of immune-related functions, it could be found that the expression of these 13 immune-related functions was all significantly different between high- and low-risk groups ($P < 0.01$), and they consistently showed a negative correlation in the high-risk groups (Figure 11(a)). Due to the importance of checkpoint inhibitor-based immunotherapy, the differences in the immune checkpoint gene expression in high- and low-risk groups of HCC patients were investigated (Figure 11(b)). The 25 immune checkpoint genes such as CD276, CD44, PDCD1, and TNFSF4 were closely related to HCC ($P < 0.001$). Combined with the expression of cuproptosis genes in HCC (Figure 12), CDKN2A, the most significantly expressed cuproptosis gene, taken as an example, the correlation between it and 8 immune checkpoint genes was explored and also a scatter plot was drawn (Figure 11). The blue line in the figure represents
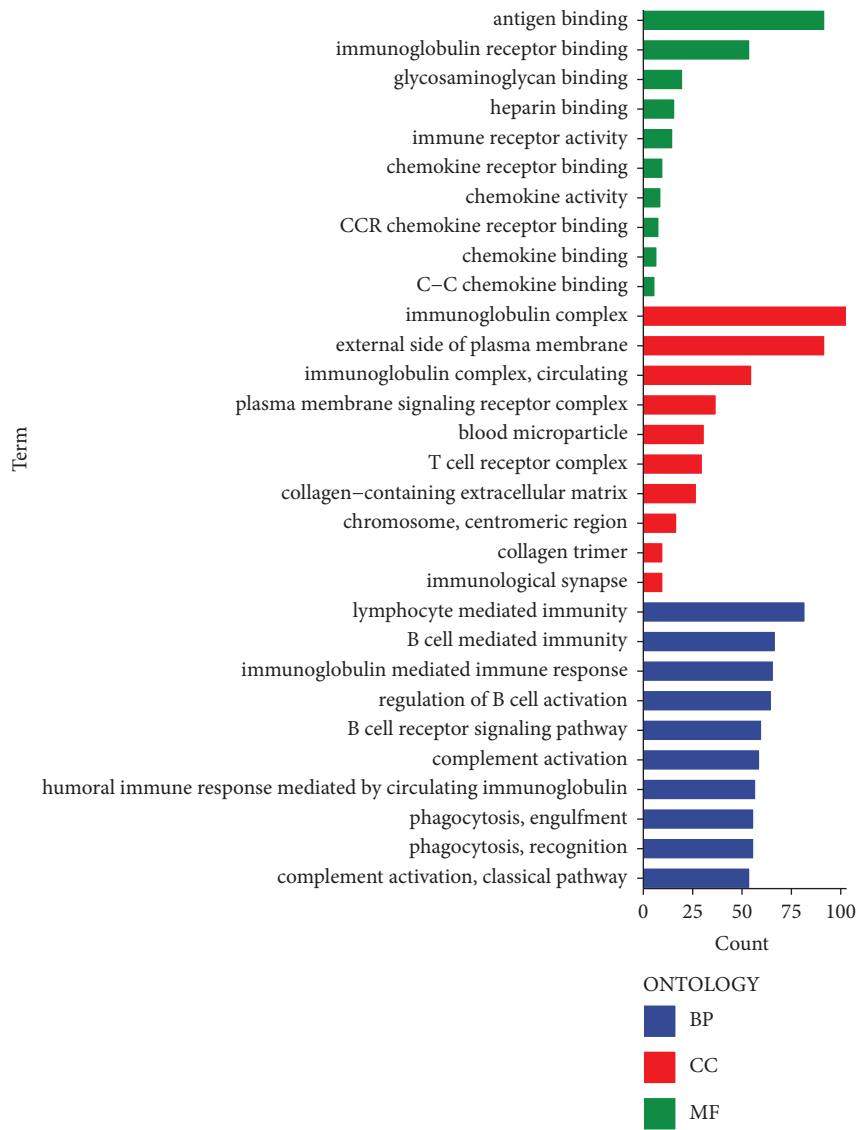
(a)

Figure 9: Continued.

(b)
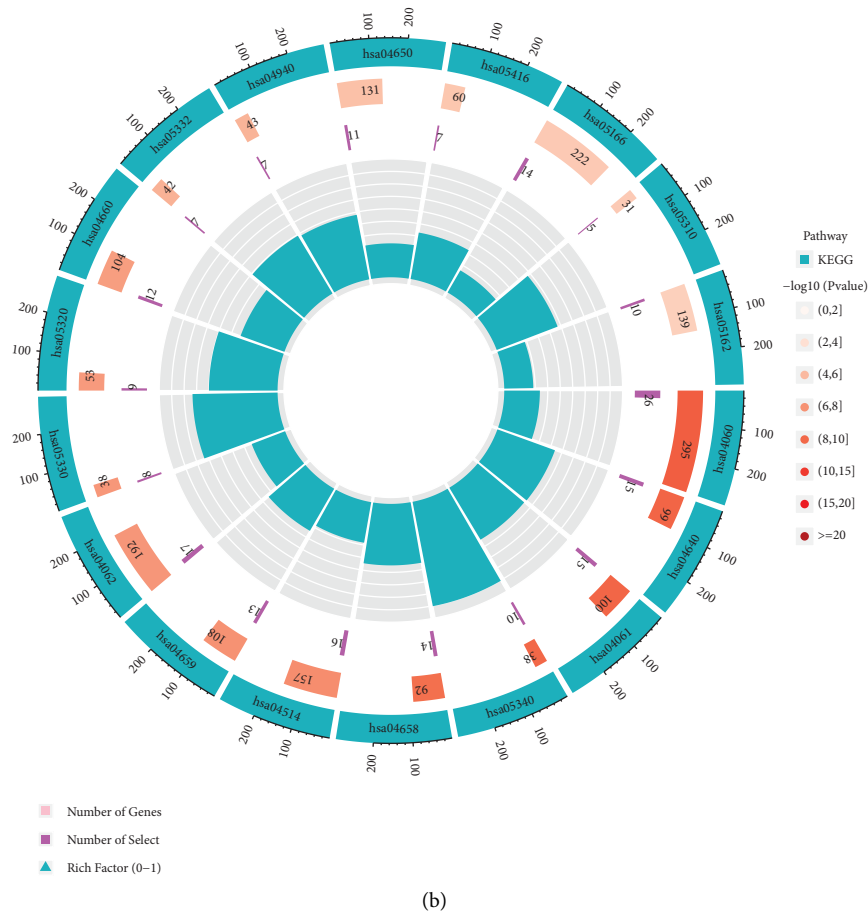
Figure 9: The enrichment analysis diagram of differential genes in high- and low-risk groups. (a) The color bar diagram of gene ontology (GO) analysis of risk differential genes, with colors representing biological function (BP, in BLUE), cell component (CC, in RED), and molecular function (MF, in GREEN), respectively (b) the circle diagram of Kyoto Encyclopedia of Genes and Genomes (KEGG) pathway enrichment analysis of risk differential genes, in which cyan represents the pathway number, different degrees of red represents significance, and purple represents the number of enriched target genes.

the trend of the correlation between CDKN2A and the corresponding immune checkpoint genes, indicating that all eight immune checkpoint genes were positively correlated with CDKN2A.

4. Discussion

Although cuproptosis was formally put forward as a newly defined programmed cell death [24], the role of copper in body cells has long been mentioned in studies by many scholars. Copper can induce various forms of cell death through various mechanisms, including apoptosis and autophagy [33] and can play a role of interfering with the progression of tumors and improving the therapeutic effect in tumors [20, 21, 34–36]. Studies have showed that tumor cells have a higher demand for copper than normal cells [37]. This phenomenon has been confirmed at the sites of many tumors, including breast cancer [38, 39], lung cancer [40], gastrointestinal tumors [41, 42], and oral cancer [43, 44]. Copper can affect the vascular endothelial growth factor [45, 46], fibroblast growth factor [47], and tumor necrosis factor [48] and also promote angiogenesis, which is conducive to the occurrence, development, and metastasis of

tumors. However, when the concentration of copper at the tumor site is abnormal, copper can regulate autophagy through ULK1 and ULK2 [49], and control protein quality through UBE2D2, which in turn affects the growth and progression of the tumor [49–51].

Therefore, in this study, bioinformatic methods were used to explore the potential role of copper and its CRGs in HCC from the perspective of cuproptosis. The expression of CRGs in HCC was determined, and 15 target genes with the significant correlation were obtained by screening. The expression levels of all LncRNAs in HCC samples were extracted, and 336 LncRNAs related to these CRGs were found through coexpression analysis. Univariate Cox regression, LASSO regression analyses, and multivariate Cox regression analysis were used to further screen out the LncRNAs (AC026412.3, AL031985.3, DDX11-AS1, AC021188.1, LINC00702, and LINC00426) with the signature expression. A prognostic model consisting of these signature LncRNAs was further constructed.

In order to verify the applicability and accuracy of this prognostic model, the sample patients were divided into high- and low-risk groups according to the risk score. By evaluating
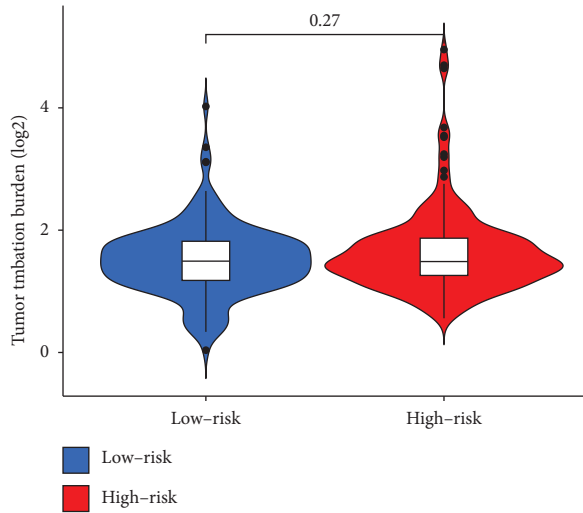
(a)
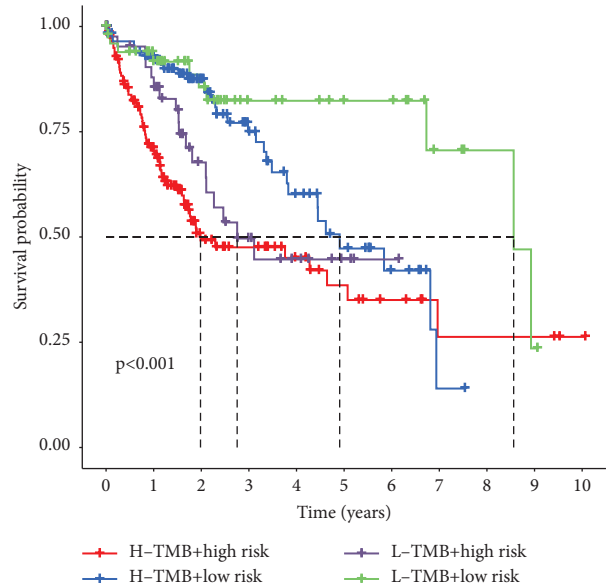
(b)
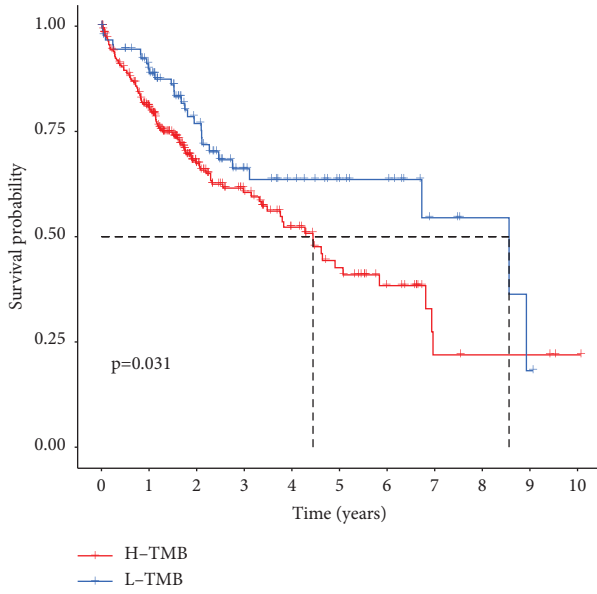
(c)
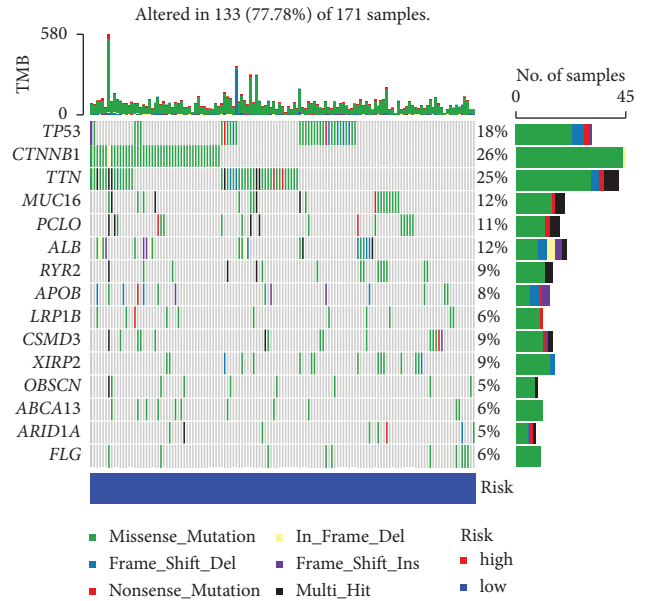
(d)

Figure 10: Continued.
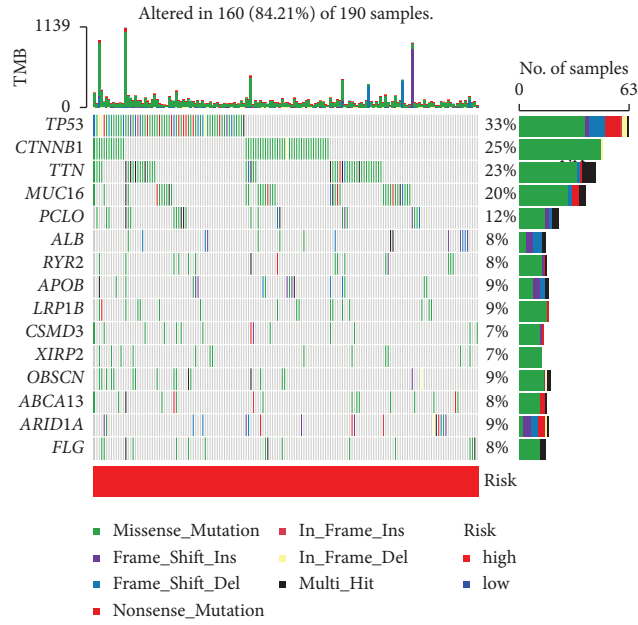
(e)

FIGURE 10: The group diagram of analysis of immune-related functions and mutated genes. (a) The violin diagram of mutation burden comparison in the high- and low-risk groups of hepatocellular carcinoma (HCC) patients; (b) the Kaplan–Meier curve for survival analysis of high and low mutation burden groups; (c) the Kaplan–Meier curve for survival analysis of high and low mutation burden groups combined with high- and low-risk groups; (d, e) the waterfall diagram of the mutation frequency of HCC tumors in both low- and high-risk groups, which shows the 15 genes with the highest mutation frequency in HCC patients, with different colors representing the mutation method of this gene.
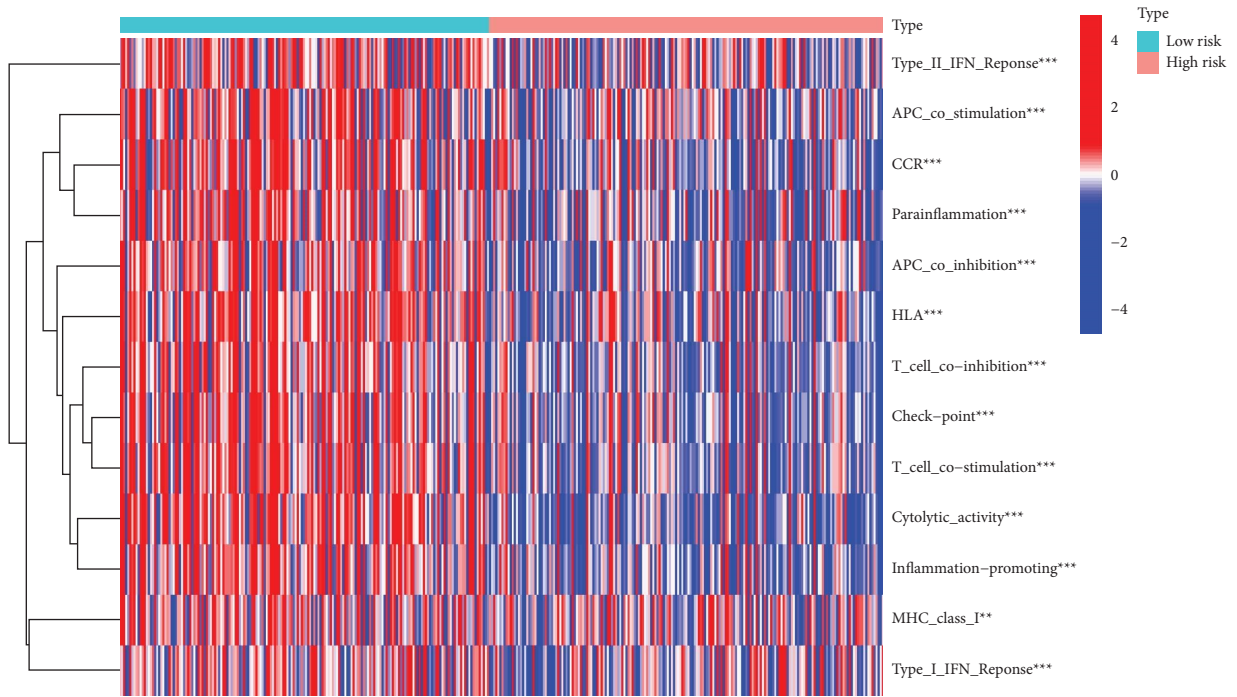
(a)

FIGURE 11: Continued.

(b)
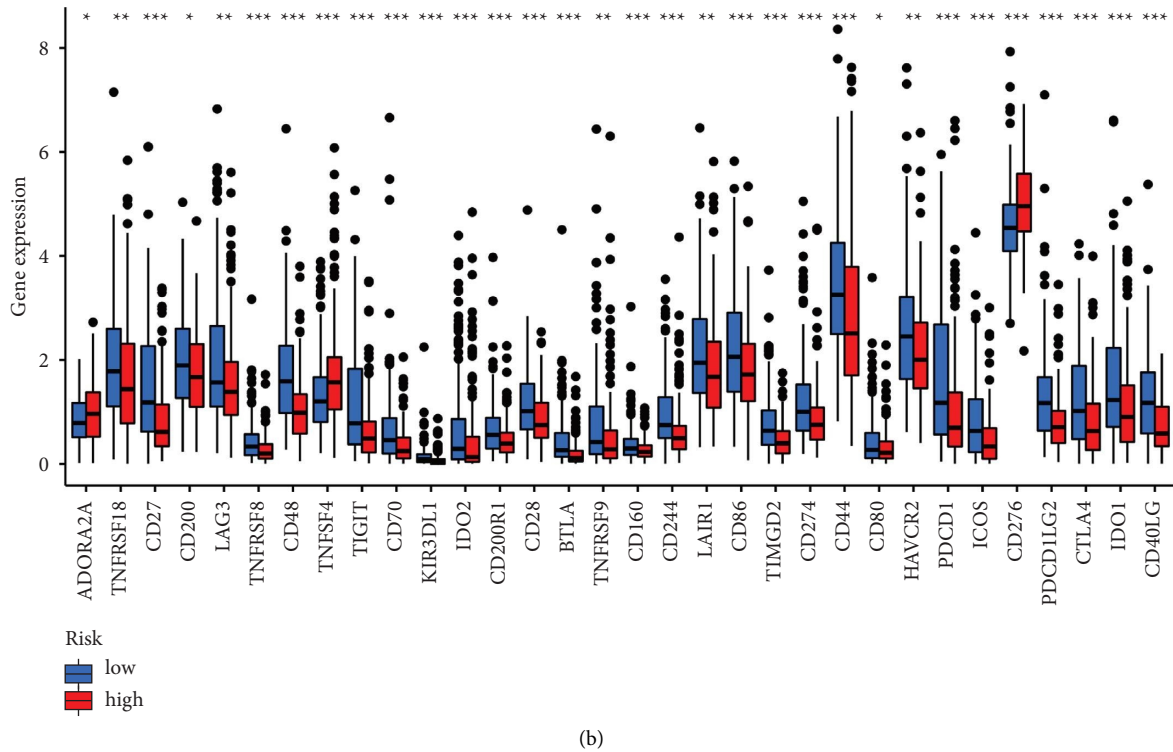
FIGURE 11: The group diagram of analysis of the immune-related function and immune checkpoint gene. (a) The expression heat map of 13 immune-related gene sets in high- and low-risk groups and (b) the box plot of differential analysis of immune checkpoint genes in patients of high- and low-risk groups.
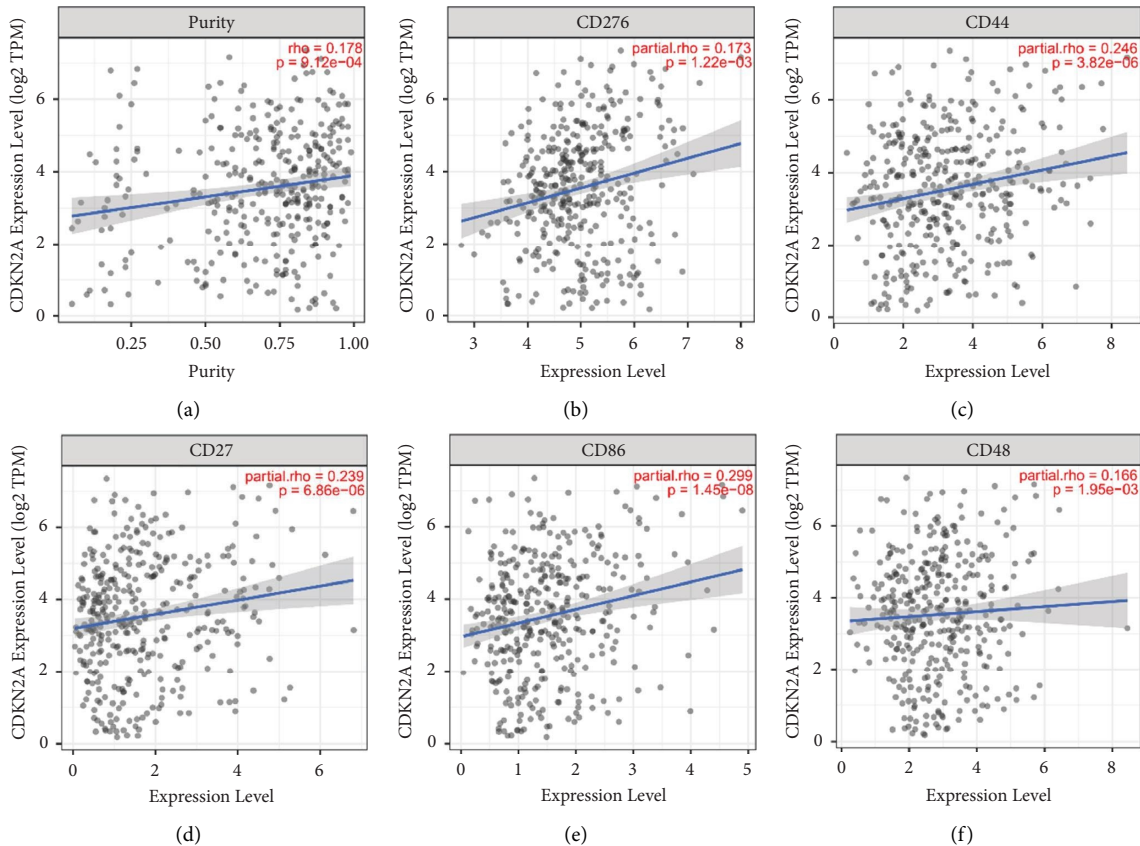
FIGURE 12: Continued.

(g) (h) (i)
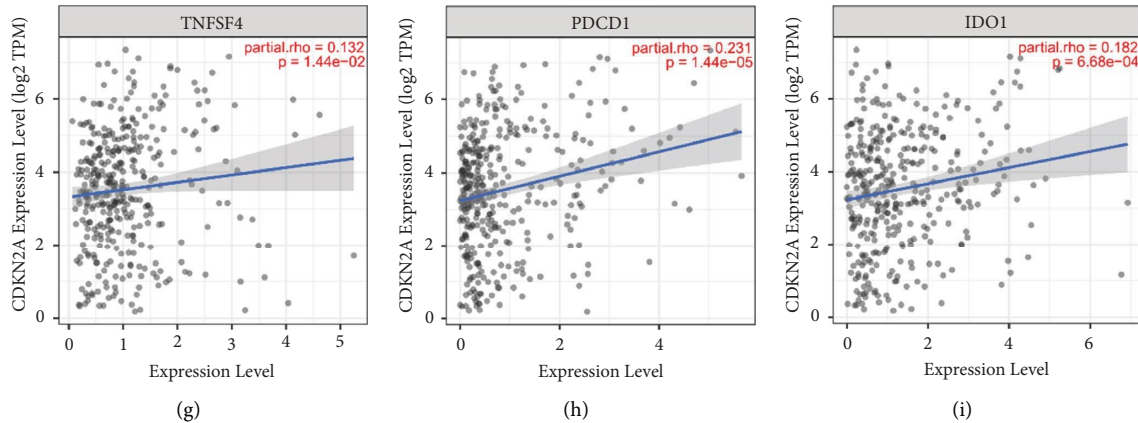
FIGURE 12: The scatter plot of correlation between the key cuproptosis gene CDKN2A and immune checkpoint genes with significant expression differences.

the survival status of patients in the high and low risk groups divided by the model, we can verify the clinical predictive ability of the model and compare the differences in immune function and tumor mutations between the two groups of patients. In the analysis of survival results of the high-risk group and the low-risk group, OS shows that the low-risk group performs better in the early years, and we think that this result is related to the insufficient sample size. HCC, as a malignant tumor with high mortality, is often found to be advanced, and because of the difficulty in treatment, the prognosis of patients is often unsatisfactory. It is found that the average life span of patients with HCC after diagnosis is only 4.9 years [52]. In order to verify the value of the prognostic model in survival, we supplemented PFS analysis. It was confirmed that this model with a good predicative ability can not only accurately predict the survival status of HCC patients, but also is more sensitive in the prediction of early HCC patients. Liu et al. have also paid attention to the significance of cuproptosis-related genes in the prognosis of liver cancer in their research, and their research samples are the same as ours. However, their research pays more attention to the analysis of cuproptosis-related immune functions, hypoxia-related genes, and tumor mutation load and drug sensitivity. Nevertheless, their research results are consistent with ours, which can prove the reliability of our conclusion to a certain extent [28].

During the analysis, it was found that the expression of the cuproptosis gene CDKN2A was the most significant in HCC and that it was closely and positively correlated with LncRNA DDX11-AS1. Studies have showed that CDKN2A is significantly expressed in multiple cancer tissues, thus affecting the prognosis of a variety of cancers. CDKN2A is negatively correlated with serosal invasion in the cervical cancer tissue [53]. Also, it can promote the angiogenic phenotype of esophageal squamous cell carcinoma and predict a poor prognosis [54]. Luo et al. reported that there is a certain correlation between the CDKN2A expression as well as immune invasion and the risk of HCC occurrence and that the

high expression of CDKN2A is negatively correlated with the overall survival rate and prognosis of patients [55], which may be related to the participation of CDKN2A in the MAPK signaling pathway and the diversity of liver cancer [56]. Additionally, Luo et al. believed that the expression of CDKN2A may help to regulate tumor-related macrophages, dendritic cells, and T cells and that CDKN2A may play an important role in immune infiltrating cells and also can be used as one of the prognostic biomarkers of HCC patients [55].

DDX11-AS1 is a newly discovered LncRNA, which is abnormally highly expressed in multiple malignant tumors [57], such as HCC, colorectal cancer, and gastric cancer. DDX11-AS1 plays its carcinogenic role by regulating the expression of related genes directly or indirectly, with the following examples given: DDX11-AS1 can bind to HNRNPC to promote the proliferation and migration of glioma cells [58] and silencing DDX11-AS1 can inhibit the growth of HCC cells by upregulating TRAF5 [59]. These results have suggested that DDX11-AS1 may play a significant regulatory role in tumors. So far, there has been no research on the relationship between CDKN2A and DDX11-AS1. We boldly inferred that there may be a positive regulatory relationship between CDKN2A and DDX11-AS1, and that silencing DDX11-AS1 can indirectly inhibit the CDKN2A expression, thereby increasing the role of copper loading in tumor cells, promoting cuproptosis, and increasing tumor cell apoptosis. However, more in-depth research and practices are still required for proving whether the fact is as we speculated.

In conclusion, a cuproptosis-related LncRNA model was constructed, which can be used for the prediction of HCC prognosis. However, there are also some limitations of this study. First, due to the currently incomplete understanding of cuproptosis, in this study, there was no guarantee that all landmark components were only related to cuproptosis, and the specific role of cuproptosis in HCC could not be independently assessed. Additionally, the prognostic ability of cuproptosis-related LncRNA in HCC was made statistically and analyzed

only through the samples in the database, but it still needs the support of massive clinical data and the verification of basic research. Nevertheless, we believe that this study may provide more ideas for improving the prognosis prediction of HCC patients.

Data Availability

The public data on HCC came from The Cancer Genome Atlas (TCGA) database, and data are available upon request to the authors.

Disclosure

Li is a master graduate student of Shandong University of Traditional Chinese Medicine, Grade 2021; Kaichao Song is a doctoral graduate student of Chinese Academy of Medical Sciences & Peking Union Medical College, Grade 2020; Wensheng Zheng is a doctor, professor.

Conflicts of Interest

The authors declare that they have no conflicts of interest regarding the publication of this article.

Authors' Contributions

All authors contributed toward data analysis, drafting, and revising the article and agreed to be accountable for all aspects of the work. Ying Li and Kaichao Song have equal contribution to this article.

Acknowledgments

Supplementary Materials

Table S1. Table of 15 CRGs and their cuproptosis death-related LncRNAs. *Table S2*. Table of KEGG pathway enrichment analysis of risk differential genes. (*Supplementary Materials*)

References

[1] F. Sun, Y. Liu, T. Gong et al., "Inhibition of DTYMK significantly restrains the growth of HCC and increases sensitivity to oxaliplatin," *Cell Death & Disease*, vol. 12, p. 1093, 2021.

[2] M. Wang, M. Wu, and T. Yang, "The synergistic effect of sorafenib and TNF-alpha inhibitor on hepatocellular carcinoma," *EBioMedicine*, vol. 40, pp. 11-12, 2019.

[3] J. A. Silva-Gomez, M. Galicia-Moreno, A. Sandoval-Rodriguez et al., "Hepatocarcinogenesis prevention by pirfenidone is PPARγ mediated and involves modification of nuclear NF-kB p65/p50 ratio," *International Journal of Molecular Sciences*, vol. 22, no. 21, p. 11360, 2021.

[4] Y. Lu, Y. T. Chan, H. Y. Tan et al., "Epigenetic regulation of ferroptosis via ETS1/miR-23a-3p/ACSL4 axis mediates sorafenib resistance in human hepatocellular carcinoma," *Journal of Experimental & Clinical Cancer Research*, vol. 41, no. 1, p. 3, 2022.

[5] X. Ren, X. Wang, Y. Yan et al., "Integrative bioinformatics and experimental analysis revealed TEAD as novel prognostic target for hepatocellular carcinoma and its roles in ferroptosis regulation," *Aging (Albany NY)*, vol. 14, no. 2, pp. 961–974, 2022.

[6] Z. Liu, J. Li, J. Li et al., "Mannan-modified Ad5-PTEN treatment combined with docetaxel improves the therapeutic effect in H22 tumor-bearing mice," *International Journal of Nanomedicine*, vol. 7, pp. 5039–5049, 2012.

[7] M. Guardascione and G. Toffoli, "Immune checkpoint inhibitors as monotherapy or within a combinatorial strategy in advanced hepatocellular carcinoma," *International Journal of Molecular Sciences*, vol. 21, no. 17, p. 6302, 2020.

[8] J. Zeng, X. Huang, L. Zhou et al., "Metabolomics identifies biomarker pattern for early diagnosis of hepatocellular carcinoma: from diethylnitrosamine treated rats to patients," *Scientific Reports*, vol. 5, no. 1, Article ID 16101, 2015.

[9] C. J. Wu, Y. T. Tsai, I. J. Lee et al., "Combination of radiation and interleukin 12 eradicates large orthotopic hepatocellular carcinoma through immunomodulation of tumor microenvironment," *OncoImmunology*, vol. 7, no. 9, Article ID e1477459, 2018.

[10] J. Liu, Z. Liu, W. Wang, and Y. Tian, "Real-time tracking and sensing of Cu(+) and Cu(2+) with a single SERS probe in the live brain: toward understanding why copper ions were increased upon ischemia," *Angewandte Chemie International Edition*, vol. 60, no. 39, pp. 21351–21359, 2021.

[11] N. Kitada, K. Takara, T. Minegaki et al., "Factors affecting sensitivity to antitumor platinum derivatives of human colorectal tumor cell lines," *Cancer Chemotherapy and Pharmacology*, vol. 62, no. 4, pp. 577–584, 2008.

[12] S. Pantoom, A. Pomorski, K. Huth et al., "Direct interaction of ATP7B and LC3B proteins suggests a cooperative role of copper transportation and autophagy," *Cells*, vol. 10, no. 11, p. 3118, 2021.

[13] Z. Tumer and L. B. Moller, "Menkes disease," *European Journal of Human Genetics*, vol. 18, no. 5, pp. 511–518, 2010.

[14] L. M. Guthrie, S. Soma, S. Yuan et al., "Elesclomol alleviates Menkes pathology and mortality by escorting Cu to cuproenzymes in mice," *Science*, vol. 368, no. 6491, pp. 620–625, 2020.

[15] Y. Wang, K. Hou, Y. Jin et al., "Lung adenocarcinoma-specificthree-integrin signature contributes to poor outcomes by metastasis and immune escape pathways," *Journal of Translational Internal Medicine*, vol. 9, no. 4, pp. 249–263, 2021.

[16] A. Pal, "Copper toxicity induced hepatocerebral and neurodegenerative diseases: an urgent need for prognostic biomarkers," *Neurotoxicology*, vol. 40, pp. 97–101, 2014.

[17] A. Pal, I. Rani, A. Pawar, M. Picozza, M. Rongioletti, and R. Squitti, "Microglia and astrocytes in alzheimer's disease in the context of the aberrant copper homeostasis hypothesis," *Biomolecules*, vol. 11, p. 1598, 2021.

[18] J. M. Hu Frisk, L. Kjellen, S. G. Kaler, G. Pejler, and H. Ohrvik, "Copper regulates maturation and expression of an MITF: tryptase Axis in mast cells," *The Journal of Immunology*, vol. 199, no. 12, pp. 4132–4141, 2017.

[19] L. Xin, X. Yang, G. Cai et al., "Serum levels of copper and zinc in patients with rheumatoid arthritis: a meta-analysis," *Biological Trace Element Research*, vol. 168, pp. 1–10, 2015.

[20] M. Yang, X. Wu, J. Hu et al., "COMMD10 inhibits HIF1α/CP loop to enhance ferroptosis and radiosensitivity by disrupting

Cu-Fe balance in hepatocellular carcinoma," *Journal of Hepatology*, vol. 76, no. 5, pp. 1138–1150, 2022.

[21] X. Ren, Y. Li, Y. Zhou et al., "Overcoming the compensatory elevation of NRF2 renders hepatocellular carcinoma cells more vulnerable to disulfiram/copper-induced ferroptosis," *Redox Biology*, vol. 46, Article ID 102122, 2021.

[22] D. Tang, X. Chen, and G. Kroemer, "Cuproptosis: a copper-triggered modality of mitochondrial cell death," *Cell Research*, vol. 32, no. 5, pp. 417-418, 2022.

[23] P. Tsvetkov, S. Coy, B. Petrova et al., "Copper induces cell death by targeting lipoylated TCA cycle proteins," *Science*, vol. 375, no. 6586, pp. 1254–1261, 2022.

[24] M. A. Kahlson and S. J. Dixon, "Copper-induced cell death," *Science*, vol. 375, no. 6586, pp. 1231-1232, 2022.

[25] S. Zhang, N. Zheng, X. Chen, K. Du, J. Yang, and L. Shen, "Establishment and validation of a ferroptosis-related long non-coding RNA signature for predicting the prognosis of stomach adenocarcinoma," *Frontiers in Genetics*, vol. 13, Article ID 818306, 2022.

[26] G. Qu, D. Wang, W. Xu, and W. Guo, "Comprehensive analysis of the correlation between pyroptosis-related LncRNAs and tumor microenvironment, prognosis, and immune infiltration in hepatocellular carcinoma," *Frontiers in Genetics*, vol. 13, Article ID 867627, 2022.

[27] S. Zhu, X. Huang, K. Zhang et al., "Low expression of long noncoding RNA CTC-297N7.9 predicts poor prognosis in patients with hepatocellular carcinoma," *Cancer Medicine*, vol. 8, no. 18, pp. 7679–7692, 2019.

[28] Y. Liu, Y. Liu, S. Ye, H. Feng, and L. Ma, "Development and validation of cuproptosis-related gene signature in the prognostic prediction of liver cancer," *Frontiers in Oncology*, vol. 12, Article ID 985484, 2022.

[29] M. Abbastabar, M. Sarfi, A. Golestani, and E. Khalili, "lncRNA involvement in hepatocellular carcinoma metastasis and prognosis," *EXCLI journal*, vol. 17, pp. 900–913, 2018.

[30] A. A. Mohamed, A. A. A. Omar, R. R. El-Awady et al., "MiR-155 and MiR-665 role as potential non-invasive biomarkers for hepatocellular carcinoma in Egyptian patients with chronic hepatitis C virus infection," *Journal of Translational Internal Medicine*, vol. 8, no. 1, pp. 32–40, 2020.

[31] A. A. Tasneem and N. H. Luck, "Autoimmune hepatitis: clinical characteristics and predictors of biochemical response to treatment," *Journal of Translational Internal Medicine*, vol. 8, no. 2, pp. 106–111, 2020.

[32] J. Xu, J. Zhang, and J. Wang, "The application of traditional Chinese medicine against the tumor immune escape," *Journal of Translational Internal Medicine*, vol. 8, no. 4, pp. 203-204, 2020.

[33] Y. Jiang, Z. Huo, X. Qi, T. Zuo, and Z. Wu, "Copper-induced tumor cell death mechanisms and antitumor theragnostic applications of copper complexes," *Nanomedicine (Lond)*, vol. 17, no. 5, pp. 303–324, 2022.

[34] C. Jin, Y. Li, Y. Su et al., "Novel copper complex CTB regulates methionine cycle induced TERT hypomethylation to promote HCC cells senescence via mitochondrial SLC25A26," *Cell Death & Disease*, vol. 11, no. 10, p. 844, 2020.

[35] L. Cui, A. M. Gouw, E. L. LaGory et al., "Mitochondrial copper depletion suppresses triple-negative breast cancer in mice," *Nature Biotechnology*, vol. 39, no. 3, pp. 357–367, 2021.

[36] F. Voli, E. Valli, L. Lerra et al., "Intratumoral copper modulates PD-L1 expression and influences tumor immune evasion," *Cancer Research*, vol. 80, no. 19, pp. 4129–4144, 2020.

[37] E. J. Ge, A. I. Bush, A. Casini et al., "Connecting copper and cancer: from transition metal signalling to metalloplasia," *Nature Reviews Cancer*, vol. 22, no. 2, pp. 102–113, 2022.

[38] Y. Feng, J. W. Zeng, Q. Ma, S. Zhang, J. Tang, and J. F. Feng, "Serum copper and zinc levels in breast cancer: a meta-analysis," *Journal of Trace Elements in Medicine & Biology*, vol. 62, Article ID 126629, 2020.

[39] D. Ramchandani, M. Berisa, D. A. Tavarez et al., "Copper depletion modulates mitochondrial oxidative phosphorylation to impair triple negative breast cancer metastasis," *Nature Communications*, vol. 12, no. 1, p. 7311, 2021.

[40] K. Zablocka-Slowinska, A. Prescha, S. Placzkowska, I. Porebska, M. Kosacka, and K. Pawelczyk, "Serum and whole blood Cu and Zn status in predicting mortality in lung cancer patients," *Nutrients*, vol. 13, no. 1, p. 60, 2020.

[41] W. Gao, Z. Huang, J. Duan, E. C. Nice, J. Lin, and C. Huang, "Elesclomol induces copper-dependent ferroptosis in colorectal cancer cells via degradation of ATP7A," *Molecular Oncology*, vol. 15, no. 12, pp. 3527–3544, 2021.

[42] Y. Liao, J. Zhao, K. Bulek et al., "Inflammation mobilizes copper metabolism to promote colon tumorigenesis via an IL-17-STEAP4-XIAP axis," *Nature Communications*, vol. 11, no. 1, p. 900, 2020.

[43] F. Chen, J. Wang, J. Chen et al., "Serum copper and zinc levels and the risk of oral cancer: a new insight based on large-scalecase-control study," *Oral Diseases*, vol. 25, no. 1, pp. 80–86, 2019.

[44] H. Mortazavi, S. Sabour, M. Baharvand, S. Manifar, and R. Akkafan, "Serum levels of ferritin, copper, and zinc in patients with oral cancer," *Biomedical Journal*, vol. 37, no. 5, pp. 331–336, 2014.

[45] I. Naletova, V. Greco, S. Sciuto, F. Attanasio, and E. Rizzarelli, "Ionophore ability of carnosine and its trehalose conjugate assists copper signal in triggering brain-derived neurotrophic factor and vascular endothelial growth factor activation in vitro," *International Journal of Molecular Sciences*, vol. 22, no. 24, p. 13504, 2021.

[46] C. K. Sen, S. Khanna, M. Venojarvi et al., "Copper-induced vascular endothelial growth factor expression and wound healing," *American Journal of Physiology - Heart and Circulatory Physiology*, vol. 282, no. 5, pp. H1821–H1827, 2002.

[47] M. Landriscina, C. Bagala, A. Mandinova et al., "Copper induces the assembly of a multiprotein aggregate implicated in the release of fibroblast growth factor 1 in response to stress," *Journal of Biological Chemistry*, vol. 276, no. 27, pp. 25549–25557, 2001.

[48] L. Qiu, L. Ding, J. Huang, D. Wang, J. Zhang, and B. Guo, "Induction of copper/zinc-superoxide dismutase by CCL5/CCR5 activation causes tumour necrosis factor-alpha and reactive oxygen species production in macrophages," *Immunology*, vol. 128, no. 1, pp. e325–e334, 2009.

[49] T. Tsang, J. M. Posimo, A. A. Gudiel, M. Cicchini, D. M. Feldser, and D. C. Brady, "Copper is an essential regulator of the autophagic kinases ULK1/2 to drive lung adenocarcinoma," *Nature Cell Biology*, vol. 22, no. 4, pp. 412–424, 2020.

[50] J. Tong, J. Lu, X. Mao et al., "Circular RNA-UBE2D2 accelerates the proliferation and metastasis of non-small cell lung cancer cells via modulating microRNA-376a-3p/Eukaryotic Translation Initiation Factor 4γ2 axis," *Bioengineered*, vol. 13, no. 3, pp. 5942–5953, 2022.

[51] C. M. Opazo, A. Lotan, Z. Xiao et al., "Nutrient copper signaling promotes protein turnover by allosteric activation of ubiquitin E2D conjugases," *bioRxiv*, Article ID 431211, 2021.

[52] A. Cucchetti, F. Trevisani, L. Bucci et al., "Years of life that could be saved from prevention of hepatocellular carcinoma," *Alimentary Pharmacology & Therapeutics*, vol. 43, no. 7, pp. 814–824, 2016.

[53] H. Y. Han, J. T. Mou, W. P. Jiang, X. M. Zhai, and K. Deng, "Five candidate biomarkers associated with the diagnosis and prognosis of cervical cancer," *Bioscience Reports*, vol. 41, no. 3, 2021.

[54] N. Zhang, J. Shi, X. Shi, W. Chen, and J. Liu, "Mutational characterization and potential prognostic biomarkers of Chinese patients with esophageal squamous cell carcinoma," *OncoTargets and Therapy*, vol. 13, pp. 12797–12809, 2020.

[55] J. P. Luo, J. Wang, and J. H. Huang, "CDKN2A is a prognostic biomarker and correlated with immune infiltrates in hepatocellular carcinoma," *Bioscience Reports*, vol. 41, no. 10, 2021.

[56] Z. Liu, Q. Zhou, Z. Wang et al., "Intratumoral TIGIT(+) CD8(+) T-cell infiltration determines poor prognosis and immune evasion in patients with muscle-invasive bladder cancer," *J Immunother Cancer*, vol. 8, no. 2, Article ID e000978, 2020.

[57] Y. Feng, M. Wu, S. Hu, X. Peng, and F. Chen, "LncRNA DDX11-AS1: a novel oncogene in human cancer," *Human Cell*, vol. 33, no. 4, pp. 946–953, 2020.

[58] Z. Xiang, Q. Lv, Y. Zhang et al., "Long non-coding RNA DDX11-AS1 promotes the proliferation and migration of glioma cells by combining with HNRNPC," *Molecular Therapy - Nucleic Acids*, vol. 28, pp. 601–612, 2022.

[59] G. Ding, Y. Zeng, D. Yang et al., "Silenced lncRNA DDX11-AS1 or up-regulated microRNA-34a-3p inhibits malignant phenotypes of hepatocellular carcinoma cells via suppression of TRAF5," *Cancer Cell International*, vol. 21, no. 1, p. 179, 2021.

Hindawi

Research Article

A Prognostic Cuproptosis-Related LncRNA Signature for Colon Adenocarcinoma

Like Zhong [ID],[1,2] **Junfeng Zhu** [ID],[1,2] **Qi Shu,**[1] **Gaoqi Xu,**[1] **Chaoneng He,**[1] **and Luo Fang** [ID][1,2]

[1]*The Department of Pharmacy, Zhejiang Cancer Hospital, Hangzhou, China*
[2]*Key Laboratory of Prevention, Diagnosis and Therapy of Upper Gastrointestinal Cancer of Zhejiang Province, Hangzhou, China*

Correspondence should be addressed to Luo Fang; fangluo@zjcc.org.cn

Background. Cuproptosis, a recently discovered form of cell death, is caused by copper levels exceeding homeostasis thresholds. Although Cu has a potential role in colon adenocarcinoma (COAD), its role in the development of COAD remains unclear. *Methods.* In this study, 426 patients with COAD were extracted from the Cancer Genome Atlas (TCGA) database. The Pearson correlation algorithm was used to identify cuproptosis-related lncRNAs. Using the univariate Cox regression analysis, the least absolute shrinkage and selection operator (LASSO) was used to select cuproptosis-related lncRNAs associated with COAD overall survival (OS). A risk model was established based on the multivariate Cox regression analysis. A nomogram model was used to evaluate the prognostic signature based on the risk model. Finally, mutational burden and sensitivity analyses of chemotherapy drugs were performed for COAD patients in the low- and high-risk groups. *Result.* Ten cuproptosis-related lncRNAs were identified and a novel risk model was constructed. A signature based on ten cuproptosis-related lncRNAs was an independent prognostic predictor for COAD. Mutational burden analysis suggested that patients with high-risk scores had higher mutation frequency and shorter survival. *Conclusion.* Constructing a risk model based on the ten cuproptosis-related lncRNAs could accurately predict the prognosis of COAD patients, providing a fresh perspective for future research on COAD.

1. Introduction

Colonic adenocarcinoma (COAD) is the most common histological subtype of colorectal cancer and is one of the leading causes of cancer mortality [1]. With the development of substantive treatment strategies, including surgery, neoadjuvant therapy, and targeted therapy, the overall prognosis for patients with COAD has significantly improved [2]. At the same time, the importance of early diagnosis of COAD for prognosis is being increasingly recognized. The 5-year survival rate of patients with early diagnosis is approximately 90%, but only 10% for patients diagnosed with advanced metastatic disease [1]. Identifying novel biomarkers for tumor diagnosis and prognosis has been shown to benefit the treatment of diverse tumor types [3–6]. Therefore, there is still an urgent need to identify novel prognostic biomarkers associated with metastasis to facilitate the timely diagnosis

and earlier application of appropriate, individualized therapy.

Long noncoding RNAs (lncRNAs) are transcripts over 200 nucleotides in length with no significant protein-coding function [7]. By modulating gene expression, lncRNAs have been reported to play important roles in many physiological processes and disease progression [8]. In COAD, a variety of lncRNAs have been reported to be highly expressed and have been associated with multiple tumor-related biological processes, including proliferation, chemical resistance, and epithelial-mesenchymal transformation [9–12]. These lncRNAs have been associated with the activation of multiple signaling pathways, including WNT, PI3K/Akt, and PPAR [13]. Considering the roles of these pathways in the occurrence and development of COAD [14, 15], lncRNAs are likely to be significant factors in tailoring individualized therapies. Several studies have identified lncRNAs as potential therapeutic targets [16–18]. Overexpression of

LINC00152 has been shown to promote the expression of fascin actin-binding protein 1 (FSCN1) by binding mir-632 and mir-185-3p, leading to proliferation and metastasis [19]. As reviewed in 2022, lncRNAs including DCST1-AS1, LINC01569, KCNQ1OT1, and LINC00997 were considered to take an active part in carcinogenesis by influencing cell metastasis, drug resistance, radio-resistance, and tumor microenvironment interaction [20]. However, the role of lncRNAs in COAD has not been completely elucidated.

Cu levels are elevated in the serum and tissues of multiple solid tumors, including colorectal tumors [21]. However, its role is not fully understood. On one hand, in addition to acting as a cofactor for key metabolic enzymes, Cu also directly promotes tumor growth by acting as a cofactor for signaling molecules such as MEK1, which transduces carcinogenic BRAF signals to ERK1/2 [22], suggesting that it may have a key role in cancer progression. On the other hand, the ion carrier elesclomol mediates copper overload in colorectal cancer cells and induces copper-dependent cell death by degrading ATP7A [23].

This cell death pathway, caused by copper levels exceeding homeostasis thresholds, is called copper death or cuproptosis [24]. It relies on mitochondrial respiration [25]. Copper binds directly to the lipid components of the tricarboxylic acid (TCA) cycle, resulting in the accumulation of lipoacylated proteins, followed by the loss of iron-sulfur cluster proteins, resulting in proteotoxic stress and cell death [26]. Cuproptosis caused by copper overload has been shown to predict tumor prognosis and judge immune and drug responses in a variety of tumors, including head and neck squamous cell carcinoma, breast cancer, and cervical cancer [27–30]. However, there is no relevant report found in COAD. Therefore, the double-edged role of copper in colorectal cancer and its influence on prognosis need to be further analyzed and understood.

In this study, we examined cuproptosis-associated lncRNAs in the clinical context of COAD using the Cancer Genome Atlas (TCGA) database. We constructed a risk model to evaluate the prognostic ability of cuproptosis-associated lncRNAs in patients with COAD. The tumor mutational burden and sensitivity analysis of chemotherapy drugs were also assessed. Taken together, our findings provide new insights into potential therapeutic strategies for patients with COAD.

2. Materials and Methods

2.1. Data Collection.
Gene expression matrices and clinical information for patients with COAD were obtained from the Cancer Genome Atlas database (https://portal.gdc.cancer.gov/). We identified 426 such samples for inclusion. The gene expression matrices were merged using a Perl script for further analysis. Genes encoding lncRNAs and mRNAs were annotated and classified using the Human Genome Browser, GRCh38.p13 (https://asia.ensembl.org/index.html). Survival time, survival status, age, sex, stage, and TNM stage were extracted from the TCGA database using Perl scripts. All data and clinical information used in this study were obtained from a public database; therefore, neither approval

from the ethics committee nor written informed consent from patients was required.

2.2. Identification of Cuproptosis-Related lncRNAs.
Expression data for cuproptosis-related genes were obtained from a previous study [26]. Expression data were extracted using Perl scripts, and Pearson's correlation algorithm was used to identify cuproptosis-related lncRNAs. With the threshold setting at |correlation coefficient| > 0.4, Pvalue <0.001 ($r > 0.4$, $P < 0.001$), 870 lncRNAs were identified as cuproptosis-related lncRNAs for further analysis (Supplementary Table 1).

2.3. Prognostic Signature Construction.
Based on univariate Cox regression analysis, the least absolute shrinkage and selection operator (LASSO) algorithm was performed using the R package "glmnet." The multivariate Cox regression analysis was used to evaluate the lncRNA signature as an independent prognostic factor for patient survival. Risk scores for each patient were calculated using the following formula: risk scores $= \sum_{i=1}^{n} \text{Coef}(i) \times x(i)$, where Coef($i$) represents the correlation regression coefficient and $x(i)$ is the expression level of cuproptosis-related lncRNAs. Patients with COAD were divided into low- and high-risk groups based on median risk scores. Kaplan–Meier survival analysis was employed to assess the difference in OS rates in the low- and high-risk groups using the log-rank algorithm. A 3D principal component analysis (3D-PCA) was conducted to assess the difference in signatures between low- and high-risk patients using the R package "ggplot2."

2.4. Consensus Clustering Analysis.
According to the prognostic cuproptosis-related genes, consensus clustering was performed using the R package "ConsensusClusterPlus." The clustering was established on the grounds of partitioning around medoids with "Euclidean" distances, and 1,000 verifications were performed. Finally, with the optimal classification of $K = 2–9$, the patients with COAD were clustered into two subtypes for further analysis.

2.5. Risk Model Independence.
The univariate and multivariate Cox regression analyses were used to assess risk scores as independent prognostic factors for COAD. A subtype analysis was conducted to confirm the independence of the risk model. To further determine whether the risk score was independent of other clinical variables, including age, Gleason score, PSA value, and T stage, patients were regrouped into new subtypes based on different clinical characteristics. According to median risk scores, patients in each subtype were stratified into low- and high-risk groups.

2.6. Somatic Mutation Analysis.
Data from the COAD samples were obtained from TCGA in "maf" format using Perl scripts. A waterfall diagram was constructed using the "Maftools" package in the R software.

2.7. Drug Sensitivity Analysis. Based on the Genomics of Drug Sensitivity Genomics in Cancer (GDSC), the drug treatment response of each patient with COAD was predicted using the R package "pRRophetic." Differences in IC_{50} values between low- and high-risk groups were analyzed using the "ggplot2" R package.

2.8. Gene Set Enrichment Analysis (GSEA). For the low- and high-risk groups, 1,000 permutations were used and screened using the largest and smallest gene set filters of 500 and 15 genes, respectively. *P* values less than 0.05 were considered to be significantly different.

2.9. Statistical Analysis. All analyses were performed using the R software (version 3.6.0) and Perl scripts. The Wilcoxon rank sum test was applied to separately conduct group comparisons with *P* values less than 0.05, which was considered to be statistically significant.

3. Results and Discussion

3.1. Identification of Cuproptosis-Related lncRNAs. A total of 14,142 lncRNAs were collected from the TGCA COAD RNA-Seq matrix. To identify lncRNAs related to cuproptosis, correlations between the expression of cuproptosis genes and lncRNAs were calculated, yielding a total of 870 candidate lncRNAs. Using the univariate Cox regression analysis, 15 cuproptosis-related lncRNAs associated with OS were selected using the least absolute shrinkage and selection operator (LASSO) algorithm (Figure 1, Supplementary Table 2).

3.2. Risk Model Construction. From the multivariate Cox regression analysis, 10 cuproptosis-related lncRNAs were selected to construct a risk model. Risk scores for each patient were calculated using the following formula: risk scores = $(0.24 \times$ expression level of AL161729.4) + $(0.35 \times$ expression level of AC068580.3) + $(0.19 \times$ expression level of AL138756.1) + $(0.1 \times$ expression level of MIR210HG) + $(0.38 \times$ expression level of EIF3J-DT) + $(0.17 \times$ expression level of LINC02381) + $(0.42 \times$ expression level of AC010973.2) + $(-0.15 \times$ expression level of TNFRSF10A-AS1) + $(0.42 \times$ expression level of ZEB1-AS1) + $(0.31 \times$ expression level of AC073957.3). Using the median risk score, the COAD patients were divided into the following two groups: 213 patients in the low-risk group and 213 patients in the high-risk group. Patients were ranked according to the cuproptosis-related prognostic signature; the resulting scatter dot plot indicated that survival time was inversely correlated with risk score (Figures 2(a) and 2(b)). The Kaplan–Meier survival analysis showed that the OS of patients with high-risk scores was significantly shorter than that of those with low-risk scores ($P = 1.553E - 08$, Figure 2(c)). A 3D principal component analysis (3D-PCA) produced a clear separation between low- and high-risk groups based on the selected lncRNAs (Figure 2(d)). Of the ten prognostic cuproptosis-related lncRNAs,

AL161729.4, AC068580.3, AL138756.1, MIR210HG, EIF3J-DT, LINC02381, AC010973.2, ZEB1-AS1, and AC073957.3 were expressed at higher levels in the high-risk group, whereas TNFRSF10A-AS1 was expressed at higher levels in the low-risk group (Figure 2(e)). These results suggested that constructing a risk model based on the ten cuproptosis-related lncRNAs is prognostic for patients with COAD.

3.3. Training and Validation Cohorts. The COAD patients were randomly classified into training and validation cohorts. In both cohorts, patients were ranked by median risk score. A scatter dot plot showed that survival times of COAD patients in the training and validation cohorts were conversely associated with risk scores (Figures 3(a) and 3(b)). The survival of patients with low-risk scores was higher than that of patients with high-risk scores in both cohorts ($P < 0.001$, Figures 3(c) and 3(d)). These results demonstrated that our risk model is accurate and reliable.

3.4. Independent Prognostic Analyses. Univariate analysis indicated that age (hazard ratio (HR) = 1.028, $P = 0.009$), stage (HR = 2.415, $P < 0.001$), T stage (HR = 3.379, $P < 0.001$), M stage (HR = 4.854, $P < 0.001$), N stage (HR = 2.083, $P < 0.001$), and the risk score (HR = 1.167, $P < 0.001$) were associated with OS (Figure 4(a)). Multivariate analysis indicated that age (HR = 1.051, $P < 0.001$), T stage (HR = 1.849, $P = 0.031$), and risk score (HR = 1.181, $P < 0.001$) were significantly associated with OS in patients with COAD (Figure 4(b)). The AUC of the signature was 0.704 (Figure 4(c)). Taken together, these results indicate that prognostic signatures based on cuproptosis-related lncRNAs are independent prognostic factors in patients with COAD.

3.5. Correlations between lncRNA Risk Scores and Clinicopathological Characteristics. Patients were classified by sex, M stage (M 0 vs. M 1), N stage (N 0 vs. N 1-2), S stage (S 1-2 vs. S 3-4), T stage (T 1-2 vs. T 3-4), and age (≥65 vs. <65). Kaplan–Meier analysis showed that survival of patients with low-risk scores was higher than that of patients with high-risk scores, based on the prognostic signature among females ($P = 5.847e - 04$), males ($P = 1.28e - 03$), M 0 ($P = 2.879e - 04$), M 1($P = 9.833e - 03$), N 0 ($P = 8.82e - 04$), N 1-2 ($P = 5.014e - 04$), S 1-2 ($P = 6.347e - 04$), S 3-4 ($P = 1.833e - 04$), T 3-4 ($P = 1.668e - 06$), ≥65 ($P = 2.7e - 05$), and <65 ($P = 2.61e - 03$). However, the survival rate was similar between T-stage groups (Figure 5). These results indicate that the prognostic signature based on cuproptosis-related lncRNAs accurately predicts prognosis relative to clinicopathological characteristics.

3.6. Consensus Clustering Analysis for Cuproptosis-Related lncRNAs associated with COAD. Thereafter, consensus clustering analysis was utilized to cluster the patients with COAD into different subgroups, and the result revealed an optimal classification for consensus clustering with $K = 2$ (Figures 6(a)–6(c)). Based on the prognostic cuproptosis-related lncRNAs, the patients with COAD were successfully

(a)

(b)

(c)

FIGURE 1: Identification and analysis of cuproptosis-related lncRNAs: (a) univariate Cox regression for 15 cuproptosis-related lncRNAs associations with COAD OS. (b-c) LASSO regression model showing coefficients and minimal lambda values.

divided into two subgroups, with 323 patients in Cluster A and 103 patients in Cluster B. The principal component analysis result illustrated a clear separation between Cluster A and Cluster B according to the prognostic cuproptosis-related lncRNAs (Figure 6(d)). The Kaplan–Meier survival curve analysis suggested that the patients in Cluster A had a higher OS rate than those in Cluster B (Figure 6(e)). These results demonstrate that the cuproptosis-related lncRNAs are associated with the prognosis of COAD.

3.7. Nomogram Construction. A nomogram was constructed to confirm the accuracy of the prognostic signature and clinicopathological characteristics (Figure 7(a)). It yielded a consistency index (C-index) of 0.727. Calibration curves indicated that the nomogram-predicted 1, 3, and 5-year survival rates were consistent with actual survival times

(Figure 7(b)). Time-dependent ROC curves revealed that the AUCs of 1-, 3-, and 5-year were 0.704, 0.731, and 0.775, respectively, indicating satisfactory accuracy of the model (Figure 7(c)).

3.8. Tumor Mutational Burden (TMB) Analysis. TMB indices for high-risk and low-risk genes were calculated. As shown in Figure 8(a), patients with high TMB had lower survival rates than those with low TMB ($P = 0.025$). The mutation frequencies of high-risk genes were higher than those of low-risk genes. Survival of the high-TMB + high-risk panel was the lowest, followed by the low-TMB + high-risk, high-TMB + low-risk, and low-TMB + low-risk panels (Figure 8(b), $P < 0.001$). A waterfall diagram (Figure 8(c)) shows the top 30 mutation frequencies. In the low-risk group, mutations were detected in 194 out of 195 samples; APC (72%), TP53 (48%),

(a)

(b)

(c)

(d)
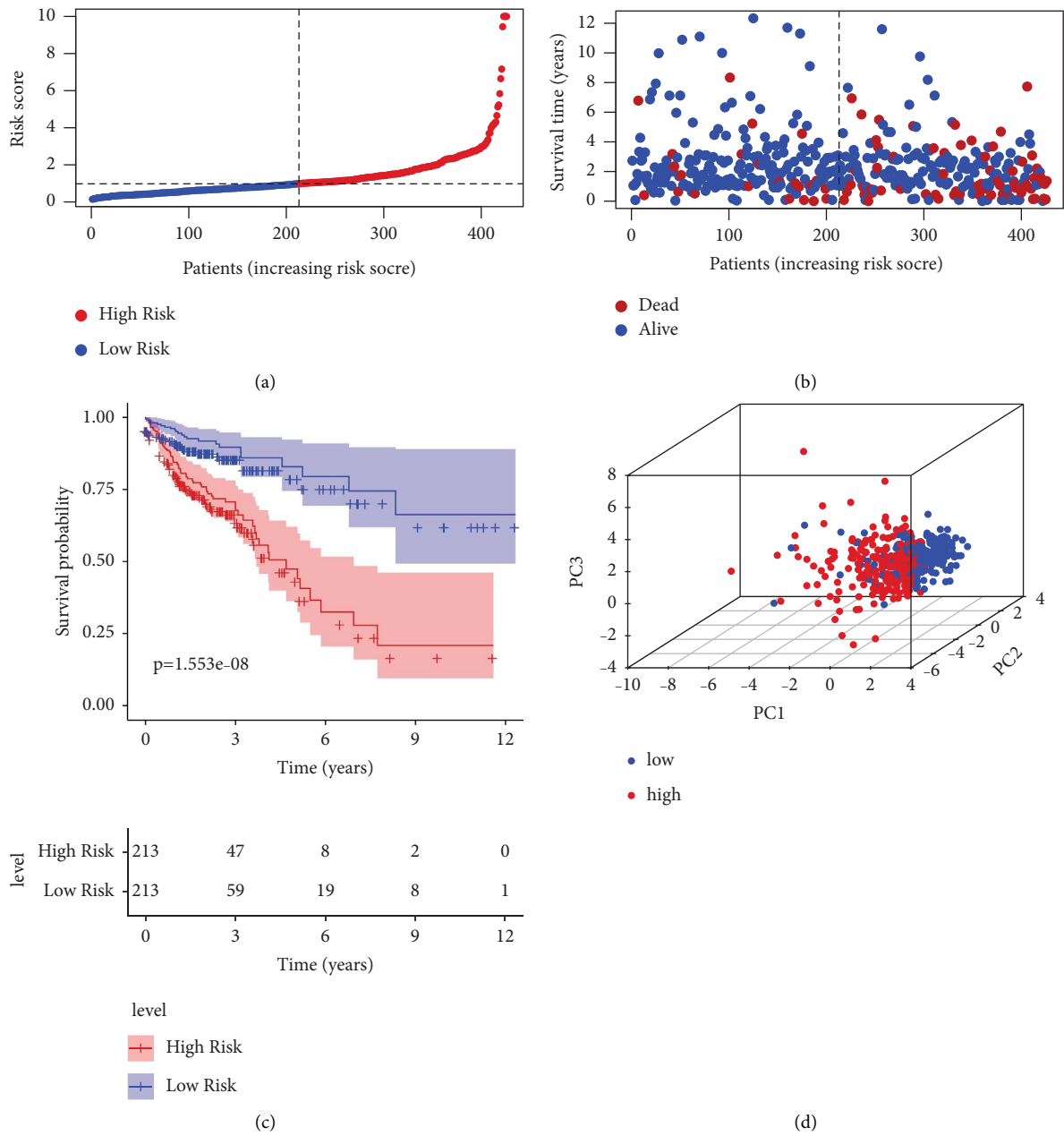
FIGURE 2: Continued.
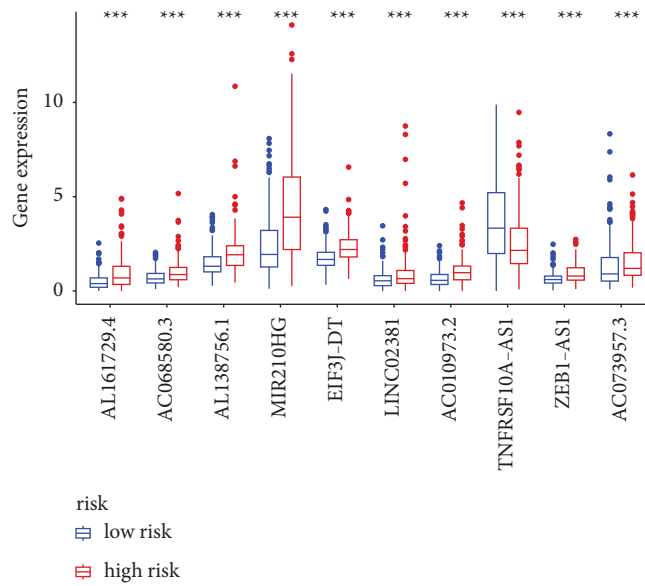
(e)

FIGURE 2: Risk model based on expression levels of ten cuproptosis-related lncRNAs: (a) distribution of risk scores; (b) scatter dot plot showing correlation of survival time and risk score; (c) Kaplan–Meier survival analysis; (d) principal component analysis (PCA) showing significant separation between low- and high-risk groups; (e) boxplot of expression levels of the ten selected lncRNAs.

FIGURE 3: Continued.

(c)
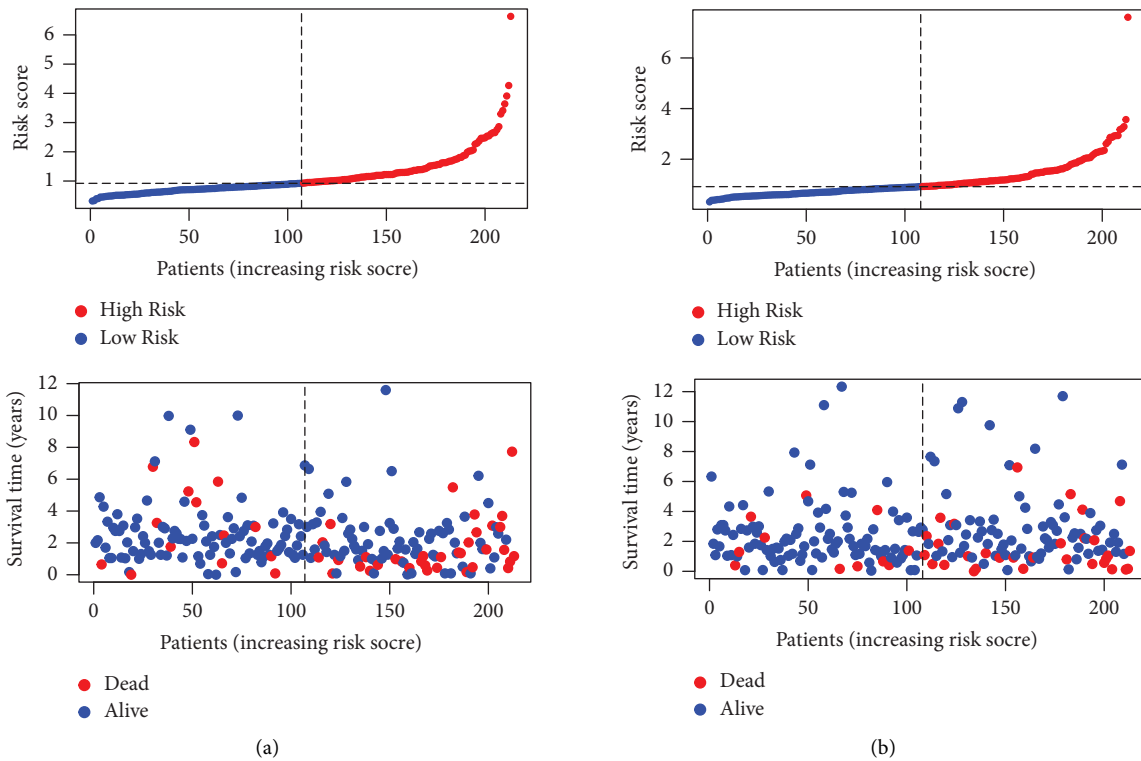
(d)
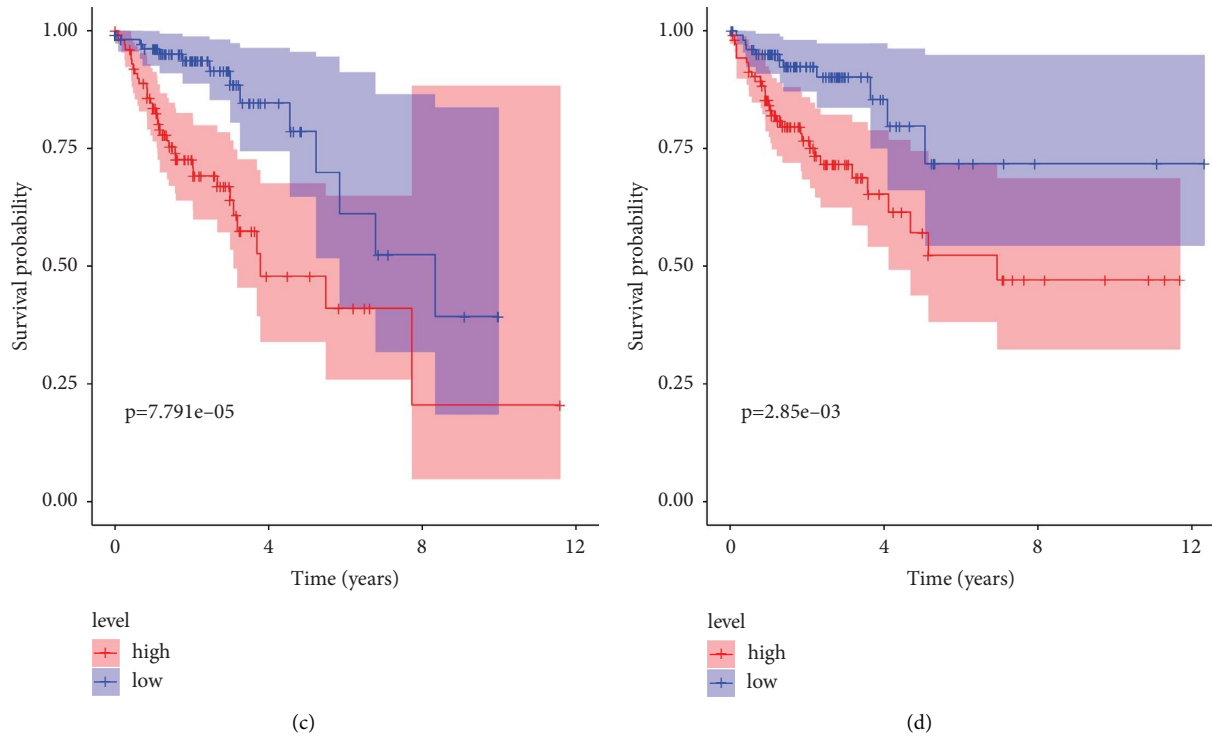
Figure 3: Testing of training and validation cohorts: (a-b) distribution of risk scores and scatter dot plots; (c-d) survival curves for training and validation cohorts.

	pvalue	Hazard ratio
Age	0.009	1.028 (1.007-1.049)
Gender	0.913	1.025 (0.654-1.607)
Stage	<0.001	2.415 (1.857-3.141)
T	<0.001	3.379 (2.148-5.318)
M	<0.001	4.854 (3.033-7.769)
N	<0.001	2.083 (1.595-2.721)
riskScore	<0.001	1.167 (1.119-1.217)

(a)

	pvalue	Hazard ratio
Age	<0.001	1.051 (1.028-1.074)
Gender	0.342	0.800 (0.505-1.267)
Stage	0.057	2.189 (0.977-4.901)
T	0.031	1.849 (1.057-3.234)
M	0.763	1.179 (0.403-3.448)
N	0.715	0.909 (0.544-1.519)
riskScore	<0.001	1.181 (1.114-1.252)

(b)

Figure 4: Continued.

(c)
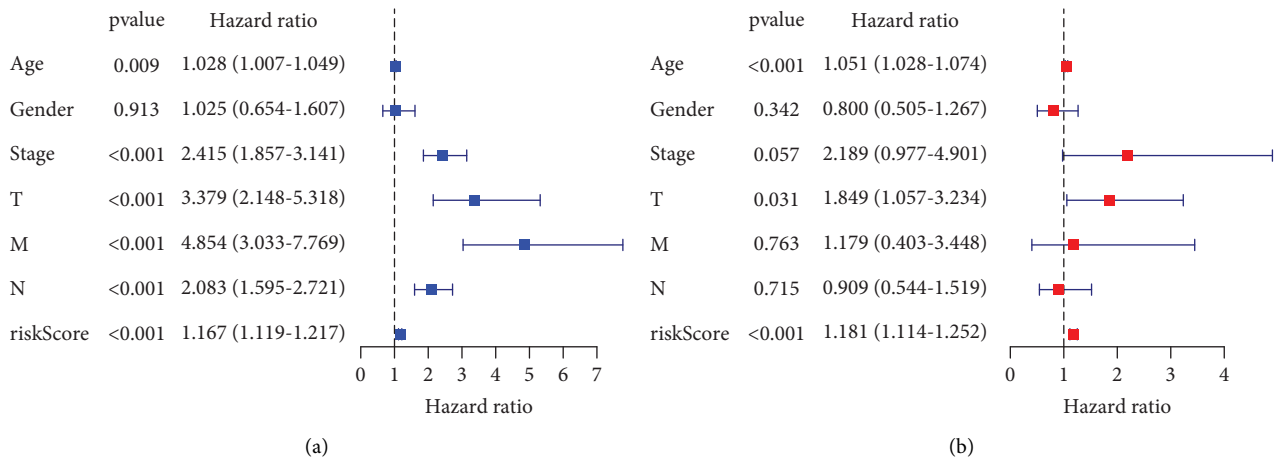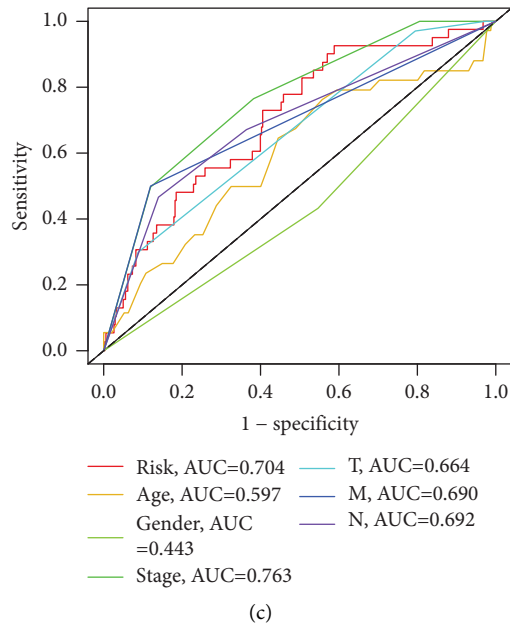
FIGURE 4: Independent prognostic analyses of the cuproptosis-related lncRNA signature: (a) univariate Cox regression showing the correlation between overall survival and clinicopathological characteristics; (b) multivariate Cox regression showing that age, T stage, and risk score are independent prognostic indicators for the overall survival; (c) receiver operating characteristic (ROC) curve analysis showing the prognostic accuracy for age, sex, stage, T stage, M stage, N stage, and risk score.

(a)

(b)

(c)

(d)

(e)

(f)

FIGURE 5: Continued.

(g)

(h)

(i)

(j)

(k)

(l)
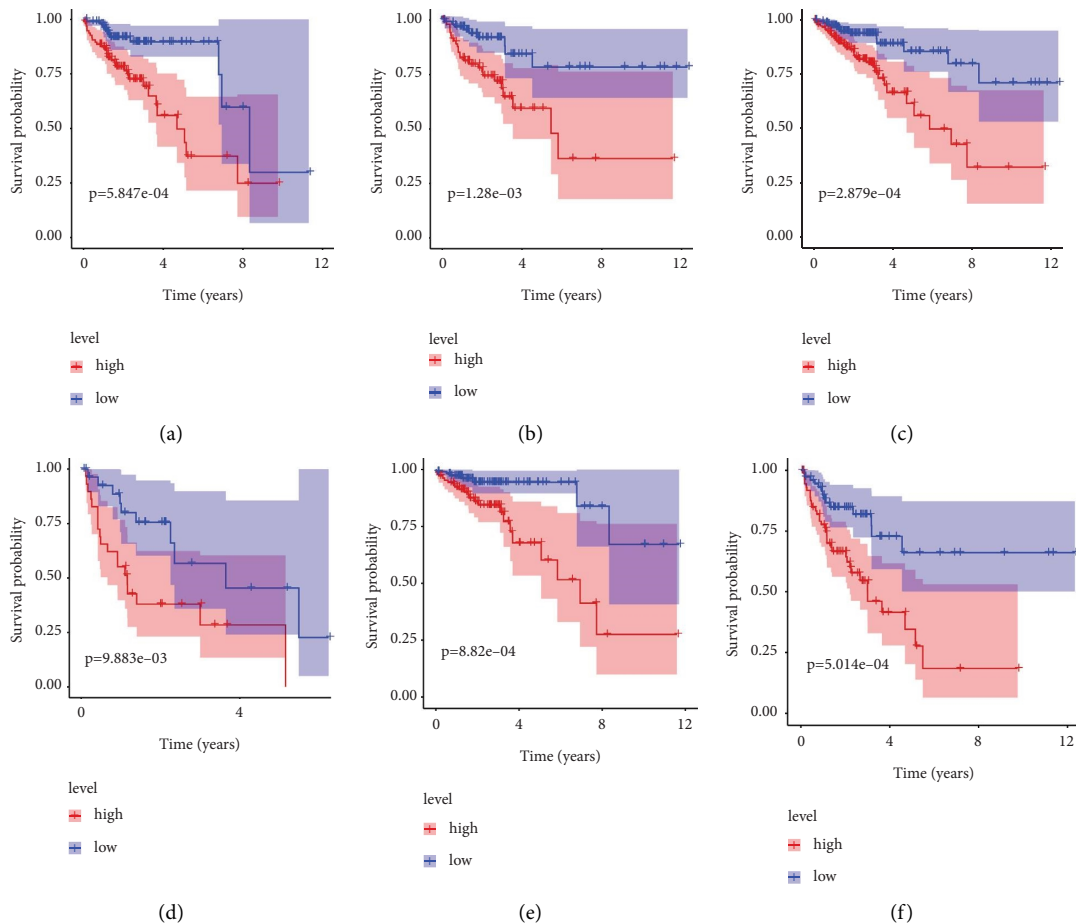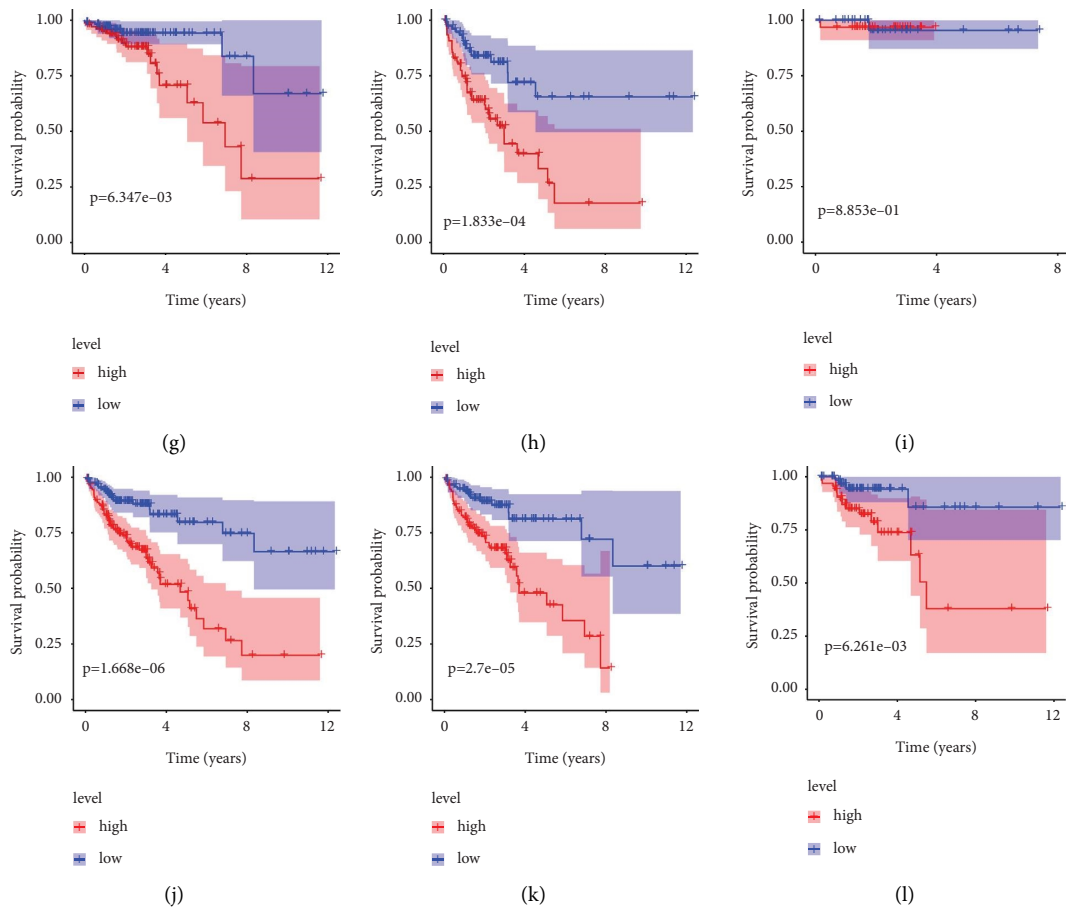
Figure 5: Kaplan–Meier analyses stratified by (a-b) sex, (c-d) M stage, (e-f) N stage, (g-h) S stage, (i-j) T stage, and (k-l) age.

(a)

(b)

(c)

Figure 6: Continued.

(d)

(e)
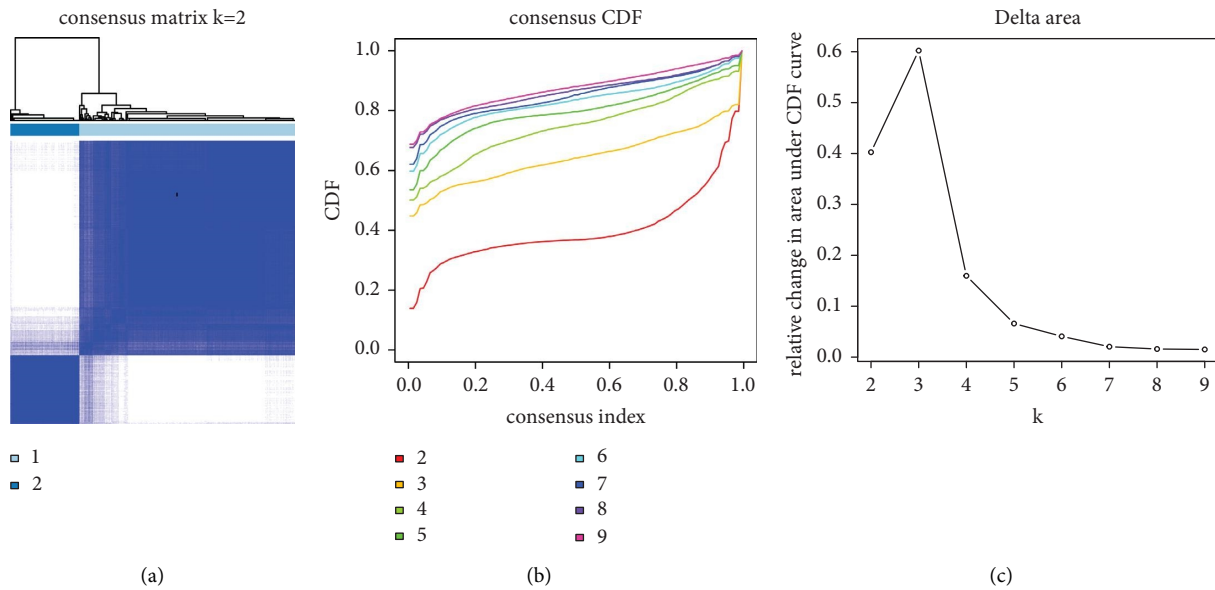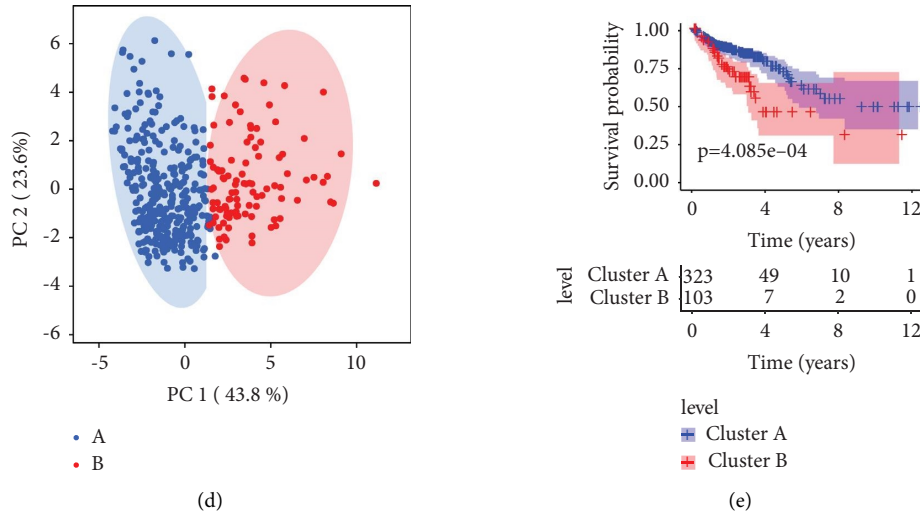
FIGURE 6: Consensus clustering analysis of patients with CM based on the ICD-related genes: (a) consensus clustering heatmap of the group at $k = 2$; (b) cumulative distribution function (CDF) curve for $k = 2–9$; (c) relative change in area under CDF curve for $k = 2–9$; (d) principal components analysis (PCA) shows a significant distribution pattern between cluster A and cluster B; (e) the Kaplan–Meier survival curve analysis reveals that the OS rate of patients in cluster A is higher than those in cluster B.

(a)

(b)

FIGURE 7: Continued.

(c)
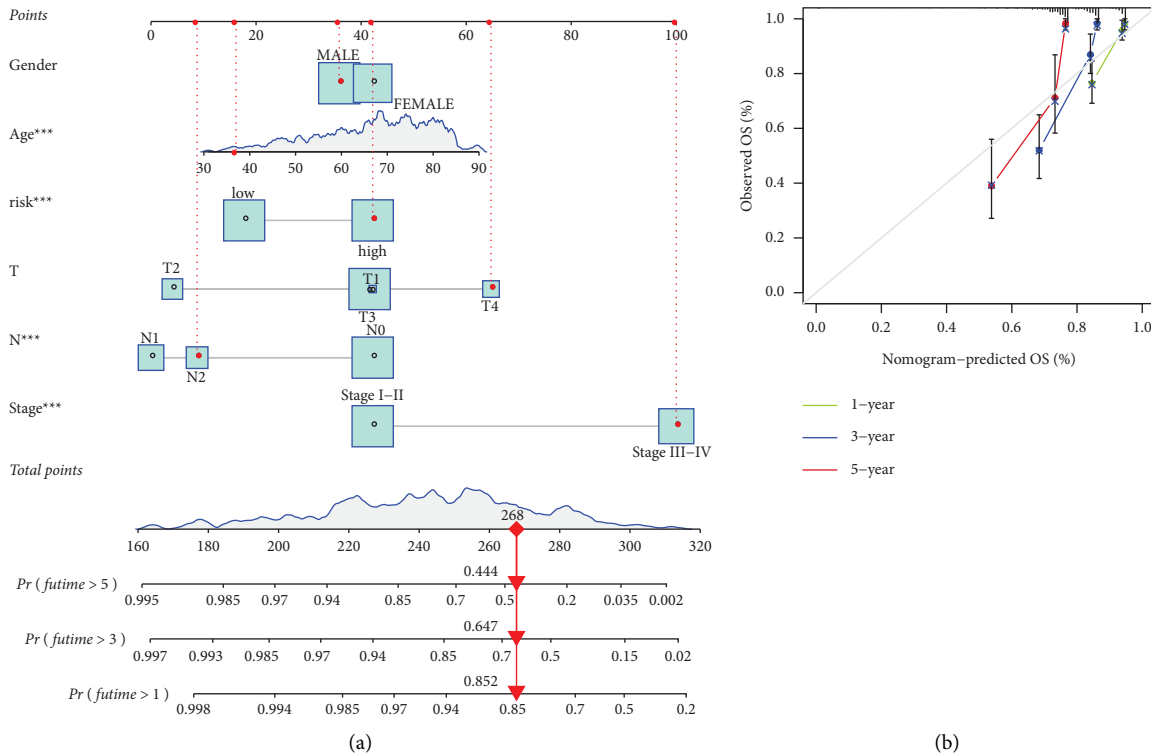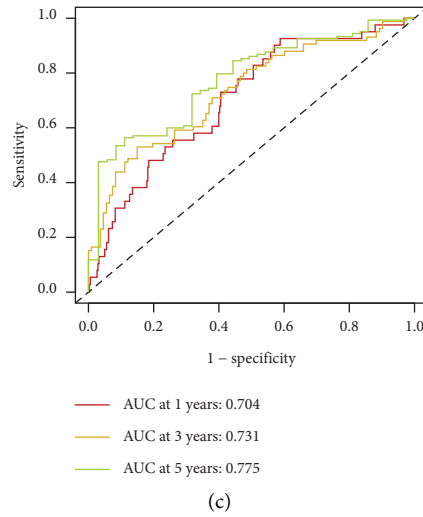
FIGURE 7: Prognostic nomogram: (a) nomogram using risk scores and clinical characteristics to predict 1-, 3-, and 5-year survival; (b) calibration curve to assess accuracy between predictive power and actual survival rates; (c) receiver operating characteristic (ROC) curve assessment of prognostic accuracy.

(a)

(b)

FIGURE 8: Continued.

(c)
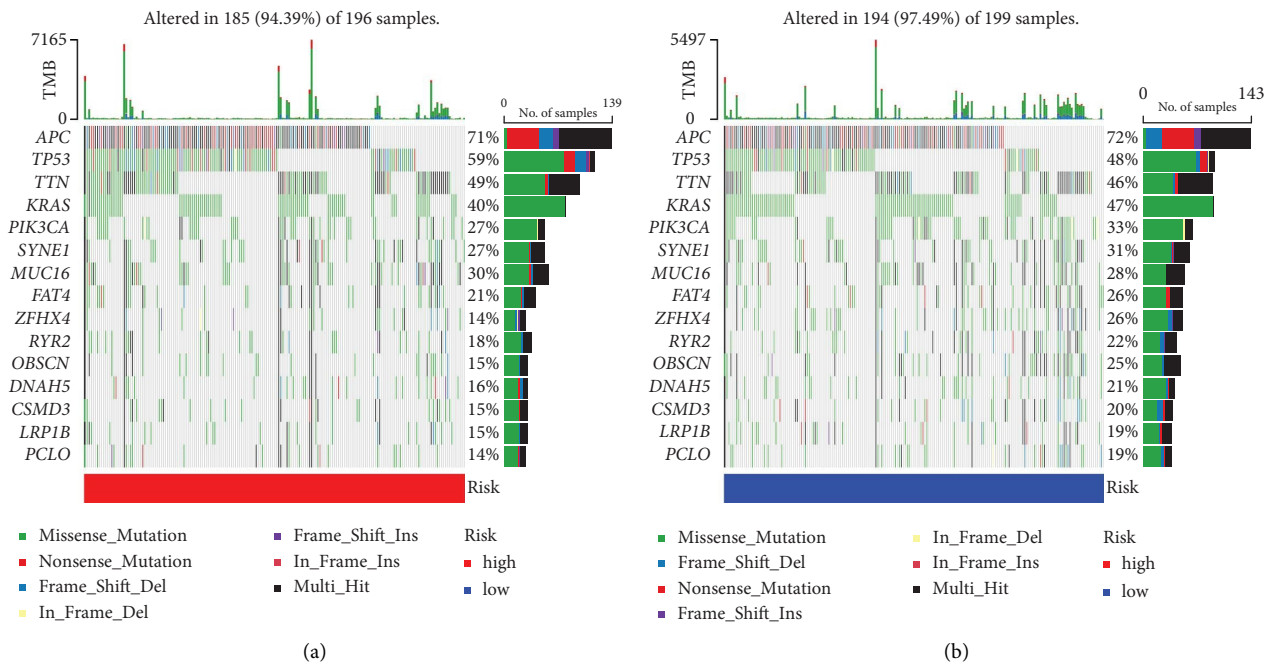
(d)
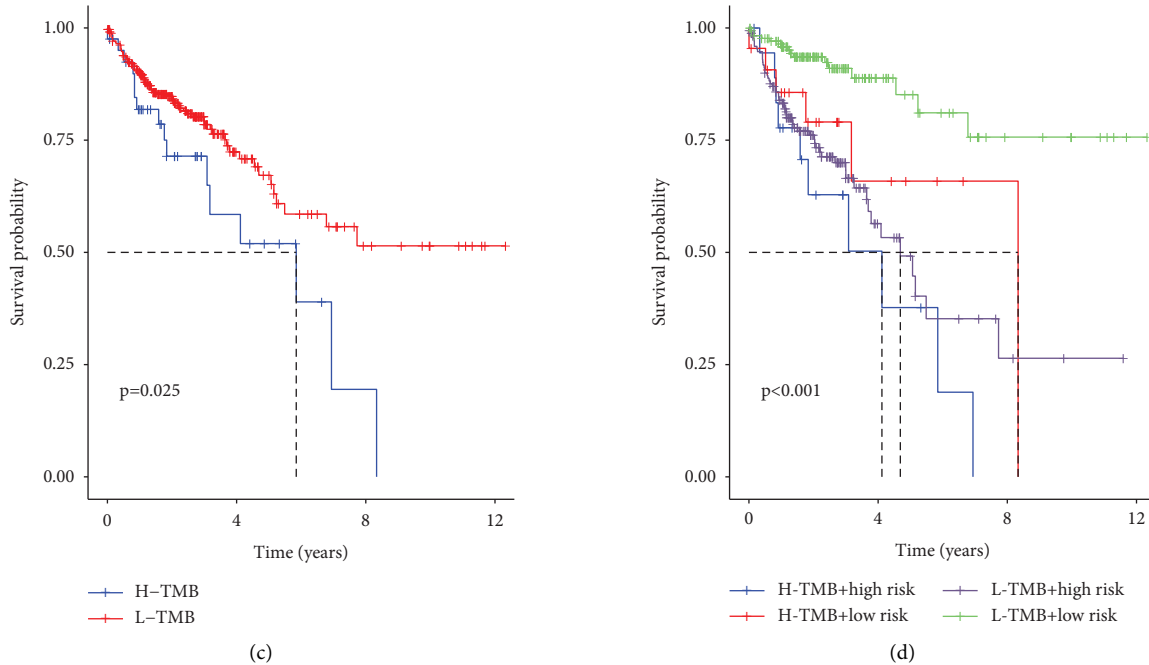
FIGURE 8: Tumor mutational burden analysis: (a) genes with the highest mutation rates in high-risk patients; (b) genes with the highest mutation rates in high-risk patients; (c) overall survival of patients with H-TMB and L-TMB; (d) overall survival of patients with L-TMB and H-TMB.

TTN (46%), and KRAS (47%) had the highest mutation frequencies. In the high-risk group, mutations were detected in 185 out of 196 samples. The mutated genes with the highest frequency in the mutation map showed no significant difference compared with the previous group (Figure 8(d)).

3.9. Sensitivity to Chemotherapeutic Agents. As chemotherapy is the primary treatment for newly diagnosed COAD, we compared IC_{50} values for several commonly used drugs between the low- and high-risk groups. IC_{50} values for high-risk COAD patients for nilotinib, rapamycin, gefitinib, salubrinal, GSK.650394, shikonin, lenalidomide, tipifarnib, and vinblastine were all lower ($P < 0.05$), while the IC_{50} for

bicalutamide was higher in the high-risk group (Figure 9). These results provide preliminary evidence for clinical drug-use guidance.

3.10. Gene Set Enrichment Analysis (GSEA). We found multiple KEGG signaling pathways that were dynamically enriched in the low-risk group compared to the high-risk group, including those involved in the citrate cycle of the TCA cycle; propanoate metabolism, arginine, and proline metabolism; alanine, aspartate, and glutamate metabolism; proteasome; and valine, leucine, and isoleucine degradation. Notably, the expression of components of the mTOR signaling pathway was significantly increased in the high-risk
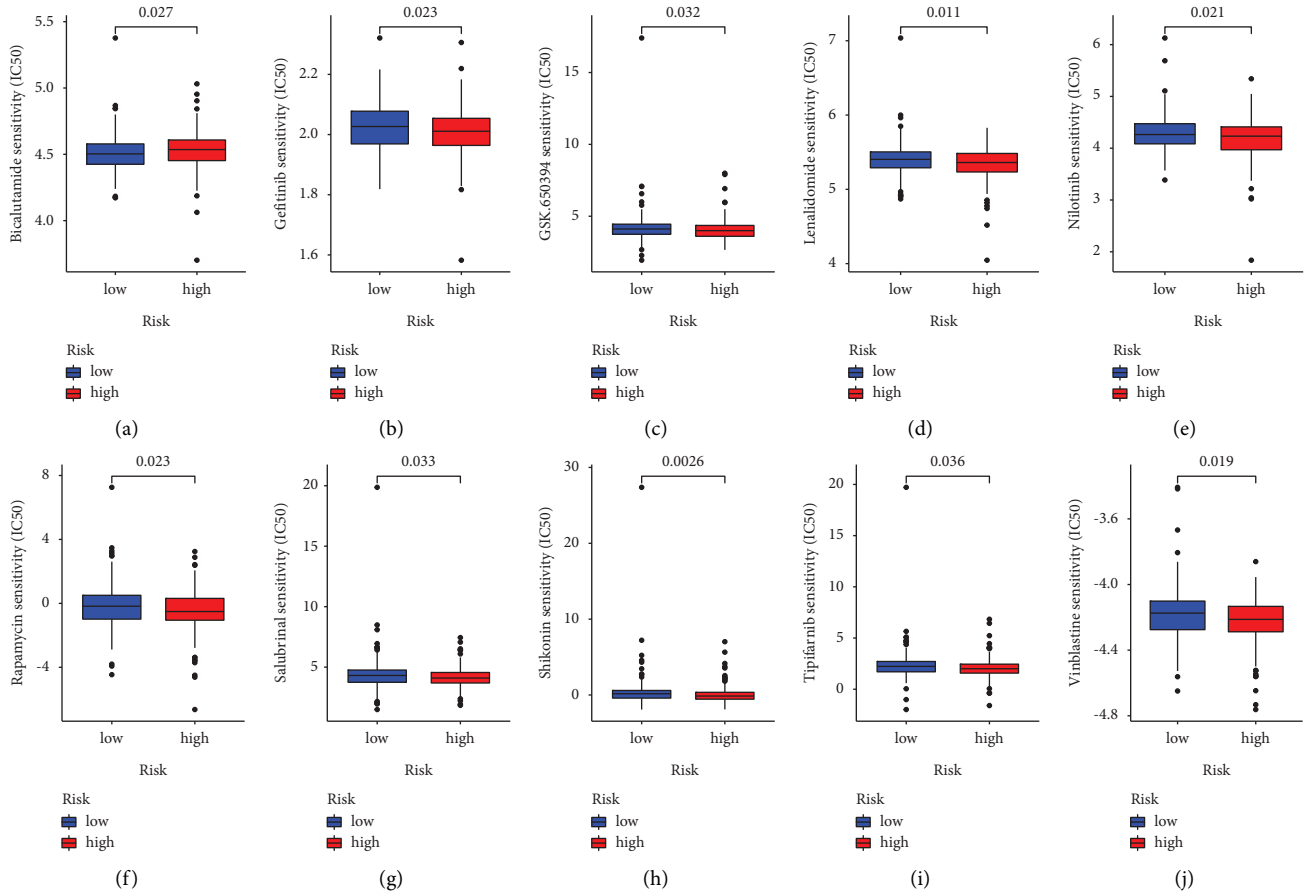
FIGURE 9: Drug sensitivities as a function of the risk group for (a) bicalutamide, (b) gefitinib, (c) GSK.650394, (d) lenalidomide, (e) nilotinib, (f) rapamycin, (g) salubrinal, (h) shikonin, (i) tipifarnib, and (j) vinblastine.
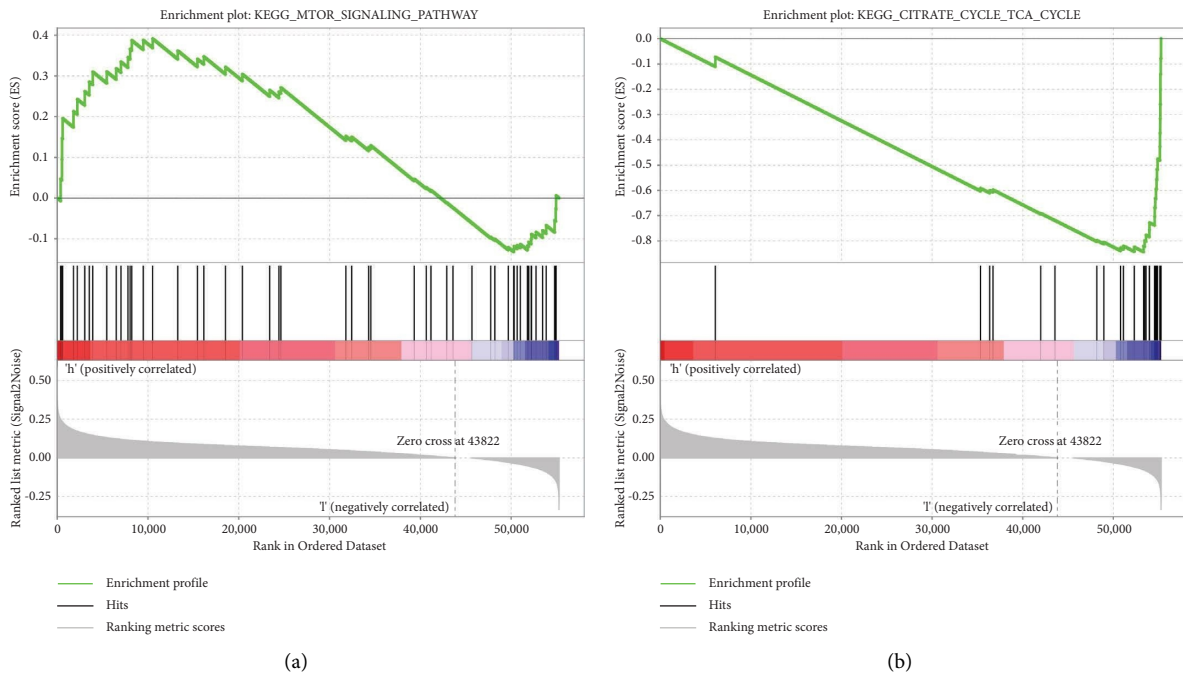
FIGURE 10: Continued.
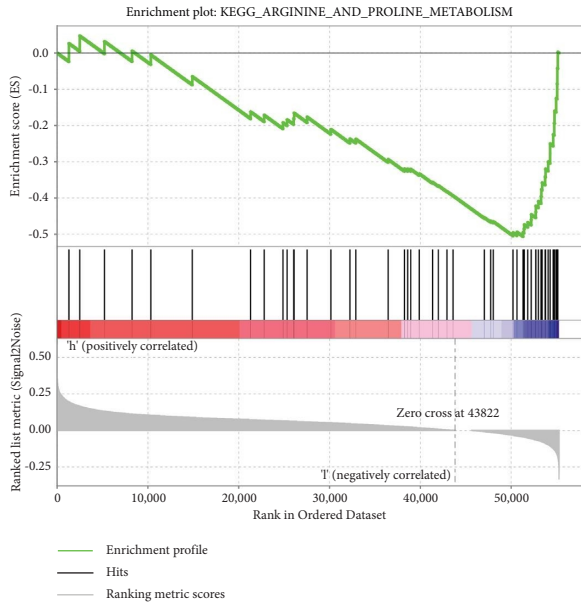
(c)
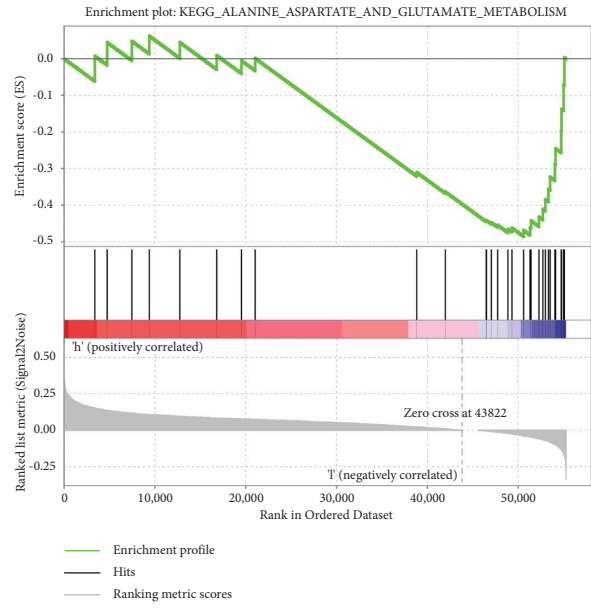
(d)
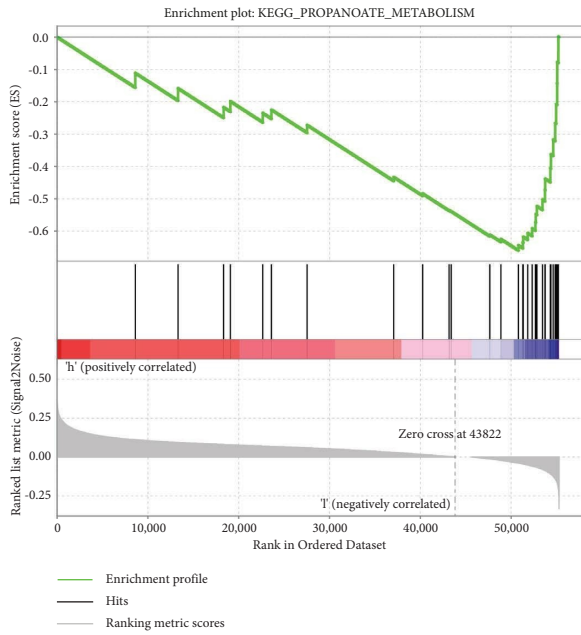
(e)
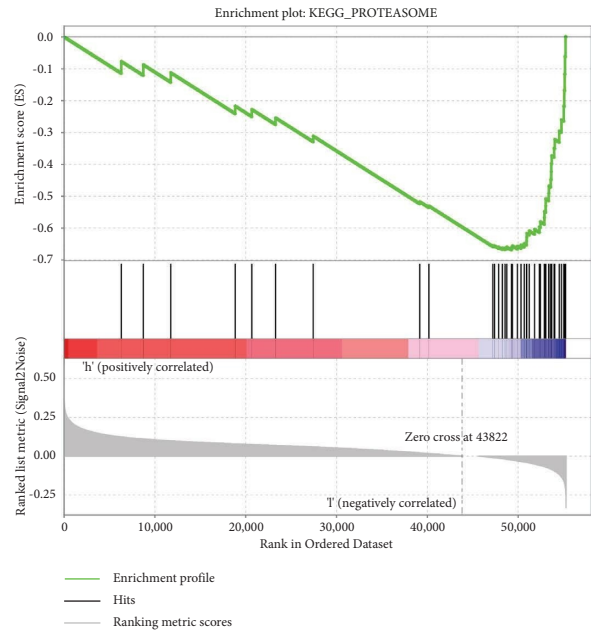
(f)

Figure 10: Continued.
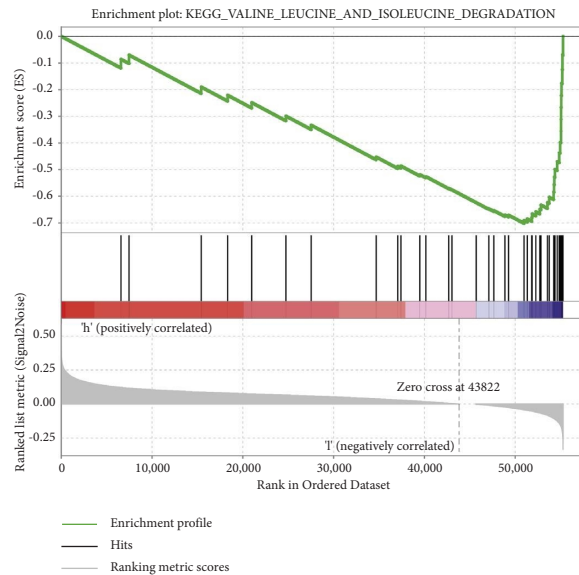
(g)

FIGURE 10: Gene set enrichment analyses: (a) mTOR signaling pathway; (b) citrate cycle TCCA cycle; (c) arginine and proline metabolism; (d) alanine, aspartate, and glutamate metabolism; (e) propanoate metabolism; (f) proteasome; (g) valine, leucine, and isoleucine degradation.

group (Figure 10). These results indicate that metabolic processes and cancer-related pathways may mediate the role of cuproptosis-related lncRNAs in patients with COAD.

4. Conclusions

Despite significant improvements in surgery, radiotherapy, chemotherapy, and immunotherapy, the 5-year COAD survival rate remains very low [1]. Therefore, it is important to identify potential biomarkers for diagnosis and treatment. In this study, we identified and validated a ten-gene feature that predicted survival in patients with COAD. This risk model may be clinically valuable for identifying patients for individualized, cuproptosis-inducing therapy.

Gene expression is regulated by the interaction of lncRNAs with RNA, DNA, and proteins through a variety of mechanisms, including regulation of transcription, mRNA stability, and translation [31]. In colon cancer, lncRNAs have been implicated in regulating cell proliferation, apoptosis, the cell cycle, cell migration and invasiveness, epithelial-mesenchymal transformation (EMT), cancer stem cells, and drug resistance [32]. Multiple types of lncRNAs have been correlated with COAD prognosis [33]. Copper-based therapies are considered to have great potential in cancer treatment; some are already in clinical trials. However, their anticancer potential has not been fully elucidated [34]. Cuproptosis is a newly discovered form of cell death that involves mitochondrial metabolic activity and has not been thoroughly studied in tumors [26]. In the current study, ten lncRNAs associated with cuproptosis were identified and included in a risk model. The Kaplan–Meier curve, time-dependent ROC curve, and Cox regression analysis all demonstrated the predictive ability of the risk model, indicating an independent predictor of COAD prognosis.

Progressive preclinical and clinical evidence suggests that targeting mitochondrial metabolism has anticancer effects [35, 36]. Cuproptosis is associated with highly reactive mitochondrial oxidative phosphorylation (OXPHOS) [26]. Despite an increasing reliance on glycolysis, cells from many cancer types still exhibit functional OXPHOS [37]. In colon adenocarcinomas, stem cells have been reported to use mitochondrial OXPHOS to produce ATP and maintain mitochondrial function via the FOXM1/PRDX3 pathway, thereby maintaining their survival and stem-cell characteristics [38].

Among the lncRNAs screened, MIR210HG, EIF3J-DT, and ZEB1-AS1 have been extensively studied in tumors. MIR210HG promotes breast cancer progression through m6A modification mediated by IGF2BP1 [39]. IGF2BP1 also plays an important role in COAD pathogenesis. Its deletion downregulates k-RAS expression downstream of β-catenin and simultaneously inhibits colon cancer cell proliferation, whereas IGF2BP1 overexpression increases c-MYC and K-RAS expression and promotes colon cancer cell proliferation [40]. Whether MIR210HG is involved in this pathway in COAD requires further investigation. In gastric cancer, EIF3J-DT is involved in the regulation of autophagy and chemical resistance of gastric cancer cells by targeting ATG14 [41], while autophagy-dependent apoptosis has been shown to be a promising therapeutic target in COAD [42]. ZEB1-AS1 is involved in the regulation of the ZEB1 pathway; its activation has been reported to promote the stem characteristics and invasiveness of COAD cells [32, 43]. The aforementioned evidence suggests functional mechanisms by which the lncRNAs we identified may be involved in COAD and suggests ways for improving chemotherapy sensitivity and prognosis. Considering our insufficient understanding of these lncRNAs, further studies on them are of clear clinical value.

We found decreased sensitivity to multiple chemotherapeutic agents in the high-risk group stratified by CPR-related prognosis. The development of chemoresistance is an important factor that limits the therapeutic efficacy of anticancer drugs and ultimately leads to the failure of COAD chemotherapy [44]. Transport-based mechanisms of cellular drug resistance play important roles [45, 46]. Through the control of entry and exit of substrates through the cell membrane by membrane transporters, such as P-gp, multiple drugs can escape from cancer cells, decreasing their intracellular accumulation, resulting in multidrug resistance (MDR) that is not limited to a specific type and confers resistance to multiple drugs [47]. Studies on MDR mechanisms and strategies for their reversal play an important role in the success of chemotherapy [48–50]. There have been studies showing that a new class of thiosemicarbazone compounds, the copper-binding di-2-pyridyl ketone thiosemicarbazones, has great promise. Through a unique mechanism, they form redox-active complexes with copper in the lysosomes of cancer cells to reduce the amount of copper in the body, thereby overcoming P-gp-mediated MDR [51]. Therefore, chelators that bind copper have been developed as anticancer agents [51]. Our data on decreased sensitivity to multiple chemotherapeutic agents in patients with COAD in the lncRNA-stratifiedhigh-risk group may also be due to higher Cu concentrations. The targeted application of chelators that bind copper to fight cancer progression and chemoresistance has significant clinical potential.

In conclusion, we identified ten cuproptosis-related lncRNAs using the multivariate Cox regression analysis and constructed a risk model that can accurately predict COAD prognosis. This evidence provides a foundation for future research on COAD. Our study had some limitations. All analyses were performed using a TCGA-COAD cohort and have not been validated against other databases. Additionally, *in vivo* and *in vitro* experiments should be performed for further validation. Further exploration of the impact of cuproptosis on prognosis and chemotherapy resistance in COAD may provide new ideas for further study and clinical applications.

Data Availability

All data and clinical information involved in this study were obtained from a public database (https://portal.gdc.cancer.gov/) approved by the ethics committee.

Consent

Written informed consent from patients was not required.

Conflicts of Interest

The authors declare that there are no conflicts of interest regarding the publication of this paper.

Acknowledgments

Supplementary Materials

Supplementary Table 1: a table includes 870 cuproptosis-related lncRNAs. Supplementary Table 2: a table includes 15 cuproptosis-related lncRNAs associations with COAD OS. (*Supplementary Materials*)

References

[1] H. Brenner, M. Kloor, and C. P. Pox, "Colorectal cancer," *The Lancet*, vol. 383, no. 9927, pp. 1490–1502, 2014.

[2] R. L. Siegel, K. D. Miller, H. E. Fuchs, and A. Jemal, "Cancer statistics, 2021," *CA: A Cancer Journal for Clinicians*, vol. 71, no. 1, pp. 7–33, 2021.

[3] A. A. Mohamed, A. A. A. Omar, R. R. El et al., "MiR-155 and MiR-665 role as potential non-invasive biomarkers for hepatocellular carcinoma in Egyptian patients with chronic hepatitis C virus infection," *Journal of Translational Internal Medicine*, vol. 8, no. 1, pp. 32–40, 2020.

[4] Y. Wang, K. Hou, Y. Jin et al., "Lung adenocarcinoma-specificthree-integrin signature contributes to poor outcomes by metastasis and immune escape pathways," *Journal of Translational Internal Medicine*, vol. 9, no. 4, pp. 249–263, 2021.

[5] Y. Liu, Y. Liu, S. Ye, H. Feng, and L. Ma, "Development and validation of cuproptosis-related gene signature in the prognostic prediction of liver cancer," *Frontiers in Oncology*, vol. 12, Article ID 985484, 2022.

[6] Y. Zhou, Q. Shu, Z. Fu et al., "A novel risk model based on cuproptosis-related lncRNAs predicted prognosis and indicated immune microenvironment landscape of patients with cutaneous melanoma," *Frontiers in Genetics*, vol. 13, Article ID 959456, 2022.

[7] M. C. Bridges, A. C. Daulagala, and A. Kourtidis, "LNCcation: lncRNA localization and function," *Journal of Cell Biology*, vol. 220, no. 2, Article ID e202009045, 2021.

[8] T. Wu and Y. Du, "LncRNAs: from basic research to medical application," *International Journal of Biological Sciences*, vol. 13, no. 3, pp. 295–307, 2017.

[9] Y. Zhu, Y. Bian, Q. Zhang et al., "Construction and analysis of dysregulated lncRNA-associated ceRNA network in colorectal cancer," *Journal of Cellular Biochemistry*, vol. 120, no. 6, pp. 9250–9263, 2019.

[10] J. Bai, J. Xu, J. Zhao, and R. Zhang, "lncRNA SNHG1 cooperated with miR-497/miR-195-5p to modify epithelial-mesenchymal transition underlying colorectal cancer exacerbation," *Journal of Cellular Physiology*, vol. 235, no. 2, pp. 1453–1468, 2020.

[11] H. Zhi and J. Lian, "LncRNA BDNF-AS suppresses colorectal cancer cell proliferation and migration by epigenetically repressing GSK-3β expression," *Cell Biochemistry and Function*, vol. 37, no. 5, pp. 340–347, 2019.

[12] S. Yang, J. Zhou, Z. Chen et al., "A novel m7G-related lncRNA risk model for predicting prognosis and evaluating the tumor immune microenvironment in colon carcinoma," *Frontiers in Oncology*, vol. 12, Article ID 934928, 2022.

[13] A. Poursheikhani, M. R. Abbaszadegan, N. Nokhandani, and M. A. Kerachian, "Integration analysis of long non-coding RNA (lncRNA) role in tumorigenesis of colon adenocarcinoma," *BMC Medical Genomics*, vol. 13, no. 1, p. 108, 2020.

[14] Z. Zhang, C. Zhou, Y. Chang et al., "Long non-coding RNA CASC11 interacts with hnRNP-K and activates the WNT/β-catenin pathway to promote growth and metastasis in colorectal cancer," *Cancer Letters*, vol. 376, no. 1, pp. 62–73, 2016.

[15] P. Han, J. Li, B. Zhang et al., "The lncRNA CRNDE promotes colorectal cancer cell proliferation and chemoresistance via miR-181a-5p-mediated regulation of Wnt/β-catenin signaling," *Molecular Cancer*, vol. 16, no. 1, p. 9, 2017.

[16] H. J. Cai, Z. C. Zhuang, Y. Wu et al., "Development and validation of a ferroptosis-related lncRNAs prognosis signature in colon cancer," *Bosnian Journal of Basic Medical Sciences*, vol. 21, no. 5, pp. 569–576, 2021.

[17] H. Liu, Y. Tian, J. Li et al., "Identification and functional analysis of lncRNAs and mRNAs between tumorigenesis and metastasis in CRC," *Aging (Albany NY)*, vol. 13, no. 24, pp. 25859–25885, 2021.

[18] H. Li, L. Liu, T. Huang et al., "Establishment of a novel ferroptosis-related lncRNA pair prognostic model in colon adenocarcinoma," *Aging (Albany NY)*, vol. 13, no. 19, pp. 23072–23095, 2021.

[19] C. Ou, Z. Sun, X. He et al., "Targeting YAP1/linc00152/FSCN1 signaling Axis prevents the progression of colorectal cancer," *Advancement of Science*, vol. 7, no. 3, Article ID 1901380, 2020.

[20] M. Entezari, A. Taheriazam, S. Orouei et al., "LncRNA-miRNA axis in tumor progression and therapy response: an emphasis on molecular interactions and therapeutic interventions," *Biomedicine & Pharmacotherapy*, vol. 154, Article ID 113609, 2022.

[21] E. J. Margalioth, J. G. Schenker, and M. Chevion, "Copper and zinc levels in normal and malignant tissues," *Cancer*, vol. 52, no. 5, pp. 868–872, 1983.

[22] D. C. Brady, M. S. Crowe, D. N. Greenberg, and C. M. Counter, "Copper chelation inhibits BRAF(V600e)-driven melanomagenesis and counters resistance to BRAF(V600E) and MEK1/2 inhibitors," *Cancer Research*, vol. 77, no. 22, pp. 6240–6252, 2017.

[23] W. Gao, Z. Huang, J. Duan, E. C. Nice, J. Lin, and C. Huang, "Elesclomol induces copper-dependent ferroptosis in colorectal cancer cells via degradation of ATP7A," *Molecular Oncology*, vol. 15, no. 12, pp. 3527–3544, 2021.

[24] M. A. Kahlson and S. J. Dixon, "Copper-induced cell death," *Science*, vol. 375, no. 6586, pp. 1231-1232, 2022.

[25] P. A. Cobine and D. C. Brady, "Cuproptosis: cellular and molecular mechanisms underlying copper-induced cell death," *Molecular Cell*, vol. 82, no. 10, pp. 1786-1787, 2022.

[26] P. Tsvetkov, S. Coy, B. Petrova et al., "Copper induces cell death by targeting lipoylated TCA cycle proteins," *Science*, vol. 375, no. 6586, pp. 1254–1261, 2022.

[27] S. Chen, P. Liu, L. Zhao et al., "A novel cuproptosis-related prognostic lncRNA signature for predicting immune and drug therapy response in hepatocellular carcinoma," *Frontiers in Immunology*, vol. 13, Article ID 954653, 2022.

[28] Q. Huang, Q. You, N. Zhu et al., "Prognostic prediction of head and neck squamous cell carcinoma: Construction of cuproptosis-related long non-coding RNA signature," *Journal of Clinical Laboratory Analysis*, vol. 36, no. 11, Article ID e24723, 2022.

[29] Z. R. Jiang, L. H. Yang, L. Z. Jin et al., "Identification of novel cuproptosis-related lncRNA signatures to predict the prognosis and immune microenvironment of breast cancer patients," *Frontiers in Oncology*, vol. 12, Article ID 988680, 2022.

[30] X. Liu, L. Zhou, M. Gao, S. Dong, Y. Hu, and C. Hu, "Signature of seven cuproptosis-related lncRNAs as a novel biomarker to predict prognosis and therapeutic response in cervical cancer," *Frontiers in Genetics*, vol. 13, Article ID 989646, 2022.

[31] N. Gil and I. Ulitsky, "Regulation of gene expression by cis-acting long non-coding RNAs," *Nature Reviews Genetics*, vol. 21, no. 2, pp. 102–117, 2020.

[32] S. Chen and X. Shen, "Long noncoding RNAs: functions and mechanisms in colon cancer," *Molecular Cancer*, vol. 19, no. 1, p. 167, 2020.

[33] F. Xia, Y. Yan, and C. Shen, "A prognostic pyroptosis-related lncRNAs risk model correlates with the immune microenvironment in colon adenocarcinoma," *Frontiers in Cell and Developmental Biology*, vol. 9, Article ID 811734, 2021.

[34] J. O. Pinho, I. V. da Silva, J. D. Amaral et al., "Therapeutic potential of a copper complex loaded in pH-sensitive long circulating liposomes for colon cancer management," *International Journal of Pharmaceutics*, vol. 599, Article ID 120463, 2021.

[35] S. Aminzadeh-Gohari, D. D. Weber, L. Catalano, R. G. Feichtinger, B. Kofler, and R. Lang, "Targeting mitochondria in melanoma," *Biomolecules*, vol. 10, no. 10, p. 1395, 2020.

[36] D. A. Wolf, "Is reliance on mitochondrial respiration a "chink in the armor" of therapy-resistant cancer?" *Cancer Cell*, vol. 26, no. 6, pp. 788–795, 2014.

[37] J. Greene, A. Segaran, and S. Lord, "Targeting oxphos and the electronic transport chain in cancer; molecular and therapeutic implications," *Seminars in Cancer Biology*, vol. 86, 2022.

[38] I. S. Song, Y. J. Jeong, and J. Han, "Mitochondrial metabolism in cancer stem cells: a therapeutic target for colon cancer," *BMB Reports*, vol. 48, no. 10, pp. 539-540, 2015.

[39] W. Shi, Y. Tang, J. Lu, Y. Zhuang, and J. Wang, "MIR210HG promotes breast cancer progression by IGF2BP1 mediated m6A modification," *Cell and Bioscience*, vol. 12, no. 1, p. 38, 2022.

[40] P. S. Mongroo, F. K. Noubissi, M. Cuatrecasas et al., "IMP-1 displays cross-talk with K-Ras and modulates colon cancer cell survival through the novel proapoptotic protein CYFIP2," *Cancer Research*, vol. 71, no. 6, pp. 2172–2182, 2011.

[41] Y. Luo, S. Zheng, Q. Wu et al., "Long noncoding RNA (lncRNA) EIF3J-DT induces chemoresistance of gastric cancer via autophagy activation," *Autophagy*, vol. 17, no. 12, pp. 4083–4101, 2021.

[42] P. Mokarram, M. Albokashy, M. Zarghooni et al., "New frontiers in the treatment of colorectal cancer: autophagy and the unfolded protein response as promising targets," *Autophagy*, vol. 13, no. 5, pp. 781–819, 2017.

[43] Y. Li, L. Wang, L. Pappan, A. Galliher-Beckley, and J. Shi, "IL-1β promotes stemness and invasiveness of colon cancer cells through Zeb1 activation," *Molecular Cancer*, vol. 11, no. 1, p. 87, 2012.

[44] N. A. Dallas, L. Xia, F. Fan et al., "Chemoresistant colorectal cancer cells, the cancer stem cell phenotype, and increased sensitivity to insulin-like growth factor-I receptor inhibition," *Cancer Research*, vol. 69, no. 5, pp. 1951–1957, 2009.

[45] D. Waghray and Q. Zhang, "Inhibit or evade multidrug resistance P-glycoprotein in cancer treatment," *Journal of Medicinal Chemistry*, vol. 61, no. 12, pp. 5108–5121, 2018.

[46] R. Zahra, M. Furqan, R. Ullah, A. Mithani, R. S. Z. Saleem, and A. Faisal, "A cell-basedhigh-throughput screen identifies inhibitors that overcome P-glycoprotein (Pgp)-mediated multidrug resistance," *PLoS One*, vol. 15, no. 6, Article ID e0233993, 2020.

[47] T. Hu, Z. Li, C. Y. Gao, and C. H. Cho, "Mechanisms of drug resistance in colon cancer and its therapeutic strategies," *World Journal of Gastroenterology*, vol. 22, no. 30, pp. 6876–6889, 2016.

[48] Y. G. Assaraf, A. Brozovic, A. C. Goncalves et al., "The multifactorial nature of clinical multidrug resistance in cancer," *Drug Resistance Updates*, vol. 46, Article ID 100645, 2019.

[49] K. Bukowski, M. Kciuk, and R. Kontek, "Mechanisms of multidrug resistance in cancer chemotherapy," *International Journal of Molecular Sciences*, vol. 21, no. 9, p. 3233, 2020.

[50] M. Wang, W. Chen, J. Chen et al., "Abnormal saccharides affecting cancer multi-drug resistance (MDR) and the reversal strategies," *European Journal of Medicinal Chemistry*, vol. 220, Article ID 113487, 2021.

[51] K. C. Park, L. Fouani, P. J. Jansson et al., "Copper and conquer: copper complexes of di-2-pyridylketone thiosemicarbazones as novel anti-cancer therapeutics," *Metallomics*, vol. 8, no. 9, pp. 874–886, 2016.

Research Article

ADRB2 Regulates the Proliferation and Metastasis of Gastrointestinal Stromal Tumor Cells by Enhancing the ETV1-c-KIT Signaling

Sijun Chen [1,2] **Feijing Wu** [3] **Jiaxuan Zhang** [4] **Jianwei Zhu** [1] **Xiaorong Zhou** [5] **and Xiaofei Zhi** [1]

[1]*Department of General Surgery, Affiliated Hospital of Nantong University, Nantong 226001, Jiangsu, China*
[2]*Department of General Surgery, The Second Affiliated Hospital of Jiaxing University, Jiaxing 314000, Zhejiang, China*
[3]*Department of General Surgery, The Second Affiliated Hospital of Fujian Medical University, Quanzhou 362000, Fujian, China*
[4]*Department of Trauma Center, Affiliated Hospital of Nantong University, Nantong 226001, Jiangsu, China*
[5]*Department of Immunology, Nantong University, Nantong 226001, Jiangsu, China*

Correspondence should be addressed to Xiaorong Zhou; zhouxiaorong@ntu.edu.cn and Xiaofei Zhi; zhi.xiaofei@ntu.edu.cn

Academic Editor: Xiaodong Li

Background. Gastrointestinal stromal tumor (GIST) originates from a pacemaker cell, the Cajal cell. However, little is known about the cancer neuroscience in GIST. In this study, we aimed to elucidate the clinical and biological roles of adrenoceptor beta 2 (ADRB2) in GIST. *Methods.* Immunohistochemistry was used to evaluate the expression of ADRB2 in GIST tissues. The biological effects of ADRB2 on GIST cell proliferation, migration, invasion, and apoptosis were explored using Cell Counting Kit −8, plate colony formation assay, transwell invasion assay, and flow cytometry. We also explored the growth and metastasis of xenograft tumors in nude mice. Western blotting was used to quantify protein expression and phosphorylation. *Results.* ADRB2 is generally highly expressed in GIST. High ADRB2 expression was significantly associated with risk level, tumor size, mitotic count, and metastasis. Overexpression of ADRB2 promoted GIST cell proliferation, migration, invasion, and apoptosis, while silencing ADRB2 expression showed the opposite effects. Furthermore, we found that silencing endogenous ADRB2 inhibited GIST progression and metastasis in nude mice. ADRB2-induced ETV1 upregulation enhanced the activation of c-KIT. *Conclusion.* ADRB2 plays an important role in the proliferation and metastasis of GIST and is expected to be a potential target for the treatment of GIST.

1. Introduction

Gastrointestinal stromal tumor (GIST), which is the most common mesenchymal tumor of the gastrointestinal tract, originates from the interstitial Cajal cells or their precursors [1, 2]. GIST usually occurs in the stomach (60%–70%) and small intestine (20%–25%) [3]. People between the ages of 50 and 70 are high-risk individuals [4]. At present, the main treatment methods for GIST are surgical resection and biological therapies, such as imatinib. However, GIST patients with recurrence and metastasis still lack effective treatments [5, 6]. Therefore, it is imperative to explore the biological

mechanism, find new biomarkers, and provide new strategies for the diagnosis and treatment of GIST.

Multiple studies have shown that tumor progression is associated with chronic stress [7–10]. The sympathetic nervous system plays an important role in chronic stress [11]. Its nerve fibers act on adrenergic receptors by releasing catechol neurotransmitters to regulate cellular function [12, 13]. The gastrointestinal tract is often injured under stress in the human body [14], such as by stress ulcers. Adrenoceptor beta 2 (ADRB2) is an important member of seven transmembrane G protein-coupled receptors that can be activated by β-agonists such as epinephrine,

norepinephrine, and isoproterenol [15]. Recent studies have found that ADRB2 signaling can regulate a variety of cells in the tumor microenvironment and activate cancer-related signaling pathways [16]. However, the role of ADRB2 signaling in gastrointestinal stromal tumors remains unclear.

In this study, we found that patients with high ADRB2 expression had a worse prognosis. We also showed that ADRB2 could promote GIST cell growth and apoptosis both in vitro and in vivo. In addition, ADRB2 enhances the ETV1-c-KIT signaling [17] by inducing ETV1.

2. Materials and Methods

2.1. Cell Lines and Cell Culture. The GIST-882 human GIST cell line was obtained from Lonza, and the GIST-T1 human GIST cell line was purchased from Cosmo Bio. The cells were incubated in RPMI 1640 (Gibco, NY, USA), supplemented with 10% FBS (Invitrogen, Life Technology, CA, USA) and 1% penicillin-streptomycin (Sigma, St. Louis, USA). All cell lines were cultured at 37°C with 5% CO_2 in an incubator.

2.2. Patients and Tissue Microarray (TMA). The GIST tissue samples used to construct the tissue microarray were collected from 122 GIST patients who underwent radical resection at the Affiliated Hospital of Nantong University (Nantong, China) from 2010 to 2018. Besides, we also collected 22 liver metastatic samples from advanced GIST patients who underwent palliative surgery. All tissue samples were identified by HE staining and immunohistochemical staining (CD117, CD34, SMA, and Desmin4). Immunohistochemical analysis and scoring were performed as previously described [18]. All participants obtained informed consent, and this study was approved by the Ethical Committee of the Affiliated Hospital of Nantong University. All experiments strictly followed the principles of the Declaration of Helsinki.

2.3. qRT-PCR. Total cellular RNA from human tissues was extracted using TRIzol (Takara, Shiga, Japan), and cDNAs were generated using PrimeScript RT reagent (Takara, Dalian, China). Subsequently, qRT-PCR was performed using the Power SYBR Green PCR master mix (Applied Biosystems, Foster City, USA) according to the manufacturer's instructions. The results were normalized to the levels of GAPDH. The primers used were as follows: ADRB2: forward 5′-AGAGCCTGCTGACCAAGAAT-3′ and reverse 5′-TAGCAGTTGATGGCTTCCTG-3′; β-actin: forward 5′-TCACCCACACTGTGCCCATCTACGA-3′ and reverse 5′-CAGCGGAACCGCTCATTGCCAATGG-3′.

2.4. Western Blotting. Total protein extraction from cells using lysis buffer (absin, Shanghai, China). Cellular proteins were separated by electrophoresis on a 10% SDS-polyacrylamide gel and then transferred to a polyvinylidene fluoride membrane by electroblotting. Following blocking with a 5% nonfat dry milk solution for 2 hours, the membrane was incubated overnight at 4°C with the appropriate primary antibody (1 : 1000 dilution). Finally, the membrane was incubated with the corresponding secondary antibody (1 : 5000 dilution) for 2 h at room temperature. The anti-c-KIT antibody was obtained from Invitrogen. Anti-p-ERK (Y204), anti-ERK, and anti-GAPDH were obtained from Cell Signaling Technology. Anti-ETV1 was obtained from Abcam. Secondary antibodies were purchased from Absin.

2.5. Cell Proliferation and Colony Formation Assay. Cells were seeded into 96-well plates at a density of 2000 cells/well and stained with Cell Counting Kit-8 (CCK-8, Dojindo, Kumamoto, Japan) according to the manufacturer's instructions. Cell viability was detected by measuring the absorbance at 450 nm. Cells (1,000 cells/well) were seeded into complete medium in 6-well plates and cultured in the incubator for 14–20 days. Then, the cells were fixed with methanol and stained with a crystal violet solution. After drying, the stained colonies in the 6-well plate were photographed and counted.

2.6. Wound Healing Assay. Cells were seeded in FBS-free medium in 6-well plates at a concentration of 5×10^5 cells per well. After the cells have filled the entire area, a yellow pipette tip was used to make a horizontal wound. PBS was used to wash the cells to remove the floating cells. Following that, the wounds were photographed using an inverted microscope at 0 and 24 h of incubation.

2.7. Transwell Invasion Assays. Transwell assays were conducted to assess cell invasion and migration capacity. Matrigel matrix (Corning, MA, USA) was placed in the upper chamber. Then, the cells were seeded into FBS-free medium in the upper chambers. A complete medium with 20% FBS was added to the lower chamber as an inducer. After 24 hours, cells were fixed with methanol and stained with a crystal violet solution. Cells on the upper surface were erased, and cells on the lower surface were photographed and counted.

2.8. Cell Apoptosis Analysis. Annexin V-FITC apoptosis assay kit (Absin, Shanghai, China) and flow cytometry were used to analyze cell apoptosis. Cells were stained with Annexin V-FITC and propidium iodide following the manufacturer's instructions. Subsequently, the cells were examined on a flow cytometer (BD Biosciences).

2.9. Cell Transfection. Full-length Small hairpin RNAs (shRNA) for ADRB2 and their corresponding negative controls were obtained from Shanghai Genechem Co. Ltd (Shanghai, China). Sequence for shRNA1 is as follows: 5′ GGACCTGAGTCTGCTATATTT 3′; Sequence for shRNA2 is as follows: 5′ AGGTACTGTGCCTAGCGATAA 3′. Sequence for negative control is as follows: 5′ GTTCTCCGA ACGTGTCACGT 3′. GIST cells were incubated with

retroviral in six-well plates according to the manufacturer's instructions. Stable cell lines expressing ADRB2 or those with ADRB2 silenced were selected using puromycin.

2.10. Immunohistochemistry.

2.10. Immunohistochemistry. Tissue sections were baked at 60°C for 1 h, followed by immersion into xylene, 100% ethanol, and then decreasing concentrations of ethanol. Antigen retrieval was done with a citric acid buffer. Sections were then blocked with 5% FBS and stained with first antibodies against ADRB2, c-KIT, and Ki67, followed by incubation with biotinylated secondary antibody and visualized by the standard avidin-biotinylated peroxidase complex method. Lastly, the tissue was counterstained with hematoxylin.

Immunoreactivity scores were assessed by the intensity of staining and percentage of positive area: − (negative staining or weak intensity under 10% aera), + (weak intensity between 10% and 100% or moderate intensity under 10%), ++ (moderate intensity over 10% or strong intensity under 90% aera), and +++ (strong intensity over 90% aera). Tissues with ++/+++ were considered as high expression, while tissues with −/+ were considered as low expression.

2.11. Animal Studies. BALB/c nude mice were provided by the Laboratory Animal Center of Nantong University. All animals were raised under pathogen-free conditions and had free access to water and food. GIST cells were injected subcutaneously into the axilla of nude mice (approximately 10^6 cells in 100 μl PBS per mouse). Tumor fragments were transplanted into the gastric wall of nude mice as previously described [18]. Tumor volume was calculated every 6 days using the following formula: Volume = (width² × length)/2. The experimental protocols were approved by the Animal Care and Use Committee of the Laboratory Animal Center of Nantong University.

2.12. Statistical Analysis. All experiments were repeated at least three times. The data were expressed as the mean ± SD. Two-tailed Student's t-test was employed to calculate the difference between two groups. The χ^2 test was performed to determine the association between patient clinical characteristics and ADRB2 expression. Spearman's correlation was used to analyze the expression of ADRB2 and c-KIT in tumor tissue samples. All statistical analyses were performed using GraphPad Prism 8.0 software and SPSS 25.0 statistical software. Two-tailed $P < 0.05$ was considered statistically significant.

3. Results

3.1. The Expression of ADRB2 Correlates with the Prognosis of Patients. To explore the expression and clinical significance of ADRB2 in GISTs, we constructed TMAs from 122 GIST patients and examined the expression of ADRB2 by immunohistochemical staining. Among 122 GIST patients, 96 (78.7%) patients had high (++/+++) ADRB2 expression in tumor tissue. Kaplan–Meier survival analysis showed that

patients with high ADRB2 expression had a worse prognosis ($P = 0.036$; Figure 1(a)). In addition, the expression levels of ADRB2 were related to risk level, tumor size, and nuclear mitotic count (Table 1). We also analyzed the differences of ADRB2 expression between radical resection samples and palliative resection samples. As shown in Table 2, high expression level of ADRB2 was significantly correlated with liver metastasis. Subsequently, we detected mRNA levels of ADRB2 in GIST frozen samples. The high immunoreactivity-score group showed significantly higher levels of ADRB2 mRNA compared to the low immunoreactivity-score group (Figure 1(b)). The mRNA levels of ADRB2 were also correlated with risk level, tumor size, nuclear mitotic count, and liver metastasis (Figures 1(c)–1(f)). These data suggested that ADRB2 may be associated with the progression of GISTs. Interestingly, we also found that ADRB2 expression showed a significant correlation with c-KIT levels (Figure 1(g)). Spearman's correlation analysis showed that ADRB2 expression was positively correlated with c-KIT expression in GIST tumors ($R^2 = 0.581$; $P < 0.001$; Table 3).

3.2. ADRB2 Modulates GIST Cell Proliferation. To further explore the function of ADRB2 in GIST cells, we ectopically overexpressed ADRB2 in GIST-882 and GIST-T1 cells (Figure 2(a)). CCK-8 assays showed that overexpression of ADRB2 promoted the proliferation of GIST-882 and GIST-T1 compared with vector-transfected cells (Figure 2(b)). Colony formation assays also indicated the similar result to the CCK-8 assays (Figure 2(c)). Furthermore, GIST-882 and GIST-T1 cells were transfected with ADRB2-sh1, ADRB2-sh2, or negative control (shNC, Figure 2(a)). Because ADRB2-sh1 has a more pronounced effect, it was selected for the following experiments. Both CCK-8 and colony formation assays suggested that knockdown of ADRB2 significantly reduced the proliferation of GIST cells (Figures 2(b) and 2(c)). These results illustrate the critical role of ADRB2 in GIST cell proliferation.

3.3. ADRB2 Promotes GIST Cell Migration and Invasion. Wound-healing assays and transwell assays were performed to analyze the effect of ADRB2 on GIST cell migration and invasion. The wound healing assay results demonstrated that overexpression of ADRB2 enhanced the migratory ability of GIST cells, whereas silencing of ADRB2 significantly reduced the migratory ability (Figure 3(a)). Transwell assays also indicated that overexpression of ADRB2 increases the number of migrating and invading GIST cells, whereas knockdown of ADRB2 had the opposite effect on GIST cells (Figure 3(b)). Overall, these data suggested that ADRB2 promotes cell migration and invasion.

3.4. ADRB2 Reduces the Process of Apoptosis. Tumor cells become resistant to apoptosis, allowing them to survive longer. Flow cytometry analysis showed that silencing ADRB2 in GIST cells resulted in a significant increase in
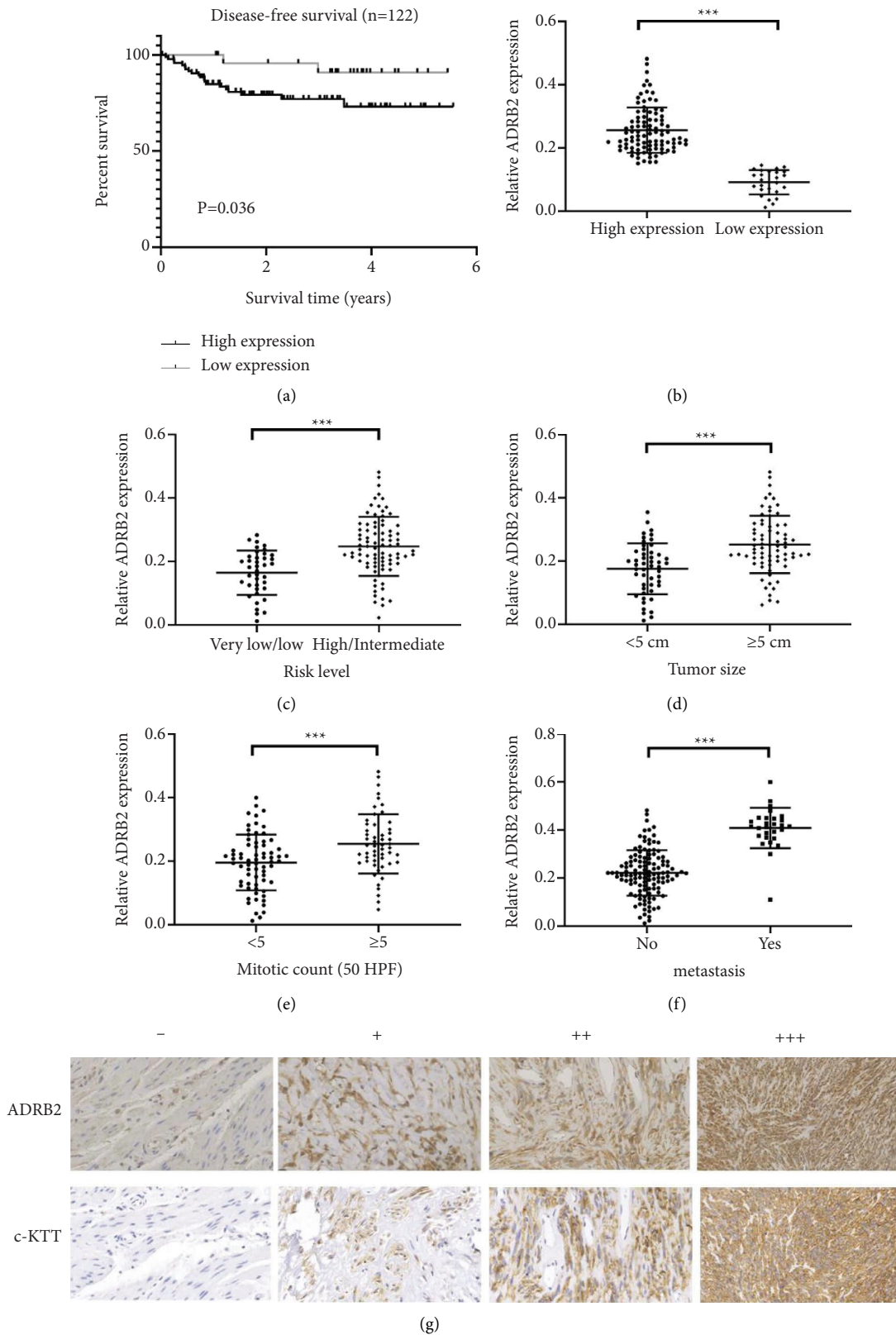
Figure 1: High ADRB2 expression is associated with prognosis in patients with gastrointestinal stromal tumors. (a) Kaplan–Meier disease-free survival curves for 122 patients with gastrointestinal stromal tumor stratified by high and low expression of ADRB2. (b) Real-time PCR was used to detect the mRNA levels of ADRB2 in high immunoreactivity-score group compared to low immunoreactivity-score group. (c–f) The mRNA levels of ADRB2 correlate with risk level, tumor size, mitotic count and liver metastasis. (g) Representative staining of ADRB2 and c-KIT in GIST tissues. Magnification: 400×; ***$P < 0.001$.

TABLE 1: Relations between ADRB2 expression and clinicopathologic characteristics of GIST patients who underwent radical surgery.

Clinicopathologic characteristics	n	ADRB2 expression		χ^2	P
		High	Low		
Ages (years)					
<60	71	59	12	1.970	0.161
≥60	51	37	14		
Gender					
Female	67	56	11	2.122	0.145
Male	55	40	15		
Tumor location					
Stomach	74	60	14	0.642	0.432
Other locations	48	36	12		
Risk level					
Very low/low	39	24	15	10.054	0.002
High/intermediate	83	72	11		
Tumor size					
<5 cm	50	33	17	8.134	0.004
≥5 cm	72	63	9		
Mitotic count (50 HPF)					
<5	71	49	20	5.578	0.018
≥5	51	47	6		

TABLE 2: Correlation between ADRB2 expression and liver metastasis.

Clinicopathologic characteristics	n	ADRB2 expression		χ^2	P
		High	Low		
Metastasis					
No	122	93	29	4.177	0.041
Yes	22	21	1		

TABLE 3: Correlation of ADRB2 expression with c-KIT level in GISTs.

ADRB2	c-KIT	No. of cases	P	R^2
−/+	−/+	15	<0.001	0.573
−/+	++	9		
−/+	+++	2		
++	−/+	7		
++	++	23		
++	+++	12		
+++	−/+	3		
+++	++	13		
+++	+++	38		

apoptotic cell death (Figure 3(c)) while the number of apoptotic GIST cells overexpressing ADRB2 was reduced compared to vector-transfected cells.

3.5. ADRB2 Promotes Tumor Proliferation and Metastasis In Vivo. We performed a subcutaneous xenograft tumor model, an orthotopic gastric tumor model, and an intravenous injection model to evaluate the role of ADRB2 in vivo. In the subcutaneous xenograft tumor model, ADRB2-silenced cells had significantly reduced ability to form tumors in nude mice compared with the NC group (Figures 4(a) and 4(b)). Similar results were observed in the orthotopic gastric tumor model (Figures 4(c)–4(e)). In addition, we found that the orthotopic tumors developed fewer liver metastatic nodes in the ADRB2-knockdown group (Figures 4(f)–4(h)). Furthermore, ADRB2-knockdown also decreased lung metastatic burden in the intravenous injection model (Figures 4(i) and 4(j)). To confirm the ability of cell proliferation, we detect Ki67 in GIST tumors with IHC. As shown in Figure 4(k), knock down of ADRB2 significantly reduced ability of tumor cell proliferation compared with the NC group.

3.6. ADRB2 Enhances the ETV1-c-KIT Signaling. We further explored the molecular mechanism of ADRB2 signaling-mediated effects. ETV1-c-KIT signaling is a key positive feedback to promote GIST progression [19]. In ADRB2-overexpressing GIST cells, ETV1, c-KIT, and p-ERK(Y204) expression were increased (Figure 5(a)). Silencing ADRB2 showed the opposite trend. When ADRB2-overexpressing GIST cells were inhibited by a c-KIT inhibitor (imatinib mesylate), it abolished the effect of ADRB2 on promoting ETV1, c-KIT, and p-ERK (Figure 5(b)). These results demonstrate that ADRB2 enhances the ETV1-c-KIT signaling by inducing ETV1 (Figure 6).

(a)

(b)

(c)
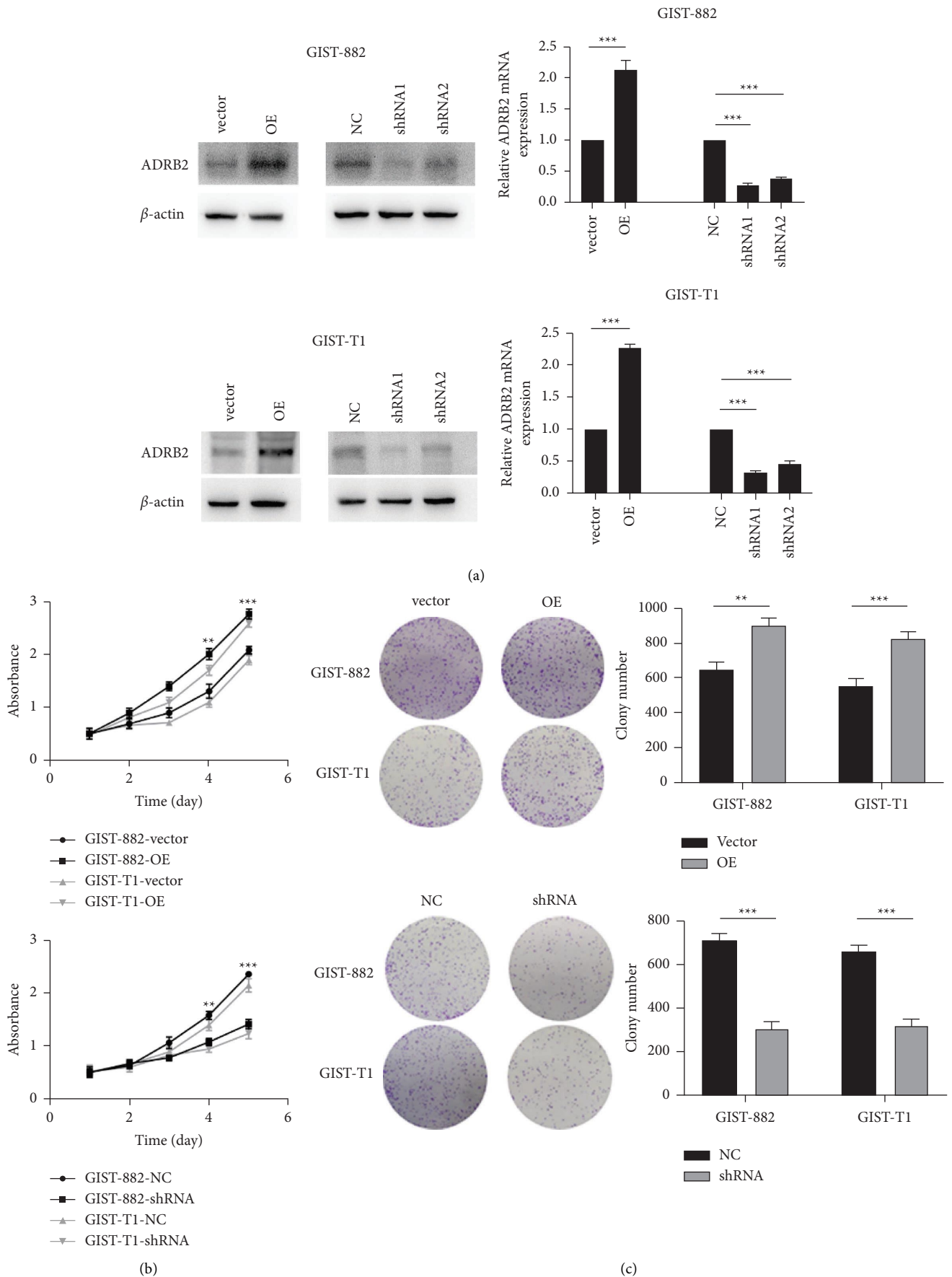
Figure 2: ADRB2 regulates tumor proliferation in gastrointestinal stromal tumors. (a) Western blot and real-time PCR confirmed overexpression and knockdown of ADRB2 in GIST-882 and GIST-T1 cells. (b, c) Cell proliferation abilities were detected by CCK-8 assay and colony formation assay. Data are presented as the mean ± SD. $^{**}P < 0.01$; $^{***}P < 0.001$.

(a)

(b)

(c)
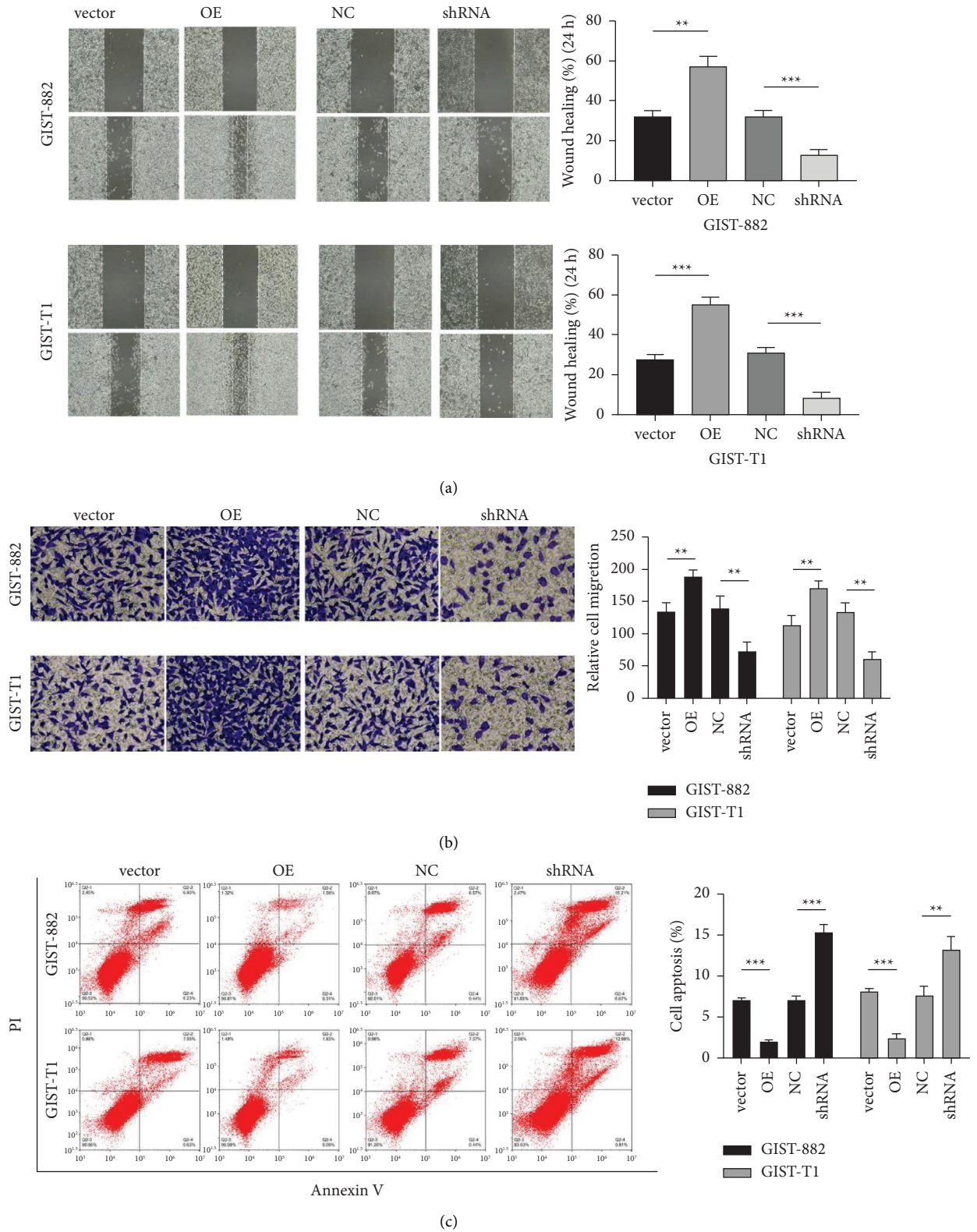
Figure 3: ADRB2 regulates GIST cell migration, invasion, and apoptosis. (a) Cell migration ability was determined by the wound healing assay; (b) transwell assay was used to determine cell invasion ability; (c) cell apoptosis was examined by staining with Annexin V/PI. Data are presented as the mean ± SD. $^{**}P < 0.01$; $^{***}P < 0.001$.

(a)

(b)

(c)

(d)

(e)

(f)

(g)

(h)

(i)

(j)

Figure 4: Continued.

(k)
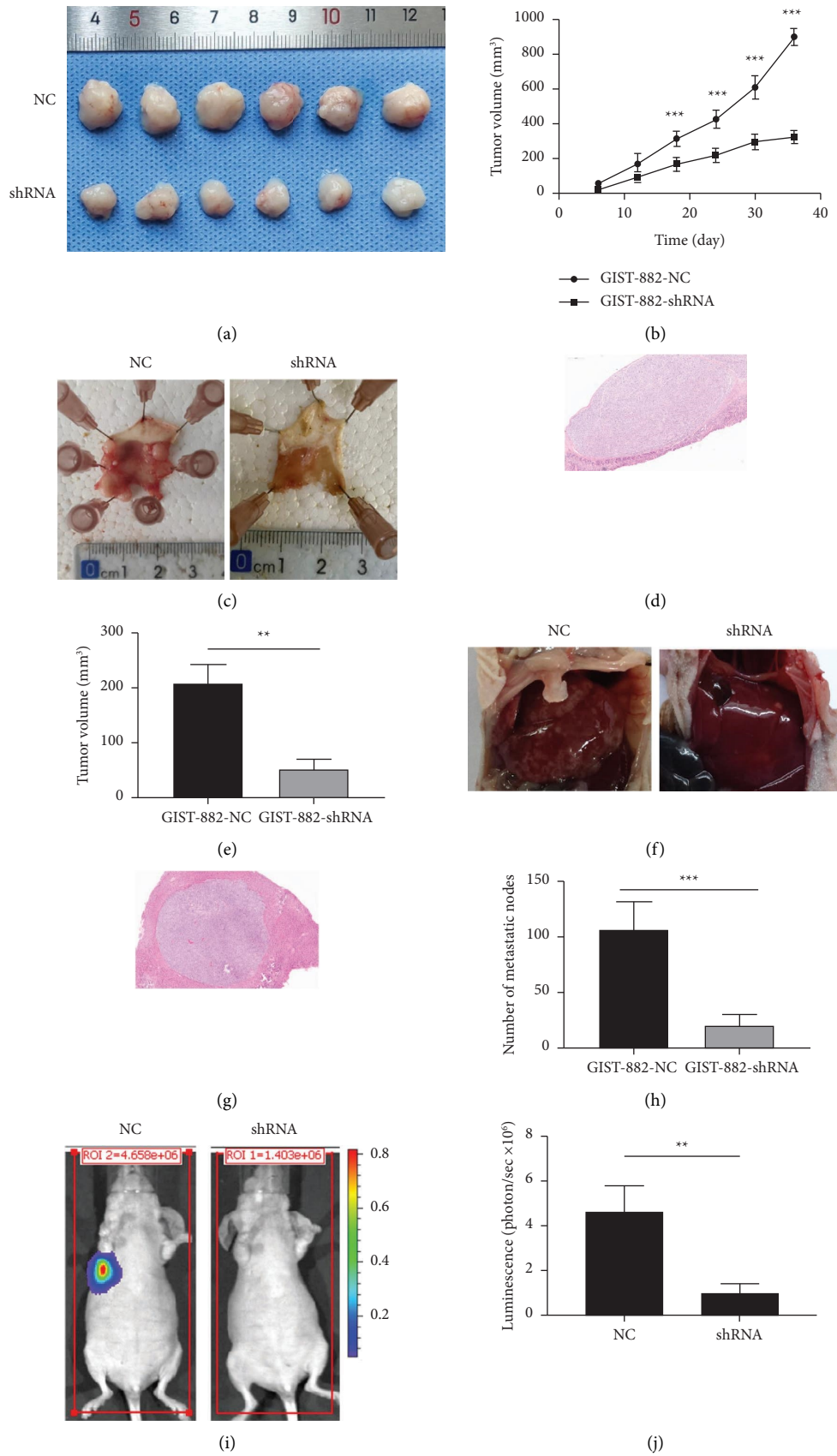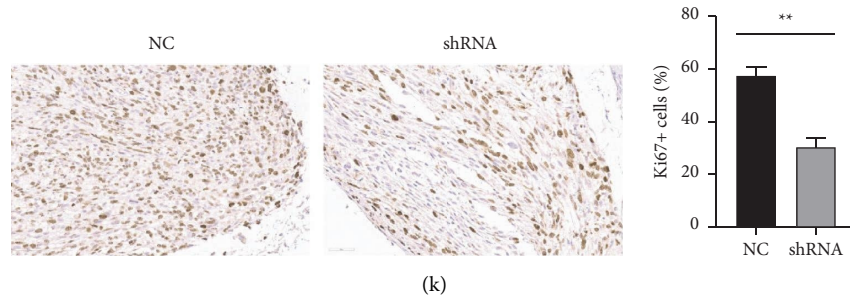
Figure 4: ADRB2 promotes the proliferation and metastasis of gastrointestinal stromal tumors in animal experiments. (a) Images of excised tumors from nude mice. (b) Tumor growth curves were used to evaluate the growth of xenograft tumors. (c) Representative images of gastric orthotopic tumors. (d) H&E staining of gastric orthotopic tumors. (e) Tumor volume of gastric orthotopic tumors. (f) Representative images of live metastasis form gastric orthotopic tumors. (g) H&E staining of liver metastasis. (h) Number of metastatic nodes. (i, j) In vivo image system was used to show the metastasis in intravenous injection model. (k) Ki67 expression was detected by IHC. Data are presented as the mean ± SD. $^{**}P < 0.01$; $^{***}P < 0.001$.

(a)

(b)
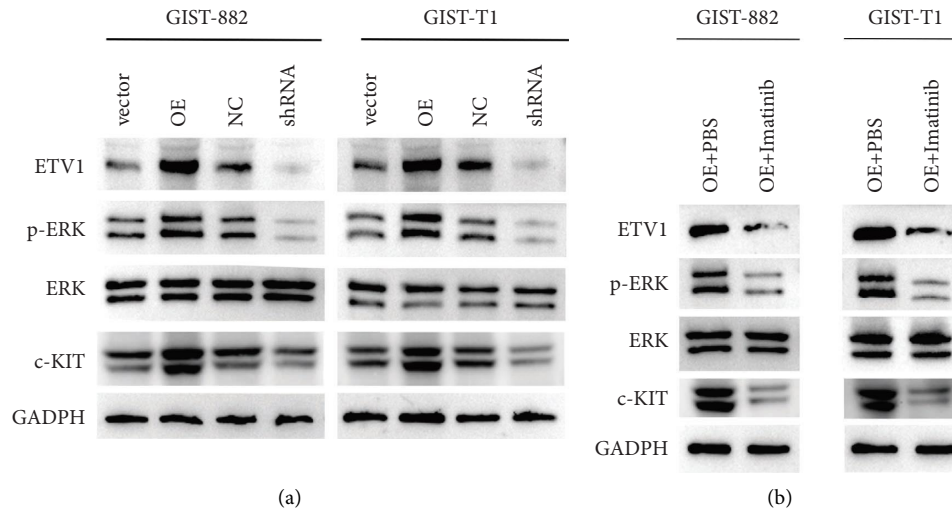
Figure 5: ADRB2 enhances the ETV1-c-KIT signaling. (a) Western blotting was used to detect the expression levels of ETV1, c-KIT, and p-ERK (Y204). (b) GIST cells were treated with or without imatinib mesylate, and ETV1, c-KIT, and p-ERK (Y204) expression levels were detected by western blotting.
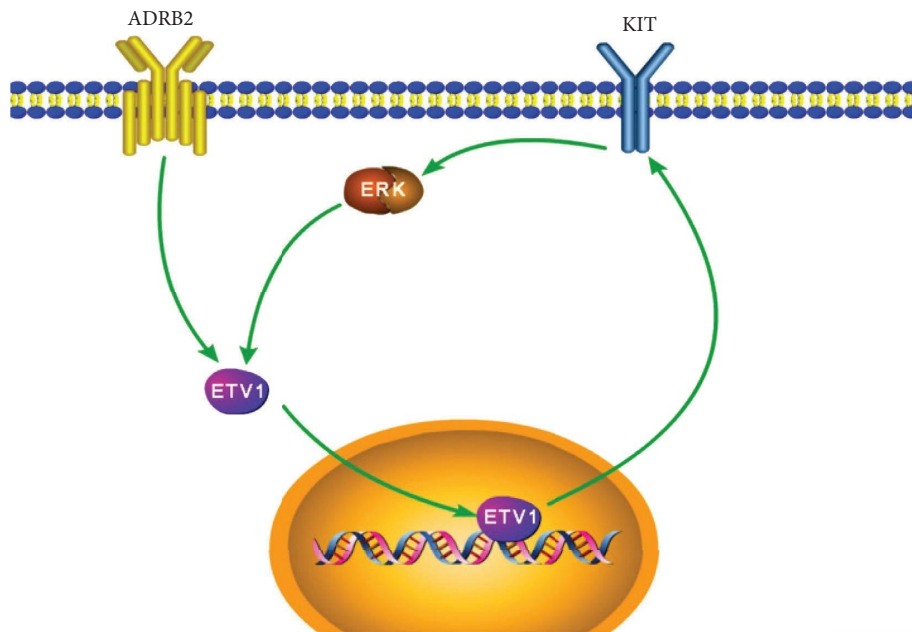
Figure 6: Schematic representation shows ADRB2 enhancing ETV1-c-KIT signaling by inducing ETV1.

4. Discussion

In this study, we found that ADRB2 was highly expressed in 78.7% of GIST tissues and co-expressed with c-KIT by TMA and immunohistochemical staining. The expression levels of ADRB2 are significantly correlated with the clinical characteristics and prognosis of GIST patients. In vivo and in vitro experiments indicated that overexpression of ADRB2 promoted GIST proliferation and metastasis, while silencing ADRB2 expression showed the opposite trend. Taken together, ADRB2 is a potential target for the treatment of GIST.

In recent years, the influence of the nervous system on tumors has gradually attracted attention [20–22]. Several studies have found that neuron-like structures exist in tumor tissue [13, 23], and the density of nerve fibers is related to the degree of tumor differentiation [24]. Sympathetic nerves release neurotransmitters such as norepinephrine, which activates receptors and then causes downstream signal transduction by binding to specific receptors on the cell surface [25]. Previous studies have found that ADRB2 is the primary receptor mediating sympathetic signaling, and ADRB2 can activate multiple downstream signaling pathways in tumors [26–28]. The crosstalk of these different signaling pathways makes the single-targeted therapies currently used in the clinic more prone to failure. Therefore, it is essential to explore new therapeutic targets for the treatment of GIST.

The ETV1-c-KIT signaling is the key positive feedback to promote GIST progression [19]. Our study reveals that ADRB2 is essential for ETV1-c-KIT feedback in GISTs. Recently, ETV1 transcription factor was found to be a major regulator of GIST-specific transcription networks, and it is highly expressed in GISTs but not in other sarcomas. More importantly, ETV1 is upregulated by MAPK-ERK signaling, which is activated by c-KIT [29, 30]. In the present study, we found that the ERK pathway is activated by ADRB2, and ETV1 expression is increased in ADRB2-overexpression cells. The effects of ADRB2 on promoting ETV1-c-KIT signaling can be abolished by the c-KIT inhibitor imatinib. These data suggest that ADRB2 plays a vital role in GIST-specific transcription networks.

The expression levels of ADRB2 vary in different cancers. Here, we show that most GIST tissues have a high expression level of ADRB2. Besides, high levels of ADRB2 are correlated with risk level, tumor size, nuclear mitotic count, and liver metastasis. Kaplan–Meier survival analysis also shows that patients with high ADRB2 expression have a worse prognosis. These data indicate that ADRB2 might be a new target for GIST treatment. The sympathetic signaling can be abnormally activated by a variety of stimuli such as chronic stress. Activation of adrenergic signaling by chronic stress leads to sympathetic and adrenal medulla secretion of catecholamines [31, 32]. ADRB2 mediates most of the effects of catecholamines in tumors. Long-term elevated catecholamine levels can also have an impact on cancer progression [33]. Therefore, the combination of ADRB2 antagonists with existing GIST treatments may have clinical implications.

In conclusion, our study confirms that ADRB2 signaling promotes GIST proliferation and metastasis in vitro and in vivo. ETV1-c-KIT feedback is regulated by ADRB2-ERK signaling. ADRB2 is a potential prognostic marker and thus may serve as a new therapeutic target for GISTs.

Data Availability

The data used to support the findings of this study are included within the article.

Ethical Approval

The experimental protocols were approved by the Animal Care and Use Committee of the Laboratory Animal Center of Nantong University. This study was approved by the Ethical Committee of the Affiliated Hospital of Nantong University.

Consent

All participants obtained informed consent.

Conflicts of Interest

The authors declare that there are no conflicts of interest.

Authors' Contributions

XZ conceptualized and designed the study. XZ and JZ were responsible for provision of study materials and patients. All authors contributed to the collection and assembly of data, data analysis and interpretation, and writing the manuscript. All authors approved the manuscript. Sijun Chen and Feijing Wu contributed equally to this work.

Acknowledgments

References

[1] G. Mastrangelo, J. M. Coindre, F. Ducimetiere et al., "Incidence of soft tissue sarcoma and beyond: a population-based prospective study in 3 European regions," *Cancer*, vol. 118, no. 21, pp. 5339–5348, 2012.

[2] P. Vandenberghe, P. Hague, S. C. Hockman et al., "Phosphodiesterase 3A: a new player in development of interstitial cells of Cajal and a prospective target in gastrointestinal stromal tumors (GIST)," *Oncotarget*, vol. 8, no. 25, pp. 41026–41043, 2017.

[3] I. Park, D. H. Chung, C. J. Yoo, and D. B. Shin, "Skull metastasis of gastric gastrointestinal stromal tumor successfully managed by surgery," *Journal of Korean Neurosurgical Society*, vol. 60, no. 1, pp. 94–97, 2017.

[4] N. Mulet-Margalef and X. Garcia-Del-Muro, "Sunitinib in the treatment of gastrointestinal stromal tumor: patient selection and perspectives," *OncoTargets and Therapy*, vol. 9, pp. 7573–7582, 2016.

[5] V. D. Pai, J. L. Demenezes, P. S. Patil, and A. P. Saklani, "Multimodality therapy of rectal gastrointestinal stromal

tumors in the era of imatinib-an Indian series," *Journal of Gastrointestinal Oncology*, vol. 7, no. 2, pp. 262–268, 2016.

[6] M. Roulleaux Dugage, R. L. Jones, J. Trent, S. Champiat, and S. Dumont, "Beyond the driver mutation: immunotherapies in gastrointestinal stromal tumors," *Frontiers in Immunology*, vol. 12, Article ID 715727, 2021.

[7] B. Kavakcıoğlu Yardımcı, F. Geyikoglu, F. Aysin, K. Koc, N. Simsek Ozek, and V. Kucukatay, "The cytotoxic and apoptotic effects of beta-blockers with different selectivity on cancerous and healthy lung cell lines," *Molecular Biology Reports*, vol. 48, no. 5, pp. 4009–4019, 2021.

[8] M. Chen, G. Qiao, B. L. Hylander et al., "Adrenergic stress constrains the development of anti-tumor immunity and abscopal responses following local radiation," *Nature Communications*, vol. 11, no. 1, p. 1821, 2020.

[9] Y. Kang, A. S. Nagaraja, G. N. Armaiz-Pena et al., "Adrenergic stimulation of DUSP1 impairs chemotherapy response in ovarian cancer," *Clinical Cancer Research*, vol. 22, no. 7, pp. 1713–1724, 2016.

[10] J. Xu, J. Zhang, and J. Wang, "The application of traditional Chinese medicine against the tumor immune escape," *Journal of Translational Internal Medicine*, vol. 8, no. 4, pp. 203-204, 2020.

[11] A. Chang, C. P. Le, A. K. Walker et al., "β 2 -Adrenoceptors on tumor cells play a critical role in stress-enhanced metastasis in a mouse model of breast cancer," *Brain, Behavior, and Immunity*, vol. 57, pp. 106–115, 2016.

[12] A. M. Decker, Y. Jung, F. C. Cackowski, K. Yumoto, J. Wang, and R. S. Taichman, "Sympathetic signaling reactivates quiescent disseminated prostate cancer cells in the bone marrow," *Molecular Cancer Research*, vol. 15, no. 12, pp. 1644–1655, 2017.

[13] Z. Xu, Y. Guo, J. Masahisa et al., "Role of the autonomic nervous system in the tumor micro-environment and its therapeutic potential," *Current Pharmaceutical Design*, vol. 23, no. 11, pp. 1687–1692, 2017.

[14] R. Tulsi, M. M. Ul Haque, F. M. Hanif, A. Devi, M. Mubarak, and N. Hassan Luck, "Metastasis of duodenal adenocarcinoma to the urinary bladder presenting as hematuria," *Journal of Translational Internal Medicine*, vol. 9, no. 2, pp. 143–145, 2021.

[15] Y. Wang and S. Jiang, "The role of ADRB2 gene polymorphisms in malignancies," *Molecular Biology Reports*, vol. 48, no. 3, pp. 2741–2749, 2021.

[16] Q. Huang, Q. Tan, K. Mao et al., "The role of adrenergic receptors in lung cancer," *Am J Cancer Res*, vol. 8, no. 11, pp. 2227–2237, 2018.

[17] Y. Hayashi, M. R. Bardsley, Y. Toyomasu et al., "Platelet-derived growth factor receptor-alpha regulates proliferation of gastrointestinal stromal tumor cells with mutations in KIT by stabilizing ETV1," *Gastroenterology*, vol. 149, no. 2, pp. 420–432.e16, 2015.

[18] X. Zhi, B. Li, Z. Li et al., "Adrenergic modulation of AMPKdependent autophagy by chronic stress enhances cell proliferation and survival in gastric cancer," *International Journal of Oncology*, vol. 54, no. 5, pp. 1625–1638, 2019.

[19] A. Duensing, "Targeting ETV1 in gastrointestinal stromal tumors: tripping the circuit breaker in GIST?" *Cancer Discovery*, vol. 5, no. 3, pp. 231–233, 2015.

[20] K. Wang, Xh Zhao, J. Liu, R. Zhang, and Jp Li, "Nervous system and gastric cancer," *Biochimica et Biophysica Acta (BBA) - Reviews on Cancer*, vol. 1873, no. 1, Article ID 188313, 2020.

[21] S. Jeong, B. Zheng, H. Wang, Q. Xia, and L. Chen, "Nervous system and primary liver cancer," *Biochimica et Biophysica Acta (BBA) - Reviews on Cancer*, vol. 1869, no. 2, pp. 286–292, 2018.

[22] S. Faulkner, P. Jobling, B. March, C. C. Jiang, and H. Hondermarck, "Tumor neurobiology and the war of nerves in cancer," *Cancer Discovery*, vol. 9, no. 6, pp. 702–710, 2019.

[23] P. Seifert, M. Benedic, and P. Effert, "Nerve fibers in tumors of the human urinary bladder," *Virchows Archiv*, vol. 440, no. 3, pp. 291–297, 2002.

[24] F. Feng, J. Yang, L. Tong et al., "Substance P immunoreactive nerve fibres are related to gastric cancer differentiation status and could promote proliferation and migration of gastric cancer cells," *Cell Biology International*, vol. 35, no. 6, pp. 623–629, 2011.

[25] E. Scott-Solomon, E. Boehm, and R. Kuruvilla, "The sympathetic nervous system in development and disease," *Nature Reviews Neuroscience*, vol. 22, no. 11, pp. 685–702, 2021.

[26] F. Q. Wu, T. Fang, L. X. Yu et al., "ADRB2 signaling promotes HCC progression and sorafenib resistance by inhibiting autophagic degradation of HIF1α," *Journal of Hepatology*, vol. 65, no. 2, pp. 314–324, 2016.

[27] X. Wei, L. Chen, A. Yang, Z. Lv, M. Xiong, and C. Shan, "ADRB2 is a potential protective gene in breast cancer by regulating tumor immune microenvironment," *Translational Cancer Research*, vol. 10, no. 12, pp. 5280–5294, 2021.

[28] Y. Xu, J. Wang, X. Wang et al., "Targeting ADRB2 enhances sensitivity of non-small cell lung cancer to VEGFR2 tyrosine kinase inhibitors," *Cell Death and Disease*, vol. 8, no. 1, p. 36, 2022.

[29] L. Ran, I. Sirota, Z. Cao et al., "Combined inhibition of MAP kinase and KIT signaling synergistically destabilizes ETV1 and suppresses GIST tumor growth," *Cancer Discovery*, vol. 5, no. 3, pp. 304–315, 2015.

[30] A. A. Mohamed, A. A. A. Omar, R. R. El et al., "MiR-155 and MiR-665 role as potential non-invasive biomarkers for hepatocellular carcinoma in Egyptian patients with chronic hepatitis C virus infection," *Journal of Translational Internal Medicine*, vol. 8, no. 1, pp. 32–40, 2020.

[31] E. V. Yang, A. K. Sood, M. Chen et al., "Norepinephrine upregulates the expression of vascular endothelial growth factor, matrix metalloproteinase (MMP)-2, and MMP-9 in nasopharyngeal carcinoma tumor cells," *Cancer Research*, vol. 66, no. 21, pp. 10357–10364, 2006.

[32] Y. Wang, K. Hou, Y. Jin et al., "Lung adenocarcinoma-specific three-integrin signature contributes to poor outcomes by metastasis and immune escape pathways," *Journal of Translational Internal Medicine*, vol. 9, no. 4, pp. 249–263, 2021.

[33] D. Luft, C. Maisch, V. Hofmann-Kruck, M. Radjaipour, and H. U. Haring, "Correlates of venous catecholamine concentrations in patients with type 1 diabetes during a cold pressor test," *Clinical Autonomic Research*, vol. 10, no. 3, pp. 131–137, 2000.

Hindawi

Research Article

Identification and Analysis of Crucial Genes in *H. pylori*-Associated Gastric Cancer Using an Integrated Bioinformatics Approach

Wei Ding [iD],[1,2,3] **Huaji Jiang,**[1,2] **Nianyuan Ye,**[1,2] **Ling Zhuang,**[1,2] **Zhiping Yuan,**[4] **Yulin Tan** [iD],[1,2] **Wenbo Xue** [iD],[1,2] **and Xuezhong Xu** [iD][1,2]

[1]*Department of General Surgery, Wujin Hospital Affiliated to Jiangsu University, Changzhou 213017, China*
[2]*Department of General Surgery, The Wujin Clinical College of Xuzhou Medical University, Changzhou 213017, China*
[3]*Changzhou Key Laboratory of Molecular Diagnostics and Precision Cancer Medicine, Changzhou 213017, China*
[4]*Department of Gastroenterology, Wujin Hospital Affiliated with Jiangsu University, Changzhou 213017, China*

Correspondence should be addressed to Yulin Tan; tanyldoctor@163.com, Wenbo Xue; xwbdoctor@163.com, and Xuezhong Xu; xxzdoctor@163.com

Background. The relationship between *H. pylori* infection and gastric cancer (GC) has been widely studied, and *H. pylori* is considered as the main factor. Utilizing bioinformatics analysis, this study examined gene signatures related to progressing *H. pylori*-associated GC. *Materials and Methods.* The dataset GSE13195 was chosen to search for abnormally expressed genes in *H. pylori*-associated GC and normal tissues. The TCGA-STAD database was chosen to verify the expression of key genes in GC and normal tissues. *Results.* In GSE13195, a total of 332 differential expression genes (DEGs) were screened. The results of weighted gene co-expression network analysis showed that the light cyan, plum2, black, and magenta4 modules were associated with stages (*T*3, *T*2, and *T*4), while the orangered4, salmon2, pink, and navajowhite2 modules were correlated with lymph node metastasis (*N*3, *N*2, and *N*0). Based on the results of DEGs and hub genes, a total of 7 key genes (ADAM28, FCER1G, MRPL14, SOSTDC1, TYROBP, C1QC, and *C*3) were screened out. These gene mRNA levels were able to distinguish between normal and *H. pylori*-associated GC tissue using receiver operating characteristic curves. After transcriptional level verification and survival analysis, ADAM28 and C1QC were excluded. An immune infiltration study revealed that key genes were involved in regulating the infiltration levels of cells associated with innate immune response, antigen presentation process, humoral immune response, or *T*cell-mediated immune response. In addition, drugs targeting FCER1G and TYROBP have been approved and are under investigation. *Conclusion.* Our study identified five key genes involved in *H. pylori*-associated GC tumorigenesis. Patients with higher levels of *C*3 expression had a poorer prognosis than those with lower levels. In addition, these key genes may serve as biomarkers and therapeutic targets for *H. pylori*-associated GC diagnosis, targeted therapy, and immunotherapy in the future.

1. Introduction

Incidence of gastric cancer (GC) is the sixth highest of all cancer types, with approximately 1,089,103 cases worldwide. GC is also the third leading cause of cancer death, with approximately 769,000 deaths each year [1]. The number of new cases of GC in China approaches 0.5 million each year [2]. Currently, the 5-year survival rate of GC patients is 32%, and more than 50% of patients are diagnosed with advanced cancer [3]. So far, surgery remains the only cure for GC [4]. The Human Genome Project is nearing completion and next-generation sequencing is being widely applied; researchers have made great progress in the study of the mechanism of GC occurrence and development [5]. The new medical model of the cross-development of sequencing technology and bioinformatics utilizes genomics and proteomics to guide targeted therapy, enabling GC patients to receive individualized and precise treatment [6]. To decrease

the high incidence and mortality of GC, early detection and diagnosis are urgently needed, as well as new biomarkers for the disease. Although technology has advanced considerably, there is still an urgent need for efficient and timely diagnostic methods and new GC-specific biomarkers.

Various risk factors affect the incidence of GC, including *Helicobacter pylori* (*H. pylori*) infection, gender, poor dietary habits, and smoking [7]. Of these, *H. pylori* infection, which often leads to gastritis, followed by gastric atrophy and gastrointestinal metaplasia, is most closely related to GC [8]. Currently, the detection of *H. pylori* and its eradication therapy can reduce the risk of GC [9]. Mechanistically, the toxic effects of *H. pylori*-producedcytotoxicity-associated gene A (CagA) and vacuolar cytotoxicity A (VacA) proteins on gastric mucosal cells can trigger a series of complex biological effects, including release of proinflammatory cytokines, recruitment of immune cells, and stimulation of the survival of gastric epithelial cells [10, 11]. *H. pylori* inhibits phagocytic activity and *T* cell function during infection, while catalyzing the formation of urea to ensure its survival in harsh low pH conditions. Furthermore, *H. pylori* metabolism byproducts damage epithelial cells of the host and contribute to the carcinogenesis of *H. pylori* infection [12]. Despite numerous studies on *H. pylori*, it remains unclear whether *H. pylori* is only involved in the initiation of gastric tumor processes, or whether it affects the mechanisms of tumor progression.

In recent years, immunotherapy, as a novel treatment method, mainly induces antitumor effects by modulating the immune system and has made revolutionary progress in the treatment of gastric cancer [13]. The tumor microenvironment (TME) is a complex ecosystem consisting of immune cells coming in many forms and other acellular components of the extracellular matrix with marked heterogeneity. In the TME, tumor cells and immunomodulators interact dynamically to produce positive immunotherapy responses [14]. The immune microenvironment of GC itself is in a dynamic change, and whether the addition of *H. pylori* will make it more complicated.

In this article, based on the GSE13195 dataset and the TCGA-STAD dataset, we used a series of bioinformatics research methods to explore the dysregulated genes and mechanisms in *H. pylori*-associated GC tissues and to find possible biomarkers and targeted drugs.

2. Materials and Methods

2.1. Data Collection and Analysis. We selected the dataset GSE13195 from the Gene Expression Omnibus (GEO, https://www.ncbi.nlm.nih.gov/geo/) for our study [15]. The dataset was derived from GPL5175 (Affymetrix Human Exon 1.0 ST Array) and contained *H. pylori*-associated GC and normal tissues from 25 patients. The dataset also included patients' pathological information, tumor stages (*T*2, *T*3, and *T*4), and lymph node metastasis (*N*0, *N*2, and *N*3). Subsequently, Sangerbox Tools (https://www.sangerbox.com/) were used for normalized raw data as well as

multiarray analysis ("lima" package) [16]. Finally, 134 downregulated genes and 198 upregulated genes were obtained according to the screening conditions of P value <0.05 and $|logFC| > 1$.

2.2. Functional and Pathway Enrichment Analysis. Genes differentially expressed were functionally enriched using DAVID v6.8 (Database of Annotations, Visualization, and Integrated Discovery, https://david.ncifcrf.gov/home.jsp) [17]. These include Gene Ontology (GO) enrichment analysis and Kyoto Encyclopedia of Genes and Genomes (KEGG) pathway analysis.

2.3. Gene Set Enrichment Analysis (GSEA). To more accurately determine the functions of differential genes, we performed GSEA using Sangerbox Tools on the basis of normal tissues and *H. pylori*-associated GC tissues [16]. The reference gene set is c2.cp.kegg.v7.0.

2.4. Screen for Tumor Progression-Related Modules and Central Genes by Weighted Gene Co-Expression Network Analysis (WGCNA). Gene co-expression networks in *H. pylori*-associated GC tissues were constructed using Sangerbox Tools [16]. First, based on Pearson correlation analysis, 25 samples were clustered to identify outliers. Then, we set the soft threshold to 5 to achieve a scale-free topology. Subsequently, using a dynamic tree-cut approach, the genes were classified into different modules based on gene expression correlations. The expression similarity of module eigen genes was further used to cluster similar modules with a height of 0.85. Module membership (MM) is the correlation of gene expression profiles with module characteristic genes, and genes with MM ≥ 0.8 are considered hub genes [18]. The protein interaction network was mapped using the String online website (https://string-db.org/).

2.5. Validation of Key Genes. Key genes were selected from abnormally expressed genes and hub genes. Receiver operating characteristic (ROC) curves were drawn to calculate specificity and sensitivity. In order to verify the accuracy and reliability of the screened key genes, the gene expression data of GC patients in the TCGA-STAD dataset (including 34 normal samples, 20 *H. pylori*-associated GC samples, 157 *H. pylori*-unassociated GC samples, and 153 other samples) were used for validation (including mRNA expression level and survival analysis) in UALCAN online website (https://ualcan.path.uab.edu/) [19].

2.6. Immune Infiltration Analysis. According to the calculation method of the immune microenvironment score of CIBERSORT, the immune microenvironment analysis of *H. pylori*-associated GC tissues and normal tissues was performed [20]. We calculated enrichment scores for each immune-related cell population using ssGSEA to examine the relationship between key genes and immune infiltration. In addition, Spearman correlations between each hub gene expression and immune enrichment scores were calculated and tested.

2.7. Target Drug. The DrugBank online analysis website (https://go.drugbank.com/) was used to find compounds that might act on key genes [21]. The flowchart of the study is provided in Figure 1.

3. Results

3.1. Data Collection and Acquisition of Differential Genes. The dataset GSE13195 from GEO was selected for this study. According to the screening conditions of $P < 0.05$ and $|logFC| > 1$, we found 332 differentially expressed genes (DEGs), including 198 that were upregulated and 134 that were downregulated (Figures 2(a) and 2(b)).

3.2. Functional and Pathway Enrichment Analysis. DAVID v6.8 was used for GO and KEGG enrichment analysis in order to better elucidate the functional and biological significance of the modules identified. GO biological process analysis showed that in terms of biological process, these differential genes were mainly related with cell adhesion, collagen fibril organization, response to drug, maintenance of gastrointestinal epithelium and detoxification of copper ion; in terms of cellular components, these differential genes were mainly located in extracellular space, extracellular exosome, extracellular region, cell surface, and basolateral plasm membrane; in terms of molecular functions, these differential genes mainly participated in extracellular matrix structural constituent, identical protein binding, protein binding, integrin binding, and collagen binding (Figure 2(c)). Furthermore, KEGG analysis revealed that these differential genes were highly involved in the regulation of gastric acid secretion, mineral absorption, protein digestion and absorption, ECM-receptor interaction, and cell cycle (Figure 2(d)).

3.3. Differential Gene Set Enrichment Analysis. GSEA was conducted to better elucidate how differential genes function. The eight KEGG pathways associated with DEGs are shown in Figure 2(e). They were melanogenesis, thyroid cancer, bladder cancer, P53 signaling pathway, glycosphingolipid biosynthesis, renal cell carcinoma, basal cell carcinoma, and endometrial cancer. Moreover, compared with normal tissues, these related pathways were hyperactivated in *H. pylori*-associated GC tissues.

3.4. Co-Expression Network Construction and Module Detection. To find modules highly correlated with the progression of *H. pylori*-associated GC, samples of cancer tissues were used to construct a network of co-expression. We investigated the relationship between the scale-free topological fit index R^2 and the soft threshold (power) in order to make the network scale-free. As shown in Figures 3(a) and 3(b), we chose a soft threshold (power) of 5 when R^2 reached 0.85 for the first time. After the adjacency matrix was constructed, we transformed it into a topological overlap matrix. Genes were then sorted into different modules, performing a dynamic tree-cutting method.

Different genes would be categorized into the same module if their expressions were significantly correlated. Finally, we got 66 modules; the module feature vector and clustering dendrogram are shown in Figures 3(c) and 3(d). Then, to identify modules that were highly correlated with the progression of *H. pylori*-associated GC, the correlation between tumor characteristics and each module was examined. As shown in Figure 3(e), among the 66 modules, modules light cyan, plum2, black, and magenta4 were most associated with stage (*T*3, *T*2, and *T*4) with *P* values below 0.05; modules orangered4, salmon2, pink, and navajowhite2 were associated with lymph node metastasis (*N*3, *N*2, and *N*0) were most correlated with *P* values below 0.05. We calculated MM and defined genes with MM ≥ 0.8 as central genes among the genes in selected modules and obtained a total of 318 hub genes. The protein interaction networks of these 318 hub genes in their respective categories are shown in Figure 4.

3.5. Acquisition and Specificity Analysis of Key Genes. Seven genes obtained by intersecting the differential genes and hub genes were defined as key genes, namely, ADAM28, FCER1G, MRPL14, SOSTDC1, TYROBP, C1QC, and *C*3 (Figure 5(a)). Their expression in the tissues of the GSE13195 dataset is shown in Figure 5(b). Among them, FCER1G, MRPL14, TYROBP, C1QC, and *C*3 were significantly highly expressed in *H. pylori*-associated GC tissues compared with normal tissues, while ADAM28 and SOSTDC1 were completely opposite. In addition, the ROC curves showed that the key genes were well predicted (AUC values: 0.957, 0.902, 0.934, 0.925, 0.862, 0.826, and 0.726, respectively) (Figure 5(c)). This suggested that seven key genes had the potential to be diagnostic markers for *H. pylori*-associated GC.

3.6. Validation and Survival Analysis of Key Genes. Based on the TCGA database, boxplots of tumor samples and normal samples (including 34 normal samples, 20 *H. pylori*-associated GC samples, 157 *H. pylori*-unassociated GC samples, and 153 other samples) were generated for further validation of the key genes. As shown in Figure 6(a), the mRNA expression levels of the five key genes (FCER1G, MRPL14, *C*3, SOSTDC1, and TYROBP) were significantly different between tumor tissues and normal tissues, while ADAM28 and C1QC showed no significant differences. In addition, FCER1G, MRPL14, and *C*3 were abnormally high in *H. pylori*-associated and *H. pylori*-unassociated GC tissues compared to normal tissues; SOSTDC1 was abnormally low in *H. pylori*-associated and *H. pylori*-unassociated GC tissues. Interestingly, TYROBPHP was abnormally high in *H. pylori*-associated GC tissues compared to normal tissues but not in *H. pylori*-unassociated GC tissues. Furthermore, the expression of TYROBP was significantly increased in *H. pylori*-associated GC tissues relative to *H. pylori*-unassociated GC tissues. The expression levels of key genes were correlated with the prognosis of GC patients through survival analysis. According to the median expression value, GC patients were divided into a high expression group and low expression group. We found that patients with GC who
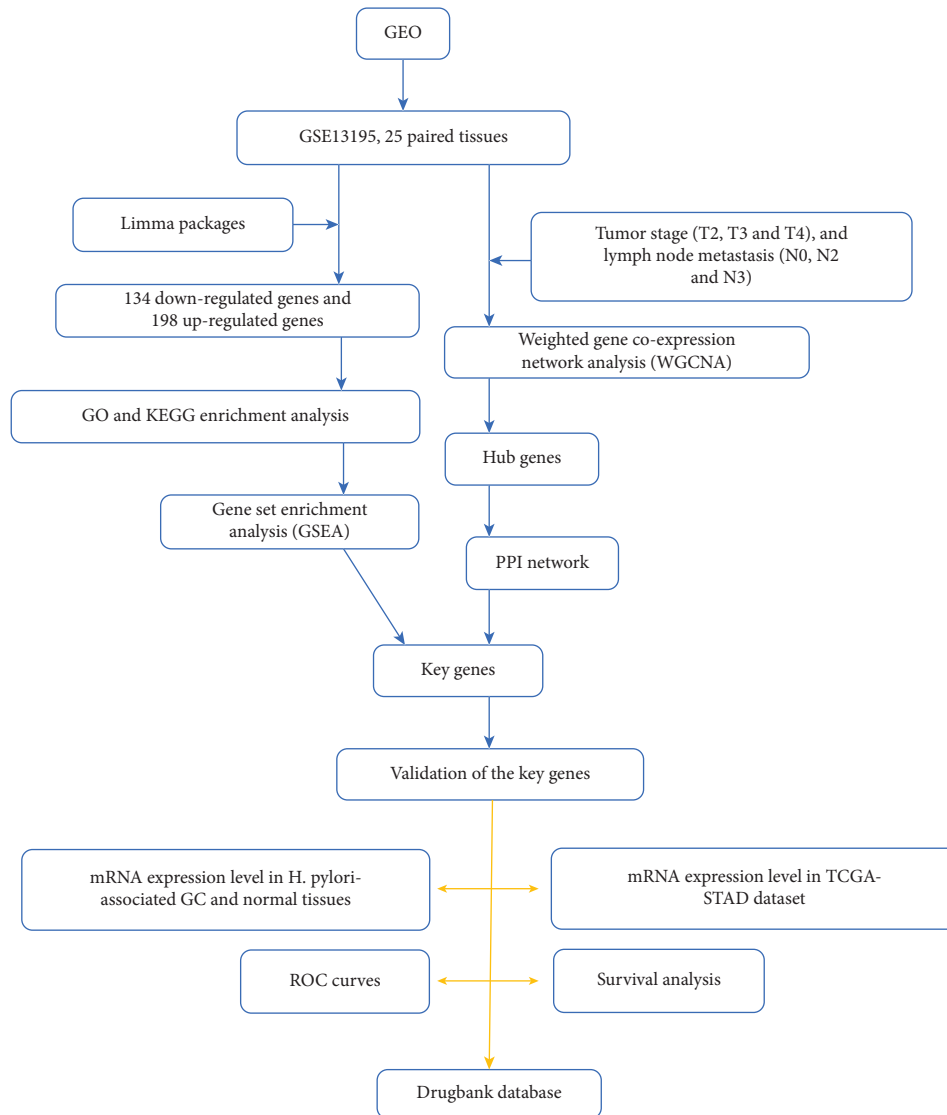
FIGURE 1: Flowchart of the study. GO: Gene Ontology; KEGG: Kyoto Encyclopedia of Genes and Genomes.

expressed high levels of *C3* had poorer overall survival, while the results of survival analysis of other genes were not statistically significant (Figures 6(b) and S1). Therefore, we removed ADAM28 and C1QC from the key genes.

3.7. Immune Infiltration Analysis. We performed immune microenvironment analysis on *H. pylori*-associated GC and normal tissues according to the CIBERSORT's calculation method of the immune microenvironment score. As shown in Figures 7(a) and 7(b), compared with normal tissues, *H. pylori*-associated GC tissues had stronger infiltration of activated NK cells, *M*0 macrophages, *M*1 macrophages, and *M*2 macrophages, but less infiltration of plasma cells and CD8 *T* cells, others are no different. We used ssGSEA to determine enrichment scores for immune-related cells. Spearman correlations

between gene expression and immune enrichment scores for each hub were calculated and tested (Figure 7(c)). The results showed that FCER1G positively correlated with the infiltration of *M*2 macrophages, *M*1 macrophages, resting mast cells and resting dendritic cells, and negatively correlated with the infiltration of plasma cells and CD8 *T* cells. MRPL14 positively correlated with infiltration of *M*1 macrophages, *M*2 macrophages, *M*0 macrophages and resting dendritic cells, and negatively correlated with infiltration of plasma cells, CD8 *T* cells, and memory *B* cells. SOSTDC1 positively correlated with infiltration of plasma cells and CD8 *T* cells, and negatively correlated with infiltration of *M*0 macrophages, *M*1 macrophages, *M*2 macrophages, and activated NK cells. TYROBP was positively correlated with *M*2 macrophages, *M*1 macrophages, resting mast cells, and delta gamma *T* cell infiltration, and negatively correlated with

(a)

(b)

(c)
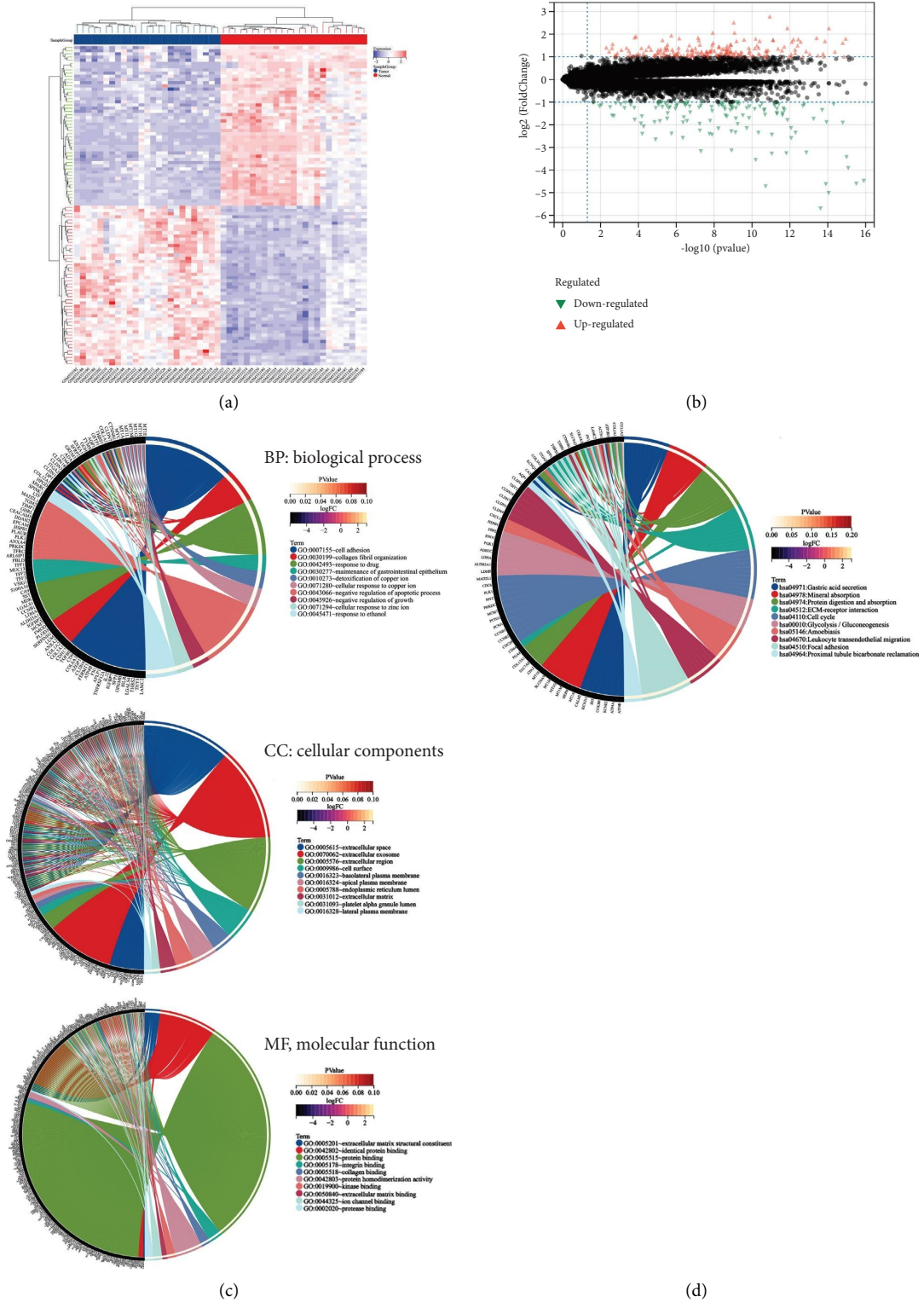
(d)
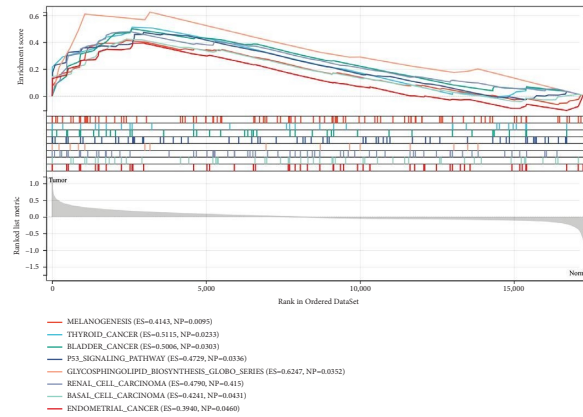
(e)

Figure 2: The analysis of differentially expressed genes. (a) Heatmap of differentially expressed genes. (b) Volcano map of differential expressed genes. (c) Gene ontology (GO) enrichment analysis (top 10). (d) Kyoto Encyclopedia of Genes and Genomes (KEGG) pathway enrichment analysis (top 10). (e) Gene set enrichment analysis.

(a)

(b)

(c)

(d)

Figure 3: Continued.

(e)

Figure 3: The weighted gene co-expression network analysis (WGCNA). (a) Analysis of the scale-free fit index for various soft-thresholding powers. (b) Analysis of the mean connectivity for various soft-thresholding powers. (c) Clustering dendrograms of GSE13195. (d) Module relationships. (e) Heat maps of the correlation between eigen gene and clinical traits of *H. pylori*-associated GC. GC: gastric cancer.

(a)

(b)

(c)

Figure 4: Continued.

(d)

(e)

(f)

FIGURE 4: Protein-protein interaction (PPI) networks. (a) *T*3-related hub genes. (b) *T*2-related hub genes. (c) *T*4-related hub genes. (d) *N*3-related hub genes. (e) *N*2-related hub genes. (f) *N*0-related hub genes.

(a)

(b)

FIGURE 5: Continued.

(c)
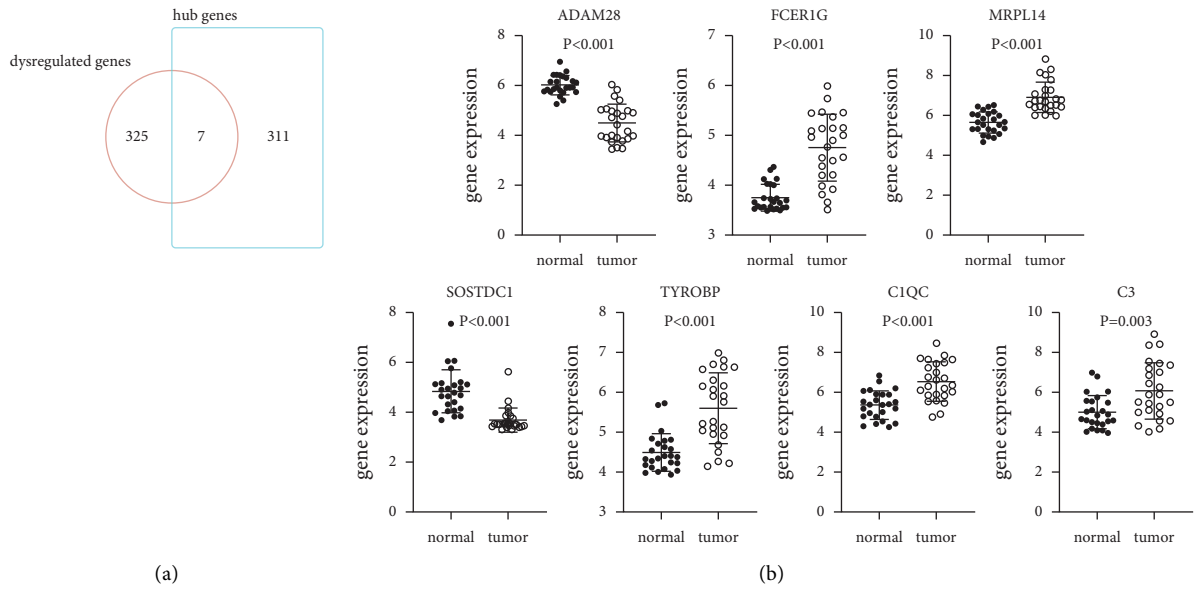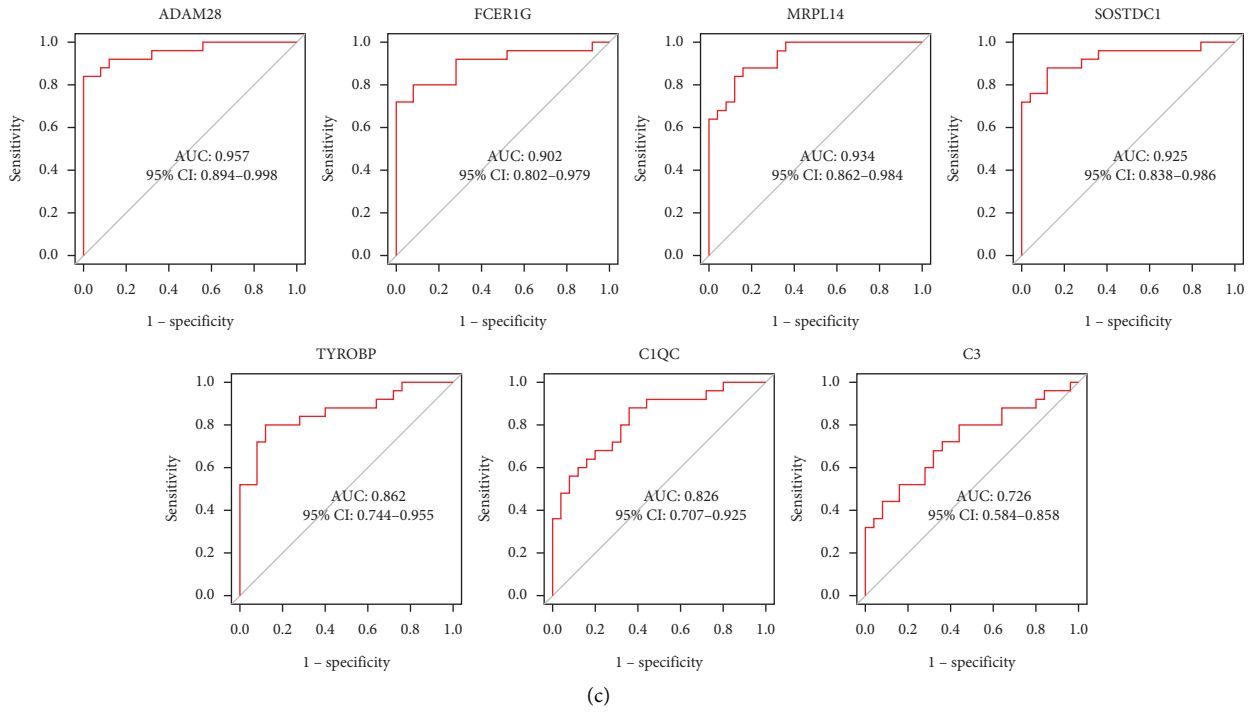
FIGURE 5: Validation of key genes in GSE13195. (a) Venn diagram. (b) mRNA expressions of key genes in GSE13195. (c) ROC curves of key genes in the diagnosis of *H. pylori*-associated GC. ROC: receiver operating characteristic. GC: gastric cancer.

(a)
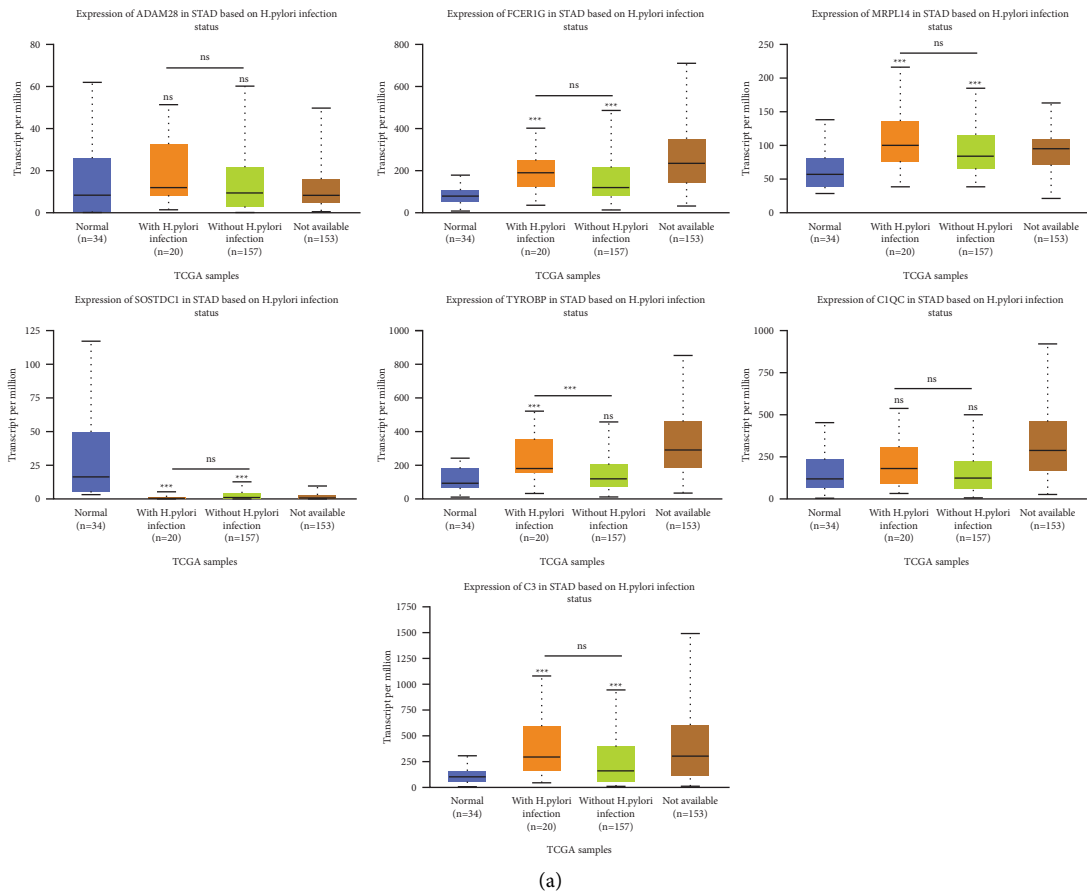
FIGURE 6: Continued.
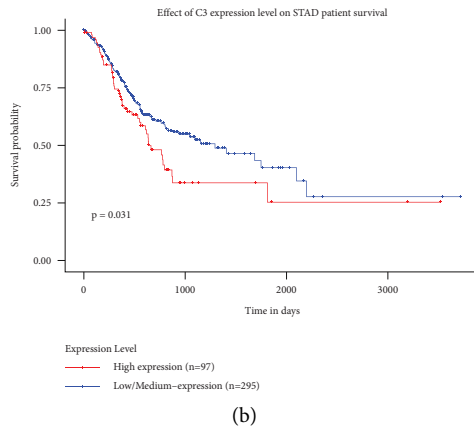
(b)

FIGURE 6: Validation of key genes in TCGA-STAD. (a) mRNA expressions of key genes in TCGA-STAD. (b) Association of *C3* gene with overall survival of patients with GC.
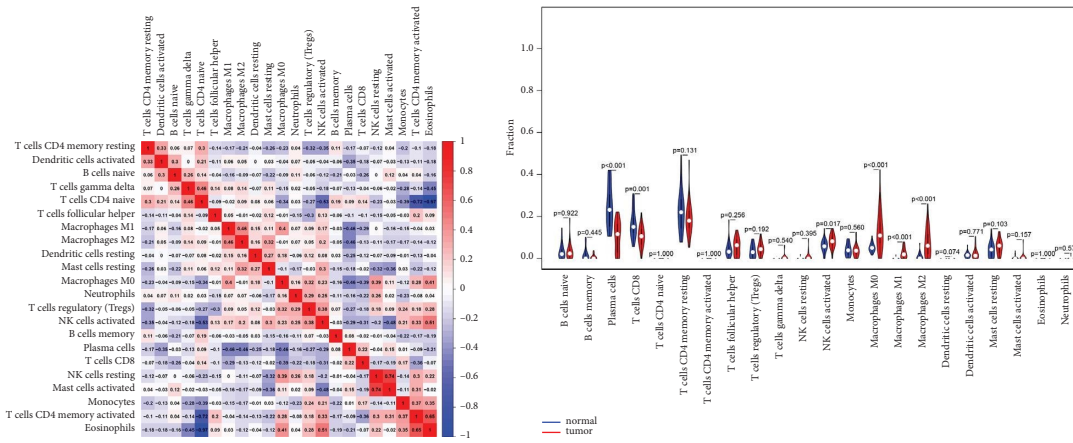
(a)
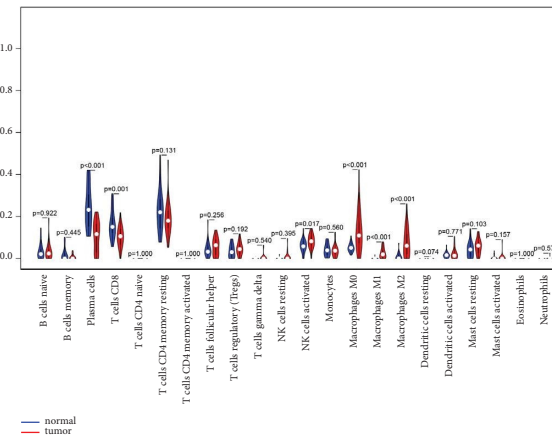
(b)
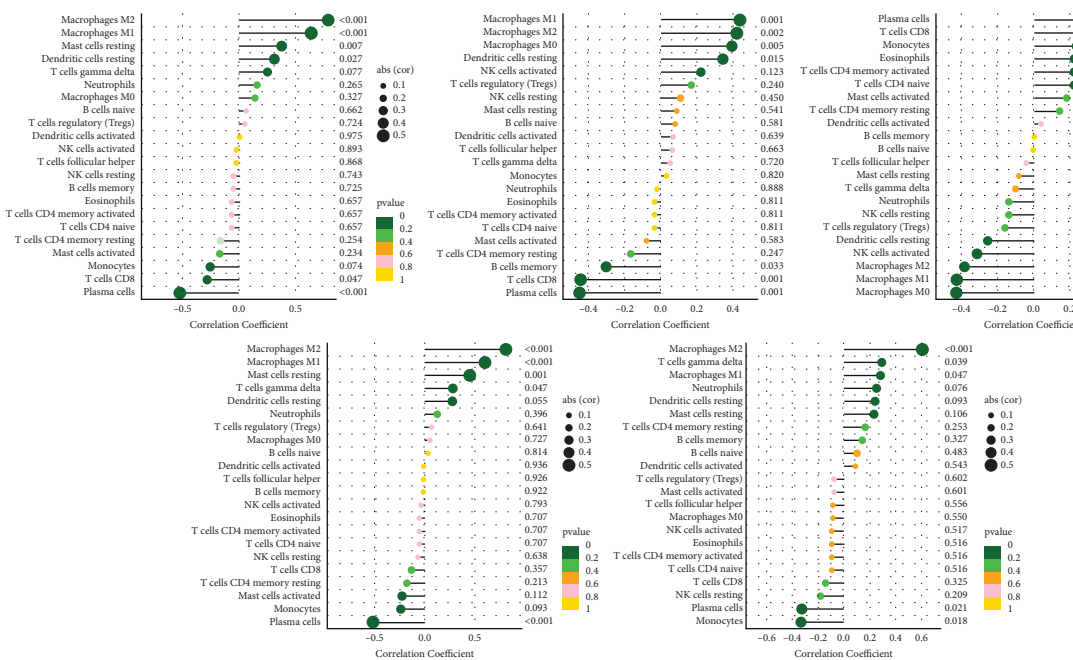
(c)

FIGURE 7: Immune infiltration analysis. The color means spearman correlation between the hub gene and the immune-related cell. (a) Correlation matrix of all 22 immune cells proportions. (b) Violin plot showed the proportions of 22 immune cells between normal tissues with *H. pylori*-associated GC tissues. (c) Influence of key genes on infiltration of 22 immune cells.

plasma cell infiltration. *C*3 was positively correlated with infiltration of *M*2 macrophages, delta gamma *T* cells and *M*1 macrophages, and negatively correlated with infiltration of monocytes and plasma cells.

3.8. Possible Targeted Drugs.

We used the DrugBank online website to search for possible targeted drugs in key genes. As shown in Table 1, for FCER1G, currently approved and under investigation drugs were benzylpenicilloyl polylysine and fostamatinib. Among them, benzylpenicilloyl polylysine acted as an agonist, while fostamatinib functioned as an inhibitor. For TYROBP, the currently approved and understudied drug was dasatinib, but it played a multi-targeted role, and the specific mechanism remained to be further studied. The remaining compounds targeting key genes were poorly studied.

4. Discussion

Globally, GC is the third most common malignancy as well as the sixth most common cause of death [1]. The recent research showed that more than half of newly diagnosed patients were from developing countries (Eastern Europe, East Asia, and Central and South America) [22]. GC can occur due to a number of risk factors, including exposure to chemical carcinogens, environmental factors, genetic susceptibility, poor diet, and excessive alcohol intake [23]. However, infection with *H. pylori* remains the main cause of GC induction [24]. Despite the rapid development of targeted therapies and immunotherapies in recent years, there was still a lack of clinical effectiveness in treating some patients with GC [25]. It would be beneficial if more methods and targets could be found for treating GC. Based on transcriptome data analysis, our study identified DEGs associated with the occurrence and progression of *H. pylori*-associated GC, and provided some potential targets for the treatment of *H. pylori*-associated GC. Based on the GSE13195 and TCGA-STAD datasets, we identified five key genes, FCER1G, MRPL14, SOSTDC1, TYROBP, and C3, which presented different expression patterns in *H. pylori*-associated GC and normal tissues, where *C*3 may affect the prognosis of GC patients.

FCER1G is located on chromosome 1q23.3 and encodes the gamma subunit of the crystalline (Fc) region (Fc *R*) of an immunoglobulin fragment involved in various immune responses such as phagocytosis and cytokine release [26, 27]. Cellular effector functions are activated by the interaction between the Fc of immunoglobulins and the Fc *R* of immune cells, which in turn trigger destructive inflammation, immune cell activation, phagocytosis, oxidative burst, and cytokine release [28, 29]. FCER1G was implicated in the progression of several cancers, such as squamous cell carcinoma, multiple myeloma, and clear cell renal cell carcinoma [27, 29, 30]. In renal cancer, the high expression of FCER1G may be a functional basis for the induction of *M*2 macrophages by the increased secretion of IL-4. In addition,

*M*2 macrophages can acquire their tumor suppressor function in part by suppressing cytotoxic *T* cells. This may explain the relevance of FCER1G to macrophage and *T* cell function [31]. These findings were consistent with our results that high expression of FCER1G was positively correlated with infiltration of *M*2 macrophages and negatively correlated with CD8 *T* cells.

MRPL14 is a highly conserved protein. One protein-binding site and two RNA-binding sites are located in the *C*-terminal region of MRPL14, which consists of a five-stranded beta barrel and two small alpha helices [32]. MRPL14 was found to be closely related to mitochondrial metabolism [33]. The conserved interaction of C7orf30 with MRPL14 promoted biogenesis of the mitochondrial large ribosomal subunit and mitochondrial translation [32]. However, research on the role of MRPL14 in cancers is currently still blank.

SOSTDC1 is a secreted protein with a glycosylated *N*-terminus that contains a *C*-terminal cysteine knot domain [34]. SOSTDC1 negatively regulates BMP (bone morphogenetic protein) signaling during cell proliferation, differentiation, and apoptosis, and also regulates various processes in development and cancer by regulating the Wnt pathway [35, 36]. Researchers have found that a lack of SOSTDC1 in GC patients was associated with a shorter survival rate. In gastric cancer, SOSTDC1 acts like a tumor suppressor, and its silencing can promote tumor growth and lung metastasis. SOSTDC1 significantly inhibits the SMAD-dependent BMP pathway, c-Jun activation, and transcription of c-Jun downstream targets [37]. In addition, SOSTDC1 regulates NK cell maturation and Ly49 receptor expression from nonhematopoietic and hematopoietic sources in a cellular-exogenous manner [38]. This seems to be contrary to the results we obtained in *H. pylori*-associated GC tissues, which needs to be further explored in the follow-up studies.

TYROBP, also known as DAP12, can noncovalently bind to activating receptors on the surface of various immune cells and mediate signal transduction and cell activation [39, 40]. There was evidence that patients with GC who overexpressed TYROBP had a poorer survival rate. Furthermore, TYROBP can stimulate macrophage activation, regulate tumor necrosis factor production, and induce tolerance [41]. TYROBP is involved in the interaction between tumor cells and macrophage *M*2 to enhance TGF-β secretion *in vitro* [42]. Our research partially confirmed this, but this part of the results still needs to be verified with large samples later.

Complement is an important part of the innate immune system. Previously, it was thought to be a network of proteins that released inflammatory mediators in response to microbial invasion [43]. A growing number of studies have shown that complement activation in the tumor microenvironment can delay local *T*-cell immunosuppression and chronic inflammation, thereby promoting tumor-promoting effects, ultimately promoting tumor immune escape, growth, and distant metastasis [44, 45]. *C*3 and downstream signaling molecules are involved in multiple biological processes of tumor cells, including tumor cell anchoring,

TABLE 1: Potential targeted drugs of key genes.

Genes	Potential drugs	Drug group	Actions
FCER1G	Benzylpenicilloyl polylysine	Approved	Agonist
	Fostamatinib	Approved, investigational	Inhibitor
TYROBP	Dasatinib	Approved, investigational	Multitarget

proliferation, tumor-associated angiogenesis, matrix remodeling, migration, and invasion [46–48]. In GC, monocytes, TAMs, M2 macrophages, DCs, Tregs, and T cell exhaustion were significantly associated with C3 expression. An immunotherapeutic approach based on C3 could provide a potential biological target for GC [49].

Although we identified and confirmed 5 key genes that were highly correlated with the progression of *H. pylori*-associated GC, we were unable to perform multifaceted validation due to the small sample size of GSE13195 and the lack of studies of the same type. In addition, we did not perform experimental tests on key genes. It is critical to conduct larger sample studies as well as multicenter clinical trials to gain a deeper understanding of how genes are involved in *H. pylori*-associated gastric cancer.

5. Conclusion

In conclusion, we identified five key genes, FCER1G, MRPL14, SOSTDC1, TYROBP, and C3, associated with the occurrence of GC in *H. pylori* infection. Among them, *H. pylori*-associated GC patients with higher C3 expression had worse prognosis than those with lower expression. In addition, in the future, *H. pylori*-associated GC may be diagnosed and treated precisely by biomarkers and therapeutic targets related to these key genes.

Data Availability

The datasets used and/or analyzed during the current study are available from the corresponding author upon reasonable request.

Conflicts of Interest

The authors declare that they have no conflicts of interest.

Authors' Contributions

DW and TY conceived and designed the project; DW, ZL, and YZP acquired the data; DW, XWB, and XXZ analyzed and interpreted the data; DW, JH, and YN wrote the paper. All authors contributed to the study and approved the submitted version. Wei Ding, Huaji Jiang, and Nianyuan Ye contributed equally to this work.

Acknowledgments

Supplementary Materials

Figure S1. Association of ADAM28, FCER1G, MROL14, SOSTDC1, TYROBP, and C1QC genes with overall survival of patients with GC. (*Supplementary Materials*)

References

[1] H. Sung, J. Ferlay, R. L. Siegel et al., "Global cancer statistics 2020: GLOBOCAN estimates of incidence and mortality worldwide for 36 cancers in 185 countries," *CA: A Cancer Journal for Clinicians*, vol. 71, no. 3, pp. 209–249, 2021.

[2] W. Chen, R. Zheng, P. D. Baade et al., "Cancer statistics in China, 2015," *CA: A Cancer Journal for Clinicians*, vol. 66, no. 2, pp. 115–132, 2016.

[3] A. Högner and M. Moehler, "Immunotherapy in gastric cancer," *Current Oncology*, vol. 29, no. 3, pp. 1559–1574, 2022.

[4] F. M. Johnston and M. Beckman, "Updates on management of gastric cancer," *Current Oncology Reports*, vol. 21, no. 8, p. 67, 2019.

[5] E. C. Smyth, M. Nilsson, H. I. Grabsch, N. C. van Grieken, and F. Lordick, "Gastric cancer," *The Lancet*, vol. 396, no. 10251, pp. 635–648, 2020.

[6] E. A. Ashley, "The precision medicine initiative: a new national effort," *JAMA*, vol. 313, no. 21, pp. 2119-2120, 2015.

[7] J. Matsuzaki, H. Tsugawa, and H. Suzuki, "Precision medicine approaches to prevent gastric cancer," *Gut and Liver*, vol. 15, no. 1, pp. 3–12, 2021.

[8] A. O'Connor, C. A. O'Morain, and A. C. Ford, "Population screening and treatment of *Helicobacter pylori* infection," *Nature Reviews Gastroenterology & Hepatology*, vol. 14, no. 4, pp. 230–240, 2017.

[9] A. C. Ford, Y. Yuan, and P. Moayyedi, "*Helicobacter pylori* eradication therapy to prevent gastric cancer: systematic review and meta-analysis," *Gut*, vol. 69, no. 12, pp. 2113–2121, 2020.

[10] R. M. Peek Jr. and J. E. Crabtree, "Helicobacter infection and gastric neoplasia," *The Journal of Pathology*, vol. 208, no. 2, pp. 233–248, 2006.

[11] P. Correa, "Human gastric carcinogenesis: a multistep and multifactorial process--first American cancer society award lecture on cancer epidemiology and prevention," *Cancer Research*, vol. 52, no. 24, pp. 6735–6740, 1992.

[12] M. J. Blaser and J. C. Atherton, "*Helicobacter pylori* persistence: biology and disease," *Journal of Clinical Investigation*, vol. 113, no. 3, pp. 321–333, 2004.

[13] R. Zappasodi, T. Merghoub, and J. D. Wolchok, "Emerging concepts for immune checkpoint blockade-based combination therapies," *Cancer Cell*, vol. 34, no. 4, p. 690, 2018.

[14] T. Wu and Y. Dai, "Tumor microenvironment and therapeutic response," *Cancer Letters*, vol. 387, pp. 61–68, 2017.

[15] E. Clough and T. Barrett, "The gene expression Omnibus database," *Methods in Molecular Biology*, vol. 1418, pp. 93–110, 2016.

[16] W. Shen, Z. Song, X. Zhong et al., "Sangerbox: a comprehensive, interaction-friendly clinical bioinformatics analysis platform," *iMeta*, vol. 1, no. 3, p. e36, 2022.

[17] B. T. Sherman, M. Hao, J. Qiu et al., "DAVID: a web server for functional enrichment analysis and functional annotation of gene lists (2021 update)," *Nucleic Acids Research*, vol. 50, no. 1, pp. W216–W221, 2022.

[18] P. Langfelder and S. Horvath, "WGCNA: an R package for weighted correlation network analysis," *BMC Bioinformatics*, vol. 9, no. 1, p. 559, 2008.

[19] D. S. Chandrashekar, S. K. Karthikeyan, P. K. Korla et al., "UALCAN: an update to the integrated cancer data analysis platform," *Neoplasia*, vol. 25, pp. 18–27, 2022.

[20] B. Chen, M. S. Khodadoust, C. L. Liu, A. M. Newman, and A. A. Alizadeh, "Profiling tumor infiltrating immune cells with CIBERSORT," *Methods in Molecular Biology*, vol. 1711, pp. 243–259, 2018.

[21] D. S. Wishart, C. Knox, A. C. Guo, S. Shrivastava, M. Hassanali, and P. Stothard, "DrugBank: a comprehensive resource for in silico drug discovery and exploration," *Nucleic Acids Research*, vol. 34, no. 90001, pp. D668–D672, 2006.

[22] M. Tyczyńska, P. Kędzierawski, K. Karakuła et al., "Treatment strategies of gastric cancer-molecular targets for anti-angiogenic therapy: a state-of-the-art review," *Journal of Gastrointestinal Cancer*, vol. 52, no. 2, pp. 476–488, 2021.

[23] J. Baj, A. Forma, M. Sitarz et al., "*Helicobacter pylori* virulence factors-mechanisms of bacterial pathogenicity in the gastric microenvironment," *Cells*, vol. 10, no. 1, p. 27, 2020.

[24] M. Pucułek, J. Machlowska, R. Wierzbicki, J. Baj, R. Maciejewski, and R. Sitarz, "*Helicobacter pylori* associated factors in the development of gastric cancer with special reference to the early-onset subtype," *Oncotarget*, vol. 9, no. 57, pp. 31146–31162, 2018.

[25] S. S. Joshi and B. D. Badgwell, "Current treatment and recent progress in gastric cancer," *CA: A Cancer Journal for Clinicians*, vol. 71, no. 3, pp. 264–279, 2021.

[26] M. Tsuji, Y. Ezumi, M. Arai, and H. Takayama, "A novel association of Fc receptor gamma-chain with glycoprotein VI and their co-expression as a collagen receptor in human platelets," *Journal of Biological Chemistry*, vol. 272, no. 38, pp. 23528–23531, 1997.

[27] L. Fu, Z. Cheng, F. Dong et al., "Enhanced expression of FCER1G predicts positive prognosis in multiple myeloma," *Journal of Cancer*, vol. 11, no. 5, pp. 1182–1194, 2020.

[28] P. Andreu, M. Johansson, N. I. Affara et al., "FcRγ activation regulates inflammation-associated squamous carcinogenesis," *Cancer Cell*, vol. 17, no. 2, pp. 121–134, 2010.

[29] S. Kraft and J. P. Kinet, "New developments in FcεRI regulation, function and inhibition," *Nature Reviews Immunology*, vol. 7, no. 5, pp. 365–378, 2007.

[30] L. Chen, L. Yuan, Y. Wang et al., "Co-expression network analysis identified FCER1G in association with progression and prognosis in human clear cell renal cell carcinoma," *International Journal of Biological Sciences*, vol. 13, no. 11, pp. 1361–1372, 2017.

[31] K. Dong, W. Chen, X. Pan et al., "FCER1G positively relates to macrophage infiltration in clear cell renal cell carcinoma and contributes to unfavorable prognosis by regulating tumor immunity," *BMC Cancer*, vol. 22, no. 1, p. 140, 2022.

[32] S. Fung, T. Nishimura, F. Sasarman, and E. A. Shoubridge, "The conserved interaction of C7orf30 with MRPL14 promotes biogenesis of the mitochondrial large ribosomal subunit and mitochondrial translation," *Molecular Biology of the Cell*, vol. 24, no. 3, pp. 184–193, 2013.

[33] C. Jacques, D. Guillotin, J. F. Fontaine et al., "DNA microarray and miRNA analyses reinforce the classification of follicular thyroid tumors," *Journal of Clinical Endocrinology and Metabolism*, vol. 98, no. 5, pp. E981–E989, 2013.

[34] M. Yanagita, "BMP antagonists: their roles in development and involvement in pathophysiology," *Cytokine & Growth Factor Reviews*, vol. 16, no. 3, pp. 309–317, 2005.

[35] M. Yanagita, M. Oka, T. Watabe et al., "USAG-1: a bone morphogenetic protein antagonist abundantly expressed in the kidney," *Biochemical and Biophysical Research Communications*, vol. 316, no. 2, pp. 490–500, 2004.

[36] K. B. Lintern, S. Guidato, A. Rowe, J. W. Saldanha, and N. Itasaki, "Characterization of wise protein and its molecular mechanism to interact with both Wnt and BMP signals," *Journal of Biological Chemistry*, vol. 284, no. 34, pp. 23159–23168, 2009.

[37] R. A. Bartolomé, L. Pintado-Berninches, M. Jaén, V. de Los Ríos, J. I. Imbaud, and J. I. Casal, "SOSTDC1 promotes invasion and liver metastasis in colorectal cancer via interaction with ALCAM/CD166," *Oncogene*, vol. 39, no. 38, pp. 6085–6098, 2020.

[38] A. J. Millan, S. R. Elizaldi, E. M. Lee et al., "Sostdc1 regulates NK cell maturation and cytotoxicity," *The Journal of Immunology*, vol. 202, no. 8, pp. 2296–2306, 2019.

[39] L. L. Lanier, B. Corliss, J. Wu, and J. H. Phillips, "Association of DAP12 with activating CD94/NKG2C NK cell receptors," *Immunity*, vol. 8, no. 6, pp. 693–701, 1998.

[40] J. Dietrich, M. Cella, M. Seiffert, H. J. Bühring, and M. Colonna, "Cutting edge: signal-regulatory protein beta 1 is a DAP12-associated activating receptor expressed in myeloid cells," *The Journal of Immunology*, vol. 164, no. 1, pp. 9–12, 2000.

[41] J. Jiang, Y. Ding, M. Wu et al., "Identification of TYROBP and C1QB as two novel key genes with prognostic value in gastric cancer by network analysis," *Frontiers Oncology*, vol. 10, p. 1765, 2020.

[42] R. Takamiya, K. Ohtsubo, S. Takamatsu, N. Taniguchi, and T. Angata, "The interaction between Siglec-15 and tumor-associatedsialyl-Tn antigen enhances TGF-β secretion from monocytes/macrophages through the DAP12-Syk pathway," *Glycobiology*, vol. 23, no. 2, pp. 178–187, 2013.

[43] D. Ricklin, G. Hajishengallis, K. Yang, and J. D. Lambris, "Complement: a key system for immune surveillance and homeostasis," *Nature Immunology*, vol. 11, no. 9, pp. 785–797, 2010.

[44] M. M. Markiewski, R. A. DeAngelis, F. Benencia et al., "Modulation of the antitumor immune response by complement," *Nature Immunology*, vol. 9, no. 11, pp. 1225–1235, 2008.

[45] E. Bonavita, S. Gentile, M. Rubino et al., "PTX3 is an extrinsic oncosuppressor regulating complement-dependent inflammation in cancer," *Cell*, vol. 160, no. 4, pp. 700–714, 2015.

[46] R. Pio, L. Corrales, and J. D. Lambris, "The role of complement in tumor growth," *Advances in Experimental Medicine and Biology*, vol. 772, pp. 229–262, 2014.

[47] D. Ajona, S. Ortiz-Espinosa, and R. Pio, "Complement anaphylatoxins C3a and C5a: emerging roles in cancer

progression and treatment," *Seminars in Cell & Developmental Biology*, vol. 85, pp. 153–163, 2019.

[48] E. S. Reis, D. C. Mastellos, D. Ricklin, A. Mantovani, and J. D. Lambris, "Complement in cancer: untangling an intricate relationship," *Nature Reviews Immunology*, vol. 18, no. 1, pp. 5–18, 2018.

[49] D. Bao, C. Zhang, L. Li et al., "Integrative analysis of complement system to prognosis and immune infiltrating in colon cancer and gastric cancer," *Frontiers Oncology*, vol. 10, p. 553297, 2020.

Research Article

Metformin Suppresses Hepatocellular Carcinoma through Regulating Alternative Splicing of LGR4

Han Zhuo [ID],[1] **Shuying Miao** [ID],[2] **Zhenquan Jin** [ID],[3] **Deming Zhu** [ID],[1] **Zhenggang Xu** [ID],[1] **Dongwei Sun** [ID],[1] **Jie Ji** [ID],[4] and **Zhongming Tan** [ID][1]

[1]*Hepatobiliary Center, The First Affiliated Hospital of Nanjing Medical University, Nanjing, Jiangsu, China*
[2]*Department of Pathology, Nanjing Drum Tower Hospital, The Affiliated Hospital of Nanjing University Medical School, Nanjing, Jiangsu, China*
[3]*The First Clinical Medical College of Nanjing Medical University, Nanjing, Jiangsu, China*
[4]*Jiangsu Breast Disease Center, The First Affiliated Hospital of Nanjing Medical University, Nanjing, Jiangsu, China*

Correspondence should be addressed to Jie Ji; jieji1989@foxmail.com and Zhongming Tan; tanzhongming@njmu.edu.cn

Background and aims. Hepatocellular carcinoma (HCC) is one of the most common causes of cancer-related deaths worldwide. The role of leucine-rich repeats containing G protein-coupled receptor 4 (LGR4) in HCC remains unclear. Metformin can prevent and control the development of a variety of cancers, especially in HCC. Alternative splicing (AS) can produce many cancer-driving genes. We aim to uncover that metformin regulates HCC development through alternative splicing of LGR4. *Methods*. First, the expression of LGR4 in HCC tumor tissues and cell lines was detected by western blotting and immunofluorescence. The ability of cell proliferation, migration, and invasion was detected with CCK8, wound-healing, and transwell assays when overexpressing LGR4 or treating with metformin. The β-catenin expression was detected by immunofluorescence. In order to investigate novel AS-associated LGR4, we discarded LGR4 isoforms from GSO databases. We used siRNA to knock down the specific isoform to check the cell proliferation, migration, and invasion when treated with metformin. *Results*. The level of LGR4 expression was higher in HCC cell lines and tumor tissues. The HCC cell proliferation, migration, and invasion were increased when over-expressing LGR4, which could be reduced by metformin treatment. The GEO database (GSE190076) showed that LGR4 had switching properties in HCC cell lines treated with metformin. We used siRNA to knock down the specific isoform, and the result showed that the specific isoform siRNA could promote the inhibition of cell invasion caused by metformin treatment. *Conclusions*. LGR4 could promote the ability of cell proliferation, migration, and invasion in HCC, which could be reduced by metformin through alternative splicing.

1. Background

Hepatocellular carcinoma is the most common type of liver cancer all over the world, especially in China [1, 2], although the treatment is still developing and includes surgery, transplantation, and local therapies. Drug therapy is also applied in clinics [2, 3]. However, the mechanism of HCC is still unclear. Metformin is a dimethyl biguanide to treat type 2 diabetes mellitus (T2DM) with few side effects. Metformin can be used to treat many types of cancer, including colorectal [4] and prostate cancers [5]. In HCC, metformin could regulate the expression of FOXO3 by apoptosis and pyroptosis to inhibit the development of hepatocellular carcinoma [6].

LGR4 belongs to the GPCRs superfamily and is recognized as a trans-membrane receptor of the LGR family. Recently, a study indicated that LGR4 could interact with PrPc to promote tumorigenesis and liver metastasis by stemness of colorectal cancer stem cells [7]. In acute myeloid leukemia, RSPO3-LGR4 signaling could be recognized as a target for treatment [8]. It also can be related to poor prognosis in ovarian cancer [9]. However, the function of

LGR4 is still unclear. Alternative splicing could produce multiple transcripts of mRNA to regulate the gene expression. An MTA1 splicing switch can be regulated by RALY to activate the cholesterol-related pathway in hepatocellular carcinoma [10]. The alternative splicing could also be regulated by DDX17 and produce a PXN-AS1 isoform in HCC. However, whether metformin could regulate gene alternative splicing is still unclear.

In our research, we investigated the function of LGR4 in the HCC, and we also found that metformin could reduce the expression of LGR4. We also indicated the mechanism of the regulatory effect of metformin. The study could provide evidence of LGR4 function, which could be recognized as a target for HCC treatment.

2. Methods

2.1. Cell Culture and Treatment. Normal cell lines (L02) and Huh-7 and HepG3B cell lines were obtained from the American Type Culture Collection (ATCC). All cells were cultured in DMEM (Invitrogen, USA) with FBS (10%), in an atmosphere containing 5% CO_2 at 37°C. The HCC cell lines were treated with metformin (20 μM) [6]. The HCC cell lines were transfected with PcDNA-LGR4 (Genewiz, China) and siRNA-LGR4 (GenePharma, China) by using Lipo 3000 (Thermo, USA). siRNA-LGR4 sequence: UGGAUGCCG CUCAUCCUAAAG.

2.2. CCK-8 Assay. According to the previous procedure [11], the treated cells were added into wells with a proper density. Two days later, the cell counting kit-8 (CCK-8) reagent was added to the wells for 2 hours. We determined the optical density (OD) at 450 nm using a multimode microplate reader.

2.3. Cell Invasion Assay. The treated cells were digested and added into the top chambers of transwell inserts with FBS-free DMEM. The cell density is 2×10^5 cells per well. And DMEM (10% FBS) was cultured in the bottom chambers. After 6 hours, 4% paraformaldehyde was used to fix the inserts and stain them with 0.1% crystal violet solution. Also, the images were obtained under a microscope.

2.4. Wound Healing Assay. The treated cells were digested and cultured in 6-well plates. After treatment, a 200 μL pipette tip was used to scratch, cells were washed, and the cell was incubated with DMEM for another 12 hours. Three random areas were photographed to assess the distance of migration.

2.5. Western Blotting. According to the previous procedure [11], proteins were isolated in RIPA buffer containing phosphatase and protease inhibitors (Roche, US). Equal total proteins were separated by SDS/PAGE gels to blot onto PVDF membranes (Millipore, USA). After blocking, the bands were incubated with an anti- LGR4 antibody (ab75501; Abcam). Finally, the blot was observed via the ECL detection system.

2.6. Immunofluorescence Assay. For β-catenin staining, the treated cells were washed with PBS three times and fixed, then treated with 0.1% Triton X (Beyotime, China). Subsequently, a blocking buffer was added and the primary antibody was incubated overnight at 4°C. The next day, the treated cells were incubated with a secondary antibody, then treated with DAPI. Finally, the images were captured by a microscope.

2.7. Bioinformatic Analysis. The GEO database (GSE190076) was used to indicate the different gene expressions. Then, the transcript was analyzed with an isoform switch analyser. A total of 480 genes underwent isoform switching. KEGG pathway analysis was also used to analyze the genes' function.

2.8. Statistical Analysis. All measurements were presented as the mean ± standard deviations (SD) from three independent experiments. Statistical significance was defined as a p value < 0.05. Differences were determined using a two-way analysis of variance (ANOVA) or unpaired Student's t-test by Prism software.

3. Results

3.1. LGR4 was Increased in HCC Tissues and Cell Lines. First, the level of LGR4 expression was detected in HCC tissues. It showed that LGR4 expression was increased in the tumor tissues (Figure 1(a)). We also used immunofluorescence to check the expression of LGR4, and it showed the same results (Figure 1(b)). Then, we checked the LGR4 expression in the HCC cell lines. The LGR4 expression was increased in Huh-7 and HepG3B cell lines (Figure 1(c)). It indicated that LGR4 expression was upregulated in tissues and at cell levels. Multivariate Cox analysis revealed that the expression of LGR4 in HCC tissues could be acting as an independent prognostic factor in HCC patients (Figure 1(d)).

3.2. LGR4 Promoted Cell Proliferation, Migration, and Invasion. To explore the role of LGR4 in HCC cell lines, we overexpressed LGR4 to check cell proliferation, migration, and invasion in HCC cell lines. First, we used RT-qPCR to check the expression of LGR4 in overexpressed cell lines (Figure 2(a)). It demonstrated that the level of LGR4 expression was much higher, indicating the successful transfection. Then, a CCK8 assay was carried out to check the cell viability, and the result demonstrated that LGR4 could promote cell proliferation (Figure 2(b)). The wound healing assay and a transwell assay also indicated the LGR4 overexpression promoted cell migration and invasion (Figures 2(c) and 2(d)). The above result showed that LGR4 could act as an oncogene in the HCC. LGR4 could activate the wnt/β-catenin pathway in many cancers. So, the immunofluorescence indicated that the β-catenin expression was higher in the LGR4 overexpressed cells (Figure 2(e)). It indicated that the LGR4 could activate the wnt/β-catenin pathway in HCC.

(a)

(b)

(c)

(d)
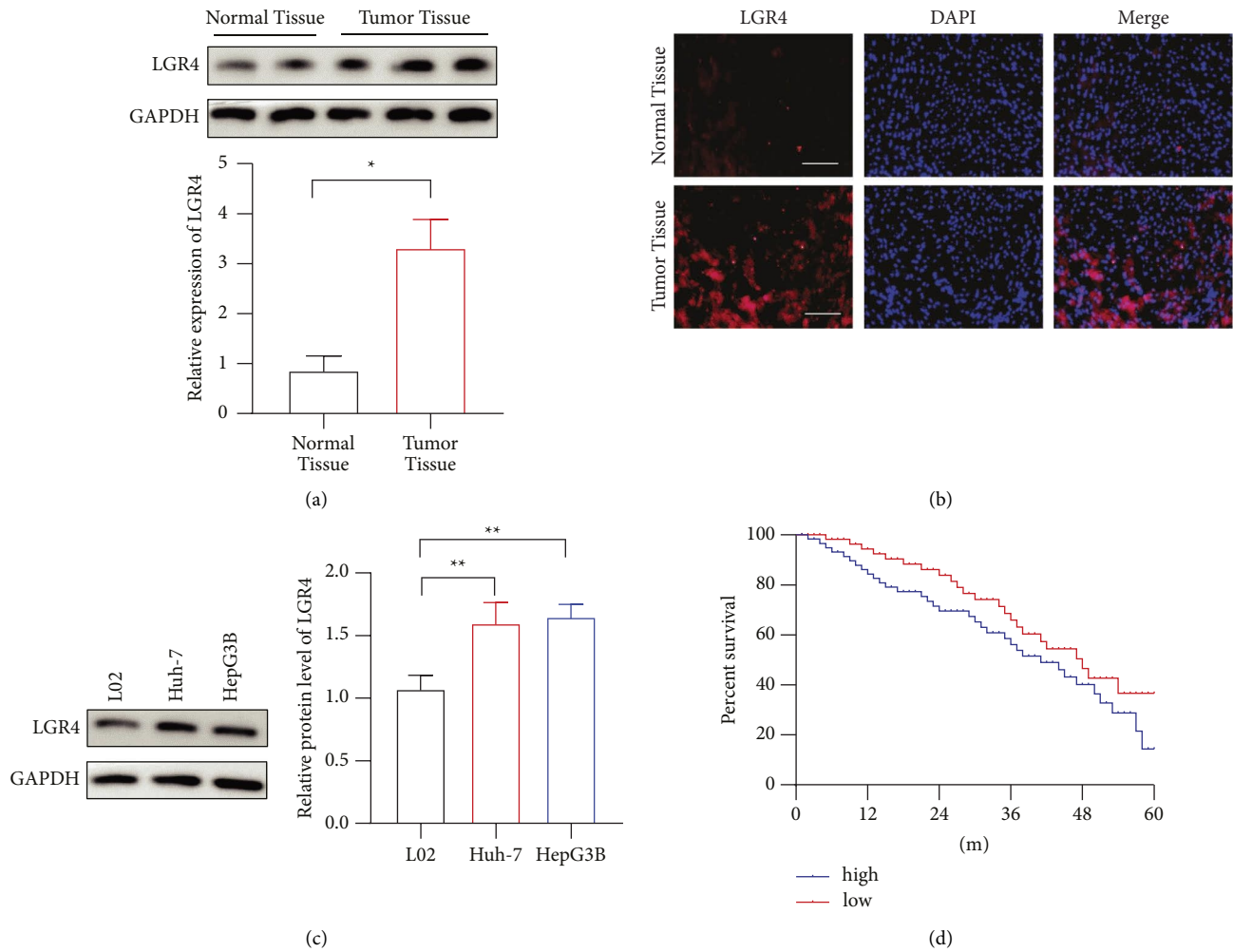
FIGURE 1: The level of LGR4 expression in HCC. (a)-(b). The level of LGR4 expression in HCC tumor tissues by western blotting and immunofluorescence. (c). The level of LGR4 expression in HCC cell lines. (d). Multivariate Cox analysis revealed that LGR4 in HCC tissues was an independent prognostic factor in HCC patients. $^*p < 0.05$, $^{**}p < 0.01$, $^{***}p < 0.001$.

3.3. Metformin Could Reduce the Cell Proliferation, Migration, and Invasion through LGR4.

Metformin, an oral hypoglycemic drug, exerts anticancer effects in many cancers, especially in HCC. To explore the effect of metformin on LGR expression, we checked LGR4 expression in HCC cell lines treated with metformin. It showed that metformin could reduce the LGR4 expression (Figure 3(a)). Then, we overexpressed LGR4 when treated with metformin to check the proliferation, migration, and invasion of cells. The results showed that metformin could reduce cell proliferation, migration, and invasion, which are counteracted by LGR4 overexpression (Figures 3(b)–3(d)). Then, we detected the expression of catenin, and it showed that metformin reduced the catenin pathway through LGR4 (Figure 3(e)).

3.4. Metformin Decreased the LGR4 Expression by Alternative Splicing.

To identify the mechanism by which LGR4 expression is regulated by metformin. We used the GEO database (GSE190076) to indicate the different gene expressions. It showed the mRNA level of LGR4 had no difference between the two groups, which meant it may be regulated by alternative splicing. Then, we analyzed transcript usage with an isoform switch analyser. A total of 480 genes underwent isoform switching (Figure 4(a)). KEGG pathway analysis also showed that the genes were enriched in spliceosome (Figure 4(b)). Interestingly, the transcript ENST00000379214 of the LGR4 gene decreased in HCC cell lines (Figure 4(c)). It indicated that metformin could reduce the level of LGR4 expression through alternative splicing.

3.5. LGR4 Switching Genes RNAi Reduce the Antitumor Effect Caused by Metformin.

Finally, we used siRNA to knock down the isoforms to observe the phenotypic change in the metformin treatment. In the CCK8 assay, it showed that metformin treatment could reduce cell proliferation, which was promoted by RNAi (Figure 5(a)). We also used the wound healing assay and the transwell assay to show that

(a)

(b)

(c)

(d)

(e)
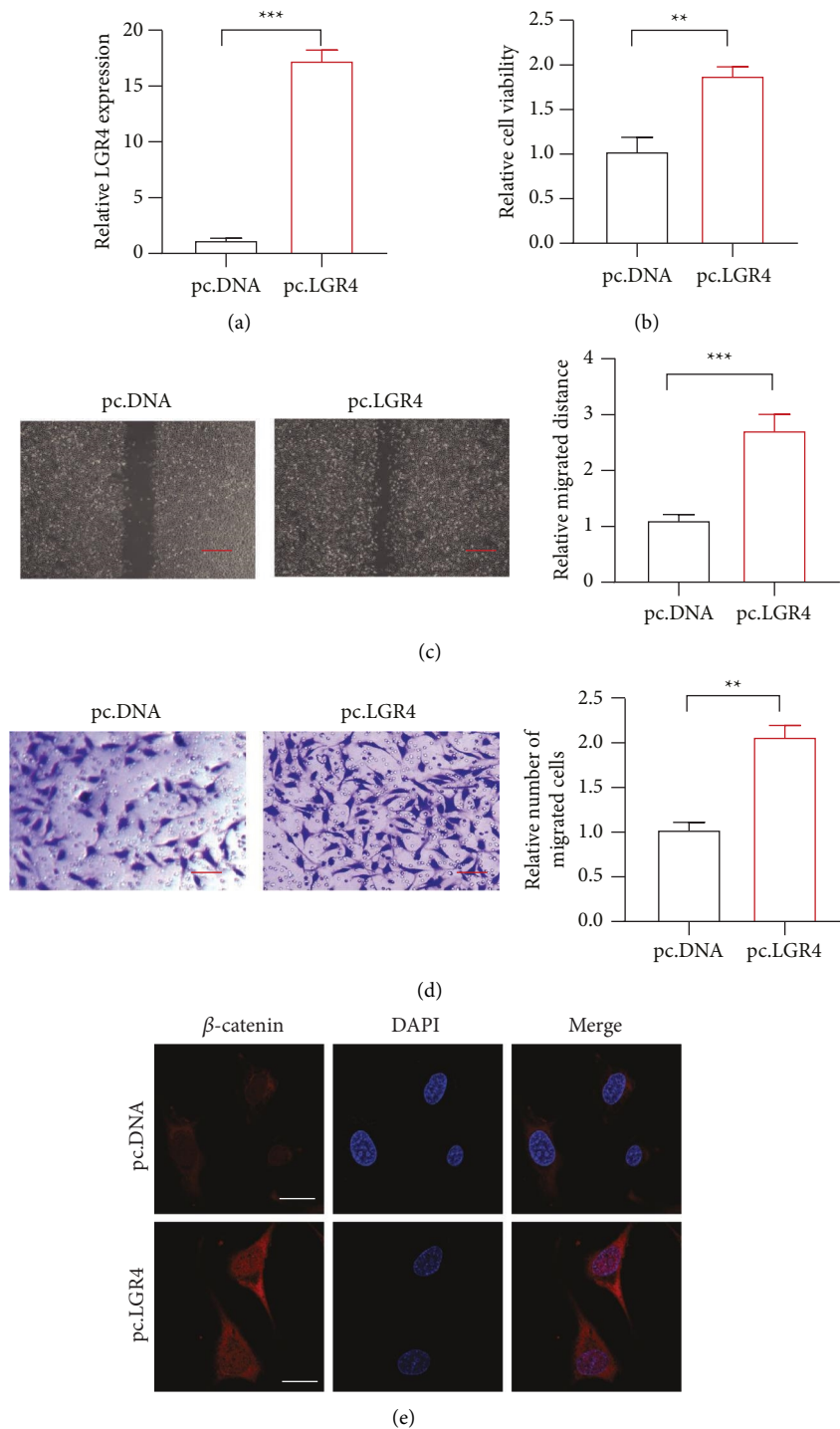
FIGURE 2: The role of LGR4 in HCC. (a) The expression of LGR4 was detected upon LGR4 overexpression. (a). The mRNA level of LGR4 in the LGR4 overexpressed cells. (b). The proliferation of HCC by LGR4 overexpression in HCC cell lines. (c). The migration of HCC by LGR4 overexpression in HCC cell lines; scar bar = 100 μm. (d). The invasion of HCC by LGR4 overexpression in HCC cell lines; scar bar = 50 μm. (e). The expression of catenin in LGR4 overexpressed HCC cell lines. $^{**}p < 0.01$, $^{***}p < 0.001$. PcDNA, an empty vector.

a specific isoform siRNA could promote the inhibition of cell migration and invasion caused by metformin treatment (Figures 5(b) and 5(c)). We also detect the β-catenin expression. It indicated that the specific isoform siRNA could also reduce the expression of catenin in response to metformin treatment (Figure 5(d)).

4. Discussion

Despite the application of surgery, transplantation, and local therapies in HCC treatment, the rate of death caused by HCC remains high. Recently, metformin, which is recognized to treat T2DM, was shown that to have antitumor

(a)

(b)

(c)

(d)

(e)
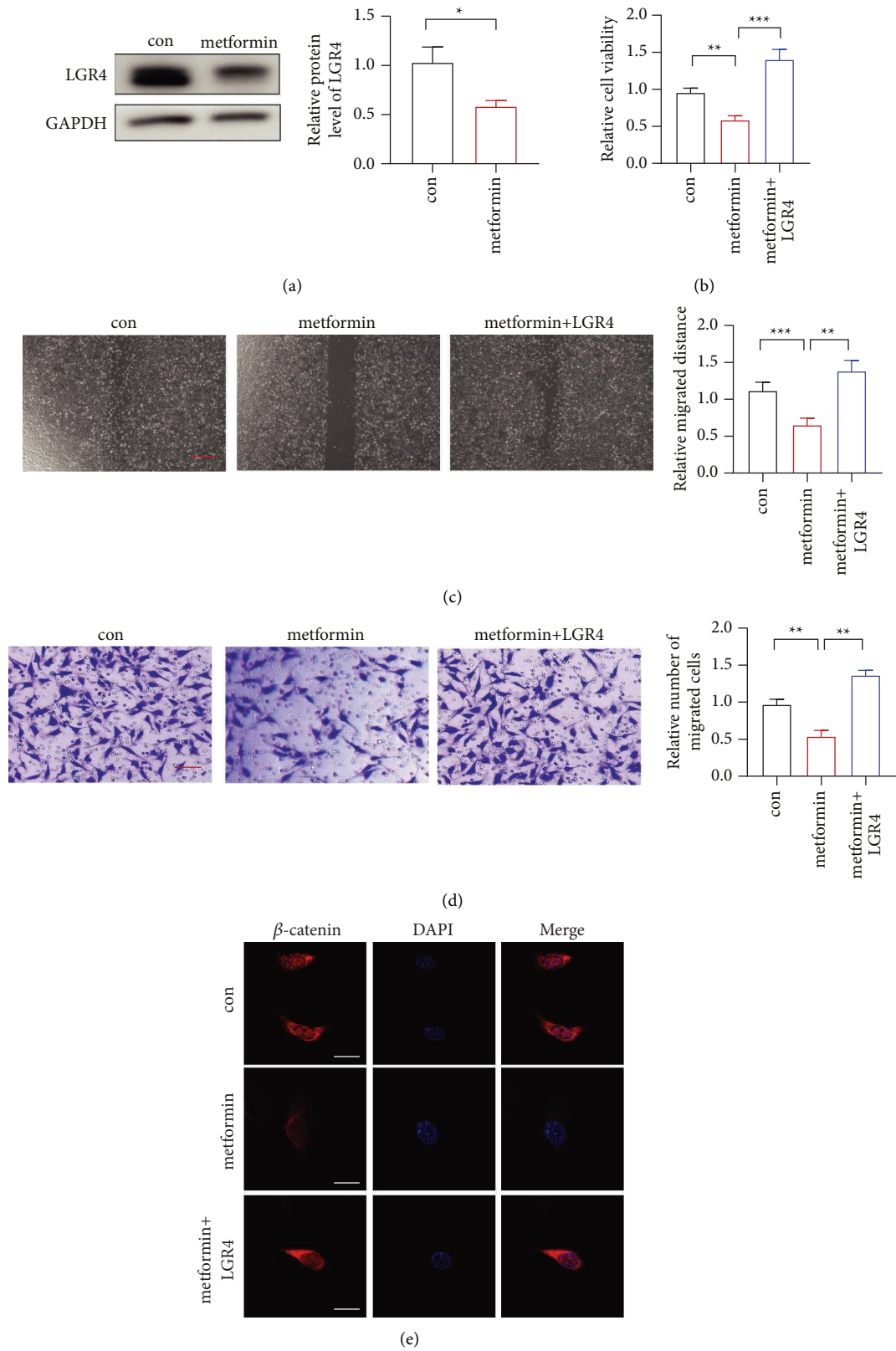
Figure 3: Metformin could reduce tumorigenesis through LGR4. (a). The expression of LGR4 was detected upon metformin treatment. (b). The proliferation of HCC by LGR4 overexpression in metformin-treated HCC cell lines. (c). The migration of HCC by LGR4 overexpression in metformin treated HCC cell lines; scar bar = 100 μm. (d). The invasion of HCC by LGR4 overexpression in metformin-treated HCC cell lines; scar bar = 50 μm. (e). The expression of catenin by LGR4 overexpression overexpressed metformin-treated HCC cell lines. $^{**}p < 0.01$, $^{***}p < 0.001$. PcDNA, an empty vector.

(a)

(b)

(c)
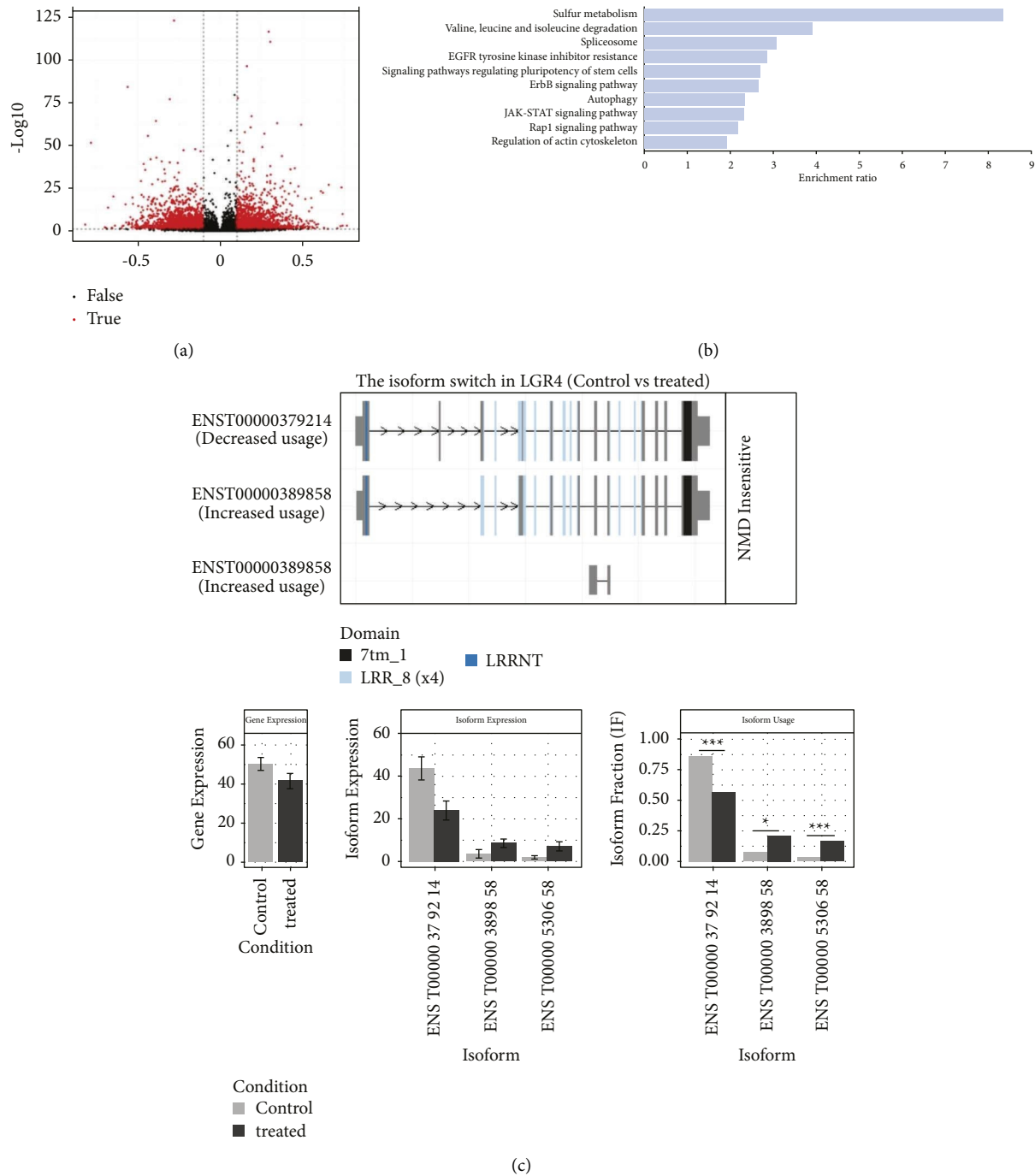
FIGURE 4: Metformin decreased the LGR4 expression by alternative splicing. (a). Volcano plots shows genes with differential transcript usage (differential isoform fraction (dIF) > 0.3 and FDR < 0.01). (b). KEGG pathways enriched for genes with differential transcript usage. (c). Visualization of switched isoform structure LGR4. Three isoforms showed differential isoform expressions, although there was no difference for the overall gene expression. Treated: metformin treatment.

effects. In colorectal cancer (CRC), the use of metformin may improve disease-free survival and overall survival in CRC patients with T2DM [12]. In bladder cancer cells, metformin improves the antitumor effect of Olaparib through the STAT3/C-MYC pathway [13]. In HCC, metformin could regulate the Hippo signaling pathway to reduce interleukin-22-induced hepatocellular carcinoma [14]. Metformin could also sensitize sorafenib-resistant HCC cells

through autophagy by AMPK activation [15]. However, the mechanism of the antitumor effect of metformin is still to be explored.

LGR4 belongs to the GPCRs superfamily and is recognized as a trans-membrane receptor of the LGR family. In this study, we found that the level of LGR4 in Huh-7 and HepG3B cell lines was much higher than that in L02 cell lines. It indicated that the LGR4 expression was increased in

(a)

(b)

(c)

(d)
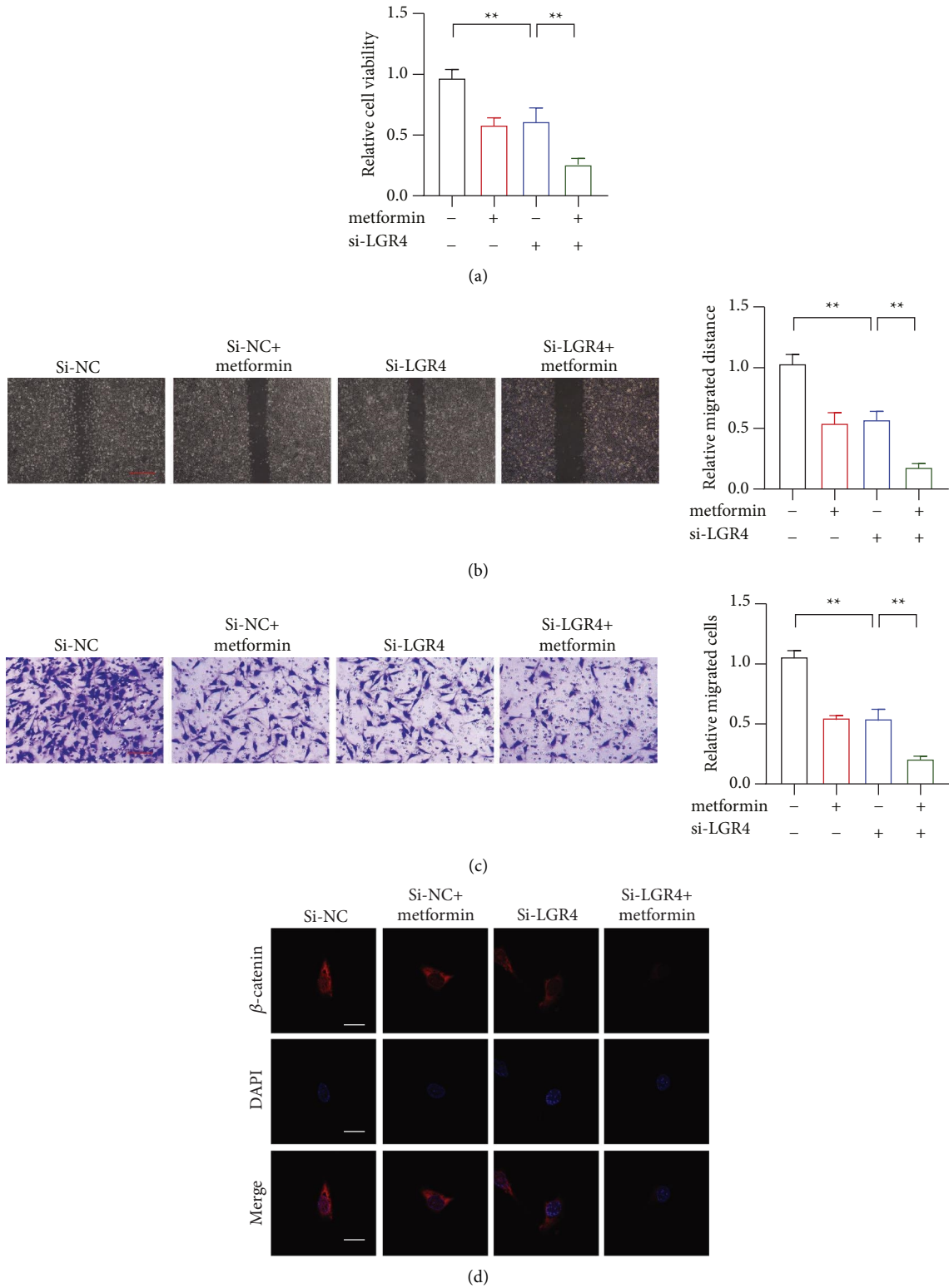
FIGURE 5: LGR4 switching genes RNAi reduces the antitumor effect caused by metformin. (a). The proliferation of HCC by LGR4 switching genes RNAi in metformin-treated HCC cell lines. (b). The migration of HCC by LGR4 switching genes RNAi in metformin-treated HCC cell lines; scar bar = 100 μm. (c). The invasion of HCC by LGR4 switching genes RNAi in metformin-treated HCC cell lines; scar bar = 50 μm. (d). The expression of catenin was induced by LGR4 switching genes by RNAi metformin-treated HCC cell lines. $^{**}p < 0.01$, $^{***}p < 0.001$. PcDNA, an empty vector.

HCC tissues and at cell levels. LGR4 overexpression could promote the processes of proliferation, migration, and invasion. Although the study indicated that Hsa_circ_0003945 could regulate the miR-34c-5p/LGR4/β-catenin axis to promote the progression of hepatocellular carcinoma [16], the exact role of LGR4 is still unclear. Mechanistically, LGR4 can activate wnt/β-catenin signaling in many diseases [16–18]. So, we detected the expression of catenin through immunofluorescence. It indicated that LGR4 overexpression could promote the catenin expression in the nucleus. Metformin treatment could inhibit the HCC tumorigenesis caused by LGR4 and also reduce the expression of β-catenin.

Alternative splicing could produce multiple transcripts of mRNA to regulate the gene expression [19]. Then, we investigated the mechanism of how metformin regulated the expression of LGR4 in HCC. We used GEO to analyze the alternative splicing. The result showed that the LGR4 gene was characterized by 3′UTR shortening upon metformin treatment in HCC cell lines. It indicated that metformin could reduce the level of LGR4 expression through alternative splicing. Finally, we used siRNA to knock down the isoforms to observe the phenotypic change in the metformin treatment. The results also showed that a specific isoform siRNA could promote the inhibition of tumorigenesis caused by metformin treatment, as well as β-catenin expression. Apart from alternative splicing, the genes also focus on sulfur metabolism pathways, and the study also indicated that sulfane sulfur metabolism could be used to treat cancers. We will also analyze sulfur metabolism in the future.

In conclusion, we demonstrated that LGR4 could promote the proliferation, migration, and invasion of HCC, which could be reduced by metformin through alternative splicing.

Data Availability

The data used to support the findings of this study are available from the corresponding author upon reasonable request.

Disclosure

Shuying Miao is the co-first author.

Conflicts of Interest

The authors declare that they have no conflicts of interest.

Authors' Contributions

Han Zhou and Shuying Miao contribute equally to this work.

Acknowledgments

References

[1] C. H. Zhang, Y. Cheng, S. Zhang, J. Fan, and Q. Gao, "Changing epidemiology of hepatocellular carcinoma in Asia," *Liver International*, vol. 42, no. 9, pp. 2029–2041, 2022.

[2] C. Wang, Y. Cao, C. Yang, R. Bernards, and W. Qin, "Exploring liver cancer biology through functional genetic screens," *Nature Reviews Gastroenterology & Hepatology*, vol. 18, no. 10, pp. 690–704, 2021.

[3] R. P. Carroll, M. Boyer, V. Gebski et al., "Immune checkpoint inhibitors in kidney transplant recipients: a multicentre, single-arm, phase 1 study," *The Lancet Oncology*, vol. 23, no. 8, pp. 1078–1086, 2022.

[4] S. Roy, Y. Zhao, Y. C. Yuan, and A. Goel, *Metformin and ICG-001 Act Synergistically to Abrogate Cancer Stem Cells-Mediated Chemoresistance in Colorectal Cancer by Promoting Apoptosis and Autophagy Cancers*, vol. 14, 2022.

[5] F. Fontana, M. Anselmi, and P. Limonta, "Exploiting the metabolic consequences of pten loss and akt/hexokinase 2 hyperactivation in prostate cancer: a new role for delta-tocotrienol," *International Journal of Molecular Sciences*, vol. 23, no. 9, p. 5269, 2022.

[6] Z. Shen, H. Zhou, A. Li et al., "Metformin inhibits hepatocellular carcinoma development by inducing apoptosis and pyroptosis through regulating FOXO3," *Aging (Albany NY)*, vol. 13, no. 18, pp. 22120–22133, 2021.

[7] Q. Cheng, H. Zheng, M. Li et al., "LGR4 cooperates with PrPc to endow the stemness of colorectal cancer stem cells contributing to tumorigenesis and liver metastasis," *Cancer Letters*, vol. 540, Article ID 215725, 2022.

[8] B. Salik, H. Yi, N. Hassan et al., "Targeting RSPO3-LGR4 signaling for leukemia stem cell eradication in acute myeloid leukemia," *Cancer Cell*, vol. 38, no. 2, pp. 263–278 e6, 2020.

[9] Z. Zeng, N. Ji, J. Yi et al., "LGR4 overexpression is associated with clinical parameters and poor prognosis of serous ovarian cancer," *Cancer Biomarkers*, vol. 28, no. 1, pp. 65–72, 2020.

[10] Y. Qiao, Q. Shi, X. Yuan et al., "RNA binding protein RALY activates the cholesterol synthesis pathway through an MTA1 splicing switch in hepatocellular carcinoma," *Cancer Letters*, vol. 538, Article ID 215711, 2022.

[11] H. Yu, C. Dai, W. Zhu, Y. Jin, and C. Wang, "PFKFB3 increases IL-1β and TNF-α in intestinal epithelial cells to promote tumorigenesis in colitis-associated colorectal cancer," *Journal of Oncology*, vol. 2022, pp. 1–8, 2022.

[12] Z. Tarhini, K. Manceur, J. Magne, M. Mathonnet, J. Jost, and N. Christou, "The effect of metformin on the survival of colorectal cancer patients with type 2 diabetes mellitus," *Scientific Reports*, vol. 12, no. 1, Article ID 12374, 2022.

[13] B. J. Chi, Y. Sun, L. L. Quan, J. T. Zhao, B. Wei, and S. Q. Wang, "Metformin can enhance the inhibitory effect of Olaparib in bladder cancer cells," *Disease Markers*, vol. 2022, pp. 1–10, 2022.

[14] D. Zhao, L. Xia, W. Geng et al., "Metformin suppresses interleukin-22 induced hepatocellular carcinoma by upregulating Hippo signaling pathway," *Journal of Gastroenterology and Hepatology*, vol. 36, no. 12, pp. 3469–3476, 2021.

[15] H. Y. Lai, H. H. Tsai, C. J. Yen et al., "Metformin resensitizes sorafenib-resistant HCC cells through AMPK-dependent autophagy activation," *Frontiers in Cell and Developmental Biology*, vol. 8, Article ID 596655, 2020.

[16] L. H. Lyu, C. Y. Zhang, W. J. Yang et al., "Hsa_circ_0003945 promotes progression of hepatocellular carcinoma by mediating miR-34c-5p/LGR4/β-catenin axis activity," *Journal of*

Cellular and Molecular Medicine, vol. 26, no. 8, pp. 2218–2229, 2022.

[17] Y. Y. Yang, Y. M. Zhou, J. Z. Xu et al., "Lgr4 promotes aerobic glycolysis and differentiation in osteoblasts via the canonical Wnt/β -catenin pathway," *Journal of Bone and Mineral Research*, vol. 36, no. 8, pp. 1605–1620, 2021.

[18] A. Ordaz-Ramos, V. H. Rosales-Gallegos, J. Melendez-Zajgla, V. Maldonado, and K. Vazquez-Santillan, "The role of LGR4 (GPR48) in normal and cancer processes," *International Journal of Molecular Sciences*, vol. 22, no. 9, p. 4690, 2021.

[19] J. Jeon, K. T. Kim, J. Choi et al., "Alternative splicing diversifies the transcriptome and proteome of the rice blast fungus during host infection," *RNA Biology*, vol. 19, no. 1, pp. 373–386, 2022.

Research Article

Identification of Key Genes in the HBV-Related HCC Immune Microenvironment Using Integrated Bioinformatics Analysis

Wei Ding [ID],[1,2,3] Zheng Zhang,[1,2] Nianyuan Ye,[1,2] Ling Zhuang,[1,2] Zhiping Yuan,[4] Wenbo Xue [ID],[1,2] Yulin Tan [ID],[1,2] and Xuezhong Xu [ID][1,2]

[1]Department of General Surgery, Wujin Hospital Affiliated to Jiangsu University, Changzhou 213017, China
[2]Department of General Surgery, The Wujin Clinical College of Xuzhou Medical University, Changzhou 213017, China
[3]Changzhou Key Laboratory of Molecular Diagnostics and Precision Cancer Medicine, Changzhou 213017, China
[4]Department of Gastroenterology, Wujin Hospital Affiliated with Jiangsu University, Changzhou 213017, China

Correspondence should be addressed to Wenbo Xue; xwbdoctor@163.com, Yulin Tan; tanyldoctor@163.com, and Xuezhong Xu; xxzdoctor@163.com

Wei Ding, Zheng Zhang, Nianyuan Ye, and Zhiping Yuan contributed equally to this work.

Purpose. Hepatocellular carcinoma (HCC) has poor prognosis and high mortality among gastrointestinal tumors because of its insidious onset and strong invasiveness. However, there was little understanding of their pathogenesis. The purpose of this study was to use bioinformatics analysis to identify genes associated with the immune microenvironment in HBV-related HCC and to develop new therapeutic targets to prevent and treat cancer. *Methods*. RNA-seq data of HBV-related HCC cases were downloaded from TCGA-LIHC database. ESTIMATE and Deseq2 algorithms were used to screen out differentially expressed genes (DEGs). WGCNA was used to construct gene coexpression networks. In key modules, functional enrichment analysis was performed. Protein-protein interaction (PPI) was used to screen hub genes, and survival analysis was conducted to assess their prognostic significance. Following, we search for key genes differentially expressed between cancerous and paracancerous tissues in GSE136247 and GSE121248 datasets. Reveal the potential links between key genes in immune infiltration by using TIMER. Finally, in TCGA-LIHC database, integration of key genes with clinical data were used to further validate their correlation with prognosis. *Results*. In the cohort of HBV-related HCC patients, immune/stromal/ESTIMATE scores were not significantly associated with patient prognosis. After bioinformatics analysis, screening out five key genes was significantly related to the prognosis of HBV-related HCC. Downregulation of SLAMF1 and TRAF3IP3 suggested poor prognosis and was related to a variety of immune cell infiltration. Furthermore, compared with adjacent nontumor tissues, TRAF3IP3 and SLAMF1 were highly expressed in tumor tissues and were linked to tumor recurrences. *Conclusion*. In conclusion, SLAMF1 and TRAF3IP3 were identified with higher expression in tumor tissues and associated with tumor recurrence. It will be a new research direction of tumor progress and treatment.

1. Introduction

About 90% of the pathological types of liver cancer were hepatocellular carcinoma (HCC) in clinical. Both morbidity and mortality are far higher than other types of tumors [1]. Gender differences (predominant in males) and geographic differences (mainly East Asia) influence the incidence of HCC [2]. The main causative factors associated with HCC

are virus (chronic hepatitis B and C), metabolism (diabetes and nonalcoholic fatty liver disease), toxicity (alcohol and aflatoxins), and immune system-related diseases [3]. Affected by these factors, the morbidity of HCC is rising continuously year by year. According to statistics data, more than half of HCC patients in the world are infected with hepatitis B virus (HBV). It is the main risk factor for human [4]. Mortality associated with HCC is also increasing. Recent
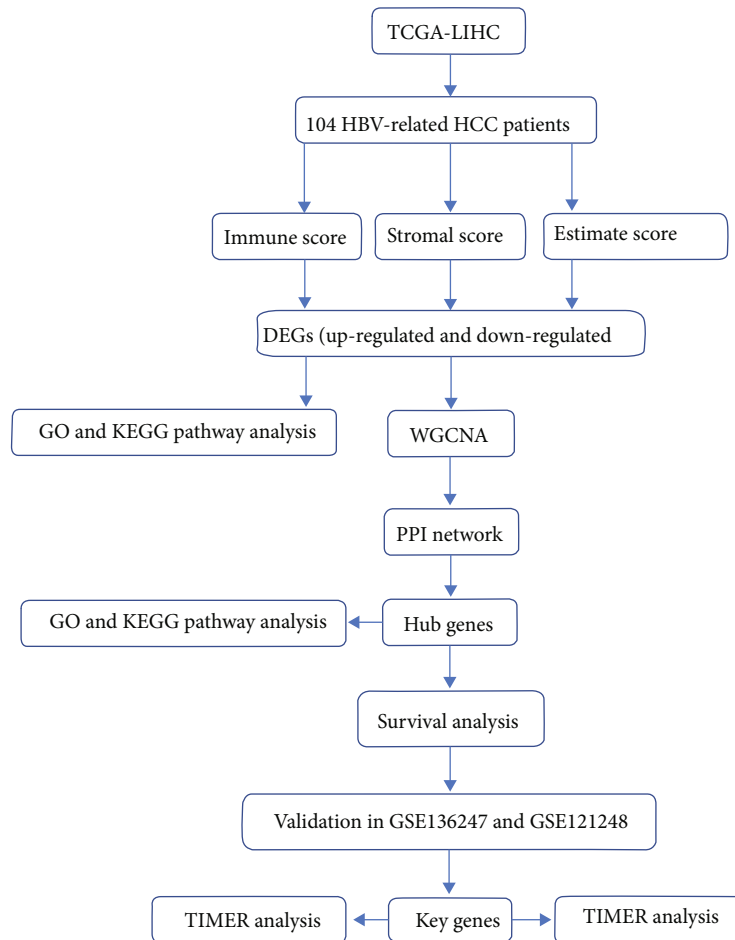
Figure 1: Flow chart of the study.

studies have shown that there were 85% of patients with cirrhosis infected with HBV, and less than 20% of people survived more than five years [5]. Reassuringly, the incidence of HCC was significantly reduced in the middle-aged population aged 30-59, largely due to the global hepatitis B virus vaccination program [6]. Liver transplantation and surgical resection are treatment options for HCC in early-stage HCC and when the tumor size is <5 cm [7]. However, because the disease is mostly asymptomatic in its early stages, most symptomatic patients are diagnosed at an advanced stage. Currently, patients with advanced HCC are mostly treated with radiofrequency ablation (RFA), transhepatic arterial chemotherapy and embolization (TACE), tyrosine kinase inhibitor (TKI), and immunotherapy, but with the emergence of drug resistance and disease recurrence, these modalities do not significantly prolong lifespan [8]. As research progresses in depth, new and diverse avenues for the treatment of HCC are being discovered.

The current study suggests that HCC is caused by HBV-induced DNA damage that triggers hepatocyte regeneration and chronic inflammation in the liver [9, 10]. The nucleocapsid of HBV-infected hepatocytes allows the virus to replicate stealthily without being recognized by type I IFN [11]. It is now widely believed that the

immune pathogenic mechanism of HCC is mainly that HBV, as a noncytopathic virus, promotes the disorder of the liver immune system and causes liver damage through abnormal immune attack. It is increasingly believed that immune pathogenesis significantly influenced the development of HBV-related HCC [12]. Although HBV was thought to contribute to HCC, there was still no clear understanding of the mechanism.

In this study, RNA-seq data and clinical feature information of HBV-related HCC patients were accessed by TCGA-LIHC. The prognosis-related DEGs and modules were screened by Sangerbox and WGCNA. In addition, Gene Ontology (GO) and Kyoto Encyclopedia of Genes and Genomes (KEGG) pathways were enriched for these DEGs and module genes and construct the PPI network to search the prognosis-related hub genes. Through the gene expression information of GSE136247 and GSE121248 in the GEO database, the possible key genes (SLAMF1 and TRAF3IP3) were finally locked. Through the TIMER database, the association between SLAMF1 and TRAF3IP3 and immune cell infiltration was analyzed. Finally, by analyzing the clinical characteristics of HBV-related HCC patients, it was confirmed that SLAMF1 and TRAF3IP3 were negatively correlated with the recurrence of patients.

(a)

(b)

(c)

(d)
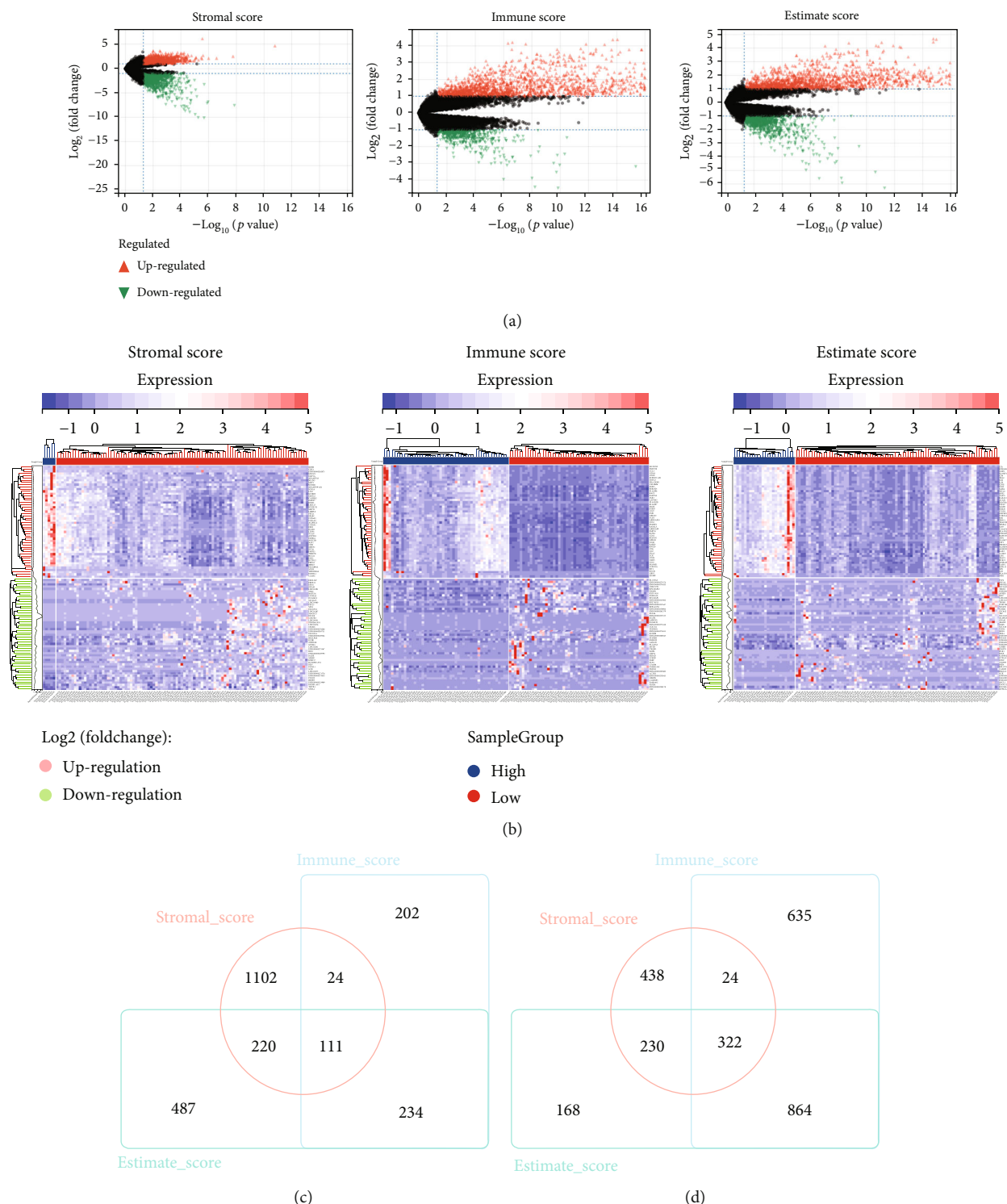
Figure 2: Identification of differentially expressed genes (DEGs) based on immune/stromal/ESTIMATE scores in HBV-related HCC. (a) Three respective volcano maps of the three groups. (b) Gene expression heat maps for three significantly differentially expressed groups. (c, d) Intersection of three groups of differentially expressed genes.

2. Methods and Materials

2.1. Data Acquisition. We gathered gene expression RNA-seq and accompanying medical data of HBV-related HCC patients from TCGA-LIHC database (https://portal.gdc.cancer.gov/) [13]. HBV-infected and noninfected patients were differentiated based on the patient's past infection history. Download gene expression data from GSE136247 and GSE121248 datasets from GEO database (https://www.ncbi.nlm.nih.gov/geo/) [14]. The GSE136247 dataset contained

(a)

(b)

(c)

Figure 3: Continued.

	Age	Gender	OS	Survival	
	0.33	−2.8e-3	0.05	0.09	Yellow
	6.6e-4	0.03	0.98	0.63 0.35	
	−0.18		0.18	0.01	Turquoise
	0.07	0.05	0.77 0.09	0.04 0.90	
	−0.08			−0.04	Red
	0.40	0.08	0.58 0.12	0.38 0.66	
	−0.07			−0.06	Green
	0.48	0.16	0.39 0.09	0.24 0.53	
	−0.24			−0.06	Blue
	0.01	0.07	0.10 0.07	0.36 0.55	
	−0.18			−0.05	Brown
	0.07	−0.09	0.51 −0.13	0.49 0.61	
	0.26			0.10	Grey
	6.8e-3		0.39	0.19 0.33	

Correlation coefficient

−0.4   −0.2   0.0   0.2   0.4

p value

0.0   0.5   1.0
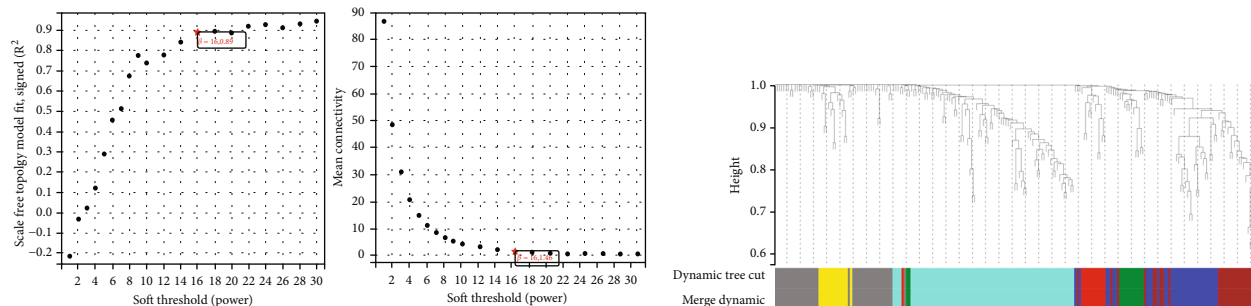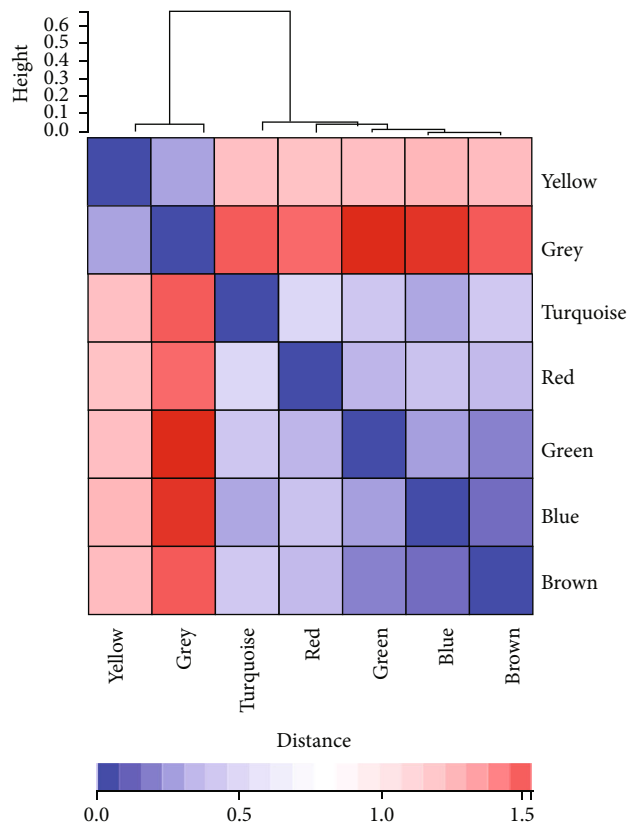
(d)
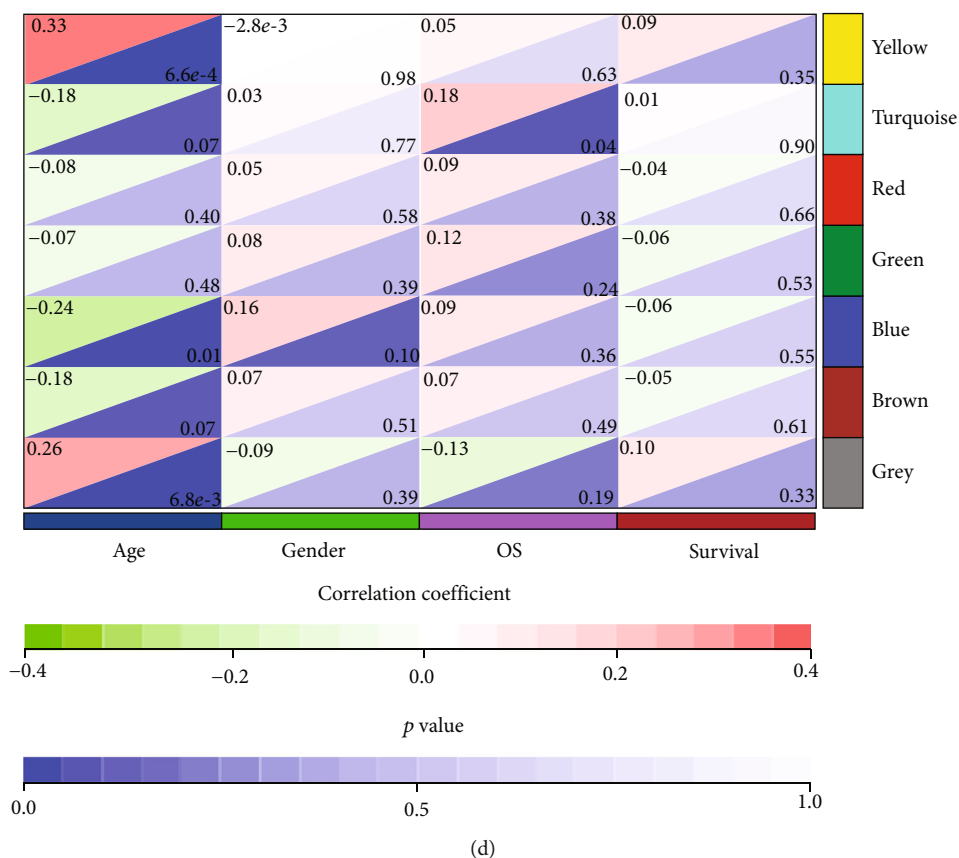
FIGURE 3: Weighted correlation network analysis (WGCNA). (a) Analysis of the scale-free fit index (left) and the mean connectivity (right) for various soft-thresholding powers. (b) Gene clustering dendrograms. (c) Topological overlap heat maps. (d) Heat map of correlations between modules and clinical features.

39 HCC tissues (25 with HBV infection) and 30 noncancerous normal tissues (19 with HBV infection) [15]. The GSE121248 dataset contained cancer and normal tissues from 37 HCC cases, and these patients had a history of HBV infection [16].

2.2. ESTIMATE Scores. The amount of tumor cells, immune cells, and stromal cells was determined using ESTIMATE (Estimation of STromal and Immune cells in MAlignant Tumor tissues using Expression data) based on the transcriptional profile of cancer samples. According to the stromal signature (stromal signature gene) and immune signature (immune cell signature gene), the stromal score and immune score were calculated by ssGSEA, respectively. Finally, the two scores were combined to generate an ESTIMATE score, which was used to analyze tumor purity. From the official website (https://bioinformatics.mdanderson.org/estimate/), matrix, immune, and ESTIMATE scores were downloaded for each sample in TCGA-LIHC cohort, and non-HBV-infected samples were excluded. In addition, this score was compared with tumor patient survival in a correlation analysis.

2.3. Acquisition of DEGs Based on Immune and Matrix Scores. All HBV-related HCC patients were divided into two groups (high vs. low) with positive and negative values.

Data analysis was performed on Sangerbox [17] using the "Deseq2" package. The filter range for DEGs were determined to be log $|FC| > 1$, $P < 0.05$.

2.4. Gene Ontology (GO) and Kyoto Encyclopedia of Genes and Genomes (KEGG) Function Analysis. Analyze the biological functions of DEGs by using the GO enrichment analysis (including BP, CC, and MF) and KEGG pathway enrichment analysis from DAVID online website tools (database annotation, visualization, and comprehensive discovery, https://david.ncifcrf.gov/tools.jsp) [18].

2.5. Weighted Correlation Network Analysis (WGCNA). WGCNA is an analytical method for analyzing gene expression patterns of multiple samples, which can cluster the similar expression gene and investigate the association between specific traits and phenotypes in modules. It will help us find relevant biomarker genes and therapeutic targets. The "WGCNA" package was used to build the DEGs coexpression network on Sangerbox to identify the modules related to prognosis.

2.6. Construction of PPI Network and Filtration of Hub Gene. The protein information and PPI network information of key modules were analyzed using String database (https://cn.string-db.org/) [19]. MCODE was a plugin for

(a)

(b)

(c)

(d)
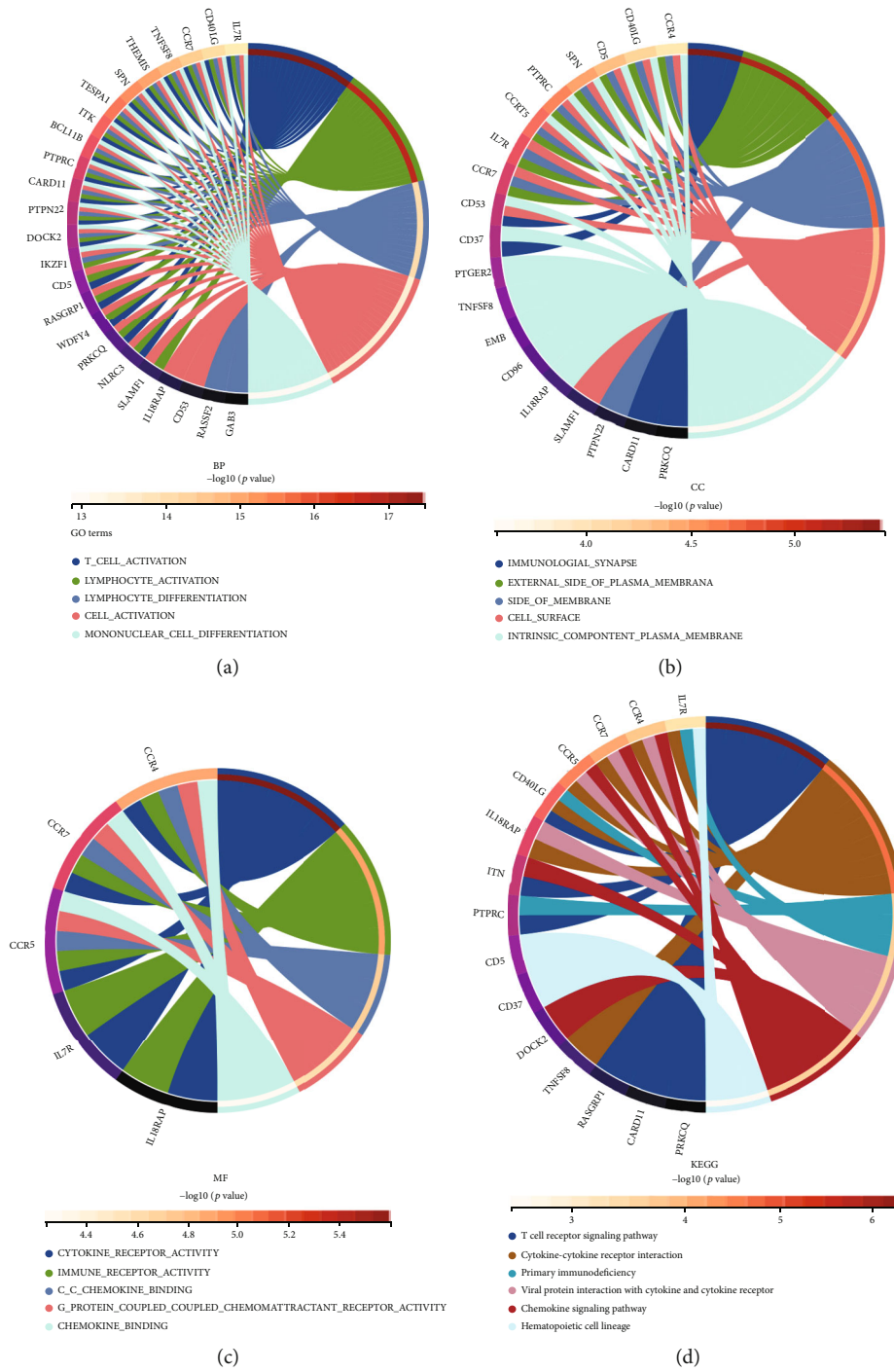
Figure 4: Chord diagram demonstrates GO and KEGG analysis of module genes. (a) Biological processes (BP), (b) cellular components (CC), (c) molecular functions (MF), and (d) KEGG pathways.

constructing functional modules of gene (protein) network clustering in Cytoscape 3.8.0. According to the analysis results, the hub gene can be determined [20].

2.7. Survival Analysis. Plot the Kaplan-Meier survival curves of these hub genes, and screen out the hub genes significantly correlated with overall survival ($P < 0.05$) by log-rank test.

2.8. Verification of the Expression of Hub Genes. Compare the previous hub genes with the expression data in

GSE136247 and GSE121248 datasets to obtain the final key genes. We used "TIMER" in Sangerbox to analyze the correlation of key genes with 6 tumor-infiltrating immune cells in HBV-related HCC tissues.

2.9. Clinical Features in Patients with HBC-Related HCC. For comparison, the basic information and medical data of HBV-related HCC patients were separated into high and low groups based on the expression of key genes.

(a)

(b)

(c)
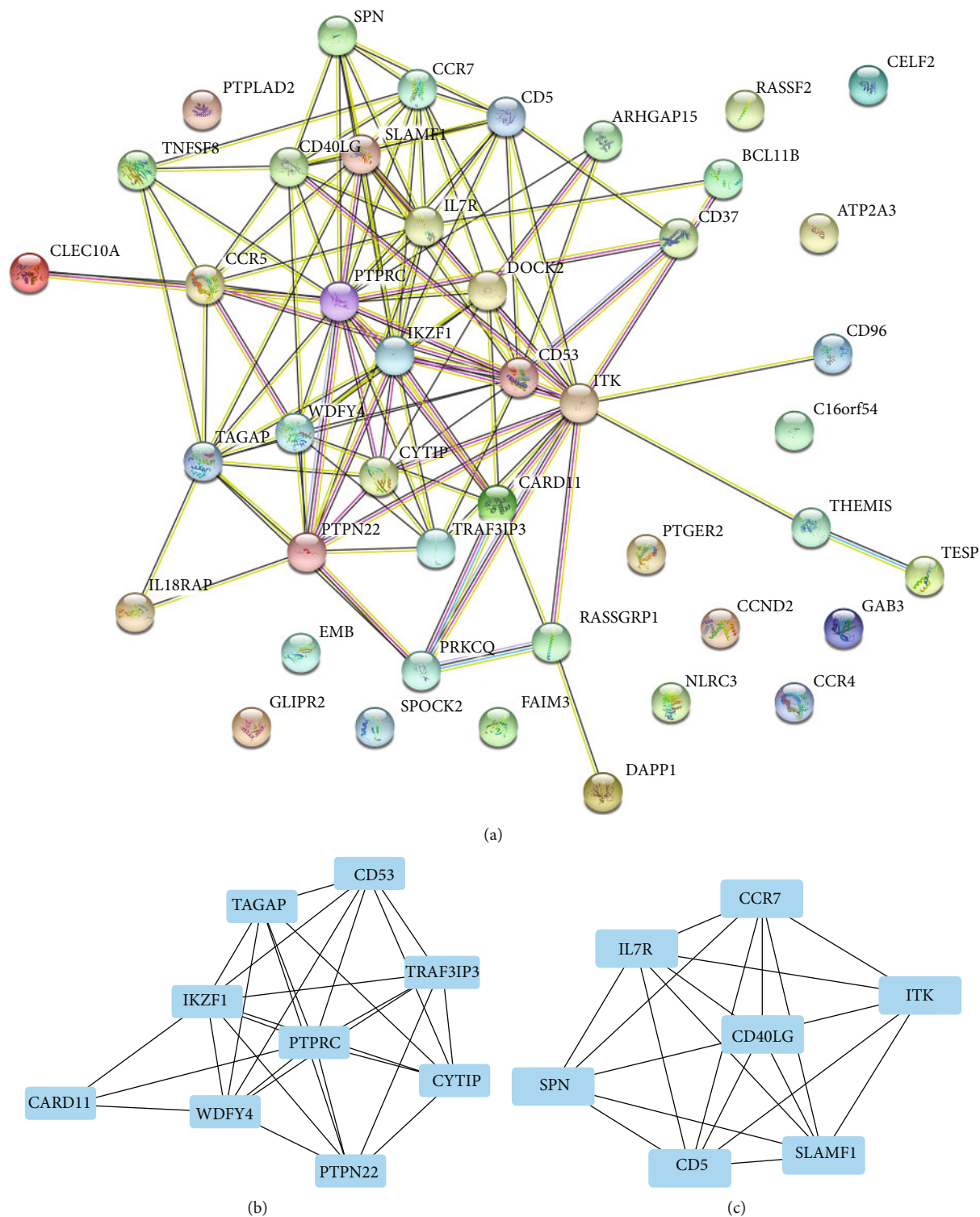
FIGURE 5: Construction of PPI network and identification of key subnetwork. (a) PPI network was constructed based on the STRING database and Cytoscape software. (b) The subnetwork contains 9 nodes and 31 edges. (c) The subnetwork contains 7 nodes and 23 edges.

2.10. Statistical Analysis. Analysis in the present study were conducted using the R package on Sangerbox and GraphPad prism 8.0.2. We used log-rank tests and chi-square tests for data analysis. A statistically significant difference was considered to be less than 0.05. The whole process of bioinformatics analysis was shown in Figure 1.

3. Results

3.1. Scores of the Immune System and Stroma Correlated with Overall Survival. Based on TCGA database, the statistical data of 104 HBV-related HCC patients were gained. Patients ranged from 23 to 83 years of age. 85 (81.7%) were male, and
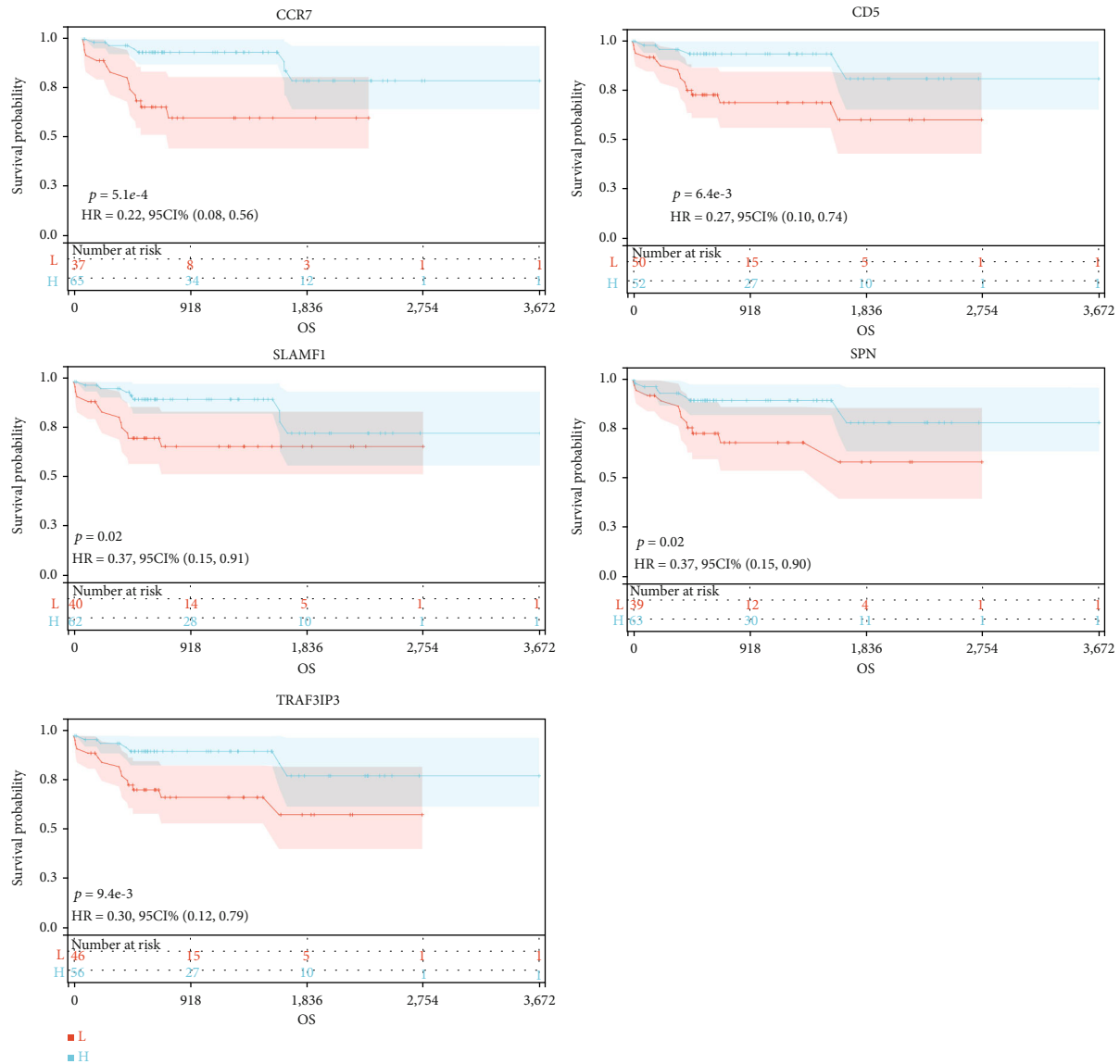
Figure 6: Survival analysis. The relations between the expression levels of CCR7, CD5, SLAMF1, SPN, and TRAF3IP3 and OS in HBV-related HCC.

19 (19.3%) were female. For each sample, ESTIMATE scores were calculated based on matrix, immune, and ESTIMATE scores. Stromal scores ranged from -1731.43 to 261.96, immune scores ranged from -964.97 to 2311.6, and ESTIMATE scores ranged from -2488.91 to 2306.2. In order to probe the possibility of the connection between immune/stromal/ESTIMATE scores and patient survival, we categorize HBV-related HCC patients into low and high groups on the basis of 0 scores. There were no positive results between the two groups (Figures S1A, S1B, and S1C).

3.2. Identification of DEGs in HBV-Related HCC. For expounding the connection between gene expression profiles and immune status, we used "DESeq2" package to identify. Genes were significantly differential expression among the three groups of scores. $|\log (FC)| > 1$ and $P < 0.05$ were as screening criteria. As shown in Figure 2(a), 571 downregulated genes and 1,845 upregulated genes were detected in

the immune score group; in the stromal score group, 1,457 downregulated genes and 1,014 upregulated genes were detected; in the ESTIMATE score group, 1,052 were detected downregulated genes and 1,584 upregulated genes. According to the heat map, there were significant differences between the three groups in the differential genes (Figure 2(b)). Through further data screening, the differential express gene in all three groups were obtained, including 111 upregulated genes and 322 downregulated genes as shown in Figures 2(c) and 2(d).

3.3. Functional Enrichment Analysis. DAVID website was used for GO and KEGG analyses. As a result of the enrichment analysis, cellular components (CC), molecular functions (MF), and biological processes (BP) were enriched by GO enrichment analysis (Figure S2). For BP, DEGs were mainly enriched in external encapsulating structure organization, biological adhesion, and collagen fibril

(a)

FIGURE 7: Continued.

(b)
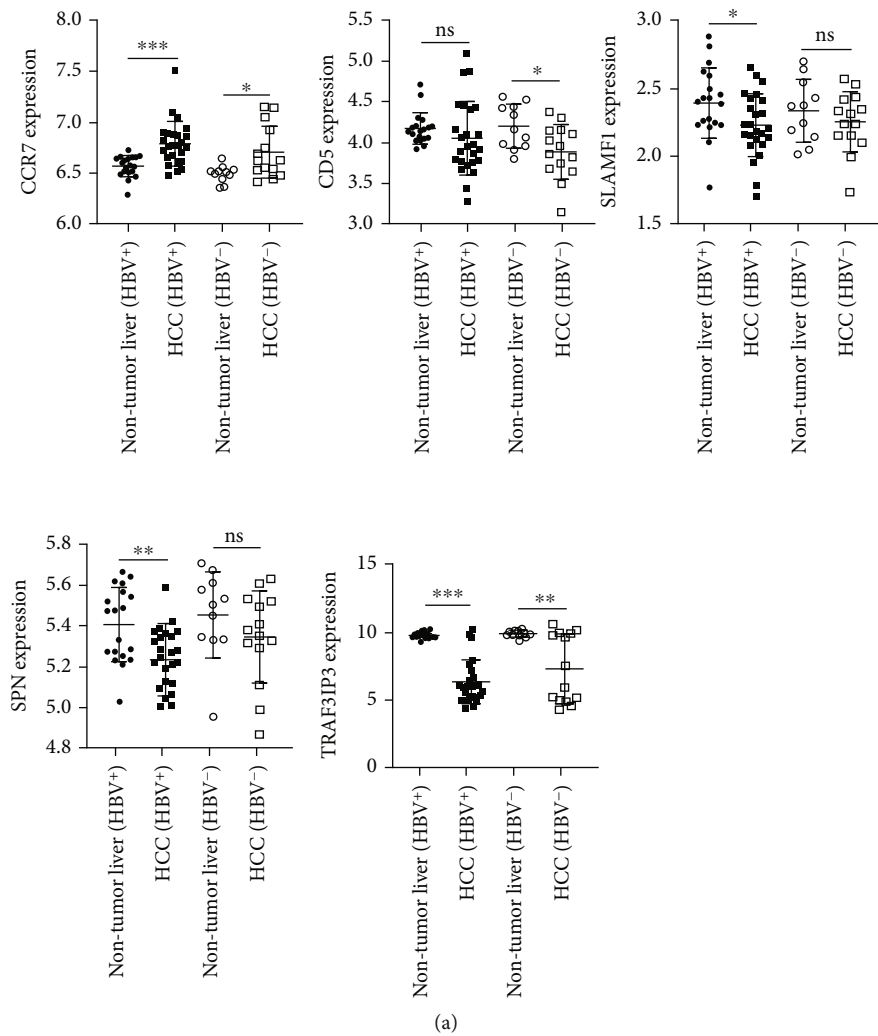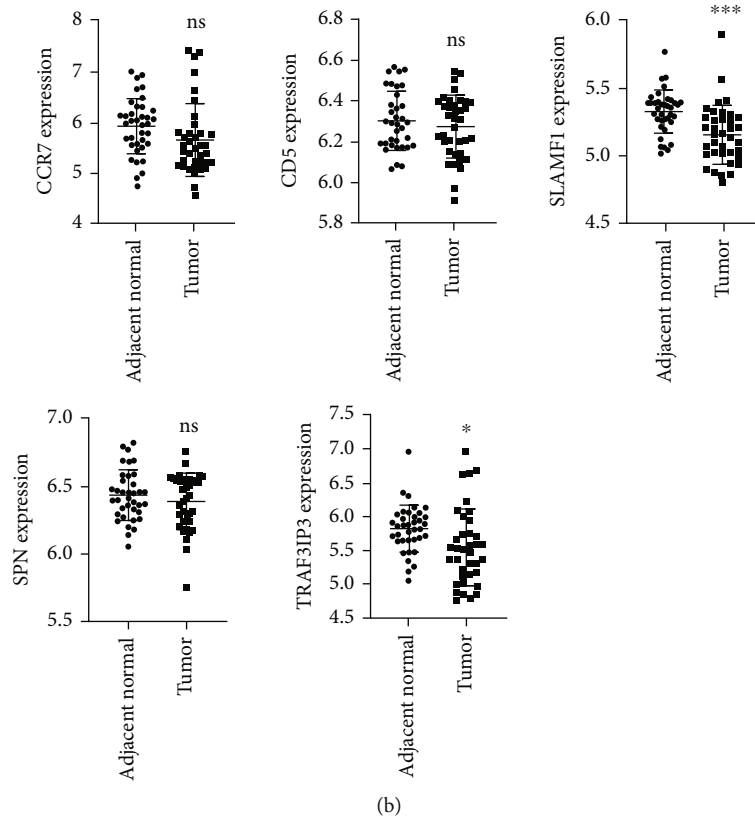
Figure 7: Hub genes were validated in the GEO database. (a) The expression levels of CCR7, CD5, SLAMF1, and SPN in GSE136247. (b) The expression levels of CCR7, CD5, SLAMF1, and SPN in GSE121248. $^*P < 0.05$, $^{**}P < 0.01$, $^{***}P < 0.001$; ns: not significantly.

organization. For CC, DEGs were mainly enriched in collagen containing extracellular matrix, external encapsulating structure, and T cell receptor complex. For MF, DEGs were mainly enriched in extracellular matrix structural constituents, glycosaminoglycan binding, and heparin binding. For KEGG, DEGs were mainly enriched in the regulation of hematopoietic cell lineage, cytokine-cytokine receptor interaction, and viral protein interaction with cytokine-cytokine receptor (Figure S2).

3.4. Weighted Correlation Network Analysis. The role network of DEGs was constructed by WGCNA analysis. With the network's soft threshold set at 16, coexpression networks resembled scale-free networks most closely (Figures 3(a)–3(c)). According to different functions, DEGs can be divided into 7 modules. Turquoise was the module with the highest significant difference over survival (OS time) (Figure 3(d)). The module contained a total of 50 genes.

3.5. Functional Enrichment Analysis of Genes in Turquoise. These genes were mostly associated with T cell activation, lymphocyte activation, and leukocyte differentiation in BP, based on GO enrichment analysis (Figure 4(a)). For CC, these genes were mainly enriched in immunological synapse, external side of plasma membrane, and side of membrane (Figure 4(b)). For MF, these genes were mainly enriched in cytokine receptor activity, immune receptor activity, and C-C chemokine binding (Figure 4(c)). For KEGG, these

genes were mainly involved in the regulation of T cell receptor signaling pathway, cytokine-cytokine receptor interaction, and primary immunodeficiency (Figure 4(d)).

3.6. Filtration of PPI Network and Identification of Prognostic-Related Genes. Through the String database, a PPI network was constructed using 50 genes (Figure 5(a)). Then, use Cytoscape 3.8.0 to further optimize the obtained PPI network, and use the MCODE plugin to draw important subnetworks (Figures 5(b) and 5(c)). There were 16 central genes (CD53, TAGAP, IKZF1, CARD11, WDFY4, PTPRC, PTPN22, CYTIP, TRAF3IP3, CCR7, ITK, IL7R, CD40LG, SLAMF1, CD5, and SPN) in the protein interaction network.

3.7. Survival Analysis in Blue Module. Identifying genes associated with overall survival in patients with HBV-related HCC was the purpose of this research. We constructed Kaplan-Meier survival curves of these genes using the prognostic information in TCGA-LIHC. Among them, the expression levels of CCR7, CD5, SLAMF1, SPN, and TRAF3IP3 were significantly associated with the prognosis of patients (Figure 6 and Figure S3).

3.8. Validation of the Analysis in the GEO Database. In addition, we determined the use of GSE136247 and GSE121248 to explore the expression of these genes in cancerous and paracancerous tissues. As shown in Figure 7(a), in GSE136247, CCR7 was expressed significantly upregulated
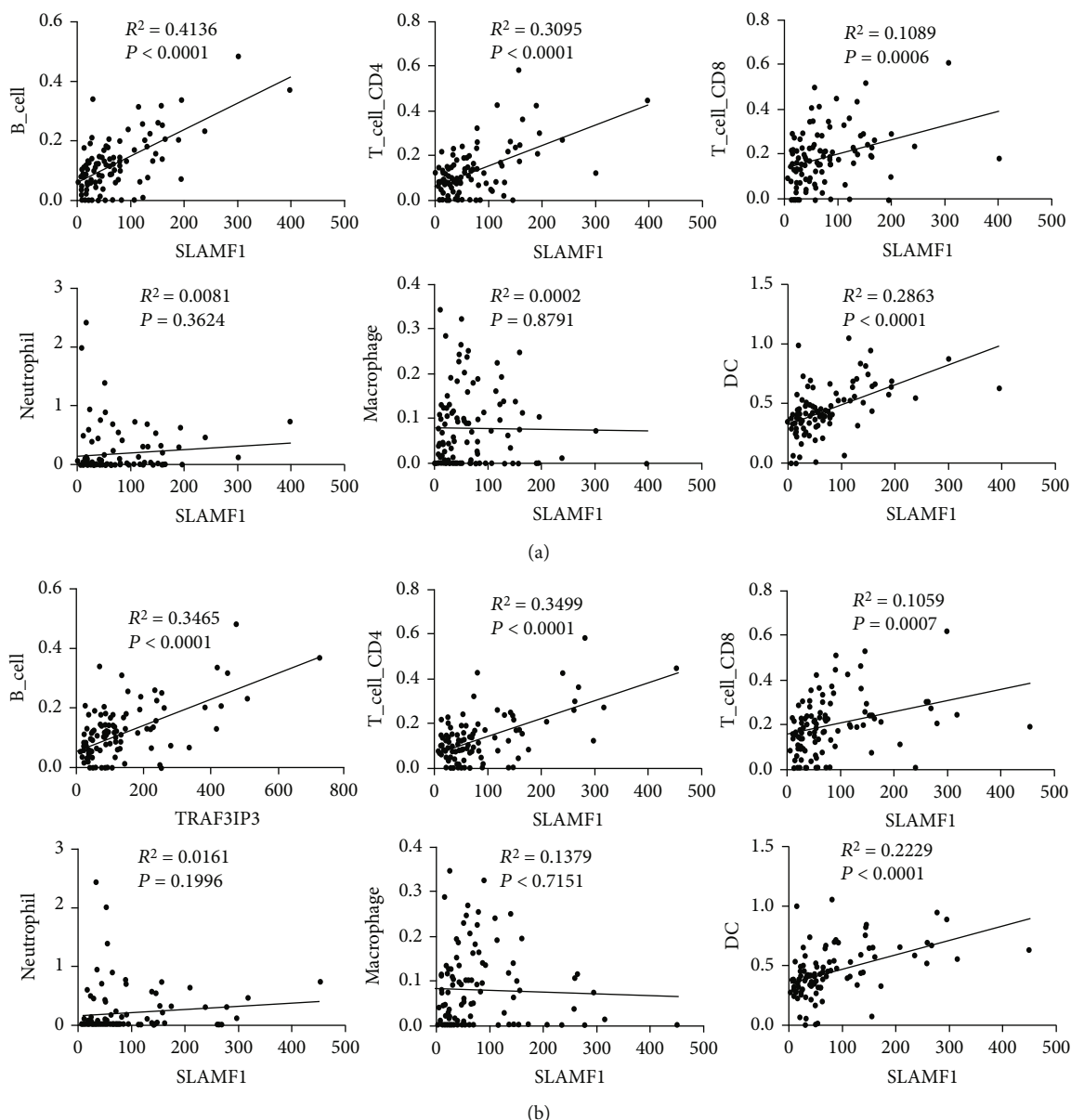
FIGURE 8: The correlation between key genes and 6 immune cell types. (a) SLAMF1; (b) TRAF3IP3.

in cancer tissues (whether or not infected with HBV) relative to adjacent tissues, whereas TRAF3IP3 was completely the opposite. In HBV-related HCC patients, SLAMF1 and SPN in cancer tissues were significantly decreased, but this phenomenon was not observed in patients without HBV infection. In addition, the expression of CD5 was significantly decreased in cancer tissues relative to adjacent tissues of HBV-uninfected patients, while in HBV-related HCC patients, the two groups did not differ significantly. As shown in Figure 7(b), in GSE121248, the expressions of SLAMF1 and TRAF3IP3 were significantly decreased in HBV-related HCC tissues relative to paracancerous tissues, while the expressions of CCR7, CD5, and SPN were not significantly different. Based on the above results, we defined SLAMF1 and TRAF3IP3 as key genes for follow-up studies.

3.9. Connection between Key Genes and Immune Infiltration. In the present study, we explored possible associations between key gene expression and the infiltration of immune cells using TIMER. A positive correlation was found between SLAMF1 and TRAF3IP3, but not between neutrophils and macrophages, with the infiltration of B cells, CD4+ T cells, CD8+ T cells, and dendritic cells (Figure 8). In light of this, key genes may play an important role in regulating immune cells.

3.10. Relationship between Key Genes and Clinical Features. Based on TCGA-LIHC database, we examined the relationship between SLAMF1 and TRAF3IP3 and HBV-related HCC clinical characteristics. The results showed that SLAMF1 and TRAF3IP3 were inversely associated with

TABLE 1: SLAMF1 and TRAF3IP3 expression and clinicopathological features in HBV-related HCC.

Variables	n	SLAMF1 expression		P value	TRAF3IP3 expression		P value
		Low	High		Low	High	
Gender							
Male	85	42	43	0.636	42	43	0.636
Female	19	10	9		10	9	
Age							
>60	33	20	13	0.140	20	13	0.140
≤60	71	32	39		32	39	
T							
T1-T2	91	44	47	0.374	44	47	0.374
T3-T4	13	8	5		8	5	
N							
N0	94	49	45	0.318	50	44	0.096
Nx	10	3	7		2	8	
M							
M0	89	45	44	0.780	46	43	0.402
Mx	15	7	8		6	9	
Recurrence							
Yes	44	27	17	0.047*	28	16	0.017*
No	60	25	35		24	36	

* represents $P < 0.05$; T: tumor stage; N: lymph node stage; M: metastasis stage.

tumor recurrence, regardless of gender, age, tumor stage (T), lymph node stage (N), and metastasis stage (M) (Table 1).

4. Discussion

HCC has a poor prognosis, killing more than 800,000 people worldwide each year [21]. In European and American countries, the prevalence of nonalcoholic fatty liver disease is rising rapidly every year, leading to the subsequent development of HCC and HCC-related death; while in developing countries in Asia, hepatitis and cirrhosis caused by viral infection are the main causes of HCC [22]. As most HCC cases are secondary to hepatitis (hepatitis B, hepatitis C, or alcoholic and nonalcoholic liver disease) or cirrhosis, HCC is now gradually considered to be the inflammatory cancer induced by chronic liver injury [23–26]. Patients with advanced HCC lack access to surgery and rely mainly on immunization or chemotherapy, example for sorafenib, a kind of the tyrosine kinase inhibitor. In recent years, several treatment options (lenvatinib, regorafenib, cabozantinib, and ramucirumab) have emerged for the various aspects' treatment of advanced HCC [27].

Cellular components of the HCC immune microenvironment (tumor cells, immune cells, stromal cells, endothelial cells, and cancer-associated fibroblasts) are critical for the response to immunotherapy [28]. Through the portal vein, antigen-rich blood from the gut is constantly exposed to the liver, which acts as a central immune organ. In order

to reduce inflammatory stimulation and tissue damage from the blood and the liver, establish an immune-tolerant microenvironment which has a strong resistance to hit and self-cleaning ability. The homeostasis of this immune microenvironment is also disrupted when hepatitis or cirrhosis or even HCC develops [29]. The TME in HCC is the hallmark of tumor, which has an important influence on tumor growth, invasion, and drug resistance [30, 31].

First, we screened out HCC patients with HBV infection from TCGA-LIHC. In the immune microenvironment of HBV-related HCC, DEGs were identified based on immunity, stroma, and ESTIMATE scores. Activation of CD4+ T cells, CD8+ T cells, NK cells, NKT cells, monocytes/macrophages, and HSCs occurs in chronic hepatitis caused by HBV. Hepatitis is further aggravated, and HCC is further encouraged by the simultaneous production of TNF-α, IFN-γ, IL-12, IL-4, and IL-13 [32, 33]. Additionally, several immunosuppressive cells, including Treg, Breg, MDSC, and Kupffer cells, inhibit immune cell activity by producing cytokines such as TGF-β and IL-10 and inducing key factors in CD8+ T and NK cell depletion, leading to immune escape of HBV and HCC tumor cell [34–37].

Additionally, we analyzed DEG enrichment. These DEGs have various biological properties and participate in various signaling pathways, such as external encapsulating structure organization, biological adhesion, T cell receptor complex, cytokine-cytokine receptor interaction, and viral protein interaction with cytokine-cytokine receptor. All of these confirmed that their involvement was in the regulation of the immune microenvironment in HBV-related HCC [38, 39]. Coexpression networks were constructed, with turquoise modules identified as key modules by WGCNA. Their main functions are to activate T cells, activate lymphocytes, and differentiate leukocytes; they are mainly located at the immune synapse, the outer and membrane sides of the plasma membrane; they mainly regulate cytokine receptor activity, immune receptor activity, and C-C chemokine binding. They are also involved in the regulation of T cell receptor signaling pathway cytokine-cytokine receptor interactions and primary immunodeficiency. A close correlation can be found between the immune regulation of HBV-related HCC and the genes of this module.

Through the PPI construction and prognostic-related genes analysis of this module, we identified five HBV-related hub genes for the prognosis of HCC patients, namely, CCR7, CD5, SLAMF1, SPN, and TRAF3IP3. On the basis of GSE136247 and GSE121248, the expression of each gene in cancer tissue and normal tissue was verified, and two key genes were finally obtained, namely, SLAMF1 and TRAF3IP3.

The SLAMF1/CD150 receptor is a member of the cell surface receptor signaling lymphocyte activation molecule (SLAM) family and is considered a marker of activated T cells, B cells, monocytes, and DCs [40, 41]. SLAMF1 is actively involved in the regulation of different types of immune responses as well as keeping the tissue microenvironment [42]. Recent studies have demonstrated that the expression level of SLAMF1 is significantly increased in liver tissue of NASH compared with non-NASH controls

and that the level of SLAMF1 was dramatically related to the seriousness of the NASH phenotype. This study was the first to identify the role of SLAMF1 in the mediating of hepatocyte death in NASH and as a measure of NASH in humans [43]. In another study, the concentration of SLAMF1 has a profound effect on the formation of cirrhosis in the plasma. But no significant difference was found between HCC and cirrhosis [44]. TRAF3IP3 (TRAF3-interacting protein 3) was identified as a TRAF3-interacting protein in original [45]. Recent studies have shown that TRAF3IP3 is involved in B and T cell development and for maintaining the functional stability of regulatory T cells [46, 47]. TRAF3IP3 has been shown to function as an oncogene in melanoma and glioma [48, 49].

Our study showed that SLAMF1 and TRAF3IP3 were lowly expressed in HBV-related HCC and positively related with the infiltration of B cells, CD4+ T cells, CD8+ T cells, and dendritic cells, but not neutrophils and macrophages. Taken together, SLAMF1 and TRAF3IP3 may contribute to the pathogenesis of HBV-related HCC. Through their effect on the immune-suppressive microenvironment, furthermore, we found that SLAMF1 and TRAF3IP3 were also associated with the recurrence of HBV-related HCC.

5. Conclusion

We used bioinformatics to comprehensively analyze the expression of immune microenvironment-related genes in HBV-associated HCC patients in TCGA. Further study of the screened DEGs yielded two genes related with prognosis. We explained that SLAMF1 and TRAF3IP3 were low-expressed in HBV-associated HCC tissues and were correlated with tumor recurrence. Our findings had clear implications for SLAMF1 and TRAF3IP3 as biomarkers for predicting the prognosis of HBV-related HCC patients and provide new research directions and diagnosis and treatment options for HBV-related HCC. However, follow-up clinical studies are required to confirm these opinions.

Data Availability

The datasets used and/or analyzed during the current study are available from the corresponding author on reasonable request.

Conflicts of Interest

The authors declare that they have no conflicts of interest.

Authors' Contributions

DW and XWB conceived and designed the project; DW, ZL, and YZP acquired the data; DW, TYL, and XXZ analyzed and interpreted the data; DW, ZZ, and YNY wrote the paper. All authors contributed to the study and approved the submitted version. Wei Ding, Zheng Zhang, Nianyuan Ye, and Zhiping Yuan contributed equally to this work.

Supplementary Materials

Figure S1: the relationship between immune status and overall survival in HBV-related HCC. (A) Kaplan-Meier curve shows the overall survival of the high and low immune score groups. (B) Kaplan-Meier curve shows the overall survival of the high and low stromal score groups. (C) Kaplan-Meier curve shows the overall survival of the high and low ESTIMATE score groups. Figure S2: chord diagram demonstrates GO and KEGG analysis of DEGs. Biological processes (BP), cellular components (CC), molecular functions (MF), and KEGG pathways. Figure S3: survival analysis. The relations between the expression levels of CD53, TAGAP, IKZF1, CARD11, WDFY4, PTPRC, PTPN22, CYTIP, ITK, IL7R, and CD40LG and OS in HBV-related HCC. (Supplementary Materials)

References

[1] J. Ferlay, I. Soerjomataram, R. Dikshit et al., "Cancer incidence and mortality worldwide: sources, methods and major patterns in GLOBOCAN 2012," *International Journal of Cancer*, vol. 136, no. 5, pp. E359–E386, 2015.

[2] E. Chakraborty and D. Sarkar, "Emerging therapies for hepatocellular carcinoma (HCC)," *Cancers (Basel)*, vol. 14, no. 11, p. 2798, 2022.

[3] L. Rinaldi, M. Guarino, A. Perrella et al., "Role of liver stiffness measurement in predicting HCC occurrence in direct-acting antivirals setting: a real-life experience," *Digestive Diseases and Sciences*, vol. 64, no. 10, pp. 3013–3019, 2019.

[4] A. P. Venook, C. Papandreou, J. Furuse, and L. Ladrón de Guevara, "The incidence and epidemiology of hepatocellular carcinoma: a global and regional perspective," *The Oncologist*, vol. 15, Suppl 4, pp. 5–13, 2010.

[5] K. O. Asafo-Agyei and H. Samant, *Hepatocellular carcinoma, in StatPearls*, StatPearls Publishing Copyright © 2022, StatPearls Publishing LLC.: Treasure Island (FL), 2022.

[6] N. E. Rich, A. C. Yopp, A. G. Singal, and C. C. Murphy, "Hepatocellular carcinoma incidence is decreasing among younger adults in the United States," *Clinical Gastroenterology and Hepatology*, vol. 18, no. 1, pp. 242–248.e5, 2020.

[7] M. Yarchoan, P. Agarwal, A. Villanueva et al., "Recent developments and therapeutic strategies against hepatocellular carcinoma," *Cancer Research*, vol. 79, no. 17, pp. 4326–4330, 2019.

[8] S. Medavaram and Y. Zhang, "Emerging therapies in advanced hepatocellular carcinoma," *Experimental Hematology & Oncology*, vol. 7, no. 1, p. 17, 2018.

[9] J. Musa, J. Li, and T. G. Grünewald, "Hepatitis B virus large surface protein is priming for hepatocellular carcinoma development via induction of cytokinesis failure," *The Journal of Pathology*, vol. 247, no. 1, pp. 6–8, 2019.

[10] M. Levrero and J. Zucman-Rossi, "Mechanisms of HBV-induced hepatocellular carcinoma," *Journal of Hepatology*, vol. 64, no. 1, pp. S84–s101, 2016.

[11] B. Rehermann and R. Thimme, "Insights from antiviral therapy into immune responses to hepatitis B and C virus infection," *Gastroenterology*, vol. 156, no. 2, pp. 369–383, 2019.

[12] Y. Chen and Z. Tian, "HBV-induced immune imbalance in the development of HCC," *Frontiers in Immunology*, vol. 10, p. 2048, 2019.

[13] Z. Wang, M. A. Jensen, and J. C. Zenklusen, "A practical guide to The Cancer Genome Atlas (TCGA)," *Methods in Molecular Biology*, vol. 1418, pp. 111–141, 2016.

[14] E. Clough and T. Barrett, "The Gene Expression Omnibus database," *Methods in Molecular Biology*, vol. 1418, pp. 93–110, 2016.

[15] J. P. Cerapio, A. Marchio, L. Cano et al., "Global DNA hypermethylation pattern and unique gene expression signature in liver cancer from patients with Indigenous American ancestry," *Oncotarget*, vol. 12, no. 5, pp. 475–492, 2021.

[16] S. M. Wang, L. L. Ooi, and K. M. Hui, "Identification and validation of a novel gene signature associated with the recurrence of human hepatocellular carcinoma," *Clinical Cancer Research*, vol. 13, no. 21, pp. 6275–6283, 2007.

[17] W. Shen, Z. Song, X. Zhong et al., "Sangerbox: a comprehensive, interaction-friendly clinical bioinformatics analysis platform," *iMeta*, vol. 1, no. 3, article e36, 2022.

[18] B. Sherman, M. Hao, J. Qiu et al., "DAVID: a web server for functional enrichment analysis and functional annotation of gene lists (2021 update)," *Nucleic Acids Research*, vol. 50, no. W1, pp. W216–W221, 2022.

[19] D. Szklarczyk, A. Franceschini, S. Wyder et al., "STRING v10: protein-protein interaction networks, integrated over the tree of life," *Nucleic Acids Research*, vol. 43, no. D1, pp. D447–D452, 2015.

[20] P. Shannon, A. Markiel, O. Ozier et al., "Cytoscape: a software environment for integrated models of biomolecular interaction networks," *Genome Research*, vol. 13, no. 11, pp. 2498–2504, 2003.

[21] F. Bray, J. Ferlay, I. Soerjomataram, R. L. Siegel, L. A. Torre, and A. Jemal, "Global cancer statistics 2018: GLOBOCAN estimates of incidence and mortality worldwide for 36 cancers in 185 countries," *CA: a Cancer Journal for Clinicians*, vol. 68, no. 6, pp. 394–424, 2018.

[22] R. L. Siegel, K. D. Miller, and A. Jemal, "Cancer statistics, 2020," *CA: a Cancer Journal for Clinicians*, vol. 70, no. 1, pp. 7–30, 2020.

[23] C. Trépo, H. L. Chan, and A. Lok, "Hepatitis B virus infection," *Lancet*, vol. 384, no. 9959, pp. 2053–2063, 2014.

[24] B. Gao and R. Bataller, "Alcoholic liver disease: pathogenesis and new therapeutic targets," *Gastroenterology*, vol. 141, no. 5, pp. 1572–1585, 2011.

[25] D. Y. Zhang and S. L. Friedman, "Fibrosis-dependent mechanisms of hepatocarcinogenesis," *Hepatology*, vol. 56, no. 2, pp. 769–775, 2012.

[26] Q. M. Anstee, H. L. Reeves, E. Kotsiliti, O. Govaere, and M. Heikenwalder, "From NASH to HCC: current concepts and future challenges," *Nature Reviews. Gastroenterology & Hepatology*, vol. 16, no. 7, pp. 411–428, 2019.

[27] B. Ruf, B. Heinrich, and T. F. Greten, "Immunobiology and immunotherapy of HCC: spotlight on innate and innate-like immune cells," *Cellular & Molecular Immunology*, vol. 18, no. 1, pp. 112–127, 2021.

[28] F. Heymann and F. Tacke, "Immunology in the liver–from homeostasis to disease," *Nature Reviews. Gastroenterology & Hepatology*, vol. 13, no. 2, pp. 88–110, 2016.

[29] J. P. Böttcher, P. A. Knolle, and D. Stabenow, "Mechanisms balancing tolerance and immunity in the liver," *Digestive Diseases*, vol. 29, no. 4, pp. 384–390, 2011.

[30] D. F. Quail and J. A. Joyce, "Microenvironmental regulation of tumor progression and metastasis," *Nature Medicine*, vol. 19, no. 11, pp. 1423–1437, 2013.

[31] M. Binnewies, E. W. Roberts, K. Kersten et al., "Understanding the tumor immune microenvironment (TIME) for effective therapy," *Nature Medicine*, vol. 24, no. 5, pp. 541–550, 2018.

[32] J. Wang, W. Zhao, L. Cheng et al., "CD137-mediated pathogenesis from chronic hepatitis to hepatocellular carcinoma in hepatitis B virus-transgenic mice," *Journal of Immunology*, vol. 185, no. 12, pp. 7654–7662, 2010.

[33] X. Hou, X. Hao, M. Zheng et al., "CD205-TLR9-IL-12 axis contributes to CpG-induced oversensitive liver injury in HBsAg transgenic mice by promoting the interaction of NKT cells with Kupffer cells," *Cellular & Molecular Immunology*, vol. 14, no. 8, pp. 675–684, 2017.

[34] Q. Wang, W. Pan, Y. Liu et al., "Hepatitis B virus-specific CD8+ T cells maintain functional exhaustion after antigen reexposure in an acute activation immune environment," *Frontiers in Immunology*, vol. 9, p. 219, 2018.

[35] N. Trehanpati and A. K. Vyas, "Immune regulation by T regulatory cells in hepatitis B virus-related inflammation and cancer," *Scandinavian Journal of Immunology*, vol. 85, no. 3, pp. 175–181, 2017.

[36] Q. F. Zhang, W. W. Yin, Y. Xia et al., "Liver-infiltrating CD11b⁻CD27⁻ NK subsets account for NK-cell dysfunction in patients with hepatocellular carcinoma and are associated with tumor progression," *Cellular & Molecular Immunology*, vol. 14, no. 10, pp. 819–829, 2017.

[37] M. Li, R. Sun, L. Xu et al., "Kupffer cells support hepatitis B virus-mediated CD8+ T cell exhaustion via hepatitis B core antigen-TLR2 interactions in mice," *Journal of Immunology*, vol. 195, no. 7, pp. 3100–3109, 2015.

[38] P. Qin, M. Zhang, X. Liu, and Z. Dong, "Immunogenomic landscape analysis of prognostic immune-related genes in hepatocellular carcinoma," *Journal of Healthcare Engineering*, vol. 2021, Article ID 3761858, 13 pages, 2021.

[39] S. Xiang, J. Li, J. Shen et al., "Identification of prognostic genes in the tumor microenvironment of hepatocellular carcinoma," *Frontiers in Immunology*, vol. 12, article 653836, 2021.

[40] V. G. Pinchouk, S. P. Sidorenko, D. F. Gluzman, E. P. Vetrova, A. G. Berdova, and L. N. Schlapatskaya, "Monoclonal antibodies IPO-3 and IPO-10 against human B cell differentiation antigens," *Anticancer Research*, vol. 8, no. 6, pp. 1377–1380, 1988.

[41] S. P. Sidorenko, E. P. Vetrova, O. V. Yurchenko, A. G. Berdova, L. N. Shlapatskaya, and D. F. Gluzman, "Monoclonal antibodies of IPO series against B cell differentiation antigens in leukemia and lymphoma immunophenotyping," *Neoplasma*, vol. 39, no. 1, pp. 3–9, 1992.

[42] I. Gordiienko, L. Shlapatska, L. Kovalevska, and S. P. Sidorenko, "SLAMF1/CD150 in hematologic malignancies: silent marker or active player?," *Clinical Immunology*, vol. 204, pp. 14–22, 2019.

[43] O. Gomez-Torres, S. Amatya, L. Kamberov et al., "SLAMF1 is expressed and secreted by hepatocytes and the liver in nonalcoholic fatty liver disease," *American Journal of Physiology. Gastrointestinal and Liver Physiology*, vol. 323, no. 3, pp. G177–g187, 2022.

[44] I. Argirion, R. M. Pfeiffer, T. K. Lam et al., "Association between immunologic markers and cirrhosis in individuals with chronic hepatitis B," *Scientific Reports*, vol. 11, no. 1, p. 21194, 2021.

[45] H. Dadgostar, S. E. Doyle, A. Shahangian, D. E. Garcia, and G. Cheng, "T3JAM, a novel protein that specifically interacts with TRAF3 and promotes the activation of JNK1," *FEBS Letters*, vol. 553, no. 3, pp. 403–407, 2003.

[46] X. Yu, X. L. Teng, F. Wang et al., "Metabolic control of regulatory T cell stability and function by TRAF3IP3 at the lysosome," *The Journal of Experimental Medicine*, vol. 215, no. 9, pp. 2463–2476, 2018.

[47] S. Peng, K. Wang, Y. Gu et al., "TRAF3IP3, a novel autophagy up-regulated gene, is involved in marginal zone B lymphocyte development and survival," *Clinical and Experimental Immunology*, vol. 182, no. 1, pp. 57–68, 2015.

[48] G. Yang, S. Tang, J. Zhang, and L. Qin, "High TRAF3IP3 level predicts poor prognosis of patients with gliomas," *World Neurosurgery*, vol. 148, pp. e436–e449, 2021.

[49] P. Nasarre, I. V. Bonilla, J. S. Metcalf, E. G. Hilliard, and N. Klauber-DeMore, "TRAF3-interacting protein 3, a new oncotarget, promotes tumor growth in melanoma," *Melanoma Research*, vol. 28, no. 3, pp. 185–194, 2018.

Research Article

Constructing and Validating a Pyroptosis-Related Genes Prognostic Signature for Stomach Adenocarcinoma and Immune Infiltration: Potential Biomarkers for Predicting the Overall Survival

Jingmin Xu,[1] **Ke Chen,**[2] **Zhou Wei** (ID),[3] **Zixuan Wu** (ID),[3] **Xuyan Huang** (ID),[3] **Minjie Cai** (ID),[4] **Kai Yuan** (ID),[5] **Peidong Huang** (ID),[5] **Jing Zhang,**[6] **and Shuai Wang** (ID)[7]

[1]*Yantai Hospital of Traditional Chinese Medicine, Shandong Province, China*
[2]*Department of Clinical Laboratory, The Sixth Affiliated Hospital of Sun Yat-Sen University, Guangzhou, 510655 Guangdong, China*
[3]*Guangzhou University of Chinese Medicine, Guangzhou, Guangdong Province, China 510006*
[4]*Shantou Health School, Shantou, Guangdong Province, China 515061*
[5]*Yunnan University of Chinese Medicine, Kunming, Yunnan Province, China 650500*
[6]*Department of Pediatrics, Shandong Second Provincial General Hospital, Shandong, China*
[7]*Department of Pediatric Surgery, Shandong Provincial Hospital Affiliated to Shandong First Medical University, China*

Correspondence should be addressed to Shuai Wang; 332002160@qq.com

Background. Stomach adenocarcinoma (STAD) is a kind of cancer that begins in the stomach cells and has a poor overall survival rate. Following resection surgery, chemotherapy has been suggested as a curative method for stomach cancer. However, it is ineffective. Pyroptosis, a kind of inflammatory programmed cell death, has been shown to play a significant role in the development and progression of STAD. However, whether pyroptosis-related genes (PRGs) can be utilized to predict the diagnosis and prognosis of gastric cancer remains unknown. *Method.* The research measured at predictive PRGs in STAD samples from TCGA and GEO. Lasso regression was used to build the prediction model. Coexpression analysis revealed that gene expression was linked to pyroptosis. PRGs were found to be overexpressed in high-risk individuals, implying that they could be used in a model to predict STAD prognosis. *Result.* Immunological and tumor-related pathways were discovered using GSEA. In STAD patients, the genes *GPX3*, *PDGFRL*, *RGS2*, and *SERPINE1* may be connected to the cancer process. The levels of expression also differed between the two risk groups. *Conclusion.* The purpose of this study is to identify and verify STAD-associated PRGs that can effectively guide prognosis and the immunological milieu in STAD patients as well as offer evidence for the development of pyroptosis-related molecularly targeted therapeutics. Therefore, PRGs and the link between immunological and PRGs in STAD may be therapeutic targets.

1. Introduction

Gastric cancer (GC), a disease with a wide range of manifestations, is the fifth most frequent cancer and the third biggest cause of cancer-related deaths globally. The most frequent histologic form of gastric cancer, stomach adenocarcinoma (STAD), is a fast developing, aggressive, and malignant GC that accounts for 95 percent of all gastric tumors. Several previous studies have found that Helicobacter pylori infection causes 90% of STAD cases [1]. Many researchers have

TABLE 1: Patients' clinical features.

Variable	Number of samples
TCGA	
Gender	
Male/female	285/158
Age at diagnosis	
≤65/>65/NA	197/241/5
Grade	
G1/G2/G3/G4/NA	Unknown
Stage	
I/II/III/IV/NA	59/130/183/44/27
T	
T1/T2/T3/T4/NA	23/93/198/119/10
M	
M0/M1/NA	391/30/22
N	
N0/N1/N2/N3/NA	132/119/85/88/19
GEO	
Gender	
Male/female	296/137
Age at diagnosis	
≤65/>65	283/150
Grade	
G1/G2/G3/G4/NA	Unknown
Stage	
I/II/III/IV/NA	Unknown
T	
T1/T2/T3/T4	11/38/92/292
M	
M0/M1/NA	Unknown
N	
N0/N1/N2/N3	80/188/132/33

recently proposed that STAD could also be brought about by autoimmunity, other bacteria, and their metabolites (such as N-nitroso compounds or acetaldehyde) [2]. STAD research has advanced to the point where it may be regarded as a collection of uncommon illnesses that risk human health [3]. Currently, the treatment of this disease is as important in the field of tumor research [4]. Chemotherapy is a significant factor of tumor treatment, but because chemotherapy drugs are cytotoxic and seem to have a lot of side effects, long-term use will cause major problems for patients. Repeated use can easily result in tumor cell drug resistance, reducing the curative effect [5]. Despite this, the absence of precise biomarkers for early tumor diagnosis, as well as restricted preclinical models, has impeded successful STAD therapeutic treatment [6, 7]. As a result, there is an urgent need to identify novel and reliable biomarkers for the early identification and prognosis of STAD. Finding treatment targets for STAD and elucidating the molecular identification of diagnostic biomarkers are critical for basic and clinical STAD research.

One of life's most fundamental challenges is cell death. The capacity to avoid cell death, which is a characteristic of cancer, not only contributes to the formation of cancer but also plays a significant role in the development of therapeutic resistance, recurrence, and metastasis [8]. The ultimate objective of cancer therapies like radiation, chemotherapy, and immunotherapy, which has recently made great progress, is to maximize tumor cell death while causing the least amount of injury to normal tissues. Tumor cells' innate genetic and epigenetic heterogeneity, as well as metabolic flexibility and other variables, provide greater adaptability to adverse tumor settings, resulting in treatment resistance and spread potential [9]. Pyroptosis is a double-edged sword that plays a twofold role in modifying tumor growth due to the ongoing activation of the inflammasome. Pyroptosis aids in the formation of a tumor-suppressive immunological milieu by unleashing inflammatory chemicals capable of directly destroying cancer cells and galvanizing an anticancer immune response [10]. Pyroptosis, a highly immunogenic form of cell death, induces local inflammation and draws inflammatory cell infiltration, offering a good chance to reduce immunosuppression of tumor microenvironments (TME) and stimulate a systemic immune response in the treatment of solid tumors [11]. In rare cases, triggering pyroptosis can directly kill tumor cells. According to new study, pyroptosis has a role in cancer formation, differentiation, invasion, and late metastasis as well as tumor sensitivity to immune medication therapy [12]. Pyroptosis-related chemicals have a crucial oncogenic function in the development of gastric cancer.

Immune checkpoint inhibitor (ICI) profiles in STAD patients may aid in diagnosing, analyzing, and anticipating therapy results [13]. The reason and methods of STAD's aberrant gene expression and pyroptosis remain unclear at this time. Understanding how PRGs regulate STAD production might result in the development of an indicator that can be employed as a therapeutic strategy.

2. Materials and Methods

We used the approaches proposed by Zi-Xuan Wu, et al. 2021 [14].

2.1. Datasets and PRGs. The Cancer Genome Atlas was used to collect STAD gene expression patterns and clinical data (TCGA) [15]. 375 STADs and 32 normal data were registered in the TCGA on May 6, 2022. The Gene Expression Omnibus (GEO) was searched for mRNA expression on May 6, 2022. Series: GSE84437. Platform: GPL6947-13512. The GEO was used to maintain 433 STAD cases [16](Table 1). We also identified 52 PRGs in total [17] (Table S1).

2.2. DEGs Linked to Pyroptosis and Mutation Rates. Perl matched and sorted transcription data and human configuration files to acquire exact mRNA data. The gene IDs were converted into gene names using information from the ensemble database. The R Limma was utilized to get the expression data for the PRGs. FDR < 0.05 and $|\log 2FC| \geq 1$ were used to evaluate if there was a significant change in PRG expression [18]. The role of differentially expressed

(a)

(b)

(c)

(d)
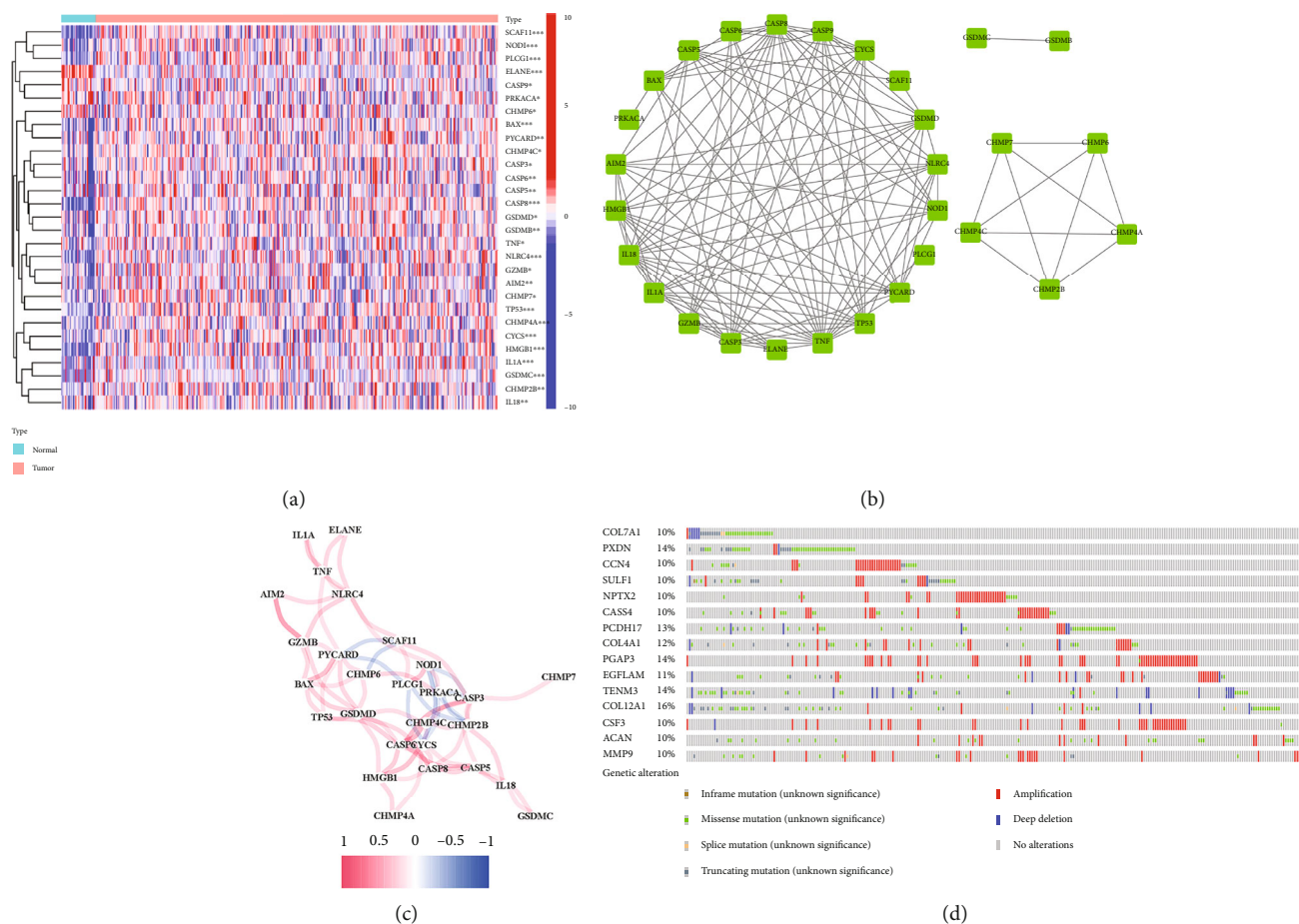
FIGURE 1: PRGs' expressions and interactions. (a) Heat map. (b) PPI network. (c) Correlation network. (d) Mutations.

PRGs that were both up- and down-regulated was investigated (DEGs). We also explored the genetic alterations in these genes. Cbioportal was used to estimate DEG mutation frequencies.

2.3. Tumor Classification Based on the DEGs. First, we used the Limma and ConsensusClusterPlus package to do cluster analysis, and we separated the prognosis-related PRGs into two clusters: cluster 1 and 2. Survminer was being used to study the survival of PRG subgroups, and survival was used to evaluate PRG's predictive validity. The pheat map was used to generate a heat map of the differential gene expression of prognosis-related PRGs, and the relationship between PRGs and clinicopathological features was explored. The limma was used to identify differences in target gene expression across categories. To study the gene interaction between STAD target genes and prognostic PRGs, the limma and corrplot programs were utilized.

2.4. Development of PRGs Prognostic Signature. Every STAD patient's risk score was also evaluated. The DEGs were divided into two groups based on their support for the median score: low-risk and high-risk. Lasso regression was shown to be associated with two risk classifications. The boldness interval and risk ratio were estimated after seeing the image, and the forest diagram was created as a conse-

quence. Survival curves for the two groups were developed and compared. To test the model's accuracy in predicting survival in STAD, the timeROC was used to generate a comparable receiver-operating characteristics (ROC) curve. The risk and survival status of PRGs were explored using the risk score's probability curve. The link between two PRGs patients was established, as was the relationship between clinical characteristics and the risk prediction model. Risk and clinical association analyses were distributed. T-distributed Neighbor Embedding (T-SNE) and Principal Component Analysis (PCA) were also examined. To determine if the prognostic model correctly classified patients into two risk groups, a representation was constructed to predict the 1-, 3-, and 5-year OS of STAD patients by the desegregation of prognosticative signals.

2.5. Functional Enrichment. The associated biological pathways were then examined using Gene Ontology (GO). BP, MF, and CC are controlled by differentially expressed PRGs. PRGs were further investigated using R based on KEGG dataset [19]. Filterpvalue < 0.05 was used to evaluate if there was a significant change in GO and KEGG.

2.6. GSEA Enrichment Analyses. GSEA was used to find related functions and route alterations in a variety of samples, while Perl was used to input data. The accompanying
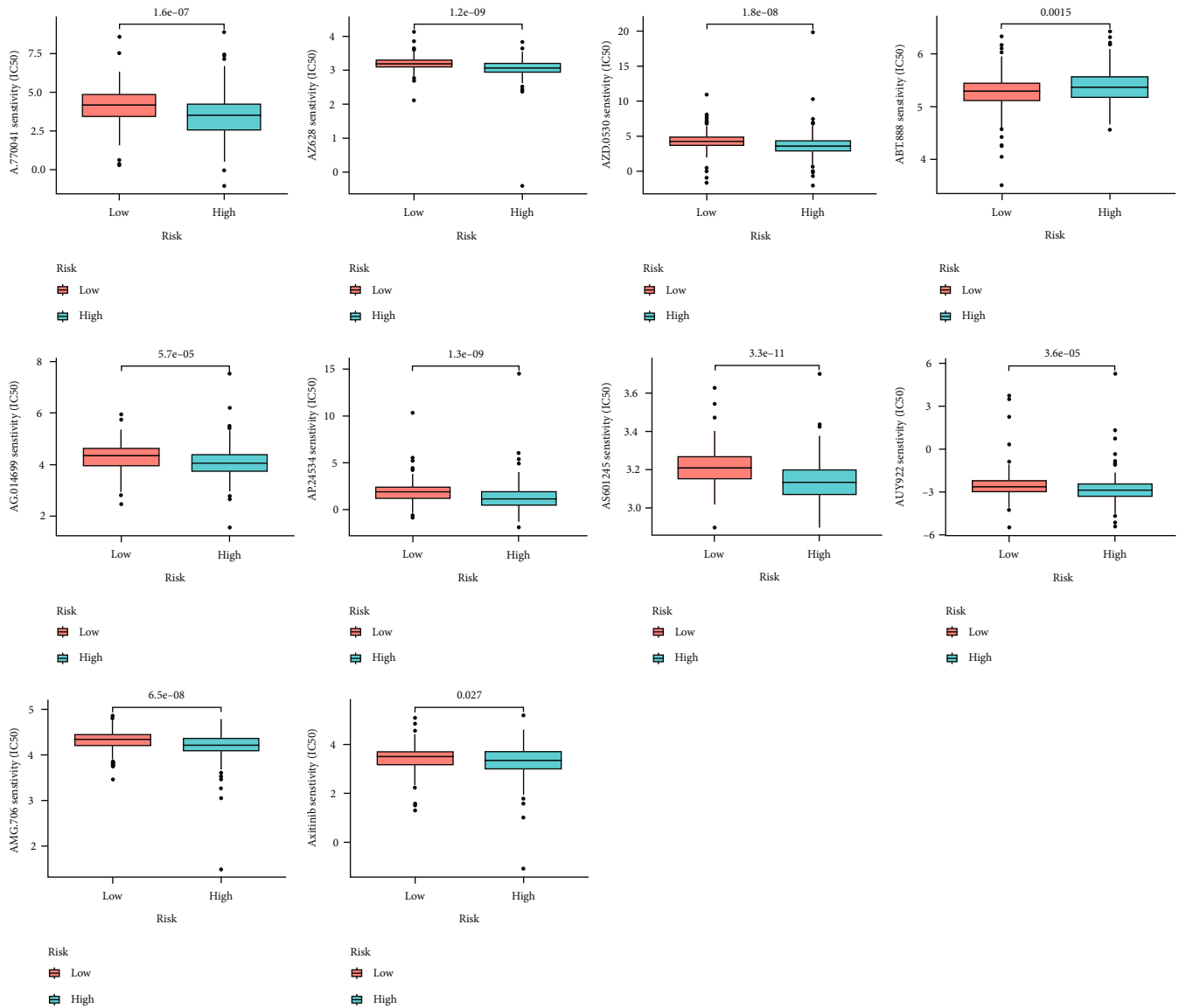
FIGURE 2: Drug prediction models.

score and graphs were used to assess whether the activities and routes within the different risk categories were dynamic or not. Each sample was assigned a 'H' or 'L' label based on whether it included a high-risk cluster of prognosis-related PRGs.

2.7. Comparison of the Immune Activity. We examined the enriched score of immune cells and activities in two risk groups using the ssGSEA in both the TCGA and GEO cohorts. We also explored the connection between PRGs, checkpoints, and m^{6}a.

3. Results

3.1. PRGs That Differ in Expression. Twenty-nine DEGs have been linked to pyroptosis (23 upregulated, 6 downregulated; Table S2). (Figure 1(a)). We conducted a protein-protein

interaction (PPI) research, the results of which are given in Figure 1(b). By setting the minimum required interaction value to 0.4, we identified that *TNF*, *CASP8*, *IL18*, *CASP3*, *IL1A*, *CASP9*, *PYCARD*, *HMGB1*, *GSDMD*, and *TP53* were hub genes (Table S3). These genes might be utilized to create independent STAD prognostic indicators. The correlation network, seen in Figure 1(c), is made up. We discovered that the gene mutations were truncating and missense variants (Figure 1(d)). 15 genes had a 10% mutation rate, with *COL12A1* being the commonly altered (16%).

3.2. Drug Prediction Models and Sensitivity Analysis. The drug prediction of the model showed that there were some genes with significant differences (Figure 2). Furthermore, the association analysis between DEG expression in the prognostic model revealed that several genes were
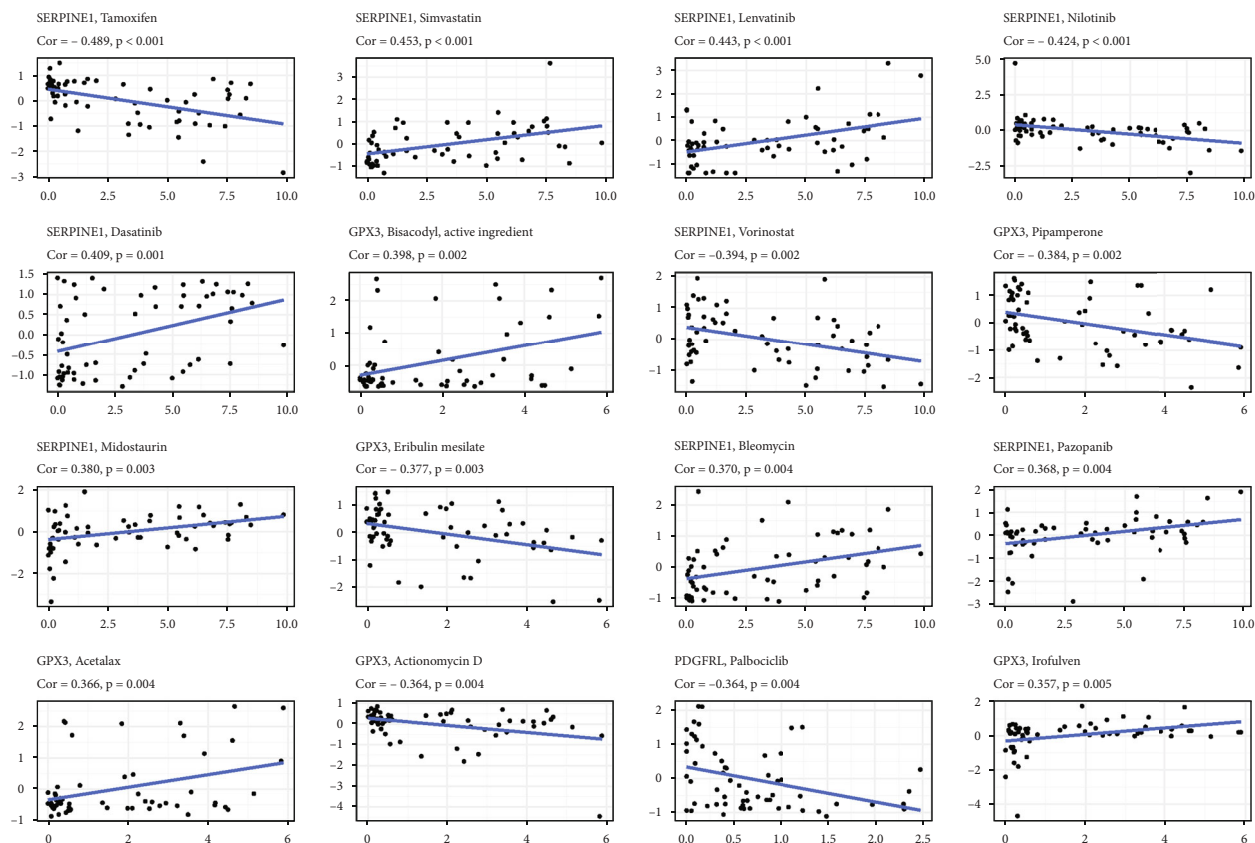
FIGURE 3: Drug sensitivity analysis.

substantially linked with medication sensitivity. For example, there was a strong association between SERPINE1 expression and Tamoxifen, Simvastatin, Lenvatinib, Nilotinib, Dasatinib, Vorinostat, Midostaurin, Bleomycin, and Pazopanib. These findings suggest possible future medication development paths (Figure 3).

3.3. Tumor Classification. In TCGA cohort, we conducted a consensus clustering analysis on 375 STAD sufferers to investigate the relationships between PRGs and STAD subgroups. The intragroup correlations were highest and the intergroup correlations were weakest when the clustering variable (k) was adjusted to 2. (Figure 4(a)). A heat map reflects both the gene expression patterns and clinical characteristics (Figure 4(b), Table S4). PRG subgroups were used in a survival study to explore the predictive capacity of PRGs, and cluster 1 had a higher survival rate ($P = 0.005$; Figure 4(c)), as shown in Figure 4(c).

3.4. In the TCGA Cohort, a Prognostic Gene Model Was Developed. Seven important PRGs were found throughout the COX investigation. These PRGs (GPX3, CD36, PDGFRL, EGFLAM, RGS2, CYTL1, and SERPINE1) were found as independent STAD prognostic markers (Figure 5(a)). The most minor absolute shrinkage and choice operator Cox regression analysis (LASSO) and the optimal value were used to build a gene signature (Figures 5(b) and 5(c)). We observed that a patient's risk score was negatively connected to STAD patients' survival using a risk survival standing plot. The presence of high-risk PRG signatures was linked to a reduced chance of survival ($P < 0.001$, Figure 5(e)). For 1-, 3-, and 5-year survival rates, the AUC of the unique PRGs signature was 0.631, 0.664, and 0.735, respectively (Figure 5(f)). Our data analysis revealed that the great majority of STAD patients lived for less than 5 years, therefore the AUC of less than 0.6 in the fifth year is a result of this. PCA and t-SNE results indicated that patients with varying risks were divided into two groups (Figures 5(g) and 5(h)).

3.5. The Risk Signature Is Externally Validated. We observed that a patient's risk score was adversely related to STAD patient survival. Surprisingly, majority of the novel PRGs discovered during this research were adversely related with our risk model, comparable to the TCGA findings (Figure 6(a)). High-risk PRG signatures were related with a lower likelihood of survival ($P = 0.011$, Figure 6(b)). The AUC of the distinctive PRGs signature was 0.594, 0.613, and 0.602 for 1-, 3-, and 5-year survival rates, respectively (Figures 6(c)). Our data analysis found that the vast majority of STAD patients lived for more than 1 years, resulting in an AUC of less than 0.7 in the fifth year. The PCA and t-SNE findings showed that patients with variable risks were efficiently sorted into two different groups (Figures 6(d) and 6(e)). We also created a heat map (Figure 6(e)).

3.6. Independent Prognostic Value of the Risk Model. In TCGA cohort, COX analysis demonstrated that the PRGs
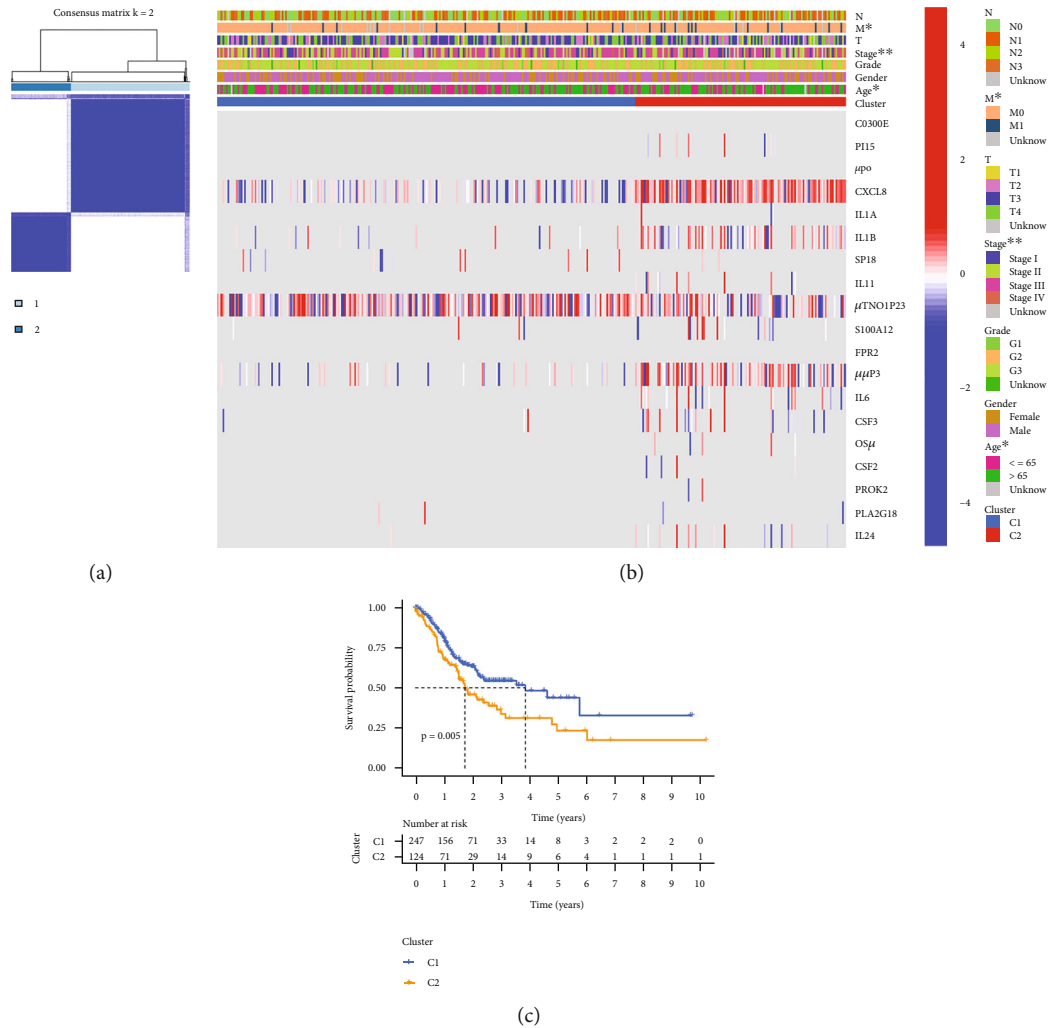
Figure 4: Tumor categorization. (a) Consensus clustering matrix. (b) Heat map. (c) Kaplan–Meier OS curves.

signature (HR: 9.629, 95CI: 2.818-32.903), Age (HR: 1.034, 95CI: 1.015-1.053), M stage (HR: 2.212, 95CI: 1.189-4.115), and N stage (HR: 1.281, 95CI: 1.088-1.508) were primarily independent predictive variables for the OS of STAD patients (Figures 7(a) and 7(b)). In GEO cohort, COX analysis demonstrated that Age (HR: 1.022, 95CI: 1.009-1.034), T stage (HR: 1.609, 95CI: 1.262-2.051), and N stage (HR: 1.526, 95CI: 1.298-1.792) were primarily independent predictive variables for the OS of STAD patients (Figures 7(c) and 7(d)). In addition, for the TCGA cohort, we constructed a heat map of clinical characteristics (Figure 7(e)) (Table S5-6).

3.7. Enrichment Analysis of Pyroptosis-Related Genes. GO enrichment analysis revealed 550 core targets, including Biological processes (BP), molecular functions (MF), and cellular components (CC). The MF mainly involves actin–binding (GO:0003779) and enzyme inhibitor activity (GO:0004857). The CC mainly involves focal adhesion (GO:0005925) and cell leading edge (GO:0031252). The BP mainly involves skeletal system development (GO:0001501), cell growth (GO:0016049), and negative reg-

ulation of hydrolase activity (GO:0051346). In addition, the main signaling pathways were identified by KEGG enrichment analysis, it revealed the over-expressed genes were mainly involved in PI3K-Akt signaling pathway (hsa04151), Proteoglycans in cancer (hsa05205), Focal adhesion (hsa04510), Vascular smooth muscle contraction (hsa04270), Protein digestion and absorption (hsa04974), and Amoebiasis (hsa05146) (Figure 8 and Table S7a-b).

3.8. Analyses of GSEA. According to GSEA, the majority of PRG prognostic signatures controlled immunological and tumor-related pathways—ecm receptor interaction, complement and coagulation cascades, hedgehog, tgf beta, jak stat, and chemokine signaling pathway, etc. Each cluster's top six enriched functions or pathways are displayed (Figure 9, Table 2). The "hedgehog signaling pathway" was the most enriched, and some of the genes were shown to be positively associated to H or L. (Table S8a-b).

3.9. Immune Activity Comparisons. We investigated the enrichment scores of 16 kinds of immune cells and the activity of 13 immune-related activities in both the TCGA and

(a)

(b)

(c)

(d)

(e)

(f)

FIGURE 5: Continued.

(g)

(h)
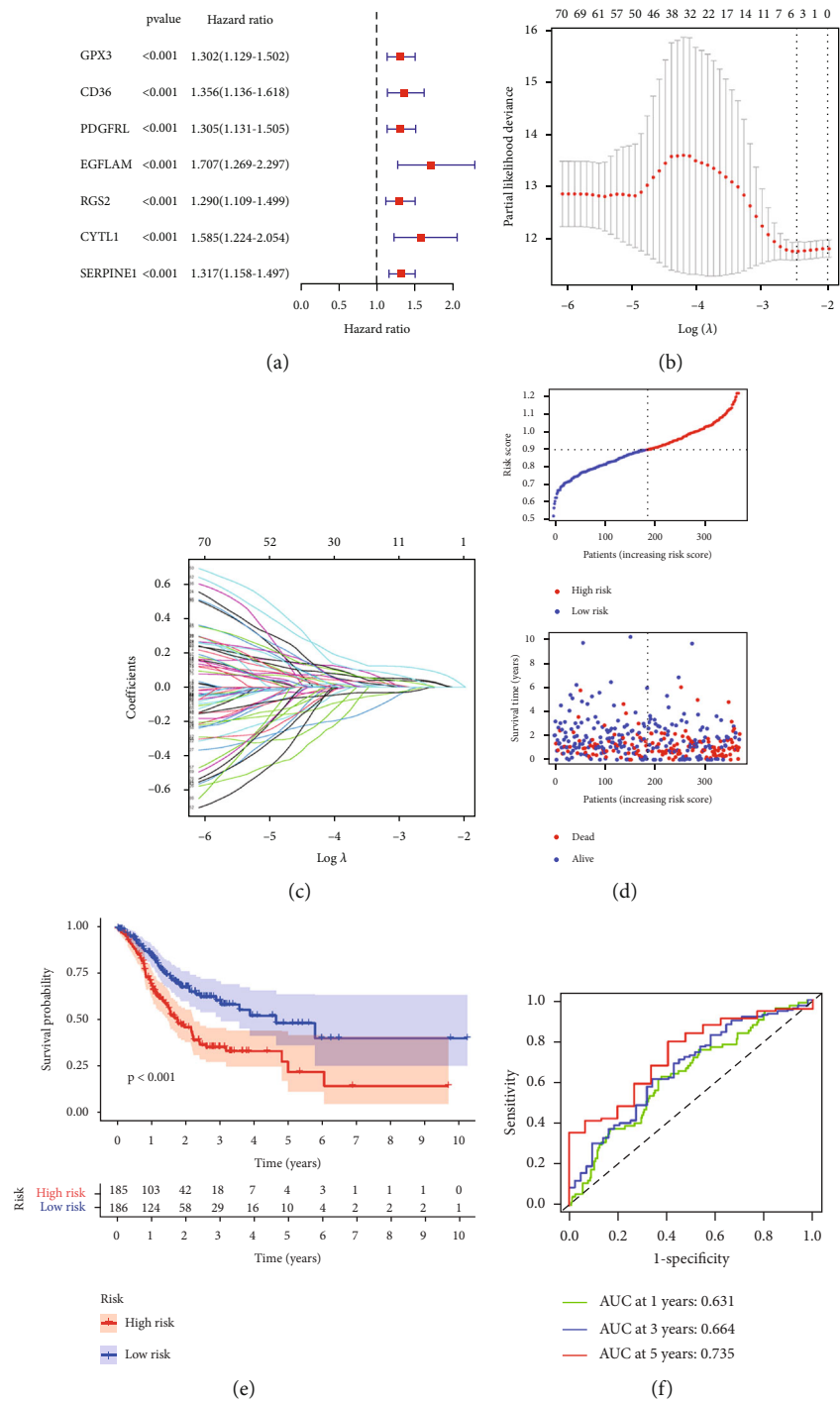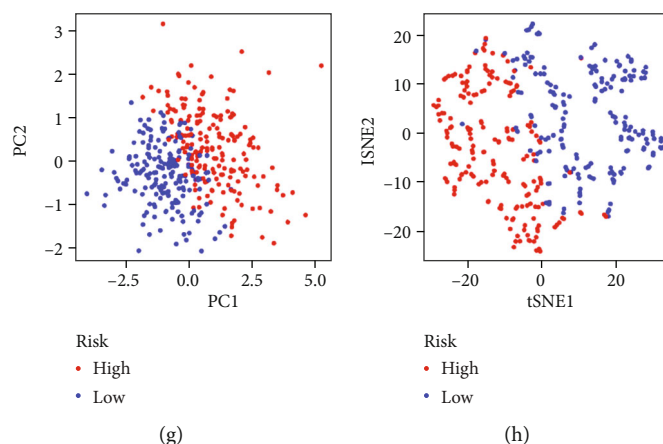
FIGURE 5: In the TCGA cohort, the formation of a risk signature. (a) Univariate cox regression analysis. (b) LASSO regression. (c) Cross-validation. (d) Survival status. (e) Kaplan–Meier curve. (f) The AUC of the survival rate. (g) PCA plot. (h) t-SNE plot.

GEO cohorts using the single-sample gene set enrichment approach (ssGSEA). In the TCGA cohort, IDCs, NK cells, and Th2 cells did not differ significantly between the two groups ($P > 0.05$). Other immune cells generally show higher levels of infiltration in the high-risk grouping (Figure 10(a)). APC coinhibition and MHC class I did not differ significantly between the two groups ($P > 0.05$). Other immune-related function generally show higher levels in the high-risk grouping (Figure 10(b)). When assessing the immune status in the GEO cohort, similar conclusions were drawn (Figures 10(c) and 10(d)).

3.10. An Examination of the Relationship between PRGs and Immunological Checkpoints and m^6a. LAIR1, CD274, HAVCR2, PDCD1LG2, TNFRSF4, and other genes were expressed differently (Figure 11(a)). When PRG expression levels were compared between the two-risk groups, *FTO* was significantly higher in the high-risk group. While *YTHDF2, RBM15, ZC3H13, METTL3, HNRNPC,* and *YTHDC1* were shown to be much more significant in the low-risk group (Figure 11(b)). The expression of *FTO* associated with m^6a modification was higher in the high risk group, indicating that it may be linked to the malignancy activity in STAD sufferers. While *YTHDF2, RBM15, ZC3H13, METTL3, HNRNPC, YTHDC1* with m^6a modifications had higher expression in the low risk group, indicating that they might be tumor suppressors.

4. Discussion

Treating STAD is a severe clinical issue because of its advanced stage and terrible prognosis. The current state of precision medicine for STAD is limited by a scarcity of powerful tumor-killing initiators and selective tumor-targeting therapeutic agents. Recent study has shown that the focused therapeutic impact of STAD may be successfully increased by modifying the process of programmed tumor cell death [20]. Pyroptosis, a recently identified process of programmed cell death, is gaining prominence in the context

of innate immunity, carcinogenesis, and patient responses to anticancer therapy [21, 22]. Pyroptosis occurs in pathogen-infected cells, causing an inflammatory reaction and cell lysis within the host body [23]. Pyroptosis manifests itself in malignancies in two ways. On the one hand, the inflammasome can efficiently promote tumor cell death by activating the pyroptosis pathway, therefore reducing tumor cell growth and invasion [24]. It is unknown how it impacts STAD development by modifying PRGs. We studied the function of critical proteins and processes in STAD prognosis and established a suitable biomarker and anticancer activity.

In a university Cox regression investigation, PRGs were found to be strongly linked with STAD prognosis. The researchers discovered four prognostic PRGs that have been expressed differently in two-risk persons. Some PRGs were identified to be highly expressed in high-risk, whereas others were seen to be differentially expressed in low-risk ($P < 0.05$). A survival analysis was used to find the prognostic capacity of PRGs after additional examination into their influence. Individuals with STAD who had low-risk PRGs survived longer. The markers *GPX3, PDGFRL, RGS2,* and *SERPINE1* were found to be significantly increased in the high-risk group, suggesting that all of these markers may be implicated in the malignancy processes for STAD patients and may be cancer-promoting factors. The findings of the above-mentioned biomarker suggest some suggestions for future work, but concrete evidence that they will be responsible for the synthesis of important transcription factors associated with pyroptosis regulation, such as *PD-L1, GSDMB,* and *ROS-NLRP3* [25–27], is lacking, necessitating further exploration.

Compared to normal tissues and cells, Gpx3 expression was lower in gastric cancer (GC) patients and GC cell lines. Cai et al. believes that Gpx3 inhibits gastric cancer migration and invasion by targeting NFκB/Wnt5a/JNK signaling [28]. When GPX3 expression in breast cancer cells and tissues was compared to normal controls, it was shown to be low. GPX3 overexpression inhibited breast cancer growth, colony
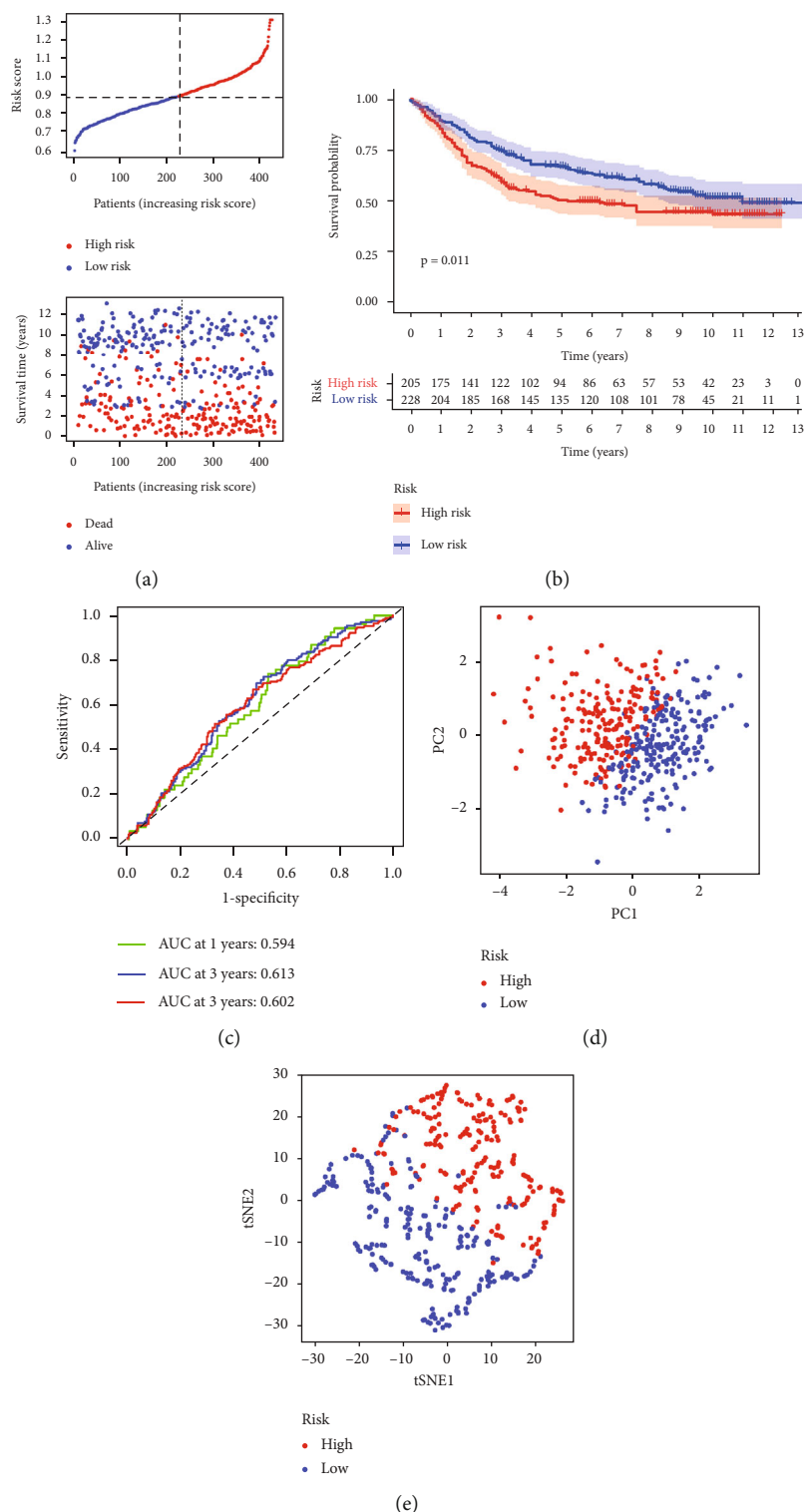
Figure 6: In the GEO cohort, the risk model was verified. (a) Survival status. (b) Kaplan–Meier curve. (c) The AUC of the survival rate. (d) PCA plot. (e) t-SNE plot.

formation, migration, and invasion in vitro. Furthermore, hypermethylation of the GPX3 promoter and suppression of hsa-miR-324-5p release have been identified as probable pathways for GPX3 downregulation in breast cancer [29]. Through bioinformatics analysis, Huo et al. discovered

PDGFRL was one of the tumor-associated macrophages (TAMs). It is vital in the progression of malignant tumors and performed well in predicting overall survival (OS) in GC [30]. Cancer cell dormancy and tumor relapse are mediated by RGS2-mediated translational control [31].
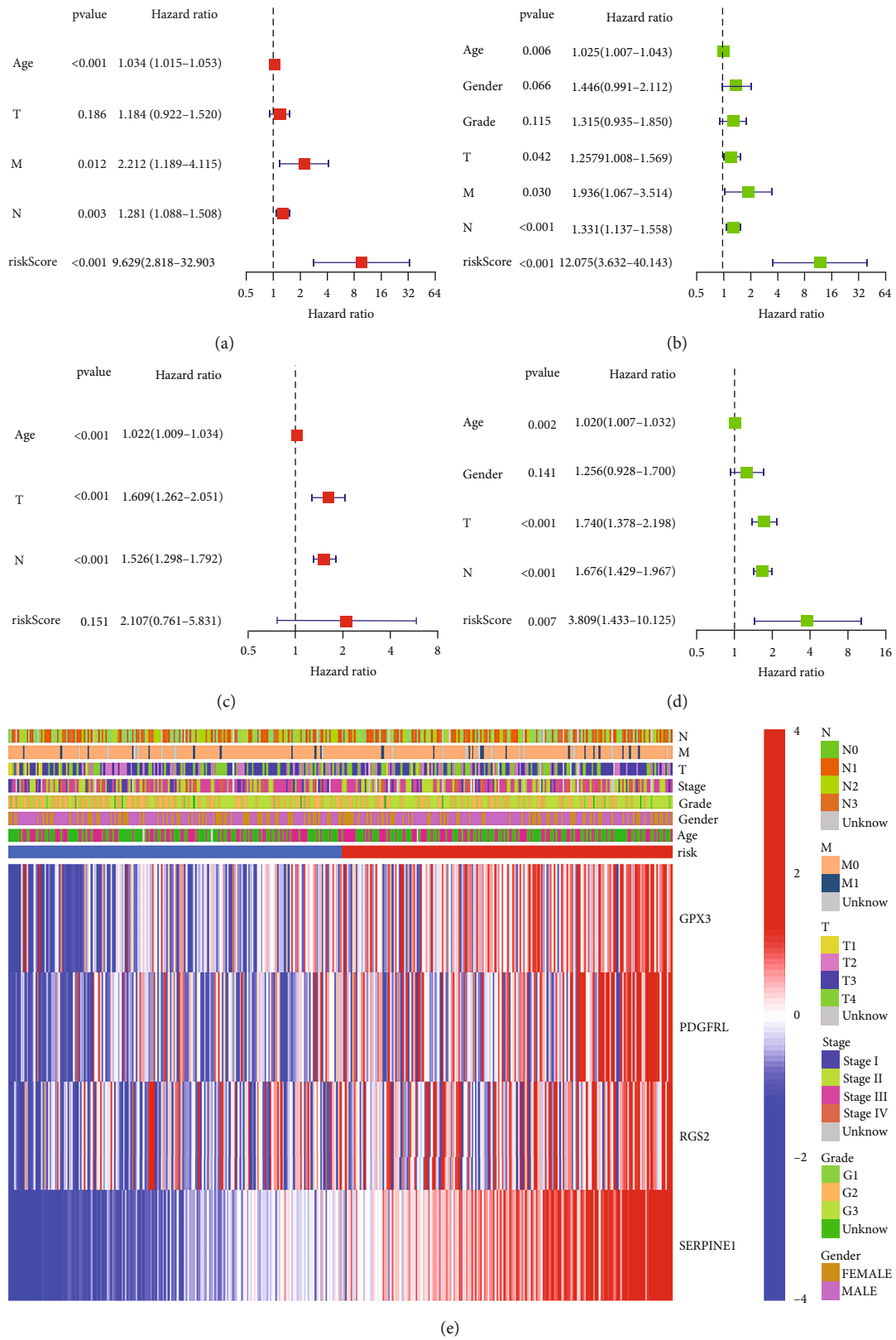
FIGURE 7: Cox regression analysis. (a,b) TCGA cohort. (c,d) GEO cohort. (a,c) Multivariate analysis. (b,d) Univariate analysis. (e) Heat map highlighting the relationships between clinicopathological characteristics and risk categories.
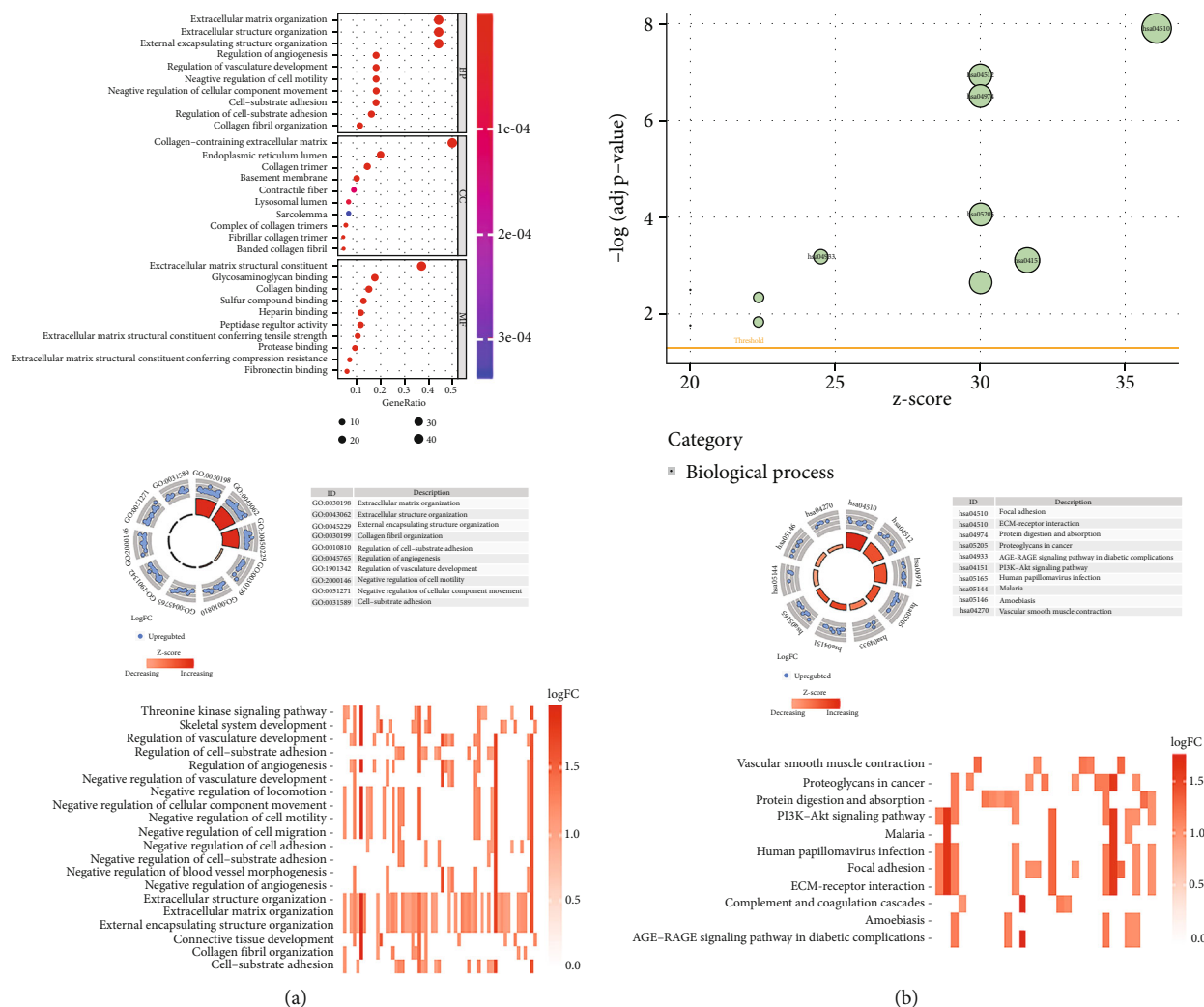
Figure 8: Enrichment analysis for PRGs. (a) GO and (b) KEGG.

SERPINE1 was found to be significantly upregulated in gastric tissues and associated with poor outcomes in a genome-scale analysis. As a result, Liao et al. thought of SERPINE1 as a diagnostic and prognostic biomarker in GC [32]. Because these PRGs appear to be associated with cancer processes in STAD patients, these studies highlight the validity and plausibility of our findings. According to the OS and ROC analyses of the GSE84437 KM-curves, a PRGs-signature might be employed as a viable predictive predictor. Only a few investigations on the gene alterations associated with pyroptosis have been conducted. More research is needed to fully understand the mechanics of PRG alteration and classification, as well as to validate our findings.

KEGG analysis found that the genes were primarily involved in PI3K-Akt signaling pathway. DHA protects against hepatic ischemia reperfusion injury by inhibiting pyrolysis and activating the PI3K/Akt signaling pathway [33]. Pioglitazone Provides Neuroprotection Against Ischemia-Induced Pyroptosis by inhibiting the RAGE pathway by Activating PPAR-ɤ [34]. Consequently, Pyroptosis

is crucial in STAD. In GSEA, the hedgehog signaling pathway was found to be the most significantly enriched pathway. Smo and Gli1 genes are components of the hedgehog signaling pathway, and their over expression can cause STAD. The degree of expression is linked to the stage and severity of STAD [35]. Furthermore, studies have shown that Hedgehog-interactingprotein (HHIP) may inhibit the growth and proliferation of STAD cell lines by blocking Hedgehog signal transduction, which may become a new biological marker for STAD and a new approach for STAD treatment by targeting the drug target of HHIP formation [36]. Overactivation of the hedgehog pathway is linked to the occurrence and progression of STAD, and specific targeted therapy targeting this pathway may become an effective new measure for clinical treatment of STAD [37]. Taking the aforementioned properties into account, PRGs may influence STAD cell migration and proliferation via modulating the nod like receptor signaling pathway.

Furthermore, our technique accurately predicts STAD patients' survival. Increases in risk score are linked to higher
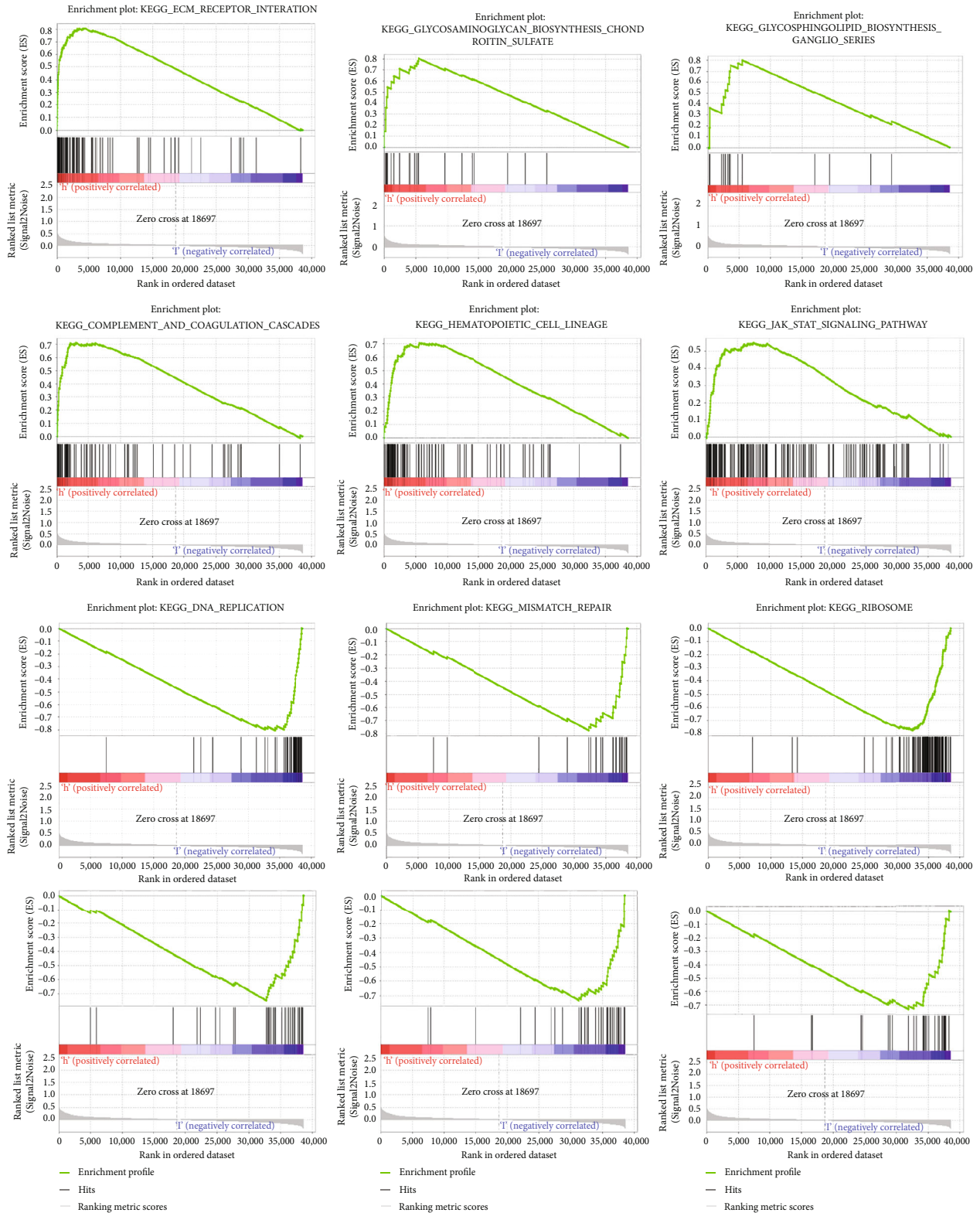
Figure 9: GSEA analyses.

TABLE 2: The top six enriched functions or pathways.

NAME	ES	NES	NOM p value	FDR q value
DNA replication	0.6792336	1.622164	0.054435484	0.67065173
Mismatch repair	0.67632705	1.6375834	0.04192872	0.75468564
Spliceosome	0.6235964	1.8821576	0.014522822	0.47306138
Homologous recombination	0.5929925	1.5829824	0.06329114	0.42215267
Cell cycle	0.5691944	1.8317317	0.024896266	0.3576104
Proteasome	0.557963	1.4626185	0.13636364	0.3447309
Other glycan degradation	-0.664515	-1.7258755	0.018480493	0.226103
Alpha linolenic acid metabolism	-0.64434105	-1.8918467	0.004106776	0.10805818
Ribosome	-0.61395043	-1.4429549	0.18145162	0.4314213
Fructose and mannose metabolism	-0.58743125	-1.8711866	0.006085193	0.08654529
Fatty acid metabolism	-0.5829716	-1.9166667	0.006097561	0.16615777
Glycosaminoglycan degradation	-0.5582348	-1.6052122	0.046511628	0.2974447
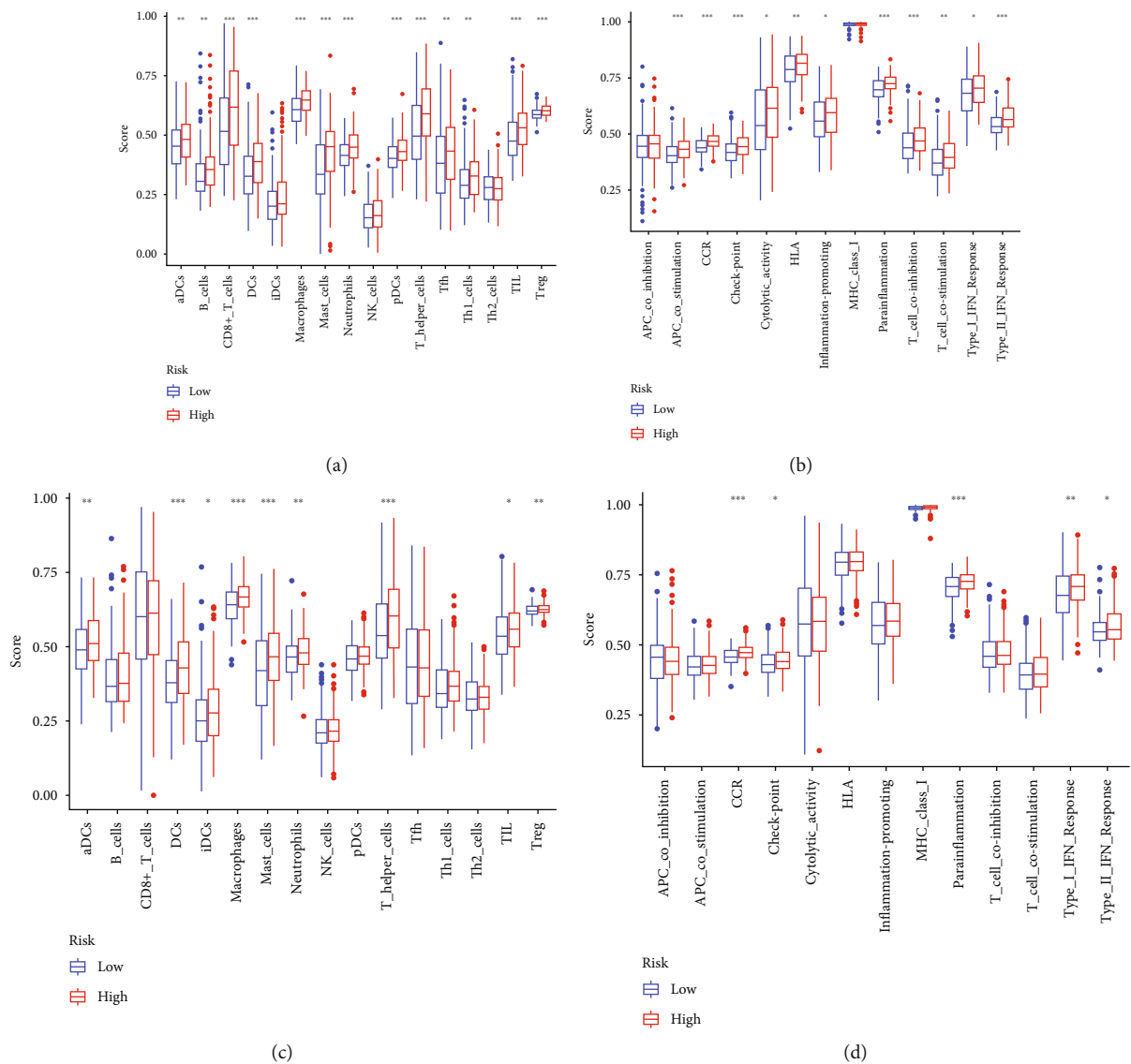
FIGURE 10: The ssGSEA scores for immune cells and immune function. (a,b) TCGA cohort. (c,d) GEO cohort.

(a)

(b)
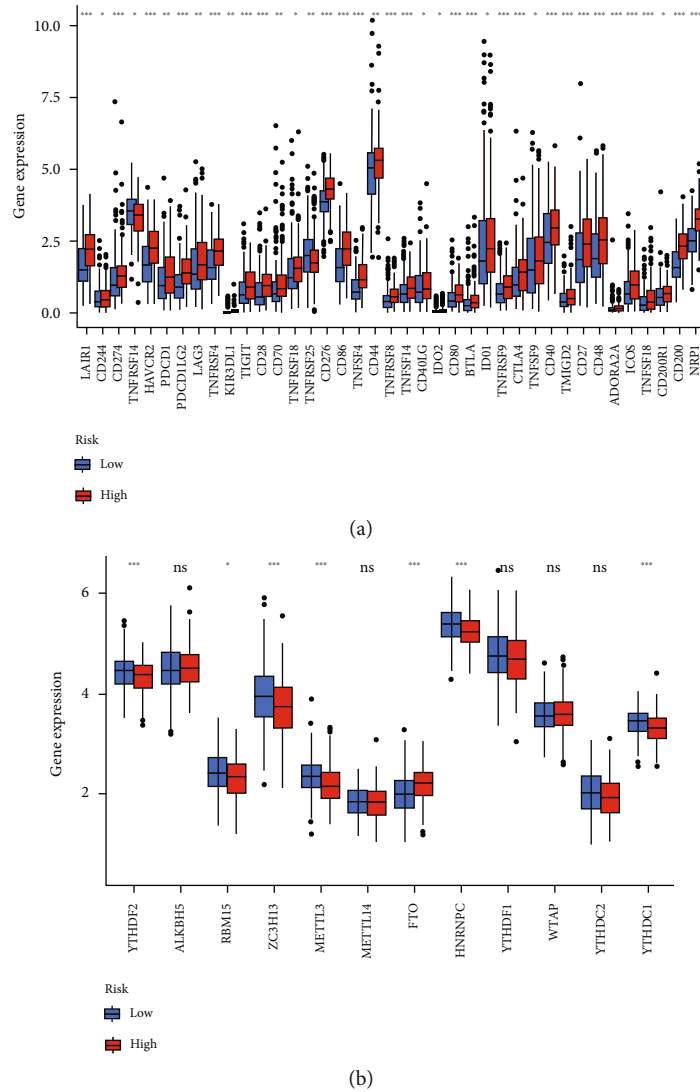
FIGURE 11: (a) Expression of immune checkpoints and (b) the expression of m⁶a-related genes.

death rates and a higher high-risk ratio. Based on our findings and data from the literature, PRGs appear to be significant biomarkers for predicting STAD patient outcomes. Recent research has discovered a link between several cell death mechanisms and anticancer immunity. Even in ICI-resistant tumors, pyroptosis, ferroptosis, and necroptosis activation in conjunction with ICIs resulted in synergistically improved anticancer efficacy [38, 39]. De novo pyroptosis in ICI-resistant cancers can produce an inflammatory milieu that mediates tumor susceptibility to immune checkpoint inhibitors (ICI), promoting pyroptosis and inhibiting tumor growth in autochthonous tumors [40]. Despite the fact that there has been minimal study on PRGs and STAD, based on the evidence presented above, it is reasonable to believe that PRG changes were associated with the onset and development of STAD.

There have been a number of publications published in recent years that examine the association between pyroptosis and STAD [41, 42]. However, when compared to other studies, the approach used in this study is novel. To begin, PRGs

in the TCGA database are routinely updated. We have made further additions to previous articles. Second, TCGA data were used as the primary analysis, with GEO data included into the common pattern for model validation. Third, GO and KEGG analyses, as well as a GSEA analysis, were performed. The conclusions of the two investigations coincided, which increased trust. Fourth, to increase the trustworthiness of the results, we employed different databases to quantify immune cells and functions.

Our analysis has the following limitations: (1) we will be unable to obtain sufficient different data sources from other publically available sites to validate the model's trustworthiness. (2) We investigated the functional enrichment processes engaged in the regulatory networks of distinct risk groups; however, their particular mechanisms in enabling pyroptosis require more exploration to corroborate our findings. (3) Although the model was validated in the GEO dataset, the prediction model developed in this work still has to be externally and practically verified before it can be used on clinical patients.

5. Conclusions

In STAD sufferers, 4 expected PRGs were discovered. The findings contribute to a better understanding of the immunological system's role in pyroptosis, perhaps paving the way for new effective treatments and prognostic biomarkers. Pyroptosis regulation may be a promising therapeutic technique for improving the result of STAD immunotherapy and providing a tailored prognostic tool for prognosis and immune response.

Abbreviations

STAD: Stomach adenocarcinoma
GO: Gene ontology
AUC: Areas under the curve
MF: Molecular functions
ICIs: Immune checkpoint inhibitors
ROC: Receiver-operating characteristics
GSEA: Gene set enrichment analyses
KEGG: Kyoto Encyclopedia of Genes and Genomes
TCGA: The Cancer Genome Atlas
PRGs: Pyroptosis-related genes
BP: Biological processes
CC: Cellular components
OS: Overall survival
GEO: Gene Expression Omnibus
DEGs: Differentially expressed genes.

Data Availability

The datasets presented in this study can be found in online repositories. The names of the repository/repositories and accession numbers can be found in the article/Supplementary Material. The [Diseases] data used to support the findings of this study have been deposited in the [GEO] repository (https://www.ncbi.nlm.nih.gov/geo/). [TCGA] repository (https://portal.gdc.cancer.gov/).

Ethical Approval

This article is not a clinical trial; hence, the ethics approval and consent to participation are not applicable.

Consent

All authors have read and approved this manuscript to be considered for publication.

Disclosure

Jingmin Xu and Ke Chen contributed equally to this article as a co-first author.

Conflicts of Interest

The authors declare that the research was conducted in the absence of any commercial or financial relationships that could be construed as a potential conflict of interest.

Authors' Contributions

Jingmin Xu, Ke Chen, and Zixuan Wu drafted the manuscript. Jingmin Xu, Ke Chen, and Zhou Wei revised the manuscript. Jingmin Xu and Zixuan Wu polished up the article. Xuyan Huang, Minjie Cai, Jing Zhang, and Kai Yuan are in charge of data collection. Shuai Wang and Peidong Huang conceived and designed this article were in charge of syntax modification and revision of the manuscript. Shuai Wang contributed to this study with funding. All the authors have read and agreed to the final version of the article. Jingmin Xu and Ke Chen contributed equally to this article as a co-first author.

Acknowledgments

Supplementary Materials

Appendix 1-52 pyroptosis-related genes. Appendix 2-DEGs linked to PRGs. Appendix 3-hub genes analysis. Appendix 4-The gene expression profile and clinical characteristics. Appendix 5-4 risk PRGs. Appendix 6-Table 6. Clinical features for the TCGA cohort. Appendix 7-GO and KEGG enrichment analysis. Appendix 8-gene set enrichment analyses (GSEA). (Supplementary Materials)

References

[1] E. M. Aydın, T. D. Demir, N. Seymen et al., "The crosstalk between H. pylori virulence factors and the PD1:PD-L1 immune checkpoint inhibitors in progression to gastric cancer," Immunology Letters, vol. 239, pp. 1–11, 2021.

[2] K. Mimura, L. F. Kua, J. F. Xiao et al., "Combined inhibition of PD-1/PD-L1, Lag-3, and Tim-3 axes augments antitumor immunity in gastric cancer-T cell coculture models," Gastric Cancer, vol. 24, no. 3, pp. 611–623, 2021.

[3] N. S. Yee, E. J. Lengerich, K. H. Schmitz et al., "Frontiers in gastrointestinal oncology: advances in multi-disciplinary patient care," Biomedicine, vol. 6, no. 2, p. 64, 2018.

[4] L. H. Eun, C. Smyrk Thomas, and Z. Lizhi, "Histologic and immunohistochemical differences between hereditary and sporadic diffuse gastric carcinoma," Human Pathology, vol. 74, pp. 64–72, 2018.

[5] G. Schinzari, A. Cassano, A. Orlandi, M. Basso, and C. Barone, "Targeted therapy in advanced gastric carcinoma: the future is beginning," Current Medicinal Chemistry, vol. 21, no. 8, pp. 1026–1038, 2014.

[6] J. Machlowska, J. Baj, M. Sitarz, R. Maciejewski, and R. Sitarz, "Gastric cancer: epidemiology, risk factors, classification, genomic characteristics and treatment strategies," International Journal of Molecular Sciences, vol. 21, no. 11, p. 4012, 2020.

[7] B. Nicola, A. Antonio, and V. Danilo, "Autoimmunity and Gastric Cancer," International Journal of Molecular Sciences, vol. 19, no. 2, p. 377, 2018.

[8] D. Hanahan and R. A. Weinberg, "Hallmarks of cancer: the next generation," Cell, vol. 144, no. 5, pp. 646–674, 2011.

[9] Y. Tan, Q. Chen, X. Li et al., "Pyroptosis: a new paradigm of cell death for fighting against cancer," *Journal of Experimental & Clinical Cancer Research*, vol. 40, no. 1, p. 153, 2021.

[10] R. Karki and T.-D. Kanneganti, "Diverging inflammasome signals in tumorigenesis and potential targeting," *Nature Reviews Cancer*, vol. 19, no. 4, pp. 197–214, 2019.

[11] P. Zhao, M. Wang, M. Chen et al., "Programming cell pyroptosis with biomimetic nanoparticles for solid tumor immunotherapy," *Biomaterials*, vol. 254, article 120142, 2020.

[12] P. Yu, X. Zhang, N. Liu, L. Tang, C. Peng, and X. Chen, "Pyroptosis: mechanisms and diseases," *Signal Transduct Target Ther*, vol. 6, no. 1, p. 128, 2021.

[13] E. Zhao, S. Chen, and Y. Dang, "Development and External Validation of a Novel Immune Checkpoint-Related Gene Signature for Prediction of Overall Survival in Hepatocellular Carcinoma," *Frontiers in Molecular Biosciences*, vol. 7, article 620765, 2021.

[14] Z. X. Wu, X. Huang, M. J. Cai, P. D. Huang, and Z. Guan, "Development and validation of a prognostic index based on genes participating in autophagy in patients with lung adenocarcinoma," *Frontiers in Oncology*, vol. 11, article 799759, 2021PMID: 35145906.

[15] Z. Wang, M. A. Jensen, and J. C. Zenklusen, "A practical guide to the cancer genome atlas (TCGA)," in *Statistical Genomics*, vol. 1418 of Methods in Molecular Biology, Humana Press, New York, NY, 2016.

[16] T. Barrett, S. E. Wilhite, P. Ledoux et al., "NCBI GEO: archive for functional genomics data sets–update," *Nucleic Acids Research*, vol. 41, no. Database issue, pp. D991–D995, 2013.

[17] D. Xu, Z. Ji, and L. Qiang, "Molecular characteristics, clinical implication, and cancer immunity interactions of pyroptosis-related genes in breast cancer," *Frontiers in Medicine*, vol. 8, article 702638, 2021.

[18] Y. Ye, Q. Dai, and H. Qi, "A novel defined pyroptosis-related gene signature for predicting the prognosis of ovarian cancer," *Cell Death Discovery*, vol. 7, no. 1, p. 71, 2021.

[19] Y. Tang, C. Li, Y. J. Zhang, and Z. H. Wu, "Ferroptosis-related long non-coding RNA signature predicts the prognosis of head and neck squamous cell carcinoma," *International Journal of Biological Sciences*, vol. 17, no. 3, pp. 702–711, 2021.

[20] Y. H. Xie, Y. X. Chen, and J. Y. Fang, "Comprehensive review of targeted therapy for colorectal cancer," *Signal Transduction and Targeted Therapy*, vol. 5, no. 1, pp. 1–30, 2020.

[21] C. B. Zhou and J. Y. Fang, "The role of pyroptosis in gastrointestinal cancer and immune responses to intestinal microbial infection," *Biochimica et Biophysica Acta (BBA) - Reviews on Cancer*, vol. 1872, no. 1, pp. 1–10, 2019.

[22] S. K. Pachathundikandi, N. Blaser, H. Bruns, and S. Backert, "Helicobacter pylori avoids the critical activation of NLRP3 Inflammasome-mediated production of oncogenic mature IL-1β in human immune cells," *Cancers*, vol. 12, no. 4, p. 803, 2020.

[23] D. A. Erkes, W. Cai, I. M. Sanchez et al., "Mutant BRAF and MEK inhibitors regulate the tumor immune microenvironment via Pyroptosis," *Cancer Discovery*, vol. 10, no. 2, pp. 254–269, 2020.

[24] J. Hou, R. Zhao, W. Xia et al., "Author correction: PD-L1-mediated gasdermin C expression switches apoptosis to pyroptosis in cancer cells and facilitates tumour necrosis," *Nature Cell Biology*, vol. 22, no. 11, p. 1396, 2020.

[25] J. Hou, R. Zhao, W. Xia et al., "PD-L1-mediated gasdermin C expression switches apoptosis to pyroptosis in cancer cells and facilitates tumour necrosis," *Nature Cell Biology*, vol. 22, no. 10, pp. 1264–1275, 2020.

[26] L. Li, Y. Li, and Y. Bai, "Role of GSDMB in pyroptosis and Cancer," *Cancer Management and Research*, vol. Volume 12, pp. 3033–3043, 2020.

[27] X. Wu, H. Zhang, W. Qi et al., "Nicotine promotes atherosclerosis via ROS-NLRP3-mediated endothelial cell pyroptosis," *Cell Death & Disease*, vol. 9, no. 2, p. 171, 2018.

[28] M. Cai, Y. Sikong, Q. Wang, S. Zhu, F. Pang, and X. Cui, "Gpx3 prevents migration and invasion in gastric cancer by targeting NFκB/Wnt5a/JNK signaling," *International Journal of Clinical and Experimental Pathology*, vol. 12, no. 4, pp. 1194–1203, 2019.

[29] W. Lou, B. Ding, S. Wang, and P. Fu, "Overexpression of GPX3, a potential biomarker for diagnosis and prognosis of breast cancer, inhibits progression of breast cancer cells in vitro," *Cancer Cell International*, vol. 20, no. 1, p. 378, 2020.

[30] J. Huo, L. Wu, and Y. Zang, "Construction and validation of a universal applicable prognostic signature for gastric cancer based on seven immune-related gene correlated with tumor associated macrophages," *Frontiers in Oncology*, vol. 11, article 635324, 2021.

[31] J. Cho, H. Y. Min, H. J. Lee et al., "RGS2-mediated translational control mediates cancer cell dormancy and tumor relapse," *The Journal of Clinical Investigation*, vol. 131, no. 1, 2021.

[32] P. Liao, W. Li, R. Liu et al., "Genome-scale analysis identifies SERPINE1 and SPARC as diagnostic and prognostic biomarkers in gastric cancer," *Oncotargets and Therapy*, vol. Volume 11, pp. 6969–6980, 2018.

[33] Z. Li, F. Zhao, Y. Cao et al., "DHA attenuates hepatic ischemia reperfusion injury by inhibiting pyroptosis and activating PI3K/Akt pathway," *European Journal of Pharmacology*, vol. 835, pp. 1–10, 2018.

[34] P. Xia, Y. Pan, F. Zhang et al., "Pioglitazone confers neuroprotection against ischemia-induced pyroptosis due to its inhibitory effects on HMGB-1/RAGE and Rac1/ROS pathway by activating PPAR-ɤ," *Cellular Physiology and Biochemistry*, vol. 45, no. 6, pp. 2351–2368, 2018.

[35] O. Abdel-Rahman, "Hedgehog pathway aberrations and gastric cancer; evaluation of prognostic impact and exploration of therapeutic potentials," *Tumor Biology*, vol. 36, no. 3, pp. 1367–1374, 2015.

[36] Y. Xu, S. Song, Z. Wang, and J. A. Ajani, "The role of hedgehog signaling in gastric cancer: molecular mechanisms, clinical potential, and perspective," *Cell Communication and Signaling*, vol. 17, no. 1, p. 157, 2019.

[37] A. I. Akyala and M. P. Peppelenbosch, "Gastric cancer and hedgehog signaling pathway: emerging new paradigms," *Genes & Cancer*, vol. 9, no. 1-2, pp. 1–10, 2018.

[38] R. Tang, J. Xu, B. Zhang et al., "Ferroptosis, necroptosis, and pyroptosis in anticancer immunity," *Journal of Hematology & Oncology*, vol. 13, no. 1, p. 110, 2020.

[39] S. K. Hsu, C. Y. Li, I. L. Lin et al., "Inflammation-related pyroptosis, a novel programmed cell death pathway, and its crosstalk with immune therapy in cancer treatment," *Theranostics*, vol. 11, no. 18, pp. 8813–8835, 2021.

[40] S. T. Workenhe, A. Nguyen, D. Bakhshinyan et al., "De novo necroptosis creates an inflammatory environment mediating

tumor susceptibility to immune checkpoint inhibitors," *Communications Biology*, vol. 3, no. 1, 2020.

[41] Y. Wang, B. Yin, D. Li, G. Wang, X. Han, and X. Sun, "GSDME mediates caspase-3-dependent pyroptosis in gastric cancer," *Biochemical and Biophysical Research Communications*, vol. 495, no. 1, pp. 1418–1425, 2018.

[42] Z. Wang, L. Cao, S. Zhou, J. Lyu, Y. Gao, and R. Yang, "Construction and validation of a novel pyroptosis-related four-lncRNA prognostic signature related to gastric cancer and immune infiltration," *Frontiers in Immunology*, vol. 13, article 854785, 2022.

Research Article

Systematic Pan-Cancer Analysis Identifies CDK1 as an Immunological and Prognostic Biomarker

Yaqi Yang, Qin Liu, Xiyuan Guo, Qing Yuan, Siji Nian, Pengyuan Kang, Zixi Xu, Lin Li[iD], and Yingchun Ye[iD]

Immune Mechanism and Therapy of Major Diseases of Luzhou Key Laboratory, Public Center of Experimental Technology, School of Basic Medical Sciences, Southwest Medical University, Luzhou 646000, China

Correspondence should be addressed to Lin Li; lilin1591905507@126.com and Yingchun Ye; yeyingchun@swmu.edu.cn

Cyclin-dependent kinase 1 (CDK1) plays an important role in cancer development, progression, and the overall process of tumorigenesis. However, no pan-cancer analysis has been reported for CDK1, and the predictive role of CDK1 in immune checkpoint inhibitors (ICIs) therapy response remains unexplored. Thus, in this study, we first investigated the potential oncogenic role of CDK1 in 33 tumors by multidimensional bioinformatics analysis based on The Cancer Genome Atlas (TCGA) and Gene Expression Omnibus (GEO) datasets. Bioinformatic analysis and immunohistochemical experiments confirmed that CDK1 is significantly upregulated in most common cancers and is strongly associated with prognosis. Further analysis indicated that CDK1 may influence tumor immunity mainly by mediating the degree of tumor infiltration of immune-associated cells, and the effect of CDK1 on immunity is diverse across tumor types in tumor microenvironment. CDK1 was also positively correlated with tumor mutational burden (TMB) and microsatellite instability (MSI) in certain cancer types, linking its expression to the assessment of possible treatment response. The results of the pan-cancer analysis study showed that the CDK1 gene was positively associated with the expression of three classes of RNA methylation regulatory proteins, and affects RNA function through multiple mechanisms of action and plays an important role in the posttranscriptional regulation of the tumor microenvironment. These findings shed light on the role of the CDK1 gene in cancer progression and provide information to further study the CDK1 gene as a potential target for pan-cancer.

1. Introduction

Cancer is the leading cause of human mortality worldwide and a significant barrier to a long life. The health and economic burdens associated with its high incidence and mortality are rapidly increasing [1, 2]. Cancer is a malignant disease and is caused by a heterogeneous population of cells with different tumorigenic abilities, phenotypes, and functions. Dysregulation of the cell cycle resulting in uncontrolled cell proliferation and genomic and chromosomal instability are common in human cancers [3–5]. Cyclins and cyclin-dependent kinases (CDKs) are the central components of the cell cycle regulatory machinery [6].

CDKs belong to the serine/threonine-specific protein kinase family, which are essential for normal cell cycle progression and are the key regulatory enzymes that drive all cell cycle transitions and coordinate the progression of the entire cell cycle in all eukaryotic cells [6–8]. Additionally, CDKs are also involved in gene transcription, mRNA processing, and cell differentiation [9, 10]. Dysregulation of CDKs leads to the sustained or spontaneous proliferation of tumor cells and accelerates the malignant growth of tumors. To date, 21 CDK and 5 CDK-like genes have been identified in the human genome based on their homologous sequences [11]. Among them, CDK1, also known as cell division cycle 2 (CDC2), is the only essential CDK in human cells. CDK1 can replace other CDKs and effectively drive the mammalian cell cycle, controlling the transition of cells from the G2 phase to the M phase [12–14]. Moreover, in malignant tumor cells, the altered expression of CDK1 and its regulators can lead to

uncontrolled CDK1 activity, which can cause uncontrolled proliferation of tumor cells and aggravate the malignancy of the tumor. Hence, CDK1 is a potential target for tumor therapy.

In advanced gastrointestinal stromal tumors [15], bladder cancer [16], non-small cell lung cancer [17], and melanoma [18], high CDK1 expression promotes the progression of malignant tumors and exacerbates the degree of proliferation of malignant tumor cells. However, current CDK1-based studies are limited to a single tumor type, and the role of the CDK1 gene in human cancers and the overall CDK1 tumor landscape are still unknown. Thus, its relationship with human cancers needs further investigation. In recent years, pan-cancer analysis has been widely used in cancer research, providing unique, detailed, and comprehensive insights into human cancers to improve the quality of cancer analysis [19–21]. Given the complexity of tumorigenesis, it is extremely important to analyze the CDK1 gene for pan-cancer expression and to assess its relationship with clinical prognosis and its relevance to the underlying molecular mechanisms.

In this study, a pan-cancer analysis of CDK1 was performed using the TCGA project and the GEO database to explore the potential molecular mechanisms of the action of CDK1 in tumorigenesis and clinical prognosis in terms of gene expression, survival status, genetic alterations, protein phosphorylation, methylation levels, immune infiltration, pan-cancer correlation with three classes of RNA methylation regulatory proteins and related cellular pathways, and to lay the foundation for future research on CDK1-based antitumor therapy.

2. Materials and Methods

2.1. Ethical Statement. This study was approved by the clinical trial ethics committee of the Affiliated Hospital of Southwest Medical University, China (ethics review number: KY2019276). Following the approval of the ethics committee, the volunteers signed the informed consent before samples were collected, and all methods were performed as per the relevant guidelines and regulations. This study was compliant with the Declaration of Helsinki.

2.2. Gene Expression Analysis. Oncomine, the classic sample database in oncology, is the largest oncogene chip database and integrated data-mining platform. It contains 86,733 samples and 715 gene expression datasets, which can be accessed to mine information related to cancer genes and can assist in screening tumor-related target molecules or predicting phenotypes [22]. Therefore, we used this online database (https://www.oncomine.org) to assess the mRNA expression levels of CDK1 in different tumors. In this study, *P* values lesser than 0.01 in the Oncomine database, a fold change of 2, and a gene ranking at 10% were set as the thresholds of significance. Additionally, we used the "Gene_DE" module of the TIMER2 [23] web server (https://timer.cistrome.org/) to determine the differences in CDK1 expression between cancer tissue and adjacent normal

tissues in TCGA tumors. We downloaded RNA-seq sequencing data from the TCGA and Genotype-Tissue Expression (GTEx) datasets from the UCSC XENA portal (https://xenabrowser.net/datapages/). The downloaded data were uniformly processed by the Toil process [24] and log2 (TPM+1) transformed for analysis to compare the CDK1 gene expression between tumor and normal tissue in multiple types of tumor.

UALCAN (https://ualcan.path.uab.edu) is a comprehensive, interactive web portal for a detailed analysis of the TCGA gene expression data [25]. We performed expression analysis on the Clinical Proteomic Tumor Analysis Consortium (CPTAC) dataset through this interactive web resource. The expression levels of CDK1 (NP_001307847.1) in total or phosphorylated proteins in primary tumors and normal tissues were explored. Valid datasets were selected from six tumors, including breast cancer, ovarian cancer, colon cancer, renal clear cell carcinoma (RCC), uterine corpus endometrial carcinoma (UCEC), and lung adenocarcinoma (LUAD). A violin plot of CDK1 expression in all TCGA tumors at different pathological stages (stages I, II, III, and IV) was obtained using the "Pathological stage map" module of the GEPIA2 web server (https://gepia2.cancer-pku.cn/#index) [26]. The log2 (TPM+1)-transformed expression data were visualized and analyzed in the form of violin plots to determine the expression of CDK1 in different pathological stages of different tumors.

2.3. Survival Prognosis Analysis. To elucidate the relationship between CDK1 regulatory genes and tumor survival prognosis, we used the "survival map" module of GEPIA2 [26] to obtain overall survival (OS) and disease-free survival (DFS) significance map data of CDK1 in all TCGA tumors. High and low cut-off (>50% or <50%, respectively) values were used as the expression thresholds for creating high-expression and low-expression cohorts. Hypothesis testing was performed using the log-rank test, and survival curves were obtained using the "survival analysis" module of GEPIA2. We used the online survival analysis tool Kaplan-Meier plotter (https://kmplot.com/analysis/) [27] to analyze the 5-year survival of patients with different tumor types using publicly available pan-cancerRNA-seq datasets to determine the effect of CDK1 gene mRNA expression levels on the OS ($n = 7,462$) and recurrence-free survival (RFS) ($n = 4,420$) of the patients.

The PronoScan database was used to determine the relationship between gene expression and patient clinical prognosis through a large collection of publicly available cancer chip datasets [28]. We used the web server of this database (https://www.abren.net/PrognoScan/) to analyze the relationship between CDK1 expression in different types of cancer and survival, such as disease-specific survival (DSS), RFS, distant recurrence-free survival (DRFS), DFS, metastasis-free survival (MFS), and distant metastasis-free survival (DMFS). The threshold was adjusted to a Cox *P* value <0.05.

2.4. Gene Mutation Analysis. The cBioPortal database contains the genomic characteristics of tumors at the DNA

level. It provides visual and multidimensional genomic data that can be used to study mechanism of tumorigenesis [29]. We performed a pan-cancer mapping study of CDK1 through the online web platform of this database (https://www.cbioportal.org/), looking at the results of mutation frequency, mutation type, and copy number alteration (CNA) in all TCGA tumors. The information on CDK1 mutation sites can be shown in protein structure schematics or 3D structures through the "Mutations" module of this database. Also, we analyzed the correlation between CDK1 gene expression and TMB and MSI in 33 tumor types using Spearman's correlation. Paired mRNA expression data for 33 tumor types ($n = 10,201$) were downloaded from the genomic data commons (GDC) data portal (https://portal.gdc.cancer.gov/) and statistically analyzed using the R package (v4.0.3); $P < 0.05$ was considered statistically significant.

2.5. Immune Infiltration Analysis. The relationship between CDK1 expression and immune infiltration in all TCGA tumors was determined using the "Immune Gene" module of the TIMER2 database web server. Tumor-associated fibroblasts, CD8+ T cells, CD4+ T cells, B cells, dendritic cells (DC), and macrophages were selected for immune infiltration assessment based on different algorithms such as TIMER, CIBERSORT, CIBERSORT-ABS, QUANTISEQ, XCELL, MCPCOUNTER, and EPIC. The P values and partial correlation coefficients (COR) were calculated by Spearman's correlation and visualized in the form of heat maps and scatter plots.

2.6. Pan-Cancer Correlation Analysis of CDK1 and RNA Methylation Regulatory Proteins. Several modified ribonucleosides including 6-methyladenosine (m6A), 5-methylcytidine (m5C), and 1-methyladenosine (m1A) have recently been shown to occur in messenger (m)RNAs and to affect their biogenesis, translation, and stability. We downloaded the uniformly normalized pan-cancer dataset from the UCSC (https://xenabrowser.net/) database. We further extracted the expression data of ENSG00000170312 (CDK1) gene and 44 regulatory proteins involved three types (*m1A, m5C, m6A*) of RNA methylation modifications in each sample, and further we filtered the samples from the following sources: primary solid tumor, primary blood derived cancer—bone marrow, primary blood derived cancer—peripheral blood. We also filtered all normal samples, and further performed log2 ($x + 0.001$) transformation for each expression value. Next, we calculated the Pearson's correlation between CDK1 and three types of RNA methylation regulatory proteins. Visual analysis was carried out in the form of heat maps.

2.7. Methylation Analysis. Methylation of DNA and histones can alter the structure of the DNA. Moreover, epigenetic regulation of gene expression might be assessed by the methylation level of the promoters. We used the TCGA dataset from the UCLAN database to analyze the CDK1

promoter DNA methylation levels in various tumors to determine the differences in the methylation levels between tumors and normal tissues. The results are presented as a box plot; $P < 0.05$ was considered statistically significant.

2.8. CDK1-Related Gene Enrichment Analysis. STRING (https://string-db.org/) is a database for predicting protein interactions. Currently the STRING database (v11.0) contains information on more than 5,000 species, more than 20 million proteins, and more than 3 billion interactions. The database can be used to understand the complex regulatory networks in living organisms [30]. We first investigated the protein-protein interactions of CDK1-binding proteins using this database, with the main parameter settings, including the meaning of the network edge ("evidence"), the active interaction sources ("experiment"), the minimum interaction required score ("low confidence [0.150]"), and the maximum number of interactors to be shown ("no more than 50 interactors"). Finally, an interaction network of 50 experimentally identified CDK1-binding proteins was obtained.

We obtained the top 100 target genes associated with CDK1 from all the TCGA tumor and normal tissue datasets using the "similar gene detection" module of the GEPIA2 database. Jvenn, an interactive Venn diagram viewer [31], was used to analyze and visualize the interactions between CDK1-interacting genes and related genes. Moreover, we combined these two sets of gene data for the KEGG pathway analysis by uploading the gene list to the web server of the DAVID database (https://david.ncifcrf.gov) with selected identifiers ("OFFICIAL_GENE_SYMBOL") and species ("*Homo sapiens*"). The Kyoto Encyclopedia of Genes and Genomes (KEGG) pathway analysis was performed to obtain the relevant KEGG data, and finally, using the "tidyr" and "ggplot2" R packages, the data were visualized. We also performed Gene Ontology (GO) functional enrichment analysis of the above genes using the Metascape database (https://metascape.org/). The data of BP (Biological process), CC (Cellular Component), and MF (Molecular Function) enrichment items were downloaded, and the results of the analysis were visualized in the form of chord and bubble diagrams.

2.9. Immunohistochemical Techniques. Immunohistochemistry was performed as described previously [32]. The cancer tissues and paraneoplastic tissues of human lung, breast, and liver cancers were fixed, dehydrated, embedded, and sectioned. The dewaxed sections were placed in hydrogen peroxide (containing 3% methanol) for 10 min at room temperature and washed with 1× PBS. The tissue sections were immersed in a 0.01 M citrate buffer solution (pH 6.0) and boiled. After cooling, the sections were washed with 1× PBS. A blocking solution (goat serum) was added dropwise for 20 min at room temperature. The CDK1 experimental group was incubated with recombinant anti-CDK1 rabbit monoclonal antibody (Abcam, Cat No. ab133327, Cambridge, UK) as a primary antibody, and the isotype control group was incubated with rabbit IgG1

antibody (Shanghaiyuanye Biotechnology, Cat No. S25766, Shanghai, China) overnight at 4°C. The goat anti-rabbit antibody (Zhongshan Jinqiao, Cat No. ZDR5306, Beijing, China) was added dropwise as a secondary antibody, incubated for 90 min at 37°C, and washed with 1× PBS after incubation. A DAB chromogenic reagent kit (Zhongshan Jinqiao, Cat No. K135925C, Beijing, China) was used to stain at room temperature. After hematoxylin counterstaining and dehydration, the sections were sealed with neutral gum. Semi-quantitative immunohistochemical detection was used to determine the CDK1 protein levels in different cancer tissues. The integrated optical density and corresponding area of the CDK1-positive region in the acquired immunohistochemical sections were determined using the Image-Pro Plus 6.0 image analysis system, and the mean optical density of the positive region in each immunohistochemical section was calculated. The measurements were repeated three times per section and averaged to accurately compare the difference in mean optical density between cancerous and normal tissues. (Ten cancer tissue sections and 10 normal tissue sections from patients with different tumors were stained for each cancer species, respectively. The isotype control group was also set up, and the number of normal and cancer tissue sections stained was five.)

2.10. Statistical Analysis. The statistical analysis was performed using Prism 8 (GraphPad Software). Data are presented as mean ± SD. Statistically significant differences between the two groups were calculated using Student's t test. For $P > 0.05$, the differences were considered to be statistically not significant (ns); $*P < 0.05$; $**P < 0.01$; and $***P < 0.001$.

3. Results

3.1. CDK1 Is Significantly Upregulated Expression in Most Common Cancers. To investigate the expression of the CDK1 gene in various tumors, we analyzed the mRNA expression of the CDK1 gene using the Oncomine database (Figure 1(a)). Based on the analysis of the Oncomine database, we found that the CDK1 gene expression was higher in a variety of malignancies than in normal tissues (Figure 1(a)): these malignancies included bladder cancer, brain and CNS cancers, breast cancer, cervical cancer, colon cancer, esophageal cancer, gastric cancer, head and neck cancer, lymphoma, liver cancer, lung cancer, melanoma, ovarian cancer, and sarcoma. However, CDK1 gene expression was lower in leukemia and myeloma than in normal tissues (Figure 1(a)). We also specifically investigated the expression of the CDK1 gene in highly prevalent malignancies such as lung, gastric, liver, colon, breast, esophageal, and pancreatic cancers (Supplementary Table 1). There was a significant upregulation of CDK1 gene expression in lung cancer tissues than in normal tissues, and the results from the TCGA dataset showed a fold change of 6.939 ($P = 4.26E - 24$) (Supplementary Table 1). The overexpression of the CDK1 gene in gastric cancer tissues showed a fold change of 2.544 ($P = 7.42E - 13$) compared to

the expression of the gene in normal tissues. Similarly, the expression levels of CDK1 gene were significantly higher in liver cancer (fold change of 5.573, $P = 1.05E - 84$), colon cancer (fold change of 2.274, $P = 6.34E - 13$), breast cancer (fold change of 2.325, $P = 2.36E - 48$), esophageal cancer (fold change of 2.929, $P = 1.54E - 26$), and pancreatic cancer (fold change of 3.888, $P = 1.37E - 7$) than in the adjacent normal tissues (Supplementary Table 1).

To further evaluate the expression of CDK1 in human cancers, we used the TIMER2 database to analyze the expression of CDK1 in different types of TCGA tumors. The differential expression of CDK1 in all TCGA tumors versus adjacent normal tissues is shown in Figure 1(b). In bladder urothelial carcinoma (BLCA), breast invasive carcinoma (BRCA), cervical squamous cell carcinoma and endocervical adenocarcinoma (CESC), cholangiocarcinoma (CHOL), colon adenocarcinoma (COAD), esophageal carcinoma (ESCA), glioblastoma multiforme (GBM), head and neck squamous cell carcinoma (HNSC), kidney renal clear cell carcinoma (KIRC), liver hepatocellular carcinoma (LIHC), LUAD, lung squamous cell carcinoma (LUSC), pheochromocytoma and paraganglioma (PCPG), prostate adenocarcinoma (PRAD), rectum adenocarcinoma (READ), stomach adenocarcinoma (STAD), thyroid carcinoma (THCA), and UCEC, among different malignancies, the expression of CDK1 in cancer tissues was significantly higher than that in the adjacent normal tissues (all P values <0.05). However, in kidney chromophobe (KICH), the expression of CDK1 in cancer tissues was significantly lower than that in the adjacent normal tissues. We compared the expression levels of the CDK1 gene in the TCGA and GTEx database integrated datasets, considering the limited paracancerous normal tissue of some cancer species in the TCGA database (Figure 1(b)). The analysis showed that CDK1 expression was significantly upregulated in various tumor tissues compared to the expression in the adjacent normal tissues (Figure 1(c)).

The results of the CPTAC database showed that the expression of total CDK1 protein in breast cancer, renal clear cell carcinoma, colon cancer, lung adenocarcinoma, and UCEC tissues was higher than that in the adjacent normal tissues ($P < 0.0001$; Figure 1(d)). We then evaluated the relationship between CDK1 expression and clinicopathological staging of patients with different tumors (Figure 1(e)). The results suggested that CDK1 expression plays an important role in the clinical progression of different malignancies such as BRCA, COAD, LUAD, and LUSC, this expression pattern is associated with good clinical application prospects.

The differential overexpression of CDK1 gene in TCGA tumors lays the foundation for its potential as a tumor therapeutic target, and this differential overexpression involves more tumor types than other tumor targets, which validates its importance at the pan-cancer level.

3.2. High Expression of CDK1 in Tumors Significantly Reduced the Survival and Prognosis of Tumor Patients. We divided tumor cases into high- and low-expression groups according to CDK1 expression levels and investigated the correlation

(a)

(b)

(c)

(d)

(e)
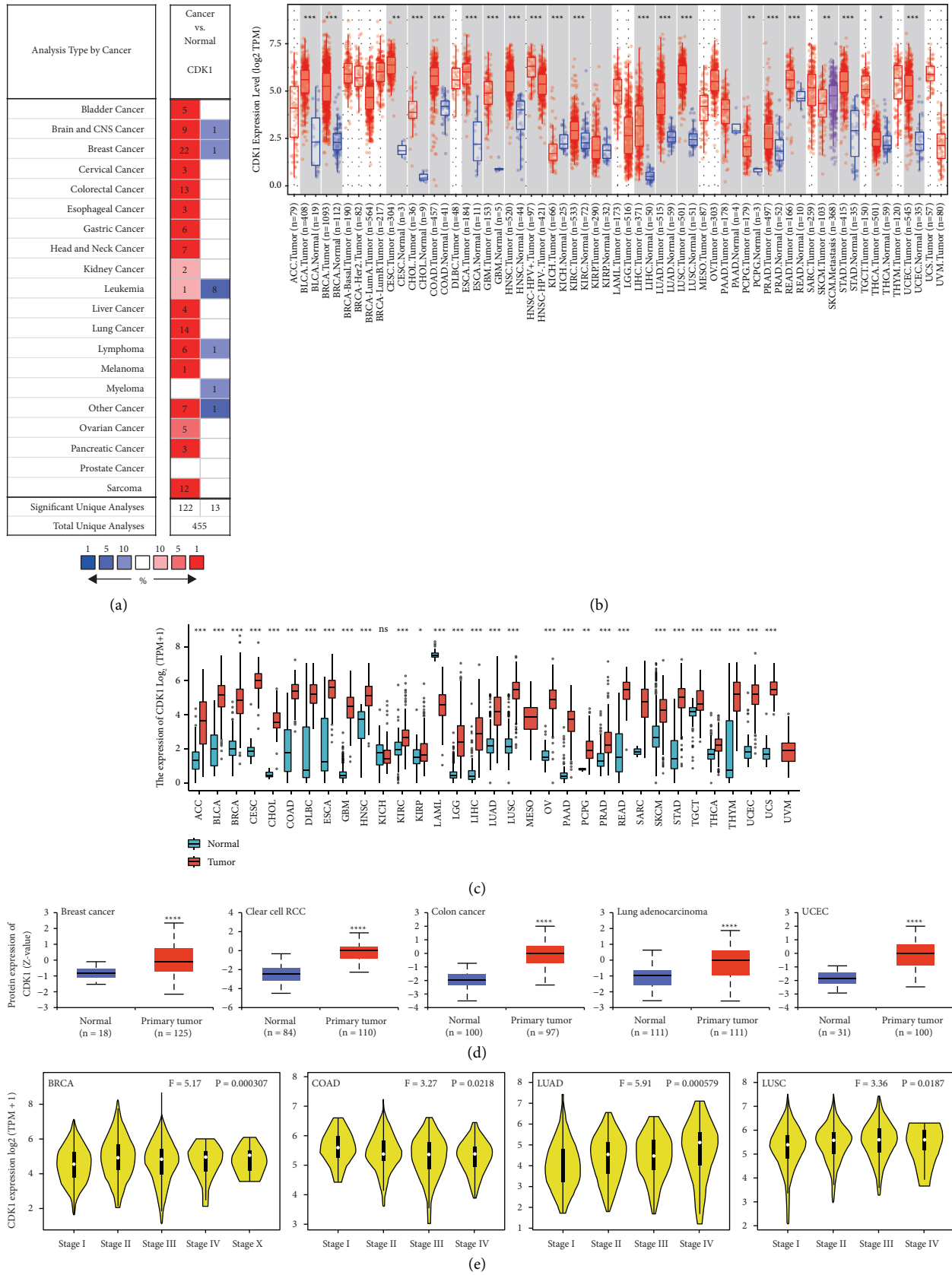
FIGURE 1: Expression levels of the CDK1 gene in different tumors and pathological stages. (a) Increase or decrease in the CDK1 levels in datasets of different cancers compared to the CDK1 levels in normal tissues in the Oncomine database. (b) CDK1 expression levels in different tumor types from the TCGA database were analyzed by TIMER2.0 ($^*P < 0.05$, $^{**}P < 0.01$, $^{***}P < 0.001$). (c) Comparison of CDK1 expression levels between tumor tissues from the TCGA database and normal tissues from the GTEx database ($^*P < 0.05$, $^{**}P < 0.01$, $^{***}P < 0.001$). (d) Based on the CPTAC dataset, the expression levels of total CDK1 protein were analyzed in normal and primary tissues of breast cancer, colon cancer, clear cell kidney cancer, and UCEC ($^{****}P < 0.0001$). (e) Correlations between CDK1 expression and tumor stage in BRCA, COAD, LUAD, and LUSC patients (Log2 (TPM + 1) was applied for log scale).

between CDK1 expression and the prognosis of patients with different tumors using the TCGA dataset. As shown in Figure 2, the OS analysis data showed that high expression of CDK1 was associated with poor prognosis of TCGA tumors (Figure 2(a)). Tumor types involved adrenocortical carcinoma (ACC, $P = 7e - 08$), KIRC ($P = 0.033$), kidney renal papillary cell carcinoma (KIRP, $P = 0.017$), brain lower grade glioma (LGG, $P = 76e - 07$), LIHC ($P = 0.00017$), LUAD ($P = 2.6e - 05$), mesothelioma (MESO, $P = 7.6e - 07$), pancreatic adenocarcinoma (PAAD, $P = 6e - 04$), sarcoma (SARC, $P = 0.0063$), and skin cutaneous melanoma (SKCM, $P = 0.037$). Data from DFS analysis showed that in TCGA tumors, ACC ($P = 0.00019$), HNSC ($P = 0.019$), KIRC ($P = 0.045$), KIRP ($P = 7.1e - 05$), LGG ($P = 0.00014$), LIHC ($P = 0.00057$), LUAD ($P = 0.027$), PAAD ($P = 0.0041$), PRAD ($P = 0.0014$), SARC ($P = 0.0022$), and uveal melanoma (UVM, $P = 0.00071$) and high CDK1 expression were associated with poor prognosis (Figure 2(b)).

We determined the association between CDK1 expression and prognosis of cancer patients using the Pronoscan database. Sixteen cohorts (GSE5287 [33], GSE13507 [34, 35], GSE2658 [36], GSE4475 [37], GSE12417-GPL97 [38], GSE4271-GPL96 [39], GSE4412-GPL96 [40], GSE1456-GPL96 [41], GSE12093 [42], GSE12276 [43], GSE12945 [44], GSE17537 [45], GSE9891 [46], GSE16560 [47], GSE19234 [48], and GSE30929 [49]) of the analytical data suggested that high CDK1 expression was significantly correlated with poor prognosis (Cox$P < 0.05$, Supplementary Figure 1A). The types of tumors included bladder cancer, blood cancer, brain cancer, breast cancer, colon cancer, lung cancer, ovarian cancer, prostate cancer, skin cancer, and soft tissue cancer. The impact on patient survival involved OS, DFS, DMFS, RFS, DRFS, DSS, and MFS. Notably, high expression of the CDK1 gene can be a protective factor for DFS in colorectal cancer patients. Additionally, we used the Kaplan-Meier plotter database to assess the prognostic relationship of CDK1 expression with a range of cancer types. The results showed that high expression of CDK1 significantly affected OS and RFS in tumor patients (Supplementary Figure 1B). In conclusion, these analyses consistently showed that the CDK1 gene is significantly associated with the prognosis of patients with different cancer types and can significantly influence the survival of patients with these tumors. First, we concluded that the CDK1 gene was differentially overexpressed in TCGA tumors. Meanwhile, this high expression status of CDK1 gene can significantly reduce survival time of tumor patients as revealed at the pan-cancer level. The above study lays the foundation for anti-CDK1 oncology therapy to extend the median survival time of tumor patients.

3.3. The Genetic and Epigenetic Features of CDK1 in Pan-Cancer.
Oncogenic mutations mainly include single-gene mutations (amplifications, insertions, deletions, etc.) and translocations (fusions). We investigated the alterations of the CDK1 gene in different tumor samples from the TCGA cohort. As shown in Figure 3(a), the highest frequency of CDK1 gene alterations (>6%) was found in uterine

carcinosarcomas with "amplification" as the mutation type. "Amplification" was also the main type of mutation in cholangiocarcinoma (>2%), pancreatic adenocarcinoma (<1%), stomach adenocarcinoma (<2%), breast invasive carcinoma (<2%), and esophageal adenocarcinoma (<2%). "Amplification" also occurred in lung squamous cell carcinoma (<1%), bladder urothelial carcinoma (<1%), prostate adenocarcinoma (<1%), ovarian serous cystadenocarcinoma (<1%), and head and neck squamous cell carcinoma (<1%). The "mutation" type of alteration was mainly seen in skin cutaneous melanoma (>2%) and colorectal adenocarcinoma (<2%). Kidney chromophobe, sarcoma, testicular germ cell tumors, and thyroid carcinoma were predominantly of the "deep deletion" type, with a frequency of less than 2%. Figure 3(b) shows the types and loci of CDK1 gene alterations. We found that the "missense" mutation of CDK1 is the main type of genetic alteration. Changes in the Pkinase domain (R275Q) detected in colorectal cancer (COAD-READ), BRCA, and GBM can induce a transcoding mutation of the CDK1 gene, which translates CDK1 from arginine (R) to glutamine (Q) at position 275. Subsequently, missense changes were found in CDK1 protein. The 3D structure of CDK1 showed the R275 site (Figure 3(c)).

We also analyzed the correlation between CDK1 expression and TMB and MSI in all TCGA tumors. As shown in Figure 3(d), ACC ($P = 1.01E - 06$), BLCA ($P = 7.20E - 07$), CHOL ($P = 0.0447$), COAD ($P = 0.0025$), HNSC ($P = 0.0137$), KICH ($P = 0.0036$), KIRC ($P = 0.0048$), acute myeloid leukemia (LAML, $P = 0.0237$), LGG ($P = 4.13E - 16$), LUSC ($P = 1.15E - 05$), PAAD ($P = 1.71E - 08$), SARC ($P = 5.50E - 06$), SKCM ($P = 1.31E - 06$), UCEC ($P = 0.0099$), and uterine carcinosarcoma (UCS, $P = 0.0021$) in CDK1 expression were positively correlated with TMB, while CDK1 expression in thymoma (THYM, $P = 4.71E - 11$) was negatively correlated with TMB. As shown in Figure 3(e), CDK1 expression in HNSC ($P = 0.0210$), MESO ($P = 0.0307$), READ ($P = 9.94E - 05$), SARC ($P = 0.0043$), STAD ($P = 1.53E - 13$), and UCEC ($P = 2.06E - 10$) was positively correlated with MSI, while lymphoid neoplasm diffuse large B-cell lymphoma (DLBC, $P = 0.0330$) showed a negative correlation between CDK1 expression and MSI.

Pan-cancer analysis of genetic and epigenetic characteristics of CDK1 gene revealed differential mutations of CDK1 in different TCGA tumors. The correlation of CDK1 with TMB and MSI in different tumors was also analyzed to provide a basis for ICIs-based therapy.

3.4. The Phosphorylation of CDK1 Protein in TCGA Tumor Tissues Was Higher than That in Normal Tissues.
We compared the differences in CDK1 phosphorylation levels in normal and primary tumor tissues using the CPTAC dataset analysis in the UALCAN database. Figure 4(a) summarizes the phosphorylation loci of CDK1 and the phosphorylation levels in specific cancer types. The phosphorylation loci with differences in the CDK1 S_TKc domain mainly included T14, Y15, and T161. Notably, analysis of the CDK1 amino acid sequence using the bioinformatics tool PhosphoNET
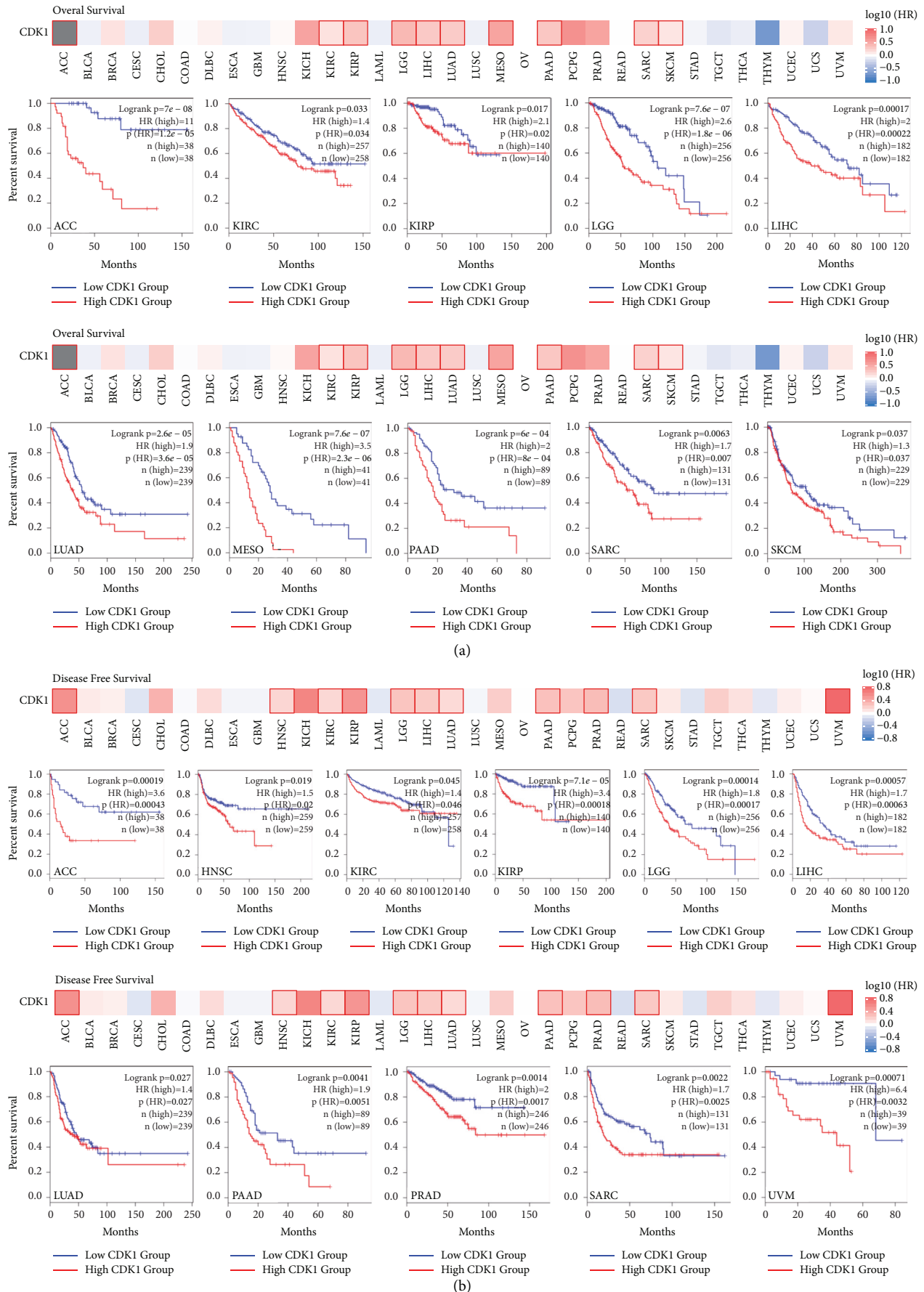
FIGURE 2: Survival analysis comparing the high and low expression of CDK1 in different types of cancer in the TCGA dataset. We used the GEPIA2 tool to perform (a) overall survival analysis and (b) disease-free survival analysis of different tumors in TCGA by CDK1 gene expression. The survival map and Kaplan-Meier curves with positive results are shown.

(a)

(b)

(c)

FIGURE 3: Continued.

(d)

(e)
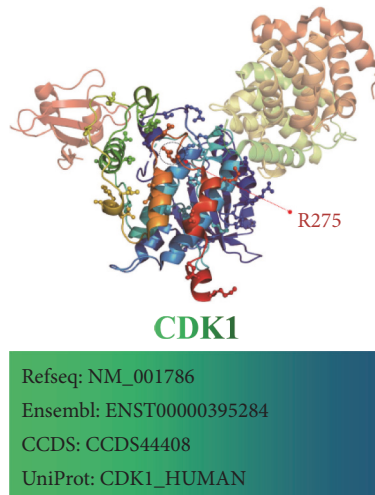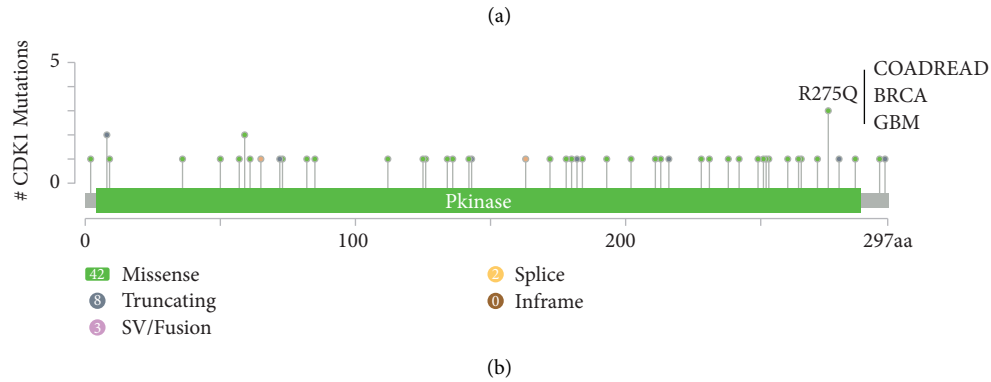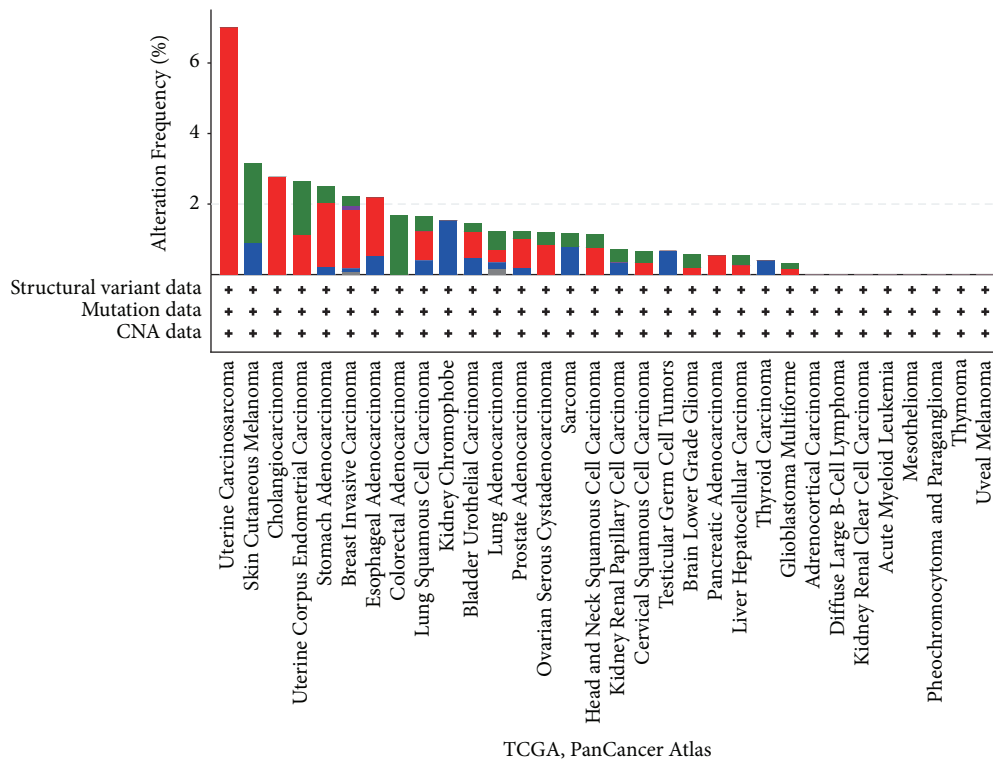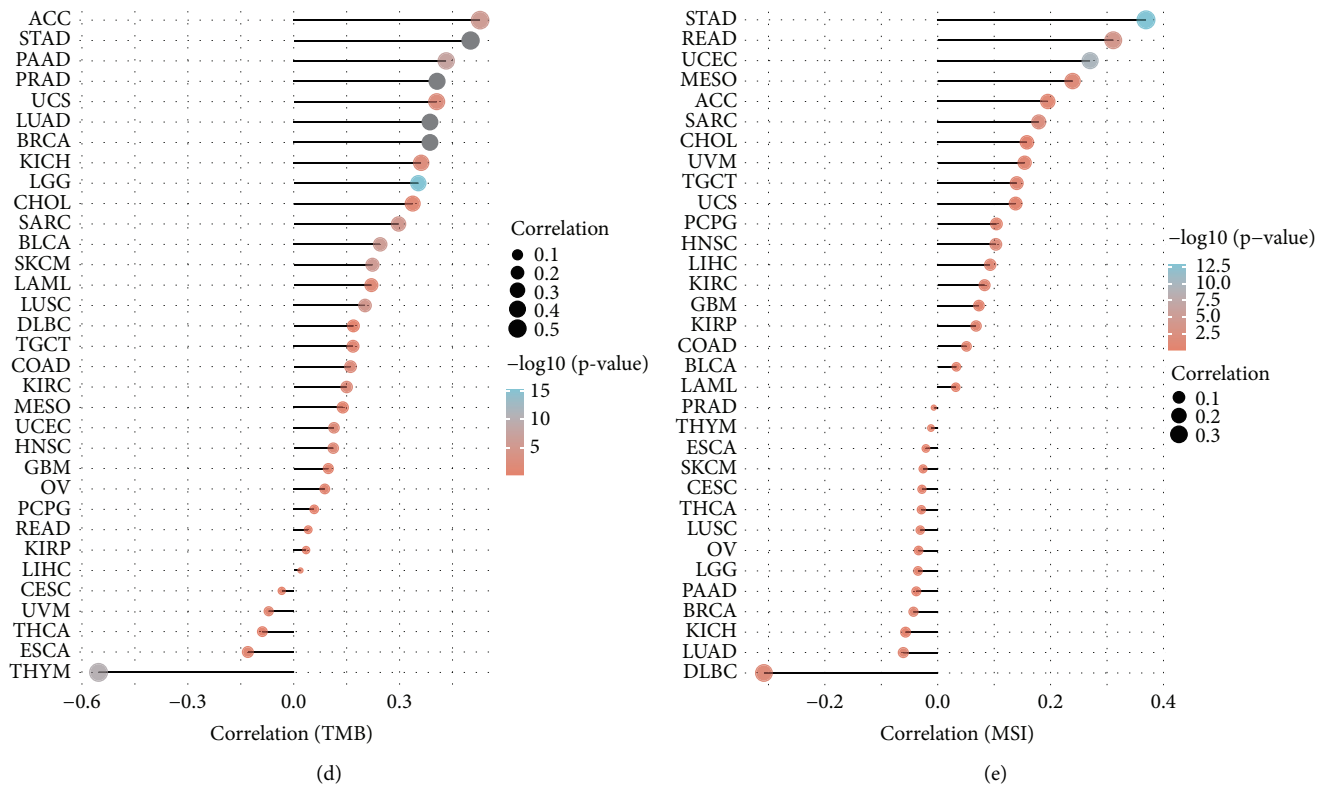
FIGURE 3: CDK1 mutation landscape. (a) The CDK1 mutation frequency in multiple TCGA pan-cancer studies according to the cBioPortal database. (b) Mutation diagram of CDK1 in different cancer types across protein domains. (c) Illustration of the three-dimensional structure of the CDK1 protein (containing the R275 mutation site). (d) Correlation between CDK1 gene expression and TCGA tumor mutation load (TMB). (e) Correlation between CDK1 gene expression and TCGA tumor microsatellite instability (MSI).

(https://www.phosphonet.ca) also identified T14, Y15, and T161 as potential phosphorylation loci. Further analysis of the above loci suggested that the phosphorylation levels of the Y15 locus were higher in primary tumor tissues than in normal tissues in ovarian, breast, LUAD, and colon cancers (all $P < 0.05$) (Figure 4(b)). The phosphorylation level of the T14 locus was also significantly higher in primary tumor tissue than in normal tissue in LUAD and colon cancer. Considering that the phosphorylation levels of the Y15 locus were significantly elevated in several primary tumor tissues, further molecular testing might help to determine the potential role of Y15 phosphorylation in tumorigenesis.

Protein phosphorylation is a common process that regulates the activity of oncogenic and tumor suppressor proteins; dysregulated protein phosphorylation is often a predisposing factor for a variety of diseases. Our results showed that protein phosphorylation levels in tumor tissues were significantly higher than those in normal tissues; dysregulation of CDK1 protein phosphorylation may alter the activity of oncogenic-related signaling pathways and contribute to the formation of associated tumor phenotypes.

3.5. Different Methylation Levels of CDK1 in Different TCGA Tumor Tissues.
DNA methylation directly affects cancer development, and hence, we investigated the DNA methylation levels of CDK1 in different tumors using the TCGA

dataset in the UCLAN database. As shown in Figure 5, the methylation levels of CDK1 were significantly lower in CHOL, LIHC, READ, testis germ cell tumor, and THCA tumor tissues compared to that in the normal tissues (all P values <0.05), whereas the methylation levels of CDK1 in COAD, ESCA, HNSC, KIRC, KIRP, LUSC, PAAD, and SARC tumor tissues were significantly higher (all P values <0.05). Due to the lack of CDK1 expression data, we did not analyze the relationship between DNA methylation and CDK1 expression. Related studies show that tumor suppressor genes can be suppressed by hypermethylation and oncogenes can be activated by hypomethylation, the differential expression of CDK1 phosphorylation in different TCGA tumors leads to genomic instability and accelerated tumor progression. Hypomethylation status of CDK1 in some tumors may lead to activation of other oncogenes, while hypermethylation status in other tumors may further exacerbate carcinogenesis by silencing tumor-associated suppressor genes.

3.6. CDK1 Expression Level Was Related to the Level of Immune Infiltration.
Tumor-infiltrating immune cells are an important component of the tumor microenvironment, and they play an important role in tumor growth, development, and drug resistance [50]. Tumor-associated fibroblasts are one of the important cells associated with tumor malignancy

(a)

(b)
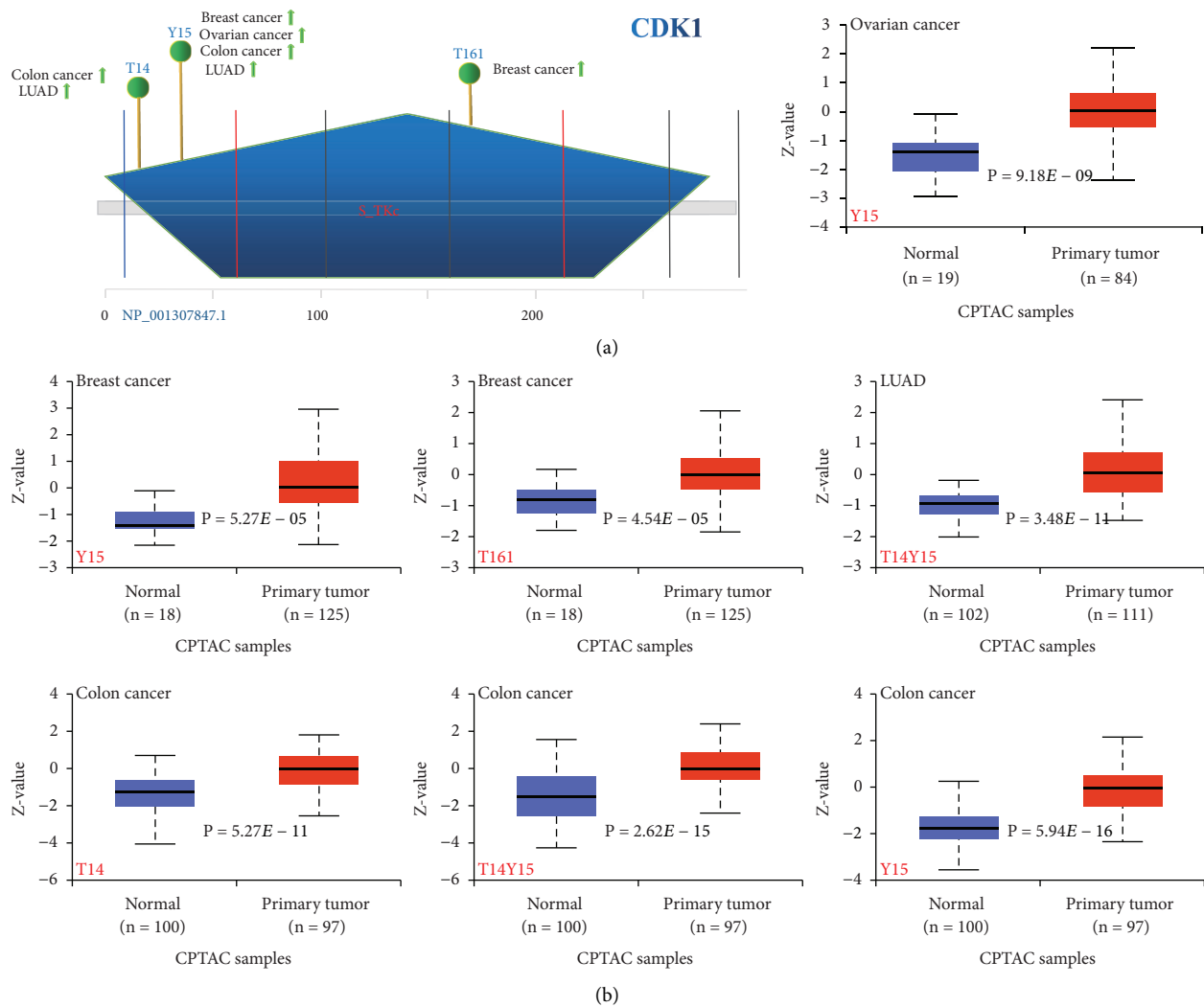
Figure 4: Phosphorylation analysis of CDK1 protein in different tumors. (a) Based on the CPTAC dataset, we analyzed the expression level of CDK1 phosphoprotein (NP_001307847.1, T14, Y15, and T161 sites) between normal tissue and primary tissue of selected tumors via the UALCAN. The phosphoprotein sites with positive results are displayed in the schematic diagram of the CDK1 protein. (b) Box plots of CDK1 protein phosphorylation in different tumors.

and are the most prominent stromal component and key players in tumor progression [51]. We used TIDE, XCELL, MCPCOUNTER, and EPIC algorithms to investigate the relationship between the level of tumor-associated fibroblast infiltration and CDK1 gene expression in different types of TCGA tumors (Figure 6(a)). Based on all or most of the algorithms, we observed a negative correlation between CDK1 expression and the infiltration values of tumor-associated fibroblasts in COAD, BRCA-Basal, THYM, HNSC, HNSC (human papillomavirus [HPV+]), LUSC, PRAD, and STAD tumors. There was a positive correlation in KICH, KIRC, KIRP, MESO, and testicular germ cell tumor (TGCT).

We also investigated the relationship between CDK1 and other immune infiltrating cells using different algorithms such as EPIC, TIMER, QUANTISEQ, XCELL, CIBERSORT, and CIBERSORT-ABS to analyze the relationship between CDK1 expression and the infiltration levels of CD4+ T cells,

CD8+ T cells, B cells, DC, and macrophages in different TCGA tumors. Specifically, as shown in Figure 6(b), CDK1 expression in BLCA and STAD was negatively correlated with the infiltration value of CD4+ T cells, whereas it was positively correlated in HNSC and HNSC-HPV F02D. Notably, in all TCGA tumors, based on the XCELL algorithm, we found a positive correlation between the infiltration values of Th2-type CD4+ T cells and the expression of CDK1. As shown in Supplementary Figure 2A, CDK1 expression in different TCGA tumors of BRCA, BRCA-lumB, HNSC, HNSC-HPV+, KIRC, LIHC, LUAD, LUSC, THCA, and THYM showed a positive correlation with the infiltration value of CD8+ T cells, while a negative correlation was observed in PAAD and UCEC. We found a positive correlation between CDK1 expression and B-cell infiltration values in HNSC, HNSC-HPV+, KIRC, LIHC, PRAD, THCA, and THYM, while CDK1 expression was negatively correlated with B-cell infiltration values in LUAD,
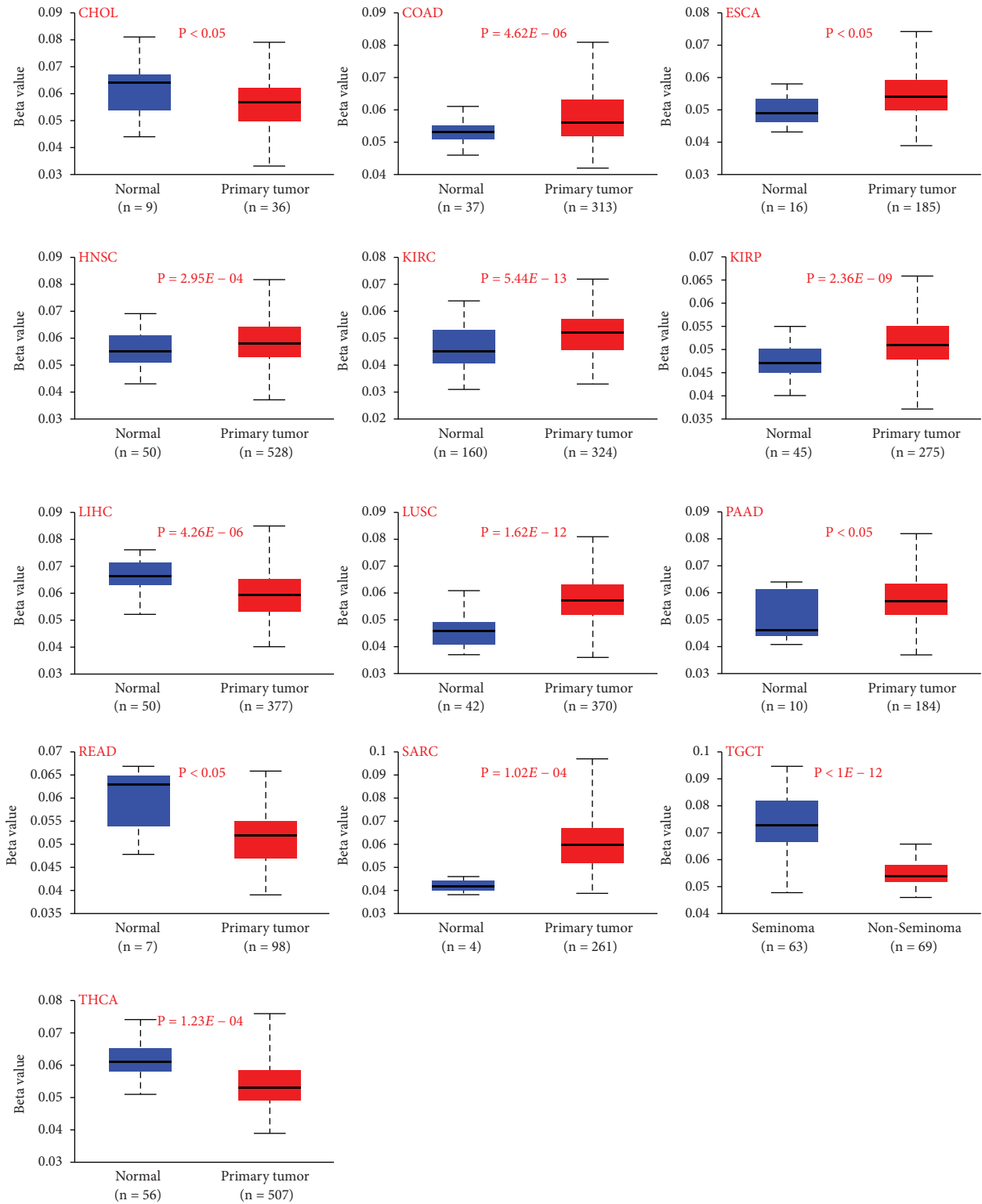
FIGURE 5: Methylation analysis of the CDK1 gene in different tumors. Box plots of methylation in different tumors, including CHOL, COAD, ESCA, HNSC, KIRC, KIRP, LIHC, LUSC, PAAD, READ, SARC, THCA, and testis germ tumor.

MESO, PAAD, STAD, and TGCT (Supplementary Figure 2B). As shown in Supplementary Figure 2C, based on most algorithms, CDK1 expression in KIRC, LGG, and THYM was positively correlated with DC cell infiltration values, while it was negatively correlated in STAD and TGCT. We also observed a positive correlation between CDK1 expression and macrophage infiltration values in BLCA, BRCA, KIRC, PRAD, and THCA tumors, and

(a)
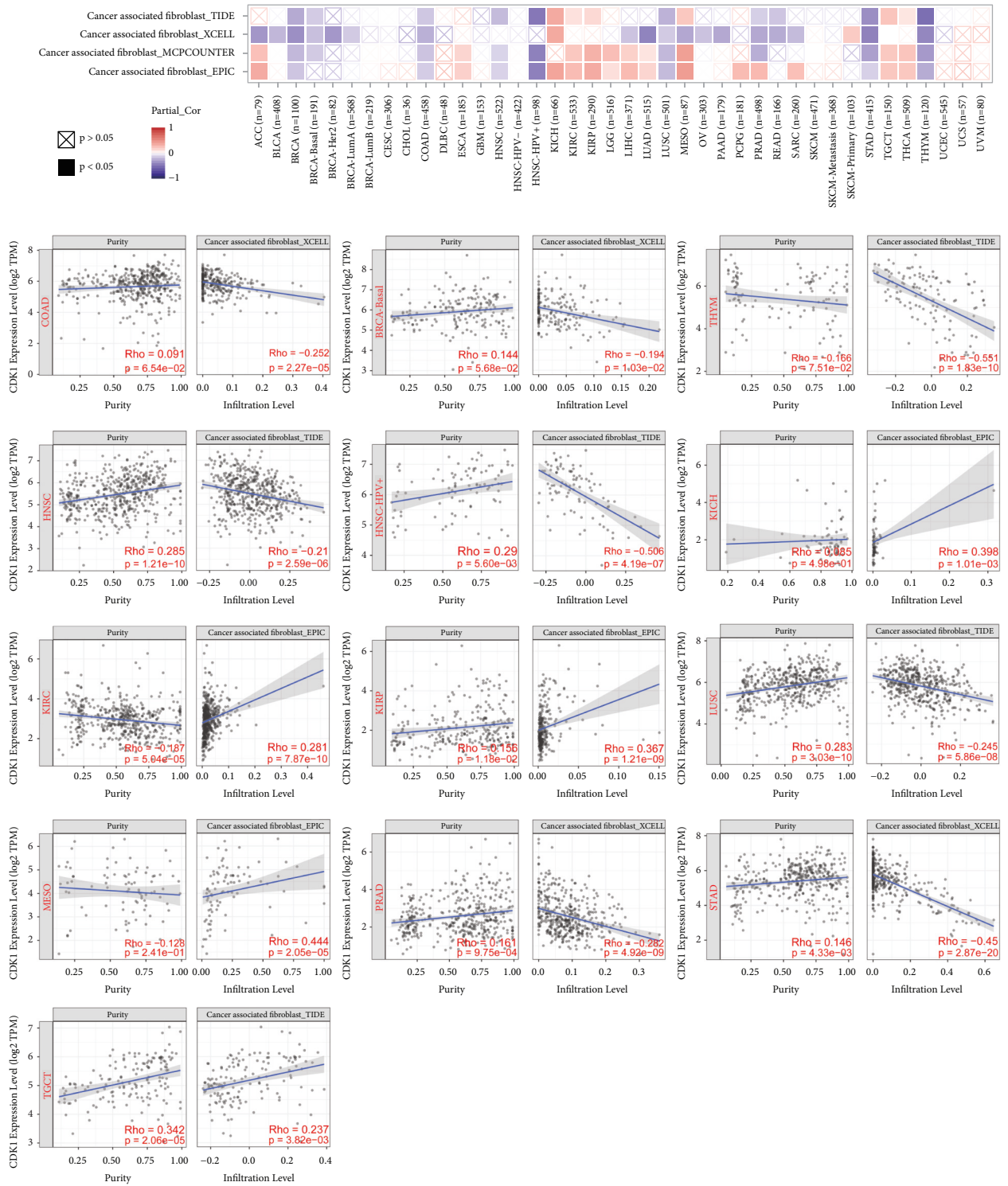
Figure 6: Continued.
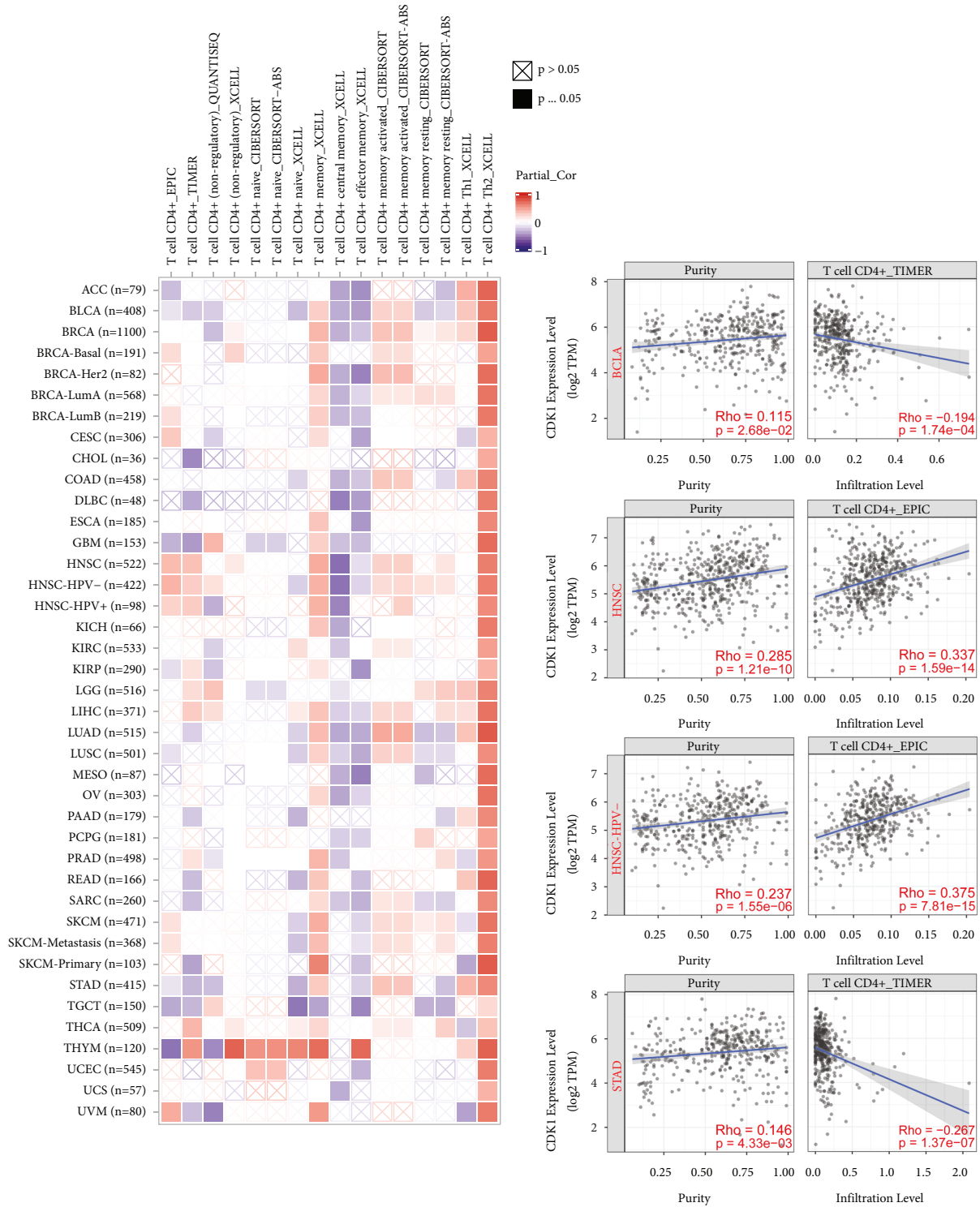
(b)

Figure 6: Correlation analysis between CDK1 expression and immune infiltration of tumor-associated fibroblasts and CD4+ T cells. (a) Different algorithms were used to determine the correlation between the expression level of the CDK1 gene and the infiltration level of tumor-associated fibroblasts across all types of cancer in TCGA. (b) Correlation of CDK1 expression with infiltrating levels of CD4+ T cells in different types of cancer.

a negative correlation in CESC, KIRP, LIHC, STAD, TGCT, and THYM tumors (Supplementary Figure 2D). These results provide strong evidence that the CDK1 gene might play an important role in tumor immune microenvironment, and CDK1 might be involved in the migration of immune cells to the tumor microenvironment. To analyze the correlation between CDK1 gene expression and tumor-infiltrating immune cells and to lay the foundation for the next antitumor immunotherapy based on CDK1 tumor targets.

3.7. The Level of CDK1 Was Positively Correlated with the Expression of RNA Methylation Regulatory Proteins in TCGA Tumors. RNA plays essential roles in not only translating nucleic acids into proteins, but also in gene regulation, environmental interactions, and many human diseases. A growing number of studies have shown that RNA methylation modification-related proteins are critical in tumor development. Our pan-cancer analysis showed (Figure 7) a significant positive correlation with expression between the CDK1 gene and three classes (*m1A, m5C, m6A*) of RNA methylation regulatory proteins. The positive pan-cancer correlations with m1A RNA methylation regulatory proteins YTHDF2 and ALKBH1, m5C methylation regulatory proteins DNMT1, DNMT3B, and ALYREF, and m6C RNA methylation regulatory proteins HNRNPC, HNRNPA2B1, and ELAVL1 were particularly significant. Our study reveals a significant positive correlation between CDK1 and RNA methylation regulatory proteins at the pan-cancer level of expression. CDK1 participates in RNA metabolic processes by affecting the expression levels of related RNA methylation regulatory proteins, this may be one of the potential mechanisms by which CDK1 exerts its corresponding oncogenic effects. Up- or downregulating the expression level of RNA methylation regulatory proteins by targeting CDK1 may become a new approach for tumor prevention and treatment.

3.8. Enrichment Analysis of CDK1-Related Partners. To further investigate the mechanism of action of the CDK1 gene in tumorigenesis, we performed functional enrichment analysis of CDK1-related binding proteins and CDK1 expression-related genes. Based on the STRING tool, we obtained 50 experimentally validated CDK1-related binding proteins and constructed a protein-protein interaction (PPI) network for these proteins (Figure 8(a)). Additionally, we obtained the top 100 genes associated with CDK1 expression using the GEPIA2 database, and a cross-tabulation analysis of the two gene sets showed that 11 genes overlapped, which included CKS1B, CDC20, CCNB1, CCNA2, CDC25C, PCNA, BUB1, CCNF, AURKA, CKS2, and CCNB2 (Figure 8(b)). We also performed a pan-cancer expression correlation analysis of CDK1 and the 11 genes using the TIMER2 database and showed a positive correlation between CDK1 and the expression of these molecules in TCGA tumors (Figure 8(c)).

We combined these two gene datasets for the KEGG and GO enrichment analysis. The results of the KEGG analysis suggested that CDK1 might be involved in different pathways such as mismatch repair, cell cycle, progesterone-mediated oocyte maturation, oocyte meiosis, DNA replication, HTLV-I infection, and pathways associated with cancer (Figure 8(d)). We found that CDK1-related genes were enriched in different pathways such as cell division, mitotic nuclear division, G1/S transition of the mitotic cell cycle, DNA repair, and G2/M transition of the mitotic cell cycle in the GO enrichment analysis category of "biological processes" (Figure 8(f)). This suggested that CDK1 plays an important role in cell cycle progression. In the GO enrichment analysis category "cellular components," CDK1-related genes were significantly enriched in different cellular components such as the nucleus, nucleoplasm, condensed chromosome kinetochore, membrane, and cytoplasm (Figure 8(g)). In the GO enrichment analysis category of "molecular function," the role of CDK1 in tumor pathogenesis might be related to protein binding, protein kinase binding, and ATP binding (Figure 8(h)). We have shown the relevant functional pathways involved in the top 20 genes associated with CDK1 as a chord plot (Figure 8(e)). The corresponding enrichment analysis of CDK1 further revealed the molecular mechanisms involved in its oncogenic role, which is involved in the malignant progression of tumors by affecting related signaling pathways or cellular functions.

3.9. In Vitro Experiments Verify the High Expression of CDK1 in Tumor Tissues. To further elucidate the difference of CDK1 gene expression in tumor tissues and normal tissues, we collected human lung cancer, liver cancer, and breast cancer tissues along with the adjacent normal tissues from the Affiliated Hospital of Southwest Medical University and conducted experimental studies on human lung cancer, liver cancer, and breast cancer tissue samples using immunohistochemical methods. The Image-pro Plus6.0 software was used for the semiquantitative analysis of different tissue specimens. Using the area of the whole image for measurement, the mean optical density values of CDK1-positive expression in the corresponding cancer tissues of lung cancer, liver cancer, and breast cancer, as well as the normal tissues, were calculated. The results showed that CDK1 was highly expressed in lung cancer tissues (Figure 9(a)), liver cancer tissues (Figure 9(b)), and breast cancer tissues (Figure 9(c)), and the difference in expression between the cancer tissues and normal tissues was significant. In contrast, there was no obvious positive staining in the rabbit IgG isotype control group. In vitro experiments confirmed the high expression status of CDK1 in tumor tissues, adding credibility to its use as a potential therapeutic target for differentially highly expressed tumors.

4. Discussion

As an important member of the cyclin-dependent kinase family, CDK1 plays a critical role in cell cycle regulation, immune checkpoint activation, and DNA damage repair. As an important locus of signaling pathways, the CDK1 gene is essential for tumor initiation and progression in different
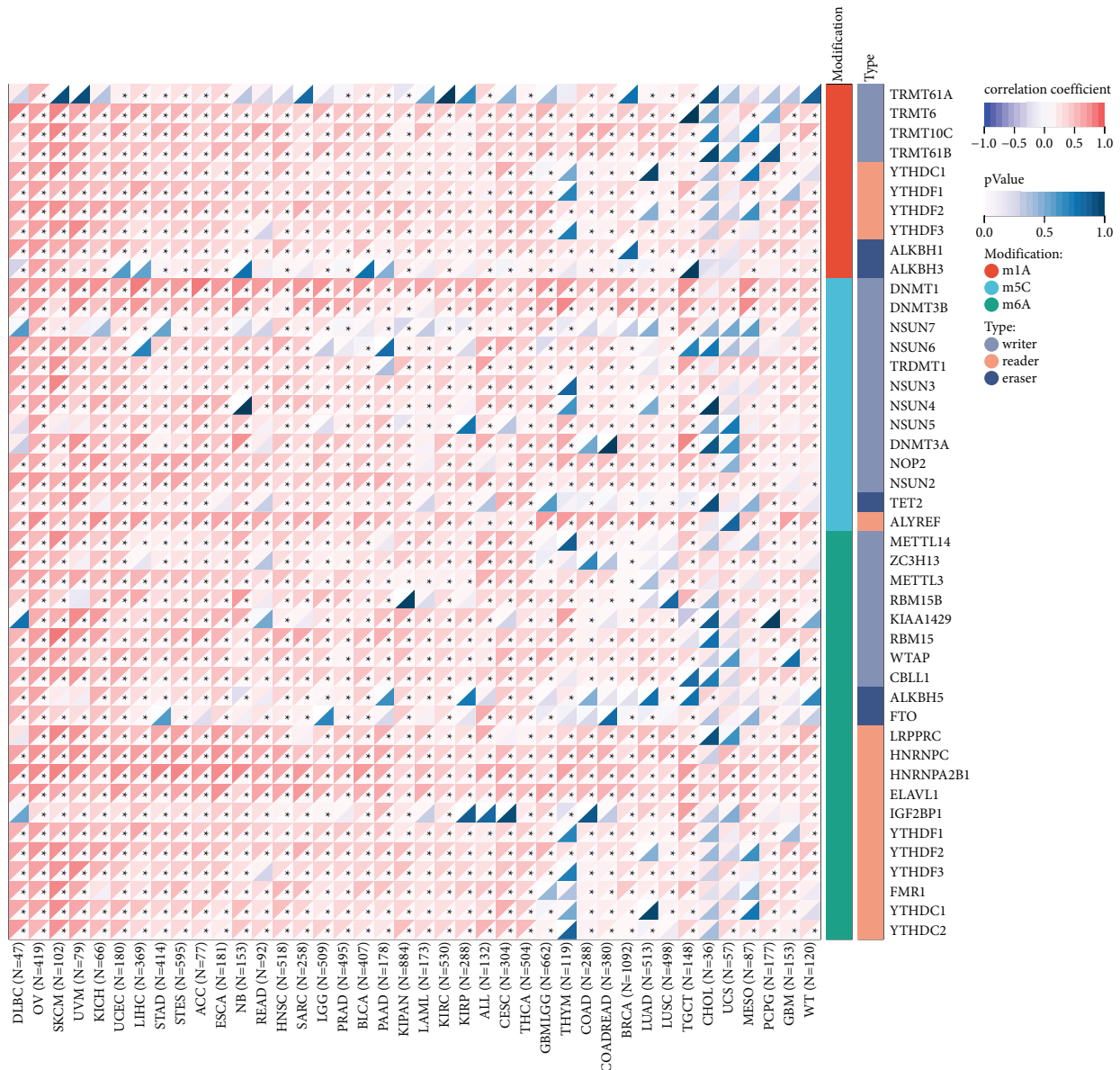
FIGURE 7: Pan-cancer correlation between CDK1 and 44 RNA methylation regulatory proteins. RNA methylation modifications are divided into three categories: m1A, m5A, and m6C; modified protein types are divided into three categories: writer, reader, and eraser.

types of cancer, promoting the progression of malignancy through different signaling pathways [52, 53]. The CDK1 protein structure is conserved from yeast to humans, suggesting that similar mechanisms may exist for the normal physiological roles of CDK1. Whether CDK1 plays a role in the pathogenesis of different tumors through some common molecular mechanisms is unknown. There are no reports of pan-cancer analysis of CDK1 from an overall perspective. Therefore, using data from various databases such as TCGA, GEO, and CPTAC, we revealed the molecular characteristics of the CDK1 gene at multiple levels, including gene expression, gene alteration, DNA methylation, and protein phosphorylation. We conducted a comprehensive investigation on the bioinformatics of the CDK1 gene in 33 tumors to elucidate its functions in the development of different tumors and potential regulatory pathways.

In this study, we first investigated the expression of CDK1 in the pan-cancer dataset (Figures 1(a)–1(d)), Supplementary Table 1). The results of the analysis of different datasets showed that the CDK1 gene was highly expressed in most tumors. CDK1 expression in different tumors was analyzed using the Oncomine database, the TIMER database, and the combined TCGA and GTEx datasets to avoid bias in the results of single dataset analysis. We also conducted in vitro experiments to select human lung, liver, and breast cancer tissues for immunohistochemical semiquantitative analysis to further validate our findings (Figure 9). Tumorigenesis is usually accompanied by abnormal gene expression, and this altered expression contributes to the development of tumors [54]. CDK1 expression and subcellular localization are regulated by RARγ and its expression level is usually positively correlated with the

(a)

(b)

(c)

(d)

Figure 8: Continued.

(e)

(f)

Figure 8: Continued.

(g)

(h)
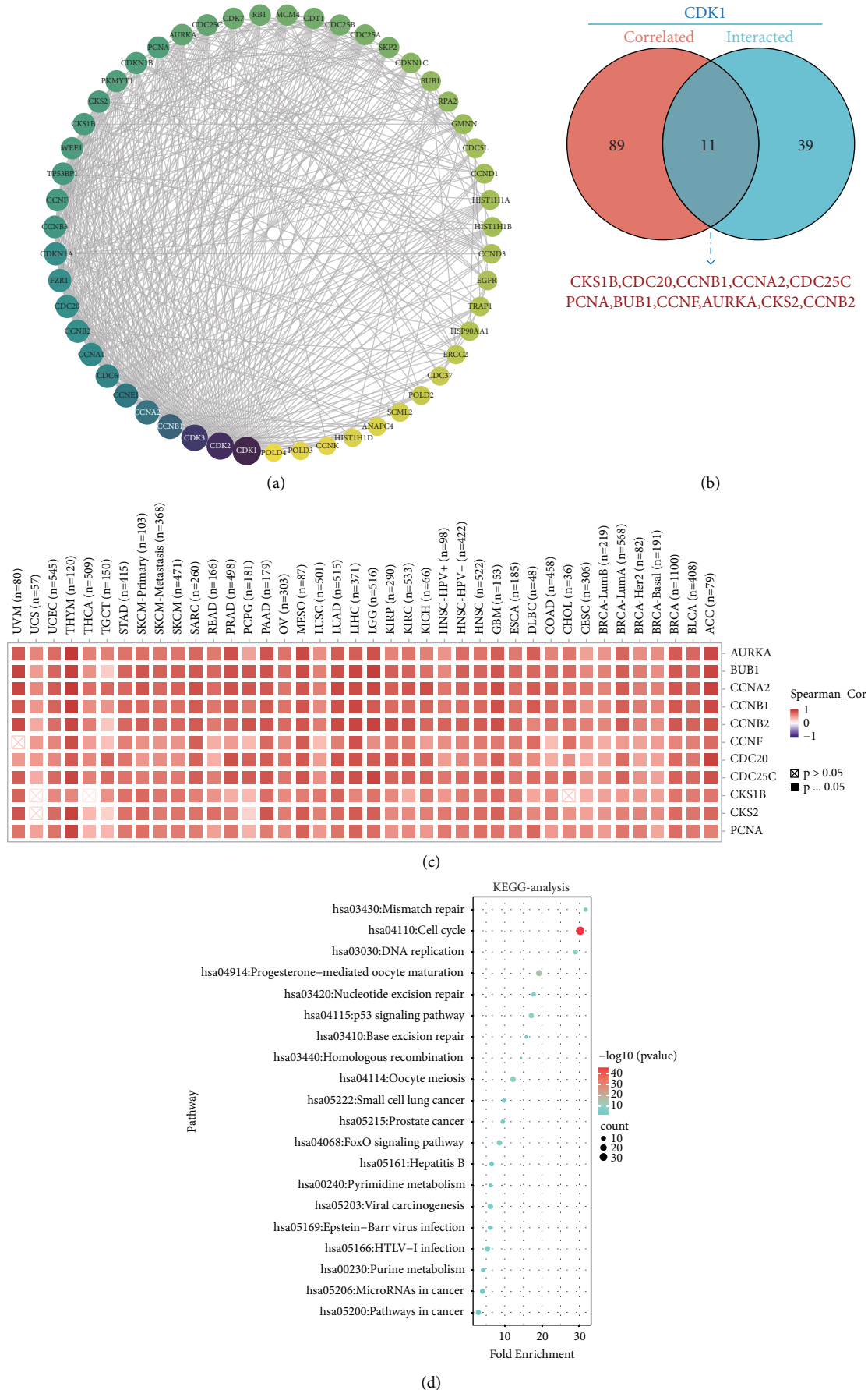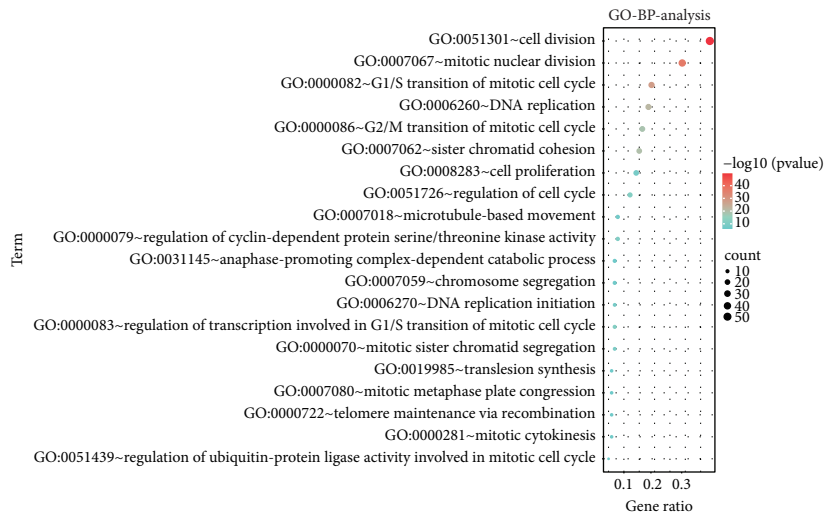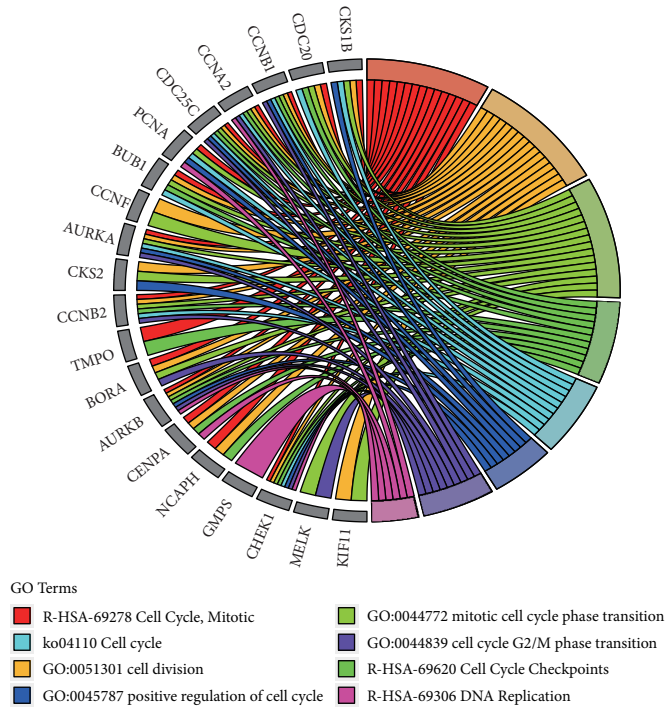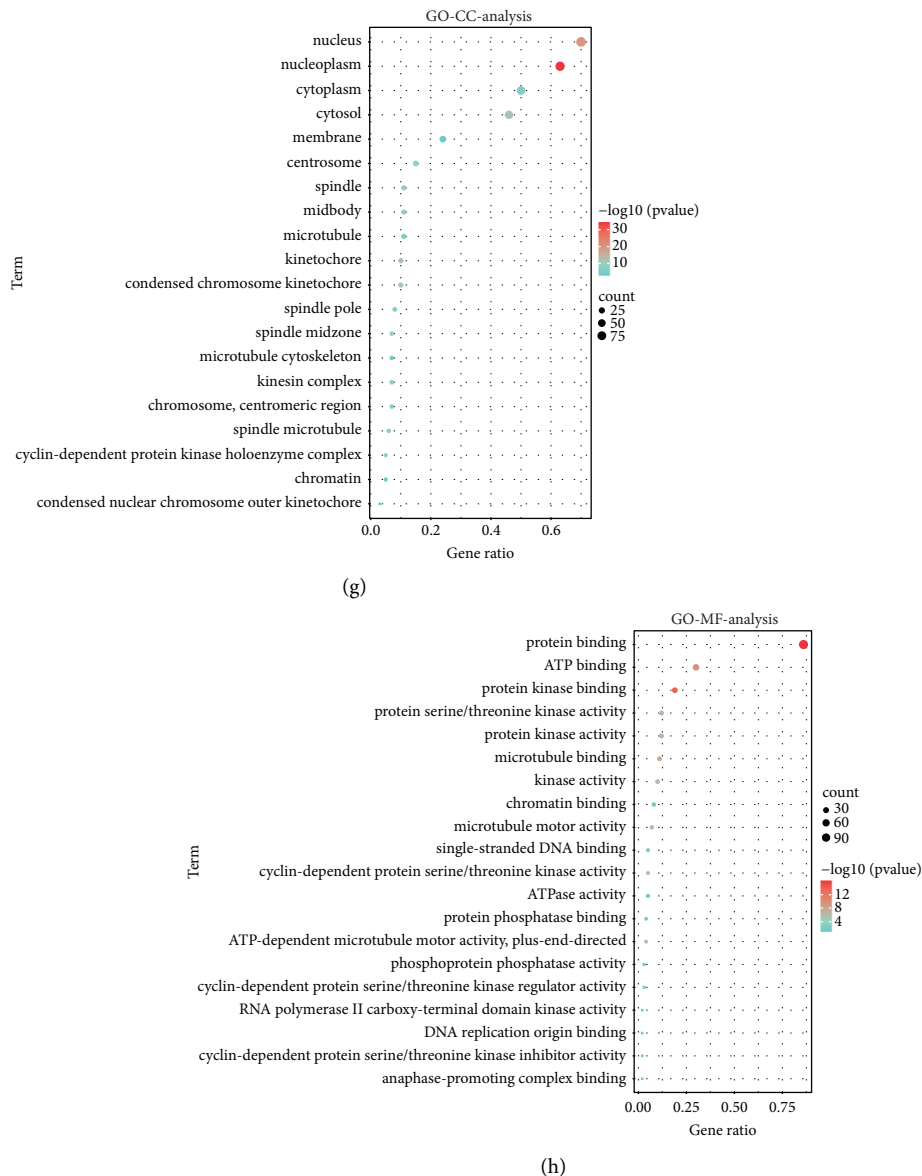
FIGURE 8: CDK1-related gene enrichment analysis. (a) PPI network analysis of CDK1-related genes. The visualizing interaction network of CDK1-binding proteins was obtained based on the STRING database. (b) Venn diagram of 50 CDK1-interacting proteins and 100 CDK1-associated genes. (c) Heat map of the gene correlation analysis. (d) KEGG analysis of CDK1-binding and interacted genes. (e) GO enrichment chord plot for the top 20 genes associated with CDK1. (f) GO-BP analysis of CDK1-binding and interacted genes. (g) GO-CC analysis of CDK1-binding and interacted genes. (h) GO-MF analysis of CDK1-binding and interacted genes.

activation of Wnt/β-catenin [55–57]. We also found that high CDK1 expression was associated with the clinico-pathological staging of BRCA, COAD, LUAD, and LUSC (Figure 1(e)).

In this study, we used independent datasets from TCGA, Kaplan-Meier plotter, and PrognoScan to determine the relationship between CDK1 expression levels and pan-cancer prognosis (Figure 2, Supplementary Figure 1). In different datasets, based on all or most tumor types, high CDK1 expression levels suggested a poor prognosis for tumor patients, affecting OS, DFS, DMFS, RFS, DRFS, DSS, and MFS survival progression in tumor patients. Previous studies have shown that high CDK1 expression is

significantly associated with reduced overall survival in patients with colon cancer [58] and hepatocellular carcinoma [59]. These results are consistent with our current findings. Notably, analysis from the Kaplan-Meier plotter dataset showed that high CDK1 expression was significantly associated with improved OS in blood cancers and improved DFS in colorectal cancers. The results of PrognoScan analysis suggested that patients with CDK1-positive esophageal squamous cell carcinoma had better OS and RFS. There were no reports on the effect of CDK1 on survival progression in blood cancer, colorectal cancer, and esophageal squamous cell carcinoma. In our study, high expression of CDK1, as a protective factor, was found to prolong the survival of

(a)

(b)

(c)
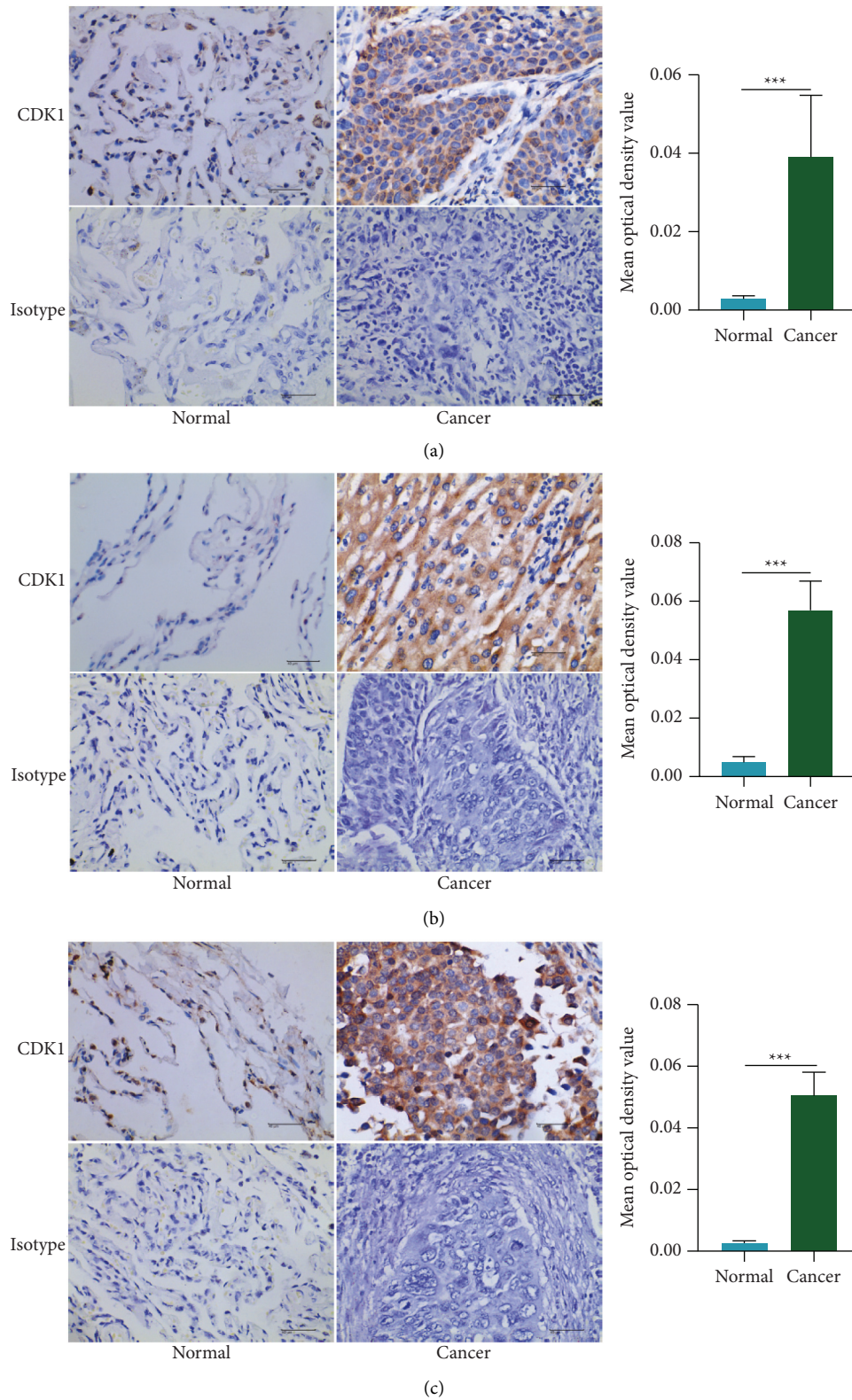
FIGURE 9: IHC verification of CDK1 gene expression in tumor tissues and normal tissues. (a) Expression of CDK1 gene in lung cancer tissues and normal tissues. (b) Expression of CDK1 gene in hepatocellular carcinoma tissues and normal tissues. (c) Expression of CDK1 gene in breast cancer tissues and normal tissues ($n = 10$ per CDK1 experiment group, $n = 5$ per isotype group; ns, not statistically significant; $*P < 0.05$; $**P < 0.01$; and $***P < 0.001$. The Student's t test was used for statistical analysis).

patients with these tumors. However, this observation needs to be confirmed with larger sample size and through other clinical characteristics of the tumor patients. Taken together, these findings provide insights into the application of CDK1 as a prognostic marker for pan-cancer in the context of immuno-oncology, thus contributing to the potential development of research on CDK1 gene-targeted therapy.

TMB refers to the number of nonsynonymous mutations in somatic cells within a given genome, which can indirectly reflect the ability and extent of neoantigen production by tumors. TMB is a potential biomarker of response to ICIs and can predict the efficacy of immunotherapy for a variety of tumors [60]. Clinical studies have shown that high TMB is associated with improved responses and survival benefits in cancer patients after ICI treatment [61–63]. In tumors, MSI is a relatively common phenomenon. The status of MSI predicts the cause and development of tumors and also plays an important role in different cancer types as an aid to diagnosis and drug guidance. A comprehensive MSI screening study showed that the degree of MSI was positively correlated with survival in cancer patients and that MSI-positive tumors generally had a better prognosis than MSI-negative tumors [64, 65]. We found that CDK1 expression was positively correlated with TMB in 15 cancers and with MSI in five cancers (Figure 3(d)). Therefore, we hypothesized that tumors with high CDK1 expression and positive TMB and MSI might have a greater survival benefit after treatment with immune checkpoint inhibitors (Figure 3(e)).

The survival, growth, migration, and dormancy of tumor cells are influenced by the surrounding tumor microenvironment, which is important for tumor progression [66–68]. In the tumor microenvironment, tumor-associated fibroblasts are a major component of the tumor stroma and are currently considered to be one of the most active cell types in the tumor microenvironment, playing a central role in tumorigenesis, progression, and metastasis [69–71]. Tumor-associated fibroblasts accumulated in the tumor microenvironment might promote the growth and migration of a variety of solid malignancies, including breast cancer [72], esophageal cancer [73], bladder cancer [74], gallbladder cancer [75], and bile duct cancer [76]. We found that CDK1 expression was negatively correlated with infiltration values of tumor-associated fibroblasts in COAD, BRCA-Basal, THYM, HNSC, HNSC-HPV+, LUSC, PRAD, and STAD tumors, whereas it was positively correlated in KICH, KIRC, KIRP, MESO, and TGCT. Meanwhile, we demonstrated the high expression status of the CDK1 gene in COAD, THYM, HNSC, HNSC-HPV+, LUSC, PRAD, STAD, KICH, KIRC, KIRP, MESO, and TGCT tumors (Figure 6(a)). Whether the CDK1 gene and tumor-associated fibroblasts have competitive inhibitory or synergistic effects on promoting tumor cell proliferation and the progression of malignancy in these tumors is unclear, and the mechanism of action between the two needs a detailed investigation.

Interestingly, we found a positive correlation between the infiltration values of Th2-type CD4+ T cells and CDK1 expression in all TCGA tumors (Figure 6(b)). There is growing evidence that CD4+ T cells play a central role in the initiation and maintenance of the immune response against

cancer or autoimmune diseases [77, 78]. As an essential component of the tumor microenvironment, it exerts powerful antitumor effects by recognizing tumor-associated MHC class II molecules. However, most solid tumors do not express MHC class II molecules, which limit the ability of CD4+ T cells to act at the tumor site [79]. CD4+ T cells are mainly composed of different cell subsets such as Th1, Th2, Th17, and Treg. Among them, Th1 cells assist CD8+ T cells in mediating immunity against tumors and viruses [80]. Th2 cells are best known for enhancing immunity against parasites, and their pathogenic role in allergic diseases has been well documented [81, 82]. However, the role of Th2 cells in the antitumor immune response is not well-understood. Th2 cells mainly secrete IL-4, IL-5, IL-6, and IL-10 cytokines [83]. IL-10 cytokines produced by Th2 cells directly inhibit Th1 cells and indirectly inhibit the activity of Th2 cells [84, 85]. Whether the high expression of CDK1 breaks the Th1/Th2 balance and increases Th2-type CD4+ T cells, leading to immune dysfunction and the suppression of the antitumor effects of Th1, needs further investigation. Our study did not find a significant effect of CDK1 expression on tumor infiltration in Th1-type CD4+ T cells. Additionally, we found that CDK1 gene expression in different tumors correlated with the infiltration of CD8+ T cells, B cells, DC cells, and macrophages. This association between CDK1 and the tumor microenvironment might be another reason for the prognostic significance of CDK1 in various cancers, where the aberrant expression of CDK1 could play a dominant role in the tumor microenvironment.

Some studies have reported that targeting CDK1 can improve the effectiveness of antitumor immunotherapy or reverse chemotherapy resistance and prolong survival time. The results of Jin Huang et al. showed that CDK1 kinase activity plays an important role in IFNG-mediated tumor immune escape. Inhibition of the kinase activity of CDK1 can prevents the expression of relevant immune checkpoints, alters the tumor microenvironment, and can significantly improve the overall survival rate in a mouse pancreatic cancer tumor model [86]. A recent report also showed that ATR inhibits CDK1-SPOP signaling and thus enhances anti-PD-L1 cytotoxicity in prostate cancer. Combination of ATR inhibitor and anti-PD-L1 therapy produces potent innate immune activation and a synergistic T-cell-dependent therapeutic response [87]. Meanwhile, CDK1 plays an important role in reversing chemotherapy resistance and improving the effectiveness of chemotherapeutic drugs. The application of CDK1 inhibitors has been reported to improve the efficacy of the chemotherapeutic drug sorafenib targeting tumor stem cells in the treatment of hepatocellular carcinoma, anti-CDK1 combination chemotherapy significantly inhibits tumor growth in hepatocellular carcinoma, while being able to overcome resistance to sorafenib [59]. Also, it has been shown that the use of CDK1 inhibitors can interfere with the proliferation of gastrointestinal mesenchymal tumor cells with high CDK1 expression. More importantly, anti-CDK1 inhibitor treatment reduced tumor growth in imatinib-resistant and imatinib-sensitive gastrointestinal mesenchymal tumor xenograft mice models, reversing the chemoresistant and

sensitive situation [15]. Based on the importance of CDK1 in antitumor immunotherapy and reversal of chemotherapy resistance, CDK1 can be an important factor in measuring the efficacy of tumor immunotherapy and chemotherapy.

We investigated the function of differentially expressed CDK1 by GO enrichment analysis and KEGG pathway enrichment analysis (Figures 8(d)–8(h)). We found that differentially expressed CDK1 is mainly associated with the regulation of the cell cycle, mismatch repair, DNA replication, G1/S and G2/M transitions of the mitotic cell cycle, protein binding, protein kinase binding, and ATP binding. Previously, CDK1 was shown to play a key role in cell cycle progression [85], which was consistent with our findings. By analyzing CDK1-related genes, we found that the positive association of CKS1B, CDC20, CCNB1, CCNA2, CDC25C, PCNA, BUB1, CCNF, AURKA, CKS2, and CCNB2 with the CDK1 gene was consistent in all TCGA tumors (Figure 8(c)). This suggested that CDK1-related enrichment pathways could serve as the underlying markers to identify patients in need of therapy.

In summary, our pan-cancer analysis of CDK1 showed a significant correlation between CDK1 expression and clinical prognosis, DNA methylation, protein phosphorylation, immune cell infiltration, RNA methylation regulatory proteins, tumor mutational load, and microsatellite instability in multiple tumors. In this study, we determined the role of CDK1 in tumorigenesis from the perspective of clinical tumor samples. Based on our established findings, the expression pattern as well as the functional importance of CDK1 make it a promising target for clinical antitumor therapy. The inclusion of CDK1 in tumor marker testing is of great significance, as well as the development of new anti-CDK1 drugs targeting CDK1, anti-CDK1 combined with immunotherapy or combined with chemotherapy, making it possible to extend the median survival time of tumor patients.

Abbreviations

CDK1:   Cyclin-dependent kinase 1
TCGA: The Cancer Genome Atlas
GEO: Gene Expression Omnibus
OS: Overall survival
DFS: Disease-free survival
DMFS: Distant metastasis-free survival
RFS: Recurrence-free survival
DRFS: Distant recurrence-free survival
DSS: Disease-specific survival
TMB: Tumor mutational burden
MSI: Microsatellite instability
CDKs: Cyclin-dependent kinases
CDC2:   Cell division cycle 2
GTEx: Genotype-tissue expression
CPTAC: Clinical Proteomic Tumor Analysis
           Consortium
RCC: Renal clear cell carcinoma
UCEC: Uterine corpus endometrial carcinoma
LUAD: Lung adenocarcinoma
CNA: Copy number alteration
GDC: Genomic data commons
DC: Dendritic cells
COR: Correlation coefficients
KEGG: Kyoto Encyclopedia of Genes and Genomes
GO: Gene ontology
BP: Biological process
CC: Cellular component
MF: Molecular function
BLCA: Bladder urothelial carcinoma
BRCA: Breast invasive carcinoma
CESC: Cervical squamous cell carcinoma and
           endocervical adenocarcinoma
CHOL: Cholangiocarcinoma
COAD: Colon adenocarcinoma
ESCA: Esophageal carcinoma
GBM: Glioblastoma multiforme
HNSC: Head and neck squamous cell carcinoma
KIRC: Kidney renal clear cell carcinoma
LIHC: Liver hepatocellular carcinoma
LUSC: Lung squamous cell carcinoma
PCPG: Pheochromocytoma and paraganglioma
PRAD: Prostate adenocarcinoma
READ: Rectum adenocarcinoma
STAD: Stomach adenocarcinoma
THCA: Thyroid carcinoma
KICH: Kidney chromophobe
ACC: Adrenocortical carcinoma
KIRP: Kidney renal papillary cell carcinoma
LGG: Brain lower grade glioma
MESO: Mesothelioma
PAAD: Pancreatic adenocarcinoma
SARC: Sarcoma
SKCM: Skin cutaneous melanoma
UVM: Uveal melanoma
COADREAD: Colorectal cancer
LAML: Acute myeloid leukemia
UCS: Uterine carcinosarcoma
THYM: Thymoma
DLBC: Lymphoid neoplasm diffuse large B-cell
           lymphoma
HPV: Human papillomavirus
TGCT: Testicular germ cell tumor
PPI: Protein-protein interaction
m1A: 1-Methyladenosine
m5C: 5-Methylcytidine
m6A: 6-Methyladenosine.

Data Availability

The original contributions presented in the study are included in the article/supplementary material. Further inquiries can be directed to the corresponding author/s.

Additional Points

The "guarantor statement" does not apply to this manuscript.

Conflicts of Interest

The authors declare that the submitted work was not carried out in the presence of any personal, professional, or financial relationships that could potentially be constructed as a conflict of interest.

Authors' Contributions

YY contributed to data analysis, methodology, figures construction, and article writing. QL contributed to investigation and validation. XG, QY, SN, PK, and ZX contributed to methodology and validation. LL and YY contributed to supervision of the article. All authors contributed to the article and approved the submitted version.

Acknowledgments

Supplementary Materials

Supplementary Table 1. Expression of CDK1 in different types of lung, stomach, liver, colon, breast, esophageal, and pancreatic cancer tissues and normal tissues. Supplementary Figure 1. Kaplan-Meier survival curves comparing the high and low expression of CDK1 in different types of cancer in the (A) PrognoScan database and (B) Kaplan-Meier plotter database. Supplementary Figure 2. Correlation between CDK1 expression in different types of cancer and infiltrating levels of (A) CD8+ T cells, (B) B cells, (C) dendritic cells, and (D) macrophages. (*Supplementary Materials*)

References

[1] H. Sung, J. Ferlay, R. L. Siegel et al., "Global cancer statistics 2020: GLOBOCAN estimates of incidence and mortality worldwide for 36 cancers in 185 countries," *CA: A Cancer Journal for Clinicians*, vol. 71, no. 3, pp. 209–249, 2021.

[2] F. Bray, M. Laversanne, E. Weiderpass, and I. Soerjomataram, "The ever-increasing importance of cancer as a leading cause of premature death worldwide," *Cancer*, vol. 127, no. 16, pp. 3029-3030, 2021.

[3] X. Wu, "Replication stress response links RAD52 to protecting common fragile sites," *Cancers*, vol. 11, no. 10, p. 1467, 2019.

[4] D. J. Gordon, B. Resio, and D. Pellman, "Causes and consequences of aneuploidy in cancer," *Nature Reviews Genetics*, vol. 13, no. 3, pp. 189–203, 2012.

[5] P. R. Prasetyanti and J. P. Medema, "Intra-tumor heterogeneity from a cancer stem cell perspective," *Molecular Cancer*, vol. 16, no. 1, p. 41, 2017.

[6] D. Martinez-Alonso and M. Malumbres, "Mammalian cell cycle cyclins," *Seminars in Cell & Developmental Biology*, vol. 107, pp. 28–35, 2020.

[7] M. Malumbres, "Cyclin-dependent kinases," *Genome Biology*, vol. 15, no. 6, p. 122, 2014.

[8] Y. Zhi, Z. Wang, C. Yao et al., "Design and synthesis of 4-(heterocyclic substituted amino)-1H-Pyrazole-3-Carboxamide derivatives and their potent activity against acute myeloid leukemia (AML)," *International Journal of Molecular Sciences*, vol. 20, no. 22, p. 5739, 2019.

[9] A. R. Nebreda, "CDK activation by non-cyclin proteins," *Current Opinion in Cell Biology*, vol. 18, no. 2, pp. 192–198, 2006.

[10] P. Loyer, J. H. Trembley, R. Katona, V. J. Kidd, and J. M. Lahti, "Role of CDK/cyclin complexes in transcription and RNA splicing," *Cellular Signalling*, vol. 17, no. 9, pp. 1033–1051, 2005.

[11] M. Malumbres, E. Harlow, T. Hunt et al., "Cyclin-dependent kinases: a family portrait," *Nature Cell Biology*, vol. 11, no. 11, pp. 1275-1276, 2009.

[12] J. Piao, L. Zhu, J. Sun et al., "High expression of CDK1 and BUB1 predicts poor prognosis of pancreatic ductal adenocarcinoma," *Gene*, vol. 701, pp. 15–22, 2019.

[13] D. Santamaria, C. Barriere, A. Cerqueira et al., "Cdk1 is sufficient to drive the mammalian cell cycle," *Nature*, vol. 448, no. 7155, pp. 811–815, 2007.

[14] N. R. Brown, S. Korolchuk, M. P. Martin et al., "CDK1 structures reveal conserved and unique features of the essential cell cycle CDK," *Nature Communications*, vol. 6, no. 1, p. 6769, 2015.

[15] X. Lu, Y. Pang, H. Cao et al., "Integrated screens identify CDK1 as a therapeutic target in advanced gastrointestinal stromal tumors," *Cancer Research*, vol. 81, no. 9, pp. 2481–2494, 2021.

[16] J. Heo, B. J. Noh, S. Lee et al., "Phosphorylation of TFCP2L1 by CDK1 is required for stem cell pluripotency and bladder carcinogenesis," *EMBO Molecular Medicine*, vol. 12, no. 1, Article ID e10880, 2020.

[17] S. Zhao, B. Wang, Y. Ma, J. Kuang, J. Liang, and Y. Yuan, "NUCKS1 promotes proliferation, invasion and migration of non-small cell lung cancer by upregulating CDK1 expression," *Cancer Management and Research*, vol. 12, pp. 13311–13323, 2020.

[18] D. Ravindran Menon, Y. Luo, J. J. Arcaroli et al., "CDK1 interacts with Sox2 and promotes tumor initiation in human melanoma," *Cancer Research*, vol. 78, no. 23, pp. 6561–6574, 2018.

[19] J. N. Weinstein, E. A. Collisson, G. B. Mills et al., "The cancer genome Atlas pan-cancer analysis project," *Nature Genetics*, vol. 45, no. 10, pp. 1113–1120, 2013.

[20] "Taking pan-cancer analysis global," *Nature Genetics*, vol. 45, no. 11, p. 1263, 2013.

[21] Z. Liu and S. Zhang, "Toward a systematic understanding of cancers: a survey of the pan-cancer study," *Frontiers in Genetics*, vol. 5, p. 194, 2014.

[22] D. R. Rhodes, S. Kalyana-Sundaram, V. Mahavisno et al., "Oncomine 3.0: genes, pathways, and networks in a collection of 18, 000 cancer gene expression profiles," *Neoplasia*, vol. 9, no. 2, pp. 166–180, 2007.

[23] T. Li, J. Fu, Z. Zeng et al., "TIMER2.0 for analysis of tumor-infiltrating immune cells," *Nucleic Acids Research*, vol. 48, no. W1, pp. W509–W514, 2020.

[24] J. Vivian, A. A. Rao, F. A. Nothaft et al., "Toil enables reproducible, open source, big biomedical data analyses," *Nature Biotechnology*, vol. 35, no. 4, pp. 314–316, 2017.

[25] D. S. Chandrashekar, B. Bashel, S. A. H. Balasubramanya et al., "UALCAN: a portal for facilitating tumor subgroup gene expression and survival analyses," *Neoplasia*, vol. 19, no. 8, pp. 649–658, 2017.

[26] Z. Tang, B. Kang, C. Li, T. Chen, and Z. Zhang, "GEPIA2: an enhanced web server for large-scale expression profiling and interactive analysis," *Nucleic Acids Research*, vol. 47, no. W1, pp. W556–W560, 2019.

[27] A. Lanczky, A. Nagy, G. Bottai et al., "miRpower: a web-tool to validate survival-associated miRNAs utilizing expression data from 2178 breast cancer patients," *Breast Cancer Research and Treatment*, vol. 160, no. 3, pp. 439–446, 2016.

[28] H. Mizuno, K. Kitada, K. Nakai, and A. Sarai, "PrognoScan: a new database for meta-analysis of the prognostic value of genes," *BMC Medical Genomics*, vol. 2, no. 1, p. 18, 2009.

[29] J. Gao, B. A. Aksoy, U. Dogrusoz et al., "Integrative analysis of complex cancer genomics and clinical profiles using the cBioPortal," *Science Signaling*, vol. 6, no. 269, p. pl1, 2013.

[30] D. Szklarczyk, A. L. Gable, D. Lyon et al., "STRING v11: protein-protein association networks with increased coverage, supporting functional discovery in genome-wide experimental datasets," *Nucleic Acids Research*, vol. 47, no. D1, pp. D607–D613, 2019.

[31] P. Bardou, J. Mariette, F. Escudié, C. Djemiel, and C. Klopp, "jvenn: an interactive Venn diagram viewer," *BMC Bioinformatics*, vol. 15, no. 1, p. 293, 2014.

[32] Y. Huang, Q. Mao, J. He et al., "Fusions of tumor-derived endothelial cells with dendritic cells induces antitumor immunity," *Scientific Reports*, vol. 7, no. 1, Article ID 46544, 2017.

[33] A. B. Als, L. Dyrskjot, H. von der Maase et al., "Emmprin and survivin predict response and survival following cisplatin-containing chemotherapy in patients with advanced bladder cancer," *Clinical Cancer Research*, vol. 13, no. 15, pp. 4407–4414, 2007.

[34] W. J. Kim, E. J. Kim, S. K. Kim et al., "Predictive value of progression-related gene classifier in primary non-muscle invasive bladder cancer," *Molecular Cancer*, vol. 9, no. 1, p. 3, 2010.

[35] J. S. Lee, S. H. Leem, S. Y. Lee et al., "Expression signature of E2F1 and its associated genes predict superficial to invasive progression of bladder tumors," *Journal of Clinical Oncology*, vol. 28, no. 16, pp. 2660–2667, 2010.

[36] I. Hanamura, Y. Huang, F. Zhan, B. Barlogie, and J. Shaughnessy, "Prognostic value of cyclin D2 mRNA expression in newly diagnosed multiple myeloma treated with high-dose chemotherapy and tandem autologous stem cell transplantations," *Leukemia*, vol. 20, no. 7, pp. 1288–1290, 2006.

[37] M. Hummel, S. Bentink, H. Berger et al., "A biologic definition of Burkitt's lymphoma from transcriptional and genomic profiling," *New England Journal of Medicine*, vol. 354, no. 23, pp. 2419–2430, 2006.

[38] K. H. Metzeler, M. Hummel, C. D. Bloomfield et al., "An 86-probe-set gene-expression signature predicts survival in cytogenetically normal acute myeloid leukemia," *Blood*, vol. 112, no. 10, pp. 4193–4201, 2008.

[39] B. M. Costa, J. S. Smith, Y. Chen et al., "Reversing HOXA9 oncogene activation by PI3K inhibition: epigenetic mechanism and prognostic significance in human glioblastoma," *Cancer Research*, vol. 70, no. 2, pp. 453–462, 2010.

[40] W. A. Freije, F. E. Castro-Vargas, Z. Fang et al., "Gene expression profiling of gliomas strongly predicts survival," *Cancer Research*, vol. 64, no. 18, pp. 6503–6510, 2004.

[41] Y. Pawitan, J. Bjohle, L. Amler et al., "Gene expression profiling spares early breast cancer patients from adjuvant therapy: derived and validated in two population-based cohorts," *Breast Cancer Research*, vol. 7, no. 6, pp. R953–R964, 2005.

[42] Y. Zhang, A. M. Sieuwerts, M. McGreevy et al., "The 76-gene signature defines high-risk patients that benefit from adjuvant tamoxifen therapy," *Breast Cancer Research and Treatment*, vol. 116, no. 2, pp. 303–309, 2009.

[43] P. D. Bos, X. H. F. Zhang, C. Nadal et al., "Genes that mediate breast cancer metastasis to the brain," *Nature*, vol. 459, no. 7249, pp. 1005–1009, 2009.

[44] E. Staub, J. Groene, M. Heinze et al., "An expression module of WIPF1-coexpressed genes identifies patients with favorable prognosis in three tumor types," *Journal of Molecular Medicine (Berlin)*, vol. 87, no. 6, pp. 633–644, 2009.

[45] J. J. Smith, N. G. Deane, F. Wu et al., "Experimentally derived metastasis gene expression profile predicts recurrence and death in patients with colon cancer," *Gastroenterology*, vol. 138, no. 3, pp. 958–968, 2010.

[46] R. W. Tothill, A. V. Tinker, J. George et al., "Novel molecular subtypes of serous and endometrioid ovarian cancer linked to clinical outcome," *Clinical Cancer Research*, vol. 14, no. 16, pp. 5198–5208, 2008.

[47] A. Sboner, F. Demichelis, S. Calza et al., "Molecular sampling of prostate cancer: a dilemma for predicting disease progression," *BMC Medical Genomics*, vol. 3, no. 1, p. 8, 2010.

[48] D. Bogunovic, D. W. O'Neill, I. Belitskaya-Levy et al., "Immune profile and mitotic index of metastatic melanoma lesions enhance clinical staging in predicting patient survival," *Proceedings of the National Academy of Sciences of the USA*, vol. 106, no. 48, pp. 20429–20434, 2009.

[49] R. M. Gobble, L. X. Qin, E. R. Brill et al., "Expression profiling of liposarcoma yields a multigene predictor of patient outcome and identifies genes that contribute to liposarcomagenesis," *Cancer Research*, vol. 71, no. 7, pp. 2697–2705, 2011.

[50] W. H. Fridman, J. Galon, M. C. Dieu-Nosjean et al., "Immune infiltration in human cancer: prognostic significance and disease control," *Current Topics in Microbiology and Immunology*, vol. 344, pp. 1–24, 2011.

[51] X. Chen and E. Song, "Turning foes to friends: targeting cancer-associated fibroblasts," *Nature Reviews Drug Discovery*, vol. 18, no. 2, pp. 99–115, 2019.

[52] R. Cong, F. Kong, J. Ma, Q. Li, H. Yang, and X. Ma, "The PVT1/miR-612/CENP-H/CDK1 axis promotes malignant progression of advanced endometrial cancer," *Am J Cancer Res*, vol. 11, no. 4, pp. 1480–1502, 2021.

[53] A. K. Schmidt, K. Pudelko, J. E. Boekenkamp, K. Berger, M. Kschischo, and H. Bastians, "The p53/p73 - p21(CIP1) tumor suppressor axis guards against chromosomal instability by restraining CDK1 in human cancer cells," *Oncogene*, vol. 40, no. 2, pp. 436–451, 2021.

[54] F. G. Haluska, Y. Tsujimoto, and C. M. Croce, "Oncogene activation by chromosome translocation in human malignancy," *Annual Review of Genetics*, vol. 21, no. 1, pp. 321–345, 1987.

[55] A. Hedblom, K. B. Laursen, R. Miftakhova et al., "CDK1 interacts with RARγ and plays an important role in treatment response of acute myeloid leukemia," *Cell Cycle*, vol. 12, no. 8, pp. 1251–1266, 2013.

[56] Y. Zhu, Y. Bian, Q. Zhang et al., "LINC00365 promotes co-lorectal cancer cell progression through the Wnt/β-catenin signaling pathway," *Journal of Cellular Biochemistry*, vol. 121, no. 2, pp. 1260–1272, 2020.

[57] Y. Zhu, Y. Bian, Q. Zhang et al., "Construction and analysis of dysregulated lncRNA-associated ceRNA network in co-lorectal cancer," *Journal of Cellular Biochemistry*, vol. 120, no. 6, pp. 9250–9263, 2019.

[58] Y. Zhu, K. Li, J. Zhang, L. Wang, L. Sheng, and L. Yan, "Inhibition of CDK1 reverses the resistance of 5-fu in co-lorectal cancer," *Cancer Management and Research*, vol. 12, pp. 11271–11283, 2020.

[59] C. X. Wu, X. Q. Wang, S. H. Chok et al., "Blocking CDK1/PDK1/β-Catenin signaling by CDK1 inhibitor RO3306 in-creased the efficacy of sorafenib treatment by targeting cancer stem cells in a preclinical model of hepatocellular carcinoma," *Theranostics*, vol. 8, no. 14, pp. 3737–3750, 2018.

[60] H. X. Wu, Z. X. Wang, Q. Zhao, F. Wang, and R. H. Xu, "Designing gene panels for tumor mutational burden esti-mation: the need to shift from "correlation" to "accuracy"," *Journal for ImmunoTherapy of Cancer*, vol. 7, no. 1, p. 206, 2019.

[61] Y. Khagi, A. M. Goodman, G. A. Daniels et al., "Hyper-mutated circulating tumor DNA: correlation with response to checkpoint inhibitor-based immunotherapy," *Clinical Cancer Research*, vol. 23, no. 19, pp. 5729–5736, 2017.

[62] M. D. Hellmann, T. E. Ciuleanu, A. Pluzanski et al., "Nivo-lumab plus ipilimumab in lung cancer with a high tumor mutational burden," *New England Journal of Medicine*, vol. 378, no. 22, pp. 2093–2104, 2018.

[63] J. Liu, W. Xu, S. Li, R. Sun, and W. Cheng, "Multi-omics analysis of tumor mutational burden combined with prog-nostic assessment in epithelial ovarian cancer based on TCGA database," *International Journal of Medical Sciences*, vol. 17, no. 18, pp. 3200–3213, 2020.

[64] R. J. Hause, C. C. Pritchard, J. Shendure, and S. J. Salipante, "Classification and characterization of microsatellite in-stability across 18 cancer types," *Nature Medicine*, vol. 22, no. 11, pp. 1342–1350, 2016.

[65] E. V. Wirta, S. Szeto, U. Hanninen et al., "Prognostic value of immune environment analysis in small bowel adenocarci-nomas with verified mutational landscape and predisposing conditions," *Cancers*, vol. 12, no. 8, p. 2018, 2020.

[66] I. J. Fidler, "The pathogenesis of cancer metastasis: the "seed and soil" hypothesis revisited," *Nature Reviews Cancer*, vol. 3, no. 6, pp. 453–458, 2003.

[67] I. J. Fidler, "The biology of brain metastasis: challenges for therapy," *The Cancer Journal*, vol. 21, no. 4, pp. 284–293, 2015.

[68] S. Alexander and P. Friedl, "Cancer invasion and resistance: interconnected processes of disease progression and therapy failure," *Trends in Molecular Medicine*, vol. 18, no. 1, pp. 13–26, 2012.

[69] S. Chen, X. Chen, T. Shan et al., "MiR-21-mediated metabolic alteration of cancer-associated fibroblasts and its effect on pancreatic cancer cell behavior," *International Journal of Biological Sciences*, vol. 14, no. 1, pp. 100–110, 2018.

[70] M. Herrera, C. Llorens, M. Rodriguez et al., "Differential distribution and enrichment of non-coding RNAs in exo-somes from normal and cancer-associated fibroblasts in co-lorectal cancer," *Molecular Cancer*, vol. 17, no. 1, p. 114, 2018.

[71] A. Katarkar, G. Bottoni, A. Clocchiatti et al., "NOTCH1 gene amplification promotes expansion of cancer associated fi-broblast populations in human skin," *Nature Communica-tions*, vol. 11, no. 1, p. 5126, 2020.

[72] S. W. Tyan, W. H. Kuo, C. K. Huang et al., "Breast cancer cells induce cancer-associated fibroblasts to secrete hepatocyte growth factor to enhance breast tumorigenesis," *PLoS One*, vol. 6, no. 1, Article ID e15313, 2011.

[73] H. Kashima, K. Noma, T. Ohara et al., "Cancer-associated fibroblasts (CAFs) promote the lymph node metastasis of esophageal squamous cell carcinoma," *International Journal of Cancer*, vol. 144, no. 4, pp. 828–840, 2019.

[74] B. Liu, S. Pan, J. Liu, and C. Kong, "Cancer-associated fi-broblasts and the related runt-related transcription factor 2 (RUNX2) promote bladder cancer progression," *Gene*, vol. 775, Article ID 145451, 2021.

[75] M. S. Pan, H. Wang, K. H. Ansari, X. P. Li, W. Sun, and Y. Z. Fan, "Gallbladder cancer-associated fibroblasts promote vasculogenic mimicry formation and tumor growth in gall-bladder cancer via upregulating the expression of NOX4, a poor prognosis factor, through IL-6-JAK-STAT3 signal pathway," *Journal of Experimental & Clinical Cancer Re-search*, vol. 39, no. 1, p. 234, 2020.

[76] S. Affo, A. Nair, F. Brundu et al., "Promotion of chol-angiocarcinoma growth by diverse cancer-associated fibro-blast subpopulations," *Cancer Cell*, vol. 39, no. 6, pp. 866–882, 2021.

[77] S. Sakaguchi, M. Miyara, C. M. Costantino, and D. A. Hafler, "FOXP3+ regulatory T cells in the human immune system," *Nature Reviews Immunology*, vol. 10, no. 7, pp. 490–500, 2010.

[78] H. Y. Wang and R. F. Wang, "Regulatory T cells and cancer," *Current Opinion in Immunology*, vol. 19, no. 2, pp. 217–223, 2007.

[79] T. M. Schmitt, D. H. Aggen, K. Ishida-Tsubota, S. Ochsenreither, D. M. Kranz, and P. D. Greenberg, "Gen-eration of higher affinity T cell receptors by antigen-driven differentiation of progenitor T cells in vitro," *Nature Bio-technology*, vol. 35, no. 12, pp. 1188–1195, 2017.

[80] X. Liu, J. Xu, B. Zhang et al., "The reciprocal regulation between host tissue and immune cells in pancreatic ductal adenocarcinoma: new insights and therapeutic implications," *Molecular Cancer*, vol. 18, no. 1, p. 184, 2019.

[81] M. Ruterbusch, K. B. Pruner, L. Shehata, and M. Pepper, "In vivo CD4(+) T cell differentiation and function: revisiting the Th1/Th2 paradigm," *Annual Review of Immunology*, vol. 38, no. 1, pp. 705–725, 2020.

[82] J. von Moltke and M. Pepper, "Sentinels of the type 2 immune response," *Trends in Immunology*, vol. 39, no. 2, pp. 99–111, 2018.

[83] A. A. Ghazy, S. Y. Abu El-Nazar, H. E. Ghoneim, A. R. M. Taha, and A. M. Abouelella, "Effect of murine ex-posure to gamma rays on the interplay between Th1 and Th2 lymphocytes," *Frontiers in Pharmacology*, vol. 6, p. 74, 2015.

[84] E. M. Savilahti, S. Karinen, H. M. Salo et al., "Combined T regulatory cell and Th2 expression profile identifies children with cow's milk allergy," *Clinical Immunology*, vol. 136, no. 1, pp. 16–20, 2010.

[85] M. Castedo, J. L. Perfettini, T. Roumier, and G. Kroemer, "Cyclin-dependent kinase-1: linking apoptosis to cell cycle and mitotic catastrophe," *Cell Death & Differentiation*, vol. 9, no. 12, pp. 1287–1293, 2002.

[86] J. Huang, P. Chen, K. Liu et al., "CDK1/2/5 inhibition overcomes IFNG-mediated adaptive immune resistance in pancreatic cancer," *Gut*, vol. 70, no. 5, pp. 890–899, 2021.

[87] Z. Tang, P. G. Pilie, C. Geng et al., "ATR inhibition induces CDK1-SPOP signaling and enhances anti-PD-L1 cytotoxicity in prostate cancer," *Clinical Cancer Research*, vol. 27, no. 17, pp. 4898–4909, 2021.

Research Article

Prognostic Value and Potential Regulatory Mechanism of H19 in Stomach Adenocarcinoma

Hongyuan Guo (ID),[1,2,3] **Xu Guo,**[1] **Yuanyuan Su,**[1] **Minghui Liu** (ID),[4] **Xi Chen** (ID),[1,2,3] **Hao Zhu** (ID),[5] **and Zheng Fu** (ID)[1,2,3]

[1]*Nanjing Drum Tower Hospital Center of Molecular Diagnostic and Therapy,*
State Key Laboratory of Pharmaceutical Biotechnology,
Jiangsu Engineering Research Center for MicroRNA Biology and Biotechnology,
NJU Advanced Institute of Life Sciences (NAILS), Institute of Artificial Intelligence Biomedicine, School of Life Sciences,
Nanjing University, Nanjing, Jiangsu 210023, China
[2]*Chemistry and Biomedicine Innovation Center (ChemBIC), Nanjing University, Nanjing, Jiangsu 210023, China*
[3]*Research Unit of Extracellular RNA, Chinese Academy of Medical Sciences, Nanjing, Jiangsu 210023, China*
[4]*School of Life Science and Technology, China Pharmaceutical University, Nanjing, Jiangsu 210009, China*
[5]*Department of Orthopedics, Affiliated Jianhu Hospital of Nantong University, No. 666 Nanhuan Road, Jianhu, Yancheng,*
Jiangsu 224700, China

Correspondence should be addressed to Minghui Liu; minghuiliu@cpu.edu.cn, Xi Chen; xichen@nju.edu.cn, Hao Zhu; medzhuhao@163.com, and Zheng Fu; zhengfu@nju.edu.cn

The first lncRNA discovered, H19, has been found to participate in the regulation of diverse biological processes, including the pathogenesis of stomach adenocarcinoma. In addition to its oncogenic function in tumor formation, a high level of H19 in tumor tissues has also been reported to be an indicator for poor prognosis. However, although many previous works have investigated the level of H19 as an independent indicator for prognosis, the real value of H19 in predicting survival has rarely been evaluated. In this study, we established a prognostic model and nomogram for stomach adenocarcinoma by combining the expression level of H19 with traditional indices, which showed the value of H19 in predicting the survival rates of patients. In addition, we investigated the mechanism underlying the correlation of the H19 level in cancer tissue with poor prognosis in patients. Our results showed that H19 could function as ceRNA by sponging five miRNAs, which may promote the progression of cancer.

1. Introduction

Gastric cancer is a prominent cancer worldwide and was responsible for over 1,000,000 new cases and estimated 783,000 deaths in 2018, making it the third leading cause of cancer death [1]. A higher incidence of gastric cancer was observed in Eastern Europe, Eastern Asia, and South America [2]. Among gastric cancers, stomach adenocarcinoma (STAD) is the most common subtype and accounts for 95% of the total number of malignancies [3]. The overall survival (OS) rate of advanced STAD remains low, with a 5-year survival rate of approximately 30% [4]. The detection of the disease at an early stage and treatment with surgical resection remains to be the optimal choice for STAD like many other kinds of cancer [5,6]. For advanced STAD, cytotoxic chemotherapy remains the main first-line treatment strategy [7,8]. Although the addition of targeted therapy in later-line treatment was proven to be beneficial when compared with chemotherapy alone [9–11], therapeutic targets for advanced gastric cancer are exceedingly rare. Therefore, the discovery of new biomarkers is likely to brew new precision treatments for treatment of STAD in the

future [12,13], and investigation into the mechanisms underlying STAD may become the key to finding novel approaches for prognosis improvement and drug development.

In recent years, long noncoding RNAs (lncRNAs) have attracted considerable attention for their role in regulating cancer-related processes such as carcinogenesis, recurrence, metastasis, and drug resistance [14–16]. However, the clinical value of lncRNAs in STAD is very incompletely understood. In this study, we used both bioinformatic and experimental approaches to identify lncRNAs with dramatically changed expression and found that H19 was dramatically upregulated in STAD tissues. Next, we analyzed the potential pathological mechanism of H19 and highlighted its interactions with five candidate miRNAs in MKN-45 cells. Additionally, we demonstrated that the interactions between H19 and these miRNAs could promote migration, invasion, and drug resistance of STAD cells and analyzed the potential downstream target genes of miRNAs. Furthermore, we discovered that H19 is an index for poor prognosis in STAD patients and functions as an important oncogenic ceRNA during the pathological process of STAD. Our findings may identify novel targets for drug development or predictive biomarkers for the prognosis of STAD patients.

2. Materials and Methods

2.1. Cell Culture. The human gastric cancer cell line MKN-45 was purchased from iCell Bioscience Inc, which was authenticated by short tandem repeats (STR) profiling and confirmed to be mycoplasma-free. MKN-45 cells were cultured in the RPMI-1640 medium (Invitrogen, CA, USA) supplemented with 10% fetal bovine serum (Gibco, Australia) and penicillin/streptomycin (Gibco, MA, USA) at 37°C in a 5% CO_2 water-saturated atmosphere. 3.

2.2. Transfection of Gastric Adenocarcinoma Cells. MKN-45 cells (5×10^5) were cultured in a 6-well plate. At 60% confluence, $6 \mu g$ of each type of RNA oligo/plasmid was utilized to transfect MKN-45 cells using Lipofectamine 2000 transfection reagent (Invitrogen, CA, USA). After 24 hours, the cells were evaluated for successful transfection.

2.3. Cell Migration Assay. MKN-45 cells were cultured in 6-well plates at a density of 2×10^5 cells/well. At 90% confluence, the cell layer was scratched with a sterile yellow $200 \mu L$ pipette tip and then washed three times in PBS. Fresh RPMI-1640 medium containing 2% FBS was then added to the cells. Three random fields of view were selected and imaged using an inverted microscope.

2.4. Cell Invasion Assay. The cell invasion assay was performed in transwell chambers. The transwell chambers were placed in a 24-well plate, and each chamber contained an insert with an $8 \mu m$ pore size polyethylene terephthalate membrane (Corning Life Sciences, MA, USA). The treated

MKN-45 cells were resuspended and seeded in the upper chambers in a serum-free medium. Cells at a density of 5×10^4 cells/well (in $200 \mu L$) were seeded in the upper transwell chambers, in which the membrane was coated with Matrigel (BD Biosciences, MA, USA) and $500 \mu L$ of complete growth medium was added to the bottom chambers. The noninvaded cells in the upper chamber were removed with cotton swabs. Invaded cells on the bottom surface of the membrane were fixed, stained with crystal violet, and observed using a microscope.

2.5. Flow Cytometry. MKN-45 cells were washed twice in cold PBS and resuspended in Annexin V binding buffer at a concentration of 1×10^6 cells/mL. Then, $100 \mu L$ of the cell suspension (1×10^5 cells) was incubated with $5 \mu L$ of FITC-Annexin V and $5 \mu L$ of propidium iodide using an Apoptosis Detection Kit (BD Biosciences, CA, USA). Then, $400 \mu L$ of binding buffer was added. The flow cytometry was used to determine the apoptosis rate.

2.6. Quantitative Real-Time PCR (RT-qPCR). The TRIzol reagent (Invitrogen, CA, USA) was used to extract the total RNA from the cells. One microgram of total RNA was reverse-transcribed into cDNA using HiScript III RT SuperMix for qPCR (+gDNA wiper) (R323-01, Vazyme). RT-qPCR was performed in a $20 \mu L$ reaction volume. Quantitative real-time PCR was performed with ChamQ Universal SYBR qPCR Master Mix (Q711-02, Vazyme) in a LightCycler 96 instrument (Roche). The relative gene expression was normalized to GAPDH and calculated by the $2^{-\Delta\Delta CT}$ method.

RT-qPCR for microRNAs was performed using a miRNA 1st Strand cDNA Synthesis Kit (MR101-01, Vazyme). Quantitative real-time PCR analysis was performed with miRNA Universal SYBR qPCR Master Mix (MQ101-01, Vazyme). The RT-qPCR was performed in a LightCycler 96 system (Roche). The primer sequences used for RT-qPCR are given in Table S2. All experiments were conducted in triplicate.

2.7. RNA Pulldown Assay. The RNA pulldown assay was performed as previously described. Briefly, biotin-labeled RNAs (antisense RNAs) were transcribed using Biotin RNA Labeling Mix (Promega Corporation). Biotinylated anti-H19 probes (5′-CTGCTGTTCCGATGGTGTCTTTGATGT TGGGCTGATGAGGTCTGGTTCCT-3′) were dissolved in binding and washing buffer and incubated with streptavidin agarose resin (Thermo Fisher Scientific Inc.). Then, MKN-45 cell lysates were incubated with probe-coated streptavidin beads and the precipitated RNAs were extracted using the TRIzol reagent. The samples were prepared for RT-qPCR analysis.

2.8. Luciferase Reporter Assay. The lncRNA H19 sequence was inserted into the pMIR-REPORT plasmid (Ambion, Austin, TX, USA). In the mutant H19 plasmid, the sequences binding to the seed sequence were mutated (Table S3) and

inserted into the pMIR-REPORT plasmid. The HEK293 T cells were seeded in 24-well plates and transfected with $0.5\,\mu g$ of this plasmid, $0.25\,\mu g$ of β-galactosidase (β-gal) plasmid, and 50 pmol of the miRNA mimic or scrambled miRNA. β-Gal expression was used for normalization. After 24 h, cells were harvested and analyzed for luciferase activity using the luciferase assay kits (Promega, WI, USA).

2.9. Public Data. Data on STAD were downloaded from The Cancer Genome Atlas (TCGA; https://portal.gdc.cancer. gov/, project: TCGA-STAD). We downloaded the expression matrices and clinical information for 442 STAD samples and removed 37 samples of cystic, mucinous, and serous neoplasms. The human gastric tissue data were downloaded from the Genotype-Tissue Expression (GTEx; https://gtexportal.org/) database.

2.10. Pancancer Analysis. The expression level of the lncRNA H19 and the correlations between the lncRNA H19 expression level and the cancer outcomes across cancer types were downloaded from the TIMER (Tumor IMmune Estimation Resource; version 2) web resource (https://timer. comp-genomics.org/) using the "Gene_DE" module and the "Gene_outcome" module.

2.11. Analysis of Differentially Expressed Genes (DEGs). A total of 379 patients included in the TCGA-STAD project were divided into an H19-high group and an H19-low group based on the median expression level of H19. DEGs between the two groups were identified using the DESeq2 package. The DEGs with $\log_2 FC \geq 1$ and P adj <0.05 were considered significant.

2.12. Enrichment Analyses. The DEGs were subjected to KEGG/GO (Kyoto Encyclopedia of Genes and Genomes/ Gene Ontology) enrichment analyses and GSEA (gene set enrichment analysis) using the clusterProfiler package and the org. Hs. eg. db package.

2.13. Prognosis Prediction. First, we integrated the disease-specific survival (DSS) times of 379 STAD patients with their clinical information. Then, we calculated the correlations of these variables with the DSS time of STAD patients with a univariate Cox proportional hazards regression model. Risk-related factors with $P < 0.1$ were included as variables in the multivariate Cox proportional hazards regression analysis. Finally, we established a prognosis prediction model for STAD by constructing a nomogram based on the results of the multivariate Cox proportional hazards regression analysis. The sensitivity of the nomogram model was evaluated with time-dependent ROC analysis using the roc package, the accuracy was evaluated with a calibration plot using the rms package, and the predictive value was evaluated by DCA (decision curve analysis) using the stdca.R function (https://www.mskcc. org/departm-ents/epidemiology-biostatistics/biostatistics/ decision-curve-analysis).

2.14. Target Prediction. We used the "Custom Prediction" module of the miRDB web interface (https://mirdb.org/) to predict the miRNAs that bind to H19 [17]. Then, we intersected the results of the miRDB prediction with the downregulated miRNAs in the STAD datasets GSE62254 and GSE15459 to obtain the target miRNAs of H19 in STAD. To predict the target genes of the H19-targeted miRNAs, we used the "Target Search" module of the miRDB web interface and the TargetScan Human online database (https://www. targetscan.org/vert_80/) [18]. We intersected the outputs of the miRDB and TargetScan predictions with the upregulated DEGs in TCGA-STAD to obtain the target genes of the predicted miRNAs in STAD. Finally, we calculated the correlation coefficients and significance between each target gene and H19 in STAD.

2.15. Statistical Analysis. All statistical analyses were performed using GraphPad Prism 8. Data were first checked for normal distribution and differences among groups were then compared by one-way ANOVA with Dunnett's test to correct for multiple comparisons. Data are shown as the means with error bars showing the SEMs. Significance was assumed for $^*P < 0.05$, $^{**}P < 0.01$, and $^{***}P < 0.005$.

3. Results

3.1. Identification of Differentially Expressed lncRNAs in GC. We downloaded STAD transcriptome data from the TCGA database and analyzed the differentially expressed lncRNAs with the DESeq2 package. The screening thresholds for differentially expressed lncRNAs (DELs) were $|\log_2 FC| > 1$ and adjusted as $P < 0.05$, and the DELs are shown in volcano plots (Figure 1(a)). Among the 3669 differentially expressed lncRNAs, 2760 were upregulated, whereas 909 were downregulated. To better visualize the relative expression levels of DELs in tumor tissues, the changes in the normalized counts of these lncRNA transcripts were calculated (Figure 1(b)). The results showed that among all the lncRNAs, lncRNA H19 was strikingly overexpressed and significantly upregulated in STAD tissues. Next, we analyzed the level of H19 with transcriptome data from both the TCGA and GTEx databases (Figures 1(c) and 1(d)). The results showed that H19 was significantly overexpressed in STAD tissues in comparison with normal adjacent tissues (NATs). The TCGA dataset analysis also showed that the H19 level was significantly higher in STAD tissues. By analyzing tumors of different stages, we found that the expression level of H19 increased moderately with increasing tumor stage (Figure S1). By applying TIMER2, we analyzed the expression level of H19 across various cancer types, and the results also indicated that upregulation of H19 was obvious in STAD in comparison with other cancer subtypes (Figure 1(e)). Based on the TCGA data, we divided the patients with each cancer subtype into the high-expression and low-expression groups according to the level of H19 and analyzed the correlation of the H19 level with prognosis (Figure 1(f)). The results indicated a strong correlation of the H19 level with prognosis in STAD patients. Kaplan–Meier

analyses of STAD patients were also performed with data from the TARGET database. Analysis of disease-specific survival (DSS) further showed that the survival rate in the H19-high group was significantly lower than that in the H19-low group (Figure 1(g)). Interestingly, in STAD patients that experienced progression after receiving adjuvant or neoadjuvant chemotherapy, the H19 level was an even more significant indicator for DSS, with a HR of 2.15 (1.16–4.00) (Figure 1(h)). These results indicated the universal overexpression of H19 in STAD and its correlation with poor prognosis in patients.

3.2. Inclusion of H19 in a Nomogram to Predict the Prognosis of GC.

To further explore the prognostic value of H19, we developed a statistical model to predict the survival of STAD patients. The univariate Cox regression analysis was utilized to screen variables that correlated with prognosis using a threshold of $P < 0.1$. Univariate analysis indicated that TNM stage, age, histologic type, radiotherapy status, and H19 level were significantly associated with OS. After Cox multivariate regression analysis, four traditional clinical variables and the expression level of H19 achieved significance of $P < 0.05$ and were identified as prognostic factors (Table S1). Next, these factors were incorporated into nomograms for predicting the survival probability of STAD patients at 1, 2, and 4 years (Figure 2(a)). The nomogram identified TNM stage as having the largest contribution to prognosis, followed by age, histologic type, radiotherapy status, and H19 level. Each value for these variables was assigned a score on a point scale. By adding up the total score and locating it on the total point scale, we estimated the probability of survival at each time point. Then, the nomogram was validated internally using the TCGA dataset. Time-dependent ROC curves for the prognostic evaluation nomogram model were generated, and the AUCs of the nomogram for predicting 1, 2, and 4-year overall survival (OS) was 0.691, 0.658, and 0.799, respectively (Figure 2(b)). As shown in Figure 2(c), the calibration plots for prediction of 1, 2, and 4-year OS in both the training and validation sets indicated excellent agreement. These findings indicate that the nomogram including H19 can accurately predict OS in STAD patients. Furthermore, the DCA curves for the STAD survival assessment model with and without incorporation of the H19 expression level are shown. Although the model including the H19 expression level had little benefit for assessing the survival of STAD patients in the first year (Figure 2(d)), an obvious positive benefit for assessing two and four- year survival was shown (Figures 2(e) and 2(f)). Altogether, our results indicated that H19 may be a promising prognostic biomarker for survival in STAD patients.

3.3. Potential Biological Function of H19 in STAD.

Since an obvious correlation between the H19 level and the prognosis of STAD was shown by our results, we further investigated the potential underlying mechanism by investigating the biological function of H19 in STAD. According to the level of H19 expression, transcriptome data for STAD samples from TCGA were used to divide the corresponding patients into an H19-high group and an H19-low group according to the median expression level of H19. Then, the differentially expressed genes between these two groups were analyzed with the DESeq2 package with a threshold of $|\log_2 FC| > 1$ and adjusted $P < 0.05$. As shown in the volcano plots in Figure 3(a), 596 genes were upregulated, whereas 173 genes were downregulated. Next, we performed KEGG and GO enrichment analyses, and the corresponding network diagrams are shown (Figures 3(b)–3(e)). As shown in the results, the biological processes "signal release," "collagen-containing extracellular matrix," "receptor ligand activity," and neuroactive ligand-receptor investigation' were enhanced in the H19-high group, while "digestion," "apical part of cell," "endopeptidase activity," and "pancreatic secretion" were suppressed. GSEA showed different gene expression patterns between the H19-high and H19-low groups (Figure 3(f)). The expression levels of genes related to the cell cycle, DNA replication, EMT, GC, and cancer pathways were positively correlated with the expression level of H19. All these pathways are related to the proliferation (cell cycle and DNA replication), invasion or migration (EMT), or maintenance (GC and cancer pathways) of malignant GC cells. These results reflected the biological effect of H19 on the transcriptome profile and justified the correlation between the H19 level and poor prognosis in STAD.

3.4. The Potential Function of H19 as a ceRNA in STAD.

According to the normalized counts of H19 transcripts in STAD tissues (Figure 1(b)), the expression level of H19 in STAD tissues should be strikingly high, indicating that it is likely to act as a molecular sponge for miRNAs. Bioinformatics analysis revealed that lncRNA H19 has putative miRNA recognition sequences for 9 miRNAs (Figure 4(a)). The minimum free energy of hybridization between each miRNA and H19 was calculated by RNAhybrid. The predicted interactions between these miRNAs and the target sites in H19 are shown in Figure S2, and all of the minimum free energies of hybridization were less than −25 kcal/mol. The RNA pulldown assay showed that the lncRNA H19 binds to miR-361, miR-519a, miR-541a, miR-516b, and miR-193a in the MKN-45 gastric cancer cell line (Figures 4(b) and S3). The knockdown of H19 expression in MKN-45 cells significantly increased the cellular levels of all 5 candidate miRNAs (Figure S4). Next, we designed luciferase reporter plasmids containing H19 with wild-type (WT) or mutant (MUT) miRNA binding sites to verify the binding capacity between H19 and the candidate miRNAs (Figure 4(c)). The luciferase assay results showed that the mimics of all five miRNAs significantly inhibited the activity of the WT luciferase reporter but not the MUT reporter. These results indicated that H19 can directly bind to these miRNAs at the predicted binding sites in gastric cancer cells.

To further validate the biological function of H19 as a ceRNA, we explored whether modulating H19/miRNA regulation affects the characteristics of gastric cancer cells. First, we investigated the influence of the H19/miRNA interactions on the invasion ability (Figures 4(d) and 4(e)). The

(a)

(b)

(c)

(d)

(e)

(f)

(g)

(h)
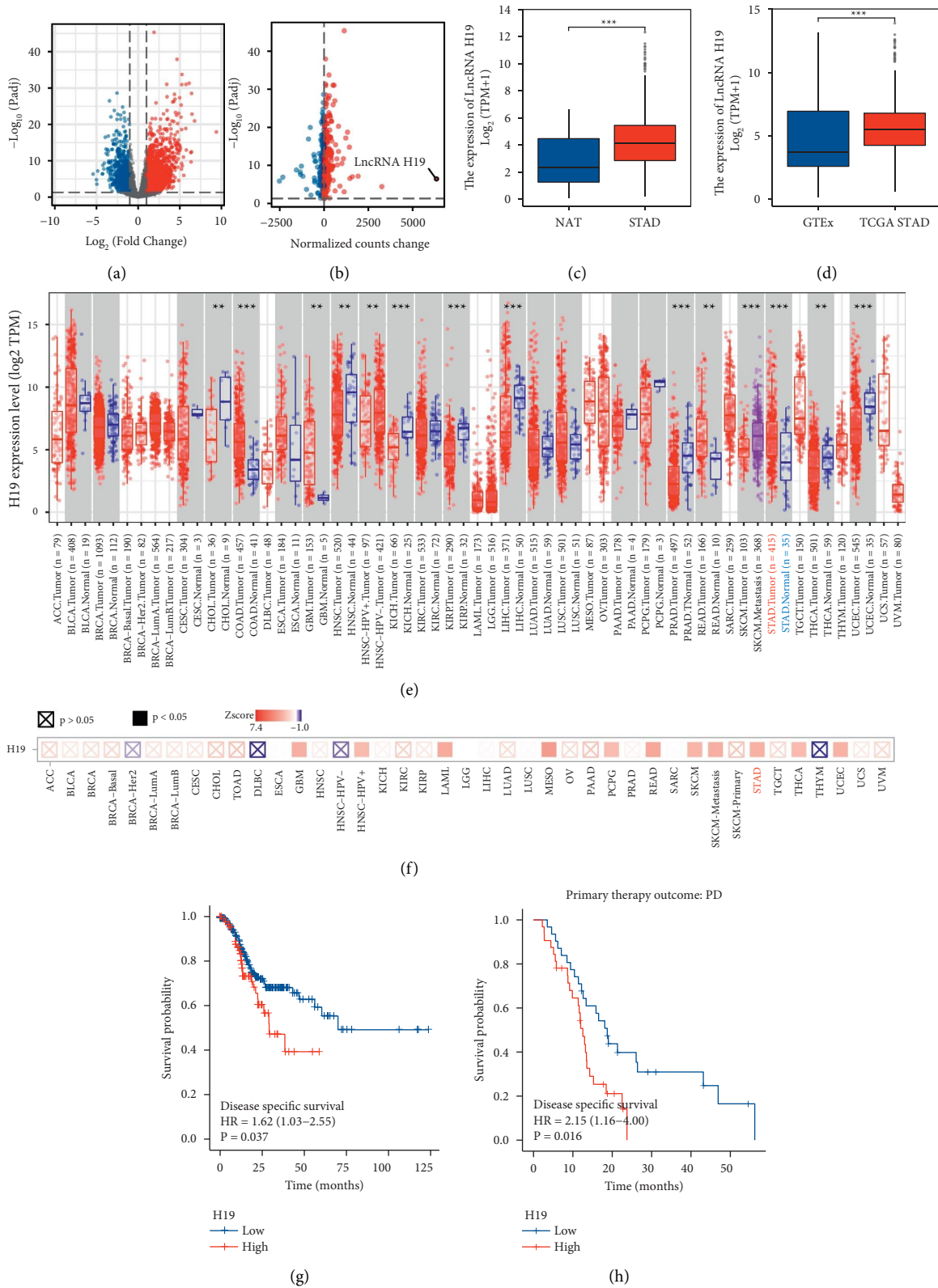
FIGURE 1: The expression of H19 in STAD and its correlation with prognosis. (a)The volcano plot of DELs between STAD and normal tissues. (b) Normalized transcript counts of significantly differentially expressed lncRNAs between STAD and normal tissues. (c) The expression level of lncRNA H19 in 379 STAD tissues and 26 normal tissues based on the TCGA database analysis. (d) The expression level of lncRNA H19 in 379 STAD tissues from the TCGA database and 174 normal tissues from the GTEx database. (e)The expression status of lncRNA H19 in different cancers and specific cancer subtypes analyzed with TIMER2. (f) The significant correlations of lncRNA H19 expression with outcomes across various cancer types visualized in the heatmap, which shows the normalized coefficient of lncRNA H19 in the Cox model. (g-h). The Kaplan–Meier curves for the DSS (c) and PD (d) of STAD patients stratified by the H19 expression level.

(a)

(b)

(c)

(d)

Figure 2: Continued.

(e)

(f)
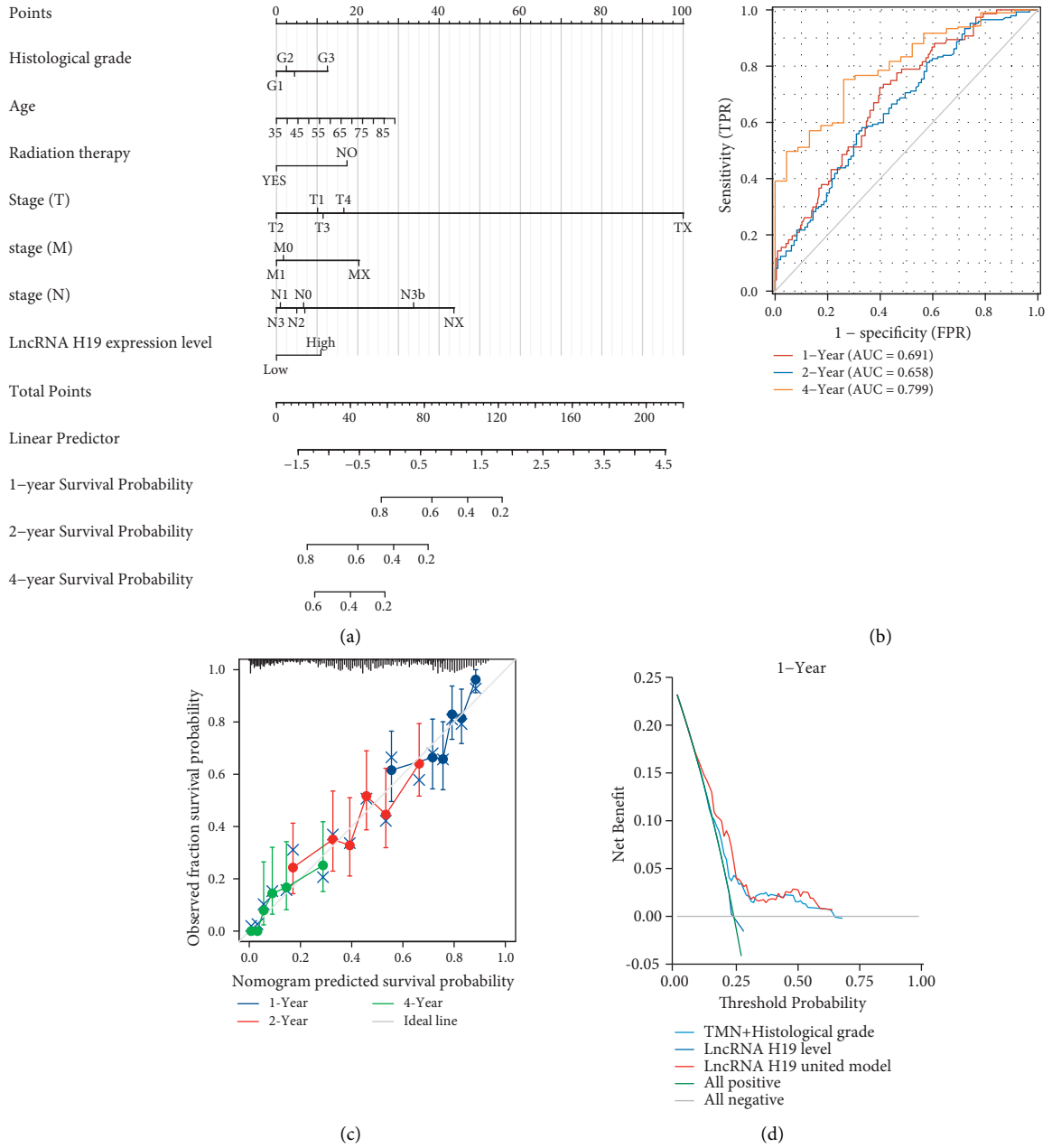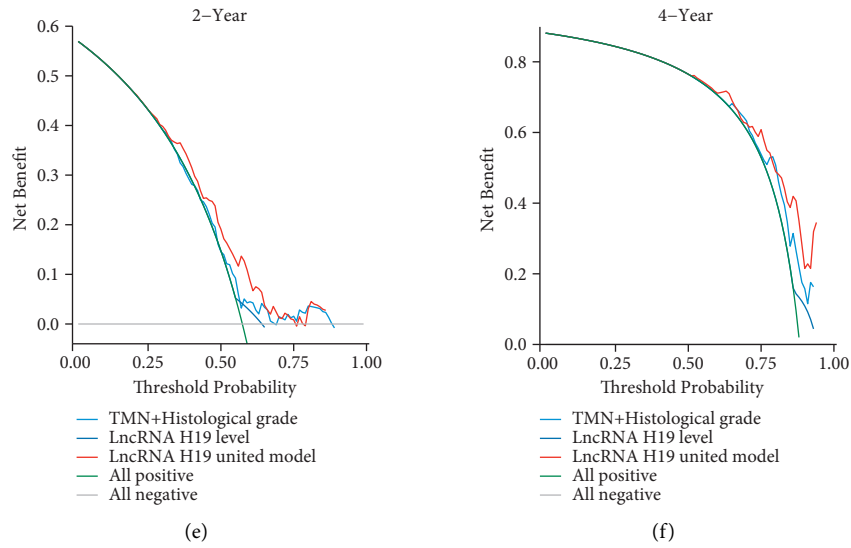
FIGURE 2: The prognostic value of H19 in STAD. (a) Prognostic nomogram for patients with STAD based on the H19 expression level. (b) Verification of the nomogram by time-dependent ROC curve analysis. (c) Calibration curves for predicting patient survival at each time point. (d–f) DCA curves showing the benefit gained from incorporation of H19 in predicting 1 (d), 2 (e), and 4 (f) year survival outcomes.
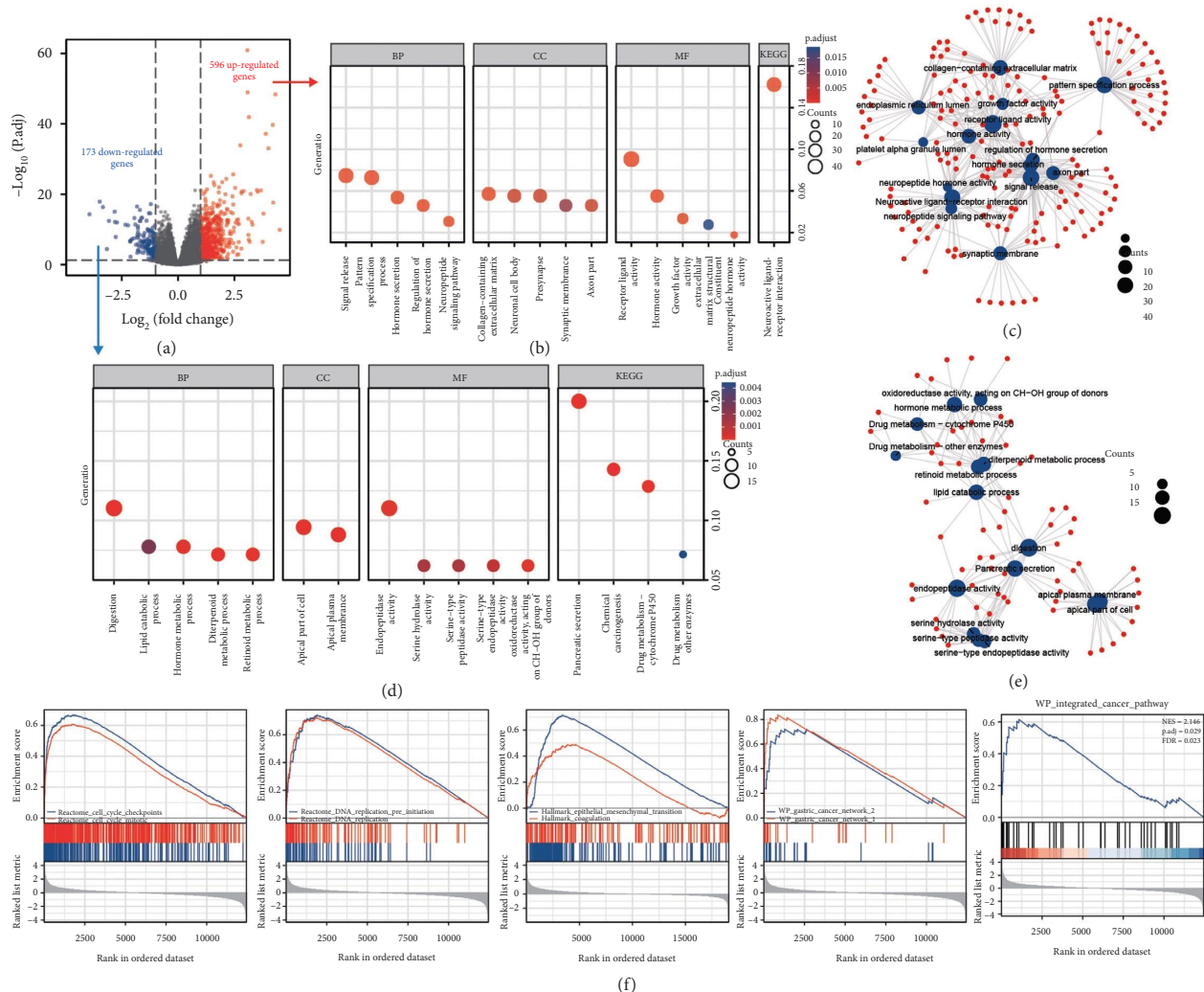
FIGURE 3: Differential expression analysis of samples with high and low H19 expression. (a) The volcano plot of DEGs between the H19-high and H19-low groups. (b–e) KEGG/GO enrichment analyses performed based on the 596 upregulated DEGs (b) and 173 downregulated DEGs (d); MF, BP, CC, and KEGG pathway analyses conducted and the corresponding networks based on the KEGG and GO analysis results constructed (c and e). (f) GSEA showing different gene expression patterns between the H19-high and H19-low groups.

(a)

(b)

(c)

(d)

(e)

(f)

(g)

(h)

(i)

FIGURE 4: Continued.

(j)

(k)

(l)

(m)

Figure 4: Continued.

(n)
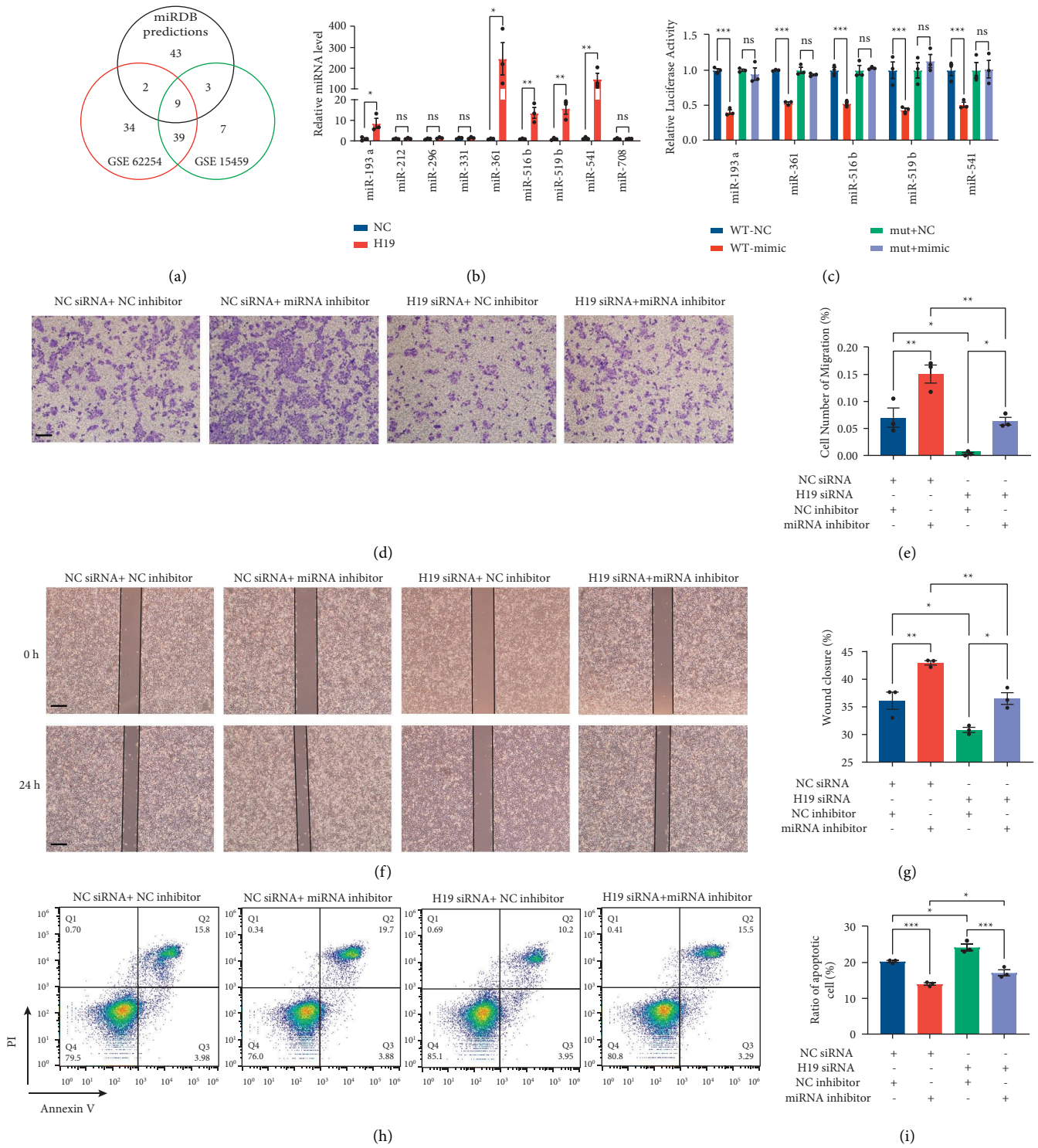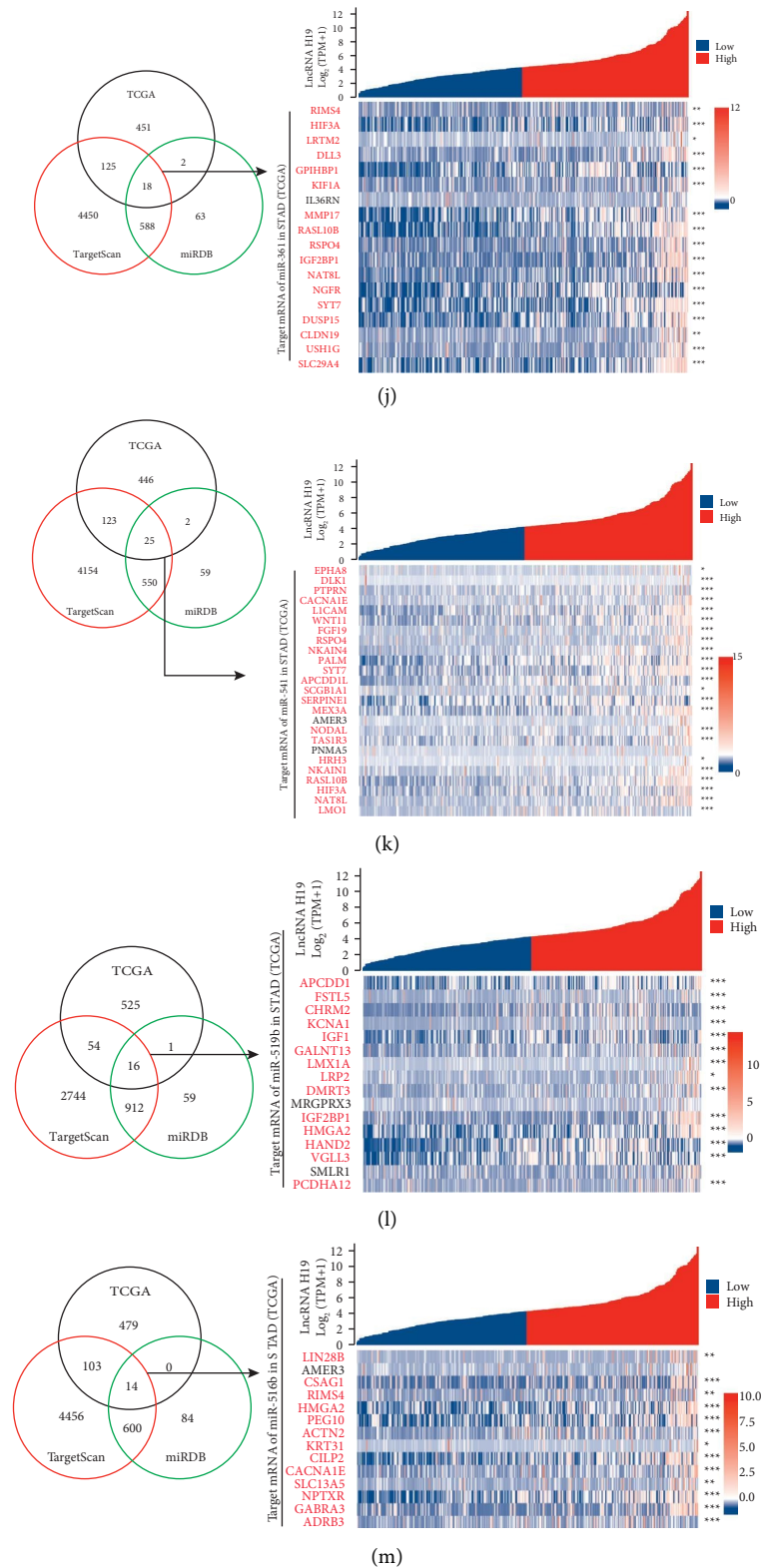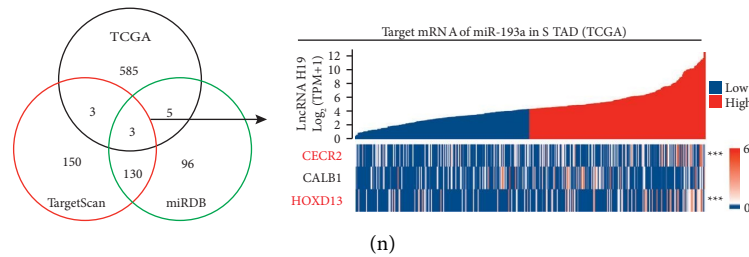
FIGURE 4: H19 promoted migration, invasion, and survival of STAD cells by binding to five miRNAs. (a) Bioinformatics analysis of 9 miRNAs potentially binding to lncRNA H19. (b) RNA pulldown assay verified the binding of 5 of the 9 miRNAs to lncRNA H19 ($n = 3$). (c) Relative luciferase activity determined to verify the binding of 5 miRNAs to H19 ($n = 3$). (d) Scratch assay showing the migration of MKN-45 cells with H19 knockdown or miRNA inhibition ($n = 3$). (e) Quantitative analysis of the wound closure rate ($n = 3$). (f) Transwell assays showing the invasion of MKN-45 cells after H19 knockdown or miRNA inhibition ($n = 3$). (g) Quantitative analysis of the number of migrated cells ($n = 3$). (h) Flow cytometric analysis of apoptosis induced by gemcitabine in MKN-45 cells transfected with H19 siRNA ($n = 3$). (i) Quantitative analysis of the percentage of apoptotic cells ($n = 3$). (j-n) Analysis of potential downstream genes regulated by five miRNAs binding to H19.

transwell assay showed that knockdown of H19 significantly inhibited MKN-45 cell invasion, while inhibition of these miRNAs significantly enhanced the invasion ability. When H19 and these miRNAs were inhibited simultaneously, the effects canceled each other out. Similar results were also observed in the scratch assay to assess the migration ability (Figures 4(f) and 4(g)). The knockdown of H19 attenuated the migration ability of MKN-45 cells, while inhibition of miRNAs promoted it. Simultaneous inhibition of H19 and the miRNAs resulted in almost complete elimination of the independent effects. Next, we evaluated the effects of H19/miRNA interactions on drug resistance in gastric cancer cells. Gemcitabine, a commonly used chemotherapeutic drug for treating STAD, was used to induce apoptosis in MKN-45 cells. The transfection of H19 siRNA significantly increased the apoptosis of MKN-45 cells and depletion of the miRNAs with inhibitors reduced apoptosis (Figure 4(h) and 4(i)). After cotransfection of H19 siRNA and miRNA inhibitors, apoptosis remained at the baseline level. These experiments covered the invasion, migration, and drug resistance properties of cancer cells and proved that H19 performed an oncogenic function by sponging these five miRNAs, which may result in the poor prognosis of STAD patients with a high H19 level. To further identify the potential target genes of these five miRNAs, we predicted their binding sites for the 3′UTRs of mRNAs in the human transcriptome with both TargetScan and miRDB (Figures 4(j)–4(n)). Then, we intersected the prediction results with the downregulated genes in H19-high tissues compared with H19-low tissues and obtained the potential genes that are affected by the overexpression of H19 in gastric cancer tissues through its action as a miRNA sponge. The lncRNA–miRNA–mRNA network was constructed to demonstrate the regulatory relationships between the miRNAs and key genes, as well as the enriched pathways and annotations of the key genes (Figure S5).

4. Discussion

In recent years, the importance of noncoding RNAs as clinical biomarkers for cancer diagnosis and prognosis has

been widely recognized [19–21]. Among the numerous noncoding RNAs, lncRNA H19 is one of the most frequently studied. Chen et al. measured the expression level of H19 in 128 pairs of STAD and adjacent normal tissues and generated ROC curves and Kaplan–Meier curves to prove its diagnostic or prognostic value [22]. Other studies have also supported H19 as a diagnostic biomarker for STAD [23,24]. However, most of these studies investigated lncRNAs as independent novel biomarkers and did not combine them with traditional variables for diagnosis. Here, we showed the real value of H19 by developing a model including relevant clinical variables for STAD prognosis. The contribution of H19 in comparison with other indices was clearly shown in the nomogram. In addition, since all the data included in the model are publicly available, the model is unbiased compared with most studies conducted with a limited cohort of samples. Our results demonstrated that H19 should be used in combination with traditional clinical indices such as TNM stage or histological grade to predict STAD prognosis. The incorporation of H19 into the model showed clear benefit for predicting the survival prognosis at 2 and 4 years and did not decrease the performance of the model in predicting 1-year survival. To our knowledge, this is the first study to integrate the clinical factors and H19 to construct a nomogram to predict the prognosis of STAD patients.

Second, we also investigated the potential biological mechanism underlying the prognostic value of H19. Through analysis of DEGs in H19-high STAD samples compared with H19-low STAD samples, we highlighted the possible biological processes and gene sets related to the poor prognosis of STAD patients. The gene sets related to the invasion, migration, and malignancy of STAD were found to be differentially regulated by H19 upregulation. These results were also supported by our in vitro experiments. Our results showed that H19 influences classical tumorigenic processes such as invasion, migration, and drug resistance. We validated the ceRNA function of H19 in MKN-45 cells and identified a panel of five miRNAs that directly bind to H19 in MKN-45 cells. Potential downstream targets were identified by combining the miRNA target prediction tools and

analysis of DEGs in the TCGA database, which provided insights for further studies.

Overall, our study verified the prognostic value of H19 in STAD and established a nomogram for predicting the survival rate of STAD patients. The validation of the nomogram demonstrated the contribution of the H19 level to increasing the accuracy of the prediction model incorporating only traditional clinical indices. We also highlighted the mechanism underlying the positive correlation between the H19 level and poor prognosis in STAD patients. Our results indicated the interactions between H19 and five miRNAs and identified candidate downstream target genes for further study of the role of H19 in STAD pathogenesis.

Data Availability

The data used to support this study are available from the corresponding author upon request.

Conflicts of Interest

The authors declare that they have no conflicts of interest.

Authors' Contributions

Zheng Fu, Hao Zhu, Xi Chen, and Minghui Liu conceived and designed the experiments. Hongyuan Guo, Xu Guo, and Yuanyuan Su performed the experiments and contributed equally to this study. Hongyuan Guo and Xu Guo contributed the materials. Hongyuan Guo, Hao Zhu, and Zheng Fu analyzed the data and wrote the manuscript. All authors read and approved the final manuscript.

Acknowledgments

Supplementary Materials

Figure S1. Relative H19 level in T1–T4 stages tumor tissues from TCGA database. Figure S2. Schematic description of the duplex formed by the binding site of lncRNA H19 and miRNAs. Figure S3. The pulldown efficacy of lncRNA H19 with biotinylated lncRNA H19 probes. Figure S4. The knockdown efficiency of lncRNA H19 in MKN-45 cells. Figure S5. The ceRNA network showing the relationship between lncRNA H19, miRNAs, and downstream target genes. Table S1. Univariate and multivariate analyses Cox proportional hazards regression analysis. Table S2. The primer sequences of RT-qPCR. Table S3. The binding site sequence and mutant sequence used for constructing luciferase reporter gene plasmids. (*Supplementary Materials*)

References

[1] J. Ouyang, X. Lei, T. Gan, and X. Yang, "Clinical crosstalk between microRNAs and gastric cancer (Review)," *International Journal of Oncology*, vol. 58, no. 4, p. 7, 2021.

[2] M. Casamayor, R. Morlock, H. Maeda, and J. A. Ajani, "Targeted literature review of the global burden of gastric cancer," *Ecancermedicalscience*, vol. 12, p. 883, 2018.

[3] B. J. Dicken, B. Cass, M. Joy, and S. M. Hamilton, "Gastric adenocarcinoma," *Annals of Surgery*, vol. 241, no. 1, pp. 27–39, 2005.

[4] X. Y. Fu, M. Chen, Y. Song, Z. Cai, Y. Ye, and S. Li, "The feasibility of applying artificial intelligence to gastrointestinal endoscopy to improve the detection rate of early gastric cancer screening," *Frontiers of Medicine*, vol. 9, Article ID 886853, 2022.

[5] Y. Wang, H. Jin, B. Tang, Q. Yang, C. Liu, and C. H. Zheng, "Lung adenocarcinoma-specific three-integrin signature contributes to poor outcomes by metastasis and immune escape pathways," *Journal of Translational Internal Medicine*, vol. 9, no. 4, pp. 249–263, 2021.

[6] P. A. Papamichalis, Z. Papamichali, I. Gatselis, and D. Koukoulis, "Promyelocytic leukemia antigen expression: a histological marker for primary biliary cholangitis diagnosis?" *Journal of Translational Internal Medicine*, vol. 9, no. 1, pp. 43–51, 2021.

[7] D. V. Catenacci, C. Muro, A.-B. Klempner et al., "Toward a treatment sequencing strategy: a systematic review of treatment regimens in advanced gastric cancer/gastroesophageal junction adenocarcinoma," *The Oncologist*, vol. 26, no. 10, pp. e1704–e1729, 2021.

[8] X. Zhao, X. Wang, B. Zhan, and K. Shu, "Deep learning-based protein features predict overall survival and chemotherapy benefit in gastric cancer," *Frontiers in Oncology*, vol. 12, Article ID 847706, 2022.

[9] K. W. Lee, K. W. Lee, C. E. Van et al., "Association of tumor mutational burden with efficacy of pembrolizumab{plus minus}chemotherapy as first-line therapy for gastric cancer in the phase iii keynote-062 study," *Clinical Cancer Research*, 2022.

[10] W. J. Zang, H. Qian, F. Liu, Y. Huang, and Z. Xue, "HDAC4 promotes the growth and metastasis of gastric cancer via autophagic degradation of MEKK3," *British Journal of Cancer*, 2022.

[11] X. Chang, X. Ge, Y. Zhang, and X. Xue, "The current management and biomarkers of immunotherapy in advanced gastric cancer," *Medicine*, vol. 101, no. 21, Article ID e29304, 2022.

[12] K. Sun, H. Lv, B. Chen et al., "Dawning precision treatment for gastric cancer: the latest biomarkers," *Journal of Translational Internal Medicine*, vol. 9, no. 4, pp. 228–230, 2021.

[13] S. Liu, X. Zhang, J. H. Walline, X. Yu, and H. Zhu, "Comparing the performance of the abc, AIMS65, gbs, and pRS scores in predicting 90-day mortality or rebleeding among emergency department patients with acute upper gastrointestinal bleeding: a prospective multicenter study," *Journal of Translational Internal Medicine*, vol. 9, no. 2, pp. 114–122, 2021.

[14] B. Yue, S. Liu, Z. Zhang, and D. Y. Yan, "Long non-coding RNA Fer-1-like protein 4 suppresses oncogenesis and exhibits prognostic value by associating with miR-106a-5p in colon cancer," *Cancer Science*, vol. 106, no. 10, pp. 1323–1332, 2015.

[15] H. Shen, W. Chen, X. Zhang, F. Wang, and W. Fan, "The prognostic value of COL3A1/FBN1/COL5A2/SPARC-mir-

29a-3p-H19 associated ceRNA network in Gastric Cancer through bioinformatic exploration," *Journal of Cancer*, vol. 11, no. 17, pp. 4933–4946, 2020.

[16] G. Zhou and X. Chen, "Emerging role of extracellular microRNAs and lncRNAs," *ExRNA*, vol. 1, no. 1, p. 10, 2019.

[17] Y. Chen and X. Wang, "miRDB: an online database for prediction of functional microRNA targets," *Nucleic Acids Research*, vol. 48, no. D1, pp. D127–D131, 2020.

[18] S. E. Mc Geary, K. S. Lin, C. Y. Shi et al., "The biochemical basis of microRNA targeting efficacy," *Science*, vol. 366, no. 6472, 2019.

[19] A. A. Mohamed, A. A. A. Omar, R. R. El-Awady et al., "MiR-155 and MiR-665 role as potential non-invasive biomarkers for hepatocellular carcinoma in Egyptian patients with chronic hepatitis C virus infection," *Journal of Translational Internal Medicine*, vol. 8, no. 1, pp. 32–40, 2020.

[20] X. Chen, Y. Ba, L. Ma et al., "Characterization of microRNAs in serum: a novel class of biomarkers for diagnosis of cancer and other diseases," *Cell Research*, vol. 18, no. 10, pp. 997–1006, 2008.

[21] P. Song, J. Liu, D. Liu, and W. Guan, "A three-lncRNA expression signature associated with the prognosis of gastric cancer patients," *Cancer Medicine*, vol. 6, no. 6, pp. 1154–1164, 2017.

[22] J. S. Chen, Y. F. Z. Wang, X. Q. Lv Zhang et al., "H19 serves as a diagnostic biomarker and up-regulation of H19 expression contributes to poor prognosis in patients with gastric cancer," *Neoplasma*, vol. 63, no. 2, pp. 223–230, 2016.

[23] M. S. Wu, H. P. Wang, C. C. Lin et al., "Loss of imprinting and overexpression of IGF2 gene in gastric adenocarcinoma," *Cancer Letters (Shannon, Ireland)*, vol. 120, no. 1, pp. 9–14, 1997.

[24] W. Wang, W. Wang, Q. Yang et al., "The rs2839698 single nucleotide polymorphism of lncRNA H19 is associated with post-operative prognosis in T3 gastric adenocarcinoma," *Clinical Laboratory*, vol. 64, no. 01+02/2018, pp. 105–112, 2018.

Research Article

PFKFB3 Increases IL-1β and TNF-α in Intestinal Epithelial Cells to Promote Tumorigenesis in Colitis-Associated Colorectal Cancer

Hongbin Yu ⓘ**, Chuang Dai** ⓘ**, Wei Zhu** ⓘ**, Yude Jin** ⓘ**, and Chunhui Wang** ⓘ

Department of General Surgery, First People's Hospital Affiliated to Huzhou Normal College, Huzhou, China

Correspondence should be addressed to Chunhui Wang; wangchunhui@zjhu.edu.cn

Colorectal cancer (CRC) is significantly correlated with inflammatory bowel disease, which usually manifests as chronic relapsing-remitting colitis. Phosphofructo-2-kinase/fructose-2,6-biophosphatase 3 (PFKFB3) can catalyze to produce fructose-2,6-bisphosphate and function as an oncogene. In this study, we revealed the function of PFKFB3 in colitis-associated CRC (CAC) and the potential mechanism. RT-qPCR and Western blot were utilized to detect the level of PFKFB3 expression. Increased PFKFB3 expression was observed in the mouse CAC model and CAC patient samples. We identified that overexpression of PFKFB3 in intestinal epithelial cells (IECs) could increase the proliferation, migration, and invasion of CRC cells by the coculture system. Mechanistically, overexpression of PFKFB3 induced phospho-p65 and promoted the expression of IL-1β and tumor necrosis factor alpha (TNF-α) in the development of colitis and CAC. In addition, PFK158, the PFKFB3 inhibitor, could reduce the CRC cell viability, migration, and invasion caused by PFKFB3 overexpression. In conclusion, overexpression of PFKFB3 promoted tumorigenesis in CAC by inducing phospho-p65 and expression of IL-1β and TNF-α. Our study suggested that PFKFB3 acted as a potential treatment target for CAC.

1. Introduction

Colorectal cancer (CRC) is becoming the third most common cancer in the world with high mortality [1]. Multistep processes are involved in colorectal carcinogenesis, including a serrated pathway, carcinoma sequential pathway, and inflammatory pathway [2]. The mechanism of the inflammatory pathway is that the inflammation process could promote cell mutation and accelerate the cycle of wounding and repair in epithelial cells, resulting in colitis-associated cancer (CAC) [3, 4].

During the pathophysiological process of CAC, the immune cells were infiltrated and the proinflammatory and anti-inflammatory cytokines secretion are imbalanced. The single cell analysis of IBD patient tissues indicated that *T* and B lymphocytes, activated dendritic cells, and macrophages consist of the network in the inflammatory process [5]. It demonstrated that macrophages could secrete a range of proinflammatory cytokines during the progression of CAC, such as IL-1α, IL-1β, and tumor necrosis factor alpha (TNF-

α). However, it has also been reported that intestinal epithelial cells expressed immunomodulatory cytokines during active ulcerative colitis and Crohn's disease. These signal pathways could activate intestinal epithelial cells (IECs) activity to induce a microenvironment transformation to develop tumor formation. It indicated that LPS-induced epithelial barrier dysfunction could be abolished by DNMT3a silencing or TNFSF13 overexpression, as well as abrogated the effect of IEC-regulated B cell differentiation [6], which indicated that LPS could induce epithelial dysfunction.

PFKFB3 (phosphofructo-2-kinase/fructose-2,6-biophosphatase 3) is an enzyme to produce fructose-2,6-bisphosphate (F-2,6-BP), involved in glycolytic activation [7]. PFKFB3 has been identified in many cancers, including breast cancer [8], pancreatic cancer [9], and gastric cancer [10]. PFKFB3 can promote cell proliferation through upregulation of cyclin-dependent kinase-1 (CDK1) and p27 [11]. Although the function of PFKFB3 in CRC cell lines has been demonstrated [12], the function of PFKFB3 in CAC

remains unclear. NF-κB plays a crucial role in inflammatory responses via regulating the synthesis and release of cytokines/chemokines, like tumor necrosis factor (TNF)-α and interleukin (IL)-1β, to promote the inflammatory responses. PFKFB3 could regulate endothelial and myocardial inflammation through the NF-κB signaling pathway [13]. From our study, the expression of PFKFB3 level in IECs was increased to exacerbate tumorigenesis. We identified overexpression of PFKFB3 in IECs could increase proliferation, migration, and invasion of CRC cells by the coculture system. Mechanistically, overexpression of PFKFB3 induced phospho-p65 and promoted the expression of IL-1β and TNF-α in the development of colitis and CAC.

2. Materials and Methods

2.1. Clinical Samples and Animal Study. A total of 20 samples were collected from patients with CAC who accepted surgery. Fresh tumor and adjacent nontumor tissue samples were blindly collected. All patients signed the consent form. The study was approved by the Ethics Committee of First People's Hospital affiliated to Huzhou Normal College.

Eight weeks old C57BL/6 mice were injected with azoxymethane intraperitoneally and treated with water containing 1.5% dextran sulfate sodium (DSS) and with regular water for 2 weeks. All animal experiments were performed according to the National Institutes of Health guide for the care and use of laboratory animals (NIH Publications, revised 1978). The study was approved by the Institutional Animal Care and Use Committee of Huzhou Normal College.

2.2. Cell Culture and Cell Transfection. CRC cell lines (Caco2) and HIEC-6 cell lines were obtained from American Type Culture Collection (ATCC). All cells were cultured in DMEM (Invitrogen, USA) with 10% FBS, with a humidified atmosphere containing 5% CO_2 at 37°C. The HIEC-6 cell lines were transfected with pcDNA-PFKFB3 (Genewiz, China) and siRNA-PFKFB3 (GenePharma, China) by using Lipo 3000 (Thermo, USA). siRNA-PFKFB3 sequence: CGCAGCAAGCAUGGCAGAAU.

2.3. CCK-8 Assay. The treated cell was digested and added with a density of 10,000 cells per well added into the top chambers of transwell inserts with FBS-free DMEM. Two days later, the cell counting kit-8 (CCK-8) reagent was added in the bottom chambers and incubated for 2 hours. We determined the optical density (OD) at 450 nm using a multimode microplate reader.

2.4. Cell Invasion Assay. The treated cells were digested and added into the top chambers of transwell inserts with FBS-free DMEM. The cell density is 2×10^5 cells per well. DMEM with 10% FBS was added to the bottom chambers. After 6 hours, 4% paraformaldehyde was used to fix the inserts, and 0.1% crystal violet solution was used to stain cells. The images were obtained under a microscope.

2.5. Wound Healing Assay. The treated cells were digested and cultured in 6-well plates. After coculture, a scratch was made with a 200 μL pipette tip. The debris was washed with PBS, and cell was incubated with DMEM for another 12 hours. At least 3 random areas were photographed to assess the closure of the gap.

2.6. RNA Extraction and RT-qPCR. TRIzol (Takara, Japan) reagent was utilized to isolate the RNA in cells and tissue. The SuperScript™ RT reagent kit (Takara, Japan) was used. Total RNA was used to reserve to synthesise cDNA templates. Expression of the mRNAs was detected with SYBR green according to the standard protocol. The primer sequences were listed: PFKFB3 forward TTGGCGTCCCCA CAAAAGT, reverse AGTTGTAGGAGCTGTACTGCTT; IL-1β forward ATGATGGCTTATTACAGTGGCAA, reverse CGTCGGAGATTCGTAGCTGGA; TNF-α forward ATGACACCACCTGAACGTCTC, reverse CTCTCCAGA GCAGTGAGTTCT; GAPDH forward TGGATTTGGACG CATTGGTC, reverse TTTGCACTGGT ACGTGTTGAT.

2.7. Western Blotting. Proteins were isolated by RIPA buffer containing phosphatase and protease inhibitors (Roche, US). Equal total proteins were separated by SDS/PAGE gels and blotted onto PVDF membranes (Millipore, USA), followed by 5% milk blocking. The membranes were incubated overnight at 4°C with anti-phospho-NF-κB p65 antibody (#3033; Cell Signaling Technology), anti-NF-κB p65 antibody (#8242; Cell Signaling Technology), anti-PFKFB3 antibody (#13123S; Cell Signaling Technology), or anti-GAPDH antibody (60004-1-Ig; Proteintech). Finally, the blot was observed via the ECL detection system.

2.8. Immunofluorescence Assay. For p65 staining, the treated cells were washed with PBS and treated with 0.1% Triton X (Beyotime, China). Subsequently, blocking buffer was added and the primary antibody was incubated overnight at 4°C. Then, cells were treated with secondary antibody and DAPI. Images were captured by a microscope.

2.9. Statistical Analysis. All measurements were presented as the mean ± standard deviation (SD) from three independent experiments. Differences were determined using a two-way analysis of variance (ANOVA) or unpaired Student's t-test by Prism software. Statistical significance was defined as a P value < 0.05.

3. Results

3.1. PFKFB3 Expression Is Increased during Colitis and Colorectal Tumorigenesis. In order to detect the expression of PFKFB3 in colitis-associated cancer, we used RT-qPCR and Western blot to observe the PFKFB3 level in colitis-associated cancer (CAC) patient samples. It demonstrated that PFKFB3 expression was upregulated in CAC (Figures 1(a) and 1(b)). Additionally, the level of IL-1β and TNF-α was also increased in colitis-associated cancer

(Figures 1(c) and 1(d)). Then, a mouse CAC model was established to detect the level of PFKFB3, and significantly increased PFKFB3 expression was detected in the inflamed, dysplastic, and carcinoma tissues (Figure 1(e)).

3.2. PFKFB3 Overexpression in IECs Exacerbates CAC Development.

As we know, IL-1β and TNF-α are important in the tumor microenvironment. First, we overexpressed or knocked down PFKFB3 in the IECs. It showed that overexpressed PFKFB3 could increase the expression of IL-1β and TNF-α (Figures 2(a) and 2(b)). Then, we established a coculture system to observe the effect of PFKFB3 in IECs on CRC cell lines (Figure 2(c)). We overexpressed or knocked down PFKFB3 in IECs and detected proliferation of CRC cell lines by CCK-8 cell lines. It showed that PFKFB3 overexpression in IECs could increase the proliferation ability of CRC cell lines (Figure 2(d)). We also detected the cell migration and invasion after PFKFB3 overexpression in IECs. The wound healing assay and transwell assay indicated that PFKFB3 overexpression in IECs could enhance the cell migration and invasion in CRC cell lines, while PFKFB3 knockdown could reduce the effect (Figures 2(e) and 2(f)). The results indicated that the PFKFB3 in IECs could induce the proliferation, migration, and invasion ability of CRC cell lines.

3.3. PFKFB3 Activated the NF-κB Signal Pathway to Induce IL-1β and TNF-α in IECs.

We detected the signal pathway in the PFKFB3 overexpressed IECs. Previously, it demonstrated that overexpression of PFKFB3 could increase the phosphorylation of p65. So, we detected the level of p65 phosphorylation in IECs. It indicated that overexpressed PFKFB3 could upregulate the phosphorylation of p65, while PFKFB3 knockdown could reduce the effect (Figure 3(a)). Then, the immunofluorescence assay was performed to reveal the p65 nuclear translocation (Figure 3(b)). It also demonstrated that PFKFB3 overexpression could increase p65 nuclear translocation. It also showed that PFKFB3 overexpression increased the level of IL-1β and TNF-α. However, the knockdown of PFKFB3 decreased the IL-1β and TNF-α levels (Figures 3(c) and 3(d)). Then, we also knocked down p65 in PFKFB3 overexpressed cells. It indicated that PFKFB3 could promote the CRC cell proliferation, migration, and invasion through NF-KB activation (Figures 3(e) and 3(f)).

3.4. PFK158 Ameliorates CAC Development.

PFK158, a PFKFB3 inhibitor, was indicated to suppress the tumor development. Then, we used LPS to treat IECs, followed by PFK158 treatment. It showed that PFK158 could decrease the evaluated IL-1β and TNF-α caused by LPS induction (Figures 4(a) and 4(b)). Then, we used the coculture system to check cell proliferation, migration, and invasion of CRC cell lines. It observed that LPS-treated IECs could enhance cell proliferation, migration, and invasion of CRC cells, which was inhibited by PFK158 (Figures 4(c)–4(e)). Finally, we detected phosphorylation of p65, and it showed that PFK158 reduced phosphorylation of p65 caused by LPS treatment (Figure 4(f)).

4. Discussion

Nowadays, more and more attention has been paid to the immunity cells in the development of CAC, such as macrophages [14]. However, the tumor microenvironment consists of many types of cells. In our study, we focused on the role of IECs in the tumor microenvironment. It was observed that the PFKFB3 level was increased in colitis-associated cancer. The abnormal interaction between IECs and CRC is unclear, and an imbalance of inflammatory cytokines has not been demonstrated clearly in CAC progression. It showed that the level of IL-1β and TNF-α was also increased in colitis-associated cancer.

PFKFB3 functions as an oncogene to enhance the glycolytic activity for production of fructose-2,6-biphosphate, which activates 6-phosphofructo-1-kinase [15]. The role of PFKFB3 has been reported in many cancers, including breast cancer, pancreatic cancer, and gastric cancer. The role of PFKFB3 has been reported in CRC. However, its role in CAC remains unclear. We focus on the role of PFKFB3 in IECs to regulate the tumor microenvironment. The results indicated that PFKFB3 in IECs could induce proliferation, migration, and invasion ability of CRC cells. NF-κB plays a crucial role in inflammatory responses via regulating the synthesis and release of cytokines/chemokines, like tumor necrosis factor (TNF)-α and interleukin (IL)-1β, to promote the inflammatory responses. PFKFB3 could regulate endothelial and myocardial inflammation through the NF-κB signaling pathway. A recent study indicated that PFKFB3 overexpression could increase immune evasion and tumorigenesis in hepatocellular carcinoma by NF-κB activation and enhance PDL1 expression [16] and could regulate the NF-κB pathways in ovarian cancer [17]. So, we detected the level of p65 phosphorylation in IECs. It indicated that overexpressed PFKFB3 could upregulate phosphorylation of p65, while PFKFB3 knockdown could reduce the effect. Then, the immunofluorescence assay was performed to release p65 nuclear translocation. It also demonstrated that PFKFB3 overexpression could increase p65 nuclear translocation.

We further assessed the therapeutic function of PFKFB3. PFK158, the PFKFB3 inhibitor, has been approved by the FDA in clinical trials with pancreatic cancers and breast cancers, as well as many other cancers. It has been reported that PFK158 could decrease tumor growth in melanoma [18]. We used LPS to treat IECs, followed by PFK158 treatment. It showed that PFK158 could decrease the elevated IL-1β and TNF-α caused by LPS induction. The coculture system indicated that LPS-treated IECs could enhance cell proliferation, migration, and invasion of CRC cell lines through phosphorylation of p65, which was

(a)

(b)

(c)

(d)

(e)
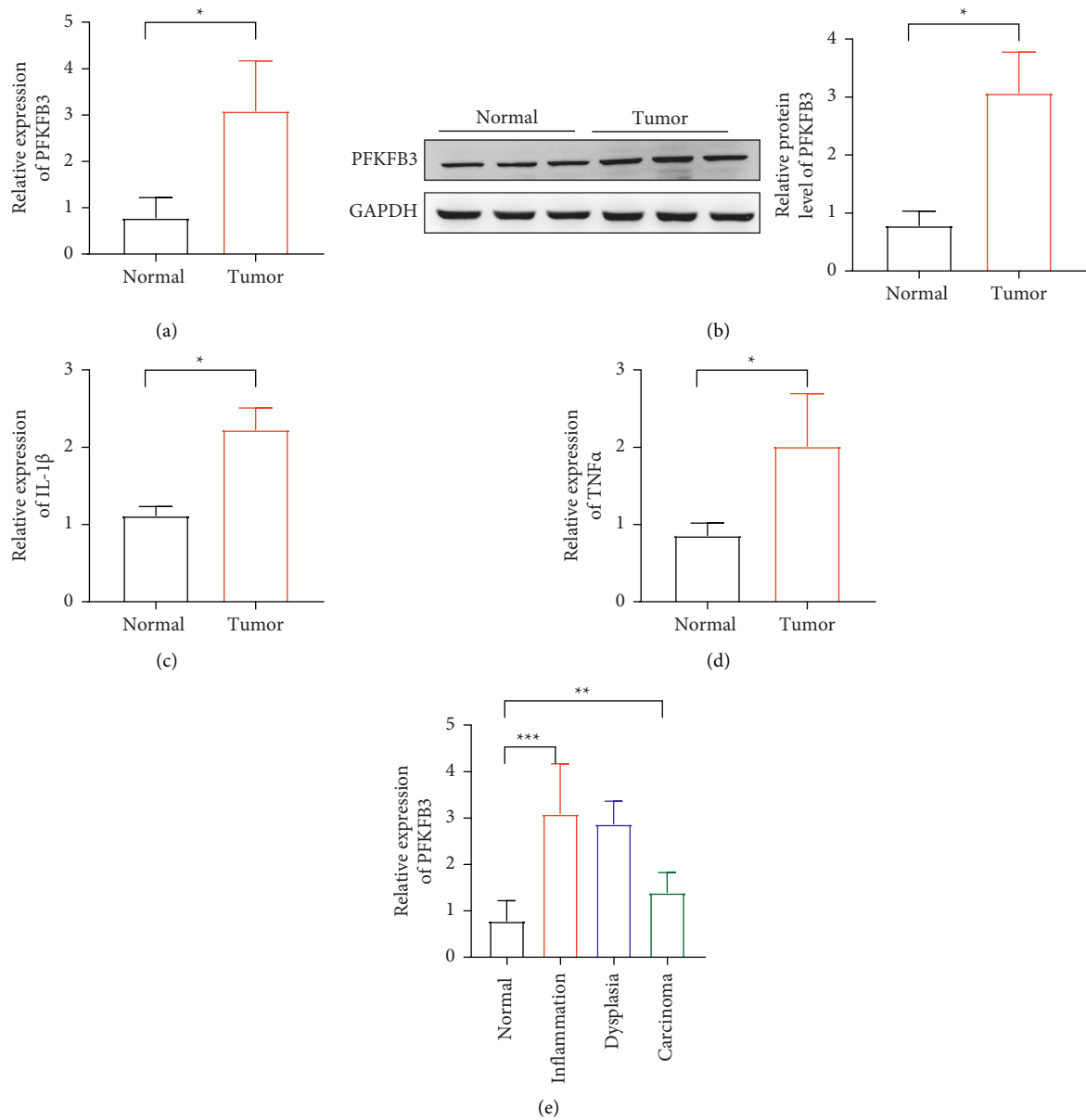
Figure 1: The level of PFKFB3 expression in CAC. (a) The expression of PFKFB3 mRNA in CRC tumor. (b) The protein level of PFKFB3 in CRC tumor. (c)-(d) The level of IL-1β and TNF-α detected in tumor by RT-qPCR. (e) Relative expression of PFKFB3 in colonic tissues from AOM/DSS-treated mice. $^*P < 0.05$, $^{**}p < 0.01$, $^{***}p < 0.001$.
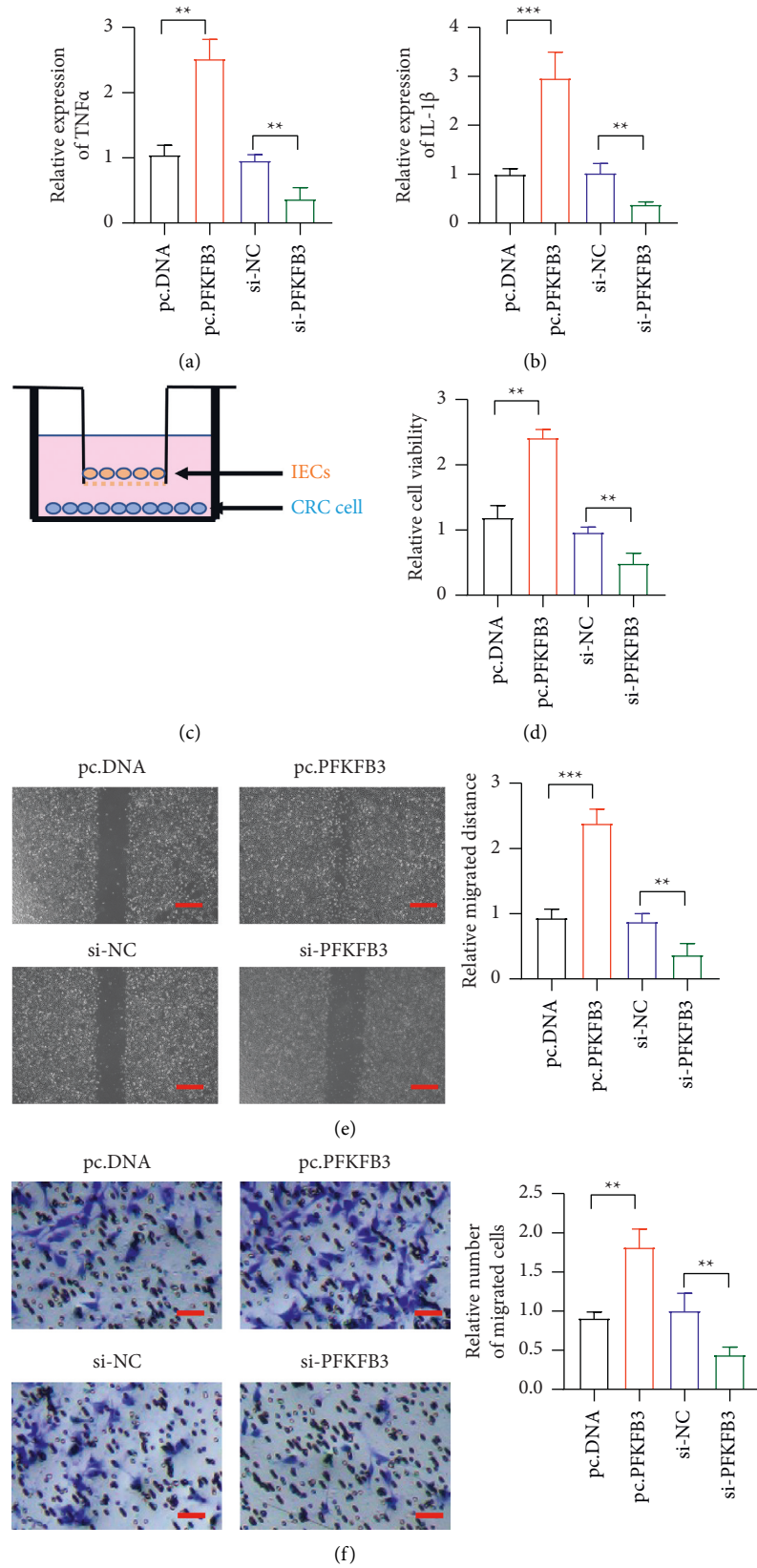
Figure 2: The role of PFKFB3 in CAC. (a)-(b) The expression of IL-1β and TNF-α level detected in PFKFB3 overexpression and knockdown. (c) The coculture assay detecting the influence of IECs on CRC cell. (d) The proliferation of CRC by PFKFB3 overexpression and knockdown in IECs. (e) The migration of CRC by PFKFB3 overexpression and knockdown in IECs; scar bar = 100 μm. (f) The invasion of CRC by PFKFB3 overexpression and knockdown in IECs; scar bar = 50 μm. $^{**}P < 0.01$, $^{***}p < 0.001$. pcDNA, empty vector; Si-NC, siRNA negative control.

(a)

(b)

(c)

(d)

(e)

(f)
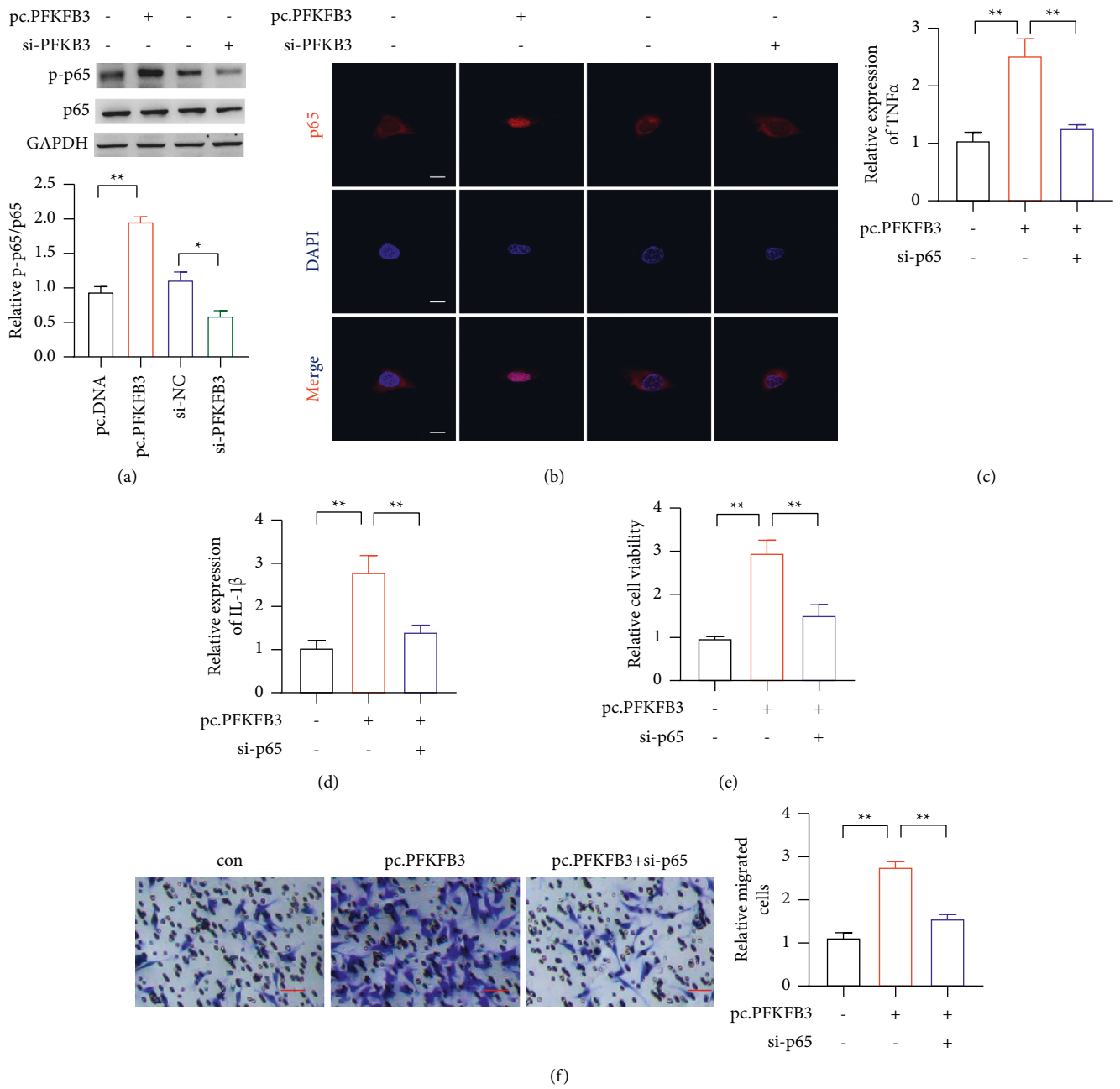
FIGURE 3: The p65 activation in CAC. (a) The phosphorylation of p65 detected in PFKFB3 overexpression and knockdown. (b) The nuclear translocation of p65 detected in PFKFB3 overexpression and knockdown; scar bar = 20 μm. (c)-(d) The expression of IL-1β and TNF-α level by PFKFB3 overexpression and p65 knockdown in IECs. (e) The proliferation of CRC by PFKFB3 overexpression and p65 knockdown in IECs. (f) The invasion of CRC by PFKFB3 overexpression and p65 knockdown in IECs; scar bar = 50 μm. $^{*}P < 0.05$, $^{**}p < 0.01$.

(a)

(b)

(c)

(d)

(e)

(f)
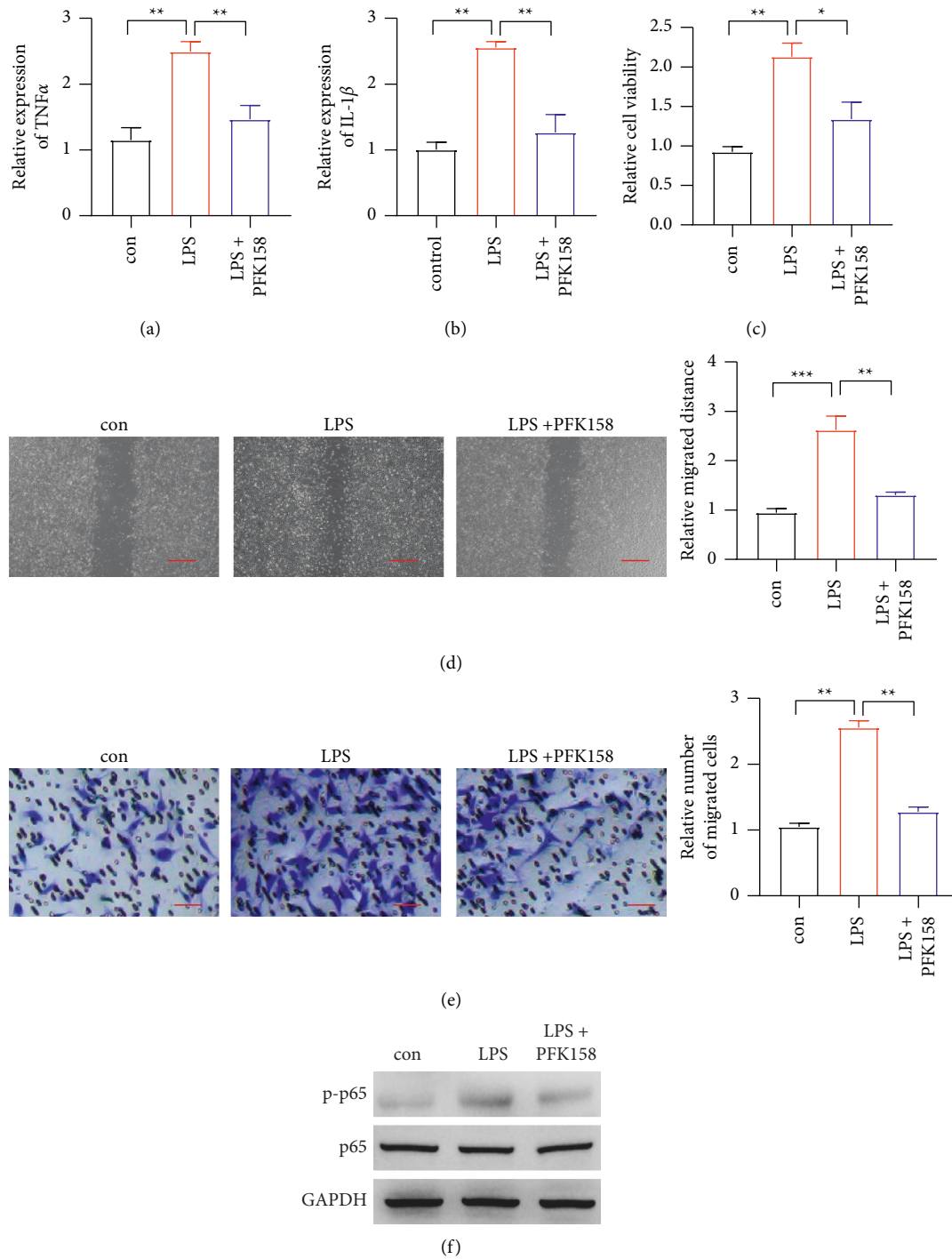
FIGURE 4: The PFK158 reduces cell proliferation, migration, and invasion. (a)-(b) The IL-1β and TNF-α expression level detected in PFK158 treatment. (c) The proliferation of CRC by LPS stimulation and PFK158 treatment in IECs. (d) The migration of CRC by LPS stimulation and PFK158 treatment in IECs; scar bar = 100 μm. (e) The invasion of CRC by LPS stimulation and PFK158 treatment in IECs; scar bar = 50 μm. (f) The p65 phosphorylation detected CRC by LPS stimulation and PFK158 treatment in IECs. $^{*}P < 0.05$, $^{**}p < 0.01$.

inhibited by PFK158. The results indicated that PFK158 was a potential candidate to treat CAC.

5. Conclusion

In conclusion, the level of PFKFB3 in intestinal epithelial cells (IECs) was increased to exacerbate tumorigenesis in mice. We identified overexpression of PFKFB3 in IECs could increase the viability, migration, and invasion of CRC cells by the coculture system. Mechanistically, overexpression of PFKFB3 induced phospho-p65 and promoted the expression of IL-1β and TNF-α in the development of colitis and CAC.

Data Availability

The data used to support the findings of this study are included within the article.

Consent

Written informed consent was obtained from all participants included in the study.

Conflicts of Interest

The authors declare that there are no conflicts of interest.

Authors' Contributions

Chunhui Wang designed the research; Hongbin Yu wrote the manuscript; Hongbin Yu and Chuang Dai performed the in vitro experiments; Wei Zhu and Yude Jin analyzed data.

Acknowledgments

References

[1] I. van den Berg, R. R. J. Coebergh van den Braak, J. L. A. van Vugt, J. N. M. Ijzermans, and S. Buettner, "Actual survival after resection of primary colorectal cancer: results from a prospective multicenter study," *World Journal of Surgical Oncology*, vol. 19, p. 96, 2021.

[2] N. Katsuya, K. Sentani, Y. Sekino et al., "Clinicopathological significance of intelectin-1 in colorectal cancer: intelectin-1 participates in tumor suppression and favorable progress," *Pathology International*, vol. 70, pp. 943–952, 2020.

[3] I. Tattoli, S. A. Killackey, E. G. Foerster et al., "NLRX1 acts as an epithelial-intrinsic tumor suppressor through the modulation of TNF-mediated proliferation," *Cell Reports*, vol. 14, no. 11, pp. 2576–2586, 2016.

[4] C. Y. Liu, N. Girish, M. L. Gomez et al., "Transitional anal cells mediate colonic re-epithelialization in colitis," *Gastroenterology*, vol. 162, 2022.

[5] J. C. Devlin, J. Axelrad, A. M. Hine et al., "Single-cell transcriptional survey of ileal-anal pouch immune cells from ulcerative colitis patients," *Gastroenterology*, vol. 160, no. 5, pp. 1679–1693, 2021.

[6] B. Cheng, A. M. Rong, W. Li, X. Bi, and X. Qiu, "DNMT3a-Mediated enterocyte barrier dysfunction contributes to ulcerative colitis via facilitating the interaction of enterocytes and B cells," *Mediators of Inflammation*, vol. 2022, Article ID 4862763, 15 pages, 2022.

[7] M. Yi, Y. Ban, Y. Tan, W. Xiong, G. Li, and B. Xiang, "6-Phosphofructo-2-kinase/fructose-2, 6-biphosphatase 3 and 4: a pair of valves for fine-tuning of glucose metabolism in human cancer," *Molecular Metabolism*, vol. 20, pp. 1–13, 2019.

[8] C. M. Galindo, F. A. Oliveira Ganzella, G. Klassen, E. A. Souza Ramos, and A. Acco, "Nuances of PFKFB3 signaling in breast cancer," *Clinical Breast Cancer*, vol. 22, 2022.

[9] S. C. Ozcan, A. Sarioglu, T. H. Altunok et al., "PFKFB2 regulates glycolysis and proliferation in pancreatic cancer cells," *Molecular and Cellular Biochemistry*, vol. 470, no. 1-2, pp. 115–129, 2020.

[10] L. Lei, L. L. Hong, Z. N. Ling et al., "A potential oncogenic role for PFKFB3 overexpression in gastric cancer progression," *Clinical and Translational Gastroenterology*, vol. 12, no. 7, Article ID e00377, 2021.

[11] A. Yalcin, B. F. Clem, Y. Imbert-Fernandez et al., "6-Phosphofructo-2-kinase (PFKFB3) promotes cell cycle progression and suppresses apoptosis via Cdk1-mediated phosphorylation of p27," *Cell Death & Disease*, vol. 5, no. 7, Article ID e1337, 2014.

[12] J. Han, Q. Meng, Q. Xi et al., "Interleukin-6 stimulates aerobic glycolysis by regulating PFKFB3 at early stage of colorectal cancer," *International Journal of Oncology*, vol. 48, no. 1, pp. 215–224, 2016.

[13] Y. X. Jiang, M. K. Y. Siu, J. J. Wang et al., "PFKFB3 regulates chemoresistance, metastasis and stemness via IAP proteins and the NF-κB signaling pathway in ovarian cancer," *Frontiers in Oncology*, vol. 12, Article ID 748403, 2022.

[14] X. M. Li, D. Y. Yuan, Y. H. Liu et al., "Panax notoginseng saponins prevent colitis-associated colorectal cancer via inhibition Ido1 mediated immune regulation," *Chinese Journal of Natural Medicines*, vol. 20, no. 4, pp. 258–269, 2022.

[15] A. Rodriguez-Garcia, P. Samso, P. Fontova et al., "TGF-β1 targets Smad, p38 MAPK, and PI3K/Akt signaling pathways to induce PFKFB3 gene expression and glycolysis in glioblastoma cells," *FEBS Journal*, vol. 284, no. 20, pp. 3437–3454, 2017.

[16] C. D. House, E. Jordan, L. Hernandez et al., "NFκB promotes ovarian tumorigenesis via classical pathways that support proliferative cancer cells and alternative pathways that support ALDH+ cancer stem–like cells," *Cancer Research*, vol. 77, no. 24, pp. 6927–6940, 2017.

[17] D. P. Chen, W. R. Ning, Z. Z. Jiang et al., "Glycolytic activation of peritumoral monocytes fosters immune privilege via the PFKFB3-PD-L1 axis in human hepatocellular carcinoma," *Journal of Hepatology*, vol. 71, no. 2, pp. 333–343, 2019.

[18] C. Casulo, M. Byrtek, K. L. Dawson et al., "Early relapse of follicular lymphoma after rituximab plus cyclophosphamide, doxorubicin, vincristine, and prednisone defines patients at high risk for death: an analysis from the national LymphoCare study," *Journal of Clinical Oncology*, vol. 33, no. 23, pp. 2516–2522, 2015.

Research Article

Construction of a Prognostic Immune-Related LncRNA Risk Model for Gastric Cancer

Wei Ding [iD],[1,2] **Pengcheng Sun** [iD],[3] **Yulin Tan**,[1,2] **Huaji Jiang**,[1,2] **Cheng Xi**,[1,2] **Ling Zhuang**,[1,2] **Yixin Xu**,[1,2] **and Xuezhong Xu** [iD][1,2]

[1]*Department of General Surgery, Wujin Hospital Affiliated to Jiangsu University, Changzhou 213017, China*
[2]*Department of General Surgery, The Wujin Clinical College of Xuzhou Medical University, Changzhou 213017, China*
[3]*Department of Oncology, The Third Affiliated Hospital of Soochow University, Changzhou 213001, China*

Correspondence should be addressed to Xuezhong Xu; xxzdoctor@163.com

Gastric cancer (GC) is one of the most common malignancies, and novel prognostic biomarkers for it are urgently required. This study is aimed at screening a group of immune-related lncRNAs (IRLs) in predicting the prognosis of GC patients. Genetic and clinical information from the 360 GC patients was included in this study. Eight IRLs in lncRNA-miRNA-mRNA network were screened out according to differential expression analysis. A novel risk score model with three IRLs (MIR4435-1HG, UCA1, and RP11-617F23.1) were identified, and patients were assigned to a high-risk group and a low-risk group. Patients in the low-risk group had a better prognosis. In addition, two nomograms were developed to predict the prognosis of GC. We evaluated the correlation between IRLs and the immune infiltration level of GC using TIMER. Furthermore, we verified that RP11-617F23.1 was significantly upregulated in human GC tissues compared with their adjacent tissues. And, patients with high RP11-617F23.1 expression in tumor tissues had poorer survival. In conclusion, we established a novel risk model based on IRLs for predicting the prognosis of GC. Meanwhile, a novel IRL, RP11-617F23.1, could serve as a predictor of prognosis for patients with GC.

1. Introduction

Gastric cancer (GC) is one of the commonest malignancies all over the world, with nearly one million new cases each year, accounting for 5.7% of all malignant tumors [1]. The incidence and mortality rate of GC, respectively, rank the 5th and 3rd among malignant tumors, and the incidence in Asia ranks the first [2]. At present, radical resection is still the most efficient option for early GC patients with low risk of lymph node metastasis. However, most patients are in moderate and advanced stages when they are diagnosed, and some patients already have local or distant metastasis because the early GC is not obvious [3,4]. Most of them are intolerance of operation, and even if they could be excised surgically, they would be prone to relapse and metastasis, with a poor prognosis, and the 5-year survival rate only reaches 30% [5,6]. Therefore, the identification of key regulators and the elucidation of the potential mechanisms for

initiating and promoting the occurrence and metastasis of GC are conducive to the formulation of a reasonable postoperative follow-up plan and the adoption of targeted interventions to improve the survival rate. It is urgently required to clarify the molecular mechanism of GC and to find ideal markers for early diagnosis and specific therapeutic targets.

As far back as 1909, Ehrlich demonstrated that the immune balance had the effect of inhibiting most tumors and played a significant role in preventing tumor progression [7]. The immune cells can specifically recognize antigens expressed on the tumor cell surface and generate immune responses via releasing cytokines to act directly on the tumor cells and inhibit tumor growth [8]. Although tumor-related immune cells within the tumor microenvironment (TME) play a role in eliminating tumor cells in the anti-tumor process, some tumor cells still escape under immune surveillance [9]. It is increasingly recognized that

the TME has an important role in tumor progression [10]. These tumor-associated immune cells may have antitumor or protumor effects. Immune escape as a new marker of cancer provides opportunities for new strategies for cancer treatment. As RNA sequencing developed, novel therapeutic biomarkers at the gene level in the TME were unearthed in abundance [11].

Long noncoding RNA (lncRNA) is a kind of RNA with a structure of more than 200 nucleotides and no functional open reading frame. Research showed that lncRNA was involved in various biological functions, including the regulation of growth, aging, differentiation, pyroptosis, apoptosis, and tumorigenesis [12]. Various lncRNAs have been found to affect tumor growth and invasion and immune response. For example, lncRNA SATB2-AS1 has been clarified to inhibit tumor metastasis and affect the TME in colorectal cancer by targeting SATB2 [13]. Mesenchymal stem cells can induce liver cancer through lncRNA-MUF interaction with miR-34a and ANXA2 [14]. LncRNA SNHG1 has been demonstrated to regulate the differentiation of regulatory T cells, thus affecting immune escape of breast cancer by targeting miR-448/IDO [15]. LncRNAs can regulate TME and have significant role in immunotherapy. However, research on immune-related lncRNA (IRL) in GC has been relatively sparse.

The purpose of our research was to screen novel immune-related lncRNAs, which might serve as predictors and therapeutic targets in GC. We performed differential expression analysis, univariate and multivariate Cox regression analysis, Kaplan–Meier survival analysis, TIMER database analysis, and other analysis to identify IRLs and evaluate the predictive ability and therapeutic potential.

2. Methods

This study was approved by the Ethics Review Committee of Wujin Hospital affiliated with Jiangsu University (no. 202121).

2.1. Data Acquisition and Preprocessing. GPL16956 Agilent-045997 Arraystar human lncRNA microarray V3 (Probe Name Version) platform was used to obtain the microarray dataset GSE122530 which was pretreated and standardized from the Gene Expression Omnibus (GEO) repository [16]. There were six paired GC and normal tissue samples. The expression of RNA sequencing and clinical data associated with GC were collected from The Cancer Genome Atlas (TCGA) [17], which included 354 GC and 41 paracancer tissue samples. Clinical information in TCGA was collected, including age, gender, tumor stage, and differentiated degree.

2.2. Data Annotation. Download the human reference genome sequence file (GRCh38.p2.genome.fa) from the GENCODE database [18]. Seqmap software was applied to match all probe sequences to the reference genome [19]. We

kept the unique mapped reads and obtained the corresponding genes of each probe. We annotate these probes according to GENCODE by using the information of the probes on chromosomes. Finally, the probes were paired with Gene Symbols, and the unpaired probes were removed.

2.3. Differential Expression Analysis. After obtaining the gene expression matrix through the previous gene annotation, Limma package [20] was used to obtain the adjusted P value and $|logFC|$ by empirical Bayes and linear regression along with Benjamini and Hochberg multiple comparison methods. Differentially expressed mRNAs and lncRNAs were identified, while adjusted P value <0.05 and $|logFC|$ >0.585; differentially expressed miRNAs were identified, while adjusted P value <0.05 and $|logFC|$ >1. After the above difference analysis, we select the intersection of differentially expressed mRNA and lncRNA in the two groups according to upregulation and downregulation to explore the common differentially expressed lncRNAs and mRNAs.

2.4. Building the ceRNA Network. The lncRNA-miRNA-mRNA network was built according to the ceRNA hypothesis [21]. In the miRNA module of miRWalk 3.0, input the miRNA list, set the species to "human," set the score value >0.85, and run to obtain the predicted miRNA-mRNA regulatory relationship pairs, which also appeared in TargetScan [22], miRDB [23], and miRTarBase [24] databases. The miRNA-related lncRNAs were predicted using Prediction Module of DIANA-LncBase Predicted v.2 database, and the regulation relationship of score greater than 0.6 was selected. According to the common differentially expressed miRNAs and miRNA-mRNA and lncRNA-miRNA regulatory relationship pairs obtained above, we built the lncRNA-miRNA-mRNA network.

2.5. Immune-Related ceRNA Network. Download the immune genes in the Immunology Database and Analysis Portal (ImmPort) from the InnateDB database [25] and match them with the ceRNA network to obtain the immune-related ceRNA network. The lncRNAs in the immune-related ceRNA network were identified as IRLs.

2.6. Univariate and Multivariate Cox Regression and Kaplan–Meier Survival Analysis. Preprocessing of survival data: to ensure the accuracy of survival time, samples with a survival status of 0 (survival) and survival time <1 month were considered a failure of follow-up in this analysis, and these samples were removed from the total samples. Finally, 339 samples were retained for overall survival (OS) data and 266 samples for disease-free survival (DFS) data. Univariate analyses from the survival package (version 3.2-7) were performed with Cox regression analysis for IRLs. After univariate Cox analysis, lncRNAs with P value <0.05 were screened out.

A novel risk model was developed for predicting the prognosis. The risk score (RS) was calculated as follows:

$$RS = \beta_{gene1} \times Expr_{gene1} + \beta_{gene2} \times Expr_{gene2} + \ldots + \beta_{genen} \times Expr_{genen}, \quad (1)$$

where β_{gene} indicated the regression coefficient β for each gene and $Expr_{gene}$ indicated the expression value of the corresponding gene for each sample.

The appellate formula was used to calculate the RS of each sample. The optimal cut-off RS point was determined using maximally selected rank statistics according to the risk model. Two groups (low-risk and high-risk groups) of patients were divided according to the optimal cut-off RS point. The two groups were used to compared by Kaplan–Meier survival analysis.

2.7. Nomogram Model Construction.
Univariate Cox regression analyses were used to sift out risk factors, based on RS, age, gender, tumor stage, and differentiated degree. Multivariate analyses were used to screen out independent risk factors with $P < 0.05$. The nomograms were constructed by using the rms package (version 6.1-0) with factors obtained above.

2.8. TIMER Database Analysis.
We analyzed the expression of IRLs obtained above in different types of cancer and the correlation with the degree of immune infiltrates, including B cells, CD8+ T cells, CD4+ T cells, macrophages, neutrophils, and dendritic cells, via TIMER database [26].

2.9. Patients and Samples.
The present study included 64 patients with gastric cancer. All patients underwent radical open gastrectomy in Wujin Hospital from January 2014 to October 2014. The inclusion criteria were as follows: [1] had detailed history, examination, and laboratory investigations; [2] did not have distant metastases; [3] no antitumor therapy was performed before surgery; and [4] complete follow-up data were available. The adjacent normal tissues were also collected 3–5 cm away from the edge of the tumor.

2.10. Quantitative Real-Time Polymerase Chain Reaction.
Total RNA was extracted using Trizol® reagent (Shanghai Pufei Biotech Co., Ltd.) based on the supplier's instruction. M-MLV kit (Promega Biotech Co., Ltd) was used to obtained cDNA by reverse transcription. qPCR was conducted using the SYBr Master Mix (Takara Biomedical Technology Co., Ltd.) and the Real-Time PCR System (LightCycler 480 II) in the $12\,\mu l$ reaction mixture with the following conditions: initial denaturation at 95°C for 30 sec, followed by 40 cycles of 95°C for 5 sec, 60°C for 30 sec, then followed by one cycle of 95°C for 15 sec, 60°C for 30 sec, and 95°C for 15 sec. The following primer information was used for qPCR: ACTB forward, 5′-GCGTGACATTAAGGAGAAGC-3′ and reverse, 5′-CCACGTCACACTTCATGATGG-3′; RP11-617F23.1

forward, 5′-ACCGCAGGCACTTGTGAAGA-3′ and reverse, 5′-AAGGGACATGCAGAGGGGAG-3′. For quantification of RNA levels, the $\Delta\Delta CT$ method was applied, and the internal reference gene ACTB was used for normalization.

2.11. Statistical Analysis.
Group differences for continuous variables were analyzed by t-test or one-factor analysis of variance (one-way ANOVA). Group differences in the distribution of categorical variables were analyzed by the chi-square test. Survival analysis was conducted by log-rank tests. Survival curves were drawn using the Kaplan–Meier method. All statistical analyses were calculated with Prism 9.0 (GraphPad Software, LLC).

3. Results

3.1. Differential Analysis of Genes.
According to the differential analysis method described in the method, the results are shown in Table 1. The volcano map of the differential genes is shown in Figures 1(a)–1(d). After intersection analysis, a total of 392 common differential mRNAs and 26 common differential lncRNAs were achieved, as shown in Figures 1(e)–1(h).

3.2. Construction of Immune-Related ceRNA Network.
The target gene prediction tool miRWalk3.0 was used to predict the common differential mRNAs associated with differential miRNAs, and a total of 29 pairs miRNA-mRNA were obtained, including 14 miRNAs and 17 mRNAs. Furthermore, according to LncBase Predicted v.2 database, 12 lncRNAs were predicted associated with differential miRNAs. Based on the obtained lncRNA-miRNA and miRNA-mRNA relationship pairs, Cytoscape was used to construct the ceRNA network. Finally, 13 miRNAs, 12 lncRNAs, and 16 mRNAs were obtained, with a total of 58 regulatory pairs. With InnateDB database matching, we obtained 4 immune-related mRNAs (CDH11, RGMB, SOX4, and ABL2). By matching the above network, an immune-related ceRNA network was built, including 8 lncRNAs, 7 miRNAs, and 4 mRNAs, with a total of 21 regulatory pairs (Figure 2). These 8 lncRNAs were identified as immune-related lncRNAs.

3.3. Development of the OS and RFS Nomograms.
One lncRNA associated with overall survival and three lncRNAs associated with disease-free survival were identified using univariate Cox analysis, and the results are shown in Table 2. The regression coefficient β was used to calculate the RS of each sample. The optimal cutoff RS points are shown in

TABLE 1: The number of differential genes.

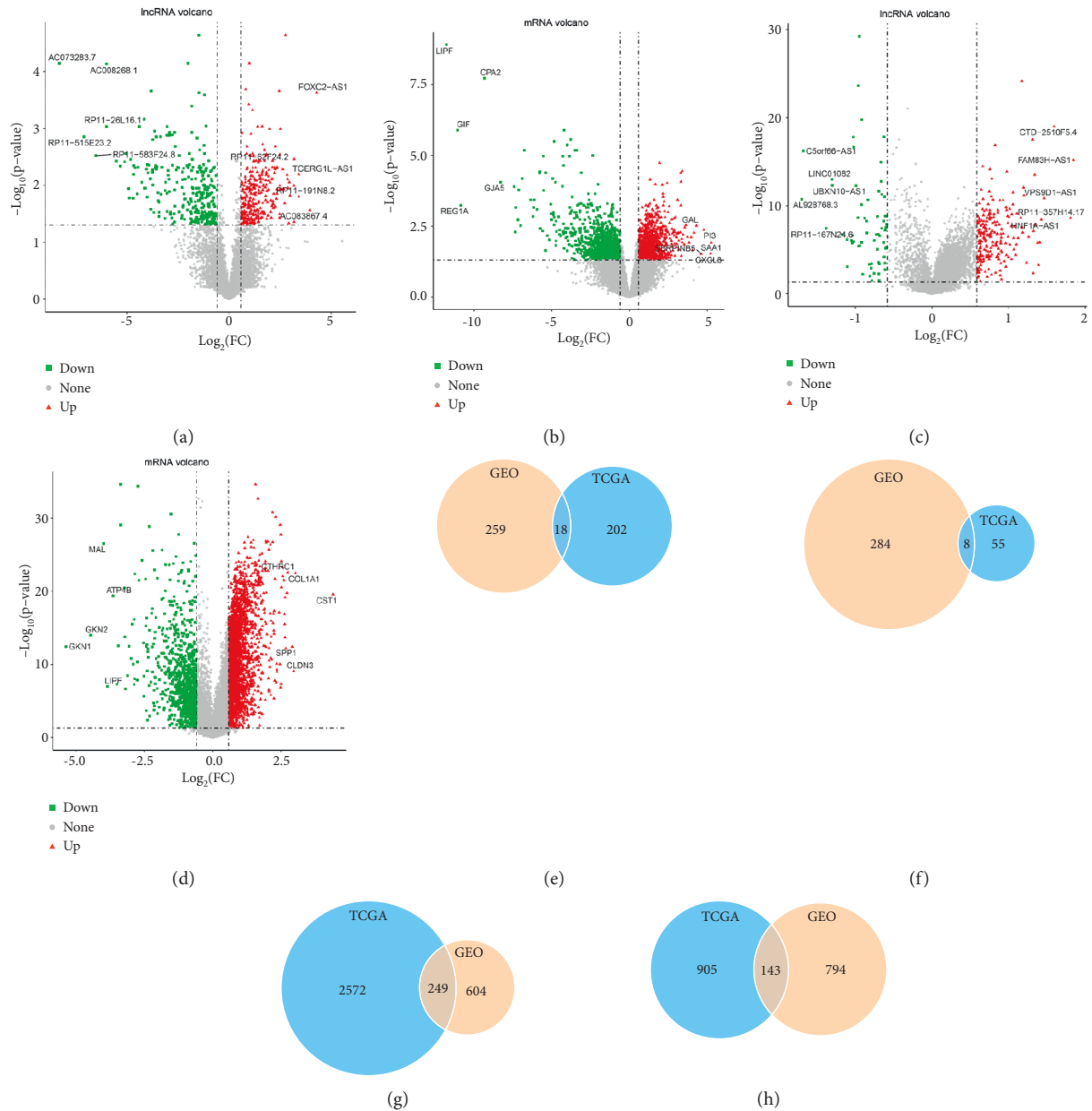|	GSE122530			TCGA		
	Up	Down	Total	Up	Down	Total
mRNA	852	936	1788	2821	1048	3869
LncRNA	277	292	569	219	62	281
miRNA	—	—	—	71	10	81

FIGURE 1: Volcano map and Venn diagram of differential genes. The volcano map of differential (a) lncRNA and (b) mRNA in GSE122530; the volcano map of differential (c) lncRNA and (d) mRNA in TCGA; (e) upregulated and (f) downregulated lncRNAs; and (g) upregulated and (h) downregulated mRNAs.

Figure 3. The patients were separated into a high-risk group and a low-risk group with the cut-off value. By survival analysis, the patients in low-risk group had significantly better OS and DFS as shown in Figure 4.

The RS was combined with clinical characteristics for univariate and multivariate regression analyses. Multivariate analysis showed that tumor stage ($P < 0.01$) and age ($P = 0.01$) were closely related to OS (Table 3), while tumor
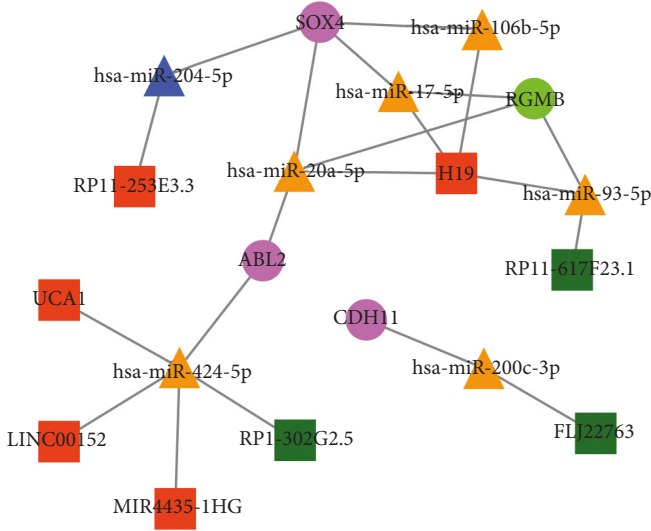
FIGURE 2: Immune-related lncRNA-miRNA-mRNA network. The pink circle stands for upregulated mRNA, the green circle stands for downregulated mRNA, the yellow triangle stands for upregulated miRNA, the blue triangle stands for downregulated miRNA, the red square stands for upregulated lncRNA, and the dark green square stands for downregulated lncRNA.

stage ($P = 0.02$) and RS ($P < 0.01$) were closely related to DFS (Table 4).

The multivariate analyses identified that tumor stage, RS, and age were independent risk factors for GC patients. To better predict the prognosis at 1-, 3-, and 5-year OS and DFS of GC patients, we constructed nomograms of the variables above (Figures 5(a) and 5(b)). The calibration plot for the probability of OS and DFS had an optimal agreement between the two nomograms for probabilities and actual observation, respectively (Figures 5(c)–5(h)).

3.4. TIMER Database Analysis.

The correlation between lncRNAs (MIR4435-1HG, UCA1, and RP11-617F23.1) and the infiltration degree of immune cells was described using TIMER database. However, only UCA1 was recorded in TIMER database. The expression levels of UCA1 in normal and primary tumor samples in all TCGA tumors are shown in Figure 6(a). The expression level of UCA1 was significantly higher in bladder urothelial carcinoma (BLCA), cholangiocarcinoma (CHOL), colon adenocarcinoma (COAD), esophageal carcinoma (ESCA), lung adenocarcinoma (LUAD), lung squamous cell carcinoma (LUSC), rectum adenocarcinoma (READ), stomach adenocarcinoma (STAD), and thyroid carcinoma (THCA) compared with adjacent normal tissues. However, UCA1 expression was significantly lower in kidney chromophobe (KICH), kidney renal clear cell carcinoma (KIRC), liver hepatocellular carcinoma (LIHC), and prostate adenocarcinoma (PRAD) compared with adjacent normal tissues. Then, we assessed the association between the immune infiltration level and the UCA1 expression level in stomach adenocarcinoma using

TABLE 2: Univariate analysis of overall survival and disease-free survival.

	Overall survival			Disease-free survival		
	HR	95% CI	P value	HR	95% CI	P value
MIR4435-1HG	1.34	[1.03–1.76]	0.03*	1.44	[1.04–1.97]	0.03*
H19	1.06	[0.98–1.14]	0.15	1.04	[0.96–1.14]	0.34
RP11-617F23.1	0.87	[0.71–1.06]	0.16	0.77	[0.59–0.99]	0.04*
FLJ22763	0.83	[0.61–1.14]	0.26	0.84	[0.58–1.22]	0.36
RP11-253E3.3	0.9	[0.63–1.28]	0.55	0.9	[0.57–1.41]	0.64
UCA1	1.02	[0.94–1.12]	0.58	1.11	[1.01–1.23]	0.03*
LINC00152	1.07	[0.83–1.37]	0.61	1.14	[0.85–1.54]	0.38
RP1-302G2.5	1.01	[0.74–1.38]	0.94	1.08	[0.76–1.54]	0.67

Note: overall survival, $\beta_{\text{MIR4435-1HG}} = 0.29$; disease-free survival, $\beta_{\text{MIR4435-1HG}} = 0.22$, $\beta_{\text{UCA1}} = 0.08$, and $\beta_{\text{RP11-617F23.1}} = -0.16$; *statistically significant.

TIMER. The results showed that the expression level of UCA1 was closely related to the infiltrating levels of CD8+ T cells, CD4+ T cells, macrophages, and dendritic cells, as shown in Figure 6(b). And, UCA1 had the highest copy number in DC cells in stomach adenocarcinoma, as shown in Figure 6(c).

3.5. The Verification of Clinical Role of RP11-617F23.1 in Gastric Cancer.

Based on the three prognostic related IRLs (MIR4435-1HG, UCA1, and RP11-617F23.1) obtained above were analyzed further. As the function of MIR4435-1HG and UCA1 has been verified before [27,28], we only tested the effect of RP11-617F23.1. First, we detected the relative expression levels of RP11-617F23.1 in GC tissues and adjacent tissues, as well as four cell lines (GES-1, NCI-N87, MKN-45, and HGC-27). As shown in Figure 7(a), RP11-617F23.1 was significantly upregulated in human GC tissues ($n = 64$) compared with their corresponding adjacent tissues ($n = 64$). Similarly, it was significantly upregulated in gastric cancer cell line (NCI-N87, MKN-45, and HGC-27) compared with gastric mucosa cell (GES-1), as shown in Figure 7(b). To further validate its clinical effect, we compared it with clinical features and survival data. Patients were separated into two groups (high and low) based on the median of the relative expression of RP11-617F23.1 in tumor tissues. As shown in Table 5, patients with higher expression of RP11-617F23.1 in tumor tissues had higher NRL value ($P < 0.001$), more advanced T stage ($P = 0.004$) and poorer tumor differentiation ($P = 0.039$) and a higher probability of lymph node metastasis ($P = 0.044$). Additionally, the prognostic value of RP11-617F23.1 for patients with GC was assessed by Kaplan–Meier survival analysis. The results identified that patients with high RP11-617F23.1 expression in tumor tissues had poorer OS and DFS than patients with low RP11-617F23.1 expression (OS: $P = 0.021$, Figure 7(c); DFS: $P = 0.004$, Figure 7(d)). Thus, our data suggested that
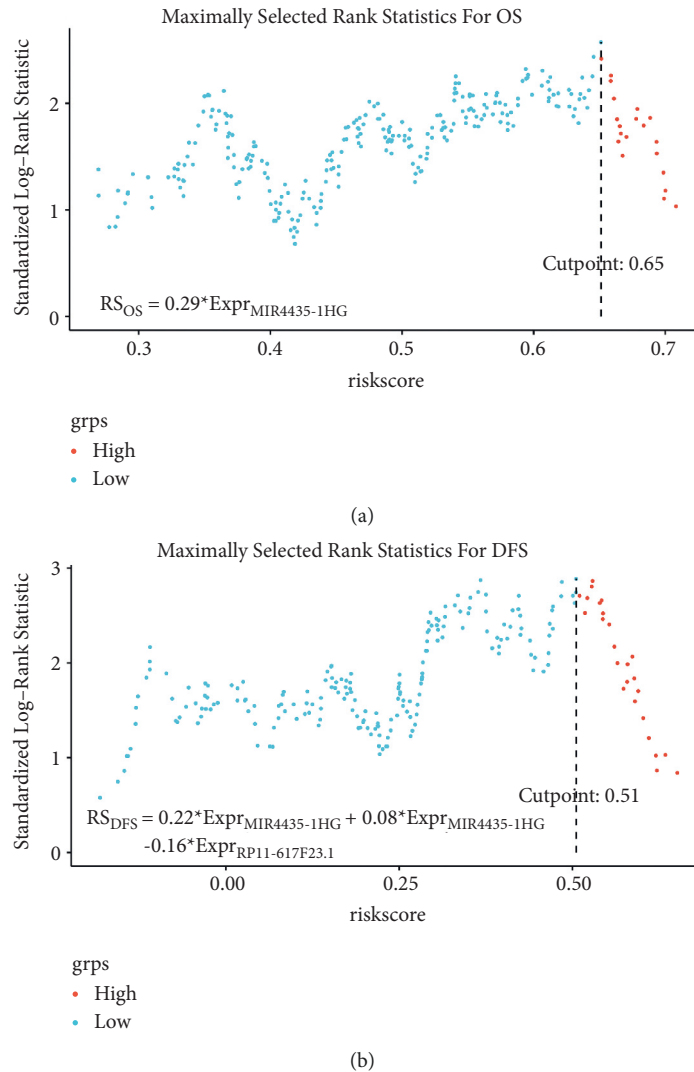
(a)

(b)

Figure 3: Maximally selected rank statistics. (a) Optimal cut-off value of RS for OS; (b) optimal cut-off value of RS for DFS (OS = overall survival; DFS = disease-free survival; and RS = risk score).

RP11-617F23.1 was a novel marker indicating poor GC prognosis.

4. Discussion

In the current study, a total of 360 GC and 47 pericarcinomatous tissues derived from two datasets (TCGA and GSE122530) were incorporated into the calculation of the differential expression lncRNAs in patients with GC. Overall, 4723 immune-related mRNAs were downloaded from the InnateDB. Three IRLs (MIR4435-1HG, UCA1, and RP11-617F23.1) were confirmed to be significantly associated with the prognosis of GC. GC patients could be separated into two groups by the risk model based on the three IRLs. The regression analyses of clinical information and RS were performed to identify the independent prognostic factors (tumor stage, age, and RS). The nomograms were constructed based on tumor stage, age, and RS to predict OS and DFS for GC patients visually. Then, the calibration plot

identified that the two nomograms had high prediction accuracy. We also found that UCA1 expression was significantly associated with various immune cells, while the other two IRLs were not recorded in the TIMER database.

In our study, MIR4435-1HG and UCA1 were identified to exhibit cancer-promoting activity, while the clinical effect of RP11-617F23.1 was contradictory. Both UCA1 and MIR4435-1HG had been previously reported in GC. In the previous study, the expression of serum UCA1 was suggested to be closely associated with the differentiation of cancer cells in GC [29]. Additionally, UCA1 could promote cell proliferation and invasion of GC by regulating the miR-590-3p/CREB1 signal pathway [30]. The upregulation of UCA1 could promote the invasion and migration in GC [31]. Recent research has shown that UCA1 would act as an antitumor miRNA inhibitor to facilitate proliferation, migration, and immune escape and inhibit apoptosis in GC [28]. And, UCA1 could increase resistance to cisplatin in GC via recruiting EZH2 and activating the PI3K/AKT pathway
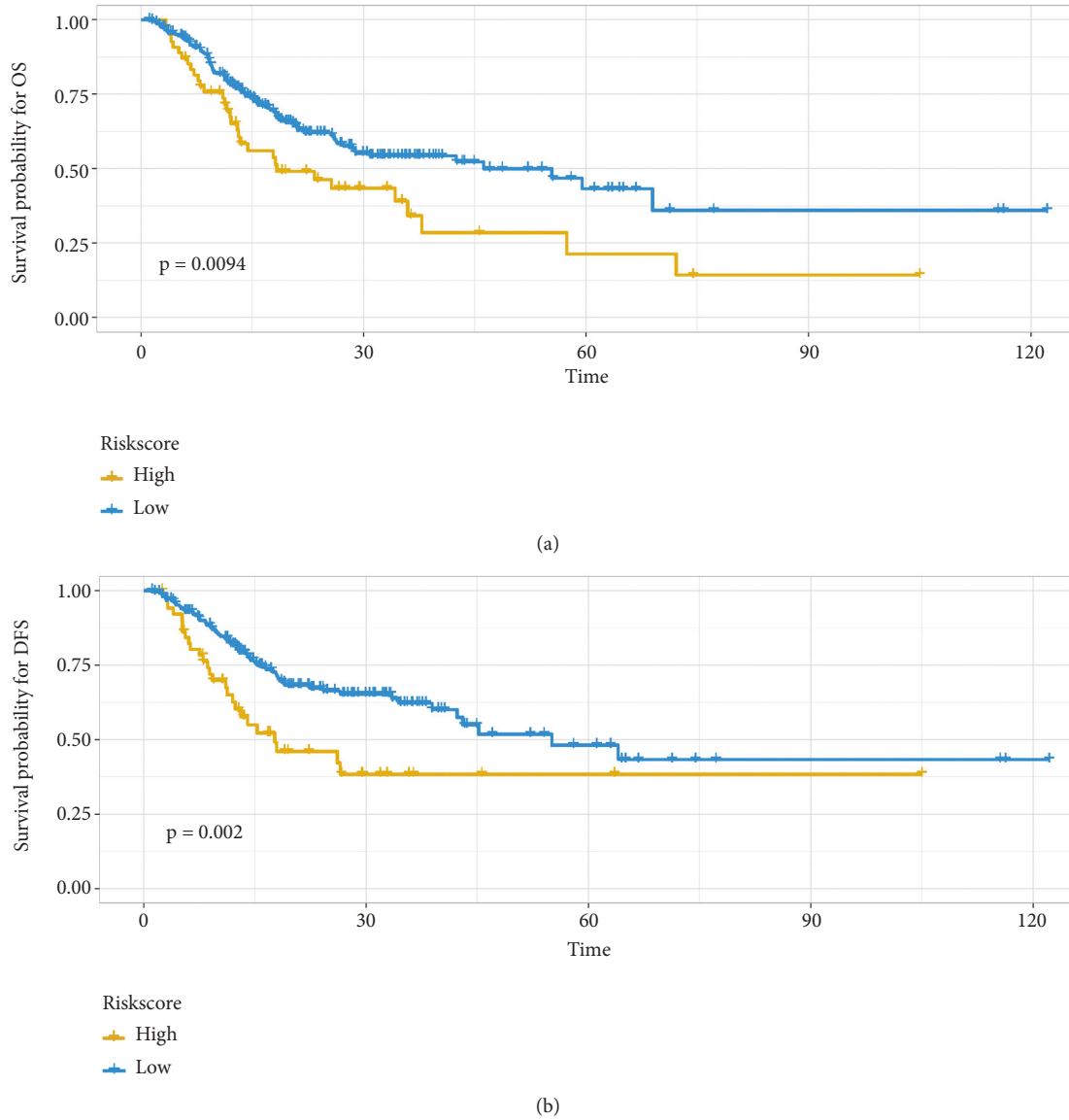
(a)

(b)

Figure 4: Survival analysis. (a) The Kaplan–Meier survival curves of OS according to RS. (b) The Kaplan–Meier survival curves of DFS according to RS (OS = overall survival; DFS = disease-free survival; and RS = risk score).

Table 3: Univariate and multivariate analysis of overall survival.

	Univariate analysis			Multivariate analysis		
	HR	95% CI	P value	HR	95% CI	P value
Tumor stage (early vs. advance)	0.553	[0.382–0.800]	0.002*	0.511	[0.355–0.736]	<0.001*
Risk score (low vs. high)	0.654	[0.434–0.985]	0.042*	0.642	[0.428–0.964]	0.033*
Age (years)	1.026	[1.008–1.044]	0.004*	1.023	[1.005–1.040]	0.011*
Differentiated degree (low vs. high)	0.744	[0.511–1.083]	0.122	—	—	—
Gender (female vs. male)	1.211	[0.830–1.768]	0.321	—	—	—

Note: HR = hazard ratio; CI = confidence interval; *statistically significant.

[32]. MIR4435-1HG was also known as LINC00978, MIR4435-2HG, and AWPPH. In the previous study, the expression level of LINC00978 has been suggested to be significantly related to tumor size, lymphatic metastasis, and tumor stage [33]. Additionally, lncRNA LINC00978 could contribute to tumor development by regulating the microRNA-497/NTRK3 axis in GC [27]. However, the upregulation of lncRNA AWPPH was demonstrated to inhibit the proliferation and invasion of gastric cancer cells via the miR-203a/DKK2 axis in another study [34]. Recent

TABLE 4: Univariate and multivariate analysis of disease-free survival.

	Univariate analysis			Multivariate analysis		
	HR	Upper 95	P value	HR	Upper 95	P value
Tumor stage (early vs. advance)	0.477	[0.298–0.763]	0.010*	0.549	[0.357–0.843]	0.006*
Risk score (low vs. high)	0.563	[0.364–0.871]	0.002*	0.492	[0.308–0.785]	0.003*
Age (years)	1.671	[1.025–2.723]	0.040*	1.647	[1.014–2.674]	0.044*
Differentiated degree (low vs. high)	0.851	[0.548–1.322]	0.472	—	—	—
Gender (female vs. male)	1.001	[0.981–1.021]	0.945	—	—	—

Note: HR = hazard ratio; CI = confidence interval; *statistically significant.

(a)
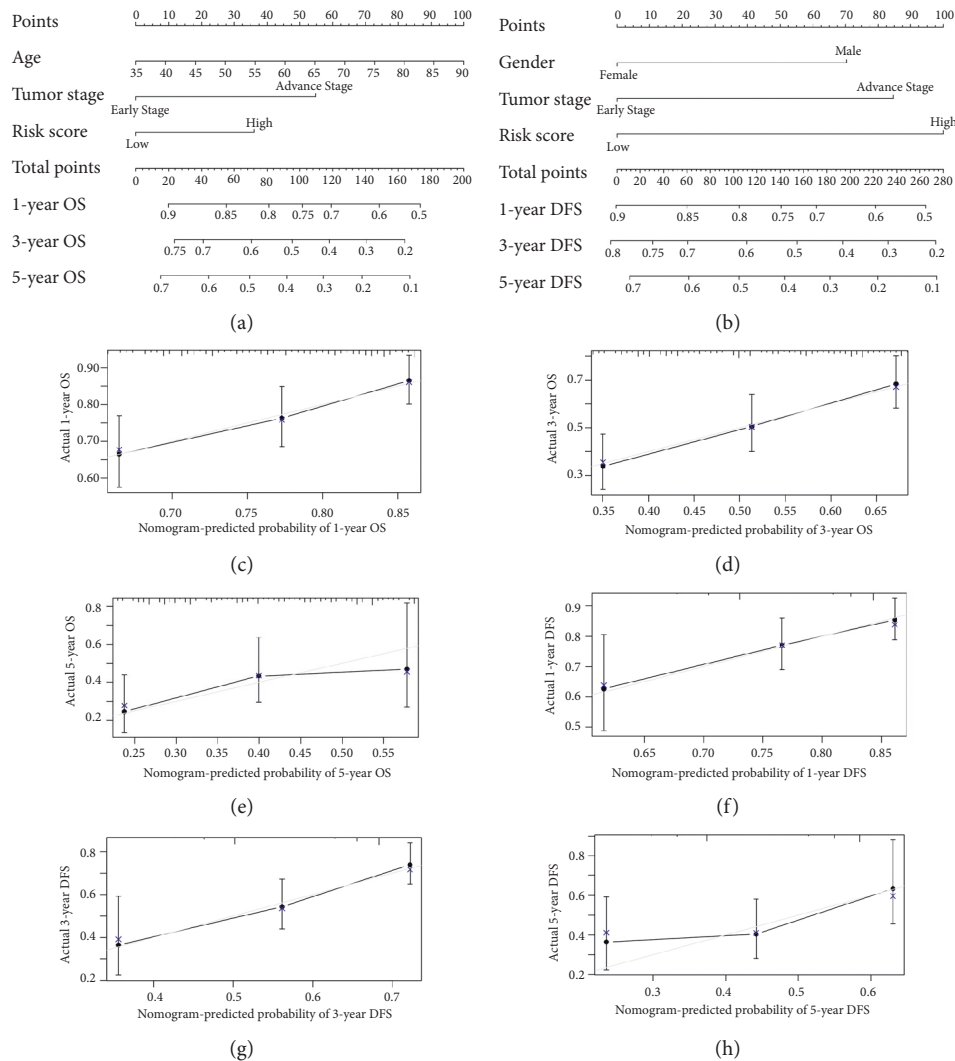
(b)

(c)

(d)

(e)

(f)

(g)

(h)

FIGURE 5: Nomograms for patients with gastric cancer. (a) The 1-, 3-, and 5-year overall survival nomogram. (b) The 1-, 3-, and 5-year disease-free survival nomogram. The calibration curves for predicting the (c–e) 1-, 3-, and 5-year overall survival and (f–h) 1-, 3-, and 5-year disease-free survival rates by nomogram prediction and actual observation in patients with gastric cancer.

study has shown that MIR4435-2HG could promote tumor metastasis in GC via targeting Wnt/β-catenin and desmoplakin. By contrast, there no reports concerning RP11-617F23.1 in GC so far. RP11-617F23.1 was also known as ZNF710-AS1-201 according to Ensembl database. Only one report concerning ZNF710-AS1-201, which demonstrated that the overexpression of ZNF710-AS1-201 was correlated with poor prognosis for patients with clear cell renal cell

carcinoma [35]. This conclusion was consistent with our verification result.

Recently, a few studies of the influence of lncRNAs on the tumor immune microenvironment of GC have been reported. HOTAIR was found to upregulate COL5A1, which was correlated with immune infiltration and promote the growth and metastasis of GC by sponging miR-1277-5p [36]. LINC00941 was correlated with the immune environment in
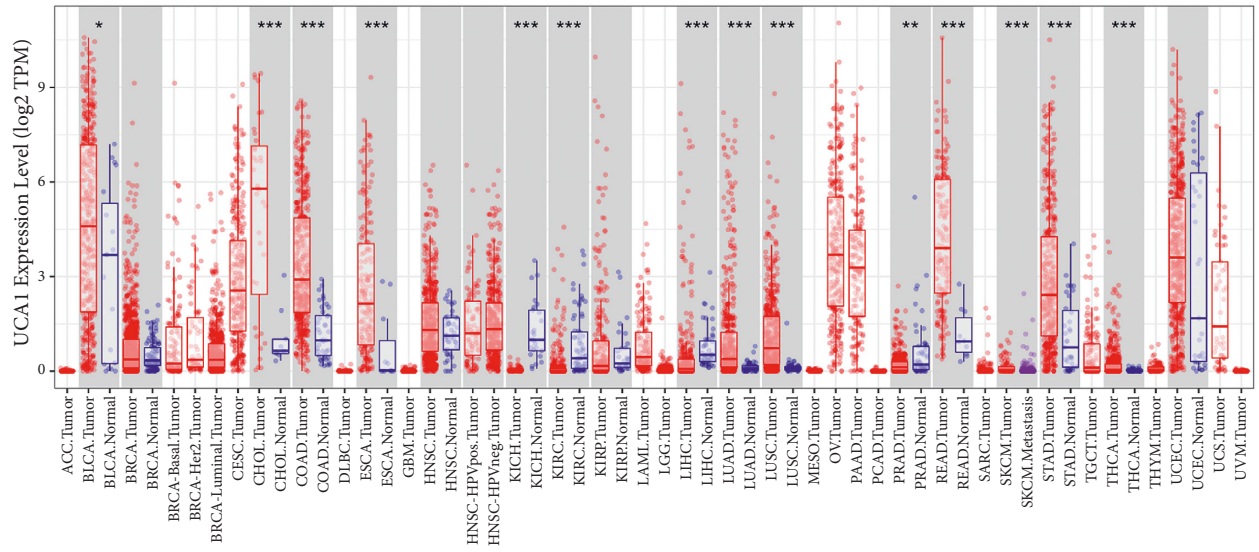
(a)
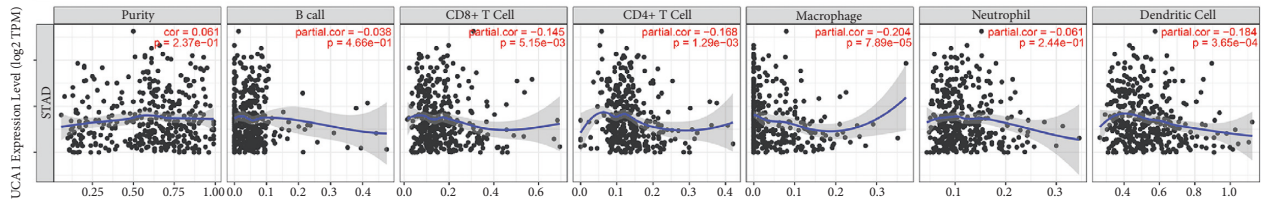
(b)
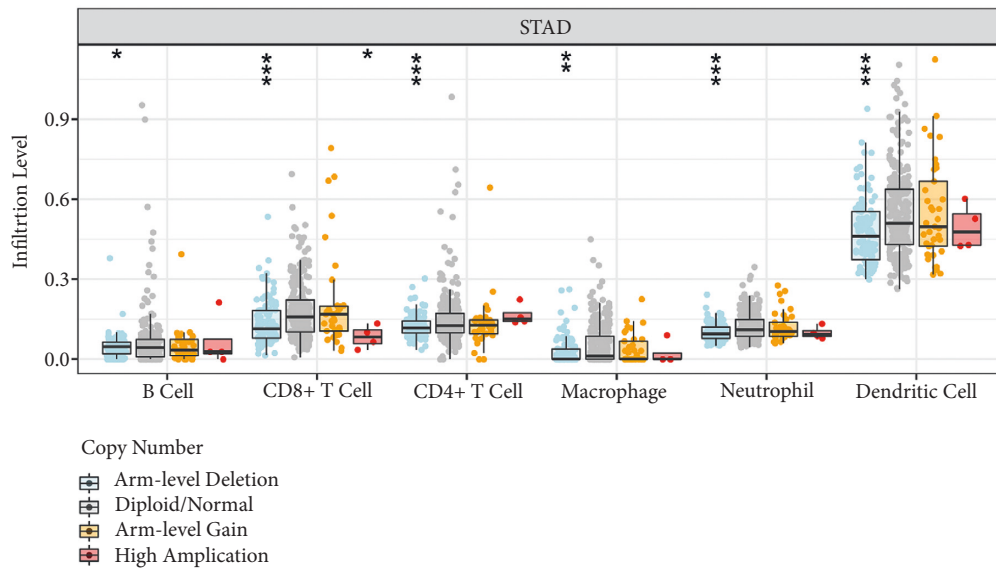
(c)

Figure 6: The association between UCA1 and the infiltration degree of immune cells. (a) Human UCA1 expression levels in different tumor types from TCGA database were determined by TIMER. (b) Correlation of UCA1 expression with the immune infiltration level in stomach adenocarcinoma. (c) Copy number distribution box plot of UCA1 in different immune cells in stomach adenocarcinoma ($*P < 0.05$, $**P < 0.01$, and $***P < 0.001$).

GC [37]. LINC00963 promoted the development of GC by targeting miR-612/CDC5L axis and mediated dendritic cell-related antitumor immune response [38]. CXXC finger protein 4 inhibited the immune escape of GC cells by acting on the ELK1/MIR100HG pathway [39]. MALAT1, as a sponge for miR-125a, regulates IL-21R signaling, participates in immune regulation of immune cells and tumor progression, and is a risk factor for survival and recurrence in GC [40]. Interestingly, RP11-617F23.1 was closely related to neutrophil-to-lymphocyte ratio (NLR) in the present
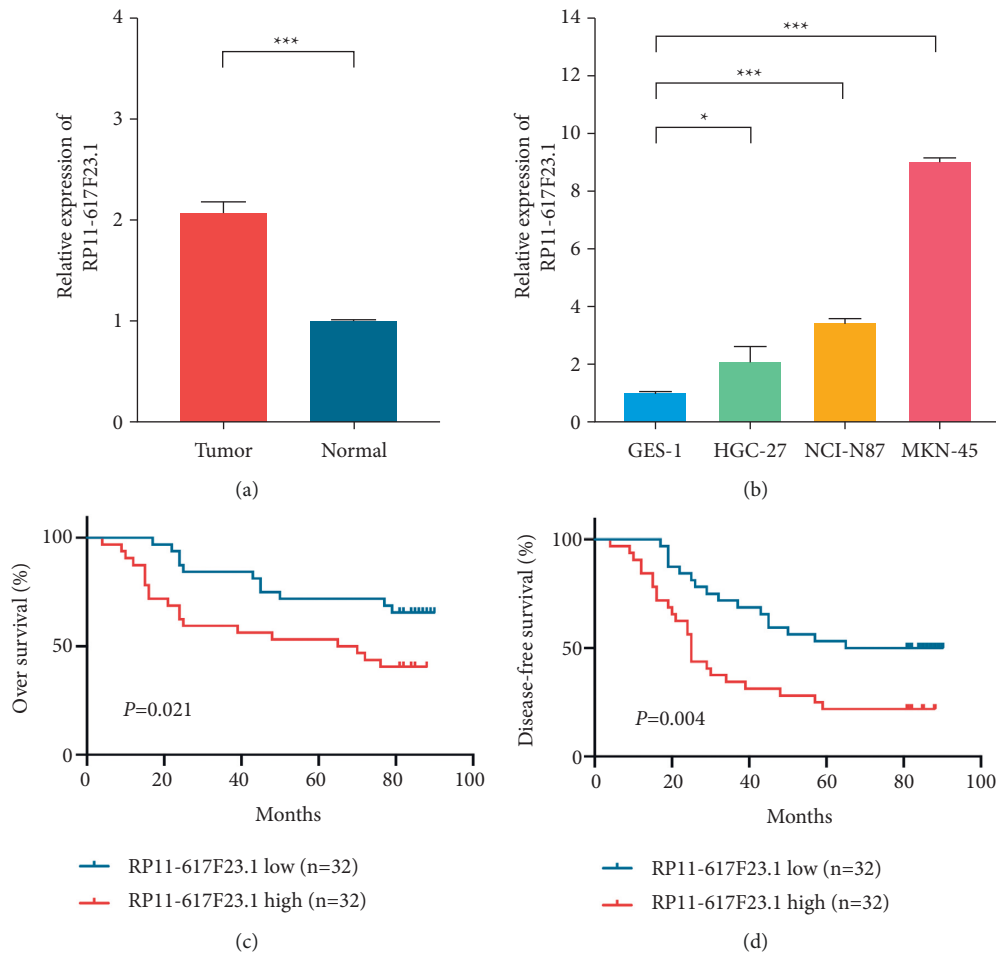
(a)

(b)

(c)

(d)

Figure 7: The verification of clinical role of RP11-617F23.1 in gastric cancer. (a) RP11-617F23.1 was significantly upregulated in human GC tissues ($n = 64$) compared with their corresponding adjacent tissues ($n = 64$). (b) RP11-617F23.1 was upregulated in gastric cancer cell lines compared with gastric epithelial cell. (c, d) Patients with high RP11-617F23.1 expression in tumor tissues had poorer overall survival (OS) and disease-free survival (DFS) than patients with low RP11-617F23.1 expression ($^{*}P < 0.05$, $^{***}P < 0.001$).

Table 5: Comparison of the clinicopathological characteristics between low and high expression groups.

Variables	RP11-617F23.1		P value
	Low expression ($n = 32$)	High expression ($n = 32$)	
Age, years	65.94 ± 6.90	67.84 ± 8.49	0.329
Sex, male	17 (53.1%)	22 (68.8%)	0.200
CEA, U/ml	20.54 ± 72.16	7.31 ± 20.63	0.692[#]
NLR	2.00 ± 0.76	3.81 ± 2.34	<0.001[#*]
Tumor differentiation, poor	16 (50.0%)	24 (75.0%)	0.039[*]
T stage, III-IV	15 (46.9%)	26 (81.3%)	0.004[*]
Lymphatic invasion, positive	14 (43.8%)	22 (68.8%)	0.044[*]

Note: mean ± standard deviation, number (percent); NLR: neutrophil lymphocyte ratio; [#]Mann–Whitney test; [*]statistically significant.

study, which reflected the immune status of patients. In addition, previous studies have identified that NRL was also significantly associated with the prognosis of GC [41]. Therefore, the molecular mechanism of RP11-617F23.1 as an IRL deserves further study, including immunoassay and immune escape.

In contrast to the previous research on IRLs in GC [42–44], the current study comprehensively evaluated the immune-related ceRNA network for the first time, established the risk model, and preliminarily validated the related lncRNAs. Additionally, the finding also suggested that RP11-617F23.1 may be used as a prognostic predictor for GC. However, the present study still had a few limitations. First, the sample size of survival analysis was not large enough. And, the detailed molecular mechanisms of RP11-617F23.1 require further investigation.

5. Conclusion

We established a novel risk model based on IRLs for predicting the prognosis of GC. Meanwhile, a novel IRL, RP11-617F23.1, could act as a predictor of prognosis for patients with GC. This provided a theoretical basis for tumor prevention and immunotherapy.

Data Availability

The RNA sequencing profiles can be obtained from The Cancer Genome Atlas (TCGA) (https://xenabrowser.net/) and Gene Expression Omnibus (GEO) (https://www.ncbi. nlm.nih.gov/geo/). The immune-related genes can be downloaded from the InnateDB database (https://www. innatedb.ca/index.jsp). The datasets used and/or analyzed during the current study are available from the corresponding author on reasonable request.

Conflicts of Interest

The authors declare that they have no conflicts of interest.

Authors' Contributions

Acknowledgments

References

[1] H. Sung, J. Ferlay, R. L. Siegel et al., "Global cancer statistics 2020: GLOBOCAN estimates of incidence and mortality worldwide for 36 cancers in 185 countries," *CA: A Cancer Journal for Clinicians*, vol. 71, no. 3, pp. 209–249, 2021.

[2] P. Karimi, F. Islami, S. Anandasabapathy, N. D. Freedman, and F. Kamangar, "Gastric cancer: descriptive epidemiology, risk factors, screening, and prevention," *Cancer Epidemiology Biomarkers & Prevention*, vol. 23, no. 5, pp. 700–713, 2014.

[3] S. Kinami, N. Nakamura, Y. Tomita et al., "Precision surgical approach with lymph-node dissection in early gastric cancer," *World Journal of Gastroenterology*, vol. 25, no. 14, pp. 1640–1652, 2019.

[4] C. Coutzac, S. Pernot, N. Chaput, and A. Zaanan, "Immunotherapy in advanced gastric cancer, is it the future?" *Critical Reviews in Oncology*, vol. 133, pp. 25–32, 2019.

[5] M. Venerito, A. Link, T. Rokkas, and P. Malfertheiner, "Gastric cancer—clinical and epidemiological aspects," *Helicobacter*, vol. 21, no. S1, pp. 39–44, 2016.

[6] L. Marano, K. Polom, A. Patriti et al., "Surgical management of advanced gastric cancer: an evolving issue," *European Journal of Surgical Oncology*, vol. 42, no. 1, pp. 18–27, 2016.

[7] P. Ehrrlich, "Ueber den jetzigen stand der karzinoforschung," *Ned Tijdschr Geneeskd*, vol. 5, pp. 273–290, 1909.

[8] J. Zheng, B. Cao, X. Zhang, Z. Niu, and J. Tong, "Immune-related four-lncRNA signature for patients with cervical cancer," *BioMed Research International*, vol. 2020, Article ID 3641231, 15 pages, 2020.

[9] X. Lei, Y. Lei, J.-K. Li et al., "Immune cells within the tumor microenvironment: biological functions and roles in cancer immunotherapy," *Cancer Letters*, vol. 470, pp. 126–133, 2020.

[10] L. Bejarano, M. J. C. Jordāo, and J. A. Joyce, "Therapeutic targeting of the tumor microenvironment," *Cancer Discovery*, vol. 11, no. 4, pp. 933–959, 2021.

[11] D. Lau, A. M. Bobe, and A. A. Khan, "RNA sequencing of the tumor microenvironment in precision cancer immunotherapy," *Trends in Cancer*, vol. 5, no. 3, pp. 149–156, 2019.

[12] M. C. Bridges, A. C. Daulagala, and A. Kourtidis, "LNCcation: lncRNA localization and function," *Journal of Cell Biology*, vol. 220, no. 2, Article ID e202009045, 2021.

[13] M. Xu, X. Xu, B. Pan et al., "LncRNA SATB2-AS1 inhibits tumor metastasis and affects the tumor immune cell microenvironment in colorectal cancer by regulating SATB2," *Molecular Cancer*, vol. 18, no. 1, p. 135, 2019.

[14] X. Yan, D. Zhang, W. Wu et al., "Mesenchymal stem cells promote hepatocarcinogenesis via lncRNA-MUF interaction with ANXA2 and miR-34a," *Cancer Research*, vol. 77, no. 23, pp. 6704–6716, 2017.

[15] X. Pei, X. Wang, and H. Li, "LncRNA SNHG1 regulates the differentiation of Treg cells and affects the immune escape of breast cancer via regulating miR-448/Ido," *International Journal of Biological Macromolecules*, vol. 118, pp. 24–30, 2018.

[16] T. Barrett, D. B. Troup, S. E. Wilhite et al., "NCBI GEO: mining tens of millions of expression profiles-database and tools update," *Nucleic Acids Research*, vol. 35, pp. D760–D765, 2007.

[17] M. J. Goldman, B. Craft, M. Hastie et al., "Visualizing and interpreting cancer genomics data via the xena platform," *Nature Biotechnology*, vol. 38, no. 6, pp. 675–678, 2020.

[18] J. Harrow, A. Frankish, J. M. Gonzalez et al., "GENCODE: the reference human genome annotation for the ENCODE project," *Genome Research*, vol. 22, no. 9, pp. 1760–1774, 2012.

[19] H. Jiang and W. H. Wong, "SeqMap: mapping massive amount of oligonucleotides to the genome," *Bioinformatics*, vol. 24, no. 20, pp. 2395-2396, 2008.

[20] M. E. Ritchie, B. Phipson, D. Wu et al., "Limma powers differential expression analyses for RNA-sequencing and microarray studies," *Nucleic Acids Research*, vol. 43, no. 7, p. e47, 2015.

[21] Y. Tay, J. Rinn, and P. P. Pandolfi, "The multilayered complexity of ceRNA crosstalk and competition," *Nature*, vol. 505, no. 7483, pp. 344–352, 2014.

[22] V. Agarwal, G. W. Bell, J.-W. Nam, and D. P. Bartel, "Predicting effective microRNA target sites in mammalian mRNAs," *Elife*, vol. 4, 2015.

[23] Y. Chen and X. Wang, "miRDB: an online database for prediction of functional microRNA targets," *Nucleic Acids Research*, vol. 48, no. D1, pp. D127–D131, 2020.

[24] C.-H. Chou, S. Shrestha, C.-D. Yang et al., "miRTarBase update 2018: a resource for experimentally validated microRNA-target interactions," *Nucleic Acids Research*, vol. 46, no. D1, pp. D296–D302, 2018.

[25] K. Breuer, A. K. Foroushani, M. R. Laird et al., "InnateDB: systems biology of innate immunity and beyond-recent updates and continuing curation," *Nucleic Acids Research*, vol. 41, no. D1, pp. D1228–D1233, 2013.

[26] T. Li, J. Fan, B. Wang et al., "TIMER: a web server for comprehensive analysis of tumor-infiltrating immune cells," *Cancer Research*, vol. 77, no. 21, pp. e108–e110, 2017.

[27] J.-Y. Bu, W.-Z. Lv, Y.-F. Liao, X.-Y. Xiao, and B.-J. Lv, "Retracted: long non-coding RNA LINC00978 promotes cell proliferation and tumorigenesis via regulating microRNA-497/NTRK3 axis in gastric cancer," *International Journal of Biological Macromolecules*, vol. 123, pp. 1106–1114, 2019.

[28] C.-J. Wang, C.-C. Zhu, J. Xu et al., "The lncRNA UCA1 promotes proliferation, migration, immune escape and inhibits apoptosis in gastric cancer by sponging anti-tumor miRNAs," *Molecular Cancer*, vol. 18, no. 1, p. 115, 2019.

[29] L. Shan, C. Liu, and C. Ma, "High expression of serum UCA1 may be a potential biomarker for clinical diagnosis of gastric cancer," *Clinical Laboratory*, vol. 65, 2019.

[30] L. Gu, L.-S. Lu, D.-L. Zhou, and Z.-C. Liu, "UCA1 promotes cell proliferation and invasion of gastric cancer by targeting CREB1 sponging to miR-590-3p," *Cancer Medicine*, vol. 7, no. 4, pp. 1253–1263, 2018.

[31] Z.-K. Zuo, Y. Gong, X.-H. Chen et al., "Retracted: TGFβ1-induced LncRNA UCA1 upregulation promotes gastric cancer invasion and migration," *DNA and Cell Biology*, vol. 36, no. 2, pp. 159–167, 2017.

[32] Q. Dai, T. Zhang, J. Pan, and C. Li, "LncRNA UCA1 promotes cisplatin resistance in gastric cancer via recruiting EZH2 and activating PI3K/AKT pathway," *Journal of Cancer*, vol. 11, no. 13, pp. 3882–3892, 2020.

[33] M. Fu, Z. Huang, X. Zang et al., "Long noncoding RNA LINC 00978 promotes cancer growth and acts as a diagnostic biomarker in gastric cancer," *Cell Proliferation*, vol. 51, no. 1, 2018.

[34] L. Li, J. Kou, and B. Zhong, "Up-regulation of long non-coding RNA AWPPH inhibits proliferation and invasion of gastric cancer cells via miR-203a/DKK2 axis," *Human Cell*, vol. 32, no. 4, pp. 495–503, 2019.

[35] G. Li, M. Xie, Z. Huang et al., "Overexpression of antisense long non-coding RNA ZNF710-AS1-202 promotes cell proliferation and inhibits apoptosis of clear cell renal cell carcinoma via regulation of ZNF710 expression," *Molecular Medicine Reports*, vol. 21, no. 6, pp. 2502–2512, 2020.

[36] Z. Wei, L. Chen, L. Meng, W. Han, L. Huang, and A. Xu, "LncRNA hotair promotes the growth and metastasis of gastric cancer by sponging miR-1277-5p and upregulating COL5A1," *Gastric Cancer*, vol. 23, no. 6, pp. 1018–1032, 2020.

[37] C. Luo, Y. Tao, Y. Zhang et al., "Regulatory network analysis of high expressed long non-coding RNA LINC00941 in gastric cancer," *Gene*, vol. 662, pp. 103–109, 2018.

[38] H. Zhu, J.-H. Tang, S.-M. Zhang et al., "Long noncoding RNA LINC00963 promotes CDC5L-mediated malignant progression in gastric cancer," *OncoTargets and Therapy*, vol. 13, pp. 12999–13013, 2020.

[39] P. Li, D. Ge, F. Hu et al., "CXXC finger protein 4 inhibits the CDK18-ERK1/2 axis to suppress the immune escape of gastric cancer cells with involvement of ELK1/MIR100HG pathway," *Journal of Cellular and Molecular Medicine*, vol. 24, no. 17, pp. 10151–10165, 2020.

[40] L. Yan, J. Zhang, D. Guo, J. Ma, S.-F. Shui, and X.-W. Han, "IL-21R functions as an oncogenic factor and is regulated by the lncRNA MALAT1/miR-125a-3p axis in gastric cancer," *International Journal of Oncology*, vol. 54, no. 1, pp. 7–16, 2019.

[41] R. Miyamoto, S. Inagawa, N. Sano, S. Tadano, S. Adachi, and M. Yamamoto, "The neutrophil-to-lymphocyte ratio (NLR) predicts short-term and long-term outcomes in gastric cancer patients," *European Journal of Surgical Oncology*, vol. 44, no. 5, pp. 607–612, 2018.

[42] J. Chen, J. G. Chen, B. Sun, J. Wu, and C. Du, "Integrative analysis of immune microenvironment-related CeRNA regulatory axis in gastric cancer," *Mathematical Biosciences and Engineering*, vol. 17, no. 4, pp. 3953–3971, 2020.

[43] Y. Wang, Y. Zou, Y. Zhang, and C. Li, "Developing a risk scoring system based on immune-related lncRNAs for patients with gastric cancer," *Bioscience Reports*, vol. 41, no. 1, Article ID BSR20202203, 2021.

[44] Y. Zhang, H. Li, W. Zhang, Y. Che, W. Bai, and G. Huang, "LASSO-based cox-PH model identifies an 11-lncRNA signature for prognosis prediction in gastric cancer," *Molecular Medicine Reports*, vol. 18, no. 6, pp. 5579–5593, 2018.